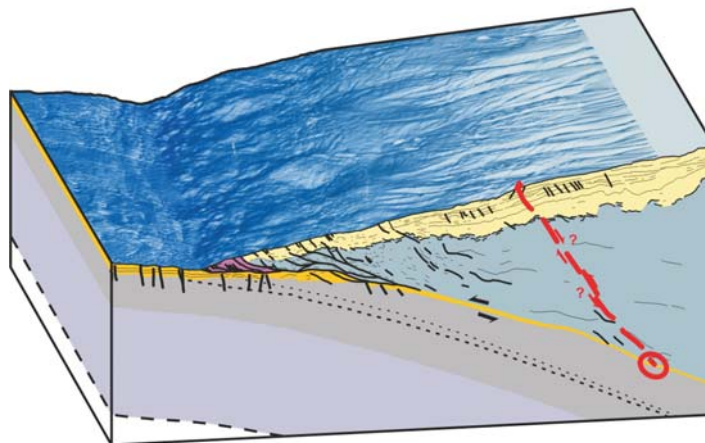


RV Meteor Cruise Report M54/2 + M54/3

Fluids and Subduction Costa Rica 2002



M54/2

Caldera - Caldera 13.8. - 7.9.2002

M54/3A

Caldera - Caldera 10.9. - 28.9.2002

M54/3B

Caldera - Curacao 01.10. - 11.10.2002

Editors

Emanuel Söding, Klaus Wallmann, Erwin Suess & Ernst Flüh
esoeding@geomar.de, kwallmann@geomar.de, esuess@geomar.de, eflueh@geomar.de

Layout and Design

Rico Wendler (rwendler@geomar.de)

Cover

Daniel Hepp, Tobias Mörz & Emanuel Söding
(dhepp@geomar.de, tmoerz@geomar.de, esoeding@geomar.de)

GEOMAR

Research Center for Marine Geosciences
Wischhofstr. 1-3
24148 Kiel
GERMANY
Tel: (49) 431- 600 2555

In memory of our colleague Sonja Klauke.

Table of Contents

1. Introduction	1
1.1 SFB Objective	1
1.2 Cruise Objectives	2
1.3 Scientific Program	4
1.3.1 Leg M54/1	4
1.3.2 Legs M54/2 and M54/3A	5
1.4 Major Geological Targets	7
1.4.1 Carbonate Mounds	7
1.4.2 Seamount Subduction	7
1.4.3 Submarine Slides	8
2. Participants	9
2.1 Scientists	9
2.2 Crew	15
2.3 Addresses of Participating Institutions	17
3. Geological Setting of the Study Area	18
3.1 Subduction of Smooth Cocos Plate Segment off Nicaragua and Northern Costa Rica	21
3.2 Subduction of Rough Cocos Plate Segment off Costa Rica	24
4. Cruise Narrative	31
4.1 Leg M54/2	31
4.2 Leg M54/3A	35
4.3 Leg M54/3B	40
5. Results	42
5.1 Seafloor Observations	42
5.1.1 Smooth Cocos Plate Segment off Nicaragua and Northern Costa Rica	42
5.1.2 Rough Cocos Plate Segment off Costa Rica	44
5.2 Heat flow studies	49
5.2.1 Smooth Cocos Plate Segment off Nicaragua and Northern Costa Rica	50
5.2.2 Rough Cocos Plate Segment off Costa Rica	52
5.3 Dredging	61
5.4 Sediment Sampling and Sedimentology	62
5.4.1 Sediment Sampling and Physical Properties	62
5.4.1.1 Sampling Techniques	62
5.4.1.2 Mounds	63
5.4.1.3 Slides and Scarps	66
5.4.1.4 Slope Profiles	68
5.4.2 Ash Layers	71
5.4.3 Structural Sedimentology of Mounds	73
5.4.3.1 Introduction	73
5.4.3.2 Indicators of Deformation and Overcompaction	73
5.4.3.3 Physical Evidence of Fluid Flow	74
5.4.3.4 Chaotic Sediment Fabric in Pipes and Flows	74
5.4.3.5 Summary and Outlook	74

5.4.4	Authigenic Carbonates	79
5.4.4.1	Introduction	79
5.4.4.2	Chemoherm and other Authigenic Carbonate Features	79
5.4.4.3	Gas Hydrate Carbonates	80
5.4.4.4	Carbonate Concretions and Cemented Sediments	81
5.4.4.5	Outlook	81
5.5.	Pore Water Geochemistry	85
5.5.1	Sampling, Processing and Analyses	85
5.5.2	Shipboard Results	86
5.5.2.1	Shelf to Deep-Sea Transects	87
5.5.2.2	Smooth Plate Segment off Nicaragua and Northern Costa Rica	92
5.5.2.3	Rough Plate Segment off Costa Rica	99
5.6.	Water Column Studies and Methane Distribution	114
5.6.1	Introduction	114
5.6.2	Material and Methods	114
5.6.3	Preliminary Results and Discussion	115
5.6.3.1	Smooth Cocos Plate Segment off Nicaragua and Northern Costa Rica	115
5.6.3.2	Rough Plate Segment off Costa Rica	116
5.7.	Biomarker Sampling	126
5.8.	Trace Element and Isotope Studies	127
5.8.1	Smooth Cocos Plate Segment off Nicaragua and Northern Costa Rica	129
5.8.2	Rough Plate Segment	130
5.9.	Lander Deployments	131
5.9.1	Smooth Cocos Plate Segment off Nicaragua and Northern Costa Rica	136
5.9.2	Rough Cocos Plate Segment off Costa Rica	138
5.10.	OBH/OBS Deployments	146
5.10.1	Computer Facilities for Bathymetry, Magnetic and Seismic Data Processing	146
5.10.2	Seismic Instrumentation	147
5.10.3	Data Conversion	150
5.10.4	Processing of JACO Network's Earthquake Data	154
APPENDIX		
A.	Station List	161
B.	Weather	183
C.	OBS/OBH/OBT Station List	197
D.	Heatflow Instrumentation, Methodology and Maps	201
E.	Core Photography	213
F.	Core Description Plates	273
G.	Logging Plates	355

1 Introduction

1.1 SFB Objective

The RV METEOR M 54 cruise is of central importance to the “Sonderforschungsbereich 574”. All subprojects were involved and participated in various aspects of the cruise. The main objective of SFB 574 is to understand the budget, reactions, and recycling of volatile elements in subduction zones and their role in climate forcing. In this way the SFB addresses the long- and short-term development of the Earth’s climate, the geochemical evolution of the hydrosphere and atmosphere, and the causes of natural disasters. These processes are all connected in one way or another with the return flow and impact of volatiles and fluids from subduction zones. The multi-disciplinary analysis of the volatile phases (water, carbon, sulfur and halogens) and their complex effects on the exosphere, is an ambitious undertaking, and one of the highest priority objectives of today’s geoscience.

The major volatile input into subduction zones are the sediments, the altered products oceanic crust, and the trench-fill from down-slope mass wasting. The output is via fluid venting at the deformation front, by gas hydrate formation/dissociation, and by volcanic degassing at the fore-arc. Inside the subduction zone the incoming material is transformed, mobilized or fractionated into different volatile reservoirs and phases. These phases are either ejected into the exosphere through the upper plate, accreted to the leading edge of the continental plate, or are transported into the lower mantle. The tectonic style of subduction, the structure of the margin wedge, and the properties and configuration of the down-going plate all exert a first order control on volatile budget, its transformation, and return pathway.

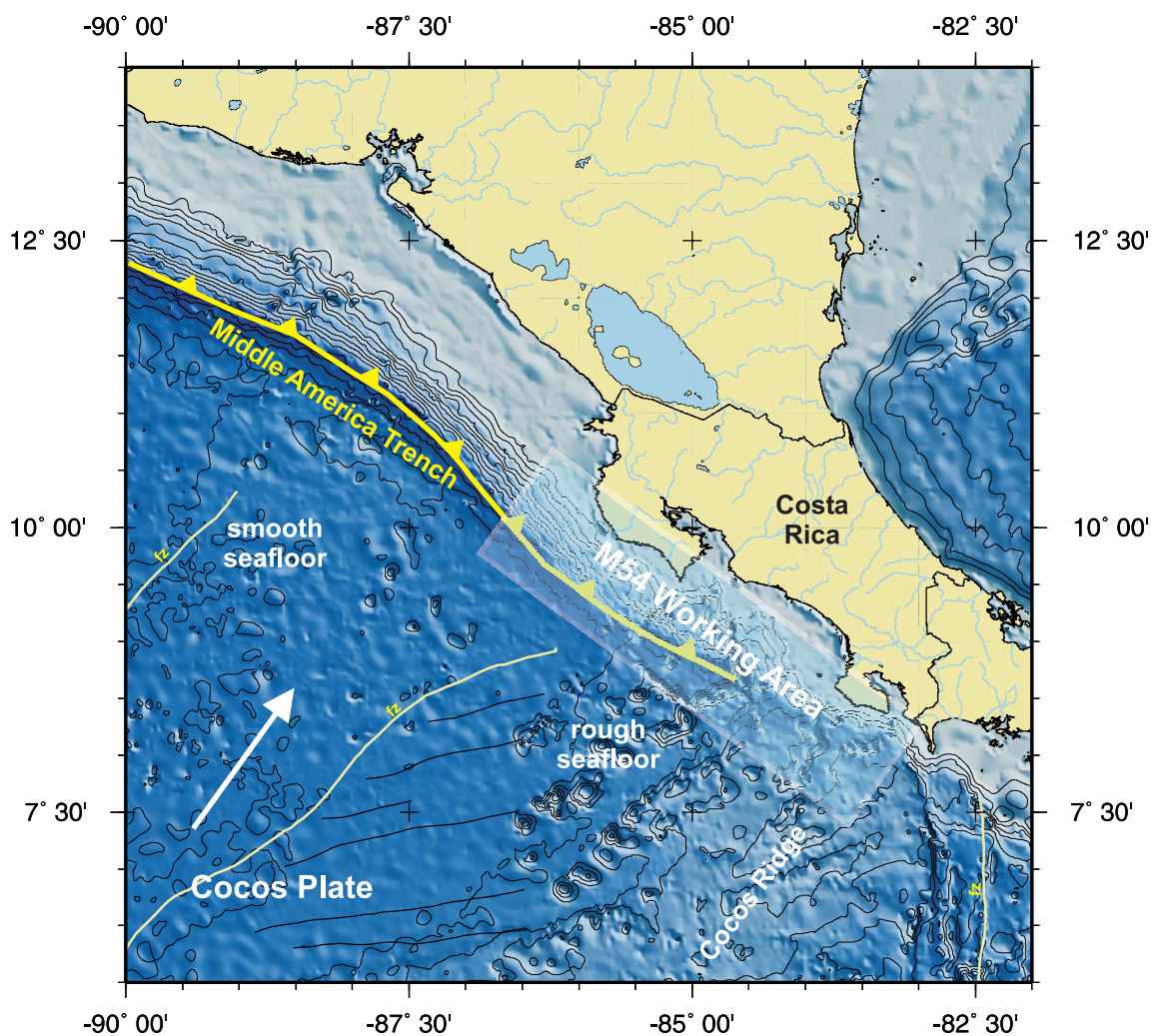


Figure 1.1: General structure of the seafloor at the Costa Rica/Nicaragua Pacific margin.

The area of investigation, the Central American fore-arc off Costa Rica and Nicaragua (Fig. 1.1 Sea floor morphology), is well suited for such an investigation because of small-scale changes of features which influence the volatile cycling; i.e. the composition and age of the incoming oceanic crust, the morphology of continental slope, and the accretionary tectonic style. Equally important are the composition of the volcanic rocks on land as well as in submarine outcrops to trace the history of volcanic emissions.

The basic data acquisition for the investigations aboard RV METEOR were geophysical surveys, multibeam and side-scan sonar surveys, sediment coring, water column sampling for methane, as well as video-guided sea floor observations and lander deployments.

1.2 Cruise objectives

During the first leg, M 54/1 (Fig. 1.2), high-resolution seismic profiles were acquired in order to obtain the geometry and thickness of the incoming sediment packages. Special attention was given to the distribution of gas hydrates as evident in the BSR, which is linked to upward fluid flow. In combination of different geophysical methods, applied to small-scale selected areas, the quantification of physical properties of the sediments and their pore fluids was attempted.

During the second leg, M 54/2, sediment coring and heat flux measurements were the main activities. The sampling was done along pre-selected profiles (Fig. 1.2). Sediment cores were used to investigate early diagenetic processes, determine the sediment physical properties, and to collect volcanic ash layers for the reconstruction of the history of explosive volcanisms. A special focus was the acquisition of heat flow profiles in order to determine the thermal structure of the lithospheric plate and thus constrain the seismogenic zone. Additionally, the thermal anomalies at and around fluid conduits and slump features were measured.

During the first part of the third leg, M54/3A (Fig. 1.2), the focus was on the identification and sampling of sites influenced by venting of methane-rich fluids. Chemoautotrophic benthic communities and carbonate chimneys, crusts and other authigenic mineral precipitates were obtained which were used as archives of the dewatering history. TV-guided deep-sea instrumentation was deployed in order to quantify the amount of fluids and dissolved gases released from the seafloor and the turnover of methane in the sediment as well as in the water column. Radiogenic and stable isotopes in fluid and solid phase samples were used along with trace element pattern to ascertain source depth and residence time of fluids. The main geological features which have shown signs of fluid venting are carbonate mounds, subducted seamount scarps and submarine land slides. These features were the main targets during leg M54/3A. During the second part of the third leg M54/3B the main task was to recover a seismic network which had been installed in April 2002 during cruise SONNE SO163-2. Recovery operation included tiltmeters, maintenance of the instruments, archive the data and re-deploy the network. The instruments will then be recovered again in summer 2003 during RV SONNE cruise SO 173-1. In addition, a benthic lander which was deployed at Jaco Scarp during leg M54/3A was recovered .

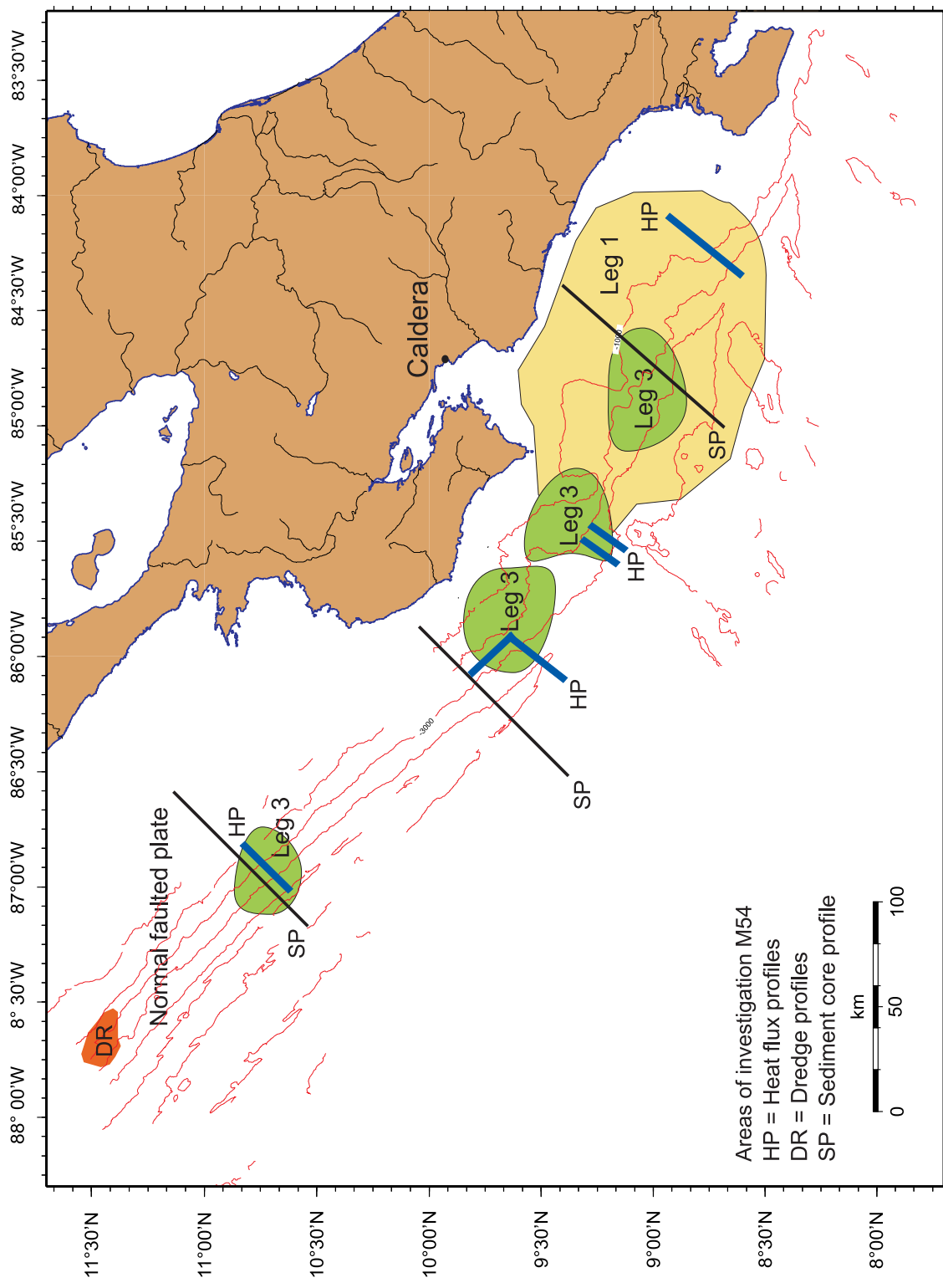


Figure 1.2: The working area of cruise M54.

1.3 Scientific programme

A coordinated scientific program was developed based on results from earlier cruises and the definition of overall and specific scientific objectives. The program was implemented in three legs, whereby the first leg was jointly carried out with members of the Earth Science Department of the University of Bremen. In general terms it was devoted to seismic imaging of venting structures and subsurface fluid pathways. The second and third leg pursued geochemical and sedimentological objectives. These were supplemented by heat flow surveys and the recovery and re-deployment of an off-shore seismic network.

1.3.1 Leg M54/1

Seismic imaging

During RV METEOR Cruise M54/1 through collaboration with the Department of Earth Science of the University Bremen seismic studies were conducted which focus on the detailed imaging of near surface sediment structures. In this way paths of fluid and gas upflow were characterized. The main part of the research program was the acquisition of 3-D seismic data in the vicinity of carbonate mounds. These surveys were complemented by simultaneous tomographic recordings of the high frequency signals with ocean bottom hydrophone systems. This approach allows the quantification of physical properties of the shallow sediment columns from seismic data. From these data it is expected to ultimately quantify the proportion of gas, gas hydrate and fluids in the sediment.

The seismic survey program addressed four different objectives, which are directly linked to the primary objectives of the SFB 574:

- Seismic imaging of the sediment column above the BSR to characterize the internal structures and to allow the reconstruction of sediment tectonics, potential fluid and gas migration pathways. In selected areas, the grid was narrowed to be able to acquire data for 3-D seismic processing and imaging.
- Seismic imaging of the detailed structure of the decollement, where high frequency signals have sufficient penetration.
- 3-D seismic imaging of carbonate mounds as the main structures related to fluid and gas venting. The objective was to better understand the geometry of pathways and faults zones as well as the relationship to the BSR reflections and shallow gas accumulation.
- Determination of seismic properties (i.e. amplitude, travelttime, attenuation, velocity) for different source signatures and frequencies from a combination of acoustic, reflection seismic and tomographic data sets. The simultaneous operation of several sources and ocean bottom systems is required to determine parameters of the BSR reflector and within the gas hydrate stability zone. Modeling of the geothermal regime could be improved by further acquisition of temperature data on such critical processes as fluid migration as well as on the morphology of the basement and the BSR-surface. Additional seismic data were collected along these geothermal transects.

In order to relate seismic information to lithology and stratigraphy in the area, several seismic lines were shot connecting the drill sites of ODP Leg 170.

1.3.2 Legs M54/2 and M54/3

A major objective of both legs M54/2 and M54/3 was the identification and sampling of venting manifestations on the seafloor which currently are or which in the past were influenced by venting of free methane or methane-rich fluids. The basis for these investigations were geophysical information, multi-beam and side-scan sonar maps as well as video sled surveys (OFOS). Sites of methane venting were found to be associated with carbonate mounds, seamount- and ridge-subduction and submarine slumps and slides. These sites were extensively sampled during both legs.

Scientific program M54/2

Geochemistry

A major goal of leg M54/2 was the investigation of sediment diagenesis in the fore-arc and the sampling of cold vents. The quantification of organic matter mineralization, secondary redox reactions, seawater-mineral interactions, as well as the determination of fluid flow and accumulation rates of volatile species in fore-arc sediments is of central importance for the element cycling. Alteration and submarine weathering of volcanic ash, biogenic opal, and clay minerals further contribute to the water cycling and solute transport in sediments. Therefore, the spatial variability and distribution of processes and chemical compounds in the fore-arc area were sampled to define the volatile input into subduction zones and to constrain the submarine volatile emissions via diffusive and focused fluid flow.

Three transects with 6 stations each were sampled perpendicular to the trench axis by piston corer, gravity corer and multi corer devices. Exact positions of the cores were determined by Parasound data showing acoustic anomaly patterns. Furthermore, sediment cores were taken at selected sites from carbonate mounds and fluid seep areas to characterize the chemical composition and the flow rates of venting fluids. After core retrieval high-resolution pore water and solid phase sampling were carried out and onboard chemical analyses of pore waters performed. From the water column an array of samples were taken to map the methane plumes and their extent around cold vent sites.

Heat flow measurements

Subduction zones are of fundamental importance in plate tectonic and a wealth of processes is inherently related to this type of destructive plate boundaries. Most important is that subduction exhibits intense seismic activity, among them the largest earthquakes in the world. The risk of hazards from great earthquakes is largest for events occurring at depth of less than 35-40 km along the fault zone between the over-riding and the down-going plate, called the seismogenic zone. The zone of stick-slip behaviour where earthquakes can nucleate may be controlled by the mechanical properties of the rock and hence temperature. Earthquakes are related to brittle deformation. At depth, however, crustal rocks deform in a ductile fashion ($T > 350-450^{\circ}\text{C}$). At shallow depth clay minerals lubricate the thrust fault ($T < 100-150^{\circ}\text{C}$). Therefore, tectonic thrust-fault earthquakes are restricted to a certain depth interval. Therefore, during leg M54/2 we obtained heat flow profiles at key locations to determine the thermal structure of the active continental margin. The profiles were obtained, in conjunction with and closely coordinated with the gravity coring operations for the geochemical objectives and hence flow paths.

Sedimentology and physical properties

Lithological core descriptions and physical property profiles are the basis for any investigations on sediment cores showing dewatering features or evidence of volatile transport. The lithological characterization was based on core descriptions and sediment physical properties. The sediment-physical work plan included the non-destructive logging part and sampling based determination of the sediment physical index parameter: water content, wet bulk density and grain density. The whole-core logging program included the following parameters: core diameter, p-wave velocity, density (GRAPE) and magnetic susceptibility. Color spectrometer data were taken on split core halves. Aim of the sediment physical working program is to establish coherent litho-physical sediment profiles by integrating descriptive and measured parameters.

Tephra-stratigraphy

Piston cores taken along transects perpendicular to the trench off Nicaragua were sampled for volcanic fallout ash layers. Sampling and analyzing these ash layers is an important addition to the field work done in subproject C4 and is aimed at reconstructing the stratigraphy of major explosive volcanic eruptions as a prerequisite to determine the temporal evolution of their volatile release into the atmosphere in the past. Sites for coring were primarily areas of undisturbed stratigraphy and selected in connection with gravity coring program for geochemical objectives.

Benthic foraminifera

Benthic foraminiferal assemblages in extreme habitats like cold vents or in regions with methane hydrate occurrences have hardly been investigated. Cold vents show a high variability of environmental conditions in a very narrow region. This leads to the formation of ecological niches and a biological zoning of meio- and macrofauna. Assemblages were taken from these ecological niches and habitat relationships were determined between single niches and between epi- and infaunal communities, live to dead assemblages. These data are going to be supplemented by stable isotope analyses and determination of organic carbon contents of the sediment.

Scientific program M54/3A

The knowledge of fluid sources, chemical composition of expelled fluids, exchange rates between basement, sediments, fluids and seawater, transport pathways and residence times of fluids are of general importance for the understanding of material budgets and cycling in subduction zones. To address these objectives during Leg 54/3A sampling by TV-guided systems was the main activity during this leg; also direct measurements by sea floor landers were carried out. Thus a variety of chemical and isotopic measurements on vent fluids, pore waters, water column samples and authigenic carbonates could be performed.

Fluid geochemistry and authigenic carbonates

In sediment layers, which are exposed to methane ascending from depths and sulfate-rich waters from above, the microbial anaerobic methane oxidation (AMO) is turnover process of first order importance. In the course of AMO bicarbonate is produced, which precipitates with calcium and magnesium from the bottom water to form so-called chemoherm carbonates. Additionally, the anaerobic methane oxidation produces sulfide that is used by chemoautotrophic bacteria as energy source. These bacteria can be free-living or symbiotic in bivalves or tubeworms and are often arranged in vertical succession above the AMO-layers. A major objective of this cruise was to quantify the amount of methane oxidized in the sediments as well as the amount of methane released into the water column. In order to estimate these fluxes three different approaches were used. If methane-rich fluids ascent through sediments, sharp concentration changes of porewater constituents develop (CH_4 , H_2S , HSO_4^- , NH_4^- , NO_3^- , alkalinity, pH). Numerical modeling of these profiles allows quantifying the biogeochemical turnover rates as well as advection rates of fluids. The second approach taken was *in situ* measurements of fluid flow rates by the VESP-Lander as well as incubation experiments by the BC-Lander. The third approach was to quantify the amount of methane from the seafloor by high-resolution, small-scale, three-dimensional mapping of methane in the water column to establish inventories.

Lander deployment

The lander deployments were unique and represent the only approach to directly measure dewatering and methane turnover at the sea floor induced by dewatering. For that program a variety of TV-guided tools were deployed which were designed to sample small-scale features such as methane vents and fluid seeps. The VESP-Lander can be lowered to and towed above the seafloor with the help of a TV-guided launcher. The lander can be separated from the launcher by an electrical release. The launcher is then retrieved while the lander is autonomously measuring the amount of expelled fluids; an option to collect water samples has also been used. After the measurements weights on the lander are released, which then ascends to the sea surface where it is recovered by the research vessel.

The deployment, autonomous measurement and retrieval of the Benthic Chamber Lander (BC-Lander) is similar to that of the VESP-Lander. This lander consists of chambers that are lowered to the seafloor in a way that a volume of bottom water and sediment are enclosed. From the enclosed volume water samples were taken at time intervals for on board analyses. The concentration change of chemical constituents (e.g. oxygen) over time allows quantification of benthic material turnover. After termination of the measurements a closing system cuts off the incubated sediment which is then brought to the surface together with the lander system.

Scientific program of leg M54/3B

The local seismological network of Costa Rica has collected sufficient data to characterize the general seismogenesis below the Middle American landbridge. However, due to its geometry, it fails to precisely define earthquake locations in the offshore area, where nearly 50% of the earthquakes occur. Therefore, the SFB 574 operates two offshore local networks for a period of about six month each. The networks were deployed such that they occupy a region first where a subducting seamount has left a prominent scar in the upper plate. The second network covers an area where from seismic reflection data a bifurcation of the decollement is observed. In addition, tiltmeters were deployed to monitor long term motion on the slope.

The first network was installed in April 2002 and recovered and redeployed during M54/3B. Recovery operation included the recovery of the tiltmeters, maintaining the instruments, archive the data and redeploy the network.

1.4 Major geological targets

1.4.1 Carbonate Mounds

Several chemoherm mounds were discovered during the SO 163 expedition (Fig. 3.1.2, 3.2.2, 3.2.3). These mounds are up to 200 - 300 m high and up to one km in diameter. They can be clearly seen on bathymetric maps at water depth between 900 and 2000 m. The mounds are readily identified on side-scan sonar maps due to the high reflectivity of outcropping hard ground. Fifteen mounds were surveyed with the video sled OFOS of which 3 were more intensively mapped. Additionally, these mounds were investigated by reflection seismic and the methane concentrations in the overlying water column measured. The preliminary results indicate that the mounds grow above the ambient niveau of the sediment surface due to the escape of methane-rich fluids. The enormous amount of carbonate, which originate probably from the anaerobic oxidation of methane, and the luxuriant chemoautotrophic communities (*Lamellibrachia* sp., *Calyptogenia* sp., *Bathymodiulus* sp.) indicate long-term methane venting. The methane concentrations in the water column above the mounds are considerably elevated compared to background levels.

Accordingly, during this leg the focus of investigations on the mounds are:

- (1) High-resolution multibeam mapping of mounds in order to understand their structure and relationship to fault pattern;
- (2) Small-scale mapping of mounds with the video sled OFOS;
- (3) Recovery of carbonates by dredging, coring and grabbing in order to elucidate the growth and development of the mounds;
- (4) In situ incubations and flux measurements by TV-guided tools (VESP, BCL, TV-MUC) and CTD as well as water and sediment sampling in order to understand the fluid geochemistry.

1.4.2 Seamount subduction

The subduction of seamounts and ridges cause prominent scars in the upper plate (Fig. 3.2.1). During the RV SONNE expeditions SO 144 and SO 163 six seamount scarps were surveyed by the OFOS. These scarps are different with respect to the shape and size of the subducted seamount or ridge as well as the time and

evolution of plate convergence. OFOS profiles revealed that at the upper plate, which is uplifted by the subducted features, massive outcrops occur. We speculate that this hard ground is authigenic carbonate precipitated in the course of methane venting. There appears to be an obvious succession in the extent of carbonate with the age of the features: the youngest structures (Small Seamount Scarp, Parrita Scarp) contain only few carbonates. At the older Jaco Scarp the carbonates cover wider parts of the seafloor, at Rio Bongo Scarp, the oldest structure, the entire top consists of carbonates, forming a plateau-like cap of nearly 1 km in diameter.

Several OFOS surveys at Jaco Scarp revealed that methane-rich fluids are associated with different areas of the feature. This may indicate that the methane and/or fluids originate from different sources: (i) decomposition of gas hydrate due to the uplift of hydrate containing sediments, (ii) methane originating from sediment strata that crop out at the area of the headwall, (iii) methane being expelled due to the internal compression of slide masses in the wake of the subducted seamount.

Based on this preliminary results the following major investigations are planned:

- (1) OFOS surveys in order to estimate the extent of carbonate and venting areas;
- (2) Sampling of vent fluids of different areas of the scarps in order to characterize the sources of methane and/or fluids;
- (3) Sampling of hard grounds of the uplifted upper plate of scarps of different ages by dredge and TV-grab in order to gain inside to origin and evolution of these features.

1.4.3 Submarine slides

Three prominent land slides were identified during previous investigations, the Nicoya landslide, the Cabo Blanco landslide and the Quepos landslide (Fig. 3.2.4). Evidence for methane-rich sediments were gained mainly at the Quepos landslide. At the base of the headwall at a water depth around 450 m extensive bacterial mats cover the soft sediment seafloor. At this depth the core of the oxygen minimum layer is situated.

Accordingly, a major goal of this leg is to characterize the source of methane and fluids and the origin of the sulfide-rich sediments; this will be achieved by:

- (1) Analyses of porewaters from sediment cores (TV-MUC, SL);
- (2) *In situ* respiration experiments, and fluid sampling with the BC-Lander.

2 Participants METEOR 54/2+3

2.1 Scientists

Leg M 54/2

1.	Wallmann, Klaus	Chief Scientist	GEOMAR
2.	Bracker, Eggo	Coring Technique	GEOMAR
3.	Deyhle, Annette	Porewater Geochemistry	SIO
4.	Domeyer, Bettina	Porewater Geochemistry	GEOMAR
5.	Gennerich, Hans-Hermann	Heatflow Measurements	GeoB
6.	Grevenmeyer, Ingo	Heatflow Measurements	GeoB
7.	Heesemann, Bernd	Heatflow Measurements	GeoB
8.	Hensen, Christian	Porewater Geochemistry	SFB
9.	Hepp, Daniel	Sedimentology	IFGK
10.	Kahl, Gerhard	Meteorology	DWD
11.	Kaul, Norbert	Heatflow Measurements	GeoB
12.	Kopf, Achim	Sedimentology	SIO
13.	Kutterolf, Steffen	Tephra Sampling	SFB
14.	Mansor, Sandra	Porewater Geochemistry	GEOMAR
15.	Marquardt, Mathias	Porewater Geochemistry	GEOMAR
16.	Mau, Susan	Methane Measurements	SFB
17.	Mörz, Tobias	Sedimentology	SFB
18.	Müller, Meino	Heatflow Measurements	GeoB
19.	Nass, Kristin	Porewater Geochemistry	SFB
20.	Ochsenhirt, Wolf-Thilo	Meteorology	DWD
21.	Ruschmeier, Wiebke	Benthic Foraminifera	IFGT
22.	Schacht, Ulrike	Sediment Geochemistry	IFGK
23.	Schmidt, Mark	Sediment Geochemistry	IFGK
24.	Schneider, Julia	Heatflow Measurements	GeoB
25.	Schupp, Jens	Sedimentology	TUB
26.	Steen, Eric	Coring Technique	IFGK

For full name of participating institutions see chapter 2.3 (page 17).



Figure 2.1: Participants of Cruise M54-2.

Leg M 54/3A

1.	Suess, Erwin	Chief Scientist	GEOMAR
2.	Albrecht, Ingrid	Sedimentology	SFB
3.	Bannert, Bernhard	Technician	OCTOPUS
4.	Brueckmann, Warner	Sedimentology	GEOMAR
5.	Fischer, York-Oliver	Sedimentology	SFB
6.	Garbe-Schoenberg, Dieter	Trace Elements	IFGK
7.	Han, Xiqu	Sedimentology	GEOMAR
8.	Hensen, Christian	Porewater Geochemistry	SFB
9.	Kahl, Gerhard	Meteorology	DWD
10.	Klauke, Sonja	Trace Elements	SFB
11.	Linke, Peter	Fluid Flow Measurements	GEOMAR
12.	Manzke, Bert	Biomarker Sampling	SFB
13.	Mau, Susan	Methane Measurements	SFB
14.	Söding, Emanuel	Parasound	SFB
15.	Nass, Kristin	Porewater Geochemistry	SFB
16.	Poser, Michael	Engineer	OCTOPUS
17.	Purkl, Stefan	Radionuclids	SFB
18.	Queisser, Wolfgang	Technician	GEOMAR
19.	Rehder, Gregor	Methane Measurements	GEOMAR
20.	Sahling, Heiko	Vent-Biogeochemistry	SFB
21.	Salazar, Marlene	Sedimentology	ICE
22.	Scholten, Jan	Radionuclids	IFGK
23.	Stange, Karen	Methane Measurements	SFB
24.	Truscheit, Thorsten	Meteorology	DWD
25.	Tuerk, Matthias	Technician	SFB

For full name of participating institutions see chapter 2.3 (page 17).



Figure 2.2: Participants of Cruise M54-3A.

Leg M 54/3B

1.	Flüh, Ernst	Chief Scientist	GEOMAR
2.	Alvarado, Guillermo	Seismology	ICE
3.	Brunn, Wiebke		IfM
4.	Goold, Sonja	Guest	ICE
5.	Gossler, Jürgen	Seismology	SFB
6.	Kahl, Gerhard	Meteorology	DWD
7.	Kopp, Heidrun	Seismology	GEOMAR
8.	Liersch, Petra		GEOMAR
9.	Rojas, Leonel	Guest	ICE
10.	Poser, Michael	Engineer	OCTOPUS
11.	Queisser, Wolfgang	Technician	GEOMAR
12.	Steffen, Klaus Peter	Technician	KUM
13.	Taylor, Waldo	Guest	ICE
14.	Truscheid, Thorsten	Meteorology	DWD
15.	Woronowicz, Tanja		GEOMAR

For full name of participating institutions see chapter 2.3 (page 17).



Figure 2.3: Participants of Cruise M54-3B.

2.2 Crew METEOR 54

Leg M 54/2

Master	PAPENHAGEN, Henning
Ch. Mate	MEYER, Oliver
1st Mate	BENDIN, Axel
1st Mate	BASCHEK, Walter
Radio Officer	KÖTHER, Wolfgang
Surgeon	Dr. SCHLENKER, Wilhelm
Ch. Engineer	SCHÜLER, Achim
2nd Engineer	BEYER, Helge
2nd Engineer	SCHMIEDESKAMP, Jan
Electrician	FREITAG, Rudolf
Ch. Electron.	HEYGEN, Ronald
Electron. Eng.	WENTZEL, Heinz
Sys.-Man.	WINTERSTELLER, Paul
Fitter	BLOHM, Volker
Motorman	SEBASTIAN, Frank
Motorman	PRINZ, Udo
Motorman	KÖRTGE, Olaf
Motorman	SONNENBERG, Ralph
Ch. Cook	TIEMANN, Frank
2nd Cook	PYTLIK, Franciszek
Ch. Steward	HORZELLA, Ernst
2nd Steward	GRÜBE, Gerlinde
2nd Steward	POHL, Andreas
2nd Steward	MÜLLER, Werner
Laundryman	HU, Guo Yong
Boatswain	HADAMEK, Peter
A.B.	HAMPEL, Ulrich-Bruno
A.B.	DRACOPOULUS, Eugenius
A.B.	KREFT, Norbert
A.B.	KUHN, Ronald

Leg M 54/3A

Master	PAPENHAGEN, Henning
Ch. Mate	BASCHEK, Walter
1st Mate	BENDIN, Axel
2nd Mate	KOWITZ, Torsten
Radio Officer	KÖTHER, Wolfgang
Surgeon	WALTHER, Anke
Ch. Engineer	SCHÜLER, Achim
2nd Engineer	REX, Andreas
2nd Engineer	SCHMIEDESKAMP, Jan
Electrician	BEKAAN, Steffen
Ch. Electron.	HEYGEN, Ronald
Electron. Eng.	ROTTKEMPER, Oliver
Sys.-Man.	WINTERSTELLER, Paul

Fitter	BLOHM, Volker
Motorman	SEBASTIAN, Frank
Motorman	PRINZ, Udo
Motorman	SONNENBERG, Ralph
Motorman	ISBRECHT, Frank
Ch. Cook	MÜLLER, Horst
2nd Cook	PYTLIK, Franciszek
Ch. Steward	HORZELLA, Ernst
2nd Steward	GRÜBE, Gerlinde
2nd Steward	MÜLLER, Werner
Laundryman	HU, Guo Yong
Boatswain	MUCKE, Hans-Peter
A.B.	HAMPEL, Ulrich-Bruno
A.B.	DRACOPOULUS, Eugenius
A.B.	KREFT, Norbert
A.B.	KUHN, Ronald

Leg M 54/3B

Master	PAPENHAGEN, Henning
Ch. Mate	BASCHEK, Walter
1st Mate	BENDIN, Axel
2nd Mate	KOWITZ, Torsten
Radio Officer	KÖTHE, Wolfgang
Surgeon	WALTHER, Anke
Ch. Engineer	SCHÜLER, Achim
2nd Engineer	REX, Andreas
2nd Engineer	SCHMIEDESKAMP, Jan
Electrician	BEKAAN, Steffen
Ch. Electron.	HEYGEN, Ronald
Electron. Eng.	ROTTKEMPER, Oliver
Sys.-Man.	WINTERSTELLER, Paul
Fitter	BLOHM, Volker
Motorman	SEBASTIAN, Frank
Motorman	RADEMACHER, Hermann
Motorman	SONNENBERG, Ralph
Motorman	ISBRECHT, Frank
Ch. Cook	MÜLLER, Horst
2nd Cook	PYTLIK, Franciszek
Ch. Steward	HORZELLA, Ernst
2nd Steward	GRÜBE, Gerlinde
2nd Steward	MÜLLER, Werner
Laundryman	HU, Guo Yong
Boatswain	MUCKE, Hans-Peter
A.B.	HAMPEL, Ulrich-Bruno
A.B.	DRACOPOULUS, Eugenius
A.B.	KREFT, Norbert
A.B.	KUHN, Ronald

2.3 Participating Institutions

DWD

Deutscher Wetterdienst
- Seewetteramt -
Bernhard-Nocht-Straße 76
20359 Hamburg / Germany

GeoB

Fachbereich 5 - Geowissenschaften
Universität Bremen
Klagenfurter Straße
28359 Bremen / Germany

GEOMAR

Forschungszentrum für marine Geowissenschaften
der Christian-Albrechts-Universität-Universität zu
Kiel
Wischhofstraße 1-3
24148 Kiel / Germany

ICE

Instituto Costarricense de Electricidad (ICE)
Red Sismologica Nacional (RSN: ICE-UCR)
UEN PySA, Oficina Sismologia y Vulcanologia
APDO 10032 - 1000 San Jose / Costa Rica

IFGK

Institut für Geowissenschaften
Christian-Albrechts-Universität zu Kiel
Ludewig-Meyn-Str. 10
24118 Kiel / Germany

IFGT

Institut für Geowissenschaften
Eberhardt-Karls-Universität Tübingen
Sigwartstr. 10
72076 Tübingen / Germany

KUM

K. U. M. Umwelt-und Meerestechnik Kiel GmbH
Wischhofstr. 1-3
24148 Kiel / Germany

OKTOPUS

Gesellschaft für angewandte Wissenschaft, innovative Technologien und Service in der Meeresforschung mbH
Kieler Straße 51
24594 Hohenweststedt

SIO

Scripps Institution of Oceanography
8602 La Jolla Shores Drive
La Jolla, CA. 92037 / USA

SIOH

Marine Geology and Geophysics
Second Institute of Oceanography
9 Xixihexia Rd.
310012 Hangzhou / China

SFB

Sonderforschungsbereich 574
Wischhofstr. 1-3
24148 Kiel / Germany

TUB

Technische Universität Berlin
Fachgebiet Grundbau und Bodenchemie
Gustav-Meyer-Allee 25
13355

3 Geological Setting of the Study Area

The working area of cruise M54 was located at the Pacific continental margin off Costa Rica and Nicaragua. This area contains the boundary between the Caribbean and Cocos plates that is marked by the Middle America Trench (Fig. 3.0.1). The Cocos Plate subducts beneath the Caribbean plate in a relatively shallow angle, dragging down crustal material as well as various kinds of sediments and fluids deposited there. The subduction, transformation, mobilization and recycling of this material results in the large well known prominent features like the back arc volcanoes, making up most of Costa Rica and Nicaragua, but also in many

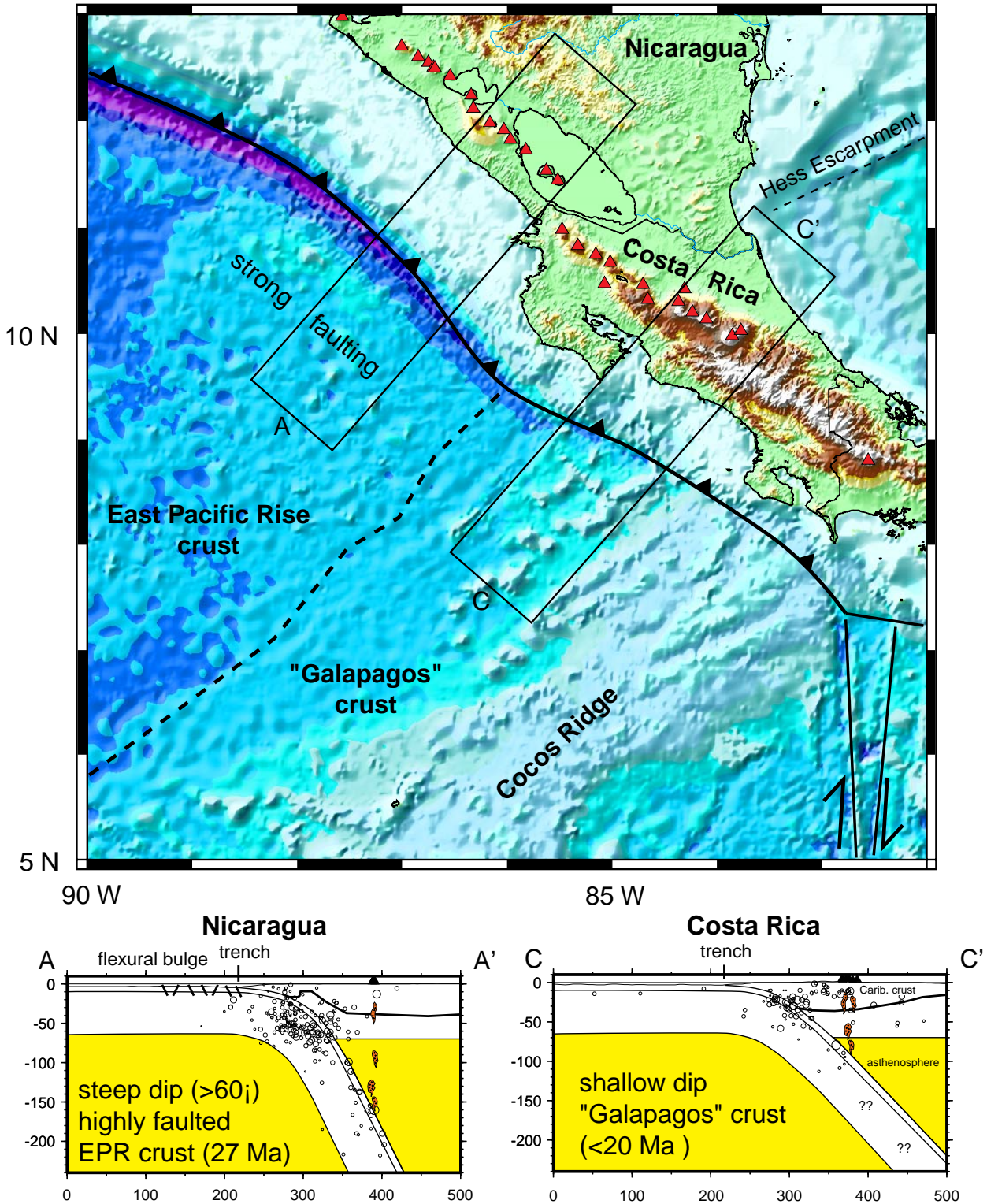


Figure 3.0.1: Geodynamic setting of Nicaragua - Costa Rica convergent margin.

small and medium type of seafloor features, like slides, mounds and margin escarpments which can be observed along the slope of the overriding plate. During M54 the latter features as sources of subducted and recycled material were of special interest for the investigations.

At the Costa Rica margin the Cocos Plate can be divided into three different areas based on morphology: 1) Northwest of Fisher Seamount, the smooth Pacific basin seafloor, created at the East Pacific Rise facing the Nicoya Peninsula is similar to the less rugged continental slope morphology; 2) Opposite the ocean floor created at the Galapagos Rift System is covered with seamounts, the continental margin has some large embayments, the continental slope is indented and has a more rugged morphology; 3) The Cocos Ridge, formed as a hotspot trace by the Galapagos Hotspot, subducts beneath a narrow continental slope that rises steeply up to a shelf of the uplifted Osa Peninsula. The general areas visited through cruise M54-2 and 3 are pictured in Figure 3.0.2, the location of stations is shown in detail on maps in sections 3.1 and 3.2. Stations not appearing on the detail maps are plotted in figure 3.0.3.

The general geologic targets of cruise M54 were features related to dewatering at the margin with one exception; i.e. an area of normal faulting on the down-going oceanic crust off Nicaragua. In order to ascertain differences in dewatering signals and activity related to tectonic style of the subducting Cocos Plate, the features situated off the northern part with smooth topography of the downgoing plate were compared to those off the southern part with rough topography.

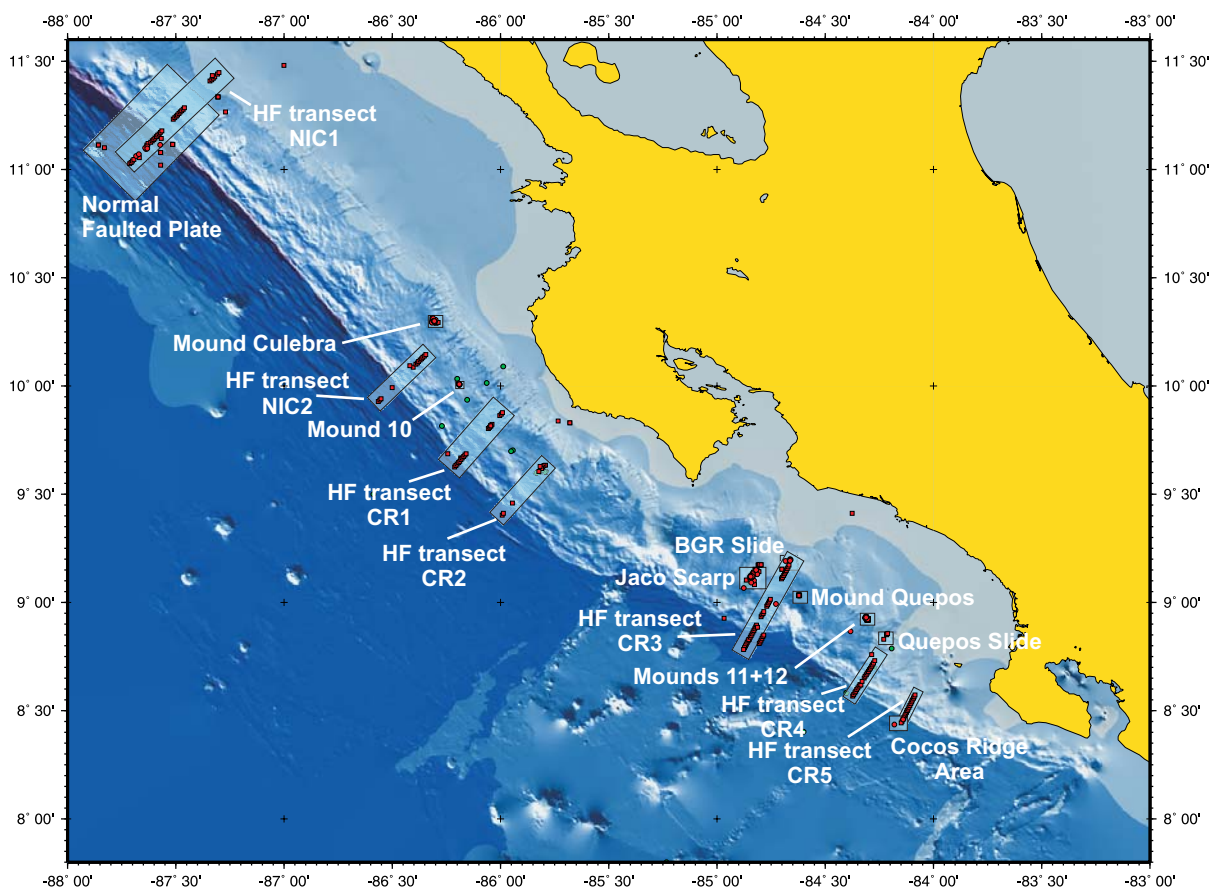


Figure 3.0.2: General areas of investigation at the Costa Rica/Nicaragua Pacific margin. Detailed maps of areas can be found in chapters 3.1 and 3.2, for the heat flow transects in Appendix D.

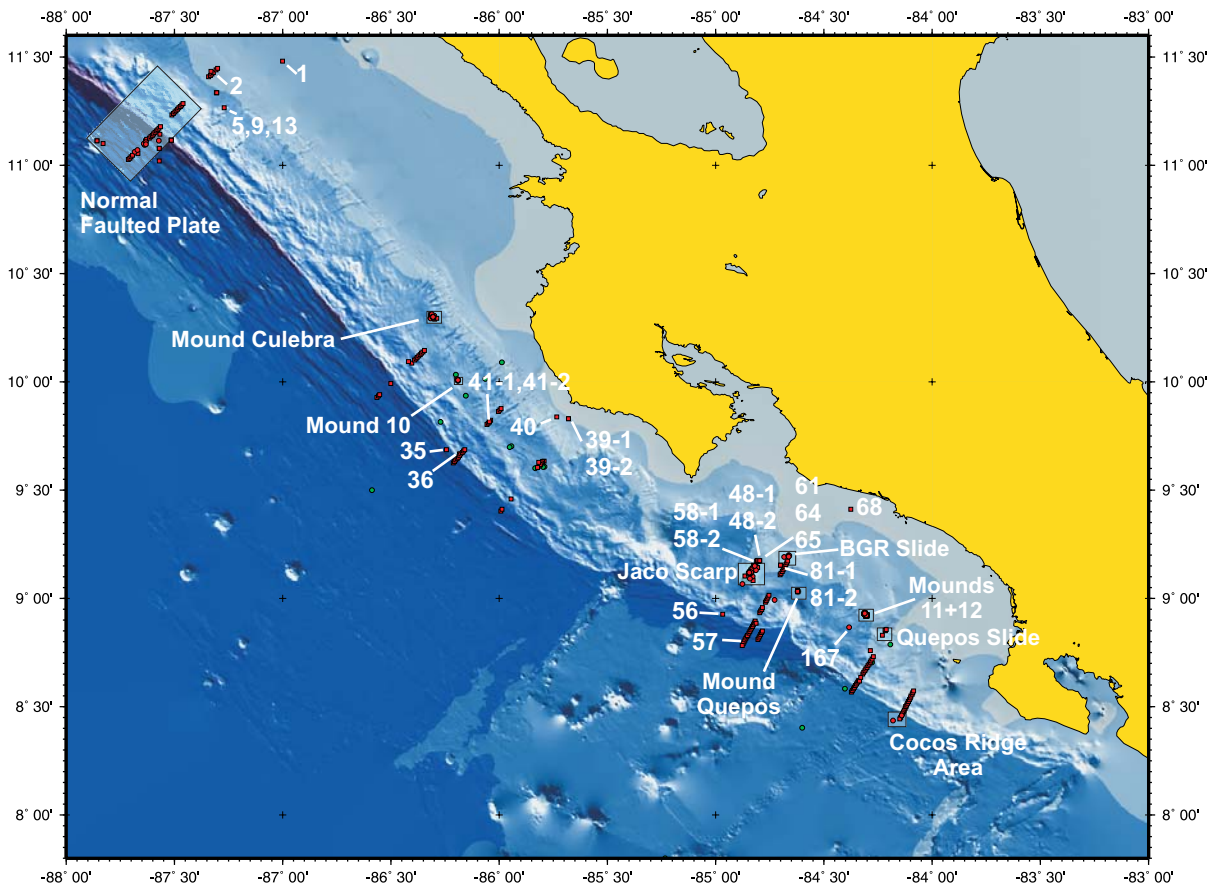


Figure 3.0.3: Stations not appearing on the following detailed area maps.

3.1 Subduction of smooth Cocos Plate segment off Nicaragua and Northern Costa Rica

On the smooth Cocos plate segment several distinct areas were investigated during cruise M54. The area of normal faulting off Nicaragua shows a system of half-grabens bordered by faults parallel to the trench, progressing downwards into the trench as the Cocos Plate subducts. These faults are likely to act as fluid venting systems, transporting material from the deeper crust to the surface. Stations performed in this area are plotted in Figure 3.1.1.

Mound Culebra is one of the biggest mounds off Nicaragua. It's about 1km² in size at a depth of approx. 1600m and was extensively swath mapped through SO163. Previous OFOS surveys revealed carbonates at the top, but no indications for mudflows. Hence it is not certain, whether Mound Culebra is actually an active mud volcano or if its development is due to some other mechanism. Stations performed on Mound Culebra are plotted in Figure 3.1.2.

Further south Mound #10 is located on the margin in about 2300m water depth. With about 300m in diameter it is relatively small compared to Mound Culebra. In contrast to most other mounds, Mound #10 has very few areas covered by carbonates. Hence when sampling at Mound #10 (Fig. 3.1.3) it was hoped to find a better environment to recover samples than elsewhere.

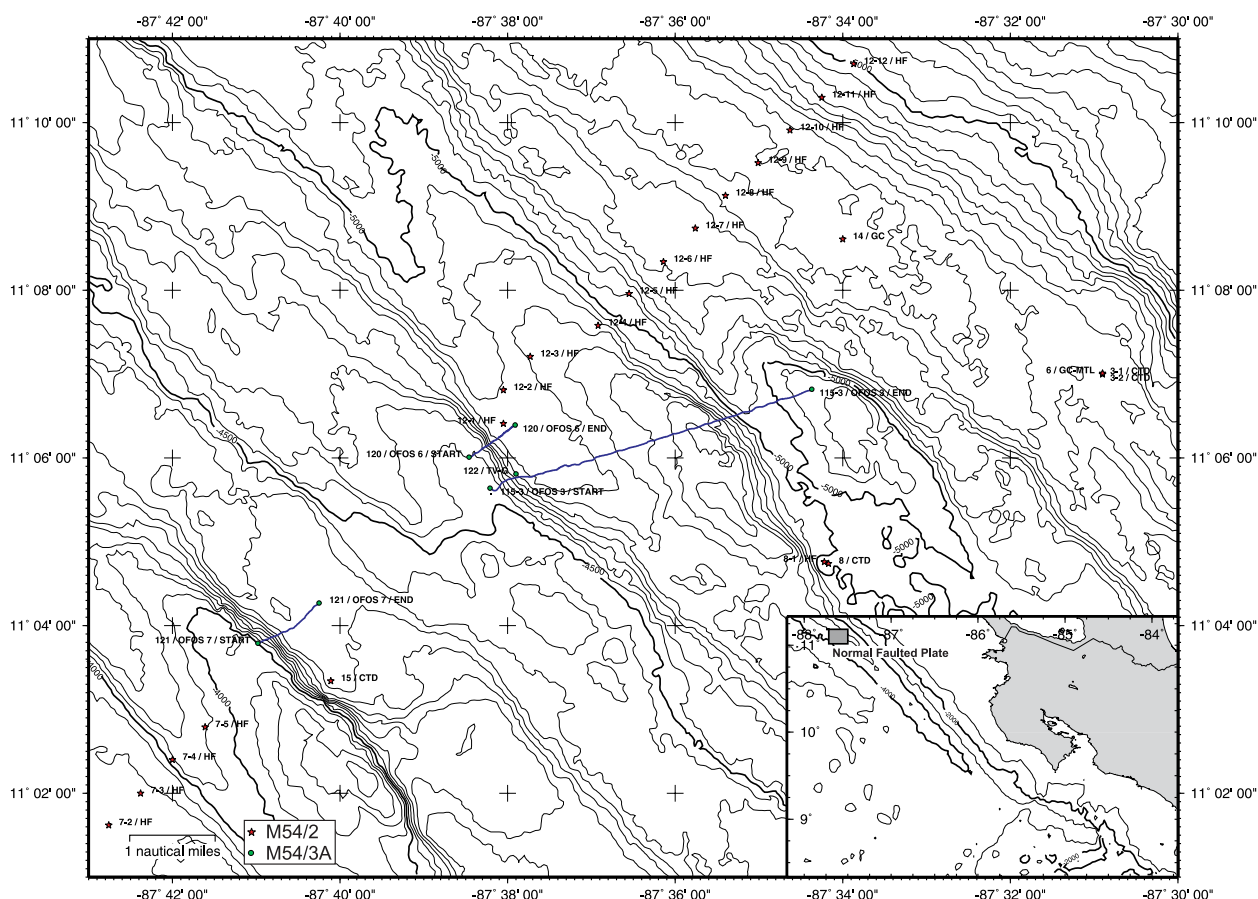


Figure 3.1.1: Stations on the normally faulted oceanic crust during M54-2 and 3.

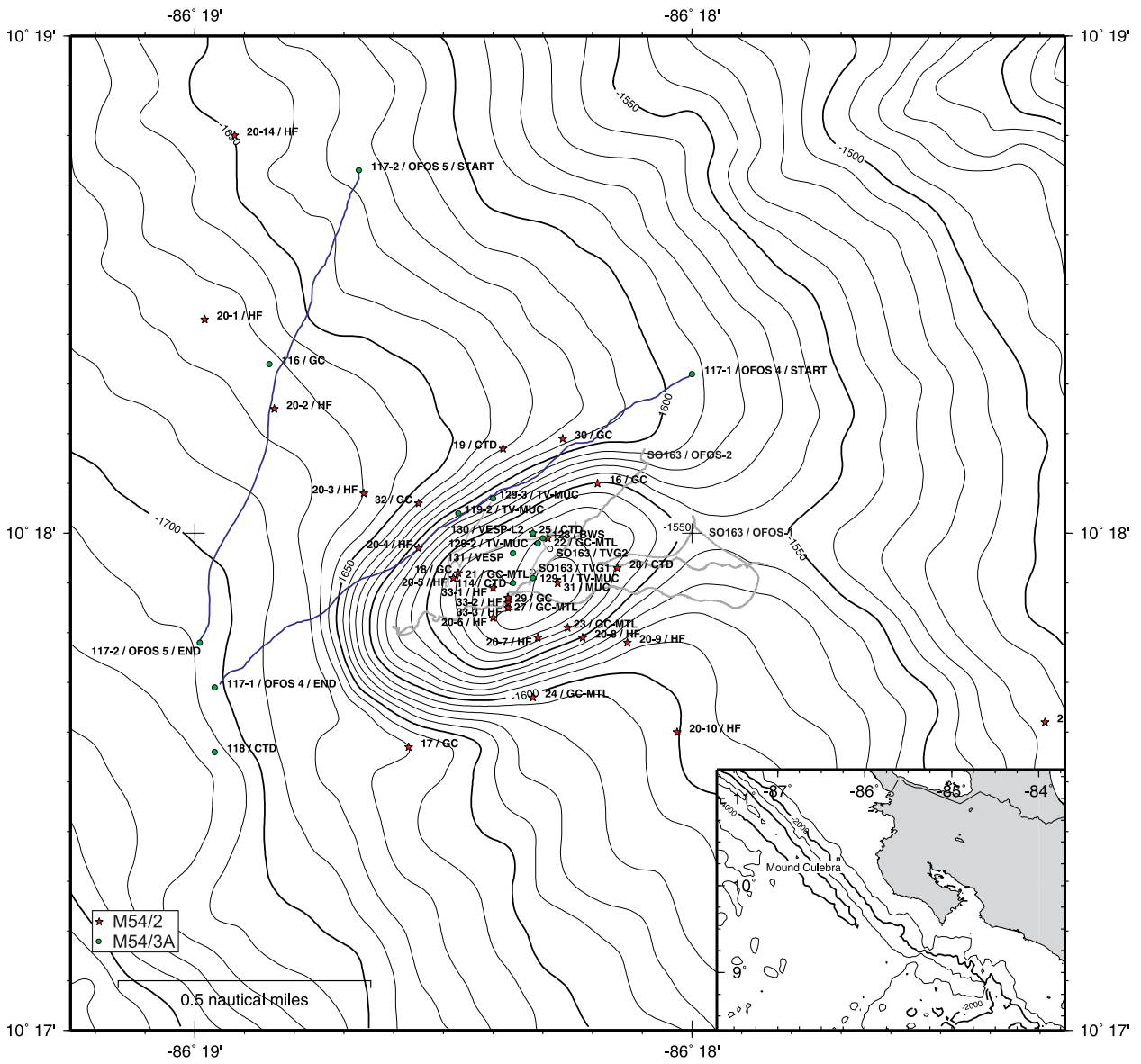


Figure 3.1.2: Stations at Mound Culebra during M54-2 and 3 and during SO163.

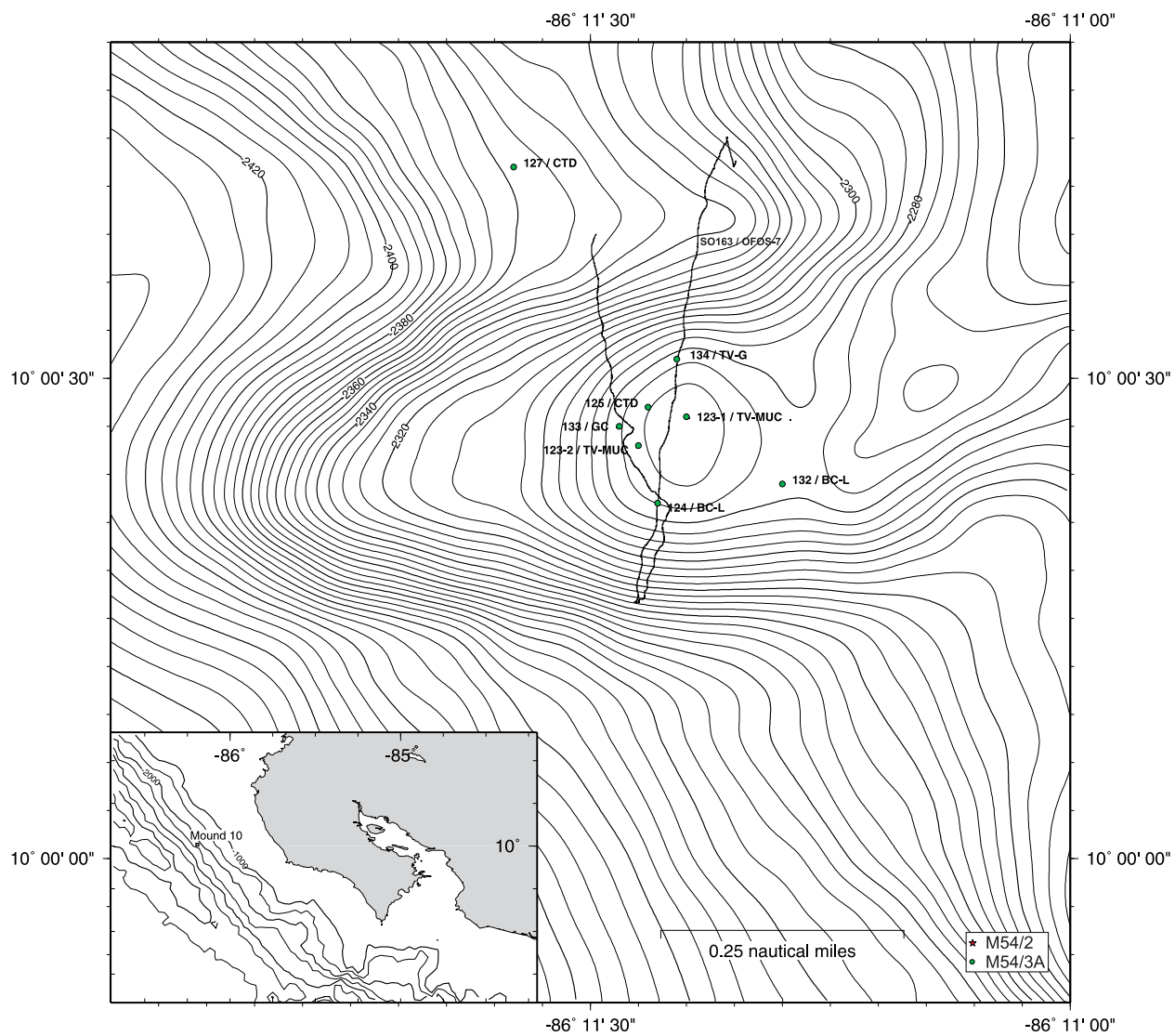


Figure 3.1.3: Stations at Mound #10 during M54-2 and 3 and during SO163.

3.2 Subduction of rough Cocos Plate segment off Costa Rica

The continental margin at the rough Cocos Plate segment shows many dents and scarps caused by the surface of the underthrusting plate. When seamounts are subducted very prominent features can be formed like Parrita Scarp or Jaco Scarp, traces in the upper plate caused by subducting seamounts. Both scarps have extensively been studied by former cruises SO144 and SO163. During M54 only Jaco Scarp was surveyed, although this was done in great detail with a variety of TV-guided devices. Locations of stations at Jaco Scarp are pictured in Fig. 3.2.1.

Mound Quepos is another relatively small mound, only about 200m in diameter and 40m high. It lies in about 1400m waterdepth. Mound Quepos is covered with a thick layer of massive carbonates, which cover the known venting areas on top, making it difficult to retrieve samples from this area. Hence sampling was mainly performed on the slope of the mound as shown in Fig. 3.2.2.

The Mounds #11 and #12 were first investigated during SO163. They are both small features, about 100m in diameter and less than 40m high. They both showed among the highest venting activities detected during cruise SO163, and were hence among the major target areas of M54. Stations on Mounds #11 and #12 are pictured in figure 3.2.3.

Another continental margin feature often connected to venting sites are submarine landslides. During M54-2 and 3 two slides were visited, the Quepos Slide in the southern part of the working area, and the "BGR"-slide, to the northeast of Jaco Scarp. The Quepos Slide was already investigated during SO144 and SO163 using the OFOS device. This survey revealed an extensive coverage with bacteria mats and clams in many areas, indicating active venting. During M54 only 5 stations were performed, at Quepos Slide as shown on Fig. 3.2.4.

The BGR-Slide is a smaller landslide detected during a BGR-cruise in 2000 in a water depth of 550 to 850m. No active venting has yet been detected here, but since the slide depthwise exactly lies within the gas hydrate stability zone, a good chance to find venting sites could be assumed. Stations performed at BGR-Slide are pictured in Fig. 3.2.5.

Cocos Ridge represents a region showing a very high relief of the seafloor and a relatively thick crust. No investigations have been undertaken there before, so only few stations were run as an initial survey (Fig. 3.2.6).

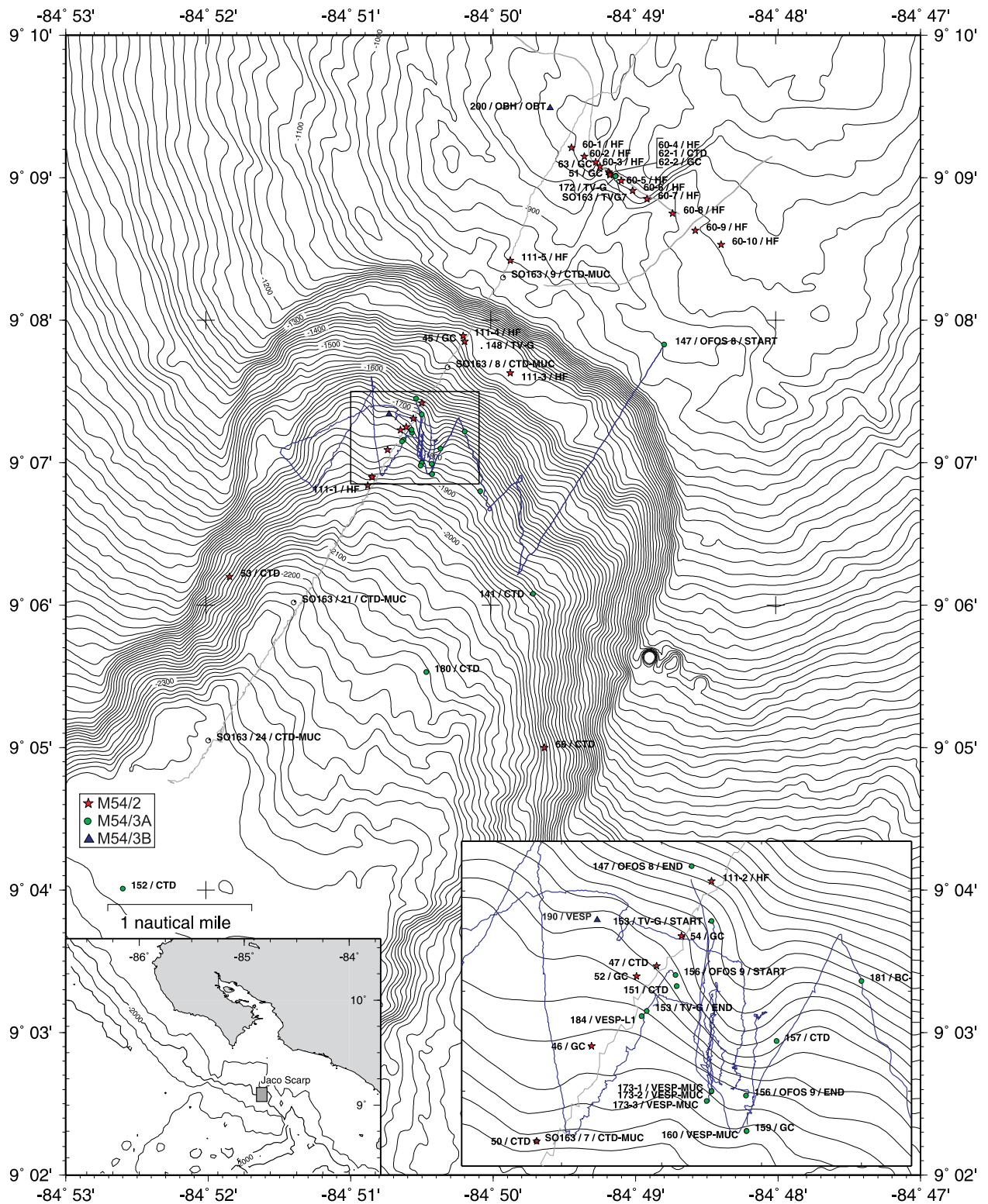


Figure 3.2.1: Stations at Jaco Scarp during M54-2 and 3.

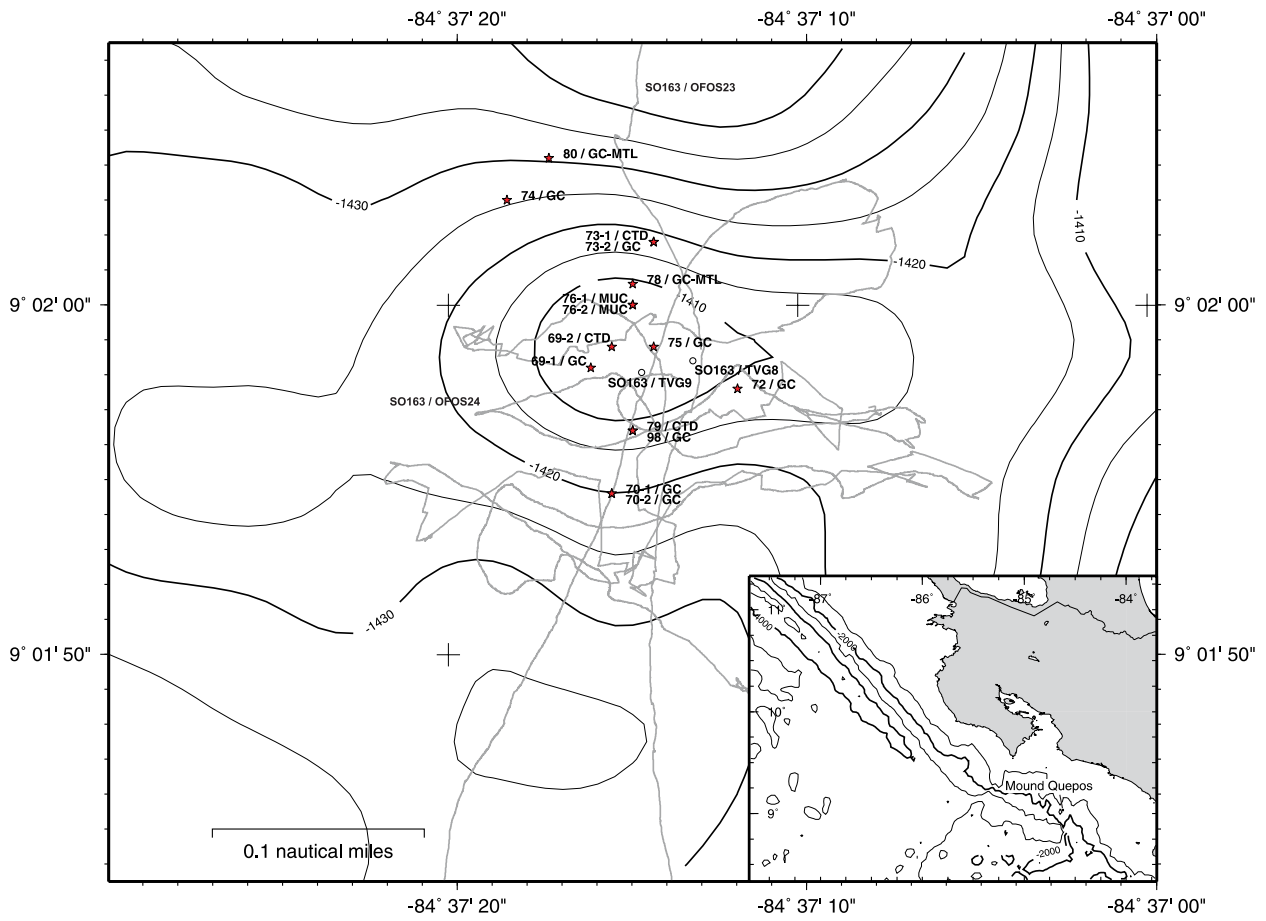


Figure 3.2.2: Stations at Mound Quepos during M54-2 and OFOS tracks from SO163.

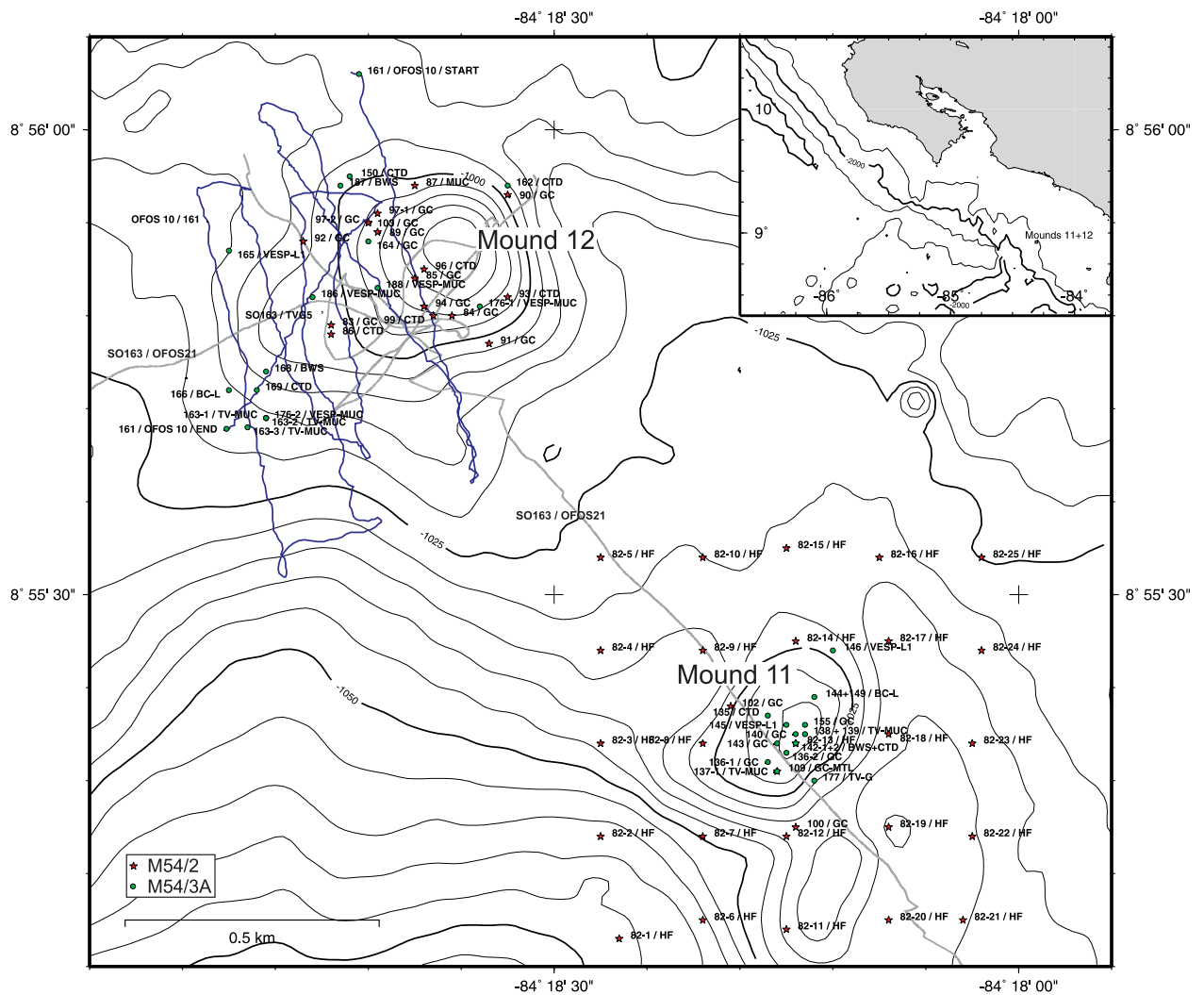


Figure 3.2.3: Stations at Mounds #11 and #12 during M54-2 and 3. Some OFOS tracks from SO163 are shown as well.

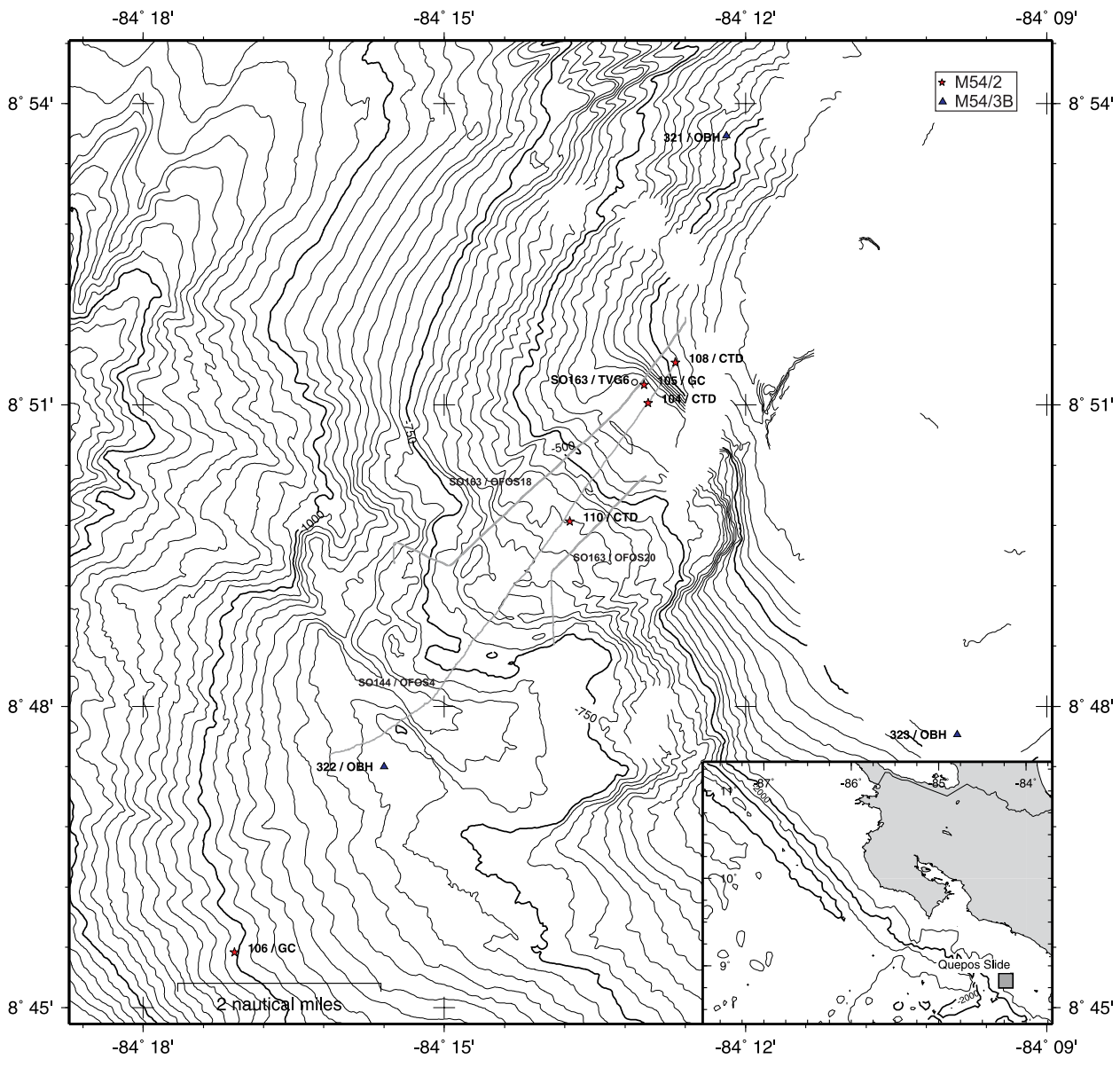


Figure 3.2.4: Stations at Quepos Slide during M54-2. Some OFOS tracks from SO144 and SO163 are shown as well.

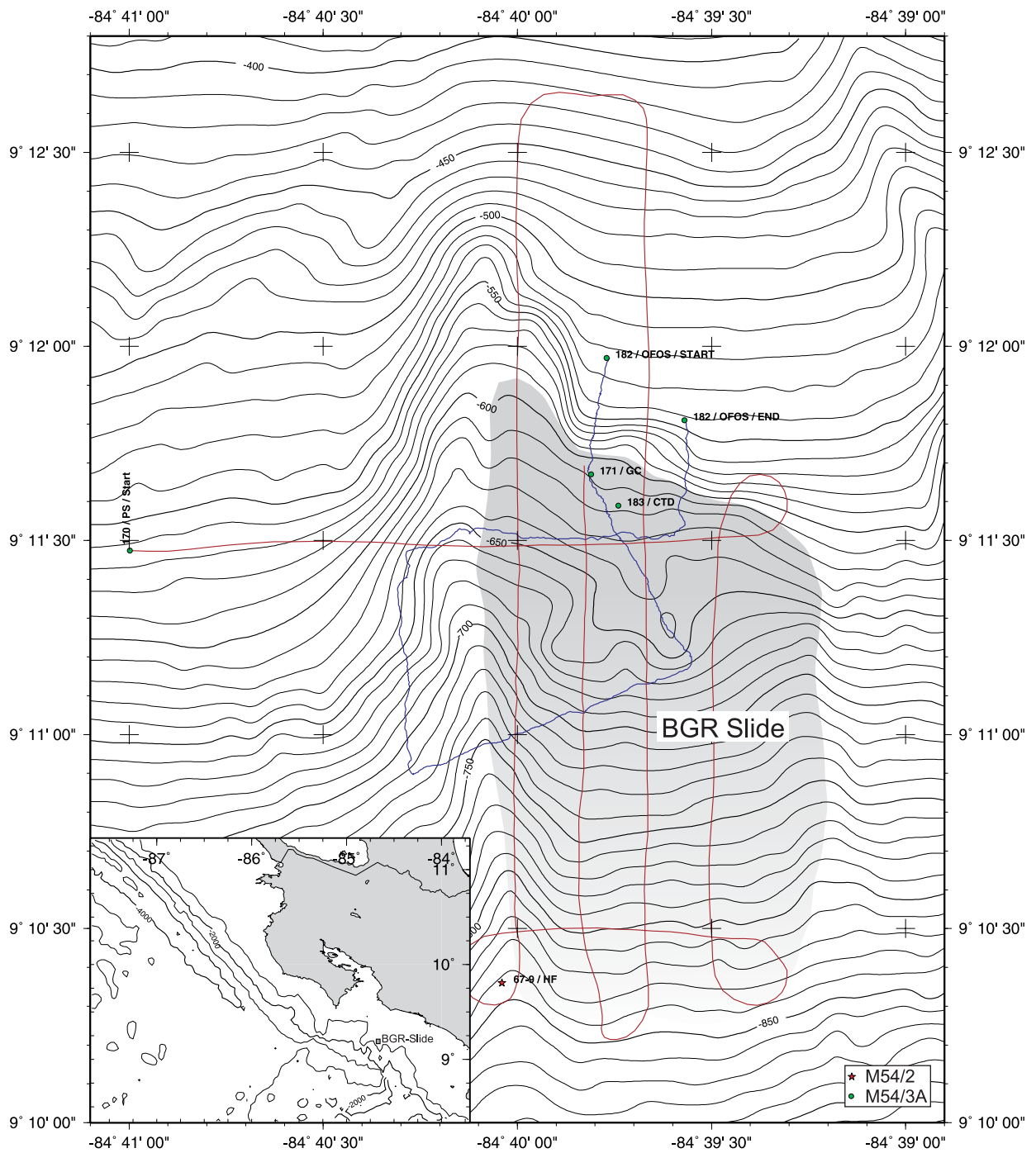


Figure 3.2.5: Stations at "BGR" Slide during M54-2 and 3.

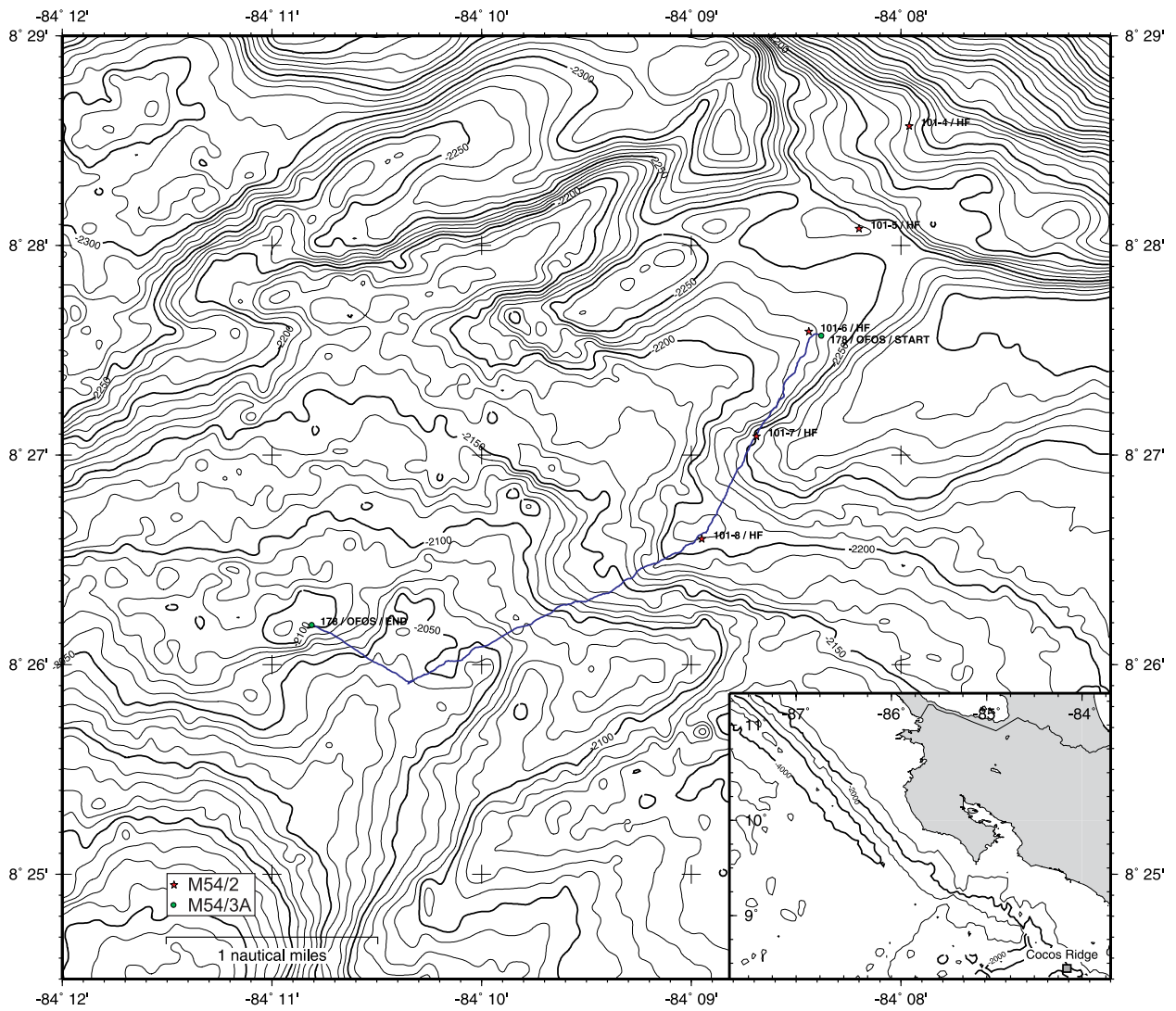


Figure 3.2.6: Stations on the Cocos Ridge during M54-2 and 3.

4 Cruise Narrative

4.1 Leg M54/2

(K. Wallmann)

During cruise M54/2 sedimentological and water column samples were taken for geochemical investigations along the Central American margin. In addition an extensive heat flow-measurement program was performed, to complement to the water and sediment data. The working area was located at the trench west of Nicaragua and spans approx. 500km to the southeast down to southern Costa Rica. The scientific work began in the northwest of the study area and was continued with stations to the southeast along the central American subduction zone the southern most locations being on the Cocos Ridge. The main areas from the northwest to the southeast were:

1. Faulted outer-flexural bulge area off northern Nicaragua,
2. the area around Mound Culebra to the west of the northern Nicoya Peninsula,
3. the deep-sea slope and trench off western Nicoya,
4. the potential vent sites at Jaco Scarp,
5. Mound Quepos,
6. Mound 12
7. Mound 11
8. and the northern part of the Cocos Ridge.

RV Meteor departed from Caldera harbor on Aug. 13 for a 15h transit to the first working area, the faulted outer-flexural bulge. The faults occur mainly in the northern part of the Cocos Plate and are orientated parallel to the subduction trench. Seismic investigations indicate existence of echelon faults, ranging very deeply through the crust into the mantle. This could result in serpentinization along these faults through in-flowing seawater, which then causes a) the production of methane in great depths and b) heat release through an exothermal chemical reaction.

Within the first six days samples were taken and measurements performed at 15 stations in this area, among them 6 gravity cores (GC), most of them equipped with a Miniature Temperature Logger (MTL), 4 heat flow profiles (HF) and 4 conductivity-temperature-depth sensors (CTD). While the CTD measurements onboard Meteor didn't show the expected increase in methane concentration in the lower part of the water column, and hence no indication for venting in these areas, the HF profiles yielded very interesting results. The values were significantly lower than expected, which led to the conclusion, that the heat flow from the basin doesn't take place in a conductive way, but rather uses convection as a mechanism, which should result in an active fluid circulation pattern within the basaltic oceanic crust. This circulation might be driven by the retained heat of the 20 million year old crust, or by an exothermal chemical reaction due to serpentinization. However, active fluid venting could not yet be confirmed in this location.

In addition a GC profile was drilled off Nicaragua, recovering sediments from shelf, slope and trench areas. Within these sediments 12 different ash layers could be distinguished, allowing us to reconstruct the history of explosive volcanism in Nicaragua, one of the important goals of the SFB. Pore water examinations yielded insight into diagenetic processes taking place within the sediments. Sulfide and methane contents indicate a more intensive diagenesis in trench sediments, compared to slope or shelf sediments. Measurements of chloride and alkalinity showed an increased influence of freshwater at the base of the gravity cores, which could be due to groundwater outflow. In situ measurements done by American colleagues also point in this direction.

On Aug. 19 the ship left the area off northern Nicaragua and steamed south to Mound Culebra, a structure approximately 1,1km² in size. It lies in a water depth of about 1600m, where it stands up about 100m over the surrounding seafloor. The top of the mound is covered with carbonates. Based on the morphology Mound Culebra had previously been interpreted as a mud volcano, however investigations using the Ocean

Floor Observation System (OFOS) during cruise Sonne 163 (SO163) revealed, that there was no indication for mudflows on the mound. The observations rather showed, that it is covered with the same terrigenous sediments found on the surrounding seafloor. In addition various vent faunas like mussel banks were identified, which indicate outflow of methane- and sulfur-rich fluids. High methane concentrations measured in the bottom water supported this assumption.

The investigations performed by M54-2 between Aug. 19 and 22 were done to approve, whether Mound Culebra is indeed a mud volcano, or what other possibilities exist to describe the development of this seafloor feature. Altogether on Mound Culebra 11 gravity cores were recovered, as well as 3 CTD stations, 2 HF profiles and 1 multicorer (MUC). While the GC's at the base of the mound contained mainly homogeneous clays, the sediments at the flank and on the top were deformed showing signs of upward mudflow from the deep. Beneath a thin layer of clay, clasts of claystone and carbonate cemented claystone up to approx. 10 centimeters in diameter were found. Most of the clays were overconsolidated, indicating an origin from greater depth. An alternation of layers containing very few clasts in some places or very many clasts in others indicates, that mudflows added material to build up the mound. Many carbonate /marl layers of various thickness and clay content as well as small carbonate "chimneys" were found as well in sulfide and methane rich cores showing evidence for high diagenetic rates in these muds. Since the sediment cover on the summit is only approximately 40 cm thick, it can be estimated, that the mud volcano has ceased to deliver mud from the deep, but is merely releasing fluids and gas to the surrounding environment for the last few thousand years.

With the exception of one station the porewater data shows, that the muds at Mound Culebra contain water carrying a signature very similar to that of the seawater. Only in one location at the summit an increased sulfur and methane concentration could be measured, however nutrients were still very low. This is probably due to methane in a gas phase being delivered to the top, while the nutrient enriched fluids stay in greater depths.

The heat flow measurements on Mound Culebra show a similar picture, with values significantly lower than the general background. Slightly higher values were only obtained from stations at the foot and the lower part of the slope. This could mean that a continuous flow of sea water goes through the whole top of Mound Culebra while salt depleted warmer fluids are escaping from the lower regions. The heat flow measurements at the location showing higher methane and sulfur concentrations had an exceptional form in that it had a clearly visible peak on the surface of the seafloor, decreasing to a minimum at approx. 1m depth. This could be due to heat produced by microbial activity oxidizing sulfide and methane.

Methane measurements in the water column at Mound Culebra confirmed, that much methane is discharged into the bottom water at this site. In contrast to measurements performed during SO163 the methane content varied dramatically within relatively small depth ranges.

We continued sampling at the western Nicoya continental slope and trench from Aug 21-24, where numerous HF profiles were measured and 6 GC's and 1 MUC taken. The heat flow profiles are in the north offshore Nicaragua as well as further south in the working areas of ODP legs 170 and 205. The results of the northern profiles show a good consistency with the models for conductive heat transport calculated for the subducted plate, while the southern profiles showed far too low values. In the northern areas approx. 90-120 mW/m² were measured over the subducted plate and approx. 40 mW/m² over the continental margin, while the values in the south were only 10 mW/m² and 20 mW/m² accordingly. Since the distance between the profiles is only about 20 nm, it may be speculated, that lateral fluid flow within the subducting plate accounts for the reduced heat flow in the southern profiles.

From Aug. 24 to 28 extensive sampling was done at Jaco Scarp, interrupted by nighttime shifts of heat flow profiles on the Costa Rica continental margin. Jaco Scarp is a very interesting feature located in approx. 800-2400 m water depth on the continental margin off Costa Rica. It's a scarp scratched into the uplifted continental plate caused by a subducted seamount. This results in a mound on the continental side and a very steep

slope on the oceanic side of the margin where blocks of sediment slide downward as the seamount carves into the overlying plate. Due to the high pressures involved as well as the intense faulting in this area highly active venting can be expected. Indeed the methane concentrations at the crest are many magnitudes higher than the background value and actually much higher than anywhere else in Central America.

The very intensive measurements in the water column in this location allowed us to precisely locate the depth horizons at the slope releasing methane into the seawater, however we were unsuccessful obtaining sediments and fluids from those areas. Several tries to recover sediments with gravity corers yielded only few relatively hard claystones without cutting through into deeper layers. Deployments were more successful on the top of the feature, where methane- and sulfide-rich sediments could be recovered as well as very much nutrient depleted, indicating a similar dilution mechanism like on Mound Culebra. The observed heat flow pattern showed lateral changes in the faulted zones on the top of Jaco Scarp, probably influenced by fluid flow in this area.

On Aug 29. the ship moved south to Mound Quepos, where several GC, MUC and CTD stations were visited during daytime until Aug. 31, while heat flow profiles were still measured during the nightshifts. Mound Quepos is a very small structure in approx. 1400m water depth, only 200m in diameter and about 40 m high. During SO163 widespread venting was observed on this location. During this cruise we were unsuccessful to push through the massive carbonate layers covering the known active venting areas on the summit of Mound Quepos. In the marginal areas several cores were taken, containing anoxic H₂S-rich sediments. The bottom water did contain an increased amount of methane, documenting the still active venting. In addition it was possible to demonstrate a clear decrease in chloride in a gravity core from the top to the bottom. The detailed analysis of the recovered salt-depleted fluids will surely help to determine the origin of these waters, and whether they are actually originating from the sediments of the subducted plate. We didn't find any indication for active mud flows, hence it is still uncertain, whether Mound Quepos is actually a mud volcano, like Mound Culebra, or built up by other processes.

The heat flow measurements in the vicinity of Mound Quepos revealed a major thermal anomaly with values approx. 4 times higher than expected. The anomaly could be traced down into the deep sea trench. It indicates, that the increased heat flow could be influenced by fluids ascending originating from the subduction zone.

The cruise continued with a short transit to the southwest, where two small submarine mounds labeled 11 and 12 were sampled from Sept. 1 until Sept. 5, again interrupted by several heat flow profiles off the Costa Rica Margin and trench, as well as 4 stations at the Quepos slide.

Similar to Mount Quepos, Mounds 11 and 12 are two small submarine features which are only 1 km away from each other. They lie in about 1000m waterdepth off the Costa Rica coast. Each of these mounds is about 100 m in diameter and 40m high. Cruise SO163 detected rich vent faunas and carbonates on these mounds, indicating active discharge of fluids into the ocean.

At Mound 12 eleven stations were visited for gravity coring, of which seven yielded excellent sediment cores. Many of the sediments had chaotic structures and big clasts of scaly clays were evidences for active mud volcanism. In one of the sediment cores the salinity dropped significantly with depth to values of about 360mM chloride, which is about 40% lower than that of the surrounding seawater. The high freshwater content could be an indicator for the very deep source of the uprising fluids, which originates from diagenetic and metamorphic processes of the subducted sediments. It is very likely that our isotope studies will shed more light on the precise source of these waters.

Mound 11 was a central area for the heat flow investigations. A 16 station 2-D grid was laid out and measured, to gain a full 3-D picture of the heat flow from Mound 11. The picture showed a maximum within an oblonged area stretching through the middle of the mound. Hence the last gravity core from the cruise was decided to be taken from this area hoping to find an area of uprising fluids. With great excitement and surprise we discovered, that in depths below 2m this core was filled with large chunks of massive gas

hydrate, several centimeters in size. Indeed the sediment there was embedded within a matrix of gas hydrate, while the upper layers contained the same muds found elsewhere, with very low salinity pore waters. Hence Mound 11 can be regarded as a mud volcano, delivering methane saturated fluids from the very deep parts of the subduction zone to the surface, resulting in gas hydrate formation at the sediment/water boundary. The presence of gas hydrates indicates a very high methane delivery rate to prevent sulfur reducing microorganisms to oxidize the methane before it forms hydrate. This peculiar feature made Mound 11 a spectacular and unique site during our cruise ensuring that further investigations will be performed here by later cruises.

On Sept. 5 and 6 the cruise continued to the southernmost region on the Cocos Ridge, to measure 2 heat flow profiles. The profiles measured yielded an extremely high temperature gradient of approx. 1000 °C/km, leading to the assumption, that warm hydrothermal fluids circulating through the crust are massively releasing heat to the ocean in this area.

Finally on Sept 6, the ship steamed north to visit the last stations at Jaco Scarp again, to measure a heat flow profile and to allow the rest of the party to pack up containers, laboratories and prepare for departure in Caldera harbor. Caldera was reached on schedule on the morning of Sept. 7, where most of the scientific party left the ship to make room for many of the already waiting participants of the following leg M54-3a. A very successful cruise came to an end, blessed by very good weather conditions, excellently working equipment and an exceptional hard working crew and scientific party who was rewarded with many truly extraordinary and thrilling scientific results.

4.2 Leg M54/3-A

(E. Suess)

During the second leg we established 6 working areas where extensive sampling and surveys were done; in addition 3 other areas were investigated with only a few stations. The main areas from north to south are:

1. Faulted outer-flexural bulge area off northern Nicaragua,
2. Mound Culebra,
3. Mound#10,
4. Jaco Scarp,
5. Mound#11 and
6. Mound#12;

the minor areas were BGR-slump, mud pie and Cocos Ridge. The nomenclature is taken from previous legs and is being used throughout the report; the areas and stations are shown in Fig. 4.2.1.

The events during the week from 09.09.2002-16.09.2002 were as follows: On September 9th we held a very successful reception on board the FS METEOR for guests invited by the local embassy of the Federal Republic of Germany. During the morning there were tours for school classes, as well as interviews with press agents and national television stations, and in the early afternoon the participation exceeded all expectations with more than 100 guests from local diplomatic, administrative and academic institutions.

The crew's outstanding preparations included not only the elegant buffet, but also help in leading tours of the ship for different groups of guests. Highlights of the occasion were the presentation of our new land-and-offshore 3-D relief map of Costa Rica to various official representatives of the country by the Chief Scientist, as well as the numerous personal contacts with colleagues and employees of relevant scientific institutions. The map was presented in the name of the SFB 574 and Christian-Albrecht-University.

During the whole time of the reception, preparations continued with setting up laboratories and equipment so that the FS METEOR could depart Caldera harbour September 10th, 10:30 local time, with 24 scientific personnel on board, setting course for the furthest northwest field of research, the 'Faulted outer-flexural bulge area off northern Nicaragua' structure offshore Nicaragua.

There, using the OFOS, three of the steep terraces next to the deep-sea trench were investigated at 4020-4350m; 4510-4750m; 4650-4950m. These almost vertically walled terraces showed spectacular exposures of basaltic crust layered over with sediment. It was surprising that the sequence of basalts was thicker than the sediments lying on top. At the bottom of the steep terraces lay strewn widespread heaps of basalt blocks and boulders. The deepest of the steep terraces seemed to be the most eroded and fractured, the middle one showed the best developed contact between sediment and basalt, and the shallowest terrace was similar to the middle terrace but heavily populated by sessile organisms. The contact on the middle terrace showed white precipitates and crusts which were initially interpreted as products deposited from ascending fluids along the contact plane. The TV-grab sampler, however, brought back only pure nannochalk from that contact depth. The precipitates could not be identified. The clear finding is that there is no indication of active fluid emission –either at the deeper end of the seaward-leaning terraces, nor at the contact between sediment and basalt.

The second half of the first week we spent investigating the northern section off Costa Rica, where the EPR-generated crust is subducted. Here two different sites were investigated in more detail. At Mt. Culebra we followed a WNW-trending fault, documented by intensive carbonate formation and populated by colonies of mussels and pogonophorans. A gravity core over an acoustic anomaly („white spots“ on the Parasound recording) showed uniform hemi-pelagic sediment. At a depth of 600 cm, however, clear chloride, CH₄- and H₂S-anomalies were measured in the pore water, which are an indication of ascending fluids. Several TV-guided MUC operations produced no recovery, either because carbonates prevented penetration or the

sediment recovered no indication of fluid movement. These operations became very time-consuming because of the poor quality of the video transmission during the TV-MUCs. It was also difficult to clearly evaluate the nature of the sea floor in vent areas. Several CTD profiles with near-bottom CH₄-maxima completed the range of samples around Mt.Culebra.

The bottom-water sampler was also deployed very successfully, showing a direct connection between methane contents of near bottom layers and those higher up in the water column. One of the VESP-Landers was deployed during the night of 5/6 September to complete the operations at Mt.Culebra. The VESP-Lander was to record expulsion activity until the end of the expedition.

The second area investigated in detail, alternately with Mt. Culebra, was Mound # 10 situated about 17 sea miles SE, at a depth of 2300 m. From earlier investigations, it was known that there was less contiguous carbonate surface, so the TV-MUC sampling was accomplished more successfully than at Mt. Culebra. This was confirmed by TV-MUC which produced a pronounced enrichment of CH₄ and H₂S and a decrease in chloride at a core depth of only 4 cm. A gravity core about 400 cm from the top of Mound # 10 showed the highest methane content so far, as well as a strong change in the methane gradient and an increase in sulfide at a depth of about 250 cm; thus ascending fluids can be assumed.

The first deployment of a Benthic Chamber Lander (BC-L) was at Mound #10. Here it was not possible to penetrate the sediment sufficiently, however after 30 hours one of the 4 samplers contained a complete time-series of samples. Two others did not function properly and a third was damaged during recovery. In the area around Mound #10 there had as yet been no CTD-survey of methane distribution in the water column. Two depth profiles, one above the top, the other at the western edge, resulted in identical patterns of methane distribution in the near-bottom water. This distribution confirmed all previous observations on CH₄-maxima directly at the bottom and a continual decrease upwards. This is to be interpreted as a fluid source and not as bubble transport of the methane.

After completing the station work, we transited to the southern area of investigation around Mounds #11 and #12. From here, all other areas could be reached within a few hours, so several investigative goals were worked on alternately. The sea was exceedingly calm so far; the temperature of 28°C and the high air humidity was not everyone's cup of tea, but this did not dampen the good spirits.

The events during the week from 17.09.2002-23.09.2002 were as follows: We spent time investigating the southern section offshore Costa Rica where the Galapagos-generated crust is subducted. We worked alternately in two areas 32 nm from each other: the Jaco Scarp and the Mounds #11 and #12. The scarps and mounds emit various types of fluids from different depths; the mechanism responsible for the fluid-movements seems to be respectively different as well. Therefore, the comparison of mounds and scarps is of high scientific priority.

Mounds #11 and #12 are gentle morphological elevations at 1000 m depth offshore Quepos, with a relief of maximum 30 m at the middle slope. Earlier OFOS observations had documented active fluid venting based on carbonate formations and vent communities. During leg M54/2 the mounds were identified as mud volcanoes with a more or less contiguous carbonate platform on top. Gas hydrates were also found about 200 cmbsf on the southern flank of Mound #11, a mound characterized by high heat flow. At the beginning of the week several gravity cores were taken at the position of the gas hydrates and in the center of the mounds. All of them terminated at about 200 cmbsf because penetration failed when they encountered compact layers of gas hydrate. Regrettably, we were not able to sample any of the gas hydrate.

All cores contained either layers of volcanic ash of different thickness (1-20 cm) cemented by carbonate, or layers of different types of carbonate concretions. TV-guided multi-corer deployments at those stations where the gravity cores failed or at positions with bacterial mats allowed an exact delineation of the pore water-concentration gradients near the surface. In general, the chloride contents decreased significantly to as low as 250 mol/L. Methane, hydrogen sulfide, and alkalinity increased significantly caused by ascending

low-salinity fluids. Freshening may, however, also be caused by dissociation of gas hydrate. Both types of chloride decrease were measured.

The second deployment of the BC-L was a remarkable success. Near bacterial mats at Mound #11, it recorded a 30-hour continuous decrease of oxygen and nitrate to values less than half those of the bottom water, with a simultaneous increase in methane. The sediment enclosed in the chamber was sampled for high-resolution pore-water chemistry. A detailed OFOS-survey of Mound #12 showed that active venting is presently taking place on the southwestern flank. Bacterial mats and carbonate-edifices (irregular chimney formations found with venting communities) are present here. Continuously younger carbonate formations extend from the top down the southwestern flank.

Platy crusts of interrelated carbonates build up the top of Mound #12. Fractures between the carbonate plates are extraordinarily densely occupied by *Bathymodiolus* colonies (vent shell) whose margins are discolored by bacterial mats. Along the downward edge of the slope fewer carbonates and more vent-organisms were observed; i.e. fragmented pieces of carbonates with dense fields of living mussels grading into fields of empty shell debris, followed by single clams and bacterial mats at the western margin of the active field.

The highest solute concentrations of pore water were obtained from sediments sampled by TV-guided multi corer at bacterial mat sites. Approximately 20 mMol/L hydrogen sulphide were measured at a depth of only 20 cmbsf; alkalinity, chloride and methane were likewise extremely high. The BC-Lander and the VESP-Lander were positioned on Mound #12 and we continued taking water column samples by using CTDs and the in situ pump. Particulate matter was collected with the in situ pump to isolate biomarkers. These are expected to be characteristic of vent-activities. Between 10-15 cm off the seafloor at Mound#11 an exceedingly high methane content of 120 mMol/L was measured as well as strong gradients. In this way we succeeded in documenting the continuous transition of the methane concentrations between the measurements of the CTD-rosette and the bottom water sampler.

Jaco Scarp represents the best-defined and, with its bathymetry, the most outstanding feature generated by seamount subduction. Along this feature a volcanic seamount originally situated on top the Galapagos-generated crust plowed into the slope sediments. Such features open up routes for fluid- and gas-emission and by this means contribute to the dewatering of subduction zones. Jaco Scarp extends from its upper edge at a water depth of 1000m down to 2300m. Inside the semi-circular scarp face there is an apron of debris and boulders which, after the passage of the seamount, were loosened from the sides and the head wall. Above 1900m the sediments of the slope are exposed and free of debris, forming several abrupt steps up to almost 1000m of water depth. From earlier investigations, we know that here fluid venting is active as shown by methane anomalies in the water column and by the presence of vent communities. Based on these results observed between 1700-1900 m, at the lower end of the exposed layers, the entire width of the caldera was searched and sampled for vent phenomena. The results indicate that venting is restricted to the center of the exposed head wall with the most active spot between 1760-1840 m. Here fluids exit horizontally from the exposed indurated layers of mud stones and support a shrubbery of pogonophoran colonies which stick out of the vertical wall. At several spots we observed caves where these colonies prosper even more than at the walls. Vent clams (*Calyptogena*) are found in the colonies as well. They are restricted to debris aprons and narrow ledges at the base of the vertical wall, primarily at a depth of about 1800 m but also around 1700m. Only at these ledges did we succeed in sampling by using the TV-grab. The material consisted mainly of mud-stone pebbles with a bit of sediment mixed in. In spite of their high permeability, and therefore the possibility of considerable admixing of bottom water, chloride values of 440 mM/L — considerably lower than seawater— were measured in the pore water of these sediments. The TV-MUC could not be used here because of the rubble, however two locations were found where the Lander could be deployed.

This week once again the sea was calm, with air temperatures decreasing slightly compared to the week

before. Also strong and frequent showers combined with thunderstorms, mostly at night, made temperatures more bearable.

The events during the week from 23.09.2002-29.09.2002 were as follows: First, following a Parasound survey, we sampled a gravity core from a small slide area on the upper slope (BGR-Slide). A reflection seismic profile of the slide area showed a chaotic development of the BSR, which suggested possible methane degassing. The 320 cm core showed 50 cm of recent sediment deposited above an erosive discontinuity of older and much more consolidated sediments below. This superposition enables us to obtain an exact dating of the slide phenomenon. At the same time, the physical characteristics of the exposed deeper sediment might allow a reconstruction of the circumstances of the slide.

Following this the older VESP-sampler modified to carry a timed sequence of 5 water samplers on a cable, took 3 profiles along the steep slope of the Jaco Scarp which was colonized by abundant pogonophora. Due to the inaccessible morphology of the fluid- and gas expulsion sites on the flank, the deployment of our usual bottom equipment was not possible. Nevertheless, in this manner described above with the modified device we obtained a composite deep profile over the whole area of expulsion. The data showed increasing methane concentrations from top to bottom of ca. 400-1.700 nMol/L. These values exceeded all the contents measured thus far during the expedition and verified the high activity of this vent site. Also a higher radon activity could be confirmed in these vent waters. A TV-grab sampler brought up large pieces of chemoherm carbonate from the flat 'roof' of the Jaco Scarp, thereby increasing the already large extent of our collection of vent carbonates.

The following day the Benthic Chamber Lander and the VESP-Lander were retrieved at Mound #12. One was placed directly in an anoxic vent field with mussel fragments and bacterial mats. The methane and hydrogen sulfide discharge and the oxygen consumption gave a consistent picture of venting. These deployments were followed by TV-MUCs along a profile on the active SW corner of Mound #12. The first deployment was in an active Bathymodiolus field and yielded high methane contents; the second, over a bacterial mat, but missed its target and showed only a moderate methane increase during deployment time. Finally, a TV-G deployment on Mound #11 to attempt again to recover some gas hydrate produced only mud with carbonate concretions and cemented sediment.

The following night, an extended OFOS-survey was carried out beyond the deep-sea trench on the oceanic plate. Here, on the flank of the Cocos Ridge, the previous leg had measured an extremely high heat flow value but nowhere along the way was there the slightest indication of fluid expulsion. After discontinuing the profile, we returned to Mound #12. However, local fishermen had laid out long lines in our working area and we could not begin. Instead we steamed to the ca. 0.5 nm diameter 'mud pie' structure, identified in the Side Scan Sonar at 2000 m depth, to obtain a gravity core. This core contained a highly carbonate cemented layer at its deepest part with shell debris and peculiar brecciated material. This fabric was overlain by hemi-pelagic sediment, which suggested a currently inactive methane vent site.

The BC-Lander was then deployed for a short station (12 hrs.) first at a narrow ledge with extended populations of vent mussels on Jaco Scarp followed by the VESP-Lander at the same site for a longer period, maximum 7 days. The deployment went smoothly, thanks to the ship's exceptional navigation skill and detailed knowledge of the steep slope that had been acquired. In the course of the day we steamed back to Mound #12 to take up the work we had not been able to carry out the previous day. The modified VESP-Sampler was deployed again at a carbonate platform densely colonized with Bathymodiolus mussels.

Here methane contents were of the same order of magnitude as at the active vent off the Jaco Scarp. This deployment was, however, mainly for measuring radon, which had also shown a slightly increased activity. Deployment of the bottom water sampler was followed early the next morning with the last instrument: The VESP-Sampler; the survey of the unknown part of Mound #12 was unspectacular, but toward the end of the profile in the SW section, the device could be deployed for the first time on top of a pogonophoran colony associated with mussels. This site turned out to be the most active one found yet for fluid venting and

dewatering. The opportunity of having sampled a 'pure' end-member type vent fluid promises exciting results for budgeting considerations of the total dewatering process in this area.

After this successful conclusion, FS METEOR set course for the position >150 nm distant to the NW to recover the VESP-Lander on Culebra Mound which had been deployed there for 10 days. This transit was a welcome change from the continuous and very extensive work for the laboratory- and equipment groups. The VESP-Lander was successfully recovered on the evening of the 27th; all systems had functioned without problems. In the early morning hours of 28th of September, all science work had ended and FS METEOR set course for Caldera. At 1230 hrs. local time the pilot came aboard and shortly thereafter at 1300 hrs FS METEOR tied up at the pier in Caldera. Thereby Leg M54/3A came to a successful end, after 17 unusually productive days. A large number of samples, analyses, measurements, and observations were collected whose evaluation will bring us a good deal closer to the central goals of SFB 574.

4.3 Agenda of the cruise M54/3B

(E. Flueh)

Cruise M54/3-B started on September 30, 2002, Caldera, Costa Rica. Altogether 11 scientists embarked on RV METEOR in Caldera, and four participants of cruise M54/3-A stayed onboard and completed the international group of scientists from Canada, Costa Rica, and Germany. All equipment needed for this short cruises was quickly installed and secured before leaving port.

At 16:30 on September 30 METEOR left the port of Caldera and steamed towards the research area offshore Pacific Costa Rica, the Jaco Scarp seismological network that was to be retrieved. This network comprised 23 ocean bottom stations which were deployed in May 2002 during cruise SO163-2 from RV SONNE (Weinrebe and Flueh, 2002). After maintenance, these stations were to be redeployed for another seismological network, the Quepos network to the southeast of Jaco Scar.p. When a waterdepth of 200 m was reached, the bathymetric data from the hydrosweep system were digitally recorded. The first instrument was reached after three hours transit, released and safely recovered at 20:30 on September 30. Subsequently, on average every two hours another instrument was recovered.

After the first ten instruments were picked up, the route was made such that five instruments (OBH301 to 305) were deployed in the Quepos network on October 01, before we continued to pick up further instruments from the Jaco network. Stations in shallow water were released using the ships hull transducer, while for instruments in deeper waters the ship stopped several miles ahead of the instrument and an active transducer was lowered on starboard side to send acoustic release commands. The operation went smoothly, and all stations responded almost instantaneously to the release commands.

On October 02 at 17:00 the VESP Lander, that was deployed during the previous leg from METEOR, was released and safely brought back to the ship. The remaining stations from the Jaco network were picked up and after service redeployed in the Quepos area. All except two stations recorded good data. One of the two tiltmeter stations was damaged, apparently a lithium battery had exploded during the recording period. Data recording had stopped in August, and the instrument could not be repaired on board for a redeployment.

After deployment of the last station (OBH323) station OBS305 was recovered to check the amplification of the seismometer. This station was placed at 1000 m waterdepth, and analysis of the data recorded in the first two days indicated that the amplification on the two horizontal components was rather high. This was changed to a lower gain and the instrument was redeployed. This terminated the planned work for this short leg, and since no problems were encountered, time was available for some bathymetric profiles to extend the coverage of high resolution bathymetry on the Pacific waters off Costa Rica. The main activity was centered on the northern end of the Panama fracture zone off the Burica Peninsula, the resulting map is shown in Fig. 4.3.1.

On 05. October at 18:00 METEOR left Costa Rican waters, and headed towards Balboa, Panama, for refuel and Panama canal passage. Some scientists left the vessel in Balboa. The canal passage was completed 08.10. by 01:00, and the final destination of this cruise, Curacao, was reached 10. October at 23:00, where cruise M54 terminated.

Details about the instruments recovered and deployed are summarized in Appendix C.

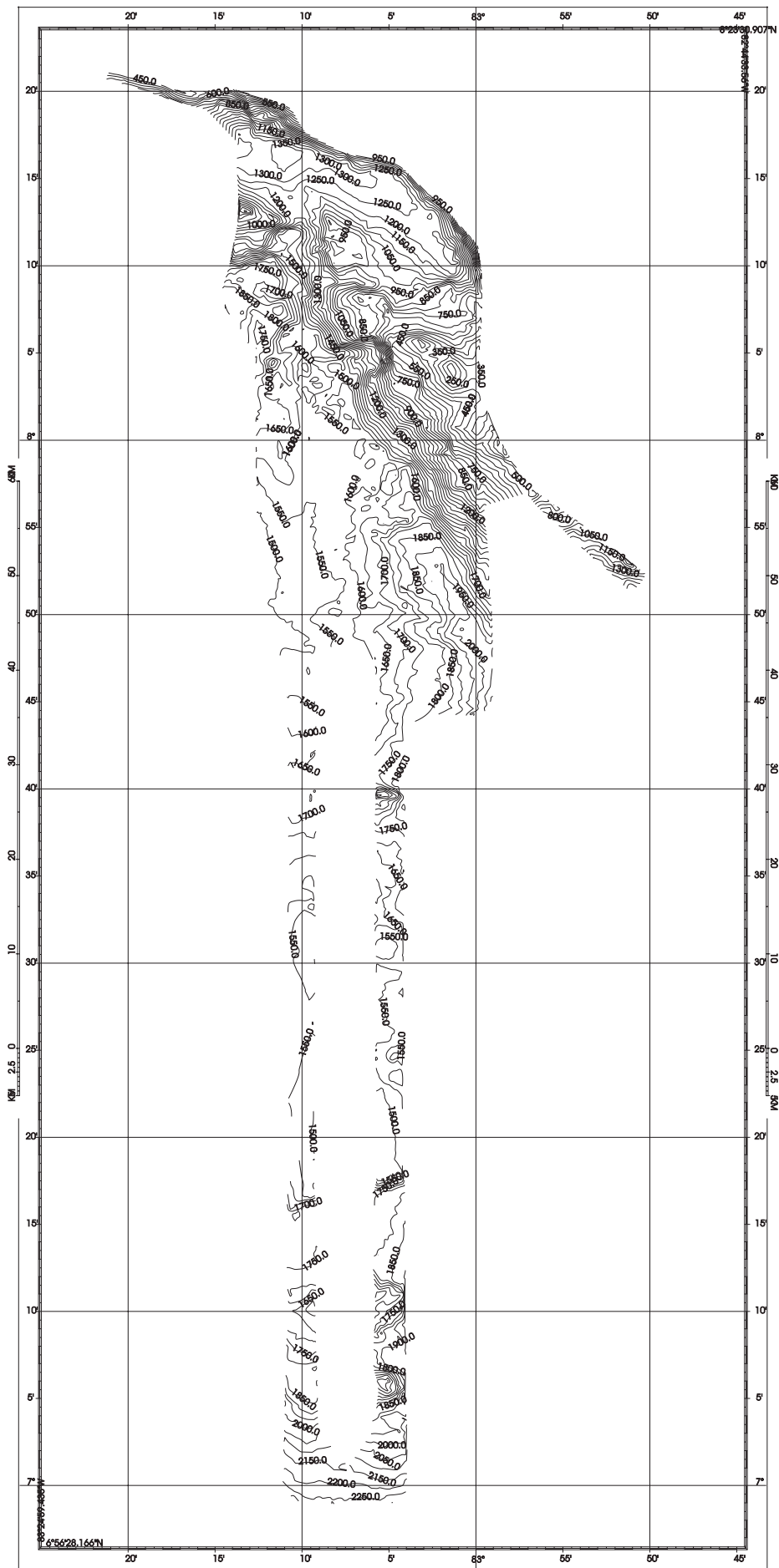


Figure 4.3.1: Results of Bathymetric profiles from M54/3B.

5 Results

5.1 Seafloor observations

(H. Sahling, W. Brückmann, J. Scholten, E. Soeding, E. Suess)

One of the major objectives of cruise M 54/3A was to identify and sample seafloor manifestations of fluid venting. For that, the video sled OFOS as well as TV-guided tools, i.e. TV-MUC, TV-G, VESP, and Landers were deployed. The seafloor observations are summarized here in order to give a comprehensive overview over fluid venting phenomena at the various geological structures surveyed during this cruise.

The technical specifications that were relevant for deployments of OFOS and TV-guided tools during this cruise on the R/V Meteor were: R/V Meteor has only a coaxial cable for the transfer of video signals, therefore, the video of all TV-guided tools was black-and-white and low quality. R/V Meteor does not have a sub positioning system for the towed tools, therefore, all coordinates given here are ship positions. The video observations were recorded on video tapes that do not contain the date and time due to additional noises caused by the inserter. OFOS is equipped with a black-and-white camera, xenon lights, a still camera (loaded with 200 ASA 30.5 m KODAK Ectachrome film for slides), flashlights, and a memory CTD (max. depth 3000m). Optimal illumination of the still images of the camera (focus: 0.8 to 1.2 m, aperture 5.6) was achieved when the weight (total length 23 cm, solid cylinder 5 x 19 cm) was hanging on a 2 meter long rope below the sled instrument deck. There was no time inserter available for the still camera.

5.1.1 Smooth Cocos Plate Segment off Nicaragua and Northern Costa Rica

Normal Faults off Nicaragua

The objective of this seafloor survey at the normal faults off Nicaragua was to identify sites of fluid venting that are related to serpentinisation processes in the upper oceanic crust. Indirect evidence for (presumed) serpentinisation and/or fluid circulation was given by a chloride anomaly that was found in a gravity corer (GC 6) taken in the sediment-filled trench during the leg M54/2. Considerable variations in the heatflow values further confirmed the presence of hydrothermal circulation in this area. However, three CTD deployments in this area did not show any methane anomalies in the water column.

Three OFOS profiles covered the landward dipping slope of three faults (Fig. 3.1.1). During this deployment we did not find any indications for methane venting. The first part of OFOS 115-3 and OFOS 120 surveyed the exposure of basalts with overlaying sediments. Some layers of the sediments were bright white and consisted of nannofossil ooze that was recovered by TVG 122. At the landward slope that was surveyed during the second part of OFOS 115-3 fractured hard rocks were exposed. With OFOS 121 a very steep slope was surveyed that consisted of hard grounds that were densely occupied by suspension feeders.

Mound Culebra

Mound Culebra is one of the biggest mounds off Nicaragua and Costa Rica. It was mapped by high resolution swath bathymetry and TOBI side scan sonar during SO 163. Two OFOS surveys during SO 163 revealed venting activity at the top of the mound. It was imaged by high resolution seismic during M 54/1. The thermal regime around the mound was studied during M 54/2. Gravity corer were taken at and around the mound during M 54/2.

During this leg various TV-guided tools were deployed (Fig. 5.1.1 and 3.1.2). These deployments revealed that carbonates and vent fauna exist at the top and at the NW flank of the mound. The observed distribution of these vent phenomena indicate that methane-rich fluids are channelled through small scale faults in the mound. The NW-SE orientation of the small scale faults probably indicate that they correspond to deeper fault patterns that run parallel to the slope. The massive carbonates that are exposed at the top area of the mound consist of several individual fields that are separated by sediment covered areas. These fields are connected to outcropping smaller-sized carbonates on the NW flank. All areas with carbonates were

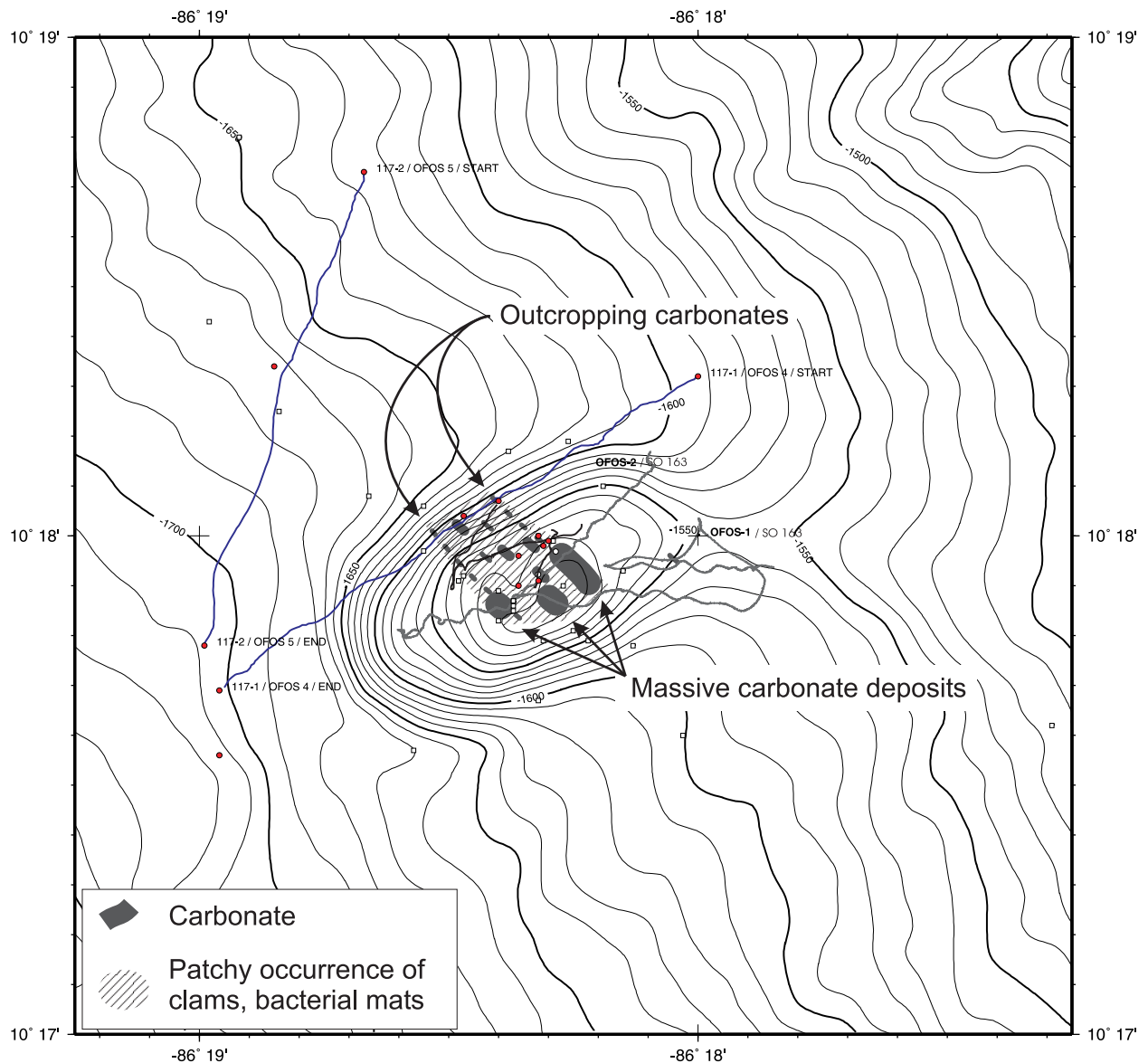


Figure 5.1.1: Simplified map showing the distribution of carbonates and vent fauna on Mound Culebra. This map is based on visual observations and the TOBI sidescan image (SO 163 cruise report p. 118).

repeatedly observed and are clearly orientated NW-SE. Chemoautotrophic organisms were concentrated in the areas between the carbonates. Several attempts to take sediment samples in scattered clam fields or bacterial mats failed, indicating widespread occurrence of carbonate concretions in the sediment. The TOBI image of Mound Culebra further confirms that small-scale NW-SE trending faults structure the mound (SO 163 cruise report, p. 118).

The objective of OFOS 117-2 was to survey an area where acoustic blanketing was observed during M 54/1 by high resolution seismic and Parasound. We found no evidence for fluid venting at the seafloor. However, the porewater extracted from a gravity corer at this site (GC 116) indicates considerable influence of low chlorinity fluids.

Mound 10

An OFOS deployment at Mound 10 (SO 163, OFOS 7) revealed that vent fauna, mainly vesicomyid clams, occur in soft sediments with, compared to other mounds, few carbonates. During the search tracks with TV-guided multicorer (TV-MUC 123-1 and -2) the general distribution could be confirmed: small clam field

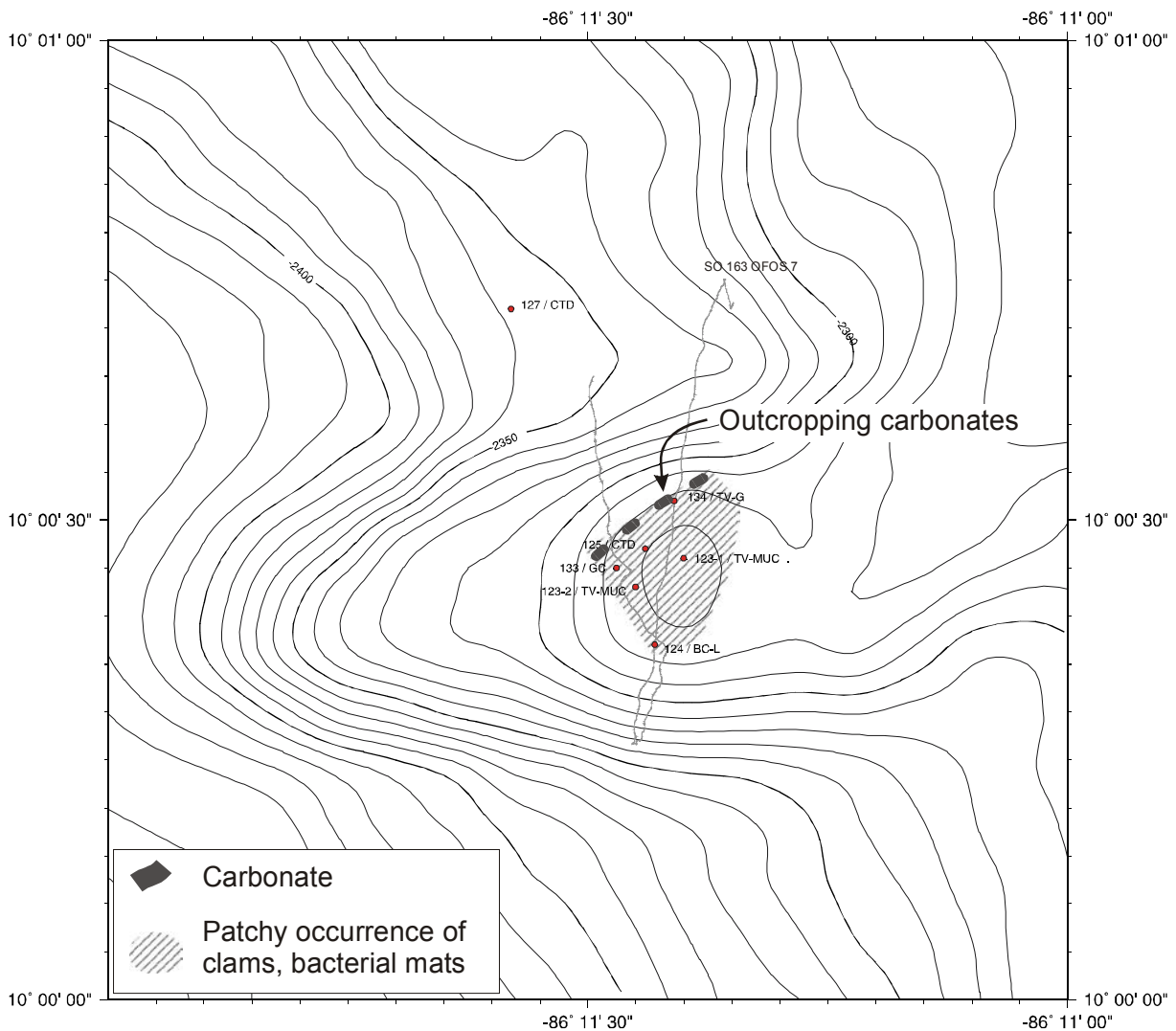


Figure 5.1.2 Location of stations and schematic distribution of carbonates and clam fields at Mound 10.

clusters occur in sediments, outcropping carbonates indicate the N limit of venting (Fig. 5.1.2 and 3.1.3). However, several sampling attempts (TV-MUC 123-2, TVG 134, BCL 124) showed that the sediments are solidified by carbonate concretions. Both TV-MUC were deployed very close to but not exactly at clam fields.

5.1.2 Rough Plate Segment off Costa Rica

„BGR Slide“

This slide was surveyed by OFOS 182 based on seismic profiles provided by colleagues from BGR / Hanover (Fig. 3.2.5). Outcrops with pretty suspension feeding organism were seen in the headwall area. The OFOS track crossed the 50m headwall in two locations and surveyed the central part of the slump mass. We found no evidence for venting activity.

Oceanic plate at Cocos Ridge

Very high heatflow values were obtained during M 54/2 on the oceanic plate at Cocos Ridge. The objective of OFOS 178 survey was to look for vent indications on the seafloor (Fig. 3.2.6). We found no evidence for venting. The seafloor morphology is generally smooth in the whole area. Beside a few outcrops and a small field with talus blocks in the area of HF 101-7 soft sediment prevailed throughout the track.

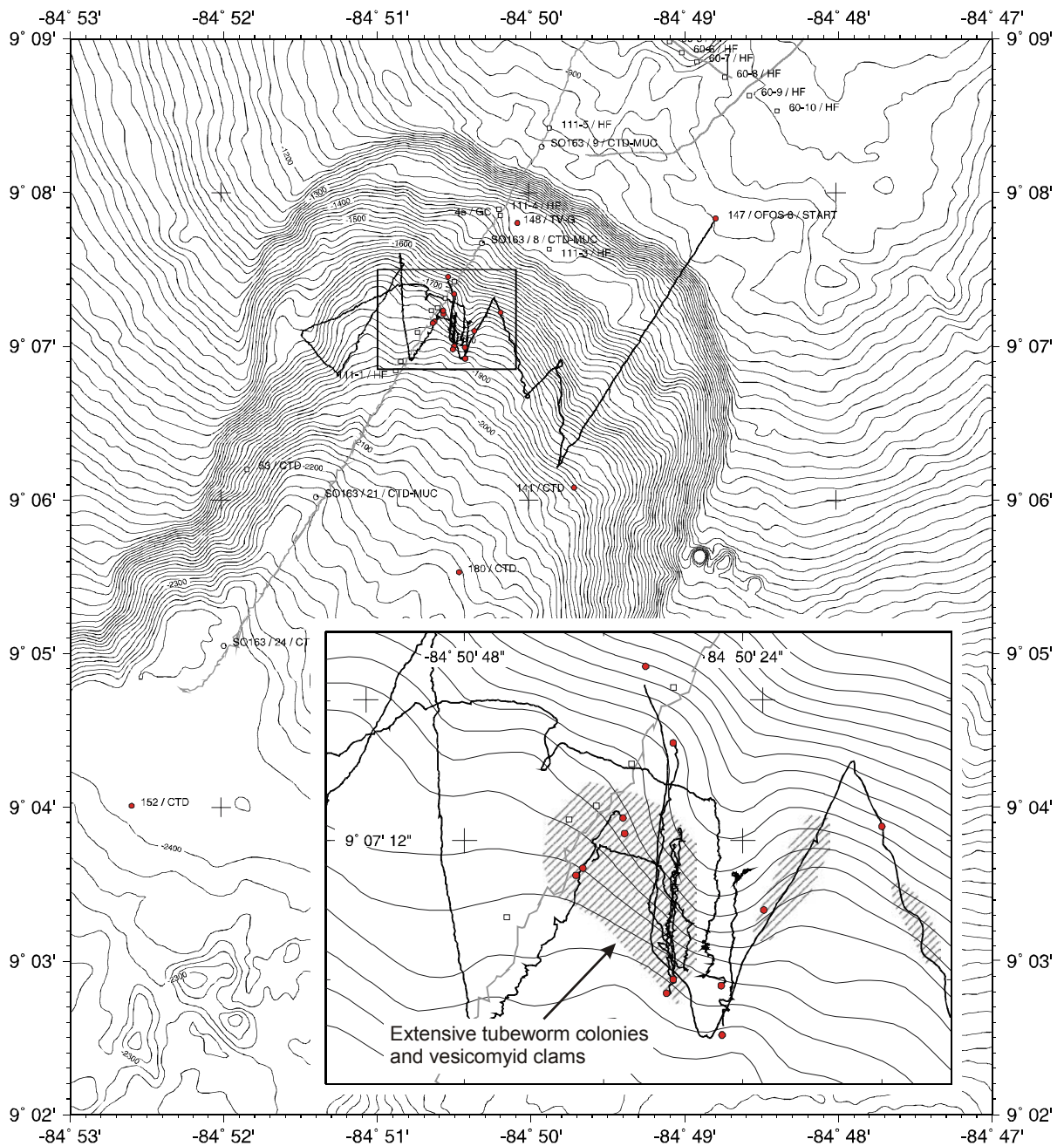


Figure 5.1.3: Stations at Jaco Scarp. Extensive fields of pogonophoran tubeworms and vesicomyid clams occur mainly on the E side of a small ledge (inset map).

Jaco Scarp

Jaco Scarp is a trace in the upper plate that is caused by a seamount that is subducting at present. This feature has been extensively studied during the cruises SO 144, SO 163 and first two legs of M 54. During this leg we extensively surveyed the scarp with OFOS and other TV-guided tools. We found abundant evidence for venting of methane-rich fluids at the base of the exposed sediment sequences in the scar (Fig. 5.1.3 and 3.2.1). The main venting area is limited to the E-side of a small ledge at a depth of around 1800 m. Pogonophoran tubeworm of the genus *Lamellibrachia* colonize the near-vertical walls while vesicomyid clams live in the talus field just below (Fig. 5.1.4). It was impossible to take samples from the tubeworm clusters. With TVG 153 we sampled vesicomyid clams and the talus that consist of pebble to cobble-size mudstones. The analyses of porewater from GC 159 revealed the seepage of low chlorinity fluids escaping the talus fields. The talus field is covered by a few cm of fine grained sediment (BCL 181).

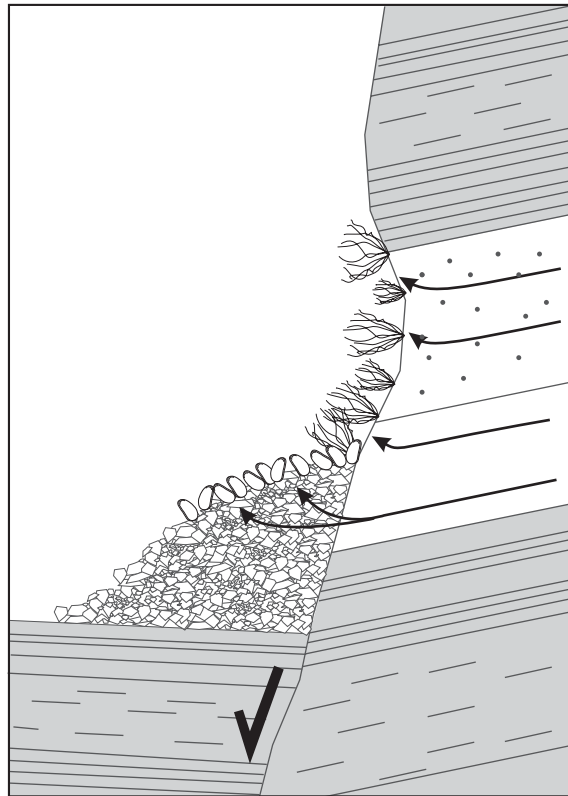


Figure 5.1.4: Schematic illustration of fluid sustaining chemoautotrophic species in the scar of Jaco Scarp: (a) sedimentary sequences are exposed after a slumping event, methan-rich fluids seep vertically;

Mound 11

Mound 11 and Mound 12 have been first detected by a TOBI sidescan sonar survey. OFOS tows during SO 163 revealed extensive venting activity. Numerous heatflow measurements were conducted around Mound 11 during leg 2. The last gravity corer of this leg recovered gas hydrate. Several TV-guided tools were deployed (Fig. 5.1.5 and 3.2.3). Mound 11 is a small feature, it rises about 20 m above the surrounding seafloor. On the slopes carbonate talus occur. Close to the top area, which is flat, carbonate pieces get more frequent and additionally clamshells were observed. The top is sediment covered with bacterial mat patches that are some square meters in size or smaller. These bacterial mats are very similar to the ones observed at Hydrate Ridge. The benthic sampling program revealed that gas hydrate occur close to the sediment surface, although we were not able to recover pieces of gas hydrate. Various multicorers deployed at bacterial mats recovered sediments that were degassing after retrieval. The porewater composition indicates ex situ dissolution of gas hydrates. Moreover, we found evidence that carbonate crusts ('gas hydrate carbonates') form on top of the gas hydrates preventing the coring devices from penetration.

Mound 12

The distribution of carbonates and chemoautotrophic fauna at Mound 12 can be explained by a model that assumes old surface expression of venting at the top with a succession towards the SSW at which the youngest surface expressions exists (Fig. 5.1.6). The top of the mound is dominated by fractured massive carbonate blocks that have probably been formed (in the sediment) and uplifted. In the fractures no living chemoautotrophic species were seen. At the slope, the carbonates form a more continuous area, the fractures

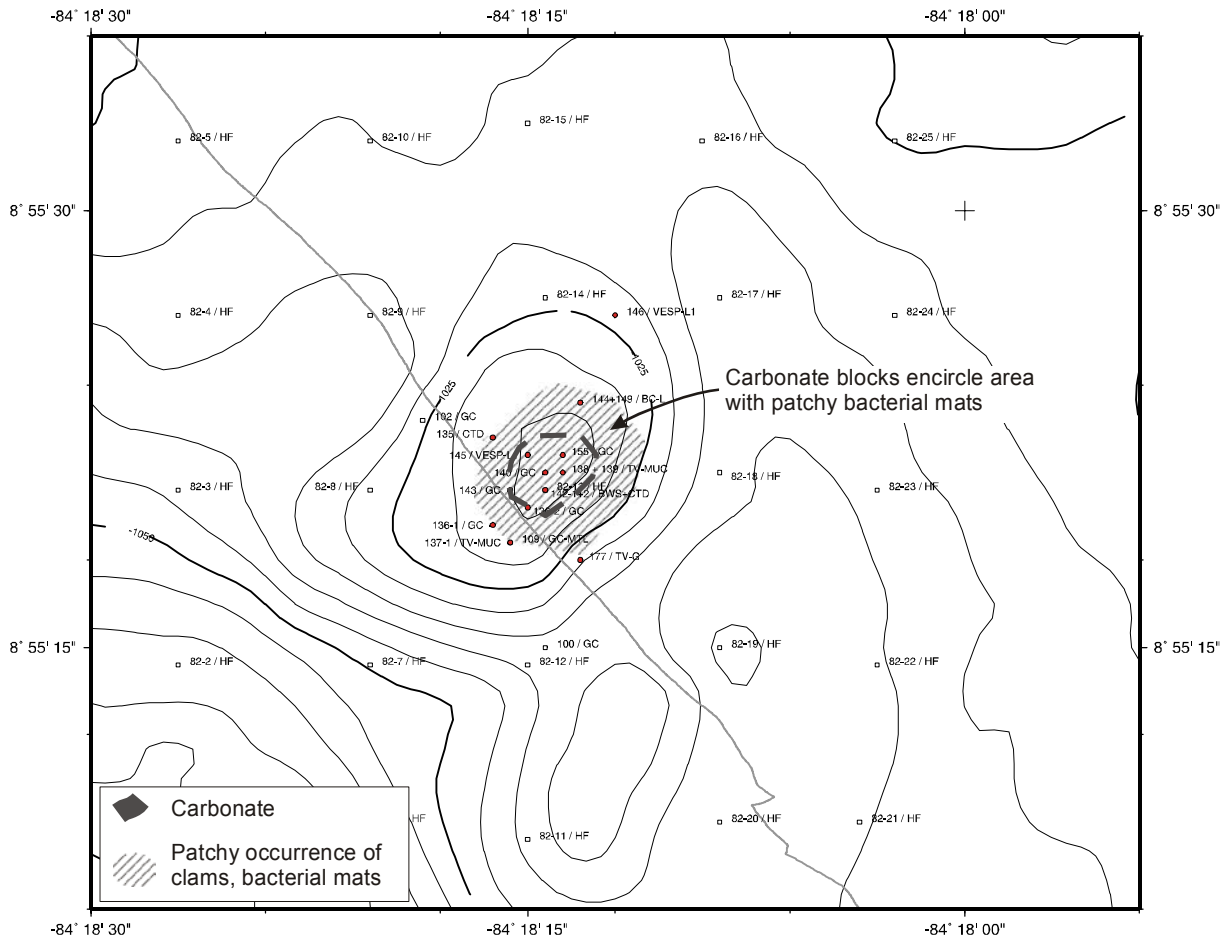


Figure 5.1.5: Location of stations and schematic distribution of carbonates at Mound 11.

are heavily populated by the mussel *Bathymodiolus*. Further to the SSW carbonate pieces in the sediment and comparable few bacterial mats occur. These may be talus blocks or sites of active carbonate formation. The most distant areas are sediment covered. Here, bacterial mats were observed and sampled. The absence of chemoautotrophic metazoans in this sediments indicates that in this areas the seepage of methane-rich fluids started only recently.

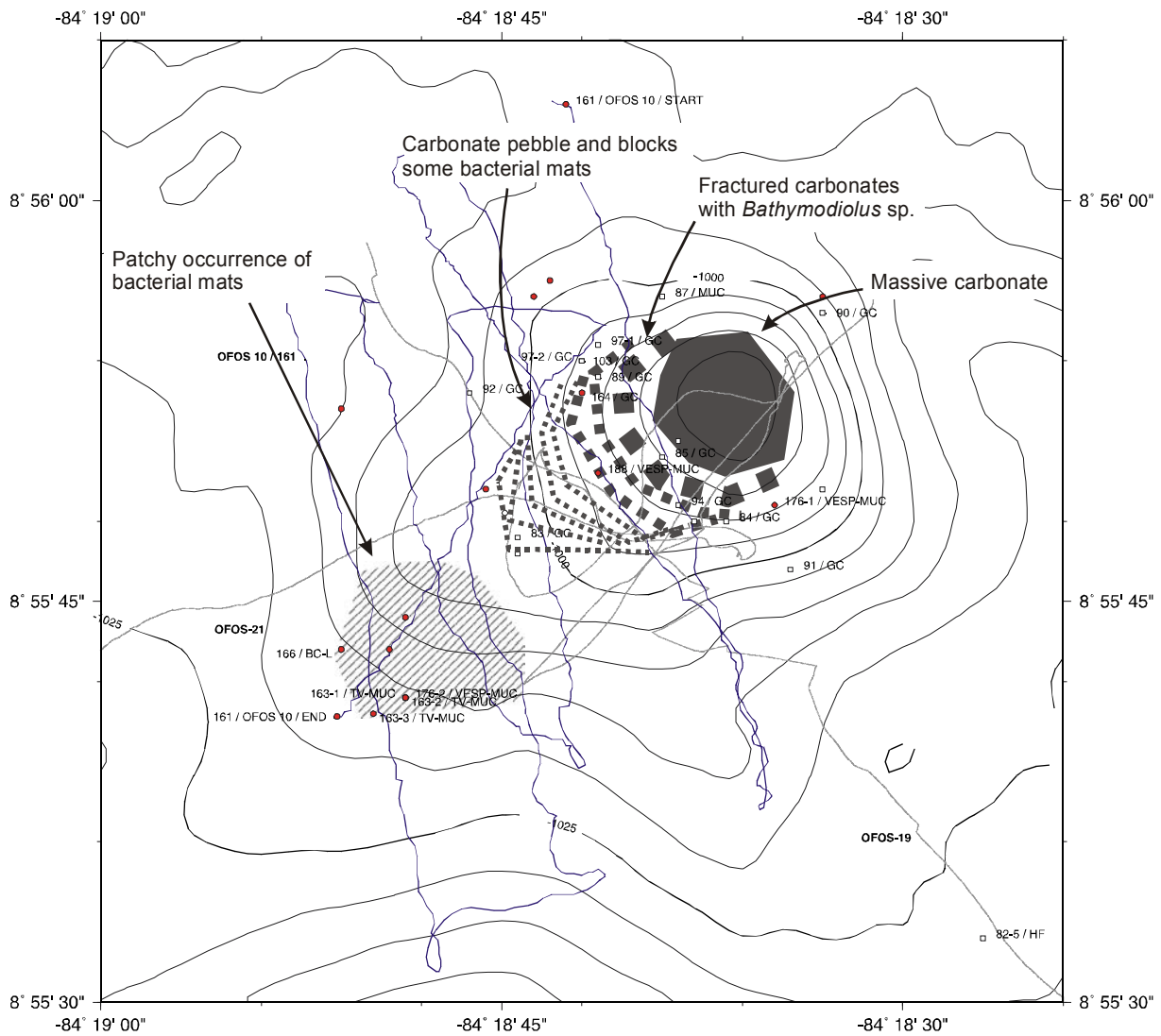


Figure 5.1.6: Schematic map of the distribution of carbonates and chemoautotrophic species at Mound 12. There is probably a time-dependent succession in the surface expression of venting: bacterial mats in soft sediments indicate that venting has started recently, massive carbonates indicate that venting has been going on for considerable time periods.

5.10 OBH/OBS deployments

(W. Brunn, E. R. Flueh, S. Goold, J. Gossler, H. Kopp, P. Liersch, T. Woronowicz)

5.10.1 Computer facilities for bathymetry, magnetic, and seismic data processing

The experiments and investigations during M54/3-B required special computing facilities in addition to the existing shipboard systems. For programming of ocean bottom stations, processing and interpretation of seismic data several workstations and a dedicated PC-laptop were installed.

Due to the large amount of data transfer GEOMAR installed a workstation cluster onboard comprising the following systems:

1	"moho"	SUN Sparc 20	2 CPU, 192 MB memory	20 GB disks, DAT, DLT, CD	Sun Solaris 2.8
2	"devonia"	SUN Ultra 60	2 CPU 1 GB memory	150 GB disks, 1x DLT, 2x DAT, 1x Exabyte	Sun Solaris 2.6
3	"hotblack"	SUN Ultra 1	1 CPU, 128 MB memory	4 GB disks, CD	Sun Solaris 2.8
4	"galicia"	SUN Sparc 10	1 CPU, 96 MB memory	12 GB disks, DAT	Sun OS 4.1.4
5	"crimea"	AMD Duron 700 MHz	1 CPU, 128 MB memory	68 GB disks, 6x PCMCIA	Windows2000
6	"pinta"	AMD Duron 700 MHz	1 CPU, 128 MB memory	68 GB disks, 6x PCMCIA	Windows2000

In addition to these computers, several laptops were used. For plotting and printing two HP Postscript Laserprinters (papersize A3 and A4) as well as the shipboard color plotters were available.

The workstation cluster was placed in the Magnetiklabor and the Reinlabor where it was set up according to a „client-server“ model, with „moho“ being the server. All important file systems from the main server at GEOMAR were duplicated onto the „moho“-disks. Using NFS-, NIS-, and automounter services the computing environment was nearly identical to that at GEOMAR, so every user found his/her familiar user interface. The convenience of network mounted file systems has to be paid for with a heavy network load, particularly during playback of OBH-data (c.f. SO123 cruise report, Flueh et al., 1997). This required a high-performance network, which was accomplished by a switched twisted-pair ethernet. A 12-port ethernet switching-hub (3COM-SuperstackII 1000) with an uplink connection of 100 Mbps to the server „moho“ and dedicated 10 Mbps ports for the client workstations maintained the necessary network performance. In order to keep the shipboard network undisturbed by the workstation cluster, but to allow for communication between them, the server „moho“ was equipped with two network interfaces and served as a router. This provided the additional benefit of a simplified network configuration. Considerable setup work was dedicated to „moho“, while the other workstations used the same IP-addresses and network configuration as at GEOMAR. In addition, „hotblack“ was set up as an redundant server, so in case „moho“ would have failed, „hotblack“ could easily switched to replace „moho“ as a server.

This network setup showed a reliable and stable performance, and no breakdowns were observed.

5.10.2 Seismic Instrumentation

The Ocean Bottom Hydrophone

The first GEOMAR Ocean Bottom Hydrophone was built in 1991 and tested at sea in January 1992. This type of instrument has proved to have a high reliability with more than 2000 successful deployments. A total of 23 instruments were available for M54/3-B. These were first recovered from the seafloor where they had been recording since about five months, and after service were deployed for a second recording period. The principle design of the instrument is shown in Figure 5.10.1, and a photograph showing the instrument upon deployment can be seen in Figure 5.10.2. The design is described in detail by Flueh and Bialas (1996). The system components are mounted on a steel pipe which holds the buoyancy body on its top. The buoyancy is made of syntactic foam and is rated, as are all other components of the system, for a water depth of 6000 m, except for the pressure cylinders holding the recording electronics. Here, various models are available for variable depths (2500 m, 3000 m, and 6000 m). Attached to the buoyant body are a radio beacon, a flash light, a flag and a swimming line for retrieving from aboard the vessel. The hydrophone for the acoustic release is also mounted here. The release transponder is a model *RT66ICE* made by *MORS Technology*. Communication with the instrument is possible through the ship's transducer system, and even at maximum speed and ranges of 4 to 5 miles release and range commands are successful. For anchors, we use pieces of railway tracks weighing about 40 kg each. The anchors are suspended 2 to 3 m below the instrument. The sensor is an *E-2PD* hydrophone from *OAS Inc.*, or the *HTI-01-PCA* hydrophone from *HIGH TECH INC.* and the recording device is a *MIS* recorder of *SEND GmbH*, which is contained in its own pressure tube and mounted below the buoyant body opposite the release transponder (see Figures 5.10.1 and 5.10.2).

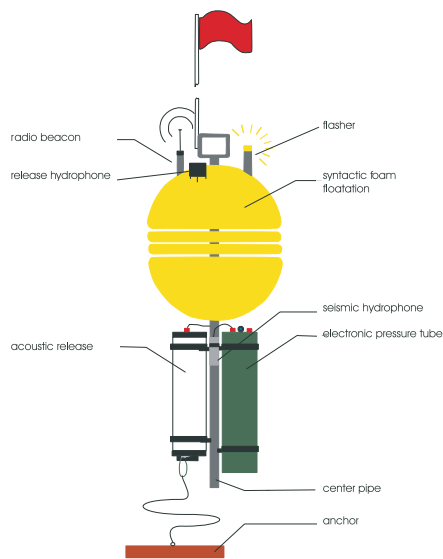


Figure 5.10.1: Principle design of the GEOMAR OBH (after Flüh & Bialas, 1996).

The design is described in detail by Flueh and Bialas (1996). The system components are mounted on a steel pipe which holds the buoyancy body on its top. The buoyancy is made of syntactic foam and is rated, as are all other components of the system, for a water depth of 6000 m, except for the pressure cylinders holding the recording electronics. Here, various models are available for variable depths (2500 m, 3000 m, and 6000 m). Attached to the buoyant body are a radio beacon, a flash light, a flag and a swimming line for retrieving from aboard the vessel. The hydrophone for the acoustic release is also mounted here. The release transponder is a model *RT66ICE* made by *MORS Technology*. Communication with the instrument is possible through the ship's transducer system, and even at maximum speed and ranges of 4 to 5 miles release and range commands are successful. For anchors, we use pieces of railway tracks weighing about 40 kg each. The anchors are suspended 2 to 3 m below the instrument. The sensor is an *E-2PD* hydrophone from *OAS Inc.*, or the *HTI-01-PCA* hydrophone from *HIGH TECH INC.* and the recording device is a *MIS* recorder of *SEND GmbH*, which is contained in its own pressure tube and mounted below the buoyant body opposite the release transponder (see Figures 5.10.1 and 5.10.2).

The Ocean Bottom Seismometer

The Ocean Bottom Seismometer (OBS) construction (Bialas and Flueh, 1999; Fig. 5.10.3) is based on the experiences with the GEOMAR OBH. For system compatibility the acoustic release, pressure tubes, and the hydrophone are identical to those used for the OBH. Syntactic foam was used as flotation again but of larger diameter due to the increased payload. In contrast to the OBH the OBS has three legs around a center post to which the anchor weight is attached (Fig. 5.10.4). While the OBH is floating about 1 m above the sea bottom, the OBS is positioned on the sea bottom to avoid collisions between the the seismometer cable and the anchor. The seismometer is deployed about 3 m to the side of the system once the OBS lands on the sea floor.

Two different types of sensors can be attached to the instrument. The „Spahr Webb“ type seismometer is based on *Mark-L4* sensors which are operated with a feedback loop to enable recordings of frequencies as low as about 60 sec. As the sensors are sensitive to



Figure 5.10.2: The GEOMAR OBH ready for deployment.

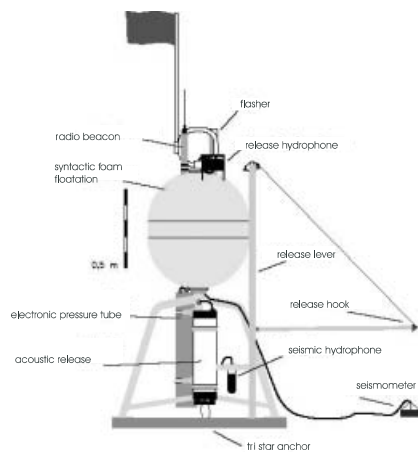


Figure 5.10.3: Principle of the GEOMAR OBS (after Flüh & Bialas, 1999).

horizontal or vertical adjustment the complete construction is fully gimballed. Tilt is measured at selected intervals and two electric motors are used to adjust and fix for a proper positioning. The second sensor is a *PMD-113* which has a flat frequency response curve from 95 sec. up to 30 Hz. This sensor type operates on the base of measuring levels within electrolytical tubes. This principle is less sensitive to its horizontal adjustment. The sensor is fixed like a pendulum while its lower third is surrounded by a viscose oil filling that gives freedom to very slow movements (within a circle of 18°) and could be assumed to be solid within the measured frequency range. Both systems are mounted within a 17" glas sphere with an additional weight at the bottom (20 kg weight in water) which should ensure a good coupling to the ground. The above described lever system was not able to handle this size of sensor and therefore a slide system was designed (Fig. 5.10.5 and 5.10.6) which allows to deploy the sensor about three meters to the side of the instrument carrier. A clock controlled burning wire is used first as release of the slide. Then the sensor is pulled by an elastic rope along the slide until it falls off at the end of the boom. Secondly the clock releases the sledge itself to enable deployment of the sensor even if it does not drop off the slide for any reason. Signals from both sensors as well as the hydrophone are recorded by use of the *Marine Longtime Recorder (MLS)* which is manufactured by *SEND GmbH* and specially designed for longtime recordings of low frequency bands. Together with the broadband sensors the fourth channel alternatively record a Differential Pressure Gauge (DPG) as described by Cox et al (1984) or a standard hydrophone.

The Marine Longtime Seismograph

For the purpose of low frequent recordings such as seismological observations of earthquakes during long term deployments of about one year time a new data logger, the Marine Longtime Seismograph (MLS) was developed by *SEND GmbH* with support from GEOMAR.

The MLS is again a four channel data logger whose input channels have been optimized for 3-component seismometers and one hydrophone channel. The modular design of the analogue front end allows to adopt for different seismometers and hydrophones or pressure sensors. Currently front ends for the Spahr Webb, PMD and Guralp seismometers as well as for a differential pressure gauge (DPG) and the OAS hydrophone are available. With these sensors we are able to record events between 50 Hz and 120 s. The very low power consumption of 250 mW during recording together with a high precision internal clock (0.05 ppm drift) allows data acquisition for one year. Data storage is done on up to 12 PCMCIA type II flashcards. The instrument can be parameterized and programmed via a RS232 interface. After low pass filtering the signals of the input channels are digitized using Sigma-Delta A/D converters. A final decimating sharp digital low-pass filter is realized in software by a Digital Signal Processor. The effective signal resolution depends on the sample rate and varies between 18.5 bit at 20 ms and 22 bits at 1 s. Playback of the data is done under the same scheme as described for the MBS above. After playback and decompression the data is provided in PASSCAL format from where it could be easily transformed into standard seismological data formats.



Figure 5.10.4: The GEOMAR OBS.

Tiltmeter

Research and surveying in risk areas such as the vicinity of volcanoes and earthquake-prone areas have been supported on land by tiltmeters for years (e.g. Decker and Decker, 1981). Small-scale as well as integral, large-scale surveys are carried out - i.e. gauges with short (ca. 2 m) as well as long (several tens to hundreds of m) base lines are being used. These systems have been successfully deployed especially in areas with tunnels and mining. The combination of tiltmeters with seismic surveys yielded good results in the field of short-term forecasts of eruptions (Dzurisin et al., 1982). Tiltmeters for marine usage have been successfully used only recently (e.g. Dünnebier and Harris, 1996; Anderson et al., 1997). Many of the systems employed up to now have been developed and constructed in academia (Simamura and Kazanawa, 1988; Wyatt et al., 1984 and 1996; Anderson et al., 1997). Short baseline systems constituted the majority among these. They are less expensive to develop, their deployment is less complicated and they can be mounted onto a variety of different platforms.

As the electronics of the referenced marine tiltmeters are all in house developments that have not been designed to be used and operated by a wide community we decided to complete a new easy-to-use instrument for the SFB574 making use of existing components as far as possible. Based on the experiences with marine long baseline instruments published by Anderson et al. (1997) we favored a short baseline solution. Future operation should then result into a larger number of instruments distributed over the area of investigation to allow minimization of station effects by an overall integration of (parts of) the deployed systems. Restricting to short baseline enables the use of the GEOMAR OBS (Bialas and Flueh, 1999) as a system carrier further using the available periphery of support (e.g. release system, relocation tools, etc.). Internet recherche and personal discussion with other long term users of tiltmeters led to the decision of selecting the type 501 and



Figure 5.10.6: The GEOMAR broadband seismometer equipped with Webb seismometer at deployment.

900-45 tiltmeters from Applied Geomechanics. The company had already been involved in marine tiltmeter developments with other customers. In general tilt values should be expected to be in the range of a few 2.5 urad to 200 urad (Wyatt et al, 1996; Tolstoy et al., 1998; a.o.) which could be easily resolved by the type 510 (+/- 1400 urad, < 10 nrad resolution). From earlier developments of a marine tiltmeter Applied Geomechanics could offer a gimballed system based on freezing Jojoba oil. Repetitive leveling would not be possible with this solution and therefore we decided to use a motor driven leveling. The basic type 510 tiltmeter was developed for drill hole deployments and could therefore compensate for a small amount of tilt only. To adopt for sea floor applications and possible larger angles of tilt caused by the slope of the sea floor the leveling system was extended to +/- 30 degrees for the GEOMAR sensor. The type 900-45 clinometer can be operated over a range of +/- 50 degrees with a resolution of 0.02 degrees. It is used to give an overall impression about the large scale tilt variations throughout the deployment. As the complete system is designed to free fall to the seafloor a C-100 compass from KVH Industries is implemented within the tiltmeter housing to allow later orientation of the tilt axis. It is well known from earlier studies that such high precision instruments are sensitive against temperature changes which requires continuous recording of this value. For data recording the easiest solution was to modify two of the long time operated MLS type seismic data loggers (Bialas et al., 2002) from SEND. X- and Y-axis of the 510 tiltmeter and temperature are permanently recorded with 1 s sample interval while the 900-45 and the magnetic compass are read after each leveling operation.

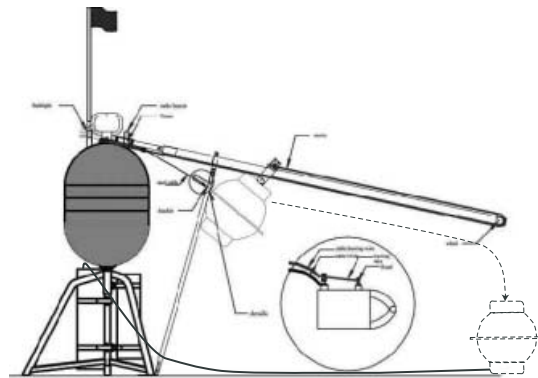


Figure 5.10.5: Sketch of GEOMAR broadband seismometer. Dashed lines indicate deployment of external broadband sensor at the seafloor.

5.10.3 Data Conversion

The OBH/OBS data are recorded in continuous mode by the MLS and MBS units. Processing of the seismic and seismological data requires a prior conversion into pseudo SEG-Y format, which is conducted based on existing REFTEK routines modified for the instrument requirements and the available hardware platforms. Figure 5.10.3.1 illustrates the processing scheme applied to the raw data onboard FS Meteor during cruise M54-3b, of which a detailed description of the main tools is presented below. Generation of the navigation file to install the correct geometry of Profiles P38-P40 was conducted during cruise SO163-1 onboard FS Sonne.

send2pas

Data recording is performed on PC cards which store the compressed data file in the MLS and MBS recorders. After recovery of the instruments, the skew of the internal clock is determined and the flash cards are then transferred to a DOS/Windows based PC. The program send2pas decompresses the data stored on the cards. send2pas contains a size option, which will split the raw data file into several decompressed individual files of the given size. The size may be estimated from the following relation:

$$\text{size} = \text{numsamples} * 16 \text{ bit} / 8 \text{ bit} = \text{numsamples} * 2 \text{ (per channel)}; \text{ numsamples} = \text{SPS} * \text{Time} / \text{s}$$

For a sampling rate of 100 Hz, which was chosen for the recording, output files covering a period of 30 days for the OBH-data recording and 10 days for the OBS data were generated.

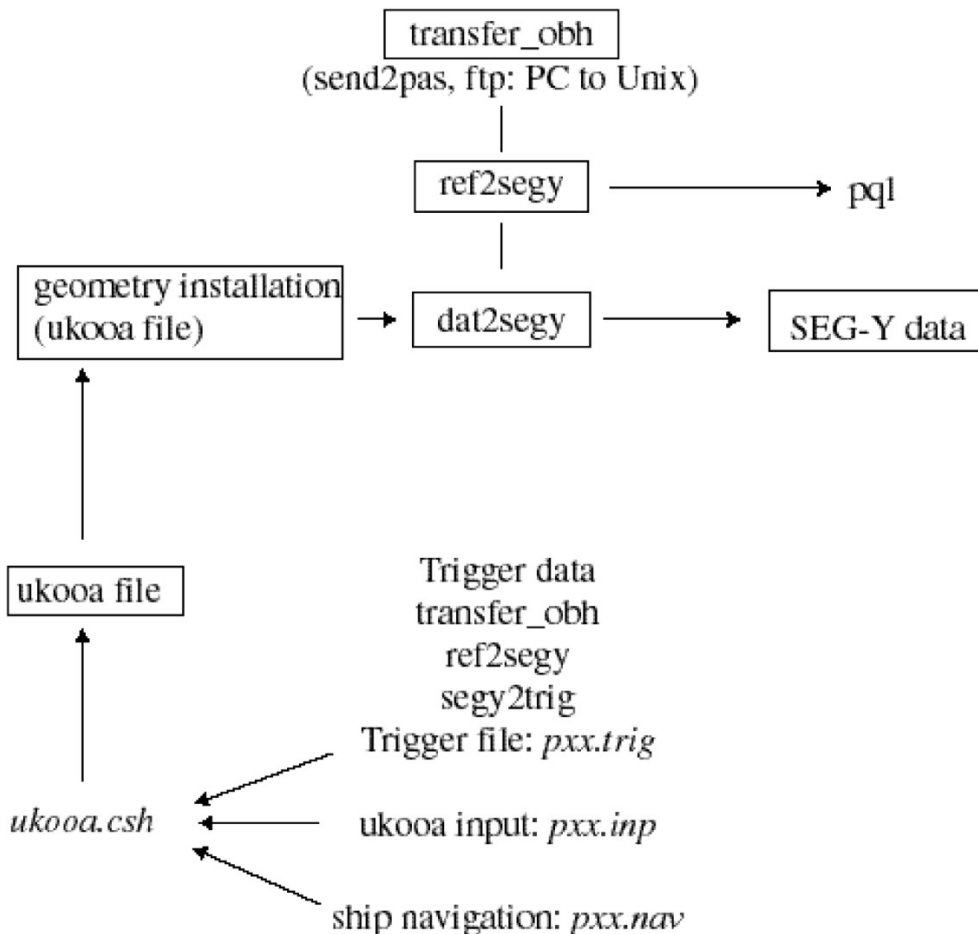


Figure 5.10.3.1: Processing scheme for conversion of raw data to SEG-Y data and geometry installation.

Subsequently, the data are converted to a PASSCAL data format in a 16 or 32 bit storage and written to the hard disk as well as copied to a SUN workstation via ftp as all other programs are UNIX based. Send2pas will also detect any possible time slip errors which may have occurred during the recording on MLS units. The time slips are caused by a mismatch of the actual sampling rate of the MLS recorder compared to the desired sampling rate. This mismatch arises because the clock rate of the crystal oscillator in the MLS recorder is temperature dependent (Klaus Schleisiek, SEND GmbH, pers. comm.). The temperature dependence is known and corrected for in the determination of the system time, but for performance reasons the sampling pulses are directly generated from the oscillator signal without any time correction. The send2pas routine detects and reports in the log-file when the accumulated inaccuracies of the sample rate cause an effective timing error of one sample. For the wide-angle data, the timing errors are considered by adding them to the skew of the internal clock, which is corrected within the dat2segy program (see below, note that the sign of skew and time slips are opposite, i.e., a negative sum of time slips corresponds to a positive skew). As each trace is at most a few tens of seconds long (vs. 1 hour and more between non-cancelling time slips), the corrected time is expected to be highly accurate with uncertainties well below one sample length.

ref2segy

The ref2segy program converts the output of send2pas to a pseudo SEG-Y trace consisting of one header and a continuous data trace containing all samples, as used by the PASSCAL suite of seismic utility programs. For each channel (consisting of pressure, vertical velocity, and velocity along two mutually perpendicular horizontal directions for OBS; pressure for OBH) one file is created with the name derived from the start time, the serial number of the Methusalem system, and the channel number. The file size of the pseudo-SEG-Y file is directly related to the recording time. For instance, a recording time of one hour sampled at 200 Hz (16 Bit) will produce a file size of 1.44 MB per channel. A record with two channels and a recording time of two days will produce a total data volume of 70 MB. After conversion to the pseudo SEG-Y trace, the seismic and seismological processing schemes diverge. The seismology data flow is described in the next section below.

pql

pql (Passcal Quick Look) is a simple display program for continuous seismic data. Its interactive zooming capability allows a rapid inspection of data quality. All data records retrieved during the cruise were visually checked before the data was stored and archived.

segy2trig

The trigger signal, provided by the airgun control system, is recorded on an additional MBS unit during the shooting period. The trigger data are treated similarly to regular seismic data and downloaded to the hard disk via the send2pas and ref2segy programs. Then, the segy2trig program detects the shot times in the data stream by identifying the trigger signal through a given slope steepness, duration and threshold of the trigger pulse. The output is an ASCII table consisting of the shot number and the shot time. Accuracy of the shot time is one of the most crucial matters in seismic wide-angle work, and must be reproduced with a precision of a few ms. Due to this demand the shot times have to be corrected with the shift of the internal recorder clock. Additionally, the trigger file contains the profile number, the start/end time of the profile and the trigger recording, which will be merged with the ukooa file that links the information with the coordinates of the source and the hydrophones.

ukooa

The ukooa program is used to establish the geometric database by calculating the positions of sources at any given shot time and offset from the ship. The source is placed on the ship track using simple degree/meter conversions and then written to a file in UKOOA-P84/1 format. Corrections for offsets between antenna and airguns as well as consistency checks are included. This file will be used when creating a SEG-Y section via the dat2segy program. The program requires the trigger file to contain the shot times, the ship's navigation, and a parameter file containing information for the UKOOA file header.

dat2segy

The dat2segy program produces standard SEG-Y records either in a 16 or 32 bit integer format by cutting the single pseudo SEG-Y trace (the ref2segy output) into traces with a defined time length based on the geometry and shooting time information in the ukooa file. In addition, the user may set several parameters for controlling the output. These parameters contain information about the profile and the receiver station, number of shots to be used, trace length, time offset of the trace and reduction velocity (to determine the time of the first sample within a record). The clock drift of the recorder (skew) and possible time slip errors are also considered. The final SEG-Y format consists of the file header followed by the traces. Each trace is built up by a trace header followed by the data samples. The output of the dat2segy program may be used as input for further processing with e.g. SEISMOS or Seismic Unix (SU).

Archiving

Data archiving was performed on DLT-Tapes using Unix tar utilities and included storage of the raw data files, the REFTEK format, and the PASSCAL data. The raw data files, and, where applicable, the REFTEK and PASSCAL data were compressed using the UNIX routine gzip. Archiving of the geometry information was already conducted during cruise SO163-1.

Profiles P38, P39 and P40

Profiles 38 through 40 were shot through the Jaco scar net during cruise SO163-2 on May 17-18, 2002, using FS Sonne as platform. A location map is given in Figure 5.10.3.2.

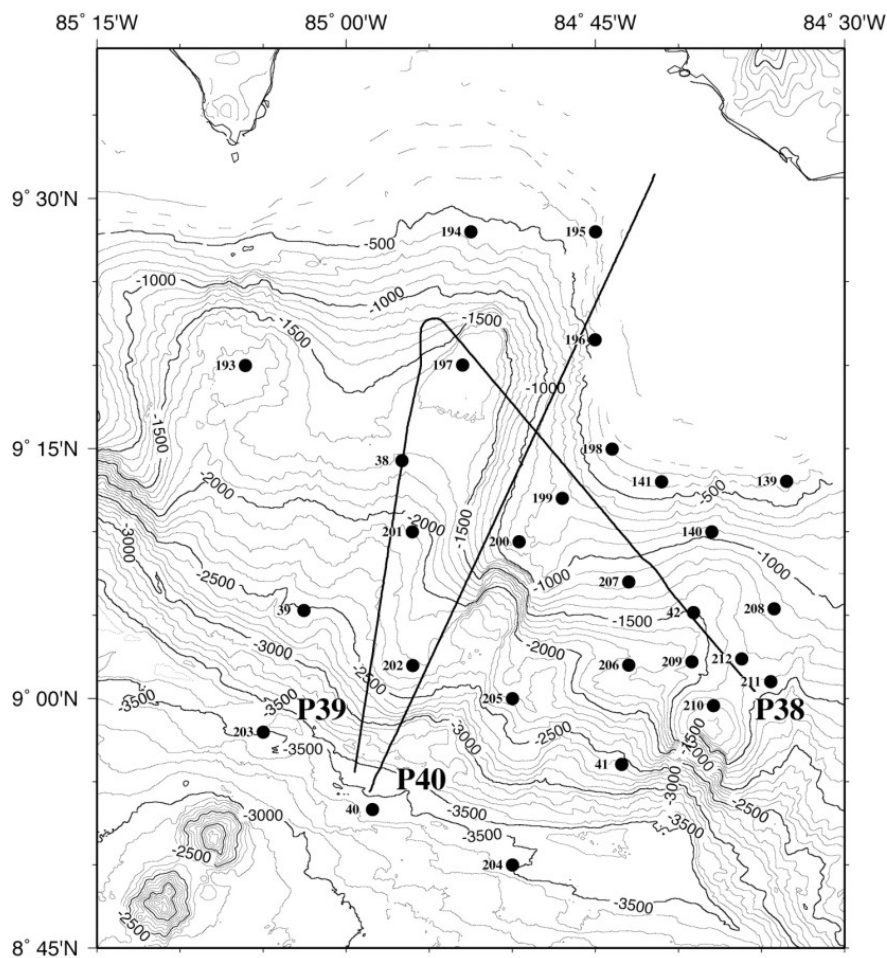


Figure 5.10.3.2: Location map of profiles P38 through P40 through the Jaco Scar Net (shot during cruise SO163-2 in May, 2002).

Figure 5.10.3.3 shows the hydrophone record section of profile P39 of station OBS201. The instrument was located approximately 2.5 km offline west of the line. Sedimentary phases are recorded to both offsets. A clear upper crustal refraction and corresponding pre-critical reflection is recognized to the northeast; these phases are also present to the southwest, however somewhat subdued. A weaker lower crustal refraction is visible to the northeast. Filtering and processing of the data will include a time-and offset-dependent frequency filter and a windowed deconvolution, which will enhance clarity.

5.10.4 Processing of JACO network's earthquake data

The initial processing of the data is identical to the processing sequence for wide angle data described in the previous section, i.e., reading of the 1 Gbyte-flashdisks, conversion into REFTEK files, and conversion into a pseudo SEGY file. Following this step, the processing sequence of the earthquake data diverges from the one for wide angle data., the further processing steps have to be.

The REFTEK files, and therefore also the single traces have been already cut into records of 30 days for OBH and 10 days for OBS stations. This simplifys the handling of a large amount of data. During former cruises, when the operating periods of the instruments were much smaller, the cutting was done after conversion into SEGY files.

A quick data quality check was made on board, to avoid bad instruments from being deployed again. The next processing steps like timing correction of data will be done at the institute at home, because of the short cruise time and the large amount of data that has to be handled. The result is shown in Table 5.10.4.1.

A short explanation of the further processing steps are given in the following part. First is the timing error correction of the data. Two timing errors need to be taken account of:

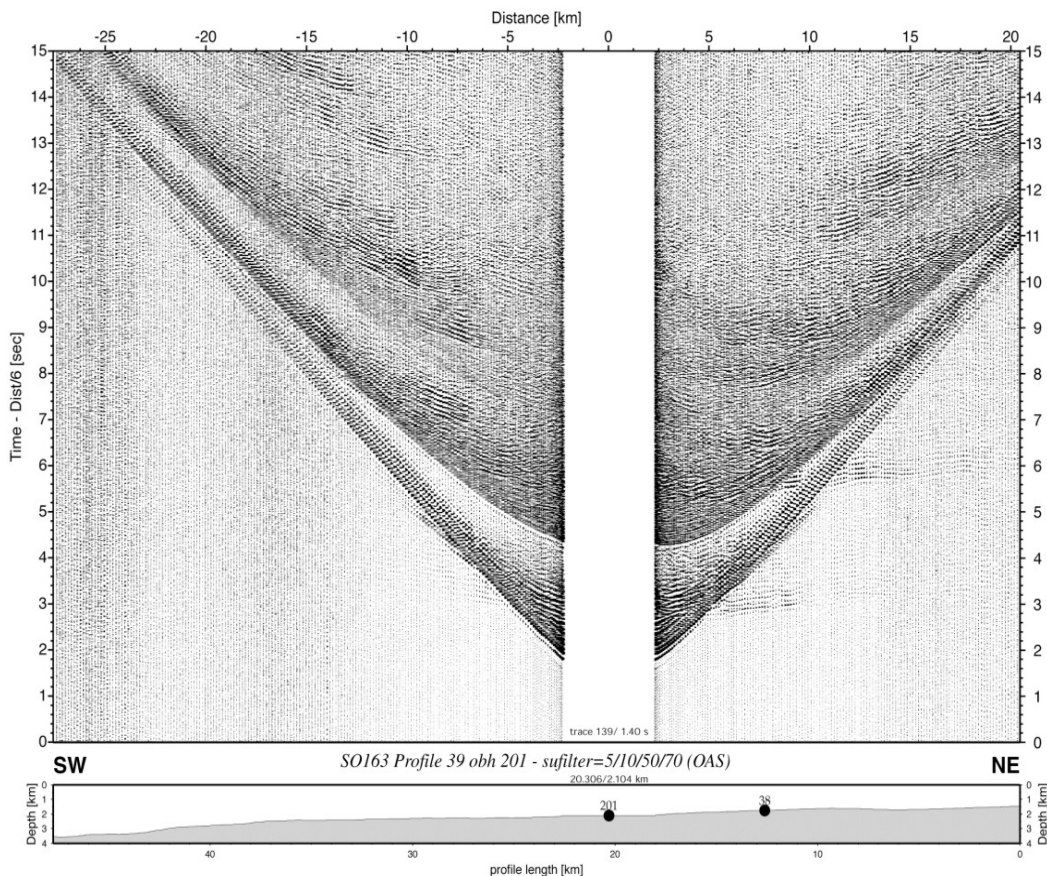


Figure 5.10.3.3: Hydrophone record section from obs 201 (OAS), Profile 39.

a) the occurrence of time slips (extra or missing samples) due to a mismatch of the desired and actual sample rates (see previous section for a more detailed discussion of time slips). The approach for correcting time slips differs from the approach used for the wide angle data because seismological analysis needs to refer back to the continuous data stream throughout. The occurrence time of all time slips is read out from the send2pas log file. The time slips before the beginning of the record are added up and applied as static shift to the start time of the record. For time slips during the record a sample is added (positive time slips) or removed (negative time slips) at the appropriate time. This procedure is only approximate (a correct treatment would require resampling of the whole record, fraught with its own difficulties), and in general the apparent time of a sample can be off by up to half a sample length due to this approximation. Relative times within the same record can be off by up to one sample length if the time span straddles a time slip.

b) the slow drift of the internal clock relative to GPS time. The system time is compared with GPS time at the beginning and end of the deployment, and a drift rate is inferred from the observed difference (skew). The time of each 25 hour record is corrected by applying the shift appropriate for the time 12.5 hours after the beginning of the record. The underlying assumption is that the system clock does indeed drift linearly, and that the drift over a 24 hour period is negligible, i.e. much less than one sample length, which was the case in this experiment. For some stations that ran out of power prematurely, no skew could be determined and therefore no drift correction carried out. Timing uncertainties for these stations accumulate at a rate 1.5-2 ms per day, starting with the first day of deployment.

A short-term-average versus long-term-average (STA/LTA) trigger algorithm is then applied to the data to find out seismic events. Trigger parameters like length of the short term (s) and long term (l) time windows, the mean removal window length (m), the trigger (t) and dettrigger ratio (d), minimum number of stations (S) and at least the time window length (M) in which trigger signals contribute to the same event must be found individually for each data set. From the first, smaller JACO network we found the following parameters to be convenient: $s = 0.5$ sec, $l = 60$ sec, $m = 500$ sec, $t = 2.8$, $d = 0.8$, $S = 3$, $M = 20$. The triggered events will be cut from the time-corrected data, and stored in subdirectories, one per event. The events will then be quality controlled again.

The SEGY traces in the event directories will be first converted into SAC, and then into SEISAN waveform format, which makes it possible to store all traces associated with an event in one file. After the conversion the data can be registered into the SEISAN database (Havskov and Ottemöller, 2001).

At least, P and when possible S phases will be picked and hypocenters preliminarily located with the program HYP, which employ an iterative solution to the nonlinear localisation problem (Lienert, 1994).

Description of the JACO and QUEPOS networks

A total of 23 ocean bottom instruments have been operated from April 28 until October 3, 2002 in a seismic network centered on Jaco Scarp. Another five OBH have been operated east of the network on Quepos Mound, which can be included into the Jaco Scarp network. The Quepos Mound stations had been recovered earlier in July 2002. The Jaco stations were recovered during RV Meteor cruise M54-3B in October 2002, and deployed in the Quepos network after retrieving the registered data (Figure 5.10.4.1 and Table 5.10.4.2). Contemporaneously with the ocean bottom deployment of the OBH, the Instituto Costarricense de Electricidad (ICE) together with GEOMAR and the University of Kiel are running a land based local earthquake network. The additional data from the land stations will be used for further constrain earthquake locations and should provide more data for focal mechanism analysis of events located nearby the marine ocean bottom array.

The Jaco Scarp region is a structural place where a seamount is subducting underneath the Caribbean Plate. As seen in the multibeam bathymetry, the subducting seamount produces an uplift of the upper part of the margin right beneath. Moreover, numerous recent fractures are cutting the Jaco uplift area at that place

Table 5.10.4.1: Station status of the JACO network, operated from April 28 to October 3, 2002.

Day of month	April		May		June							July							August			September			Oct.		Remarks						
	28	29	30	9	10	11	12	13	14	15	16	17	18	19	20	21	22	23	24	25	26	27	28	29	28	29		30	1	2	3		
Julian day		120	129	129	130	140	145	164	165	170	175	180	209	210	209	215	215	269	270	269	270	270	275	275	275	275	275	275	275	275	275	275	
OBH38	s	x	x	x	x	x	x	x	x	x	x	x	x	x	x	x	x	x	x	x	x	x	x	x	x	x	x	x	x	x	x	x	hydrophone, spiky
OBH39	s	-	-	-	-	-	-	-	-	-	-	-	-	-	-	-	-	-	-	-	-	-	-	-	-	-	-	-	-	-	-	-	DPG, clipped
OBH40	s	x	x	x	x	x	x	x	x	x	x	x	x	x	x	x	x	x	x	x	x	x	x	x	x	x	x	x	x	x	x	x	DPG, very noisy
OBH41	s	x	x	x	x	x	x	x	x	x	x	x	x	x	x	x	x	x	x	x	x	x	x	x	x	x	x	x	x	x	x	x	DPG, ok / spiky
OBH42	s	x	x	x	x	x	x	x	x	x	x	x	x	x	x	x	x	x	x	x	x	x	x	x	x	x	x	x	x	x	x	x	DPG, ok / noisy
OBH139																																	hydrophone, ok
OBH140																																	hydrophone, ok
OBH141																																	hydrophone, ok
OBH193																																	hydrophone, ok
OBH194																																	hydrophone, ok
OBH195																																	hydrophone, ok
OBH196																																	hydrophone, ok
OBH197																																	only hydrophone ok
OBH198																																	hydrophone, ok
OBH199																																	hydrophone, ok / noisy
OBH200																																	tiltmeter, ok
OBH201																																	bad hydrophone
OBH202																																	tiltmeter, malfunction
OBH203																																	only hydrophone ok, offset since July 30
OBH204																																	hydrophone, noisy
OBH205																																	hydrophone, ok
OBH206																																	hydrophone, ok
OBH207																																	hydrophone, offset since June 26
																																	only hydrophone, spiky, offset since June 17
																																	Hydrophone, ok / noisy

x operating
s deployment/recovery
- inaccurate recording, so that data cannot be used
blank not recording

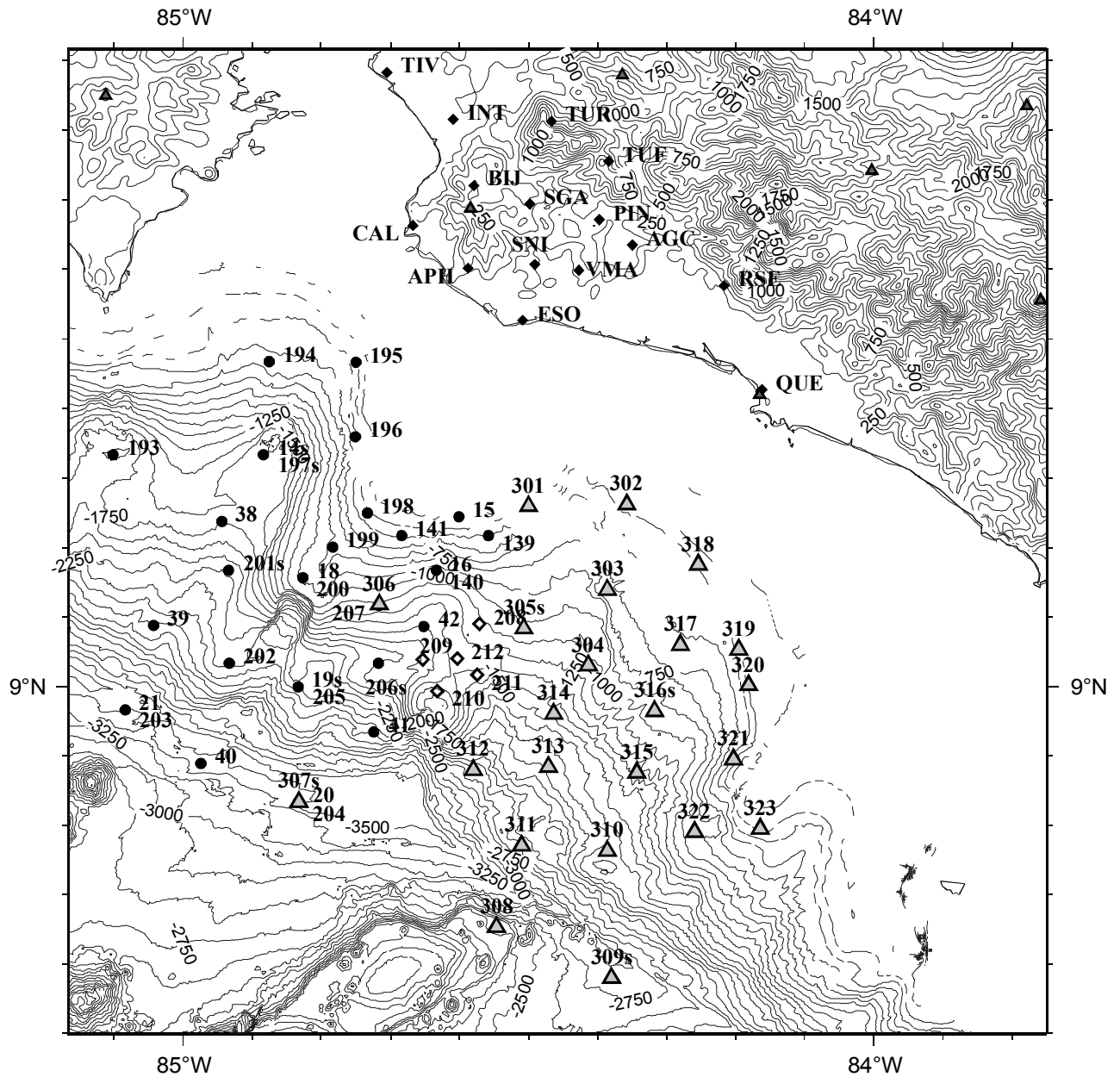
(Figure 5.10.4.2).

The main objectives of this passive seismological experiment is to detect and register the seismicity induced by the convergent dynamics between the subducting seamount and the Caribbean Plate. The spatial dimensions of the joined marine and land network are designed to register local tectonic events of the subducting plate.

Additionally two tiltmeters were operated in the JACO network at position 199 and 200, and have been redeployed in the QUEPOS net. Unfortunately only one instrument worked correctly. A data example is shown in Figure 5.10.4.3.

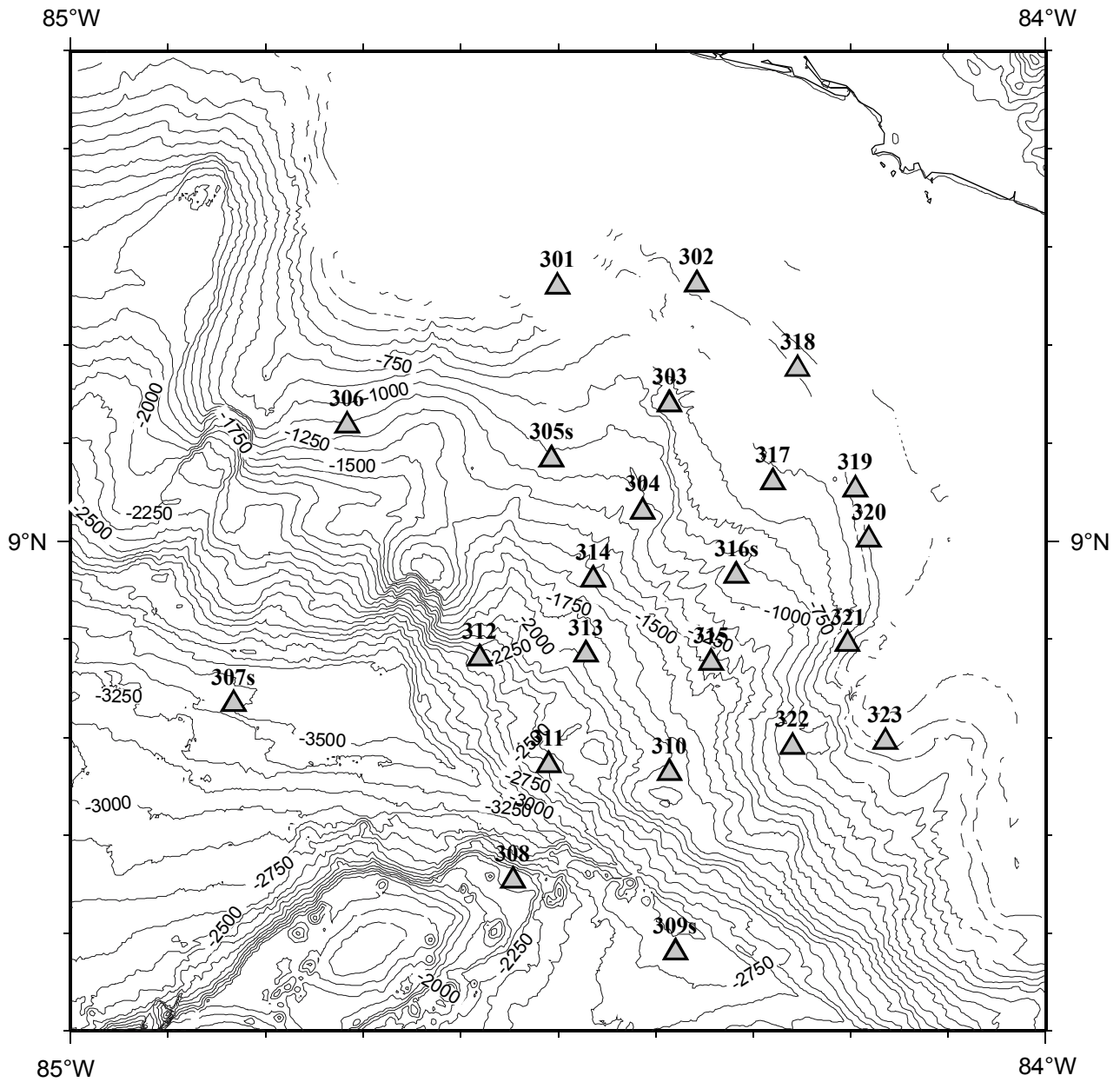
Table 5.10.4.2: The QUEPOS network ocean bottom stations.

Station	Latitude (N)	Longitude (W)	Depth (m)	
obh301	9 15.56	84 30.03	311	
obh302	9 15.71	84 21.48	326	
obh303	9 08.36	84 23.15	656	
obh304	9 01.81	84 24.81	1156	(ex obh101 Megalense)
obs305	9 05.01	84 30.40	1038	(ex obh64 Megalense)
obh306	9 07.06	84 42.99	1157	(ex obh207 JACO net)
obs307	8 50.03	84 49.96	3488	(ex obh204 JACO net)
obh308	8 39.20	84 32.78	2167	
obs309	8 34.80	84 22.79	2840	
obh310	8 45.81	84 23.16	1849	
obh311	8 46.26	84 30.60	2550	
obh312	8 52.81	84 34.81	2613	
obh313	8 53.05	84 28.29	1993	(ex obh59 Megalense)
obh314	8 57.66	84 27.84	1617	(ex obh104 Megalense)
obh315	8 52.55	84 20.60	1312	
obs316	8 57.88	84 19.04	909	(ex obh71 Megalense)
obh317	9 03.60	84 16.80	519	
obh318	9 10.53	84 15.27	354	(ex obs48 Megalense)
obh319	9 03.16	84 11.74	283	
obh320	9 00.08	84 10.89	220	
obh321	8 53.69	84 12.20	284	(ex obh75 Megalense)
obh322	8 47.41	84 15.60	796	
obh323	8 47.72	84 09.89	206	



- ▲ permanent CRSN land stations
- ◆ JACO land stations
- JACO ocean net (recovered)
- ◇ QUEPOS MOUND subnet (recovered)
- △ QUEPOS ocean net

Figure 5.10.4.1: The combined land and seafloor seismic network of the JACO and QUEPOS area. The land stations have been installed in April 2002. The JACO ocean bottom instruments have been deployed during RV Sonne cruise SO 163-1 and SO 163-2. The QUEPOS ocean bottom stations have been setup during RV Meteor cruise M54-3B. The land network was moved from the Jaco area to Quepos in October 2002.



△ QUEPOS ocean network

Figure 5.10.4.2: The QUEPOS ocean bottom network, consisting of 23 OBH and OBS stations.

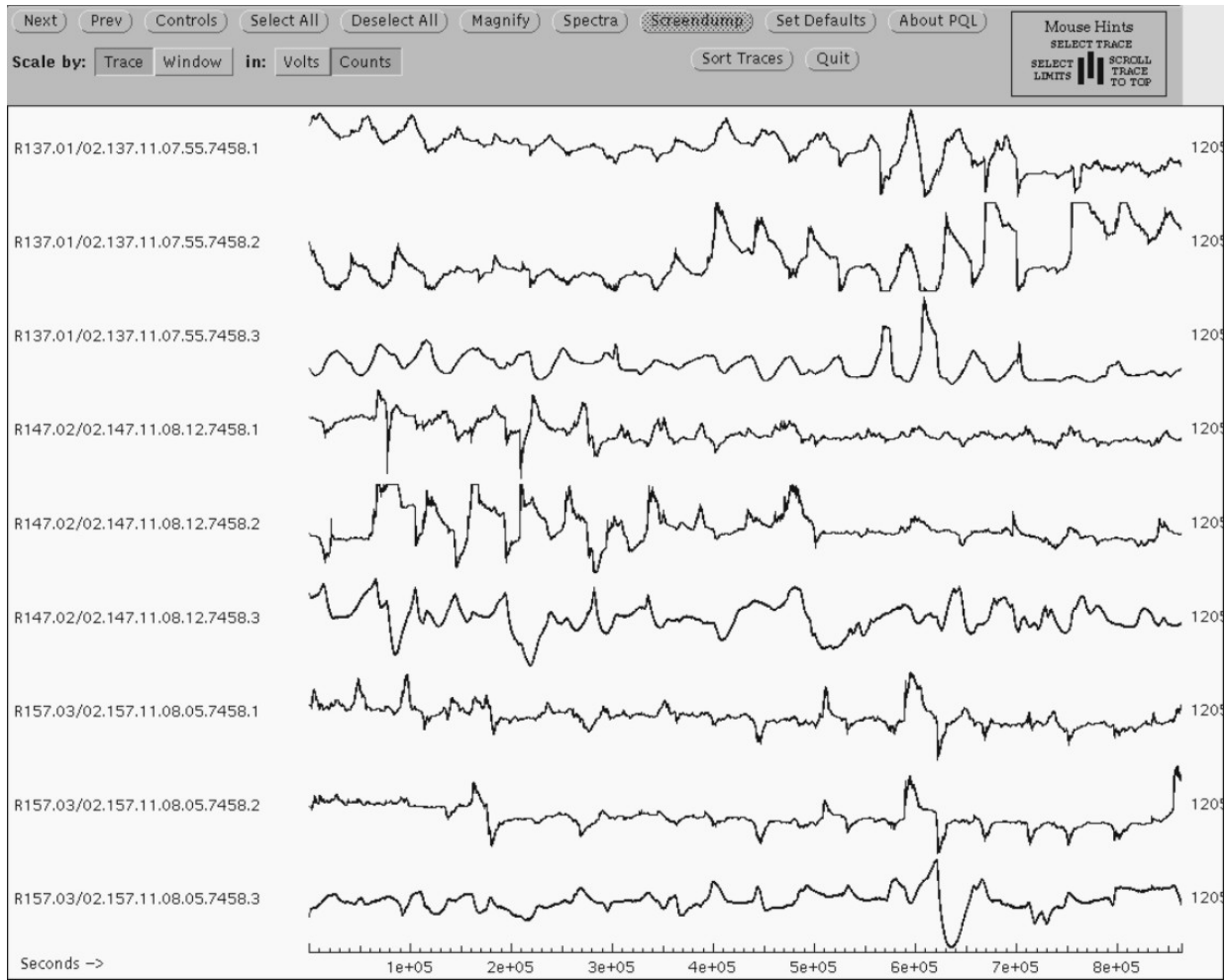


Figure 5.10.4.3: Data example of the tiltmeter station obt199 of the JACO network. A time period of 30 days is presented starting on May 17, 2002. The tiltmeter signal is shown on traces #1. The other traces show other parameters like temperature.

5.2 Heat flow studies

(I. Grevemeyer, N. Kaul, H.-H. Gennerich, B. Heesemann, M. Heesemann, M. Müller, J. Schneider)

The Earth's heat loss or heat flow is an important parameter to reveal geodynamic processes occurring in the Earth's interior and to characterize shallow fluid flow. Heat flow, however, is not measured directly, but calculated from the geothermal gradient dT/dz and the thermal conductivity k of near-surface material. Two different techniques have been used to derive the in situ thermal gradient offshore Costa Rica and Nicaragua: (i) Lister-type heat probes of the violin-bow design (Lister 1979; Hyndman et al. 1979), and (ii) outriggers mounted on the core barrel of a gravity corer.

Two different Lister probes were used (see Appendix for details). A 3m long probe, which has been successfully used over the last 10 years by the Fachgebiet Meerestechnik und Sensorik of Bremen University (e.g., Grevemeyer et al., 1999; Kaul et al., 2000; Villinger et al., 2002) and a new 6m long probe, which was deployed the first time. The instruments measure the temperature gradient with 11 and 22 termistors, respectively. The termistors are mounted in a lance that penetrates into the sedimented seabed. After penetration a pulse of fractional heating and its decay is recorded while the probe remains for 7-10 minutes in the seafloor. Generally, equilibrium temperatures were reached within this time interval. However, they can also be calculated by extrapolating the decay of the fractional heating pulse. Data from individual termistors were monitored in real time using the ship's coaxial cable connecting the probe with a computer on the vessel. Additionally, all data were stored on harddisk in the heat probes. Measurements with the Lister probes were carried out in the so called pogo style, performing several penetrations in a row at small distances and hence providing densely spaced heat flow measurements. On regional transects the spacing was 1000 m, while on some profiles investigating shallow fluid flow the separation of individual penetrations was only 50 m.

In addition to measurements along heat flow profiles, some geothermal gradients were obtained during gravity coring (Tab. 5.2.0.1). So called Miniature Temperature data Logger (MTL) were mounted as outriggers on gravity corers. The MTLs were developed in the Fachgebiet Meerestechnik und Sensorik of Bremen University. A detailed description is given elsewhere (Pfender and Villinger, 2002). To measure the gradient, the gravity corer has to remain for 7 minutes in the seabed. Like for the measurements with the Lister probes, the decay of the fractional heating pulse has been inverted to obtain equilibrium in situ temperatures.

The thermal conductivity can either be measured in situ at the location of temperature measurements or by subsequent measurements on material recovered from the seabed, generally provided by gravity or piston

Table 5.2.0.1: Geothermal gradients derived from outriggers attached to gravity corers.

Station number	Heat flow station number	geothermal gradient [°C/km]
M54/2	HF01	28.0
M54/6	HF03	14.7
M54/11	HF07	-
M54/21	HF10	-
M54/22	HF11	47.7
M54/23	HF12	38.6
M54/24	HF13	28.7
M54/27	HF15	-
M54/39	HF21	-
M54/56	HF26	216.0
M54/57	HF27	531.0
M54/78	HF33	67.1
M54/80	HF34	61.2
M54/109	HF40	-

Table 5.2.0.2: Summary of thermal conductivity measurements on core material.

Station	Depth [cm]	N	mean k [W/mK]	std k [W/mK]
M54/1	3.5-466.5	25	0.88	0.10
M54/2	1.0-702.5	40	0.76	0.05
M54/6	23.0- 416.0	24	0.72	0.05
M54/11-2	4.0-440.0	25	0.74	0.04
M54/13	3.0-344.5	20	0.79	0.05
M54/14	0.0-965.0	50	0.73	0.05
M54/17	204-767.5	30	0.80	0.06
M54/18	4.5-532.0	30	0.82	0.08
M54/21	3.5-463.0	25	0.83	0.06
M54/21	core catcher	5	0.89	0.17
M54/24	65-495.0	10	0.78	0.06
M54/32	17.0-553.0	30	0.83	0.10
M54/35	5.5-748.0	40	0.83	0.10
M54/41-1	20.0-160.0	5	0.79	0.02
M54/48	15.0-244.0	15	0.88	0.08
M54/56	4.0-571.0	30	0.87	0.11
M54/57	13.5-709.0	40	0.82	0.09
M54/61	3.5	25	0.87	0.10
M54/62-2	52.0-270.0	15	0.89	0.11
M54/78	4.0-562.0	30	0.84	0.08
M54/80	10.0-850.0	50	0.84	0.06
M54-109	9.0-230.0	13	0.90	0.09

cores. In situ measurements were obtained with the Lister probes (Lister 1979; Hyndman et al. 1979) by monitoring and inverting the decay of a calibrated heat pulse fired at every second to third penetration. A similar technique is used to yield the thermal conductivity from the sediments samples using the needle probe method (von Herzen & Maxwell 1959). 577 measurements were performed in the recovered sediments from the 21 gravity cores listed in table 5.2.0.2. The mean thermal conductivity of all measurements is 0.82 W/mK.

Heat flow was yielded from thermal gradients and thermal conductivity measurements using the approach described by Hartmann and Villinger (2002).

5.2.1 Smooth Cocos Plate Segment off Nicaragua and Northern Costa Rica

In the northern segment three regional transects were surveyed to reveal the regional thermal temperature field of the incoming oceanic plate and the thermal state of the subduction thrust fault, in which the risk of hazards from great subduction zone earthquakes is largest. The most northwestern transect near 11°N was called NIC1 (Fig. 5.2.1.1). Transect NIC2 was located to the northwest of Nicoya Peninsula, and transect CR1 was placed along the drill sites of Ocean Drilling Program (ODP) Legs 170 and 205, hence offshore Nicoya Peninsula. In addition, a detailed heat flow study of a mud dome immediately to the northwest of transect NIC2 investigates the advective heat transfer of the feature, which is believed to be related to fluid back flow out of the deep subduction zone.

Heat flow transect NIC1

Four heat flow stations have been surveyed along RV Ewing Line NIC80. Station HF04 (M54-7) and HF08 (M54-12) were located on the incoming plate, while stations HF02 (M54-4) and HF06 (M54-10) investigated the thermal state of the continental slope (see detailed map in Appendix D). Unfortunately, because of technical problems with the new 6m probe, data from station HF08 could not be downloaded. However, all

other stations provided data useful for geophysical interpretation. Interestingly, heat flow on the incoming plate is well below values expected from conductive cooling of 24 m.y. old lithosphere created at the East Pacific Rise to the west (Fig. 5.2.1.2). Thus, heat flow data support mining of heat by hydrothermal activity. However, values over the descending plate on the slope are consistent with conductive heat transfer out of the subducting plate, suggesting that as the plate is forced under the margin wedge the hydrothermal circulation system is turned off.

Heat flow transect NIC2

The second heat flow transect is co-located with line BGR99_39, northwest of Nicoya Peninsular. Only two stations have been obtained: HF18 (M54-34) on the incoming plate and HF14 (M54-26) on the slope (see detailed map in Appendix). Value seaward of the deformation front are scatter about the expected conductive heat flow out of the incoming oceanic lithosphere and agree quite well with a conductive heat transfer on the middle slope (Fig. 5.2.1.2). Further landward heat flow stations HF09 (M54-20) and HF16 (M54-33) surveyed Mound Culebra, a mud volcano or diapir. Here, values are somewhat higher than those expected from conductive cooling and therefore may indicate advective transport of heat.

Heat flow transect CR1

Heat flow stations HF22 (M54-42), HF19 (M54-37), and HF20 (M54-38) were carried out along seismic line BGR99_44, which is coincident with the Ocean Drilling Program (ODP) transect of ODP leg 170 and 205 offshore Nicoya Peninsular. Station HF22 covers the incoming plate and the lower slope and surveys the heat flow pattern across the drill sites of leg 205 (see detailed map in Appendix). Values are well below the expected conductive heat flow (Fig. 5.2.1.2). This trend is also evident further landward. All measurements, including data from Langseth and Silver (1996) support a common trend, suggesting that heat is removed by circulating fluids. Discharge sites, however, have not been sampled.

Mound Culebra

Mound Culebra is an oval shaped (~1200 m SW-NE-oriented long axis, ~500 m NW-SE-oriented short axis), about 120 m high feature at 1500 m water depth on the continental slope northwest off Nicoya Peninsular. The mound is believed to be related to mud volcanism or diapirism, and hence perhaps to dewatering processes and fluid return flow out of the subduction zone. From CTD measurements and methane sampling in the water column it is well known that the mound is venting methane. Heat flow stations HF09 (M54-20) and HF16 (M54-33) (Fig. 5.2.1.3 and Fig. 5.2.1.4) as well as measurements with outriggers on gravity corers surveyed the heat flow pattern of the mound.

Away from the mound and on its flanks all measurements were successful. On the crest, however, the probe or the gravity corers were not always able to penetrate the seafloor, possibly related to massive carbonates outcropping on the seafloor. However, the data show a systematic trend along the survey line and increase from background values of ~36 mW/m² at approximately 2 km distance from the mound to ~40-50 mW/m² at the foot and steep slope. Surprisingly, heat flow on the mound and uppermost slope generally equals approximately background values (Fig. 5.2.1.4). The only exception is a single site on the top (M54/22 – HF11) where outriggers made successful measurements. Heat flow is well above the background flux suggesting that the anomaly might be caused by both conductive and advective effects. If the probe did not sample the vent site itself, the total heat flux from the vent could be even higher than the measured 41.5 mW/m². We believe that it might be reasonable to suggest that the high heat flow site is related to one of the locations where Mound Culebra is releasing methane into the bottom water.

5.2.2 Rough Plate Segment off Costa Rica

In the second segment, crust was not created at the East Pacific Rise to the west, but at the Cocos-Nazca spreading ridge to the south. Both spreading ridges run roughly perpendicular to each other. Thus, while

seafloor spreading anomalies and hence isochrons of crustal age run parallel to the continental margin offshore Nicaragua and northern Costa Rica, anomalies run normal to the strike offshore southern Costa Rica. In addition, except for heat flow transect CR2 offshore Nicoya Peninsular, the seafloor is dominated by seamounts and aseismic ridges (Fig. 5.2.1.1), which have been formed by the Galapagos hotspots millions of years ago.

Three regional transects survey the region where the hotspot features enter the subduction zone. Detailed surveys has been performed to study the thermal state and hydrogeological system of the incoming plate. Stations on the incoming plate are supplemented by profiles on the slope to reveal thermal properties in the seismogenic zone. Additionally, potential sites of fluid back flow were sampled by high resolution heat flow surveys.

Heat flow transect CR2

Heat flow transect CR2 is to the southeast of the plate boundary separating crust created at the Cocos-Nazca-spreading-ridge and at the East Pacific Rise (Barckhausen et al., 2001), but still on relatively smooth terrain. Station HF23 (M54-43) sampled a too high heat flow on the incoming plate (see detailed map in Appendix D), while station HF43 (M54-113) on the slope has values lower than those expected by conductive heat transfer out of a descending plate (Fig. 5.2.1.2). However, in between both stations data collected previously (Silver, personal communication) are in agreement with a conductive model.

Heat flow transects CR3, CR4 and CR5

Heat flow transect CR3 was located northward of Quepos Ridge and was composed of five stations, HF24 (M54-49), HF25 (M54-55), HF30 (M54-67), HF31 (M54-71), and HF32 (M54-77). Transect CR4 was between Quepos Ridge and Cocos Ridge. Transect CR5 was on the northwestern flank of Cocos Ridge. CR4 includes stations HF36 (M54-88) and HF37 (M54-95); CR5 includes stations HF38 (M54-101) and HF39 (M54-107). All transects were located on seismic lines shot during cruise SO81. Heat flow measurements on transects CR3, CR4 and CR5 were placed on seismic lines SO81p02, SO81p05 and SO81p18, respectively (see detailed map in Appendix D).

Along the transects similar heat flow pattern were detected (Fig. 5.2.2.1). Overall, heat flow is too low on the middle slope, but increase towards the deformation front. However, the highest heat flow anomaly is not detected at the deformation front, where offshore Costa Rica the decollement reaches the seafloor, but seaward on the incoming plate. On transect CR3 the highest values occur on the first fault block on the incoming plate; thus, may indicate fluid flow trough the permeable uppermost basement rather than along the decollement. However, high heat flow close to the deformation front (300-900 mW/m²) is interpreted to indicate advective heat transfer out of the subduction zone into the ocean.

Jaco-Scarp Area

The Jaco Scarp is related to the subduction of a seamount. The underthrusting of the seamount caused landsliding and fracturing on the margin wedge, which are clearly imaged by remote sensing techniques. Three stations were conducted in the Jaco Scarp area. Station HF28 (M54-59) and HF29 (M54-60) surveyed features on the top of a dome like feature above the seamount, while station HF41 (M54-111) was running across the Jaco Scarp itself, covering the steep slope; water depth ranges from ~2000 m to < 1000 m (Fig. 5.2.2.2). All stations were located on tow-tracks of the OFOS video system (see Appendix for details).

On the dome like feature little evidence for fluid flow was detected. Heat flow was generally close to 40 mW/m² (Fig. 5.2.2.3 and Fig. 5.2.2.4). A single penetration of HF28 yielded 20 mW/m², and may therefore indicate fluid recharge, though. However, station HF41 provided high heat flow values (180-200 mW/m²) between 1800-1700 m water depth (Fig. 5.2.2.5), suggesting that heat is transferred advectively. At the

same location, observations with OFOS and a prominent methane anomaly in the bottom water provided clear evidence for fluid venting.

Mound 11

The mound belongs to a chain of small mounds at water depths of approximately 1000 m offshore the Costa Rican town Quepos. A grid of heat flow penetrations (25 penetrations) was placed on the feature to reveal its 3D heat flow signature. Heat flow is generally between 44 and 62 mW/m². The lowest values occur to the east and northwest of the mound, while the highest values occur on the feature and immediately to its south (Fig. 5.2.2.6) and may indicate diffusive fluid discharge. However, the morphology of the structure suggests that at least episodically focused mud flow must occur. A gravity corer deployed on the feature in the high heat flow region sampled natural gas hydrates close to the seafloor.

Acknowledgements

The heat flow survey of the Fachgebiet Meerestechnik und Sensorik of Bremen University was funded by the Deutsche Forschungsgemeinschaft through Grant Vi 133/7-1.

References

- Barckhausen, U., C.R. Ranero, R. von Huene, S.C. Cande, and H.A. Roeser, Revised tectonic boundaries in the Cocos plate off Costa Rica: implications for the segmentation of the convergent margin and for plate tectonic models, *J. Geophys. Res.*, 106, 19207-19220, 2001
- Grevemeyer, I., N. Kaul, H. Villinger, and W. Weigel, 1999. Hydrothermal activity and the evolution of the seismic properties of upper oceanic crust. *J. Geophys. Res.*, 104, 5069-5079
- Hartmann, A. and H. Villinger 2002, Inversion of marine heat flow measurements by expansion of the temperature decay function, *Geophys. J. Int.*, 148, 628-636
- Hyndman, R.D., E.E. Davis, and J.A. Wright 1979, The measurement of marine geothermal heat flow by a multi-penetration probe with digital acoustic telemetry and in situ thermal conductivity, *Mar. Geophys. Res.*, 4, 181-205
- Kaul, N., A. Rosenberger, and H. Villinger 2000, Comparison of measured and BSR-derived heat flow values, Makran accretionary prism, Pakistan, *Mar. Geol.*, 164, 37-51
- Lister, C.R.B. 1979, The pulse probe method of conductivity measurements, *Geophys. J. R. astr. Soc.*, 57, 451-461
- Pfender, M. and H. Villinger 2002, Miniatrized data logger for deep sea sediment temperature measurements, *Mar. Geol.*, 186, 557-570
- Villinger, H., and E.E. Davis 1987, A new reduction algorithm for marine heat flow measurements, *J. Geophys. Res.*, 92, 12,846-12,856
- Villinger, H., I. Grevemeyer, N. Kaul, J. Hauschild, and M. Pfender 2002, Hydrothermal heat flux through aged oceanic crust: where does the heat escape?, *Earth Planet. Sci. Lett.*, 202, 159-170
- von Herzen, R., and M.E. Maxwell 1959, The measurement of thermal conductivity of deep sea sediments by a needle probe method, *J. geophys. Res.*, 64, 1557-1563

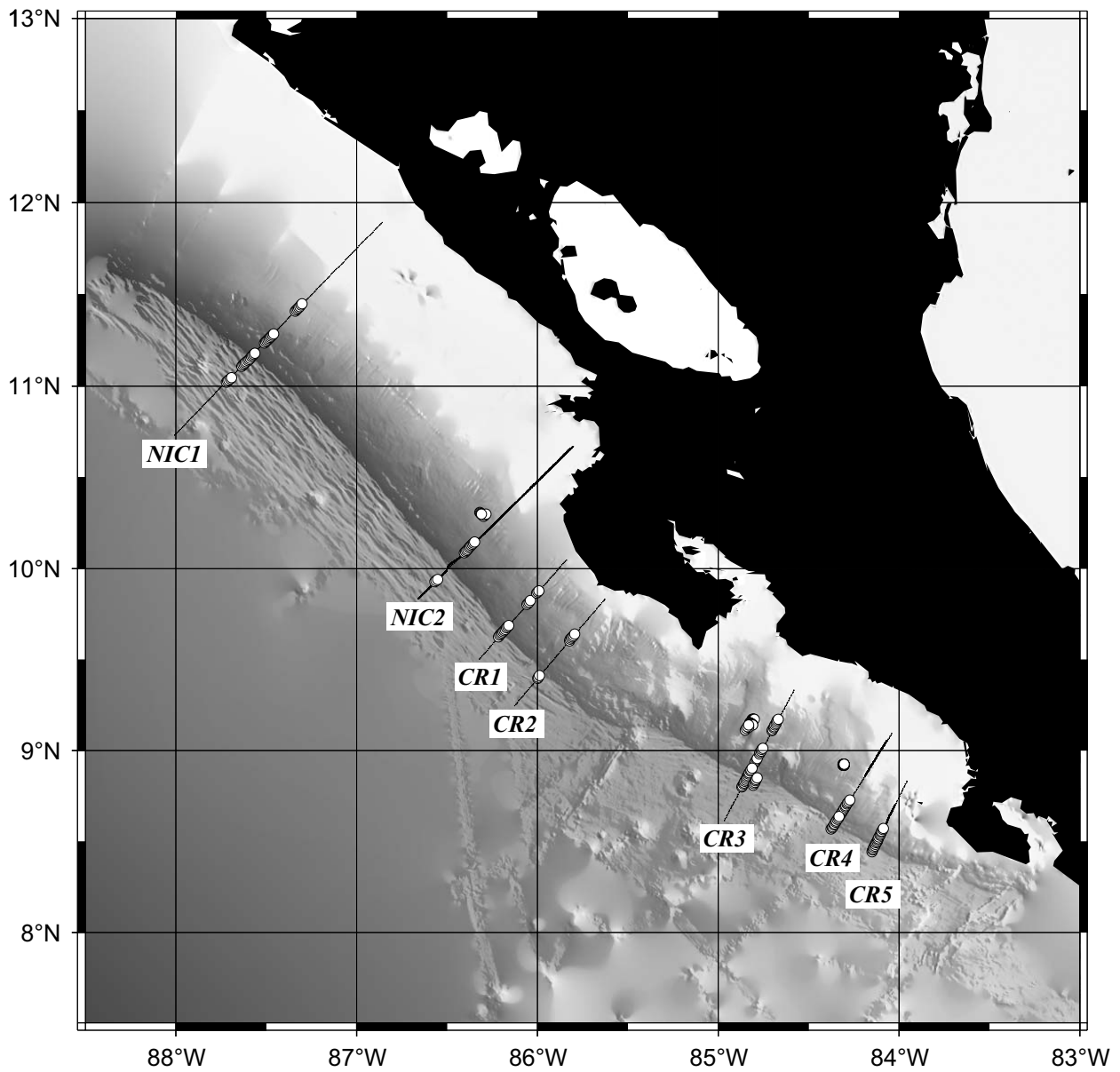


Figure 5.2.1.1: Location map of heat flow surveys conducted during M54-2.

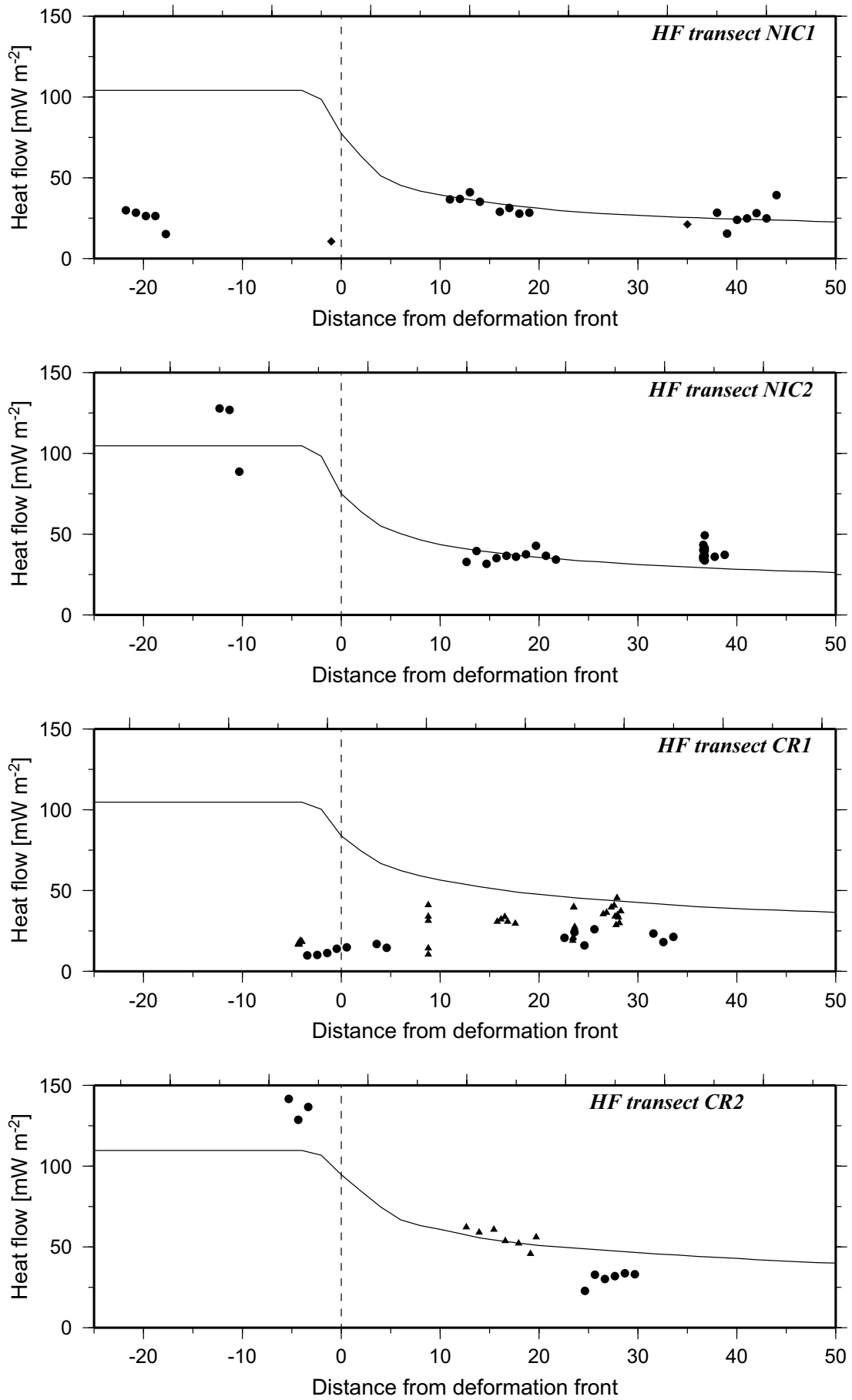


Figure 5.2.1.2: Heat flow anomaly as a function of distance along the transects on the ,smooth' Cocos plate segment.

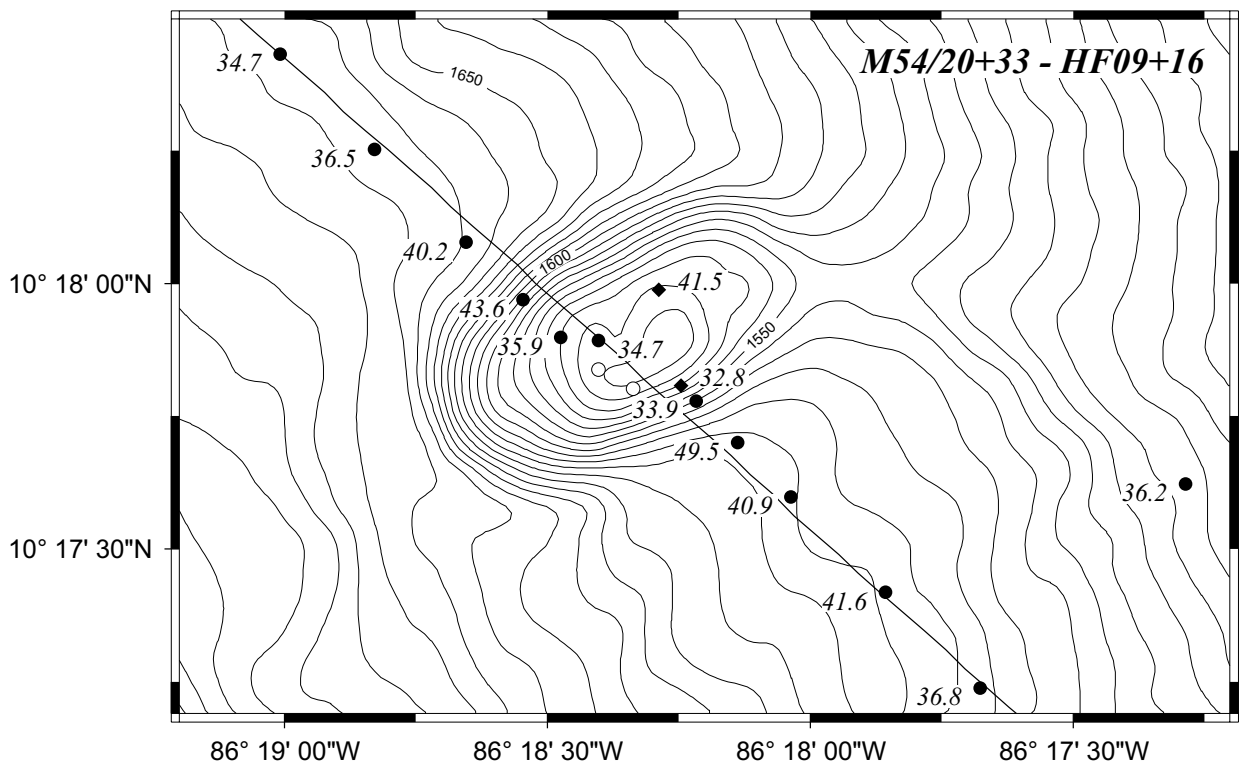


Figure 5.2.1.3: Heat flow transect (with heat flow in mW/m^2) across mud dome Mound Culebra.

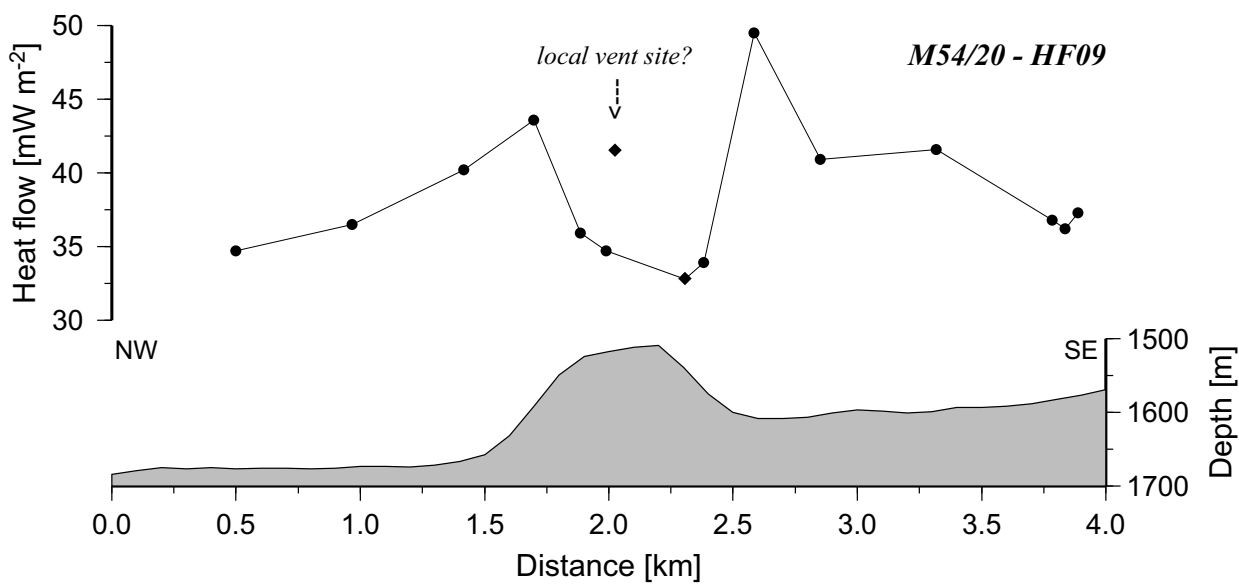


Figure 5.2.1.4: Heat flow anomaly as a function of distance across Mound Culebra.

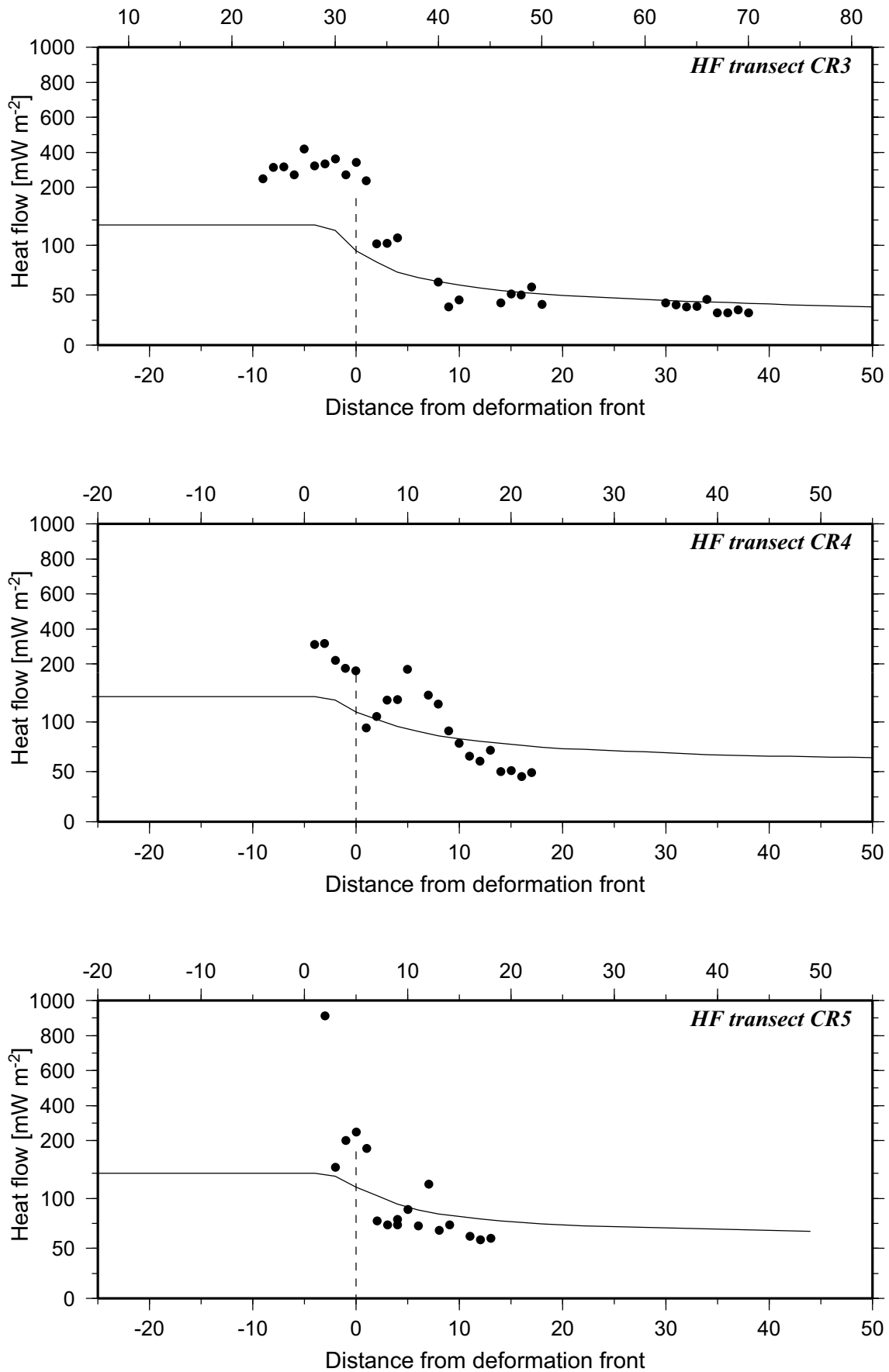


Figure 5.2.2.1: Heat flow anomaly as a function of distance along the transects on 'rough' plate segment offshore southern Costa Rica.

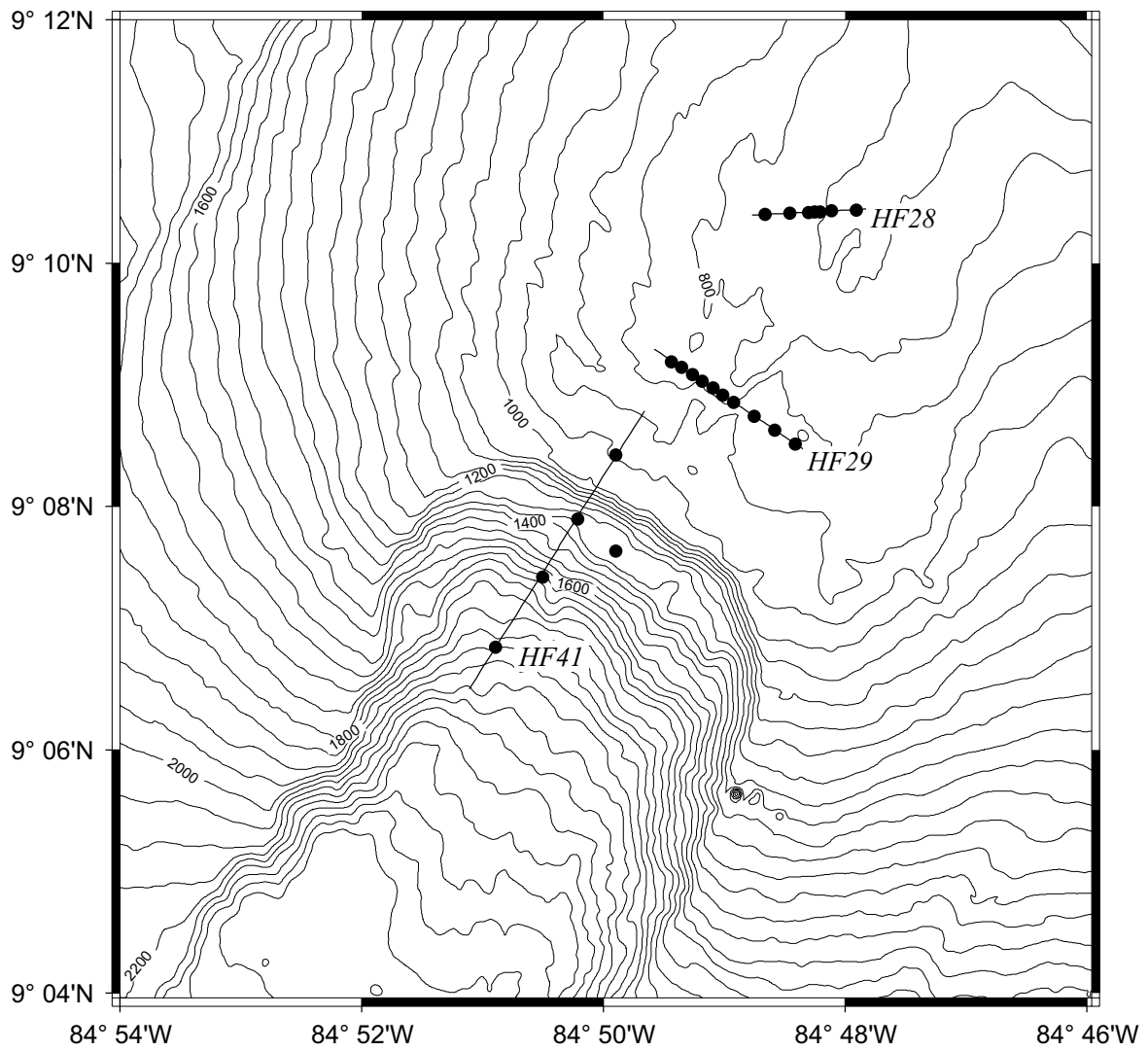


Figure 5.2.2.2: Heat flow stations in the Jaco Scarp area.

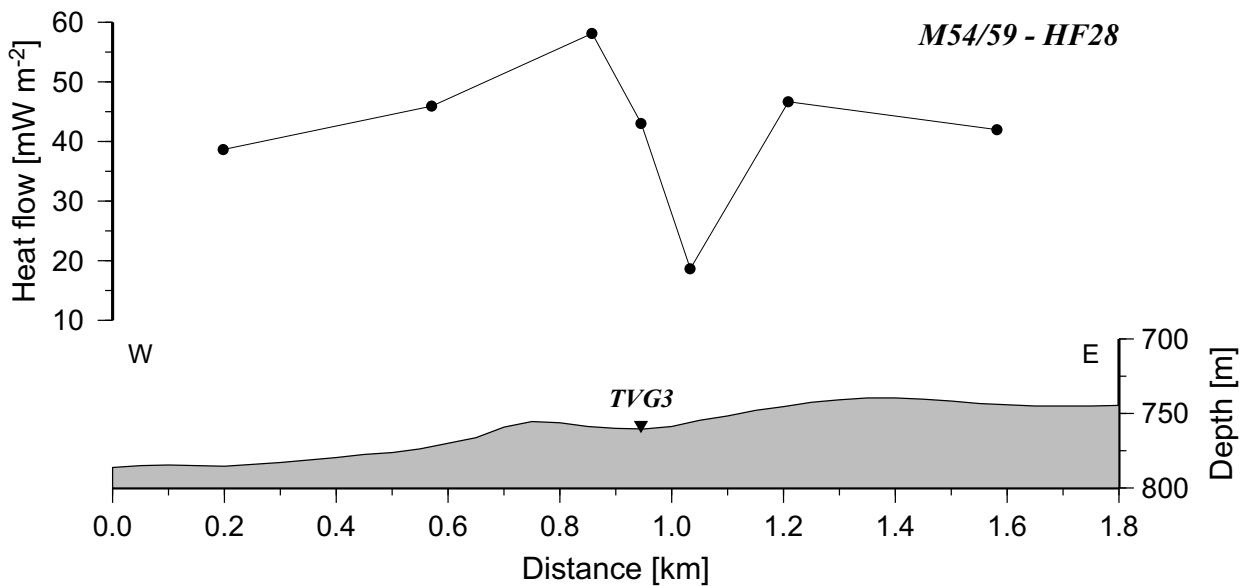


Figure 5.2.2.3: Heat flow anomaly along station M54/59-HF28.

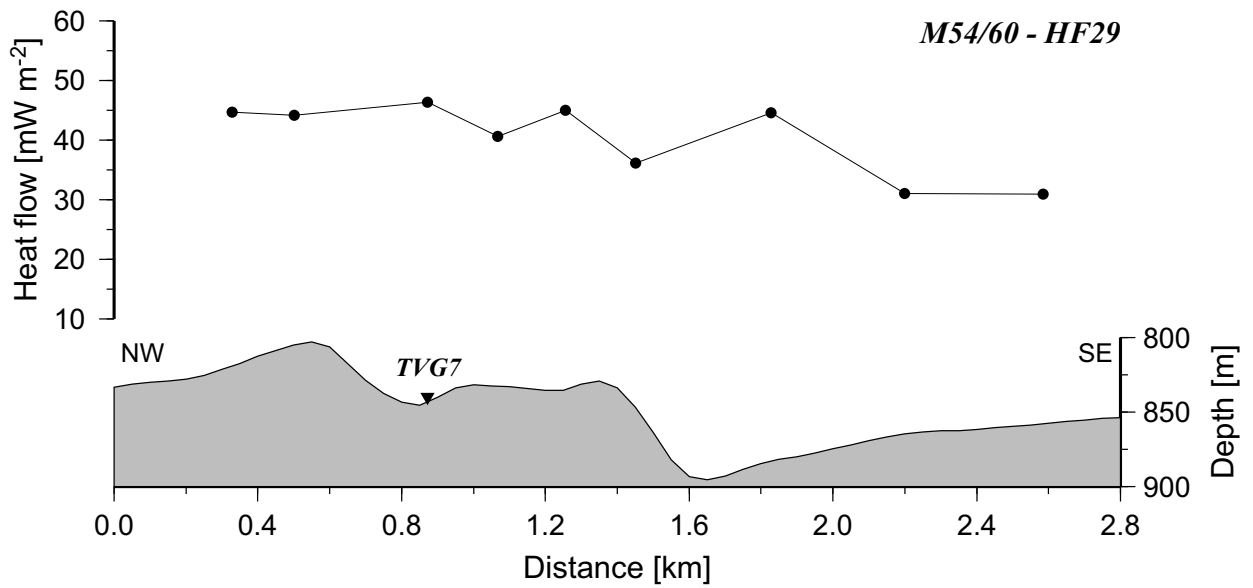


Figure 5.2.2.4: Heat flow anomaly along station M54/60-HF29.

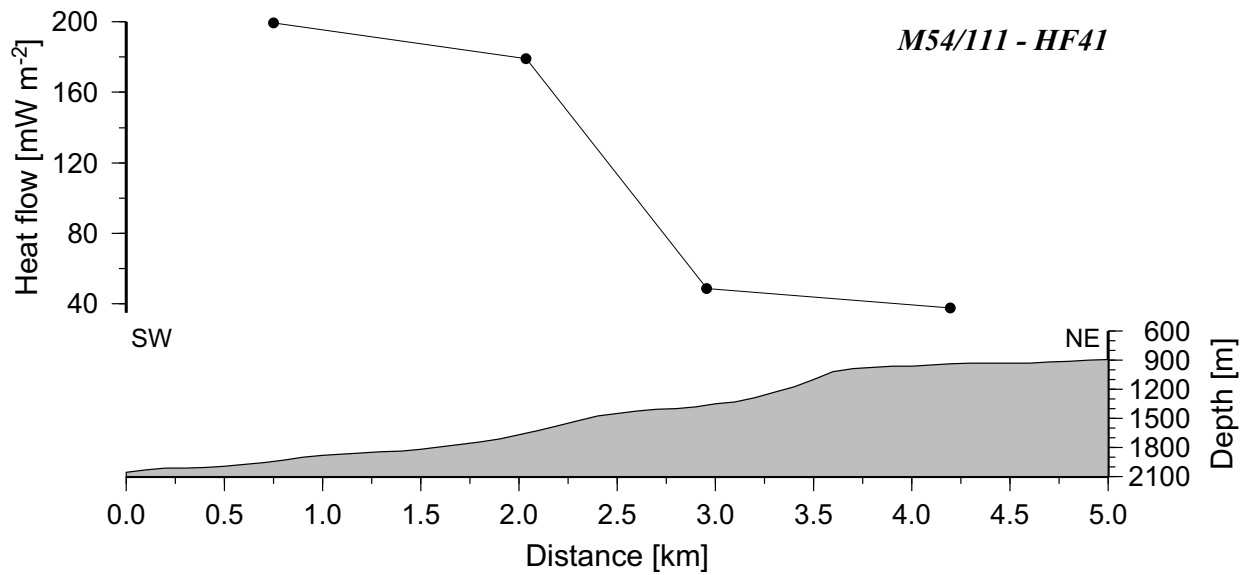


Figure 5.2.2.5: Heat flow anomaly along station M54/111-HF41 across the Jaco Scarp.

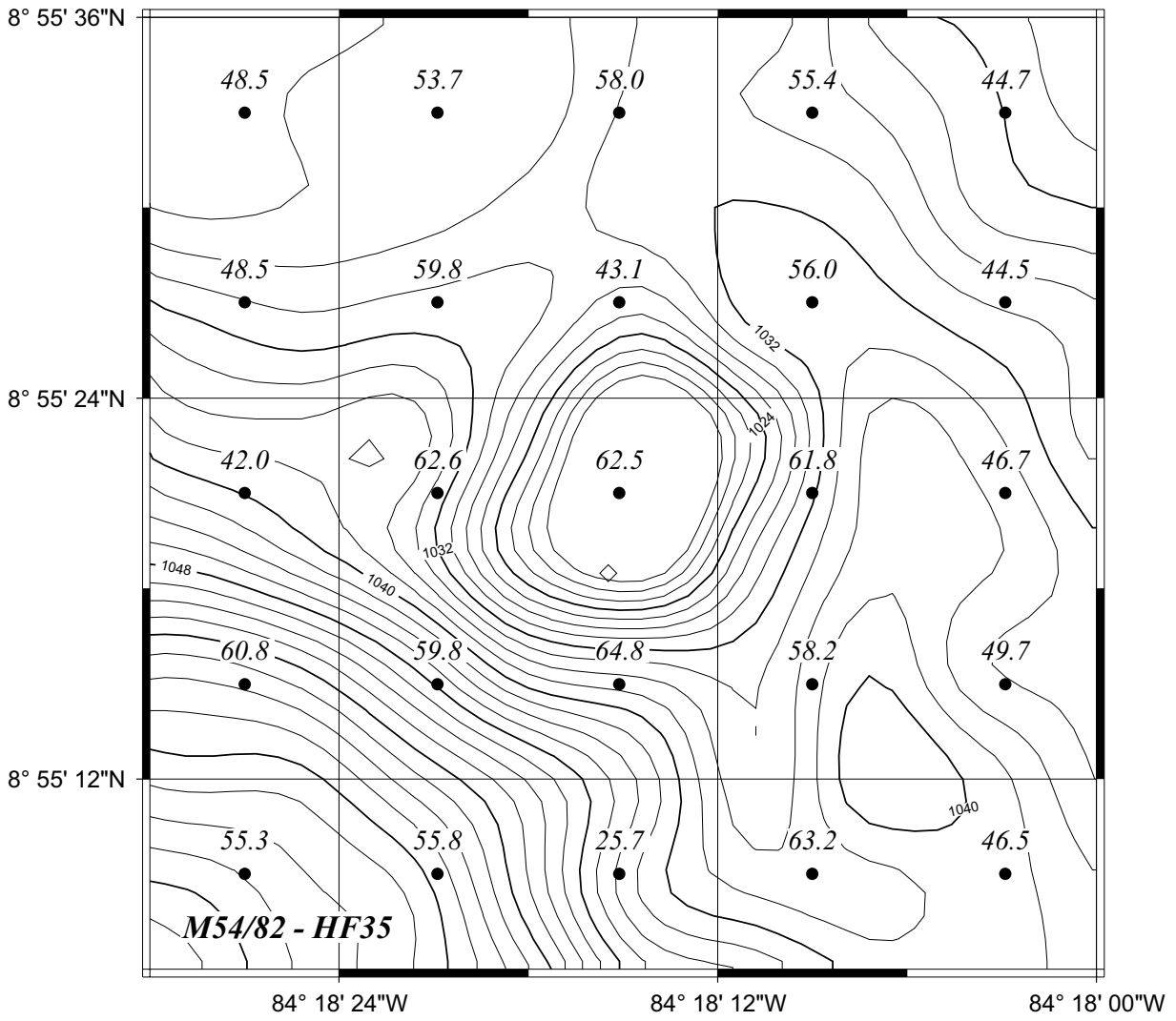


Figure 5.2.2.6: Heat flow survey (with heat flow in mW/m²) on the mud dome "Mound11".

5.3 Dredging at the Nicaraguan slope

(S. Kutterolf)

At station M54/5 we have tried to dredge some igneous rocks (basalts, gabbros) from scarp walls at the Nicaraguan slope. We started the dredge line at $11^{\circ}11.44/87^{\circ}21.24$ at the base of a deep scarp in the slope. The end of the dredge line on the top was at the position $11^{\circ}16.01/87^{\circ}16.16$. The water depth varies between 2947 m at the base and 1718 m at the top of the scarp. Through the dredging we only recovered clay-stones and carbonates. No igneous rocks have been found.

5.4 Sediment sampling and sedimentology

5.4.1 Sediment sampling and physical properties

(W. Brückmann, M. Schmidt, T. Mörz, S. Kreiter, A. Deyhle, A. Kopf)

5.4.1.1 Sampling techniques

65 sediment cores of 2 to 12 m (total length) were taken by box corer (BC) and a piston corer (PC) during M54 cruises in the Costa Rica and Nicaragua fore arc area. The box corer device was equipped with a 2 to weight attached to the top of a 3 to 18m steel tube surrounding an inner 3-18m PVC-tube. The piston corer was additionally equipped with a piston running in the PVC-tube upwards while the corer is running downwards during sediment penetration. Miniature Temperature Logger (MTL), measuring the in situ temperature of sediment during contact of the corer with the sea floor, were attached in specific intervals to the outer metal tube of the coring device.

As soon as cores arrived on deck, they were cut into approx. 1 m long segments after recovery and the segments were sampled at both ends for gas-geochemical investigations prior to cutting. The core segments were then stored in a 4°C cooled container until core logging was performed using a GEOTEK Multi Sensor Core Logger. Logged sediment cores were split into archive and work halves under nitrogen atmosphere and work halves were immediately sampled for further geochemical analyses. The archive halves were described by means of sedimentological characteristics based on Munsell Color Chart and ODP lithology classification. Photographs of 1 m sediment segments and close-up photographs of particular features were taken with a Nikon Coolpix 995. Colour scans of archive halves were made with a Minolta Colorscanning System.

In order to assess the geotechnical properties of sediments from locations off Costa Rica and Nicaragua the undrained shear strength „cu“ was determined in three different experiments. The undrained shear strength determines such processes as sliding and slope failure.

Two different vane shear and one falling cone measurements were conducted, to minimize the limitations of a single test. The tests were carried out in the undisturbed parts of the working halves, after the geochemistry-samples had been obtained.

Vane tests

The vanes were lowered cautiously into the sediment until the top of the vane and the sediment were at the same level. The vanes were rotated with 30°/min while the torque was continuously registered. After reaching the peak-value the experiment was terminated. From the peak value the undrained shear strength was calculated assuming a simultaneous failure on a cylindrical surface without a top-face, according to the equation:

$$cu = \tau_{\max} = \frac{T_{\max}}{\pi r^3 \left(2 \frac{h}{r} + \frac{2}{3} \right)}$$

where cu is the undrained shear strength, τ_{\max} is the maximum shear stress on the cylinder, Tmax is the maximum torque, r is the radius and h the height of the vane used.

The vane-shear tester from Pero was used with a vane of 4 cm height and 1 cm radius. The vane used with the Haake Rotoviskosimeter RV20 had a height of 0.8 cm and a radius of 0.5 cm. The difference between them the both is the measurement range and accuracy. While the Pero tester can measure materials with high shear strength the Haake Rotoviskosimeter is limited to a cu of 30 kPa with a better resolution.

Fall-cone Test

The fall-cone test were conducted with a „Strassentest“ Kegelfallpenetrometer (fall cone tester). The cone

has an angle of 60 ° and a mass of 85 g. The cone was lowered carefully to the surface of the sediment and then fell free for five seconds until no further movement could be expected. Finally the depth of penetration was measured with a dial gauge. The undrained shear strength was determined with the equation of Hansbo (1957) with the coefficients from Houlsby (1982):

$$c_u = \frac{k \times M}{h^2}$$

where k is an empirical Factor determined by the cone angle, M is the mass of the cone and h is the penetration of the cone.

The advantage of this method is that only a small sample volume is required so that differences in adjacent regions of one core can be measured. The experiment is considerably faster but the results have a slightly greater scatter. All the results are plotted together with the core logs.

In addition to box and piston coring activities, surface sediment (0—80cm) was sampled by 9 multicorer (MUC) stations. The MUC was equipped with eight sampling tubes of 80 cm length. The soft and muddy sediment was directly sampled after arrival on deck in 1 cm intervals for further investigations (see chapter: Geochemistry and Micropaleontology).

Furthermore, one dredge station located near the deep sea trench in the Nicaragua fore arc area was performed with a “chain sack” dredge (DR).

5.4.1.2 Mounds

A large number of mounds were discovered during earlier cruises to the Costa Rica margin, especially during the SO144 and SO163 SONNE cruises nearly 30 of these features were mapped. They occur over a wide range of water depths, they are commonly circular in shape and up to a mile in diameter. Their structure and geological setting are described elsewhere (chapter 3. of this cruise report). During cruises M54/2 and M54/3a the largest of these features, Mound Culebra, Mound Quepos and unnamed mounds #10, #11#, and 12 were sampled with densely spaced gravity and piston cores. The results of the geological sampling are summarized here, a detailed description of structural, sedimentological, and stratigraphic features is given in Appendix E+F.

Mound Culebra

ME54-17 (10°17.57'N 86°18.57'W, 1673mbs)

Recovery of 200-770cm sediment from SW-slope of Mound Culebra, mainly consisting of silty to sandy clay. Some altered volcanic clasts (serpentinites, chloritoides, zeolites) were identified by smear slides below 376cm sediment depth. Scaly clay was found in the core catcher.

ME54-18 (10°17.92'N, 86°18.47'W, 1551mbs)

540cm sediment was recovered at western rim of the top of Mound Culebra. The upper part consists of consolidated scaly clay and the lower part of clay. The clayey part is filled by fluid channels consisting of fluidized sandy (volcanic clasts) clay.

ME54-21 (10°17.91'N, 86°18.48'W, 1548mbs)

470cm of consolidated clay and scaly clay filled with fluid channels and fluid pores filled with sandy (volcanic clasts) clay and water. Station was located near ME54-18.

ME54-22 (10°17.99'N, 86°18.29'W, 1532mbs)

Northern rim of top of Mound Culebra. 465cm of consolidated and scaly clay. Few carbonate clasts (1-3mm) and no appearance of fluid channels.

ME54-23 (10°17.81'N, 86°18.25'W, 1530mbs)

Consolidated and scaly clay (0-240cm) was found at the SW-rim from top of Mound Culebra. Some small (1-3mm) carbonate clasts and one approx. 8cm carbonate concretion were found.

ME54-24 (10°17.67'N, 86°18.32'W, 1615mbs)

The southern slope of Mound Culebra at station ME54-24 consist of clayey sand with altered volcanic clasts within the first 120cm. Underlying sediment composition down to 540cm consists of consolidated and scaly clay.

ME54-27 (10°17.86'N, 86°18.37'W, 1530mbs)

Only 35cm of bioturbated sediment could be recovered from the top of Mound Culebra at station ME54-27. Calyptogena shell fragments, fluid channels and carbonate concretions mixed with silty clay (exchanged to scaly clay towards greater depth).

ME54-29 (10°17.87'N, 86°18.37'W, 1529mbs)

Mainly sandy clay (0-176cm) is mixed with clay lenses, carbonate clasts and fluid channels at station ME54-29 located on top of Mound Culebra.

ME54-32 (10°18.06'N, 86°18.55'W, 1656mbs)

The upper 200cm of sediment at station ME54-32 (NW-slope of Mound Culebra) consist of sandy clay, which exchange to consolidated clay down to 540cm. Volcanic clasts of mm-size and reworked volcanic ash layers were found in the sediment.

ME54-133-GC (10°18.34'N, 86°18.85'W, 1682mbs)

Due to coring difficulties only the interval from 275 to 838cm was cored. The dominant lithology is olive green calcareous clay with with lenses and layers of greenish black sandy silt throughout the recovered interval. A strong H₂S smell was noticed at the bottom of the core.

Mound 10

ME54-133-GC (10°00.45'N, 86°11.47'W, 2298mbs)

400cm of sediment were sampled at Mound#10 with a dominant lithology of calcareous silty clay, with abundant carbonate concretions throughout the core. Strong H₂S smell was noticed, between 210 and 262cm and 288 and 340cm small gas bubbles were visible on the core surface.

Mound 11

ME54-100 (08°55.25'N, 84°18.24'W, 1044mbs)

Silty/sandy clay is mixed with clay/sand/carbonate mud lenses (chaotic structure) at station ME54-100 on the southern slope of Mound 11. The core recovery was 280cm.

ME54-102 (08°55.38'N, 84°18.31'W, 1039mbs)

The western slope of Mound 11 consists of silty and sandy clay within 0-280cm at station ME54-102. Carbonate mud, shell/shale fragments and carbonate concretions (<6cm) are abundant.

ME54-109 (08°55.31'N, 84°18.26'W, 1000mbs)

The sandy to silty clay matrix is filled with fluid channels between 60-124cm and covered with 60cm reworked (mixed) lenses of clay at station ME54-109 (top of Mound 11). Reworked carbonate mud and concretions are abundant between 124 and 216cm. Gas hydrate mixed with silty clay was found between 216 and 242cm.

ME54-164-GC (08°55.69'N, 84°18.82'W, 1022mbs)

300cm sediment was recovered 150m W of the top of Mound 11, primary lithology is green calcareous clay with abundant layers, nodules, and spots of fine greyish black ash below 150cm. At the bottom of the core strong H₂S smell was noticed.

Mound 12

ME54-84 (08°55.80'N, 84°18.61'W, 980mbs)

Stiff carbonate layers are intercalated with silty and sandy clay between 0 and 282cm. Carbonate chimneys of various size were found. The station is located at the southern slope of Mound 12.

ME54-89 (08°55.89'N, 84°18.69'W, 997mbs)

The core recovery from the NW-slope of Mound 12 was about 243cm. The silty clay is exchanged to consolidated (scaly) clay at 170cm down to 243cm. Carbonate concretions and carbonate mud layers are abundant throughout the whole sediment core.

ME54-90 (08°55.93'N, 84°18.55'W, 1009mbs)

NE-slope of Mound 12 was covered with 294cm of sandy clay at station ME54-90. The sandy clay is filled with small fluid channels at 108-177cm.

ME54-91 (08°55.77'N, 84°18.57'W, 1010mbs)

343cm of sandy and silty clay is mixed with some carbonate mud lenses and carbonate clasts. The station is located at the SE slope of Mound 12.

ME54-92 (08°55.88'N, 84°18.77'W, 1012mbs)

Silty clay (mainly carbonate mud) is filled with channel structures (bioturbation?) between 127 and 250cm. Black ash layers were found at 250-260cm. The core recovery was 268cm. The station is located at the western slope of Mound 12.

ME54-94 (08°55.81'N, 84°18.64'W, 994mbs)

362cm of silty and sandy clay (carbonate mud) was recovered at station ME54-94 from the southern slope (near top) of Mound 12. Carbonate concretions and shell fragments are abundant throughout the sediment core.

ME54-97-2 (08°55.90'N, 84°18.70'W, 1001mbs)

The sediment at station ME54-97-2 (NW slope of Mound 12) consist of silty clay exchanged with scaly clay at 285cm down to 383cm. Carbonate concretions, fluid pores and –channels are abundant. Gas content of the sediment was high (degassing bubbles on sediment surface after core splitting).

ME54-136-2GC (08°55.33'N, 84°18.25'W, 1023mbs)

Located near the top of Mound 12 this core's dominant lithology is light grey to dark green calcareous clay. Many horizontal to subhorizontal unfilled tubes were observed throughout the core.

ME54-140-GC (08°55.35'N, 84°18.24'W, 1018mbs)

This core recovered 190cm of calcareous silty clay at the top of Mound 12 with frequent carbonate pebbles and few carbonate cm-sized concretions.

ME54-143-GC (08°55.33'N, 84°18.26'W, 1021mbs)

This core recovered 157cm of dark green calcareous clay from the top of Mound 12. Indirect evidence, such as an interval with soupy sediment interval from 119 to 126cm and aragonitic crusts, points to the occurrence of a thin gas hydrate layer over this interval. Between 80 and 100cm light gray, micritic carbonate nodules were observed.

ME54-155-GC (08°55.33'N, 84°18.25'W, 1018mbs)

The core recovered 174cm of olive green calcareous clay at the top of Mound 12 with few cm-sized carbonate nodules and ash lenses. H₂O smell was observed throughout the core.

Mound Quepos

ME54-69-1 (09°01.97'N, 84°37.27'W, 1427mbs)

Core recovery from top of Mound Quepos was 111cm at station ME54-69-1. The sediment mainly consists of sandy clay and a few shell fragments and carbonate concretions.

ME54-73-2 (09°02.03'N, 84°37.24'W, 1450mbs)

Sediment (161-426cm) consisting of mainly silty clay was recovered from the northern slope of Mound Quepos at station ME54-73-2. The matrix is mixed with shell fragments, wood fragments, carbonate concretions and fluid pores.

ME54-74 (09°02.05'N, 84°37.31'W, 1445mbs)

Silty/sandy clay was recovered from NW-slope of Mound Quepos. Wood fragments were found in the sediment (130-397cm) and degassing occurred between 300 and 407cm.

ME54-75 (09°01.98'N, 84°37.24'W, 1430mbs)

The top of Mound Quepos at station ME54-75 consists of sandy/silty clay between 140 and 414cm. The matrix is mixed with shell fragments, wood and a few carbonate concretions.

ME54-78 (09°02.01'N, 84°37.25'W, 1447mbs)

561 cm sediment mainly consisting of silty/sandy clay was recovered from northern slope of Mound Quepos at station ME54-78. The matrix was mixed with wood, shell fragments and lenses filled with fluids and carbonate mud.

ME54-80 (09°02.04'N, 84°37.29'W, 1448mbs)

853cm (total core length) sediment was recovered from the NW-slope of Mound Quepos at station ME54-80. Degassing through core catcher was observed on deck (decomposing gas hydrates?). Strong H₂S odor was detected; pyrite needles were abundant in the whole core.

5.4.1.3. Slides and Scarps

Jaco Scarp was formed as an erosional feature following the subduction of a seamount on the oceanic plate that collided with the Costa Rica continental margin. The collision led to a circular uplift with faulting at the upper plate (dome). Seaward the process is associated with sedimentary landslides, leading to the formation of steep scarps. Several sea mounts can be seen in different stages of collision with the margin. This indicates that sea mount subduction is a continuing process that not only strongly modifies slope morphology and slope stability, but also moderates the overall devolatilisation and material recycling at the subduction zone.

Jaco Scarp

ME54-48-1 (09°10.41'N, 84°48.25'W, 761mbs)

Sediment NE of Jaco scarp consists of clayey sand exchanging to silty clay and consolidated clay from top to bottom at station ME54-48-1. The total core recovery was 260cm. Reworked black ash layers and porous lenses and tubes of carbonate are abundant.

ME54-48-2 (09°10.41'N, 84°48.25'W, 760mbs)

Consolidated and scaly clay was recovered at station ME54-48-2 (same position as station ME54-48-1!). The total core recovery was about 280cm. Carbonate and clayey clasts are abundant. Carbonate chimneys were found between 150 and 180cm. H₂S-odor was observed throughout the whole core.

ME54-56 (08°55.61'N, 84°58.01'W, 3535mbs)

590cm sediment could be recovered from the deep sea trench (SW of Jaco scarp) at station ME54-56. Mainly clay dominates the upper 4m of sediment. Up to 5 turbidites could be identified in the range of 400-590cm. This lower segment was also characterised by abundant black ash layers.

ME54-61 (09°10.46'N, 84°47.76'W, 744mbs)

Station ME54-61 is located NW of Jaco scarp. The sediment matrix consists of clayey sand and silty clay (474cm total core length). Pyrite, clay clasts and carbonate clasts could be identified in the whole core.

ME54-62-2 (09°09.02'N, 84°49.18'W, 825mbs)

Clayey sand changing to silty/sandy clay was determined in a 278cm sediment core recovered from NE of Jaco Scarp at station ME54-62-2. Carbonate clasts and fluid channels were found in the sediment.

ME54-63 (09°09.11'N, 84°49.28'W, 815mbs)

Mainly silty clay (324cm) was found at station ME54-63 NE of Jaco Scarp. The matrix is intercalated by a black ash layer (126-128cm) and a carbonate concretion (190-198cm).

ME54-64 (09°10.54'N, 84°48.27'W, 750mbs)

Coral fragments, altered glass, volcanic clasts, pyroxene, olivine, foraminifera, and carbonate clasts could be identified within the upper 86cm silty sand. Silty clay and clay is dominating the lower core segment down to 536cm. Pyrite needles are abundant between 86 and 536cm. The station ME54-65 is located NE of Jaco Scarp.

ME54-159-GC (09°07.20'N, 84°50.63'W, 1816mbs)

Only 58cm of olive green sands and gravel could be recovered from the Jaco Scarp slide mass.

Quepos Slide

ME54-105 (08°51.20'N, 84°13.01'W, 414mbs)

Clayey sand changing to scaly clay from 80cm down to 263cm depth (total core length). Shell fragments and carbonate clasts are abundant. High gas content was degassing bubbles in the sediment.

Mud Pie

ME54-48-1 (09°10.41'N, 84°48.25'W, 1938mbs)

The dominant lithology in this 200cm core is homogenous olive green calcareous clay with occasional silty clay. Several horizontal to subvertical unfilled tubes were observed, which are interpreted as worm burrows.

BGR Slide

ME54-171-GC (09°11.67'N, 84°39.81'W, 610mbs)

312cm of sediment was recovered close the head wall of the BGR slide, a 1 by 4km wide small scale slump feature near the Costa Rica shelf edge. The top 53cm of sediment consist of green calcareous clay with a sharp erosive contact at 54cm, presumably the base of the sliding plane, overlying well indurated dark green calcareous clays.

5.4.1.4. Slope profiles

Determining the contribution of sediment and volatiles from deep sea plain and continental slope/shelf to the subducted sediment is a major subject in the SFB 574. Three bathymetric profiles perpendicular to the Middle America Trench were sampled by sediment coring. The profiles are crossing different tectonic elements (A, B, and C in Fig. 5.4.1) providing different material inputs and different volatile/material reflux situations. Core locations have been selected at the deep sea plain, the trench, slope and shelf area. E.g. core locations and bathymetry of profile 1 (area A) are shown in Fig. 5.4.2. Brief descriptions of all “profile” sediment cores are given in this chapter. Detailed core descriptions (lithology, photography, core logging data) are shown in the appendix.

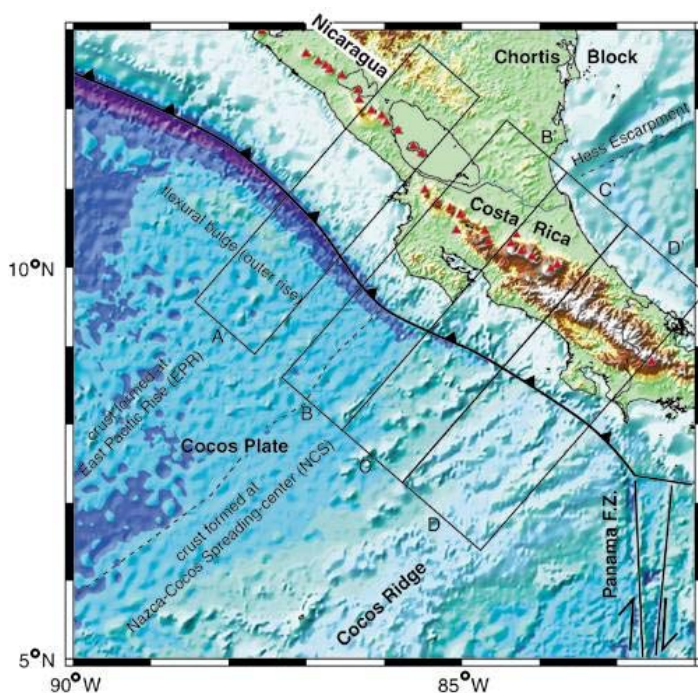


Figure 5.4.1: Geodynamic setting of Central America (Suess et al., 2000).

All cores have been sampled in detail for further investigations of pore water, sediment physical properties and sedimentology/geochemistry of solids (see Appendix D+E for tables).

Core descriptions :

Profile 1 (area A)

ME54-01 (11°28.91'N, 87°00.02'W, 148mbs)

Total core recovery was 500cm. The matrix mainly consists of sand and silt, and bioturbation was visible throughout the whole core. Shell and shell fragments were abundant between 50 and 500cm. The station ME54-01 is located on the Nicaragua shelf.

ME54-02 (11°20.11'N, 87°18.35'W, 1205mbs)

Station ME54-02 is located on the continental shelf of Nicaragua. The total core length is 734cm. Mainly silty clay is intercalated with numerous black and white ash layers in the whole core.

ME54-13 (11°20.12'N, 87°18.30'W, 1200mbs)

358cm of silty/sandy clay intercalated with black and white ash layers were recovered from the continental slope near Nicaragua at station ME54-13.

ME54-06 (11°07.01'N, 87°30.91'W, 5320mbs)

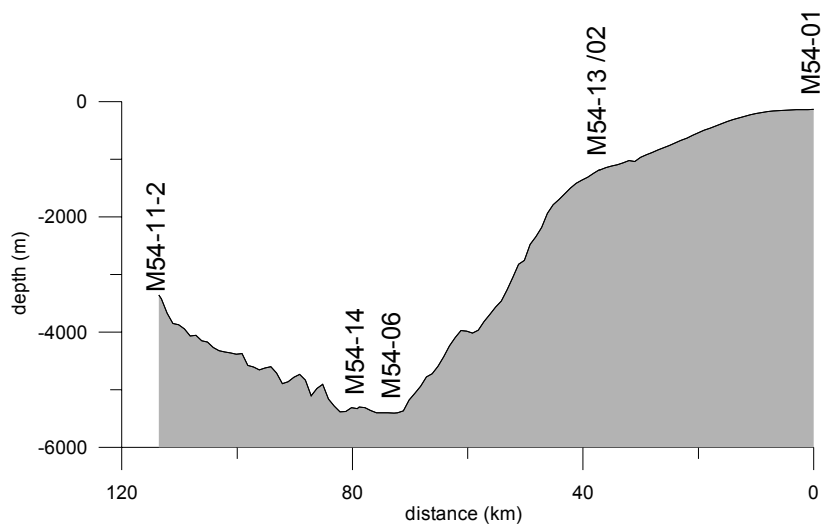


Figure 5.4.2: Bathymetry along Profile 1 from 11°06.03'N/ 87°49.82'W to 11°28.91'N/ 87°00.02'W. The positions of core stations are labeled.

436cm of sandy silt to clay were recovered from the deep sea trench near Nicaragua at station ME54-06. Reworked black ash lenses and turbidites could be identified.

ME54-14 (11°08.61'N, 87°34.00'W, 5412mbs)

Surface sediment from the deep sea trench near Nicaragua at station ME54-14 consists of silty clay changing to clay at about 3 m sediment depth. The clay matrix is mixed with turbidite sequences down to 970cm (total core length). Black ash layers (partially reworked) are abundant.

ME54-11-2 (11°06.03'N, 87°49.82'W, 3334mbs)

The sediment core (0-436cm) recovered from oceanic plate off Nicaragua mainly consists of silty

and sandy clay at station ME54-11-2. The matrix is intercalated with black and white ash layers (thickness up to 18cm).

Profile 2 (area B)

ME54-35 (09°41.20'N, 86°14.58'W, 4403mbs)

760cm of sediment could be recovered from the trench SW Nicoya Peninsula at station ME54-35. The upper 6m are mainly characterised by turbidite sequences. The lower part consists of clay and silty clay. Thin reworked ash layers could be found in the core.

ME54-36 (09°40.02'N, 86°11.02'W, 4183mbs)

Silty and sandy clay (0-572cm) was recovered from the trench SW Nicoya Peninsula at station ME54-36. Basalt and clay clasts (1-2mm) are abundant. Reworked ash and carbonate lenses were found.

ME54-40 (09°50.27'N, 85°44.07'W, 230mbs)

270cm of sediment was recovered from the shelf area SW Nicoya Peninsula. The matrix mainly consists of consolidated clay. Holes (cm-range) filled with shell fragments indicate strong bioturbation processes.

ME54-41-1 (09°48.99'N, 86°02.68'W, 2422mbs)

Station 54-41-1 is located on the continental slope of Costa Rica (SW Nicoya Peninsula). Total core recovery was about 560cm. Silty/sandy clay and consolidated clay is characterizing the slope sediment. Reworked black ash was found in the consolidated clay segment.

ME54-81-1 (09°09.20'N, 84°41.97'W, 931mbs)

Sandy and silty clay down to 626cm was recovered from the continental slope SW Nicoya Peninsula at station ME54-81-1. Carbonate mud layers, shell- and shale fragments are found in the sediment.

Profile 3 (area C)

ME54-57 (08°49.70'N, 84°51.21'W, 3462mbs)

732cm of silty clay and clay mixed with turbidite sequences were recovered from deep sea trench (SW of Quepos/Costa Rica) at station ME54-57. Reworked ash and carbonate clasts could be identified. Flame

structure at 415-433cm.

ME54-68 (09°24.71'N, 84°22.51'W, 54mbs)

Silty clay changing to clay at 200cm down to 568cm (total core length) was recovered from the shelf SW of Quepos/Costa Rica at station ME54-68. Pyrite needles, shell and shale fragments are abundant.

References:

Hansbo, S., 1957, A new approach to the determination of the shear strength of clay by the fall-cone test.: Proceedings of the Royal Swedish Geotechnical Institute, v. 14, p. 5-47.

Houlsby, G.T., 1982, Theoretical analysis of the fall cone test: Géotechnique, v. 32, p. 111-119.

Suess et al. 2000, "Volatiles and Fluids in Subduction Zones : Climate Feedback and Trigger Mechanisms for Natural Disasters." SFB 574-Proposal. Christian-Albrechts-Universität Kiel, 518 pages.

5.4.2 Ash Layers

(S. Kutterolf)

On RV METEOR cruise M54/2 ash-layers or ash remnants were found in most of the cores. In part they looked like primary ash-deposits from a volcanic eruption which reached a thickness of 1 to 14 cm; in part ash lenses and ripped-up clasts of older ash layers occurred.

A clear difference between the coring areas in front of Nicaragua and Costa Rica, was evident off Nicaragua a lot of primary mafic and felsic ash layers were found whereas off Costa Rica the majority of the volcanic material as reworked mafic ash lenses and ash layers.

Because of the good stratigraphic features and the good differently evolved ash layers in profile 1 at the Nicaraguan slope we will focus in the following part on the cores M54-2, M54-11-2, and M54-13. The cores M54-1, M54-6 and M54-14 contained no prominent ash layers, only reworked traces of ash layers. As you can see in Figure 5.4.2.1 cores M11-2, M2, M13 contain different ash layers in different depths. The cores are all situated in a different distances to the volcanic chain. The sedimentation rate decreases from the cores in the slope area to the cores near or on the opposite of the trench. With this information we will try to correlate between the cores. There are prominent ash layers in the upper and middle part of the sections, which can be correlated in all cores and are marked with closed lines. The more speculative correlations in the lower part of the sections are marked with dashed lines. The difference between the depths and the development of the ash layers in the different cores can be lead back to the different sedimentation rates and styles (grade of disturbance) at the slope and the decreasing mass of ashes in the increasing distance to the eruption centres.

This correlation could be confirmed by the petrographic analysis of some thin sections (e.g. Table 5.4.2.1). The mafic ash layers have a smaller amount of glas fragments which are seldom vesicular. Whereas the felsic ash layers have mostly a high content of glas fragments which can form very vesicular structures and elongated bubble remnants, although they differ in the types of crystals. Within the felsic ash layers it is possible to distinguish between the ashes due to their glas and crystal content, the content of pumice fragments and the type of crystals.

Table 5.4.2.1: *Petrographic features of different ash layers of the cores M54-2, M54-11-2 and M54-13. The coloured columns show possible correlations.*

	Size of glas fragments	Glas content %	Crystal content %	Mafic glas	Pumice fragments	fluidal structures in pumice fragments	Crystals: x = many y = abundant ? = few				
							Green hbl	Brown hbl	cpx	opx	ol
M11-2_59-62	middle	60-70	30-40		abundant	few	x	y	y	y	
M13_30-34	fine-middle	80-90	10-15	few	abundant	abundant	x	y	x	x	
M-2_238-244	middle	80-90	10-15	few	abundant	abundant	x	y	x	y	?
M13_41-46	fine	50-60	30-40	few	many	abundant	x	y	x		?
M11-2_83-86	middle-coarse	60-70	30-40		many	many	?		x	y	?
M11-2_234-242	coarse	90-95	5-10	few	abundant	few	x		y		
M13_238-240	fine-middle	70-80	20-30	abundant	abundant	abundant	x				
M2_295-300	fine-middle	60-70	20-30	few	many	abundant	x	y	x	y	
M11-2_311-230	fine-middle	70-80	20-30	few	many	abundant	x	y	x	y	
M13_283-286	middle	60-70	20-30		abundant	abundant	x		y		
M11-2_12-70	middle	20-30	10-20	-----	few	few	?		x	x	?

All the felsic ash layers contain amphiboles with the exception of one layer in the upper part of the core M54-13. This ash layer differs in the high content of pumice remnants and as well as in the fluidal structures within these pumice clasts.

This first analysis lead us to conclude, that we can see approximately 7-8 different eruptions in the ash layers of the cores. Because of the similar mineralogy of the most ash layers it is necessary to analyse the glass chemistry to distinguish between different eruption phases of one or more eruption centres. These analyses will be compared to the data from the pumice layers on land and probably be correlated. Until now we can only assume 3 different eruption centres. One mafic and two felsic eruption centres which differ in the content of amphibole and pumice fragments.

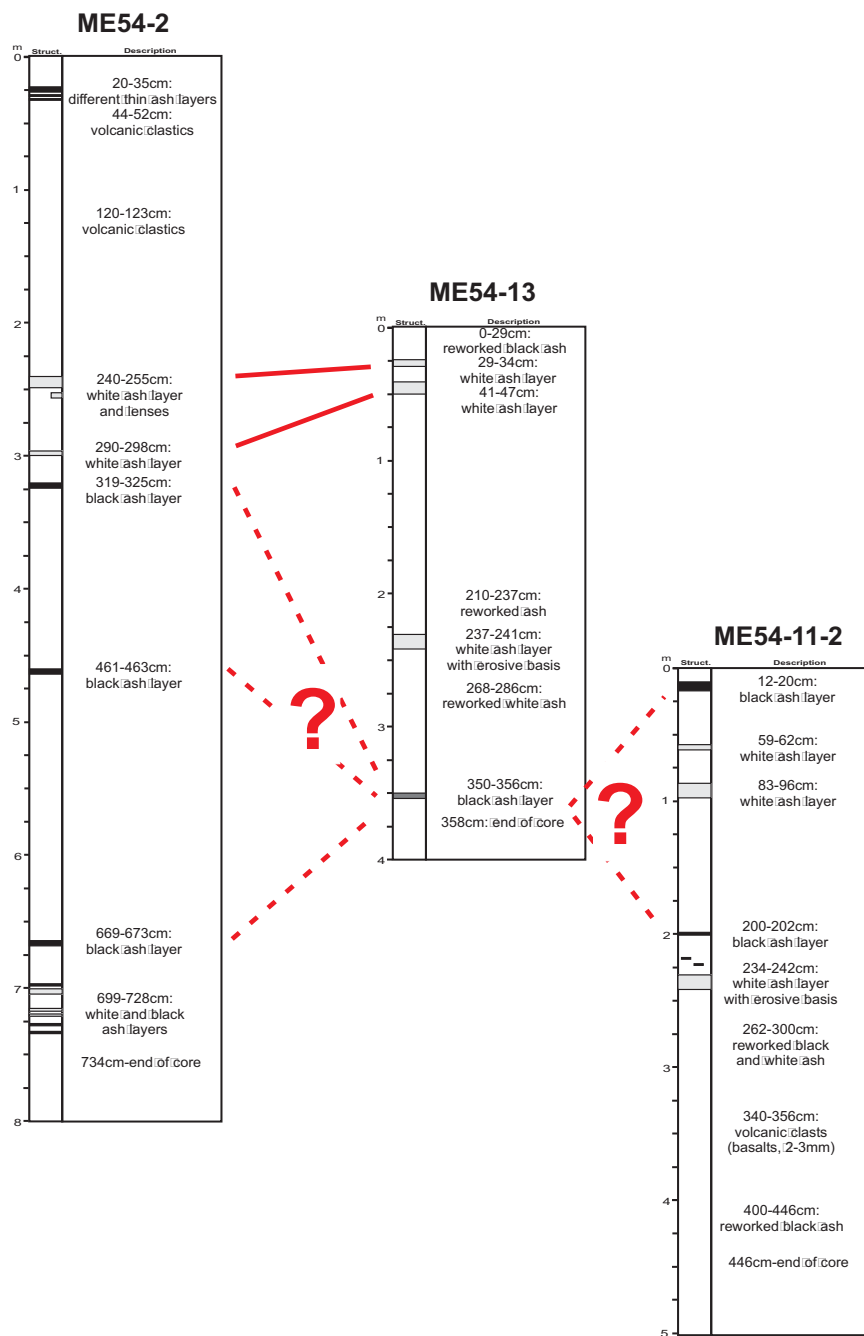


Figure 5.4.2.1: Correlation off ash-layers through cores M54-2, M54-13 and M54-11-2.

5.4.3 Structural Sedimentology of Mounds

(T. Mörz, A. Kopf & W. Brückmann)

5.4.3.1 Introduction

More than 30 mounds were discovered and bathymetrically mapped off Costa Rica during the SO 144 and 163 expeditions (Bohrmann et al, 2002; Weinrebe & Flüh, 2002 and pers. com. Sahling). Commonly, these mounds are nearly circular in shape, several tenths of meters high with an average diameter of several hundred meters and occur in water depths between 900 and 2000 m. One of the most spectacular structures of this type is 1.5 km in diameter and more than 100 m high (Mound Culebra, position 10° 18' N, 86° 18.3' W at a water depth of 1,600 m, Weinrebe & Flüh, 2002). Investigations with the TOBI side scan system (Weinrebe & Flüh, 2002) yielded high backscattering for the mounds and subsequent OFOS surveys revealed the presence of authigenic carbonates and carboniferous vent fauna communities partially covering the tops and slopes. No indicators of recent mud flow activity were found. This in turn questioned the previous interpretations of the mounds as being mud volcanoes (e.g. Shipley et. al, 1992, Kimura et al., 1997 or Bohrmann et al, 2002). The earlier interpretations were based on 3D seismic work related to ODP Leg 170, whereas the later interpretations by Bohrmann et al, 2002 is based on extensive video surveys revealing crater like central depressions and faunal communities similar to those found on mud volcanoes off Barbados (Bohrmann et al, 2002, pers. com. Sahling).

Therefore the working hypothesis prior to M54/2 was that the mounds are chemoherm buildups made up entirely of carbonates. Four such mounds (Mound Culebra, Mounds #10, #11 and #12) were sampled in detail by gravity-, piston-, and multi corer and video grab sampler during Legs 54/2 and 54/3A. Recovering overcompacted and tectonically deformed clays, various allochthonous fragments, fluid and mud channels (partially calcified) and rare chaotic mud flows. These findings together with a large collection of sediment physical property data made it necessary to reevaluate our working hypothesis and eventually revert to an interpretation of diapiric origin of the mounds.

5.4.3.2 Indicators of deformation and overcompaction

Indurated, stressed, or brecciated clays were recovered on top of Mound Culebra (e.g stations. M54-18, 21, 22) and Mound 12 (M54-92). The basal section of Core M54-18 (core catcher) of central Mound Culebra is a good example of an overcompacted and tectonically deformed clay body. It is characterized by undrained shear strength values > 100 kPa and abundant stress induced brittle deformation features. The stiff clay is intensely structured by closely spaced micro fault planes of various orientations. The micro fault planes are either very even or covered by well expressed slickensides indicating net movement along some of the fault planes (Fig. 5.4.3.1A, B). Coatings of carbonate (?), manganese or salt on some cleavages and fault planes are direct evidence of preferential fluid flow along tectonically induced pathways (Fig. 5.4.3.1C).

The orientation of the fault planes can not be explained by a single deformational regime. The multidirectionally stressed material with high shear strength indicates origin from greater depth and possible rotation during ascent and deformation.

Allochthonous fragments (clasts) are abundant in mound top and slope sediment cores. Four types of clasts have been observed during core evaluation.

- * Core scale angular mud clasts with no difference in composition to the surrounding matrix. These clasts often grade into true mud breccias (e.g. M54-22).
- * Core scale well rounded mud clasts with differentiating composition compared to the matrix (e.g. M54-18, Fig. 5.4.3.2A).
- * Large off core scale clay fragments (M54-18) with angular contacts to the surrounding matrix (Fig. 5.4.3.2B).

- * Dark, indurated (crystalline ?) rock fragments occurring in nests or single clasts within fluid channels (M54-18, 21, 22; Fig. 5.4.3.2C, D).

Preferred horizontal orientation of mud clasts is seen only in mound slope locations of Mound 11 and 12 (e.g. M54-100). These core sections are preliminarily interpreted as mud flows (Fig. 5.4.3.4C).

5.4.3.3 Physical evidence of fluid flow

Venting and rapid focussed dewatering is evident in largely open channels with mud suspension filling in a commonly coarser channel matrix. Part of the channels are also filled with (clear) water and sand fraction grains. Channel orientation is commonly sub vertical (Fig. 5.4.3.3A, B). Part of the channels also occur in an echelon like orientation with angles of 20-25 degrees off the core axis (Fig. 5.4.3.3C). A tectonic control of the location and orientation of the channels is evident, as channels follow fault plane intersections and micro brecciated sections of the structured clays (Fig. 5.4.3.3B). The structural control on the channel location is also expressed in a strong cross-sectional variance in channel geometry of single channels along the core. An biological origin of the observed structures has been also discussed.

5.4.3.4 Chaotic sediment fabric in pipes and flows

Chaotic sediment fabric has been observed in most of the central mound stations. Brecciation, unoriented clasts and crosscutting dewatering and venting structures are commonly seen in cores below 2 mbsf (Fig. 5.4.3.4A). The uppermost homogeneous meters might in part represent slope or hemipelagic sedimentation. Indicators for rapidly deposited mud flows with debris flow structures are absent at slope and basal coring locations of Mound Culebra (e.g. M54-32, 27 etc.). This might be a sign of inactiveness of the mound in terms of rapid, large scale extrusion or the mound represents a diapiric mud dome with dominantly steady, low viscous mud extrusion that mixes with hemipelagic and slope background sedimentation.

Evidence of rapidly deposited mud flows has been found on the flanks of Mound 11 and 12 (Fig. 5.4.3.4B, C). Coarse basal layers of turbidites, sections dominated by chaotic carbonate fragments (shells and concretions) are alternating with clay-rich packages that are characterized by soft sediment deformation. Related sedimentary processes are turbidites and debris flows of local origin. The carbonate fragments are likely remnants of vent fauna and chemohierms formed higher up on the mounds near active expulsion sites. The presence of mud flows is indicative of more active and rapid rise of high viscous material within the domes and subsequent periodic failure of the dome top.

5.4.3.5 Summary and Outlook

Presented evidence of allochthonous material from greater depth, evidence of transportation fragmentation and deformation found in mound sediments point toward an interpretation as exposed mud diapirs or diapiric mud pipes with no or limited associated flows. Further work will focus on the

- determination of the material source and source depth (biostratigraphy of clasts, consolidation testing, illite-crystallinity, petrography of clasts)
- Understanding of eruption mechanism (diapirism, fluid-gas and mud-suspension venting, understanding of the pathways (conduits))
- Quantification of eruption rates and frequencies (C^{14} , rheology of extruded materials, determination of hydraulic conductivities, hints from fossil calcificated chimneys).

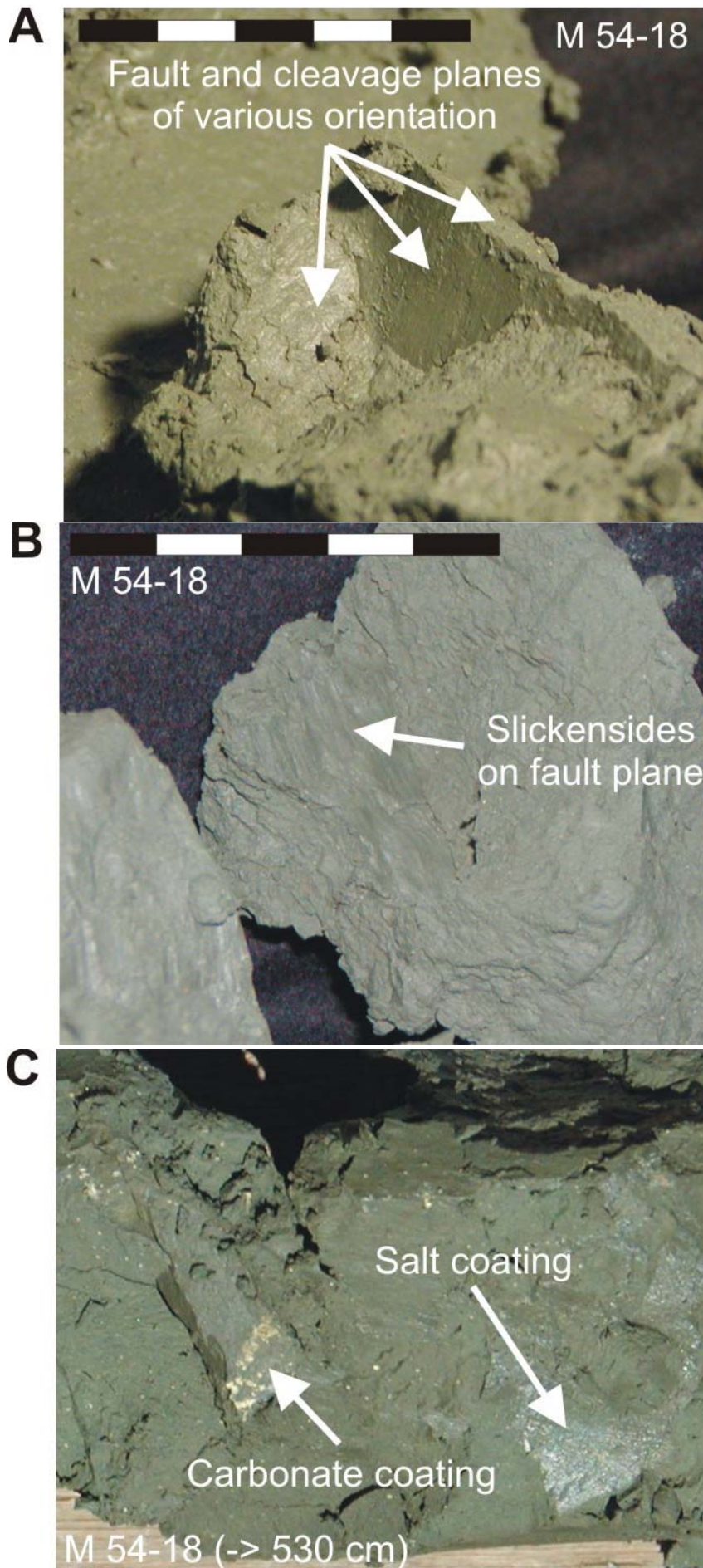
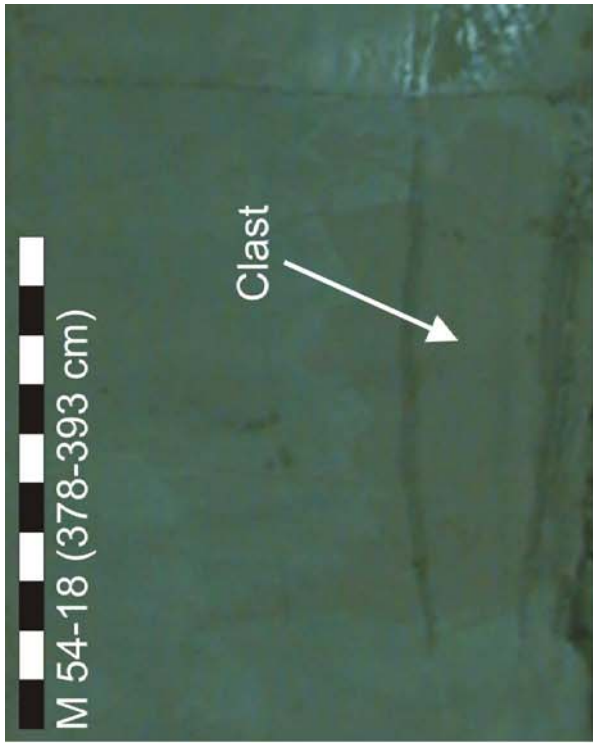
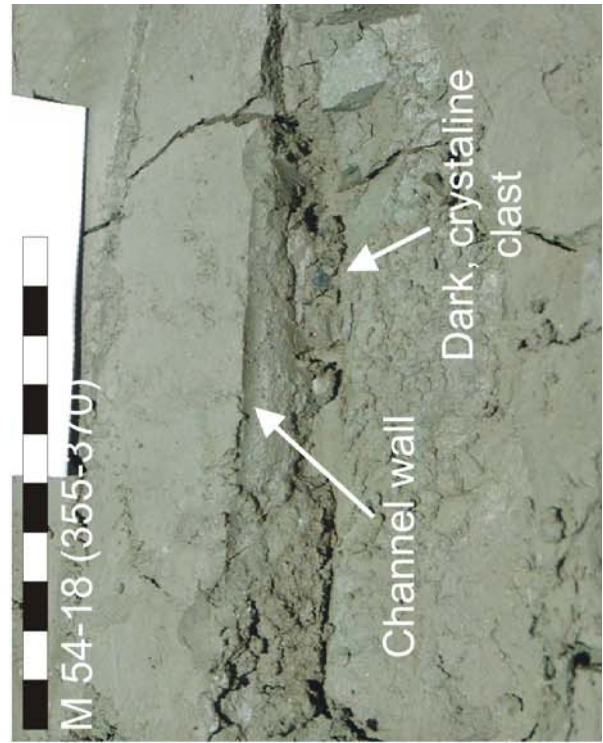


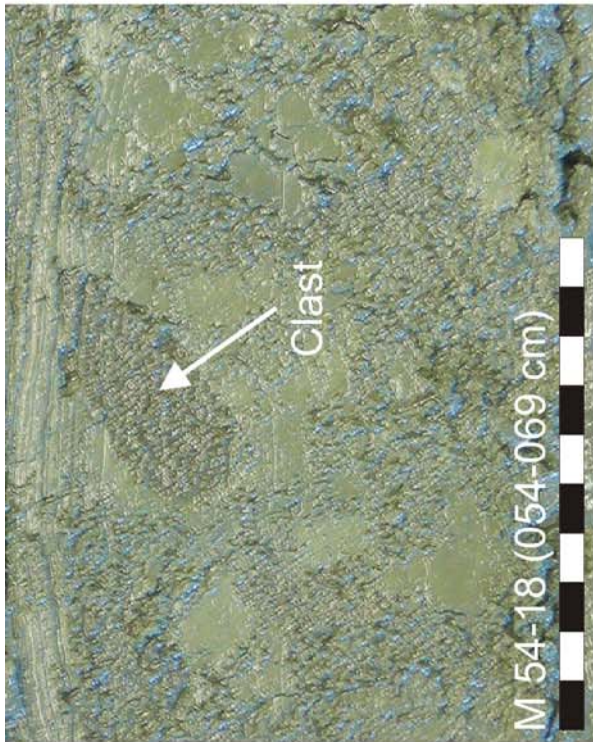
Figure 5.4.3.1: Indicators of intense brittle deformation. A, B Fault planes, in part covered with slickensides. C Coating on fractures.



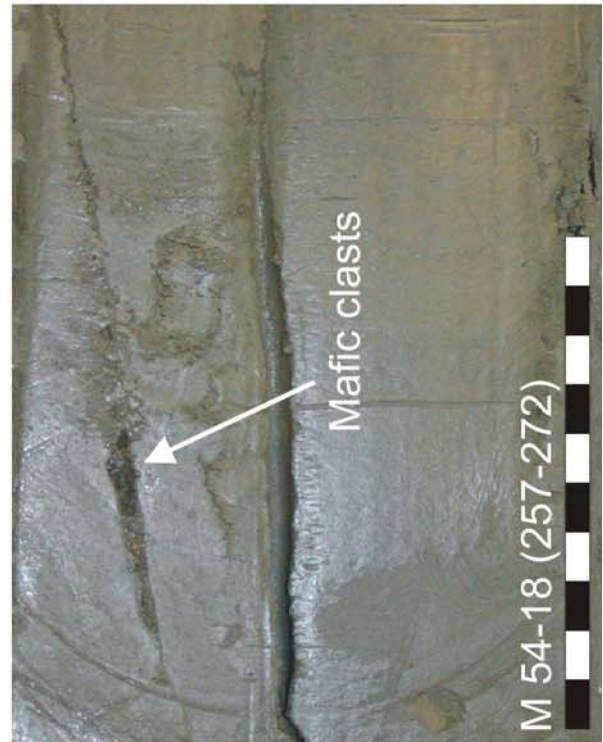
B



D

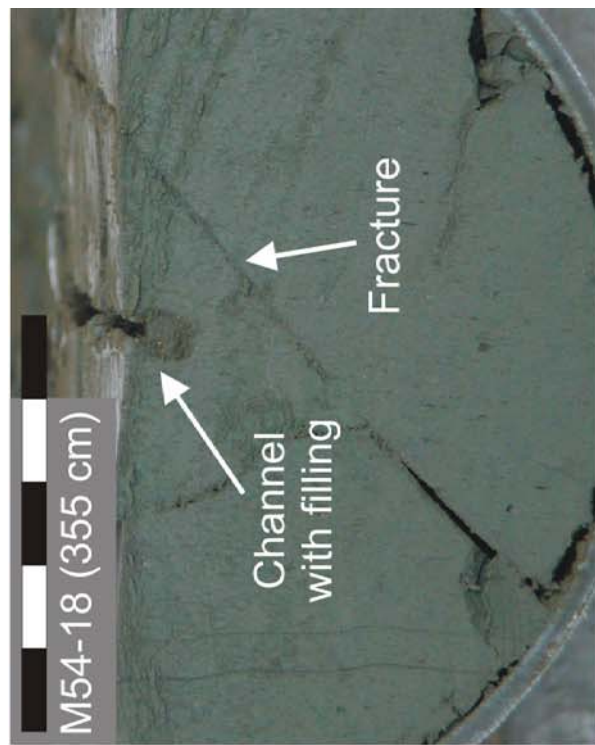


A

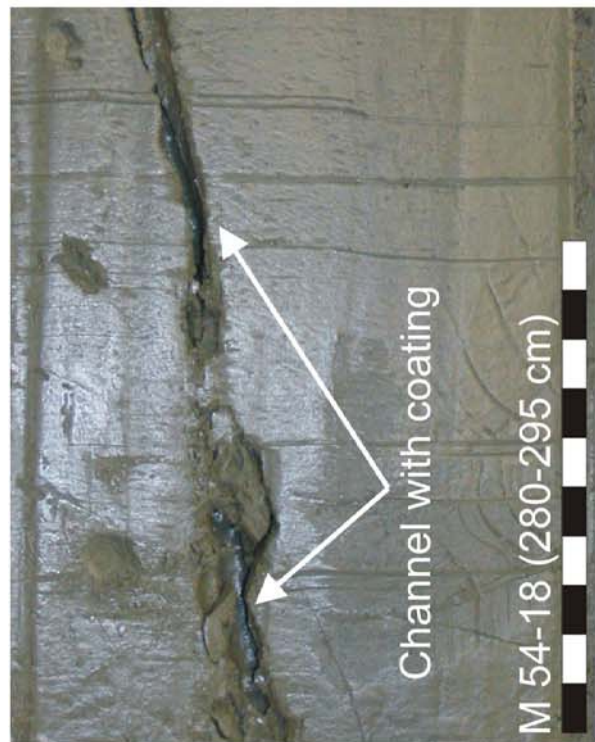


C

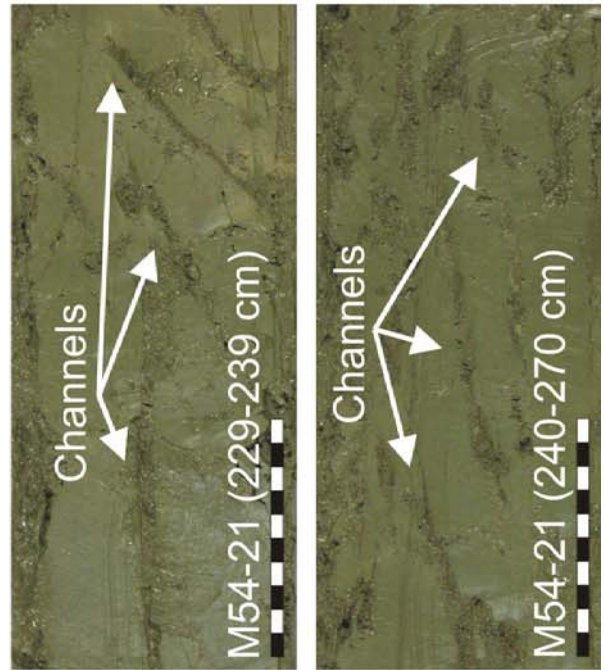
Figure 5.4.3.2: Various clast types. A Rounded clasts. B Subangular off core scale clasts. C, D crystalline clasts in channels and pockets.



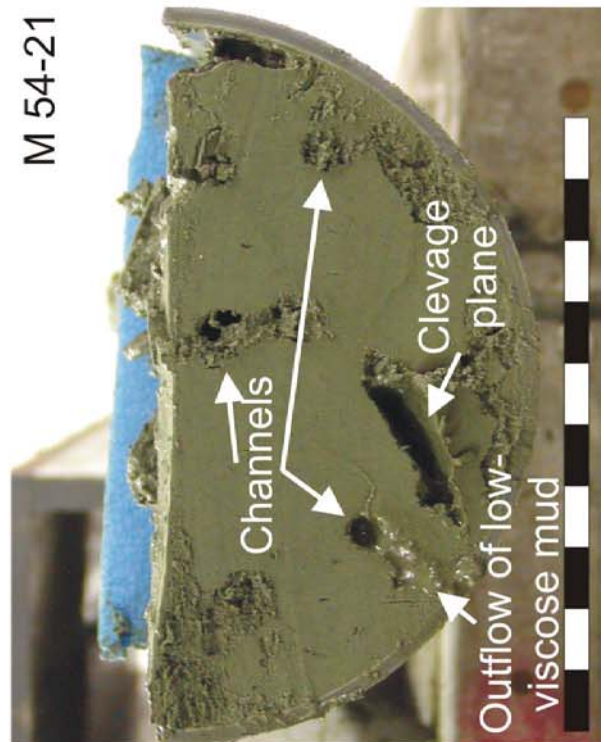
B



A



C.2



C.1

Figure 5.4.3.3: Examples of fluid migration pathways. A: Channel with dark coating, originally filled with clear water. B: Core cross sections with filled channels and fractures. C: An echelon like channel orientation.

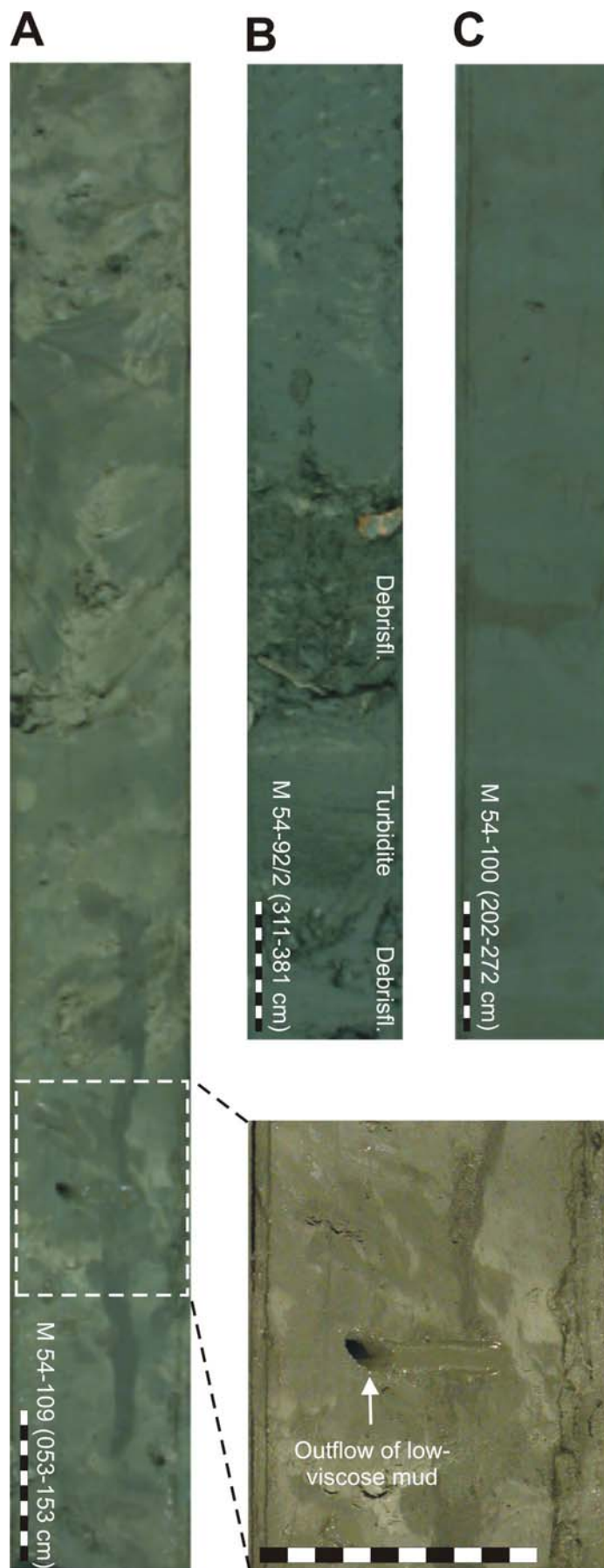


Figure 5.4.3.4: Example of different mud diapir fabric types. A chaotic fabric of the central Mound 11 with vertical mud escape structures. B Example of a mud flow sequence. C Mud flow with oriented mud clasts.

5.4.4 Authigenic Carbonates

(X. Han, E. Suess, T. Mörz, A. Deyhle, A. Kopf)

5.4.4.1 Introduction

Mud mounds, some of which are covered with chemoherm, were discovered off Costa Rica during the SO 144 and 163 expeditions (Bohrmann et al, 2002a; Weinrebe & Flüh, 2002). These mounds are up to 200-300 m high and up to one km in diameter. They are clearly recognized on bathymetric maps at water depth between 900 and 2000 m. OFOS surveys established that they are partially covered by an impenetrable cap of carbonate but it remained unclear whether or not they are solid carbonate throughout or if the interior consists of fluidized mud. The mounds are readily identified on side-scan sonar maps due to the high reflectivity of the outcropping hard ground caps (Weinrebe & Flüh, 2002) and over-compacted clays. Extensive coring revealed that the internal structure of some mounds is dominated by compacted clays.

Four such mounds were surveyed by OFOS and sampled in detail during Legs 54/2 and 54/3A (Mound Culebra, Mounds #10, #11 and #12). Additional authigenic carbonates were sampled from the top of the Jaco Scarp, where also wide-spread carbonate hard-grounds occur without a significant morphological expression. Previous expeditions had established that such hard-grounds are also present at most other scarps and appear connected to fault patterns in the upper plate caused by uplift from seamount subduction.

Isolated crusts, concretions, chimneys and carbonate-cemented sediment layers of high permeability either as conduits, breccias and fault planes were also recovered during Legs M54/2 and /3A from throughout the gravity cores, multi-cores and grab-samples.

Chemoherms, hard-grounds, isolated concretions, and carbonate-cemented sediments are characteristic for all tectonic features related to fluid venting. Generally, the carbonate results from the bacterially-mediated oxidation of methane, either supplied by ascending fluids from depth or by dissociating methane hydrates. Although at the present time no C-isotope data are available from any of these samples, it is highly likely that their origin as derived from methane, will be confirmed shortly.

5.4.4.2 Chemoherm and other authigenic carbonate features

Chemoherm carbonates have been defined recently in analogy to bioherms but emphasizing that they are primarily the result of chemical precipitation caused by fluid venting (Bohrmann et al., 1998). Hereby carbonate supersaturation is induced by anaerobic methane oxidation (Suess et al, 1999; Greinert et al., 2001). An additional essential feature appears to be that shell debris from vent clams are incorporated into the body of a chemoherm in various proportions and that the body of the chemoherm itself forms in contact with and is exposed to the bottom water, however carbonate chimneys and carbonate concretions have been found in various depths in the sediments (Fig 5.4.4.1 B, Fig 5.4.4.4). In case the carbonate body constitutes an elevated feature standing above the surrounding seafloor it may be termed chemoherm or chimney but if no such morphological expression exists the carbonate body may be termed cap or platform carbonate.

The condition under which chemoherm, chimneys, platform or cap carbonates form appears to be related to the type and degree of fluid venting with all gradations between them. Focussed flow from point sources over long periods of time tend to form chimneys and morphologically elevated chemoherms; flow out of fault zones tend to form platform carbonates and flow out of generally circular mud diapirs tend to form cap carbonates.

Typical chemoherm/platform carbonates were sampled from above the Jaco Scarp (Sta. M54/TV-G 172) presumably formed by methane-rich fluids emanating from fault zones. Figure 5.4.4.1A-C show different

chemoherm carbonates with little or no sediment incorporated but abundant shell debris (Bathymodiolus fragment; Fig. 5.4.4.1B), filled-in fluid conduits (Fig. 5.4.4.1A) and several generations of carbonate layers lining free void spaces (Fig. 5.4.4.1C). Another type of chemoherm carbonates was observed and recovered from Mound #12. Here flat carbonate slabs form a closely connected hard ground were recovered where Bathymodiolus colonies crowd into every available fracture between the slabs. The population resembles that of vent clams observed in the fracture space between pillow basalt at mid-ocean ridge hydrothermal systems. Such dense biomass attests to high flux rates of venting fluids.

Chimney-like cylindrical structures were found embedded into the clay-rich muds in several cores (e.g. M54-29, M54-62-2, M54-84). Only features with an open, tube-like central conduit have been termed chimneys. The features were found in various stages of lithification, some of which were just slightly more indurated than the surrounding matrix, while others had rigid carbonate walls. The biggest intact example in a gravity core is shown Fig. 5.4.4.4. The chimneys vary in colour from mostly dark brown to dark and middle gray. Most of them are cylindrical, although the diameter is rather oval in the majority of the cases. The outer diameter of the chimneys is several mm to several cm for the intact examples, but may be limited by the diameter of the gravity corer. The walls of the chimneys can be several cm thick (e.g. M54-84), but are usually 1 cm or less. In some cases, only fragments were found, which were related to a chimney because of their arcuate shape. Given the components incorporated into the chimney walls as well as the variable lithification, it is assumed that the chimneys form by calcifying the sediment. Consequently, what is now recovered as a chimney has been a fluid pathway earlier, with the methane being oxidized and precipitated due to oversaturation. As a consequence of being a fluid flowpath, it is mostly coarse-grained permeable material which builds the chimneys, whereas the surrounding matrix consists of less permeable clay-rich material. Some chimney walls show fragments of mm-sized claystone clasts which may have been transported upward with the ascending fluid or mud (e.g. M54-62-2). Rigid, fully cemented chimney walls probably reflect areas with enhanced fluid flow over long periods of time while softer chimney structures may attest that fluid migration here is fairly recent. Some of the chimneys are filled with fluidized, often coarse grained mud while others are empty and may actually been inactive at the time of recovery. No matter how well lithified the chimneys are, they remain macroscopically porous. Zonation is inferred from macroscopic inspection, and shore-based geochemical analyses will test whether there have been changes in fluid composition with time. The best example for a yellowish white cement at the inner wall of an otherwise middle grey chimney has been found at station M54-92.

5.4.4.3 Gas hydrate carbonates

Gas hydrate carbonates are equally a newly defined type of authigenic lithology related to methane oxidation (Bohrmann et al., 1998). Hereby methane is generated from dissociating gas hydrates and the mineral precipitation occurs in the immediate vicinity of and sometimes still in contact with solid gas hydrates. This type is characterized by layered aragonite growing into the open void space which is left by dissociating gas hydrates, by imprints of the hydrate fabric onto the carbonate surfaces, and brecciated fabric presumably caused by the break-up of gas hydrate layers (Suess et al., 2001; Bohrmann et al., 2002b). Such pieces of suspected gas hydrate carbonate was recovered from the Mound #11 area, where gas hydrates were also found in near-surface sediments during Leg M54-2. The characteristic features are aragonite layers lining the inside of an open chimney which formed under sediment cover (Fig. 5.4.4.2A). A highly brecciated carbonate horizon was cored 200 cm below sea floor at a circular shallow mound feature identified by side scan sonar survey (Sta. 179 GC) whose origin might be related to gas hydrates. Again, C- and O-isotope data are currently not available but should surely soon document whether or not gas hydrate carbonates presently form at these mounds.

Core 143-GC contained an interesting assemblage showing the relationship between the occurrence of carbonate concretions, cement, and sediment texture as well as accessory authigenic minerals which may be used as gas hydrate indicators. The interval between 99-134 cmbsf contains at first abundant shell fragments

(99-108 cm) followed at 104-110 cm by a black tabular carbonate cemented sandstone crust (110-119 cm). Its surface appears granular and easy to be flaked off. Powder scraped from the surface is composed of aragonite needles. Below the crust there was a big void filled with water and surrounded by soft volcanic ash containing sandy sediments (110-126 cmbsf). Authigenic framboidal pyrite is abundant and green glauconite is common among the heavy minerals of the sediments. Probably this void was originally filled with gas hydrate, which disappeared when the hydrate became exposed to air. Above and below the void there were also several carbonate concretions, the host sediment appeared very dry as if dewatered by gas hydrate formation. Fig. 5.4.4.3 shows schematically this sequence.

5.4.4.4 Carbonate concretions and cemented sediments

Abundant samples of carbonate-cemented sediments were recovered from just about each gravity and multi-core. There are isolated patches of elongated concretions, resembling bone-beds (Fig.5.4.4.2B; Sta.M54 TV-G 134) which either are cemented burrows or fluid conduits. The latter interpretation is more likely because of their preferred occurrence with vertical and sub-parallel conduits and other tectonically related dewatering features. Buried chimneys therefore represent the carbonate-cemented sections of feeder channels. Some of them show diffuse, root like structures before they coalesce into the actual, focused carbonate chimney. Abundant mussel shell fragments characterize the root zone of this chimney, some of them are integrated into the carbonate structure (Fig. 5.4.4.4). Similar carbonate chimneys have been recovered at almost every mound location investigated and vent locations related to tectonic faults e.g. core M54-62/2.

Odd-shaped black or dark olive colored carbonate-cemented mud stones were common (Fig. 5.4.4.2C). Some of these contained shell fragments others appeared completely micritic giving off a petroliferous smell from freshly broken surfaces. Their distribution in cores appeared random with sharp contacts towards the host sediment. Another type of carbonates recovered from sediments was large scoria-like pieces of highly porous material associated with very soft mud. The carbonate constitutes an irregular fragile framework enclosing lumps of mud (Fig. 5.4.4.2D). The largest pieces of this type were recovered at Sta. TV-G 177 from Mound #11. The crater-like mound morphology and the intimate association of sediment and carbonate texture and fabric suggest that these lithologies might have formed inside a mud volcano.

5.4.4.5 Outlook

Results obtained so far by the SFB 574 have documented a vast variety of authigenic carbonates, their regional distribution and their as yet unknown depth of occurrence throughout the upper plate of the Central American subduction zone. This situation emphasizes the enormous importance of the authigenic carbonate-C reservoir as part of the volatile budget escaping from the fore-arc. Moreover, we believe that the varied carbonate mineralogy, detailed C-, O-, Ca-, Sr-, Th-, and U-isotopic make-up along with trace element and enclosed biomarker composition represent an as yet untapped archive of information on fluid source, fluid depth, fluid residence time, and fluid interaction with biota, sediment, and lower and upper crust lithologies. The luxuriant chemoautotrophic communities (*Lamellibrachia* sp, *Calyptogena* sp., *Bathymodiolus* sp.) associated with the authigenic carbonates indicate long-term methane venting. The methane concentrations in the water column above the mounds are considerably elevated compared to background levels indicate presently active authigenic carbonate formation. Taking into account these circumstances, the significance of authigenic carbonates for the volatile budget is tremendously increased and their analyses demand center-stage for achieving one of the major objectives of the SFB 574.

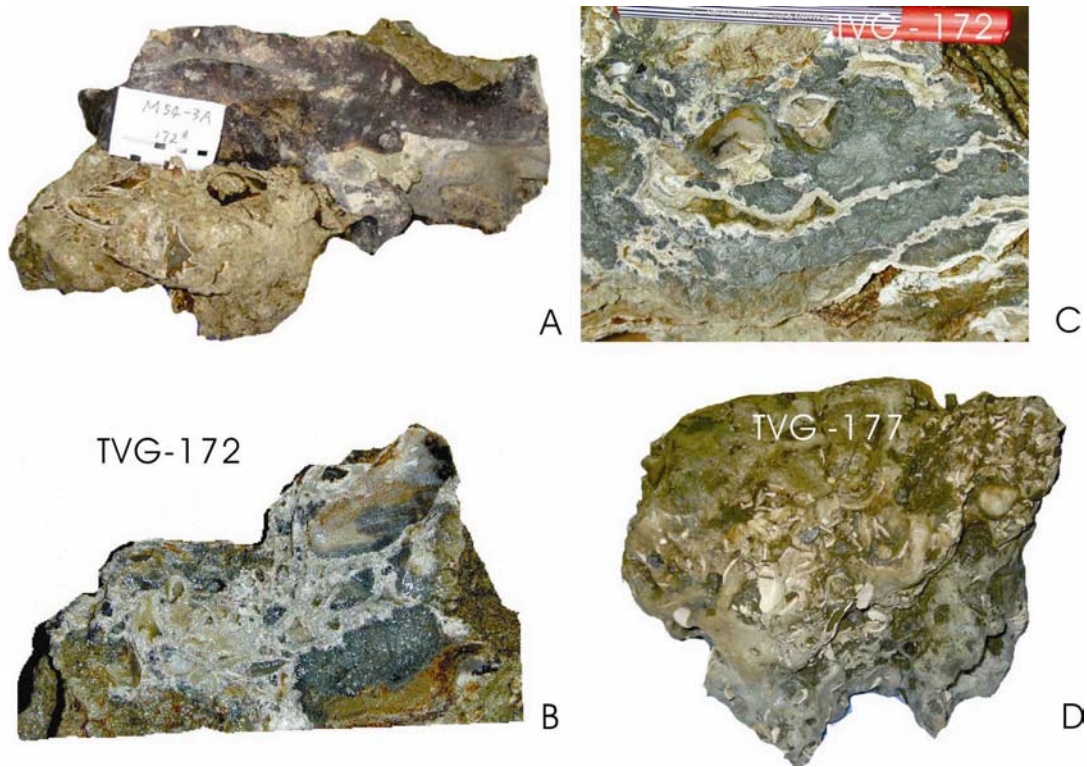


Fig. 5.4.4.1 Typical chemoherm carbonates; A = cemented fluid channel in micritic matrix; B = Cemented Bathymodiolus fragment; C = Several generations of cement in void filling; D = Carbonate cemented shell debris and sediment

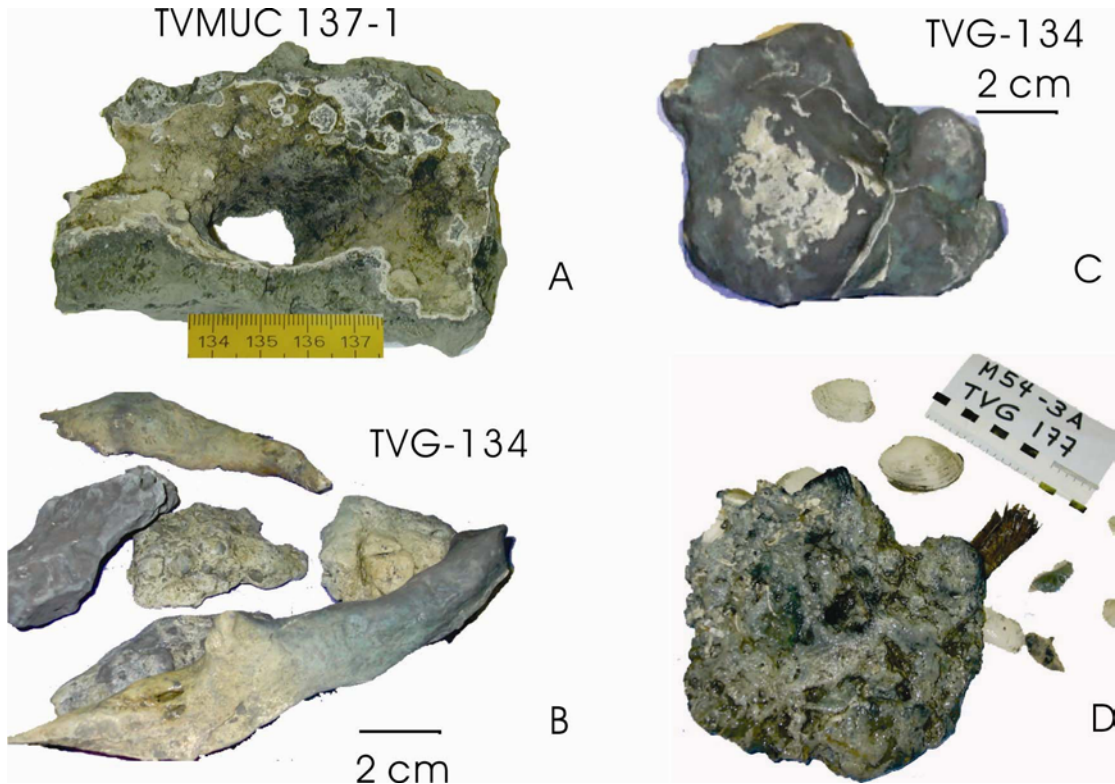


Fig. 5.4.4.2 Typical carbonate concretions;
 A = Probable gas hydrate carbonate with aragonite lined void space and gas/fluid escape channel;
 B = Elongated carbonate concretions (bone-bed type); C = Concretion with carbonate cemented vein filling; D = Fragile carbonate framework containing uncemented mud clasts.

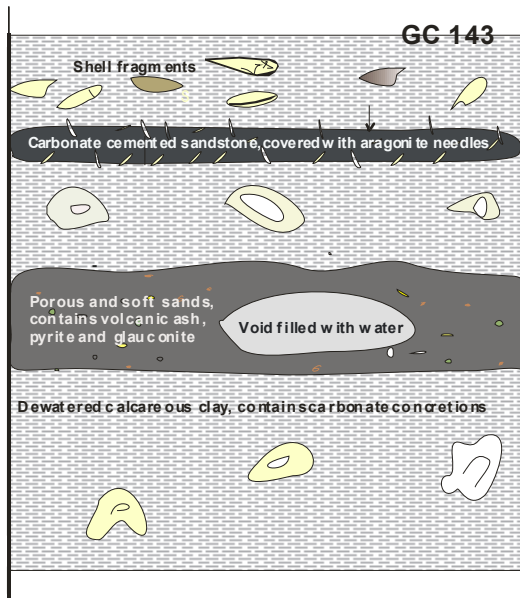


Fig. 5.4.4.3 Schematic sequence of authigenic mineral assemblage associated with gas hydrate cemented porous sediments; St. M54 GC-143.

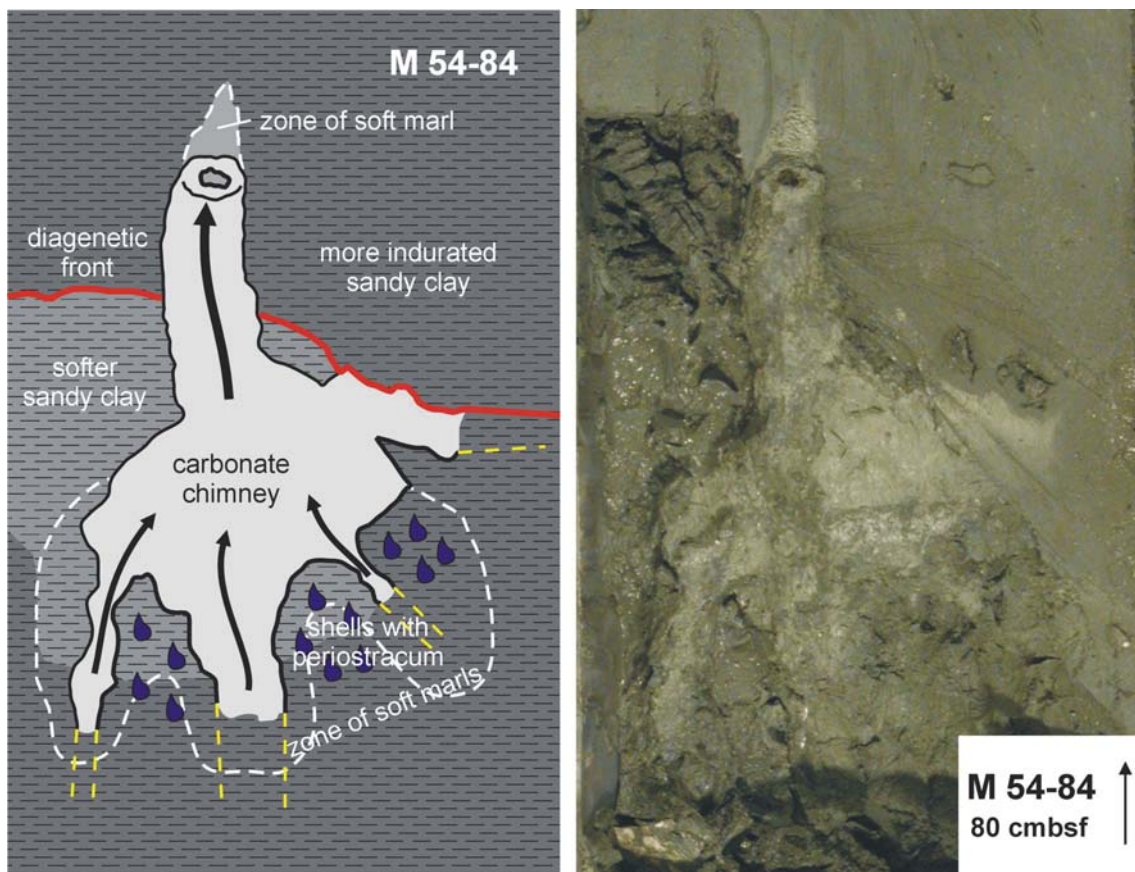


Fig. 5.4.4.4 Example of a buried carbonate chimney. The chimney has been found 80 cmbsf in core M54-84. Arrows indicate possible flow or migration paths. The open portion of the tube extends only over the distance indicated by the upper arrow.

References:

- Bohrmann, G., J. Greinert, E. Suess, and M. Torres, 1998. Authigenic carbonates from the Cascadia subduction zone and their relation to gas hydrate stability. *Geology*, 26 (7): 647-650.
- Bohrmann, G., K. Heeschen, C. Jung, W. Weinrebe, B. Baranov, B. Cailleau, R. Heath, V. Hühnerbach, M. Hort, and D. Mason, 2002a. Widespread fluid expulsion along the seafloor of the Costa Rica convergent margin. *Terra Nova* 14, (2) 69-79
- Bohrmann, G., E. Suess, J. Greinert, B. Teichert, T. Naehr 2002b. Gas hydrate carbonates from Hydrate Ridge, Cascadia margin: Indicators for near-seafloor clathrates. *Proc. 4th Intl. Gas Hydrate Research Conf. Yokohama*, 102-107.
- Greinert J, Bohrmann G, Suess E (2001) Gas hydrate-associated carbonates and methane venting at Hydrate Ridge: Classification, distribution and origin of authigenic lithologies. In: C. Paull and W. Dillon (eds.) *Natural Gas Hydrates: Occurrence, Distribution, and Detection*, Washington, American Geophysical Union, Monograph Series 124: 99-113.
- Suess, E., M. E. Torres, G. Bohrmann, R. W. Collier, J. Greinert, P. Linke, G. Rehder, A. Tréhu, K. Wallmann, G. Winckler, and E. Zuleger, 1999. Gas hydrate destabilization: enhanced dewatering, benthic material turnover and large methane plumes at the Cascadia convergent margin. *Earth Planet. Sci. Lett.*, 170: 1-15.
- Suess, E., G. Bohrmann, D. Rickert, W.F. Kuhs, M. Torres, A. Trehu, and P. Linke 2002. Properties and fabric of near-surface methane hydrates at Hydrate Ridge, Cascadia margin. *Proc. 4th Intl. Gas Hydrate Research Conf. Yokohama*, 740-744.
- Weinrebe, W., and E. Flüh (eds.), 2000. R.V. SONNE Cruise Report SO-163, SUBDUCTION I (March 13 - April 20, 2002; Balboa - Balboa). *GEOMAR Report 106*, Kiel, 530 pp.

5.5 Pore-water geochemistry of surface sediments

(C. Hensen, A. Deyhle, B. Domeyer, Y.-O. Fischer, D. Garbe-Schönberg, M. Inthorn, S. Klauke, S. Mansor, M. Marquardt, K. Nass, and U. Schacht)

Investigations of the geochemical composition of pore-waters provide information to investigate the forces and impacts driving redox-, and mineralization processes within the upper sediment column. During the cruises M 54/2 and 54/3A the pore water composition of surface sediments was investigated at more than 80 locations to characterize and quantify sediment diagenetic processes and fluid geochemistry along the active continental margin off Costa Rica. Concentration vs. depth profiles of pore-waters were determined for major nutrients, total alkalinity, chloride, hydrogen sulfide, and methane to identify locations influenced by seepage and to assess the effect of methane formation and decomposition processes.

Below we first give a short overview on the procedures of sediment retrieval, pore water processing, and geochemical laboratory methods followed by a selection of major results obtained during both cruises.

5.5.1 Sampling, processing, and analyses

Sediments were generally retrieved by use of a multicorer (TV-guided during M 54 3A) and a gravity corer. On M54/3 additional sediment samples were obtained from Benthic Chamber Lander and TV-Grab deployments.

To prevent a warming of the sediments after retrieval all cores were immediately placed in a cooling room and maintained at a temperature of about 4°C. Supernatant bottom water of the multicorer-cores was sampled and filtered for subsequent analyses. The multicorer-core was processed immediately after recovery, mostly, in a glove box under argon atmosphere. For cores with high amounts of methane and/or gas-hydrates a faster sampling procedure outside the glove box was preferred and sub-samples for methane analyses were taken. Each core was cut into slices for pressure filtration with a minimum depth resolution of 0.5 cm. Gravity cores were cut lengthwise after recovery. On the working halves pH and Eh were determined and sample intervals between 10-50 cm were taken for pressure filtration. At sampling locations where methane was expected to be present, syringe samples were taken on deck from every cut segment surface. Occasionally, higher resolution sampling for methane analysis was carried out in the cooling laboratory immediately after storing by sawing 4×4 cm rectangles into the PVC liner and taking syringe samples of 3 ml sediment every 30-40 cm and injected into 24 ml septum vials containing 9 ml of a concentrated NaCl-solution. After closing and subsequent shaking methane becomes enriched in the headspace of the vial. One replicate was taken and poisoned with a saturated NaOH solution for subsequent isotopic analyses.

Each sample depth for pore water squeezing was additionally sampled for (1) the calculation of sediment density and (2) for determination of redox-sensitive elements. Porosity sub-samples were filled into pre-weighed plastic vials and redox-samples were kept in specific gas-tight containers under argon atmosphere for subsequent analyses in the home laboratory.

For pressure filtration Teflon- and PE-squeezers were used. The squeezers were operated with argon at a pressure gradually increasing up to 5 bar. Depending on the porosity and compressibility of the sediments, up to 30 ml of pore water were received from each sample. The pore water was retrieved through 0.2 µm cellulose acetate membrane filters.

Pore water analyses of the following parameters were carried out during both cruises: nitrate, ammonia, phosphate, alkalinity, ferrous iron, hydrogen sulfide, chloride, methane, fluoride, silicate, calcium, Eh, and pH. The analytical techniques used on board to determine the various dissolved constituents are listed in Table 5.5.1.1. Modifications of some methods were necessary for samples with high sulfide concentrations. Detailed descriptions of the methods are available on http://www.geomar.de/zd/labs/labore_umwelt/Analytik.html.

Table 5.5.1.1: Techniques used for pore water analyses.

Constituent	Method	Reference
Nitrate	Autoanalyzer / Spectrophotometry	Grasshoff et al. (1997)
Alkalinity	Titration	Ivanenkov and Lyakhin (1978)
Silicate	Spectrophotometry	Grasshoff et al. (1997)
Phosphate	Spectrophotometry	Grasshoff et al. (1997)
Ammonium	Spectrophotometry	Grasshoff et al. (1997)
Chloride	Titration	Gieskes et al. (1991)
Hydrogen sulphide	Spectrophotometry	Grasshoff et al. (1997)
Methane	Gas chromatography	Niewöhner et al. 1998
Ferrous iron	Spectrophotometry	http://www.geochemie.uni-bremen.de/links/links.html
Fluoride	Ion-sensitive electrode	http://www.geochemie.uni-bremen.de/links/links.html
Calcium	Titration	Grasshoff et al. (1997)
pH	Electrode	Dickson (1993)
Redox potential (Eh)	Electrode	-

Nitrate, ammonium and phosphate were measured photometrically (with help of an autoanalyser in case of nitrate) using standard methods described by Grasshoff et al. (1997). Samples of the sediment pore water for total alkalinity measurements were analyzed by titration of 0.5-1 ml pore water according to Ivanenkov and Lyakhin (1978). Titration was finished until a stable pink color occurred. During titration the sample was degassed by continuously bubbling nitrogen to remove the generated CO₂ or H₂S. The acid was standardized using a IAPSO seawater solution. The method for sulfide determination according to Grasshoff et al. (1997) has been adapted for pore water concentrations of S²⁻ in the range of millimolar amounts. For reliable and reproducible results, an aliquot of pore water was diluted with appropriate amounts of oxygen-free artificial seawater; the sulfide was fixed by immediate addition of zinc acetate gelatin solution immediately after pore-water recovery. After dilution, the sulfide concentration in the sample should be less than 50 µmol/l. Chloride was determined by titration with AgNO₃ standardized against IAPSO seawater. High concentrations of H₂S (> 1mM) in the sample affect the measurements. Therefore, these samples were pre-treated with a 1:1 dilution of 0.01 N suprapure HNO₃ and stored for 1-2 days, without lid, in a cool room. For the analysis of iron concentrations sub-samples of 1 ml were taken within the glove box and immediately complexed with 20 µl of Ferrozin and afterwards determined photometrically. Fluoride was determined in 1.5 ml sub-samples by an ion-sensitive electrode.

Acidified sub-samples (35µl suprapure HCl + 3 ml sample) were prepared for ICP analyses of major ions (K, Li, B, Mg, Ca, Sr, Mn, Br, and I) and trace elements. Sulfate, DIC, d¹⁸O and d¹³C of CO₂ will be determined on selected sub-samples in the shore-based laboratories.

5.5.2 Shipboard results

The major goals of the pore water geochemistry working-group were different between M 54/2 and M 54/3A mainly due to different instrumentation on-board ship. During M 54/2 it was attempted to obtain an overview of the general pore water systematic within the slope sediments (i.e. changes along shelf to deep-sea transects) and of the geochemical characteristics of methane-rich fluids that were expected at a number of mound-like structures and seamount scars along the slope. On M 54/3A those structures were re-visited and a number of specific samples could be taken directly at active vent sites (i.e. marked by living bivalves or bacterial mats) by means of TV-guided instruments.

5.5.2.1 Shelf to deep-sea transects

During M 54/2 15 stations (M 54: 1, 2, 6, 11/2, 13 (piston core), 14, 35, 36, 39-2, 40, 41/1, 56, 57, 68, and 81/1) were sampled by gravity corer along three transects almost perpendicular to the coastline off S-Nicaragua, along the ODP Leg 170, and off S-Costa Rica (see Figure 3.0.1). These were supplemented by three multicorer deployments: M 54: 9, 41/2, 81/2. Overall, the general pattern for the whole area is that the mineralization intensity increases from the shelf downslope into the deep-sea trench, which can be observed at best for the parameters alkalinity, methane, and ammonia. Representatively, this is displayed for three stations along the S-Nicaraguan transect in Figures 5.5.2.1.1-5.5.2.1.3. E.g. alkalinity levels increase from almost seawater levels at M 54-1 to nearly 80 meq/l at depth at station M 54-14 (Figures 5.5.2.1.1-3), where the high alkalinity level corresponds with high amounts of dissolved methane and ammonia. Obviously, the major part of the reactive organic material is deposited at lower slope depths and in the trench, which is supported by a larger number of turbidites (see section 5.4), indicating vast accumulation rates along the trench axis. Additionally, the high methane levels at M 54-14 suggest that high amounts of hydrogen sulfide should be present as well.

Since this is not the case, we assume that the supply of reactive iron (immediately trapping free H_2S) clearly exceeds the production level of hydrogen sulfide in these sediments.

Apart from the generally low reactivity of the shelf sediments, two interesting observations could be made, however, at M 54-1 (Figure 5.5.2.1.1): (1) There seems to exist a more reactive top layer indicated by the peak of hydrogen sulfide. (2) The chlorinity decreases significantly with depth, possibly indicating a fresh water advection into the surface sediments.

A distinct exception of all transect stations is M 54-6 also located within the trench axis off Nicaragua (Figure 5.5.2.1.4). The most striking differences between all other trench locations (i.e. Figure 5.5.2.1.3) are (1) a decrease in chlorinity over depth, (2) comparatively low alkalinity levels of about 30 meq/l at maximum, and (3) significant levels of hydrogen sulfide in the lower part of the core. Additionally, alkalinity does increase with depth, but shows a distinct maximum at about 2.5 mbsf (probably within the zone of sulfate reduction).

The working hypothesis for these observations (which has to be proven by additional analyses) is that a low-chlorinity / high calcium fluid is ascending into the sediments. Also calcium has not been measured yet, it is most likely that higher concentrations of dissolved calcium are controlling the alkalinity level below 2.5 mbsf. Due to fluid advection it can be assumed that the reaction rates of anaerobic methane oxidation must to be higher compared to other trench locations, which is most likely the explanation for detectable hydrogen sulfide concentrations, exceeding the reaction capacity of reactive iron minerals.

**M 54-1 SL
Shelf / Nicaragua (148 m)**

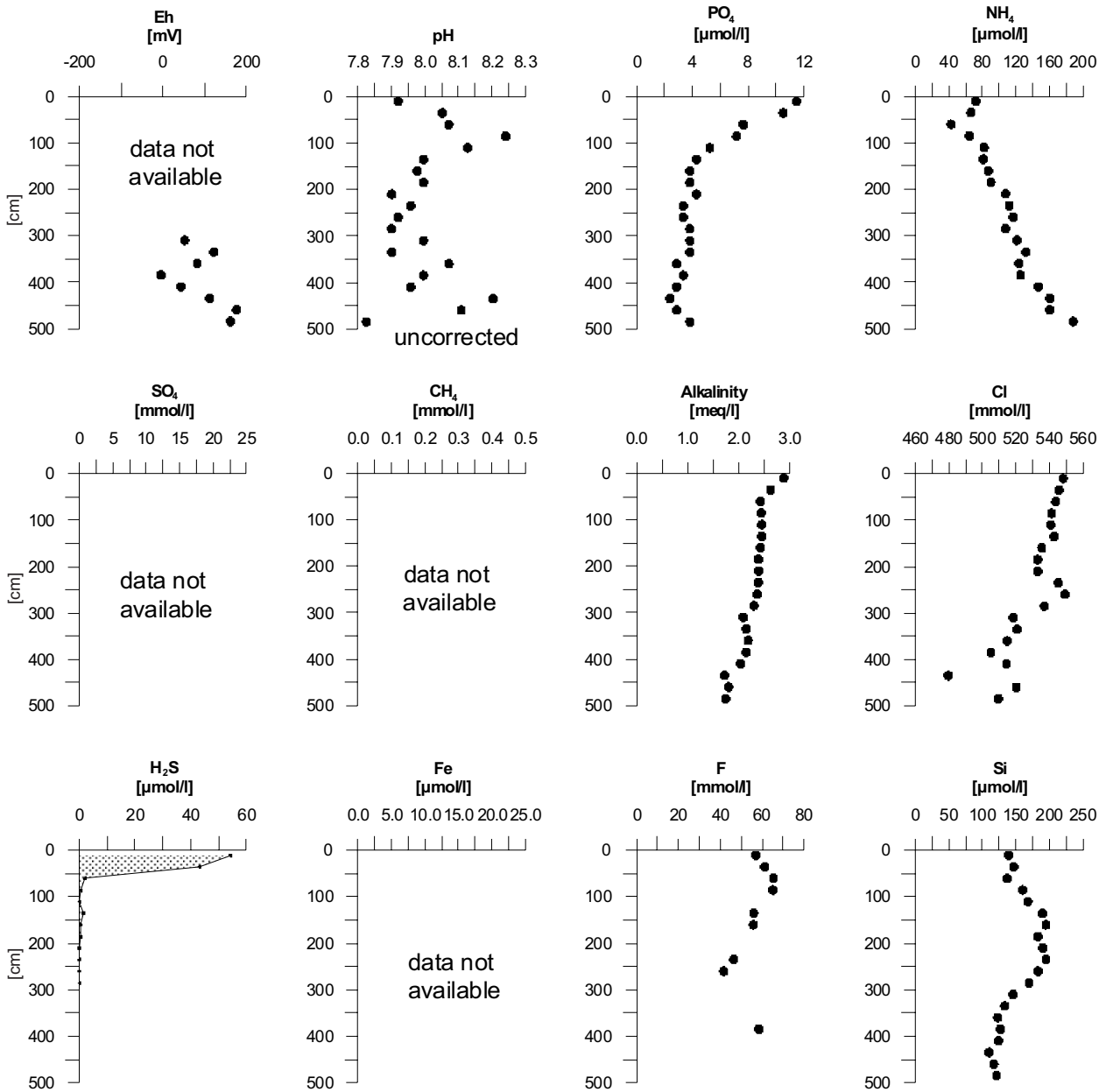


Figure 5.5.2.1.1: Pore water profiles of gravity core M 54-1.

M 54-13 KL Slope / Nicaragua (1200 m)

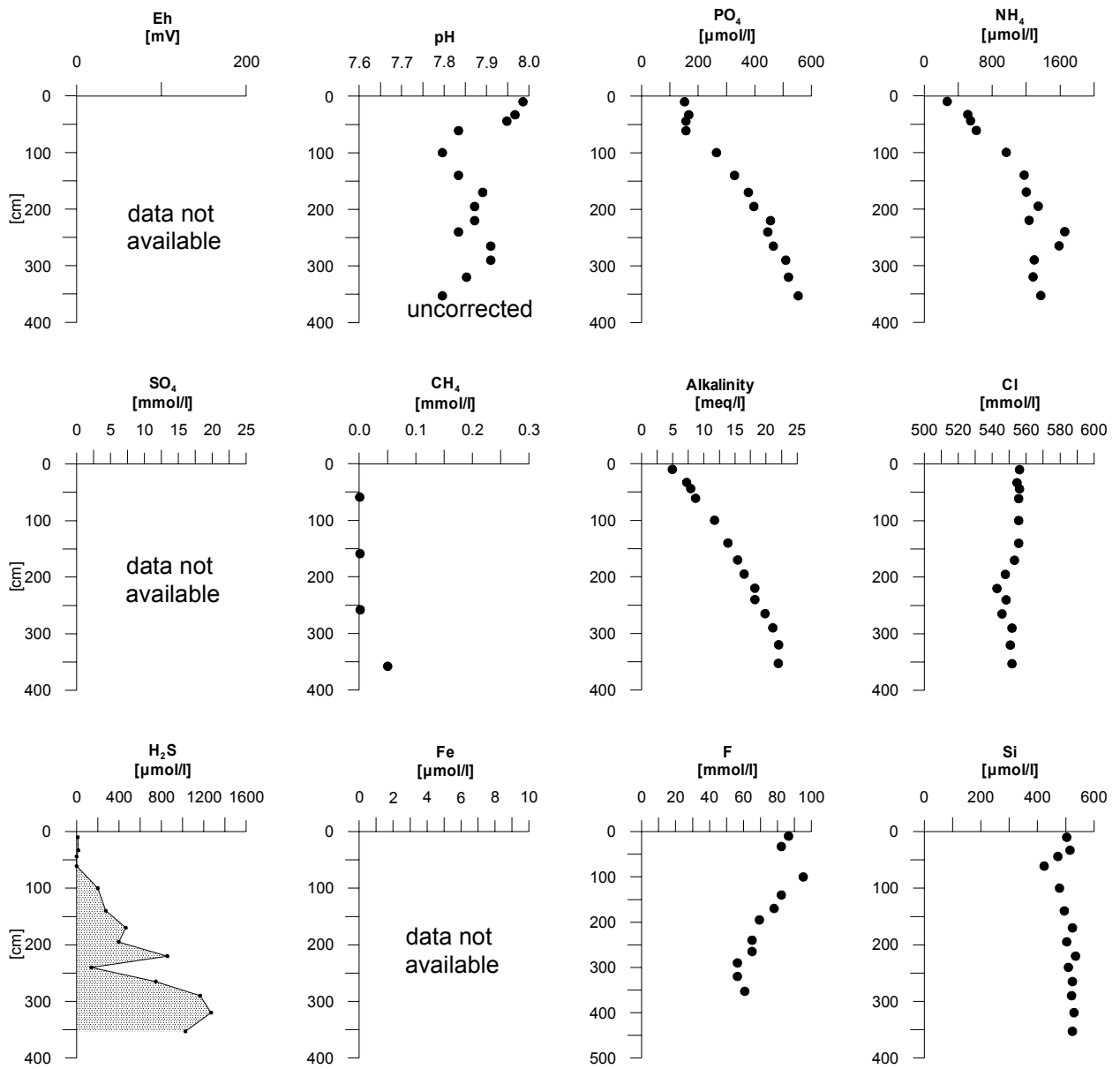


Figure 5.5.2.1.2: Pore water profiles of piston core M 54-13.

M 54-14 SL
Trench / Nicaragua (5412 m)

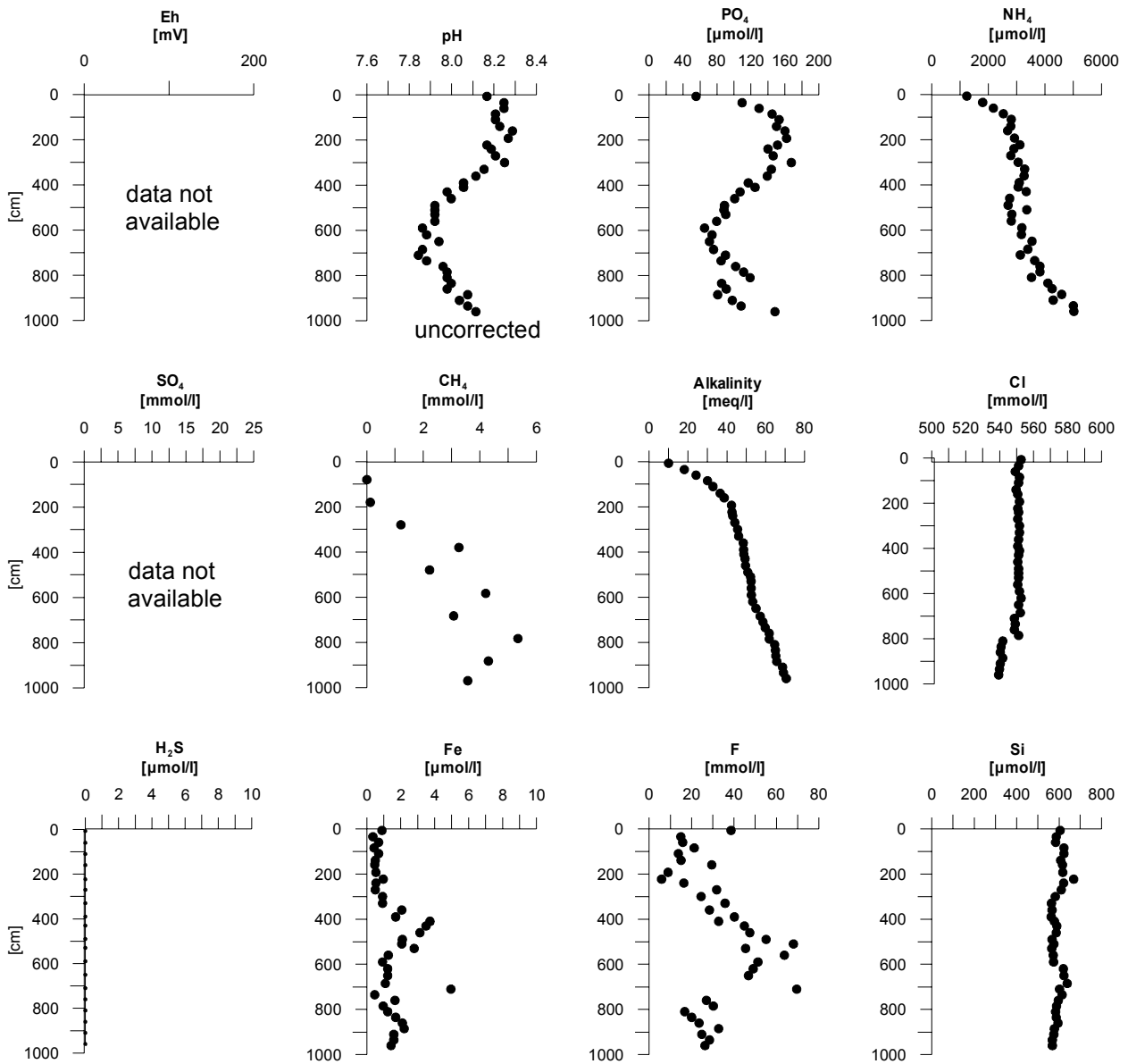


Figure 5.5.2.1.3: Pore water profiles of gravity core M 54-14.

M 54-6 SL
Trench / Nicaragua (5320 m)

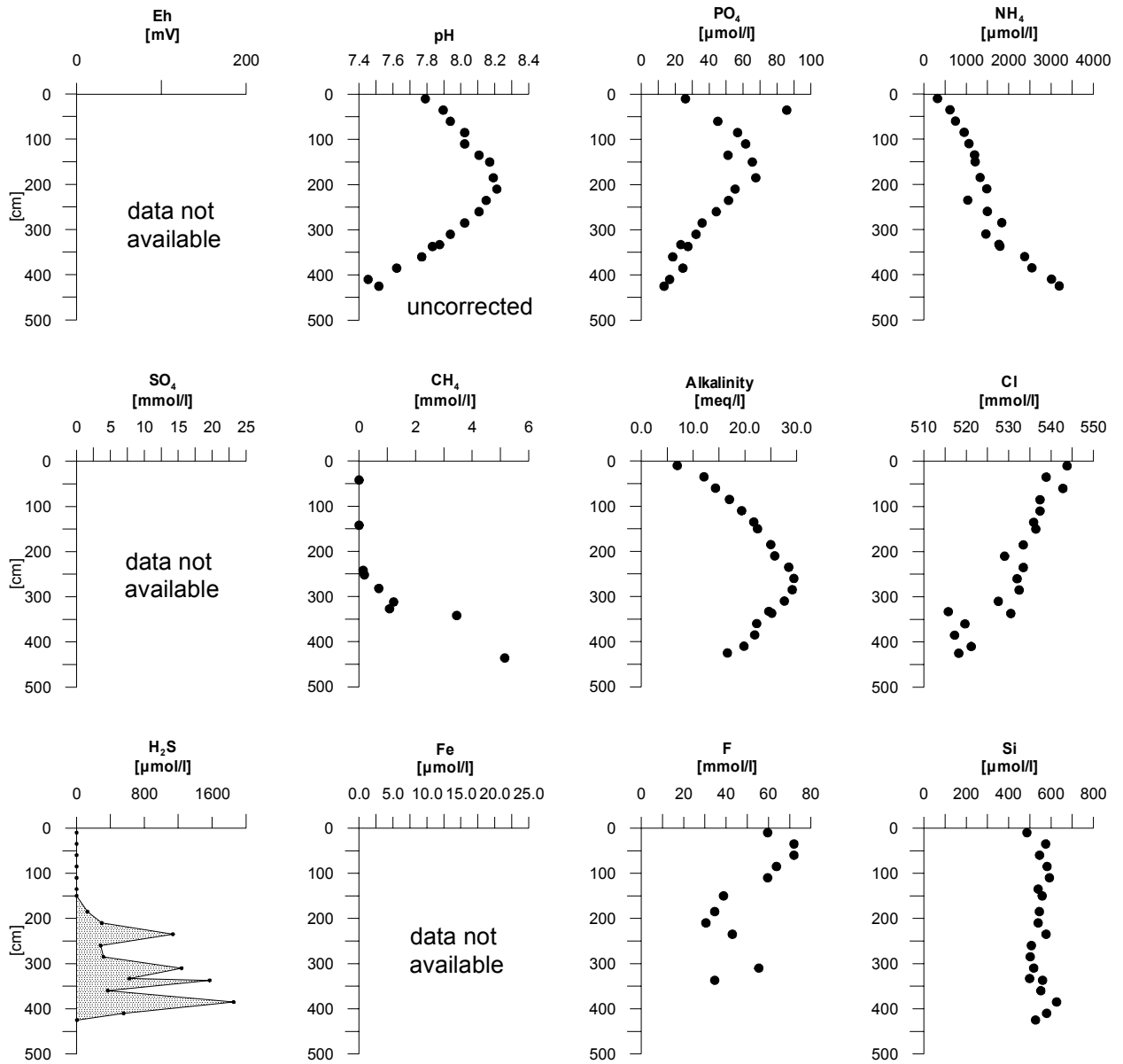


Figure 5.5.2.1.4: Pore water profiles of gravity core M 54-6.

5.5.2.2 Smooth Plate segment off Nicaragua and Northern Costa Rica

Mound Culebra

Mound Culebra with a diameter of roughly 0.8 nautical miles and an elevation of more than 100 m above the surrounding sea floor is the largest mound structure visited during M 54. On total, 11 gravity cores and 3 MUCs (2 TV-guided) were sampled here (see Figure 3.1.2). Since the TV-MUC did not strike active vent sites at this location the most intriguing information comes from the gravity cores. The pore water profiles plotted in Figures E-G summarize the variability of fluid compositions on the plateau and along the slope of the mound.

On top of Mound Culebra there is as well evidence for active flow of methane rich fluids from below almost reaching the top of the sediment surface at M 54-29 (Figure 5.5.2.2.1) as for seawater penetrating the sediments surface marked by a number of constituents almost remaining on bottom water levels over the whole length of the core (Figure 5.5.2.2.2). The sediments showing the observed in- and outflow pattern might belong to a more complex hydrological system. Interestingly, pore waters at the active vent sites (M 54-27 and 29) do not show prominent variations in chlorinity, which, in turn, could be observed at stations (M 54-17 and 32; Figure 5.5.2.2.3) on the slope and along a fault line (M 54-116; TOBI observation). The low-chlorinity fluids, however, could only be detected at depth in the gravity cores covered by sediments with normal saline pore waters.

There was no indication for ascending fluids reaching the sediment surface in the slope region of Mound Culebra. Summarizing the concentration profiles of alkalinity, hydrogen sulfide, and ammonia of all gravity cores of the Mound Culebra area (Figure 5.5.2.2.4), it is possible to categorize them into more or less three groups. The recharge group (1) has no hydrogen sulfide and very low alkalinity / ammonia concentrations. In the H₂S discharge group (2) we find extremely high values of alkalinity and hydrogen sulfide together with low ammonia concentrations. Finally, the low chloride group (3) has intermediate concentrations of alkalinity / hydrogen sulfide and the highest amounts of ammonia.

The main characteristics of the H₂S discharge group are high advection rates at least of methane (driving high concentrations of alkalinity and hydrogen sulfide almost to the sediments surface) together with a nutrient depletion can possibly be best explained by the occurrence of gas venting at certain locations on the plateau. Unfortunately, significant amounts of methane could only be determined at M 54-27. Most of the methane at M 54-29 has probably escaped during core retrieval.

Mound 10

Mound 10 is a much smaller structure southeast of Mound Culebra (see Figure 3.1.3). Pore water samples were collected only during M 54/3A. Below we show the results of a TV-MUC and a gravity corer deployment (Figure 5.5.2.2.5-5.5.2.2.6). The TV-MUC was placed on a vent site close to the top of the structure. The results plotted in Figure 5.5.2.2.5 are from two tubes (D and E) sampled at the same deployment. The differences in alkalinity, chlorinity and hydrogen sulfide profiles are indicative for the small-scale variability in vent-affected sediments.

The general pattern is that methane rich and nutrient poor fluids ascend to the sediment surface, where the methane is oxidized by sulfate to produce CO₂ (alkalinity) and hydrogen sulfide. The high peaks of nitrate may be indicative for the occurrence of H₂S-oxidizing bacteria (i.e. *Beggiatoa*). A similar pattern, even though at a greater sediment depth, can be observed at station M 54-133 at the western slope of the mound. Hydrogen sulfide concentrations are continuously high over the whole length of the core. The main zone of methane oxidation is between 2.5-3 mbsf.

**M 54-29 SL
Mound Culebra
Centre (1529 m)**

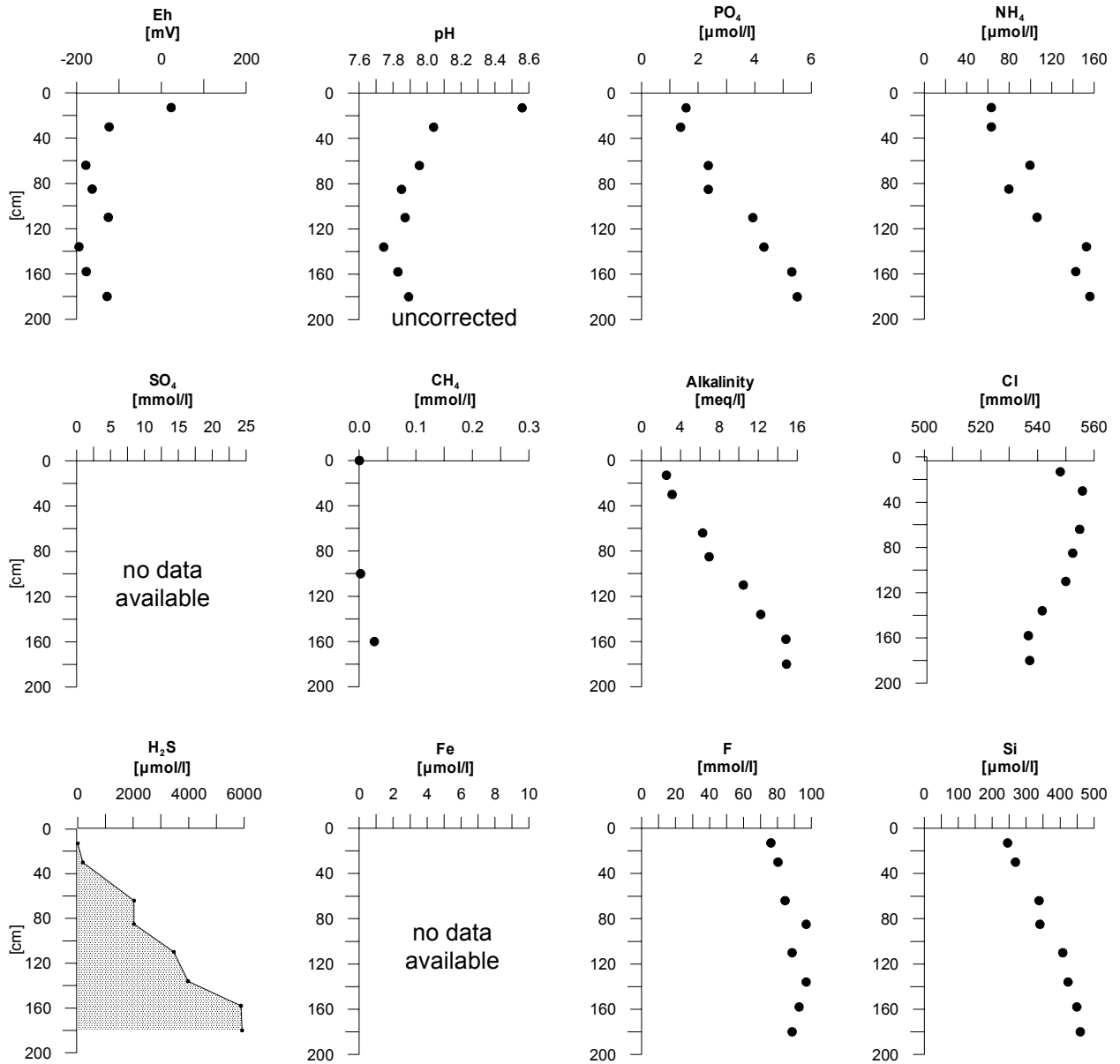


Figure 5.5.2.2.1: Pore water profiles of gravity core M 54-29.

**M 54-21 SL
Mound Culebra
W-Centre (1548 m)**

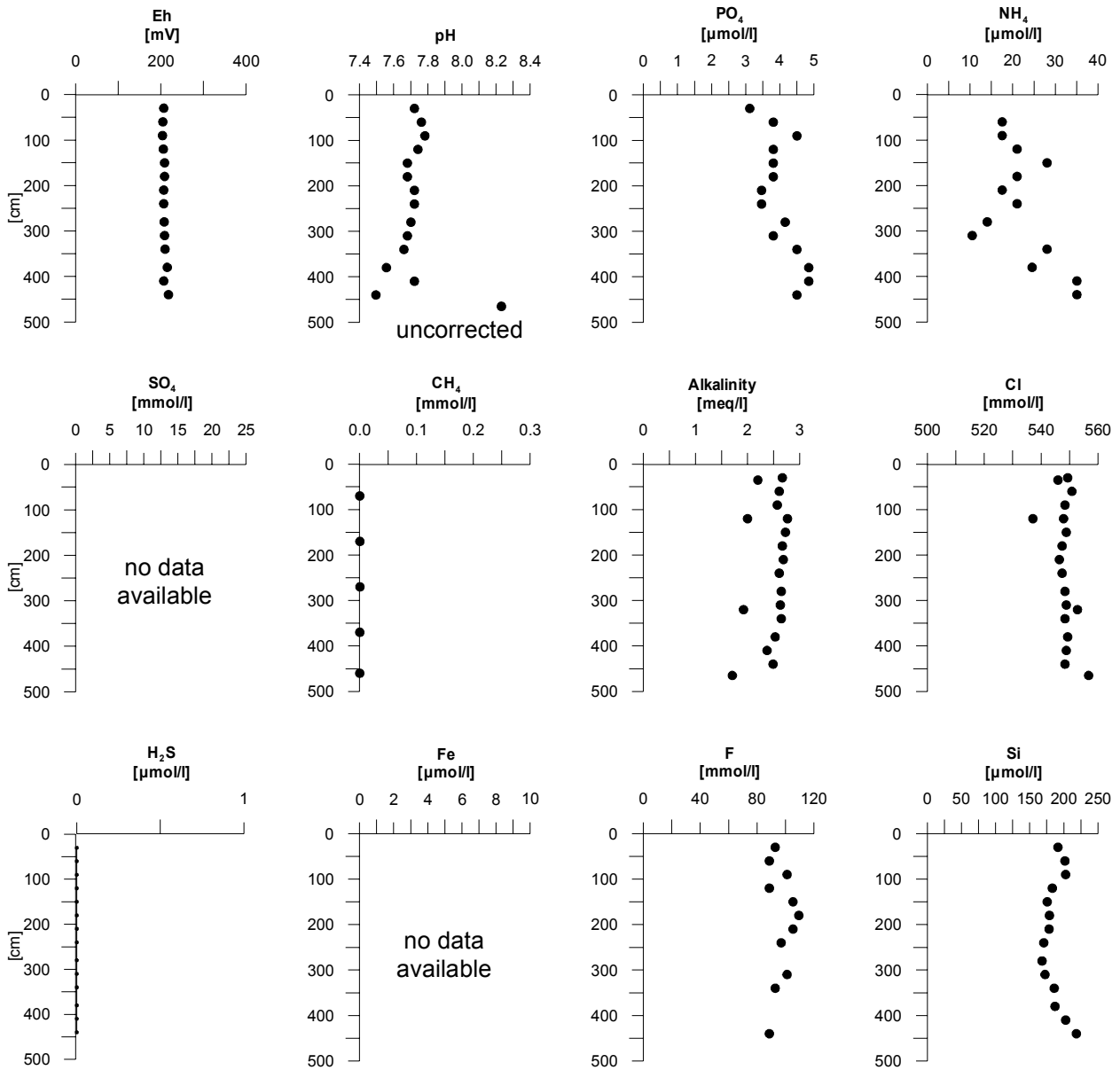


Figure 5.5.2.2.2: Pore water profiles of gravity core M 54-21.

M 54-32 SL
Mound Culebra
NW-Slope (1656 m)

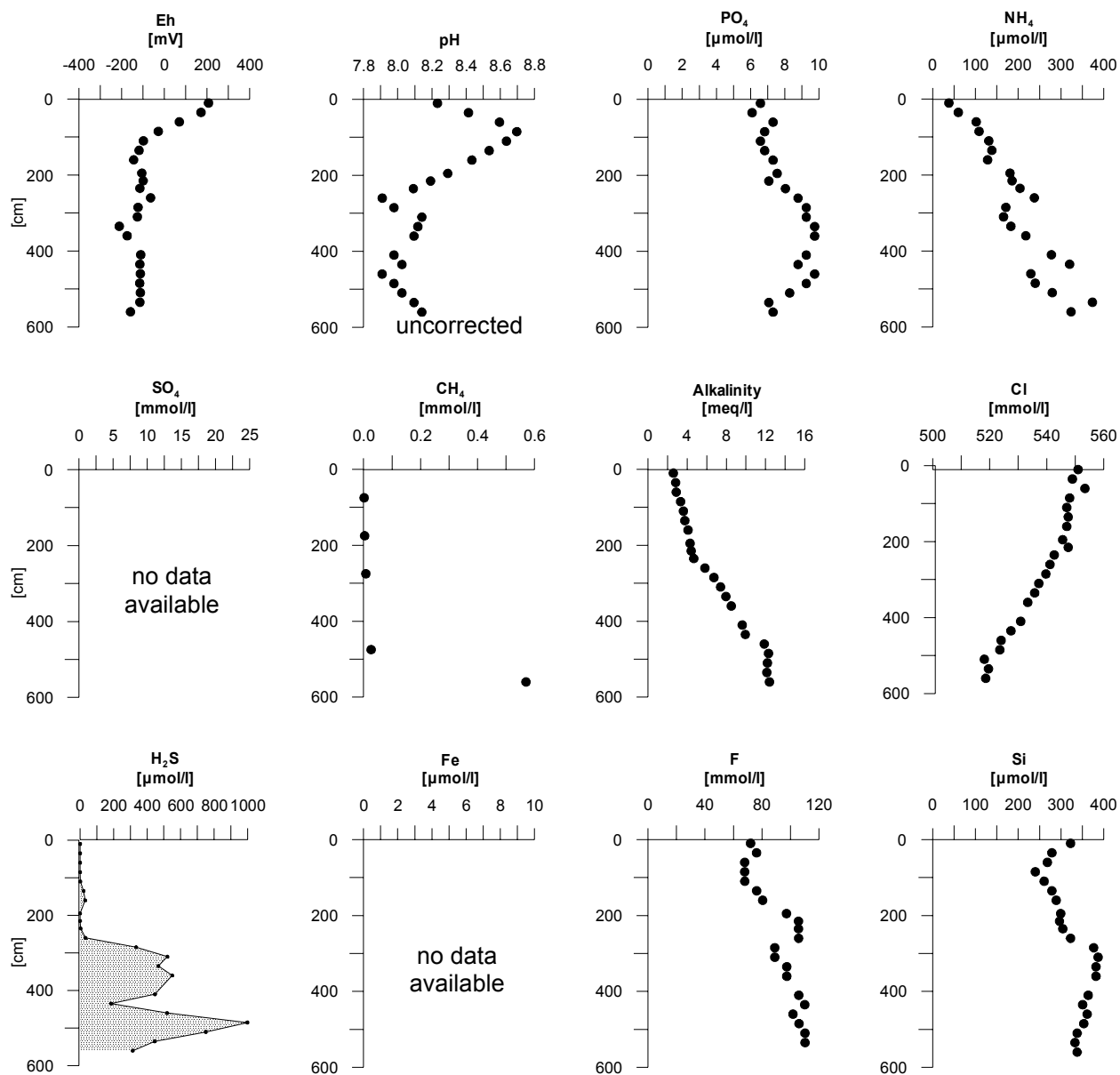


Figure 5.5.2.2.3: Pore water profiles of gravity core M 54-32.

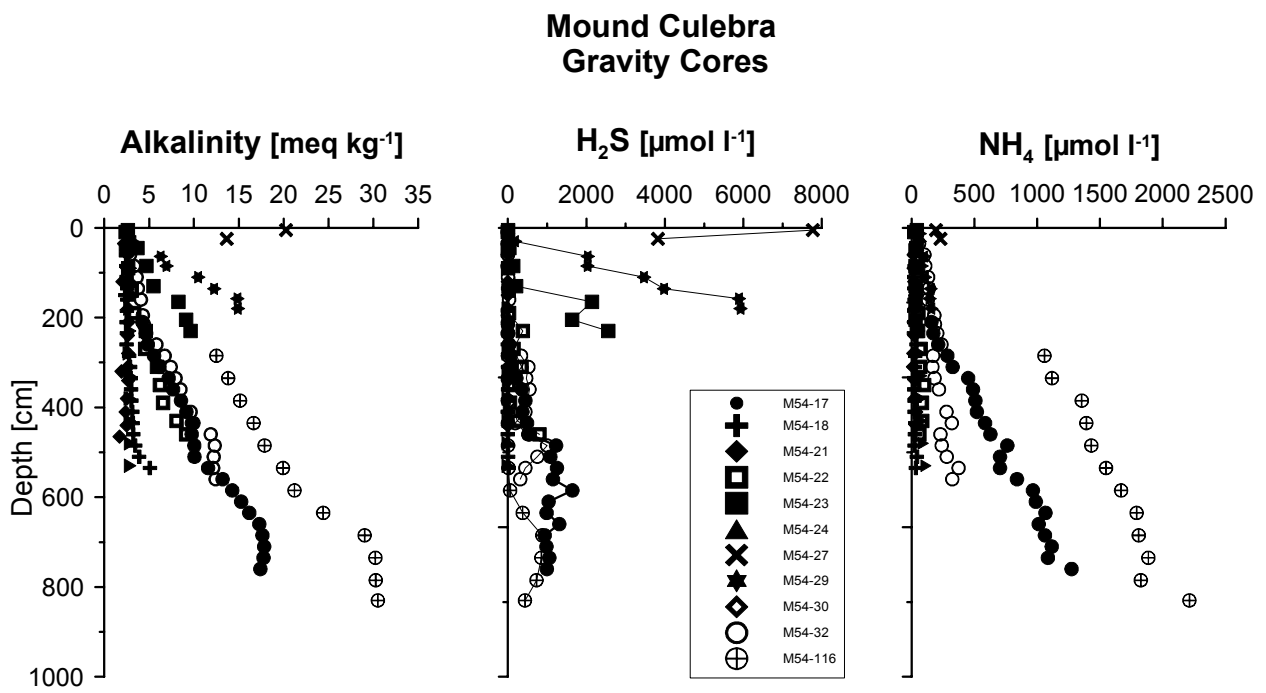


Figure 5.5.2.2.4: Selected pore water profiles of all gravity cores at and around Mound Culebra.

**M 54-123/1D-E TV-MUC
Mound 10
Top (2268 m)**

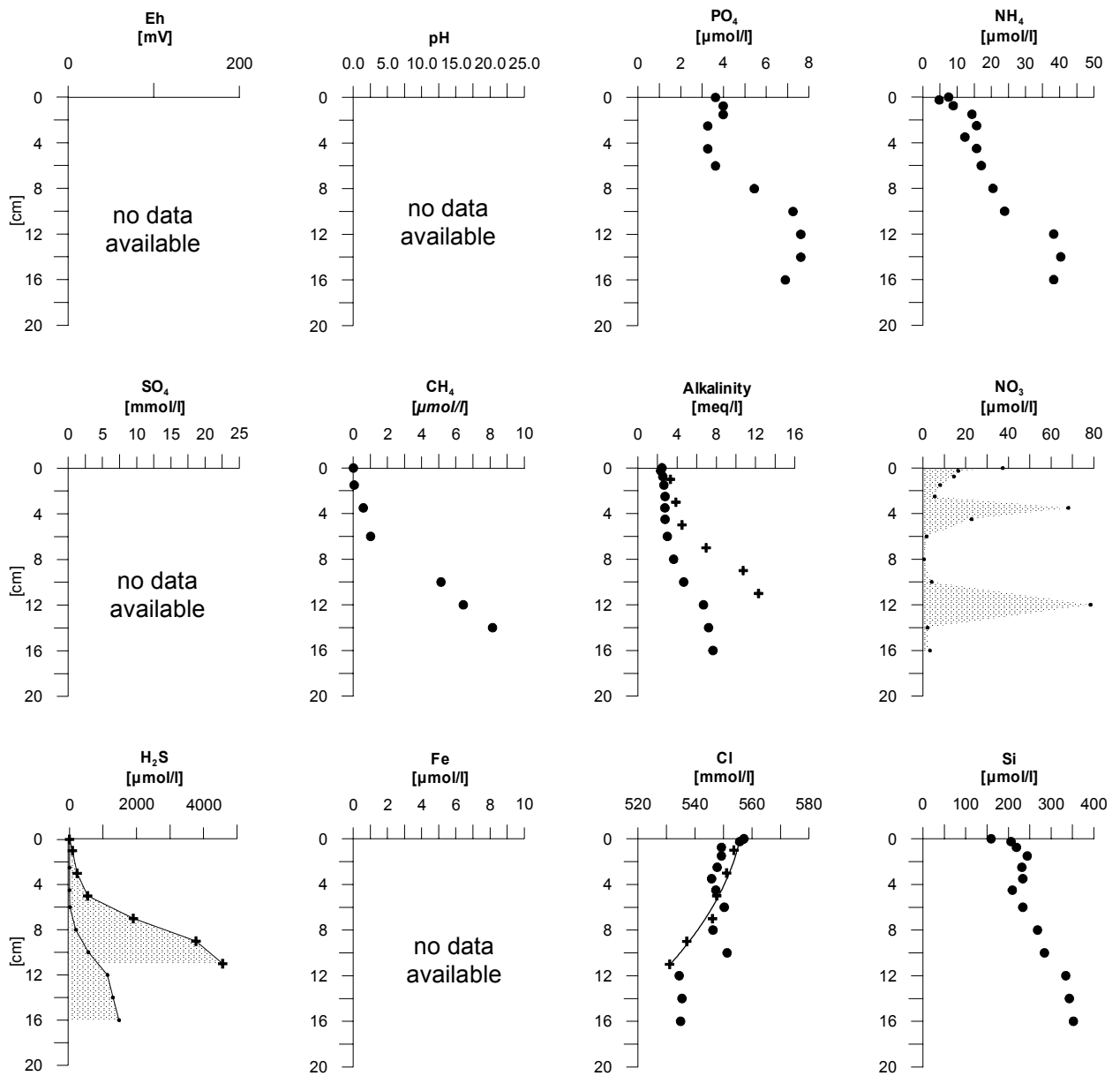


Figure 5.5.2.2.5: Pore water profiles of TV-MUC M 54-123/1.

**M 54-133 SL
Mound 10
W-Slope (2298 m)**

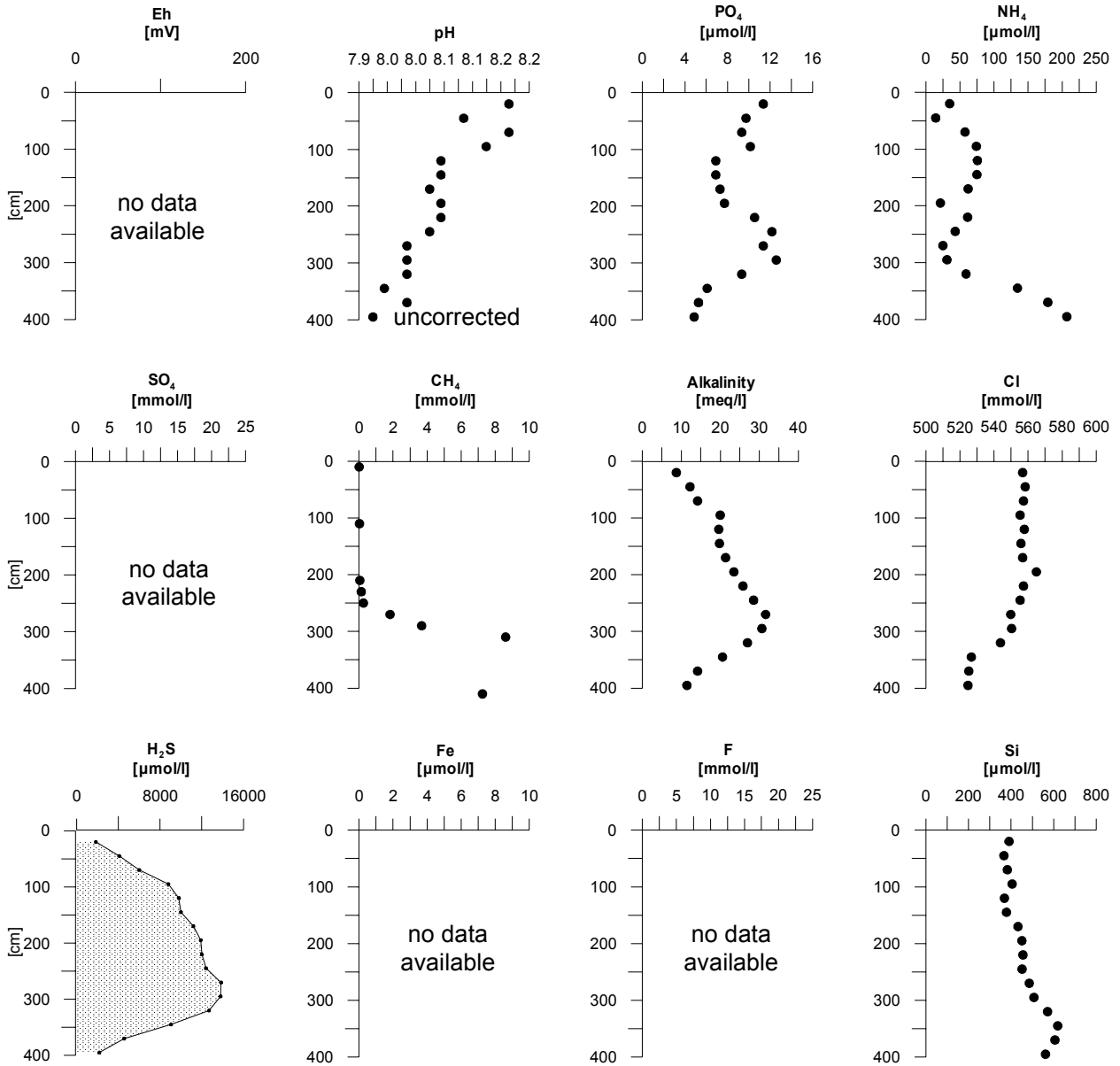


Figure 5.5.2.6: Pore water profiles of gravity core M 54-133.

5.5.2.3 Rough Plate segment off Costa Rica

Jaco Scarp

An extensive pore water program was conducted around this area of seamount subduction (Figure 3.2.3). The cores sampled at the plateau show a similar variety in pore water geochemistry as it was observed at Mound Culebra pointing to locally ascending methane-rich fluids (Figure 5.5.2.3.1) and recharge locations with concentrations of the main constituents only slightly above bottom water levels (Figure 5.5.2.3.2). However, pore waters at both types of locations have very low nitrogen and silicate inventories, pointing to the fact that ascending fluids are depleted in nutrients. Due to the tectonic stress of seamount subduction a fault pattern was created, which probably allows fluid circulation in hydrologic system within the upper-plate sediment cover on top of the seamount. At the slope below the headwall and along the slide mass the geochemical situation is quite different, because older, consolidated sediments are exposed at the seafloor. Extended vent fields could be observed on several OFOS-tracks (section 5.1) and methane concentrations in the water column are very high in this region (section 5.6.3.1).

The main pore water information comes from only two short gravity cores (M 54-52 and 159; Fig. 5.5.2.3.3), because the consolidated sediment was difficult to sample and pore water processing was only possible in certain layers. In consistency to the OFOS observations and the methane enrichments in the water column the sediments contain high amounts of methane close to the sediment surface. In addition, at M 54-159 a slight chloride depletion could be detected. The very high concentrations of ammonia (up to 6000 $\mu\text{mol/l}$ at M 54-52) are strongly characteristic for the origin and thus the state of burial of sediments. The observed ammonia levels are comparable to those of upper plate sediments drilled on ODP Leg 170 (Kimura et al., 1997)

Mound Quepos

Mound Quepos is a structure located north of Parrita Scar and probably associated to a regional fault system (Figure 3.2.2). Seven gravity cores on Mound Quepos were sampled during M 54/2. Figures 5.5.2.3.4 and 5.5.2.3.5 are characteristic for the two end member types of the pore water geochemistry found there. At the top of the structure (Figure 5.5.2.3.4) the sediments obviously experienced only a weak diagenetic overprint. Methane and hydrogen sulfide are absent to a depth of about 4 mbsf.

Thus, there is no evidence for fluid advection at this site. At the stations further to the north and west, the sediments are increasingly affected by fluid flow. At station M 54-80 (Figure 5.5.2.3.5) there is clear evidence for the existence of a low-chlorinity fluid. Over a depth of 6 m the chlorinity decreases by about 30%. The cross in the chloride-profile indicates a sub-sample from a fluid channel (see section 5.4), which is further depleted in chloride as the surrounding sediment. In contrast to many other fluid affected sites, however, the pore fluids are not significantly depleted in nutrients.

Mound 11 and 12

Mounds 11 and 12 on the continental slope off S-Costa Rica at a water depth of about 1000 m are two small, closely adjoining, smooth mound structures with only a slight elevation above the surrounding seafloor. In terms of venting these otherwise inconspicuous elevations are among the most active locations in the whole working area, which resulted in a high sampling density (see Figure 3.2.3). One of the most interesting gravity corer was retrieved closely the center of Mound 11 (Figure 5.5.2.3.6). The lowermost 20 cm of the 2.30 m long core consisted of massive gas-hydrate layer. According to subsequent gas-hydrate dissolution pore water constituents are strongly diluted at this depth.

At about 1.5 mbsf the zone of methane oxidation is located, which can be deduced by the peaks in alkalinity and hydrogen sulfide. Interestingly, all pore water constituents show that the upper 1.2 m of the sediment are completely mixed. The mechanism driving the pore water mixing is not known yet, but it might also indicate a non-steady-state situation of pore water geochemistry caused by a recent upward movement of the methane oxidation front.

Two vent locations at Mound 11 (M 54-137/1 and 138) could be sampled very successfully by means of the TV-MUC (Figure 5.5.2.3.7 and 5.5.2.3.8). At both locations finely dispersed gas-hydrate was present at least within the upper 10 cm of the sediment, which is the reason for otherwise unusually high methane concentrations of more than 8-10 mmol/l.

In both cases methane oxidation takes place close to the sediment surface (peaks in alkalinity and hydrogen sulfide). An additional reaction front below the sampled depth at station M 54-137/1 is likely because of further increasing gradients of alkalinity and hydrogen sulfide. The most interesting feature might, however, be the chloride profiles. Especially, the exponentially shaped profile at M 54-138 may be useful to calculate the advection rate of the fluids, if the Cl-depletion is not caused by the dissociation of gas-hydrates, which in turn seems to be unlikely due to the inhomogeneous distribution of gas-hydrates. At station M 54-137/1 the Cl-depletion in the upper part of the profile might be explained by the dissolution of gas-hydrate, but this is contradictive to other pore water profiles (i.e. Si), which are not indicative for any dilution.

At Mound 12 again a large variety of gravity cores was retrieved from different locations ranging from not affected (Figure 5.5.2.3.9) to largely affected (Figure 5.5.2.3.10) by low chlorinity fluids. Most indications for active venting were preferably found at the western part of the structure, which seems to be a common feature for most of the sampled mounds.

At core M 54-97/2 we find again almost no deviations from bottom water concentrations for all constituents within the upper 1.5 mbsf above the zone of methane oxidation indicating homogeneously mixed pore waters. Since there was no gas-hydrate, the slight concave shape of the lower part of the Cl-profile would make a calculation of the advection rate possible at this site.

Station M 54-163/3 was obtained from a TV-MUC deployment at a vent site clearly marked by the occurrence of bacterial mats at the seafloor (Figure 5.5.2.3.11). Apart from the steepest gradients between bottom water and the sediment of alkalinity and hydrogen sulfide a significant, non-linear increase of the chloride concentration with depth could be observed. A suitable explanation for this observation is a recent formation of gas-hydrate below the sampled sediment depth. Again, the shape of the Cl-profile would enable us to calculate the advection rate of the fluid at this site.

BGR Slide

The so-called BGR-Slide is a small slide structure northeast of Jaco Scarp (see Figure 3.2.5 and section 5.4.1.3). The core was taken below the headwall of the slide, which has removed several tens of meters of sediment by one event. The core has a total length of 3 m of which about 2.5 m consist of old, consolidated material and the upper 0.5 m are deposited after the slide occurred. This transition is clearly visible in the pore water profiles of Figure 5.5.2.3.12. Since the sediment / pore water system at this site is expected to be diffusion controlled, it is possible to determine the timing of the occurrence of the slide by subsequent modeling of pore water profiles, which can be calibrated by stratigraphic methods.

References

Gieskes, J. M., Garno, T., and Brumsack, H. 1991 Chemical methods for interstitial water analysis aboard Joides Resolution. Ocean Drilling Program, Texas A & M Univ.

Grasshoff, K., Ehrhardt, M., and Kremling, K. 1997 Methods of seawater analysis. Verlag Chemie.

Ivanenkov, V. N. and Lyakhin, Y. I. 1978 Determination of total alkalinity in seawater. In: Bordovsky, O.K. and Ivenenkov, V. N. (eds.): Methods of hydrochemical investigations in the ocean, Nauka Publ. House, Moscow, 110-114 (in Russian).

Kimura, G., Silver, E., Blum, P., et al., 1997. Proc. ODP, Init.Repts., 170: College Station, TX (Ocean Drilling Program).

**M 54-48/2 SL
Jaco Scarp
Plateau (760 m)**

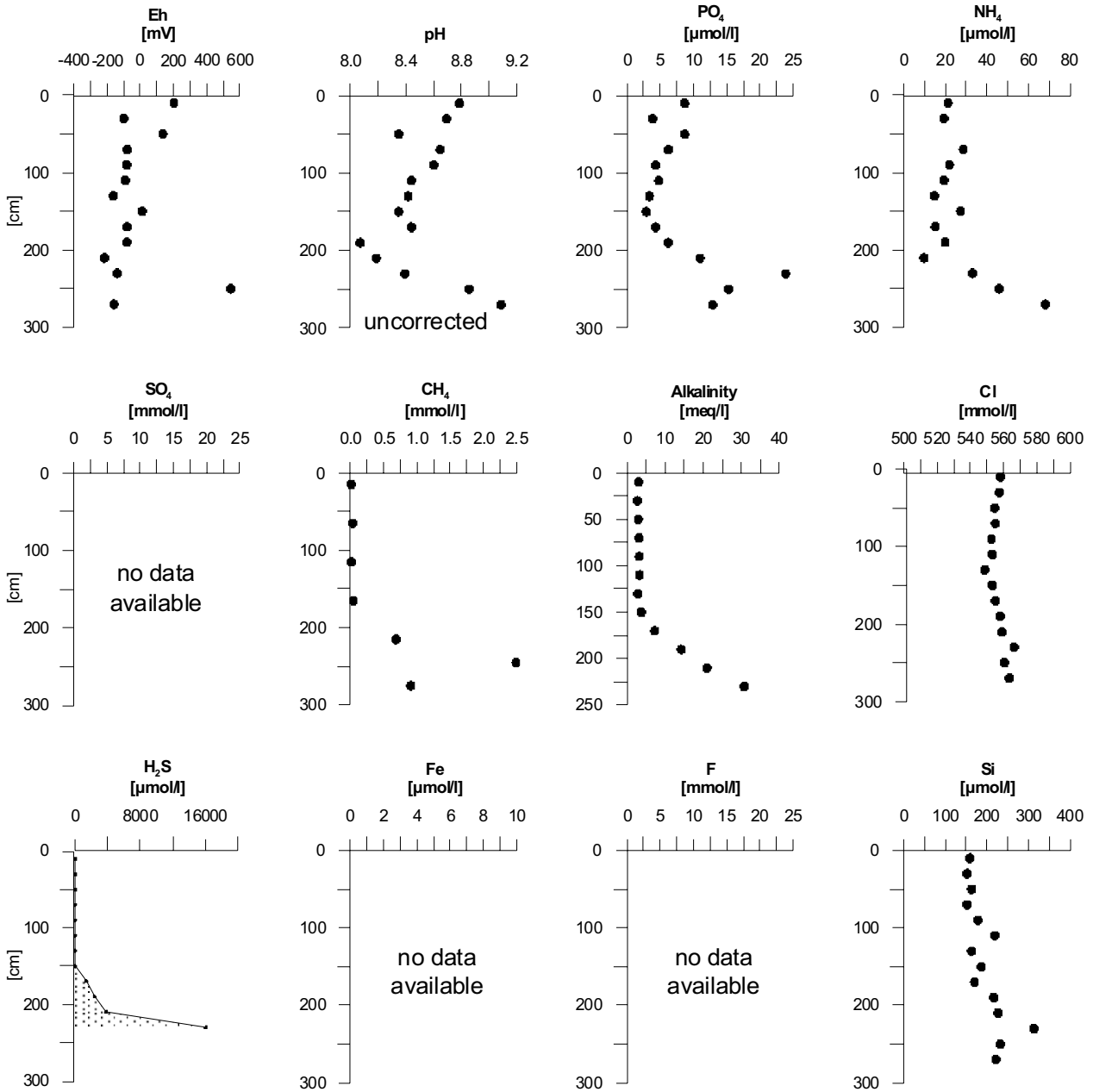


Figure 5.5.2.3.1: Pore water profiles of gravity core M 54-48/2.

**M 54-62/2 SL
Jaco Scarp
Plateau (825 m)**

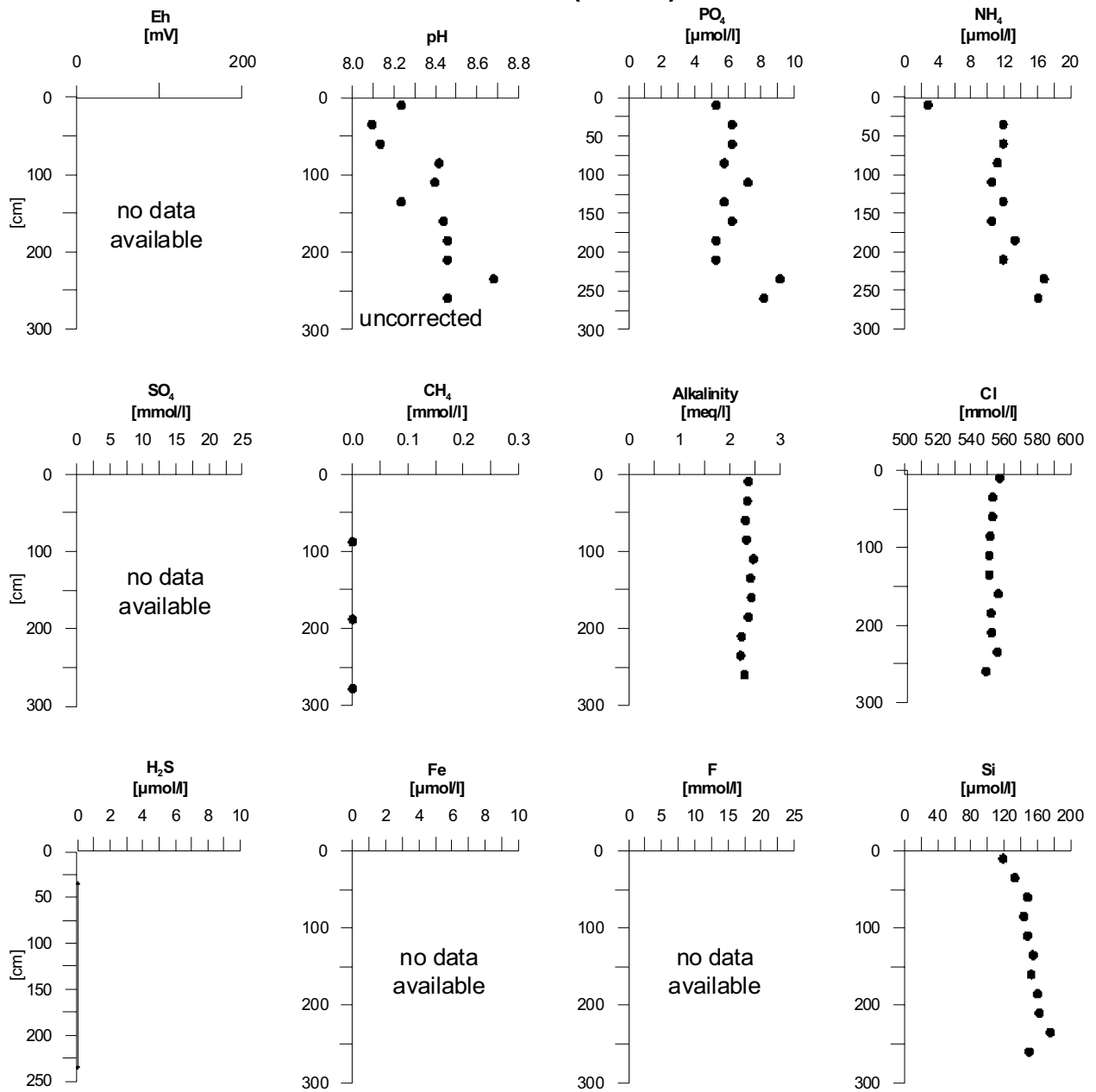


Figure 5.5.2.3.2: Pore water profiles of gravity core M 54-62/2.

**M 54-159 SL
Jaco Scarp
Slope (1800 m)**

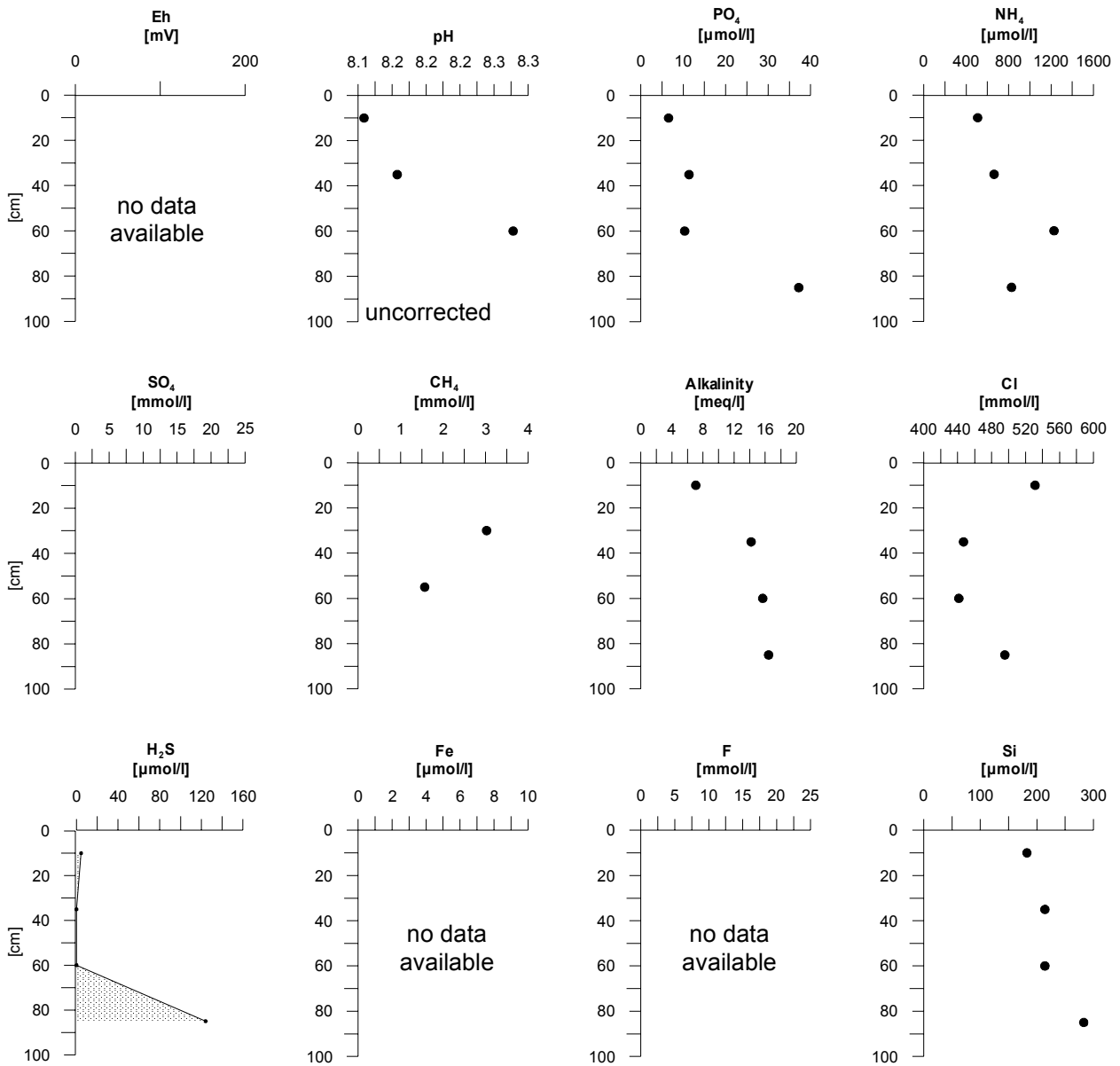


Figure 5.5.2.3.3: Pore water profiles of gravity core M 54-159.

M 54-75 SL Mound Quepos Top (1430 m)

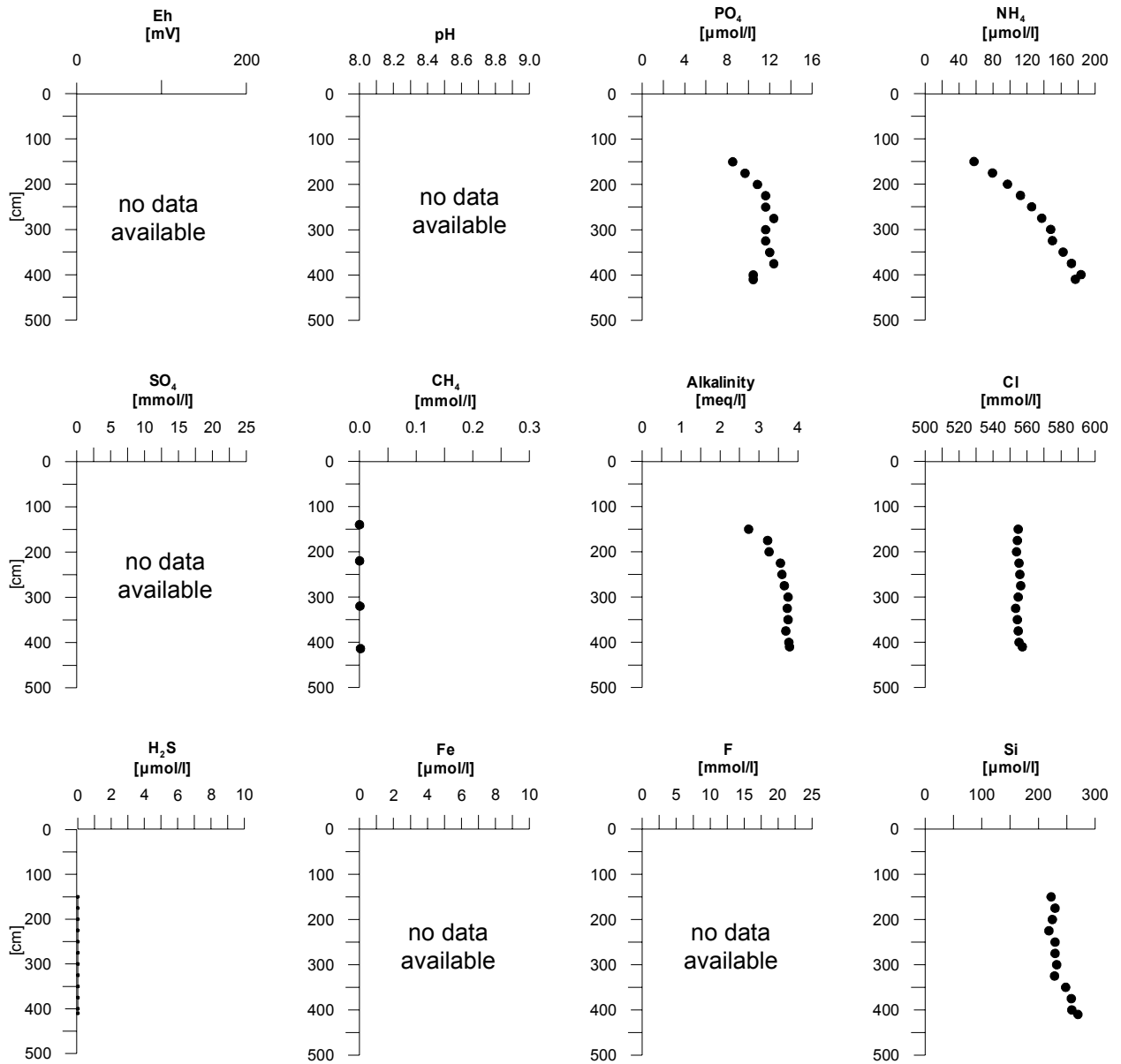


Figure 5.5.2.3.4: Pore water profiles of gravity core M 54-75.

**M 54-80 SL
Mound Quepos
W-Slope (1448)**

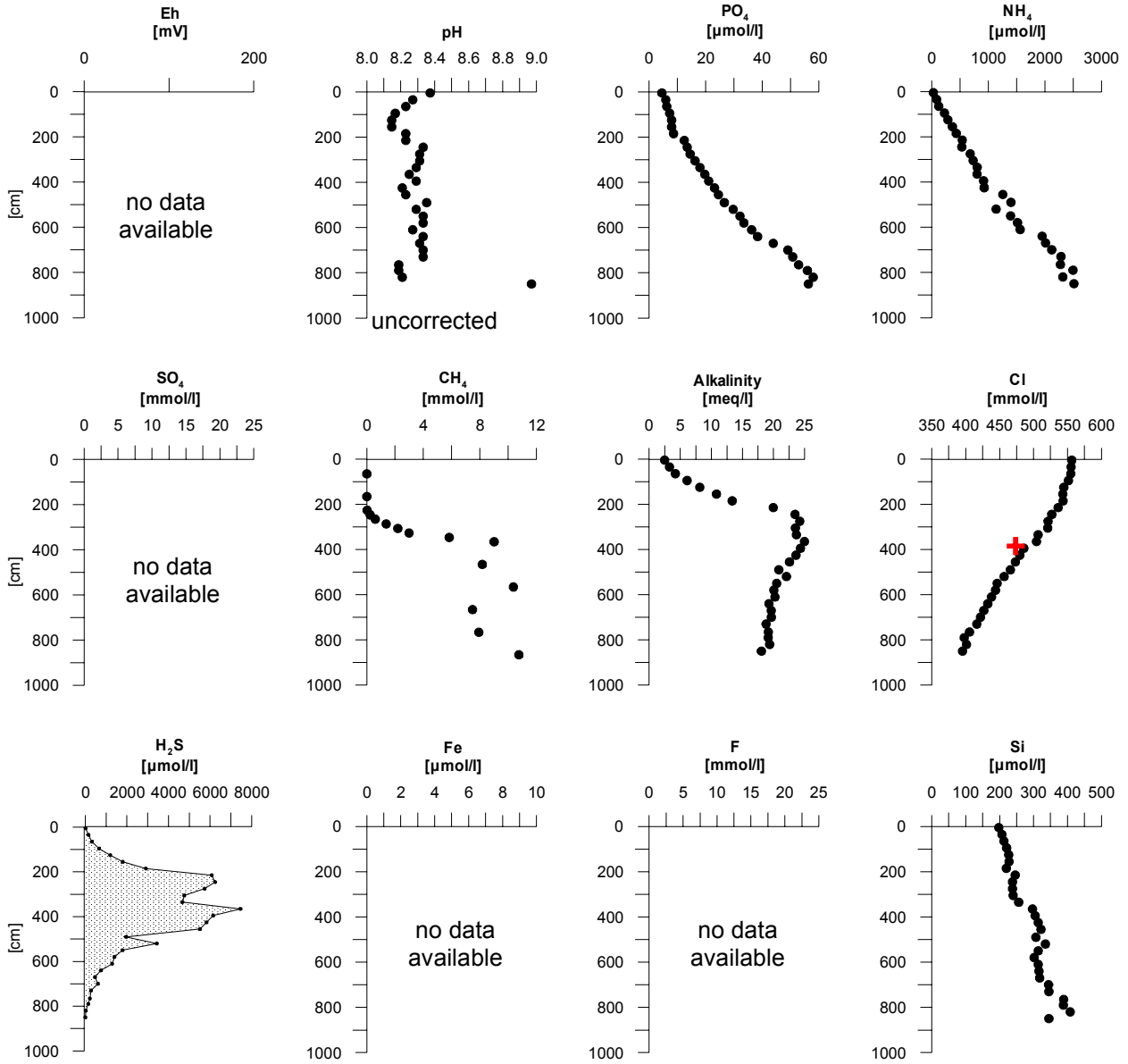


Figure 5.5.2.3.5: Pore water profiles of gravity core M 54-80.

**M 54-109 SL
Mound 11
SW-Slope (1000 m)**

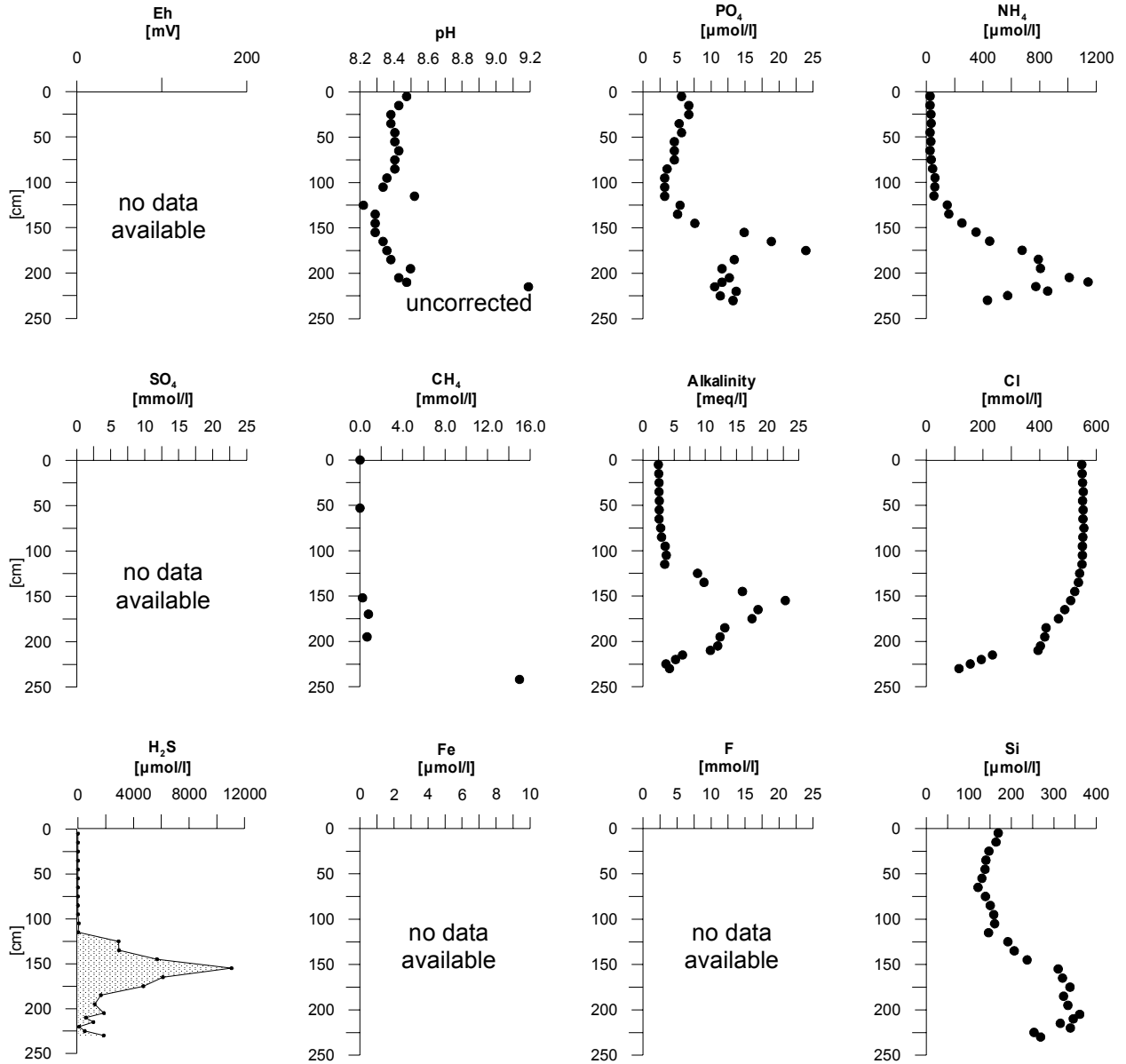


Figure 5.5.2.3.6: Pore water profiles of gravity core M 54-109.

**M 54-137/1 TV-MUC
Mound 11
Top (1024 m)**

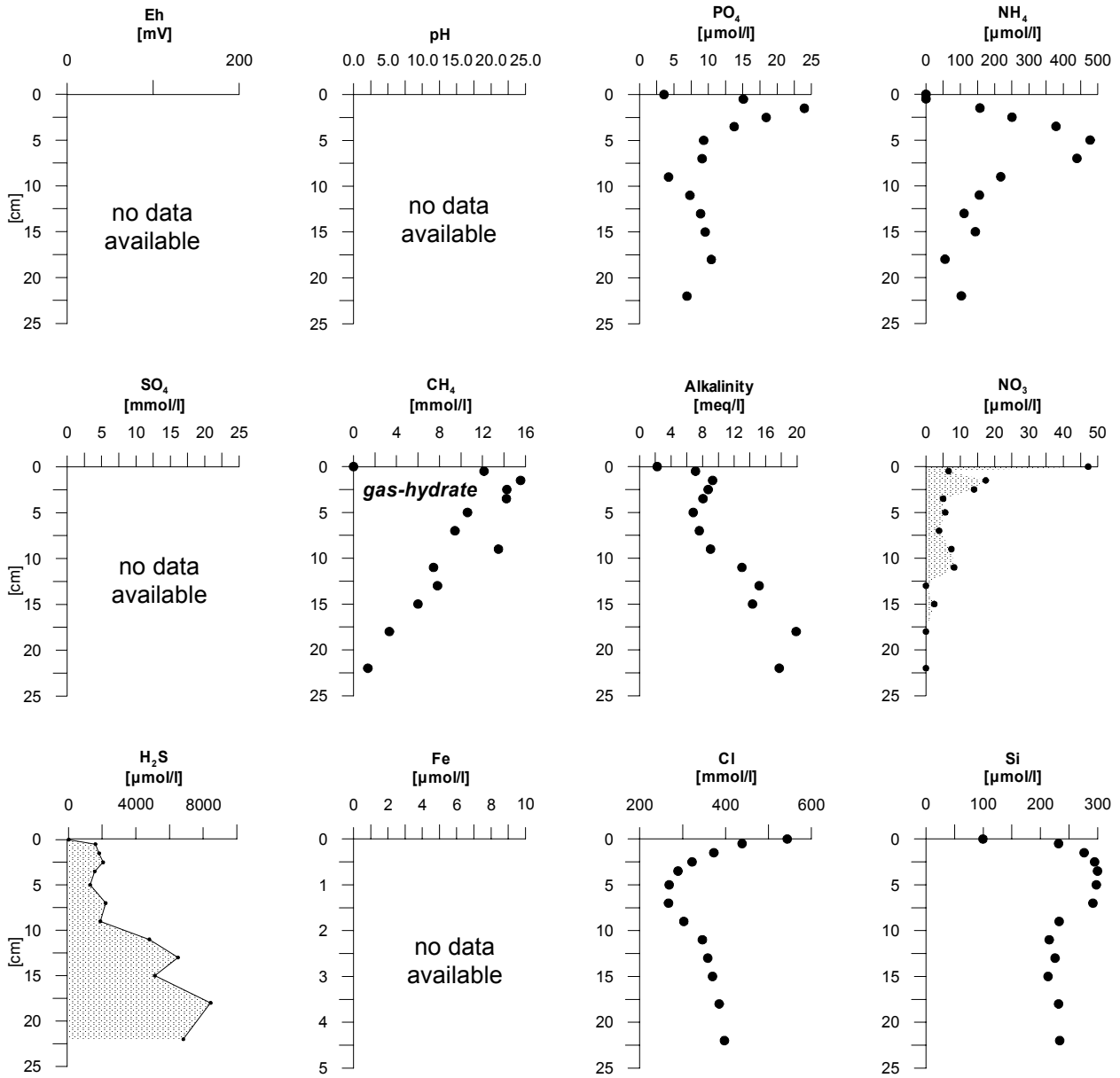


Figure 5.5.2.3.7: Pore water profiles of TV-MUC M 54-137/1.

**M 54-138 TV-MUC
Mound 11
Top (1024 m)**

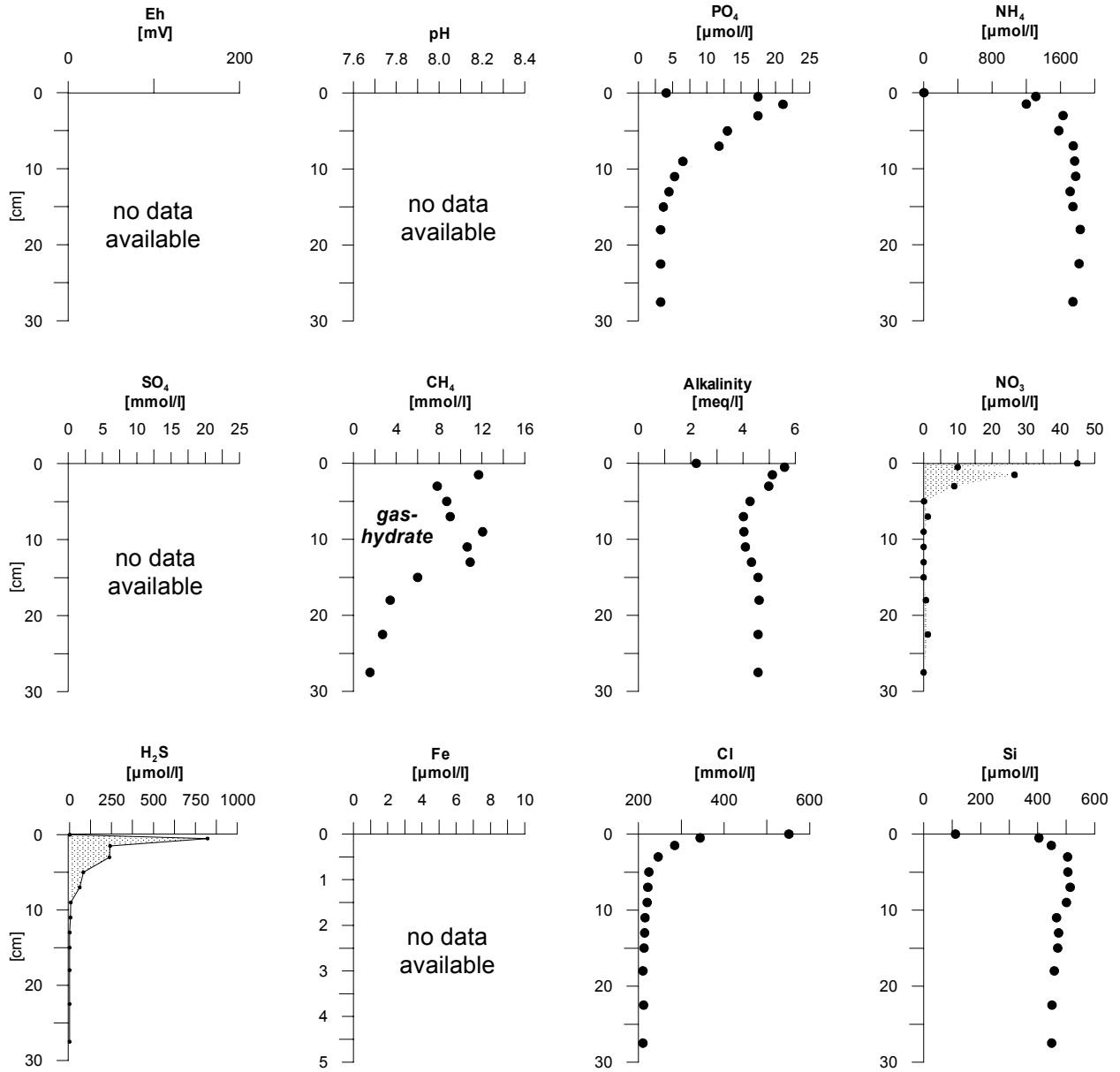


Figure 5.5.2.3.8: Pore water profiles of TV-MUC M 54-138.

**M 54-84 SL
Mound 12
S-Slope (980 m)**

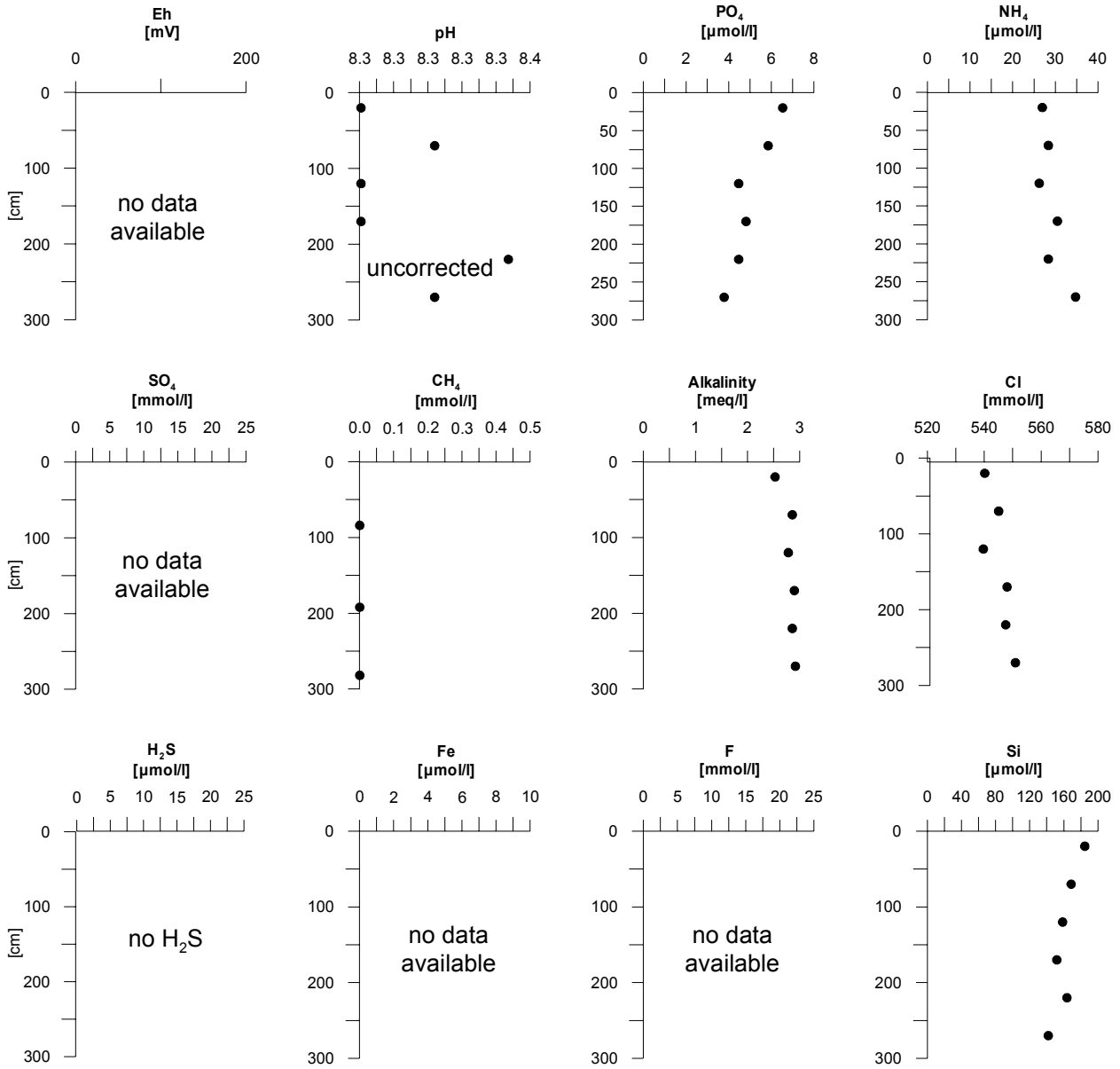


Figure 5.5.2.3.9: Pore water profiles of gravity core M 54-84.

**M 54-97/2 SL
Mound 12
W-Slope (1001 m)**

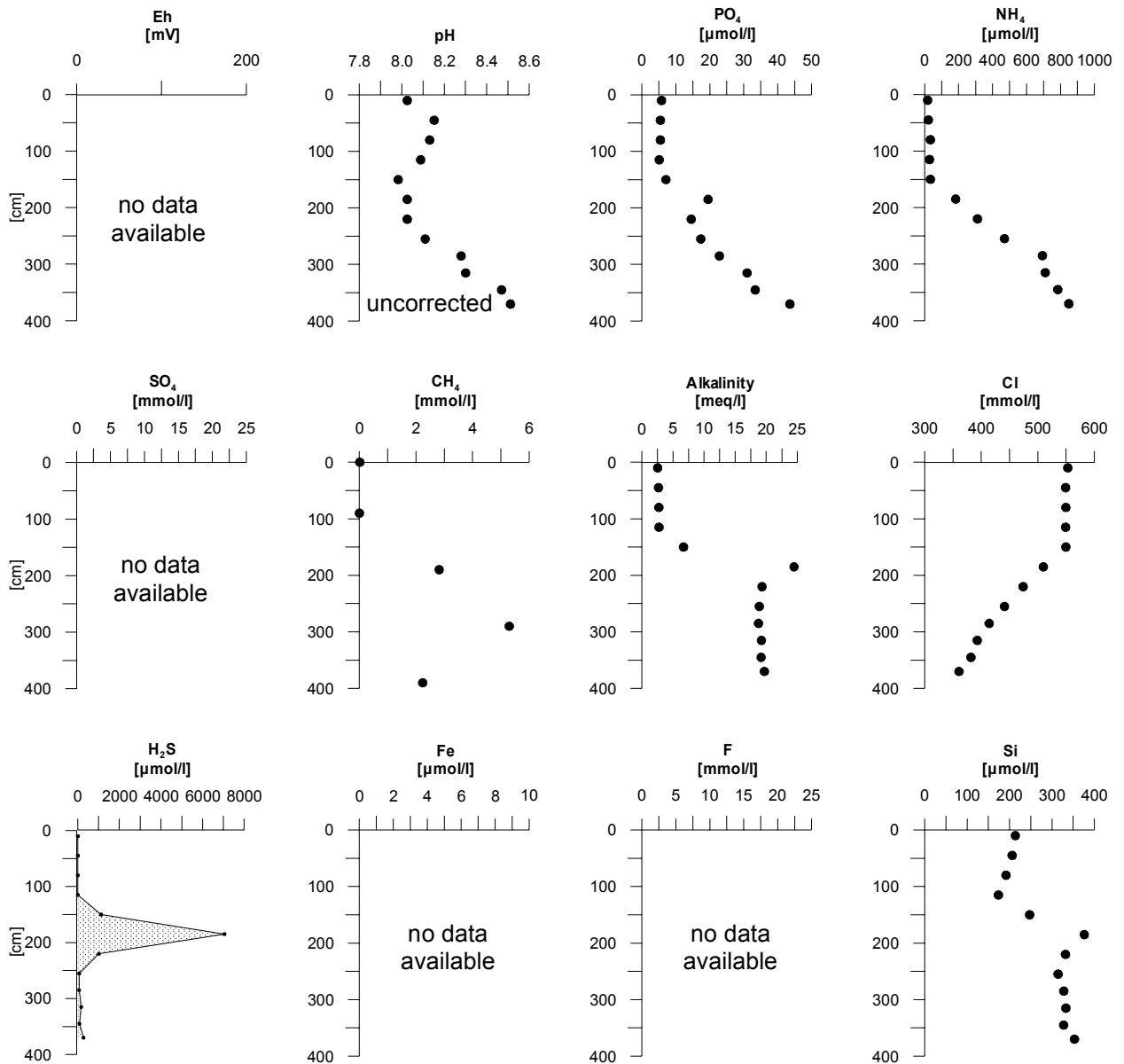


Figure 5.5.2.3.10: Pore water profiles of gravity core M 54-97/2.

M 54-163/3 TV-MUC SW Mound 12 (1024 m)

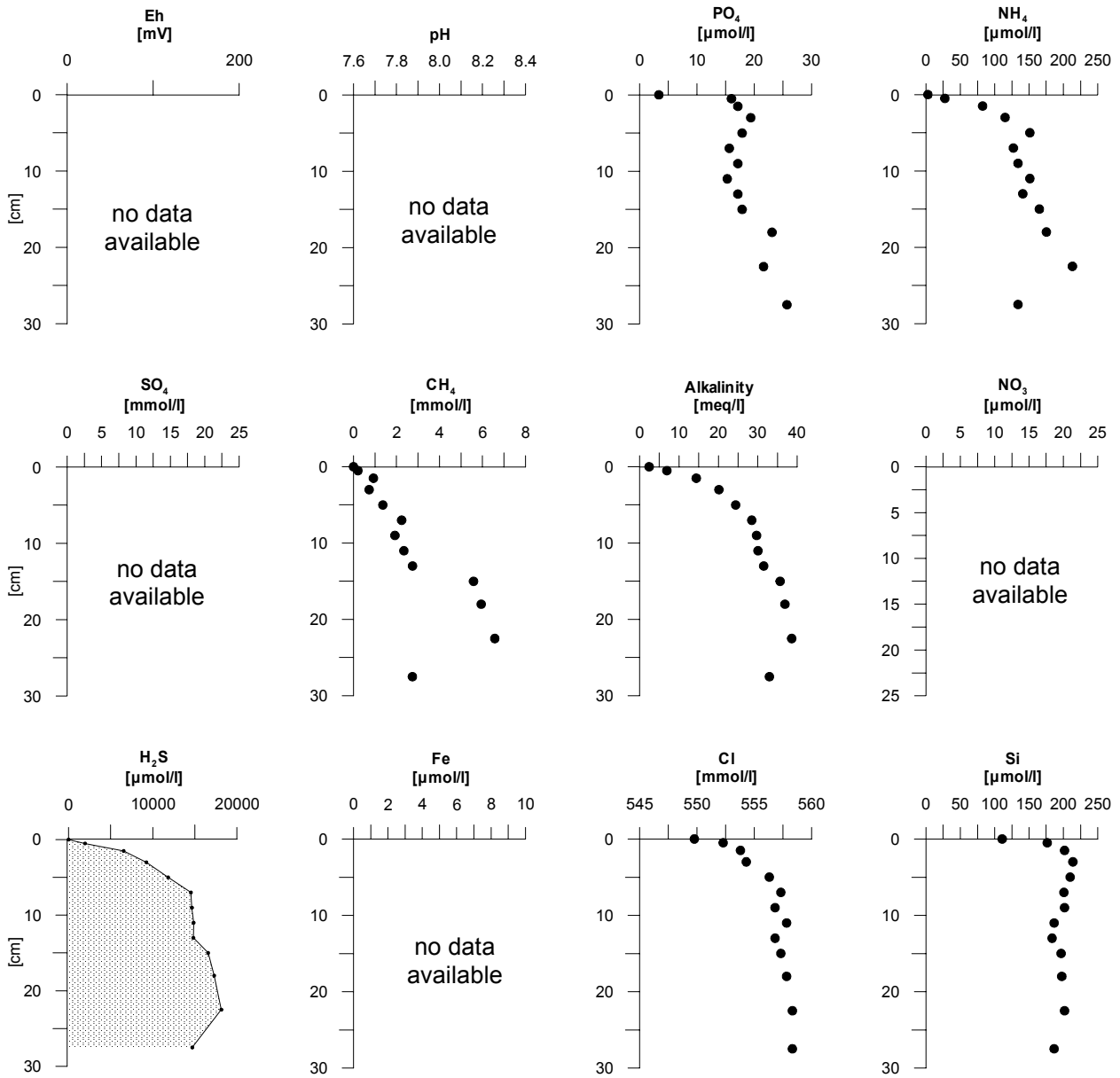


Figure 5.5.2.3.11: Pore water profiles of TV-MUC M 54-163/3.

**M 54-171 SL
BGR Slide
Below Headwall (611 m)**

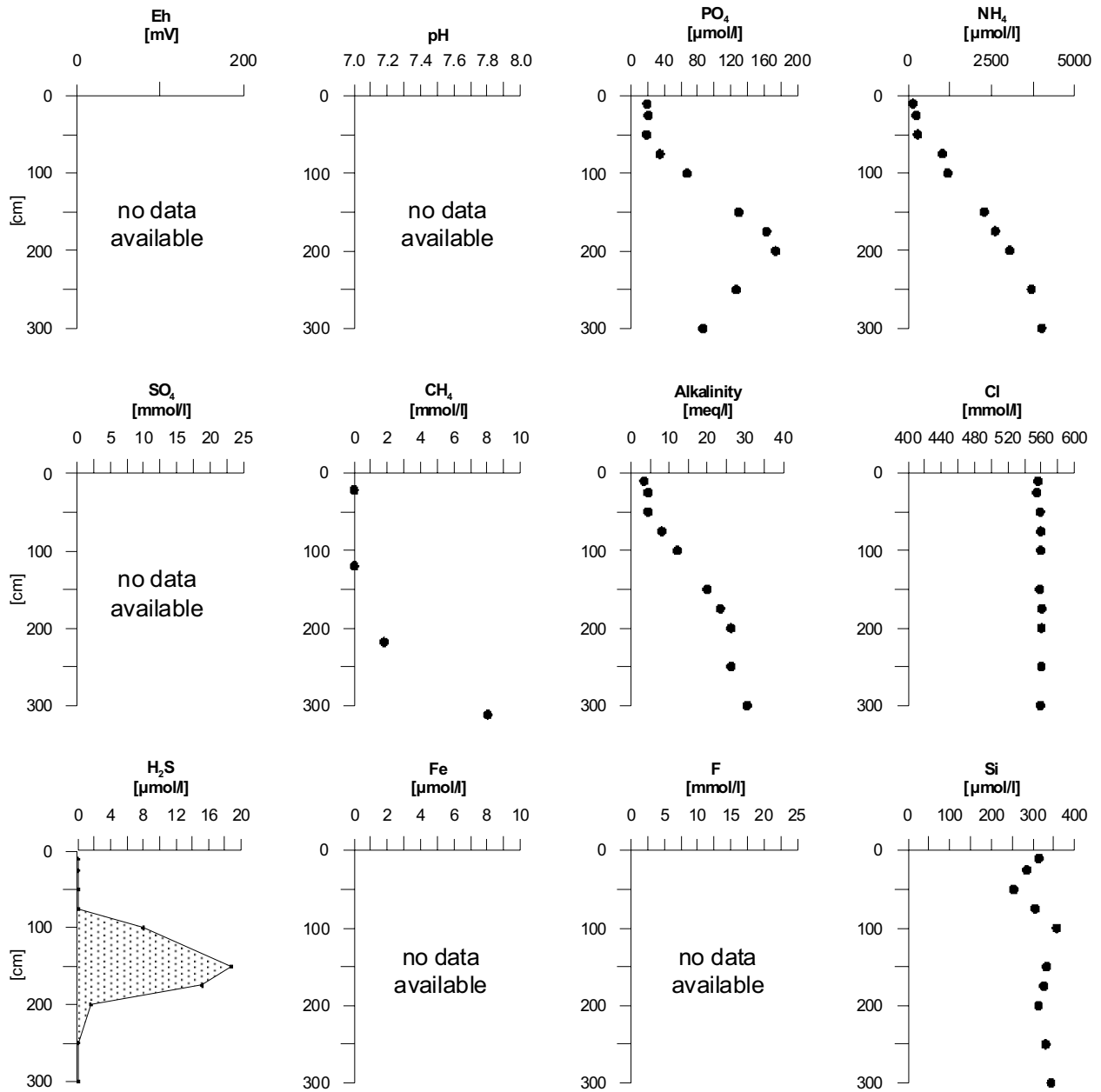


Figure 5.5.2.3.12: Pore water profiles of gravity core M 54-171.

5.6 Water column studies and methane distribution

(S. Mau, G. Rehder, J. Michels and K. Stange)

5.6.1 Introduction

The investigation of methane in the water column provides valuable insight in the processes of dewatering at active continental margins, because methane belongs to the cycled key components. Methane injection into the water column is just one process in the carbon budget at active seep sites. Due to its relatively short lifetime and its generally low background in deep waters this injected methane is ideally suited to locate currently active vent sites and the extension of the generated methane plumes. Measurements of the concentration in the water column and investigations of the isotopic composition of this methane will allow to yield info in the formation and further development of it as well as in the processes controlling the methane pathways in the water column. Hence, the intensive sampling program during Meteor54/2+3a was performed in the research area of the SFB 574 to gather more information on the methane cycle in the ocean.

5.6.2 Material and Methods

Water for methane analyses was sampled by a 24-bottle rosette including a CTD-unit (CTD), a bottom water sampler (BWS), and a video controlled vent sampler (VESP-MUC). CTD, BWS, and VESP-MUC were used for mapping the distribution of methane in the water column. The latter was also applied to measure outflow rates at one location over time. At all stations, samples were taken for shipboard analysis of methane and during M54/3a for oxygen measurements, too. Additionally, two sets of 250 ml water samples were filled into crimp cap glass bottles sealed with a butyl rubber septum and poisoned with 0.5 ml of a saturated HgCl₂-solution for further analysis in Kiel.

The oxygen content was determined using the method developed by Winckler as described in Grasshoff et al. (1997). Usually, three Niskin bottles were sampled twice to control reproducibility of the measurements. The oxygen sensor of the CTD-unit Neil Brown Mark III worked well throughout the cruise, but its results show higher values than the ones of the titration. Further comparison of the oxygen data with the density data will be performed to solve this problem.

For CH₄-analysis aboard, a modification of the vacuum degassing method described by *Lammers and Suess* [1994] was used [Rehder et al., 1999]. 1600 ml of water were injected into pre-evacuated 2200 ml glass bottles, which leads to almost quantitative degassing. The gas phase was subsequently recompressed to atmospheric pressure and the CH₄ mole fraction of the extracted gas was determined by gas chromatography. A Shimadzu GC14A gas chromatograph equipped with a flame ionization detector was used in connection with a Shimadzu CR6A Integrator. Nitrogen was used as carrier gas. Separation was achieved using a 4 m 1/8" SS column packed with Porapak Q (50/80 mesh) run isothermally at 50 °C. The total gas content of the sample was calculated from the measured dissolved oxygen concentration assuming that N₂ and argon are 100% saturated relative to their atmospheric partial pressures [Weiss, 1970]. The dissolved methane concentration was estimated as the product of the mole fraction in the extracted gas phase and the amount of total gas (STP) in the sample. For calibration, mixtures of 1.936 ppm ± 0.003 ppm and 9.854 ± 0.006 ppm of synthetic air (Deuste Steininger, calibrated against NOAA/CMDL standards at the Institute for Environmental Physics, Heidelberg) were used.

The two sets of 250 ml water samples will be transported to Kiel at 4 °C. One set will be used to measure methane concentrations with a standard purge and trap technique for intercomparison. The other will be used for the analysis of the stable carbon isotopic ratio of methane (δ¹³C) using the new MAT 253 Mass Spectrometer.

5.6.3 Preliminary Results and Discussion

5.6.3.1 Smooth Cocos Plate segment off Nicaragua and Northern Costa Rica

Mound Culebra

Mound Culebra is located at a water depth of about 1600 m and its western flank is elevated more than 100 m relative to the surrounding seafloor. The structure has a diameter of about 0.8 nm (nautical miles). OFOS investigation during SO163/1 have revealed massive carbonates exposed both at the flanks and the top of the mound. At the top, chemautotrophic communities that are typical for vents have been observed. On SO163, first measurements of the methane plume above this structure had been performed which have been extended on this cruise. A NW-SE and NE-SW-Profile of the results is shown in Figure 5.6.1.

The area had been investigated during SO163/2 by sampling at the top and on the NW-flank of the mound. On M54 we started at the same position as during SO163/2, aiming at the development of vent sites with time. The analyzes showed almost the same methane concentrations (about 25 nmol/l) as in May (Fig. 5.6.2), but the sharp decline with decreasing depth was not found anymore, that is values typical for background of 1 nmol/l were reached at 1350 m water depth (M54-25), whereas the measurements of May showed such values at 1450 m depth. This could suggest a changing activity at the vent site with time. Further CTD-deployments on top of the mound showed values ranging from 10 nmol/l to 25 nmol/l near the seafloor which are similar to the ones found at station M54-25. The lower methane concentration was found at station 114 located in the southwestern part of the top-area whereas 25 nmol/l were found at station 25 and 28 which are situated in the NE-part. To date one could assume a decreasing methane concentration from NE to SW, although the differences could result from varying activity as well. The highest methane concentration was determined in bottom water which was sampled by the bottom water sampler (BWS) reaching 31 nmol/l at the same location as M54-25 (Fig. 5.6.2). BWS and CTD-rosette were often used together at one position to get a continuous profile from the sediment-water interface into the water column until background values were resolved.

To gain knowledge of the further distribution of the plume above Mound Culebra, we took water samples NW and SW of the mound. Station 19 (NW) and 118 (SW) showed no bottom sources, but at station 19 the content of methane reached up to 45 nmol/l 30 m above ground. In contrast, the findings in May suggest a methane plume on the NW-flank which was located 60 m above ground. Future interpretation of the CTD-results will possibly explain this inconsistency. However, both stations at the NW-flank hinted at another source at this flank. Furthermore, the results of station 19 and 118 show a methane plume in a water depth of about 1500 m. The sources on the top are located at the same depth, therefore, the methane could originate from there. This assumption has been confirmed by the values of profiles 19 and 118 where the concentrations are lower than the ones of the bottom sources due to mixing with ocean water.

An additional methane enrichment was found at 1400m water depth, that is 100m above the mound, at station 28, 114, and 118. One possible explanation for this anomaly is a source area further away from the mound, at a higher site at the continental slope.

Mound 10

Indications of venting have been observed during SO163 on top of Mound 10 and on its northern flank. These findings agreed with the study of methane concentrations in the water column above this mound. Two CTDs were deployed in this area. The one on top of the mound (M54-125) shows a methane enrichment close to the seafloor with maximum values of 19 nmol/l (Fig. 5.6.3). The other station (M54-127) was chosen NW of the mound, because of the assumption made during SO163 that ocean currents flow from SE to NW. At this station methane concentrations reach values of 14 nmol/l located at the same depth range as

the anomaly at station 125. Therefore, it is probably a result of the venting at the top of the mound. Another enrichment of methane was determined at both locations at a depth of 2050 m. The source of this anomaly, 220 m above the top of the mound, is presumed to lay further away of the mound, at about this depth range.

5.6.3.2 Rough Plate segment off Costa Rica

Mound Quepos

Quepos Mound is a small-scale structure extending less than 30 m above the surrounding seafloor, with a diameter of less than 200 m. During SO163 (OFOS 23 &24) an active vent field together with an associated methane anomaly in the lower water column was observed, but the measured concentrations are quite low compared to the other mounds. The three stations deployed on M54/2 do not differ much (Fig. 5.6.4), hence there has not been a variation with time. The highest values of about 1.5 nmol/l were found near the sea floor with a maximum of 2 nmol/l on the northern flank. In the vicinity, i.e. on the northwestern edge of the mound, maximum concentrations of 6 nmol/l have been detected on SO163/2. On this cruise (M54-73/1) the highest methane inventory was observed 15 m above the sea floor suggesting a source at the flank. In summary, methane enrichment above Mound Quepos does exist, even though the values reach only about 2 nmol/l whereas the ambient background has a value of 1 nmol/l.

Mound 11

The presence of gashydrates as detected during M54/2 raised the interest to investigate the methane distribution in the water column above this mound. Therefore, water from above the mound (M54-142/2) and from the northwestern edge of the mounds top (M54-135) was sampled and analyzed. Both profiles show small excursions in a water depth of 700 to 850 m with a maximum value of 10 nmol/l (Fig. 5.6.5). Sudden changes in concentration like these excursions could result from gaseous venting. Though examination using parasound which would show low density anomalies could not prove this view. Values of 5-6 nmol/l were reached at station 142/2 right above the sea floor suggesting a source there. Apart from these exceptions methane concentrations were slightly higher than the background value of 1 nmol/l till 670 m water depth.

Mound 12

Like Mound 11, Mound 12, which is situated 0.5 nm to the NW of Mound 11, is covered with chemoherm-like carbonates and abundant seep fauna consisting of pogonophorans and bivalves. At this site, the 24-bottle rosette (CTD), BWS, as well as the VESP-MUC were used for sampling along a NW-SE and NE-SW profile (Fig. 5.6.6).

Bottom sources at Mound 12 were found at its NW-, SW-flank, and on top with values of 16 nmol/l to 110 nmol/l. At two locations, CTD and BWS were used in combination to record a water column profile beginning closest to the seafloor. At station 168 and 169, the data of CTD and BWS match. In contrast, lesser values of bottom water at BWS 187 and the higher ones in the water column at CTD 150 do not fit indicating either small source areas or variability of venting over time.

At Mound 12 the largest methane content was determined in water samples taken by VESP-MUC at a site with abundant seep fauna. After the VESP had been left at the same location for 45 min, the concentration of methane was measured to 4000 nmol/l (Fig. 5.6.7), the highest value at a vent site off Costa Rica so far. The jump in the methane concentrations illustrates a decrease of mixing with ocean water as well as a decrease of oxygen in the barrel of the VESP-MUC. This barrel surrounds five bottles used for sampling

water. After about 30 min, a nearly constant methane concentration of 3000-4000 nmol/L was measured some centimeters above the sediment-water interface.

Jaco Scarp

The Jaco Scarp is formed as a consequence of the subduction of a seamount on the oceanic plate. This leads to a circular uplift with faulting at the upper plate (dome). Seawards the process is associated with sedimentary landslides, leading to the formation of steep scarps. The profile of the water column within Jaco Scarp showed the highest methane inventory of all stations investigated during the Paganini expedition in 1999 (SO144, CTD02) [Bohrmann, 2002 #525]. The observed plumes were localized at depths below 1680 m. A first hydrocast at the same position during the 2002 field work confirmed this finding (SO163/2-CTD07). Hence, high priority was given to the assessment of the inventory and the localization of the sources of the methane plumes within the sampling program of the water column.

During the expeditions M54/2+3a, a total of eight hydrocasts were taken, and the methane distribution within the water column investigated. In addition, the 5-bottle rosette of the VESP-MUC was used two times for video-controlled water-sampling immediately above extensive fields of pogonophora which were discovered during OFOS observations (M54-OFOS 147).

A section of five stations (SO163/2) along the axis of the scarp (Fig. 5.6.8), mainly following the track of an OFOS investigation in 1999 (SO144 OFOS2), was accompanied by three more stations in order to monitor the NE-SW extension of the plume (Fig. 5.6.9). Within this section, the highest values (up to 400 nmol/l) were detected at station M54-47, where anomalous high CH₄-concentrations were observed up to a depth level of 1550m. The enrichment of methane between 1600 m and 1900 m found in May of this year (SO163/2) could be confirmed by data of this cruise. However, the depth of the maximum concentrations and the fine structure of the plume varies considerably. Detailed investigation of the density distribution within Jaco Scarp will be needed to understand whether this observation is related to a variety of sources or rather a product of hydrographic processes (bending of isopycnical surfaces or internal waves). The CH₄ inventory and the video surface mapping (OFOS) indicates that the latter scenario seems more likely.

With the aim to localise this plume along the rim of the scarp, a series of four hydrocasts was taken, roughly following the 1900 m isobath (Fig. 5.6.8, and Fig. 5.6.10). Station M54-53 in the east shows a broad layer of methane-enriched waters from the bottom up to 1650 m, with concentrations up to 45 nmol/l and without layers of distinctly higher concentrations. Station M54-50, near the most active vent area (see below) has the highest CH₄ inventory along the section, with sharply bounded methane-rich layers centred around 1850 m and 1700 m water depth. Similar to station 53, station M54-141 lacks a fine structure of the methane-rich layer, but has a higher inventory. At the western station (M54-066), the plume between 1750 m and 1900 m which dominates the methane distribution at the other stations, is almost completely missing. In contrast, the station shows the most prominent plume around 1700 m.

Based on these results, M54/147 OFOS (Fig. 5.6.8) was deployed to search for signs of fluid venting along the headwall of the Scarp focusing on the depth range from 2000 m to 1700 m. A small stretch with an extremely high abundance of vent-associated biota was localized in the north-western region of the scarp at depths between about 1750 m and 1850 m (Fig. 5.6.8, 5.6.11). As other biologic evidence for seepage during the extensive OFOS surveys had been scarce, this site possibly generates most of the widespread methane anomaly within this depth range. Three water samples taken from a hydrocast deployed for the sampling of biomarkers showed bottom-near methane concentrations of more than 1000 nmol/l, about three orders of magnitude more than natural background.

Two hydrocasts were deployed next to faults at the uplifted plate. Both stations show slight CH₄ enrichments close to the seafloor (Fig. 5.6.12). These could suggest venting of deep seated fluids, but in comparison to the sources described above, they play a minor role in the methane budget of this area.

BGR-Slide

The BGR-Slide is a landslide situated at 9°11.61 N and 84°39.73 W in shallow water of about 620 m depth. This site was chosen for observations, because BGR-results revealed that the bottom-simulating-reflector (BSR) does appear close to the sediment surface which indicates occurrence of gashydrates.

Only one CTD was deployed near the bottom of the slides headwall. Methane concentrations between 300 and 400 m water depths do not differ much compared to values from the two hydrographic sections measured during the SO163/2 (Fig. 5.6.13). In contrast, values from 500 m to 600 m water depths show two to three times higher concentrations (up to 20nmol/l). According to the profile at the BGR-Slide, there is no bottom source at this location, but probably close to it. Furthermore, the profile reveals sudden changes of methane concentrations in the water column. The jumps from low to high values and the other way around could be a consequence of gaseous venting or more than one source on the slope. Therefore, this site should be one of the targets of future research in this area.

Quepos Landslide

The Quepos Landslide is situated in about the same water depths as the BGR-Slide. Observations by OFOS during SO163/1 revealed bacterial mats covering the sediments just below the headwall and few bacterial mats on the slide mass. Sediments which were taken close to the headwall were degassing when brought up to the surface.

The water column above Quepos Landslide was sampled by one CTD-station on top of the slide (M54-108), one on the bottom of the headwall (M54-104), and one on the talus of the slide (M54-110). Methane was slightly enriched on the top and values increased with decreasing depths (Fig. 5.6.14). The same trend was shown by profiles of two hydrographic sections measured during SO163/2. The water from the bottom of the headwall, i.e. 15 m above the ground, had a CH₄-content of up to 17 nmol/l. Whether this is the result of active venting or due to methane enrichment as a consequence of the oxygen minimum zone, which is located at a depth of about 400 m, is not known to date. Interestingly, even though few signs were found on the slide mass by OFOS, at station 110 methane concentrations were as high as 15 nmol/l right above the sea floor suggesting a vent site at about this location. In this area, more measurements of the background are needed to distinguish between methane derived from the oxygen minimum zone and methane resulting from fluid seepage.

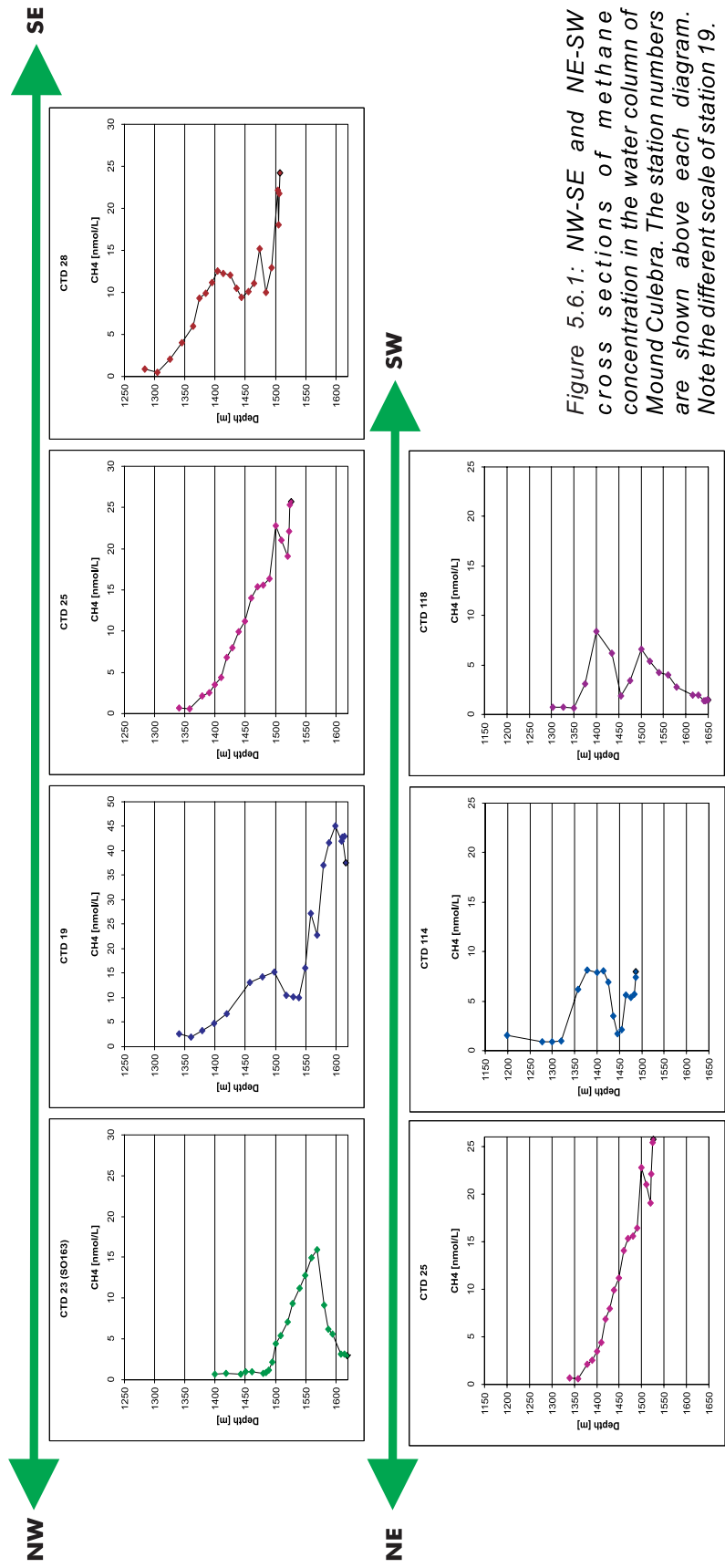


Figure 5.6.1: NW-SE and NE-SW cross sections of methane concentration in the water column of Mound Culebra. The station numbers are shown above each diagram. Note the different scale of station 19.

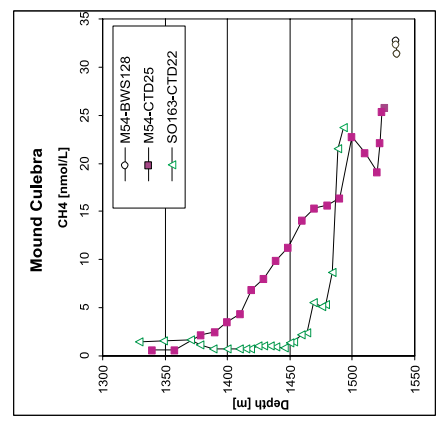


Figure 5.6.2: Methane content in water sampled in immediate vicinity on top of Mound Culebra. Compared are the measurements from May 2002 (SO163/2) and August 2002 (M54). The latter was accompanied by bottom water samples (BWS).

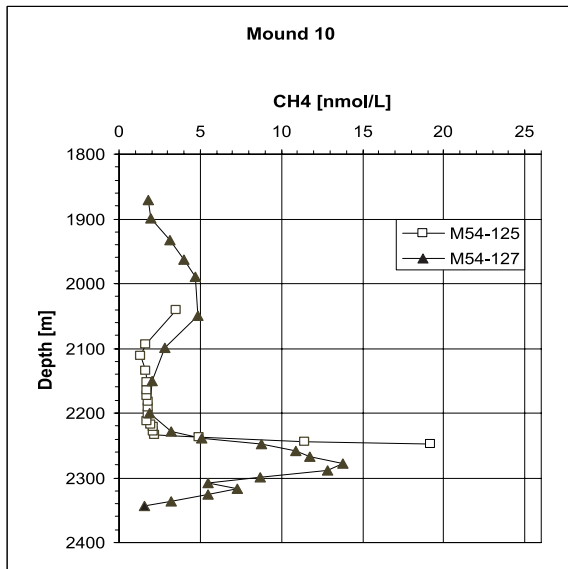


Figure 5.6.3: Methane concentration vs depth for station 125 and 127 at Mound 10.

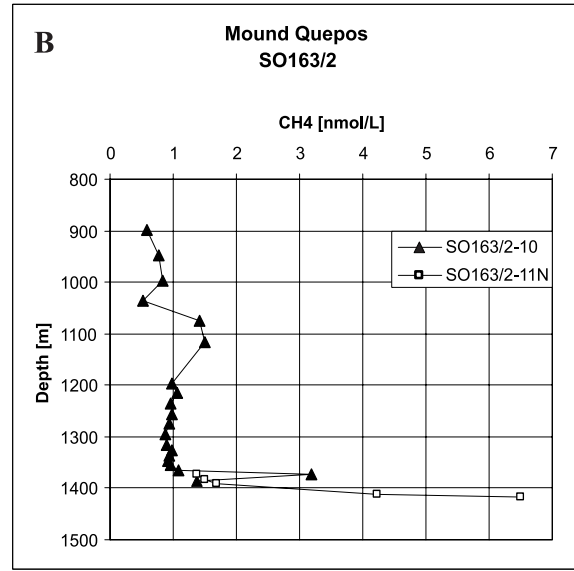
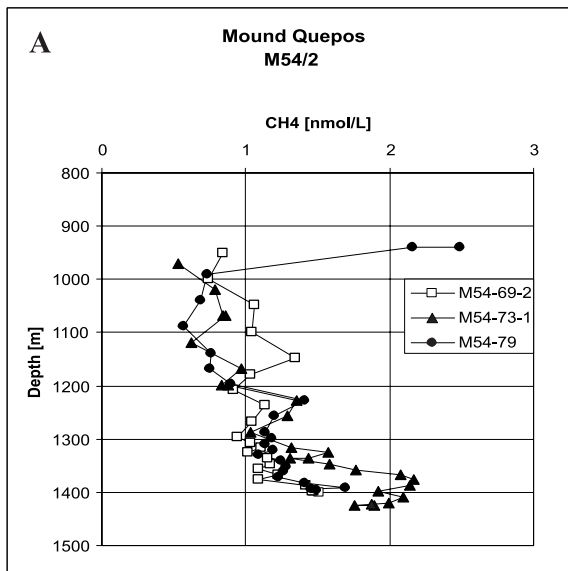


Figure 5.6.4: Depth profiles of the methane inventory in the water column above Mound Quepos. (A) Measurements taken during M54/2, and (B) some examples of values from SO163/2.

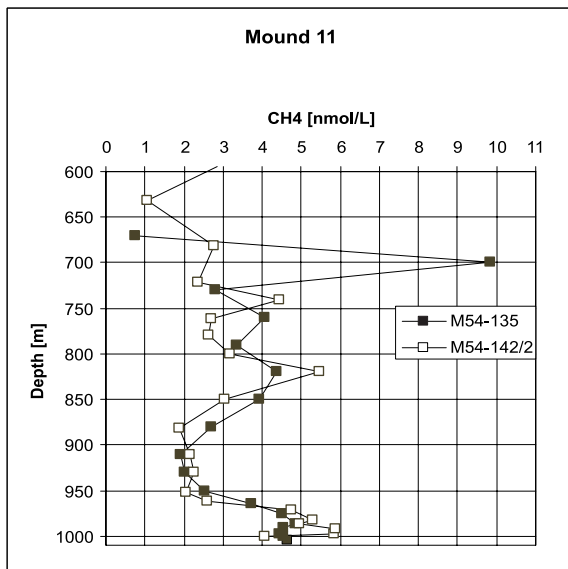


Figure 5.6.5: CH₄ concentrations in the water column at Mound 11. Station 142/2 is situated at the top of the mound and station 135 at the northwestern edge of the top.

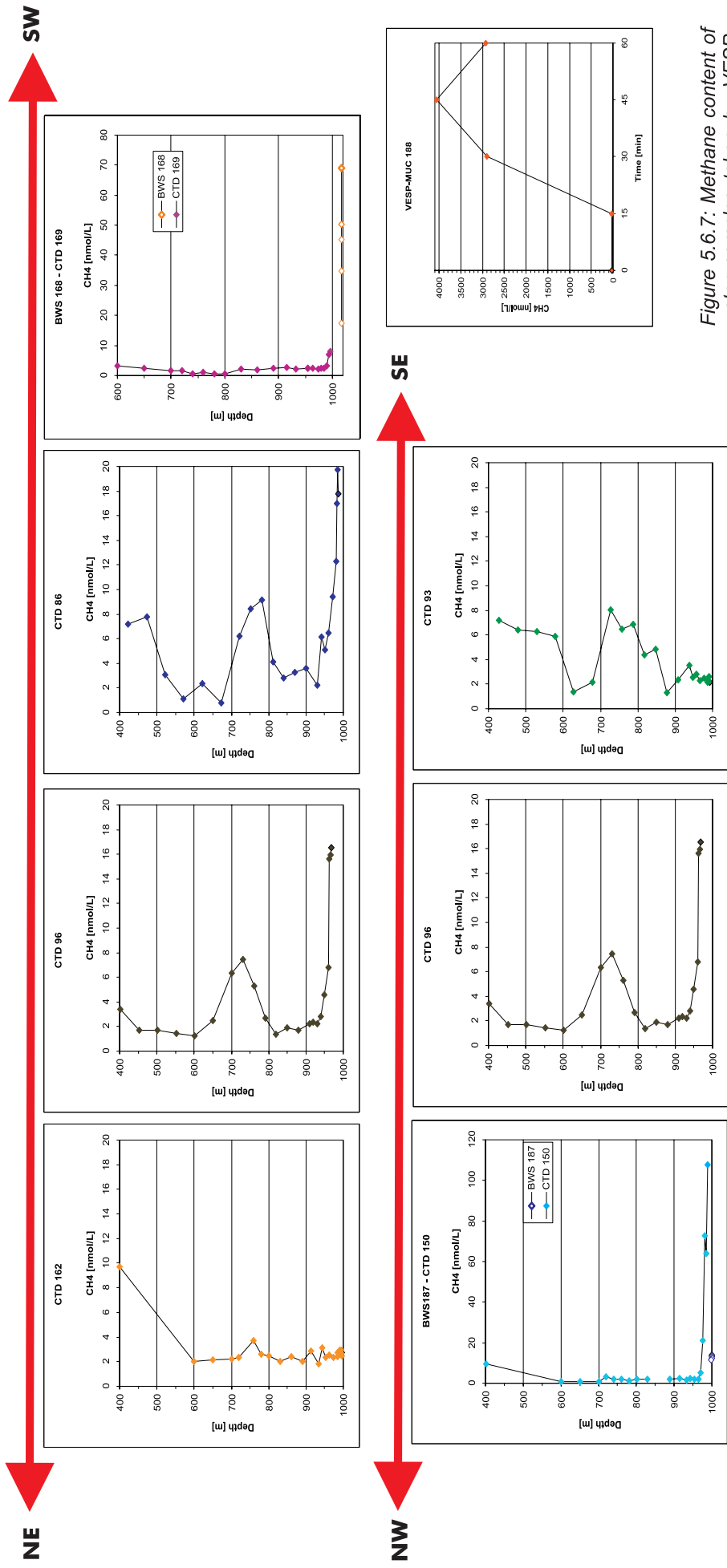
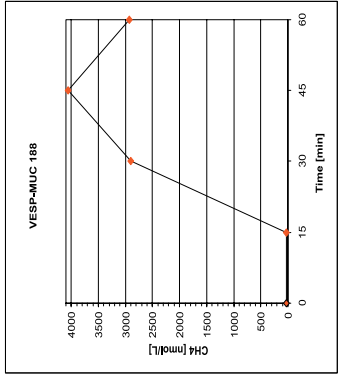


Figure 5.6.6: NW-SE and NE-SW cross sections of methane concentration in the water column of Mound 12. The station numbers are shown above each diagram. Note the different scale of stations BWS168-CTD169 and BWS187-CTD150. These diagrams include a CTD-profile and values of bottom water (BWS) taken at nearby sites.

Figure 5.6.7: Methane content of water samples taken by VESP-MUC at Mound 12 which was set up on the seafloor. The water was sampled every 15 min for a period of one hour.



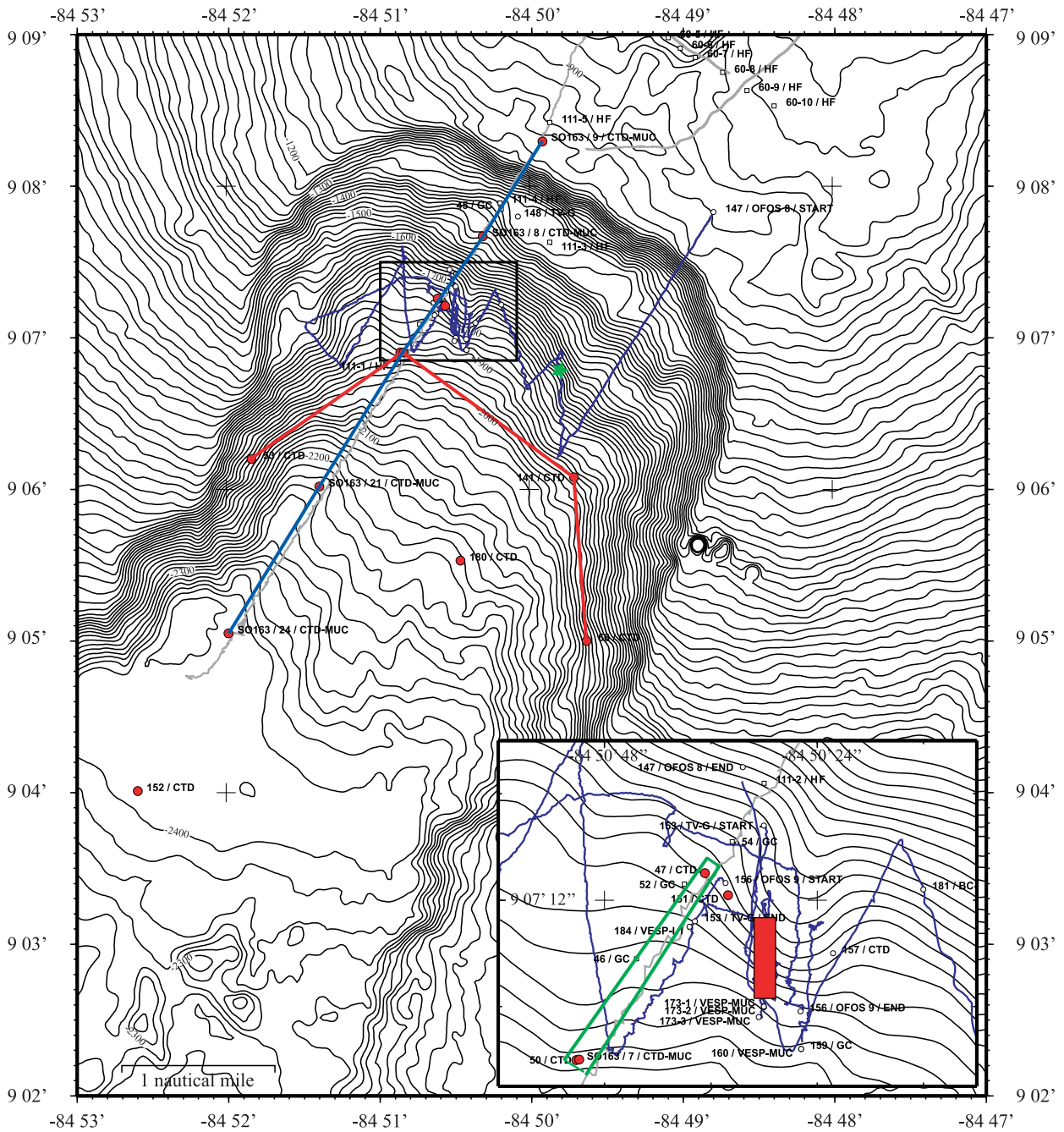


Figure 5.6.8: Map of Jaco Scarp with bathymetry. The dots indicate CTD stations. The data from CTD-station SO163-9 to SO163-24 along a straight line in direction of seamount subduction is represented in Figure 5.6.9; CTD-stations (53, 50, 141, and 66) taken roughly at the 1900m isobath are represented in Figure 5.6.10. The thin line represents the track of the video guided investigations with OFOS or the towed VESP-MUC. Insert Map: The open rectangle surrounds the methane-rich CTD casts near the area of high abundance of pogonophora, which is indicated by the filled rectangle. Sampling with the towed VESP-MUC was performed within this area.

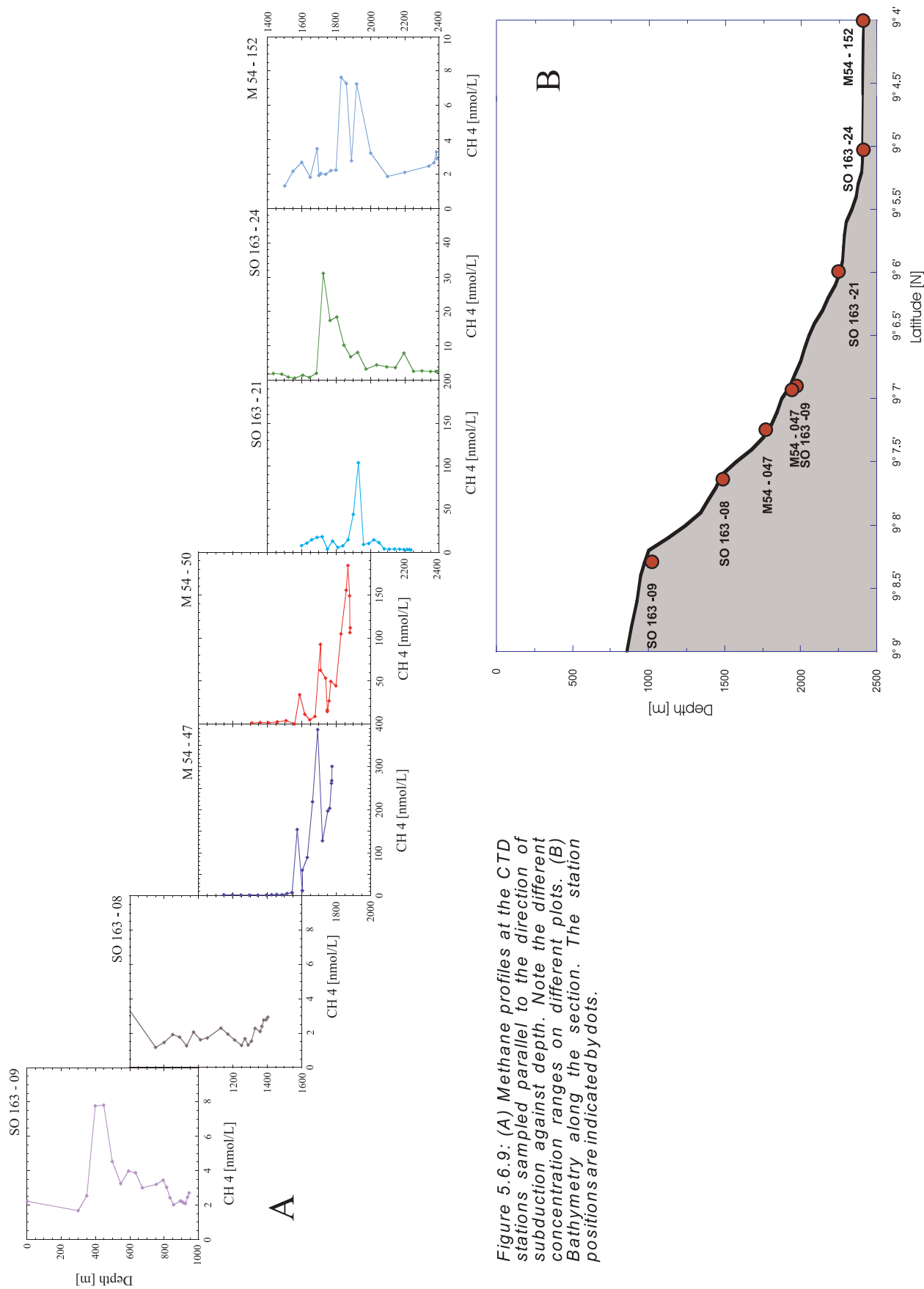


Figure 5.6.9: (A) Methane profiles at the CTD stations sampled parallel to the direction of subduction against depth. Note the different concentration ranges on different plots. (B) Bathymetry along the section. The station positions are indicated by dots.

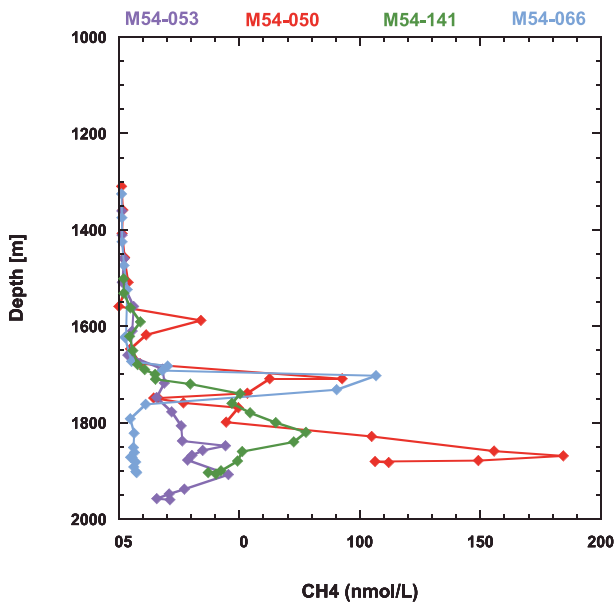


Figure 5.6.10: Methane profiles along the 1900m isobath within Jaco Scarp. For location of stations, see Figure 5.6.8.

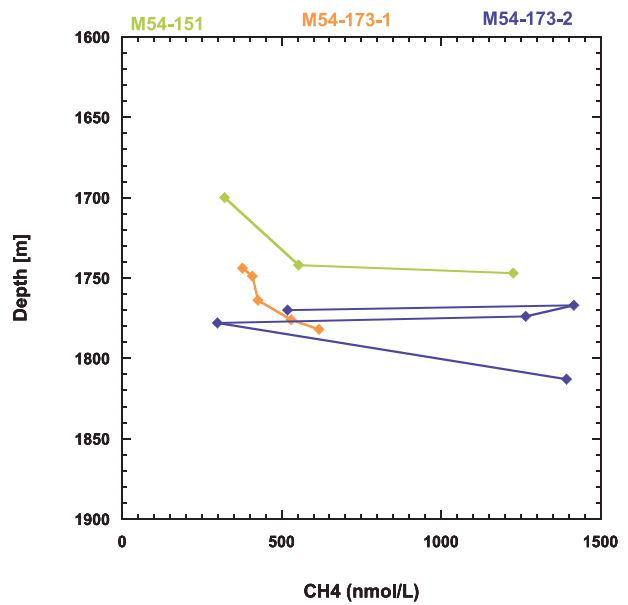


Figure 5.6.11: Methane concentrations in immediate vicinity of the vent sites. For stations M54-173 (1, 2) the video-guided VESP-MUC was used for a bottom-near sampling above the vent-indicating fauna. Highest concentrations are three orders of magnitude above natural background.

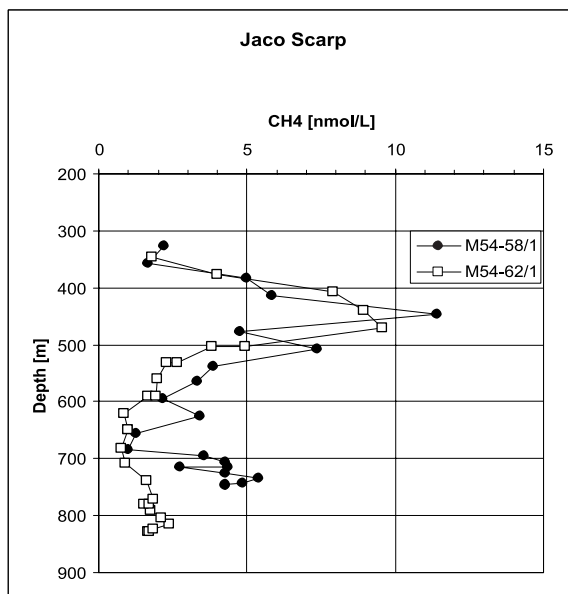


Figure 5.6.12: CH₄ concentration vs depth for station 58/1 and 62/1 at the dome (uplifted plate) of Jaco Scarp.

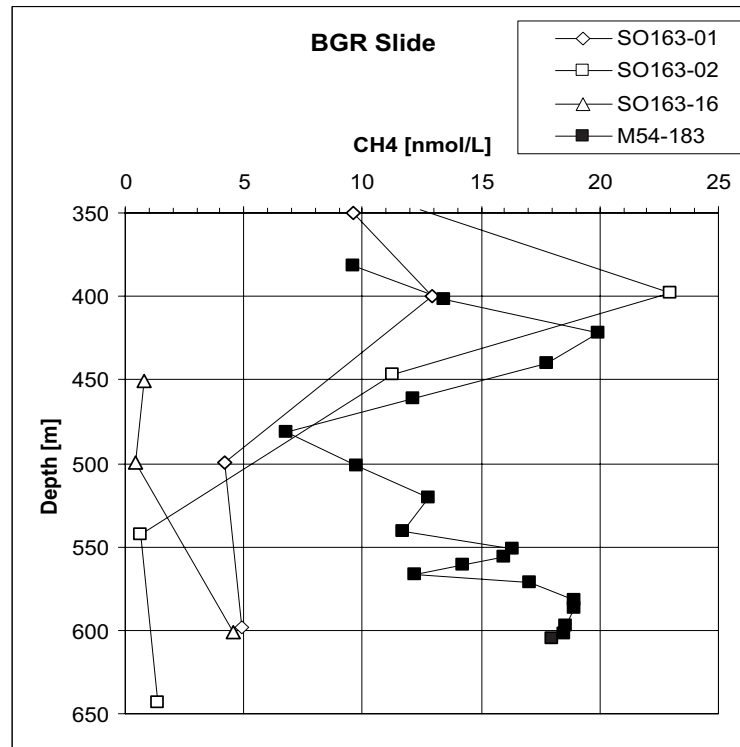


Figure 5.6.13: Methane concentration vs depth for station 183 at the BGR-Slump. The station is situated at the bottom of the headwall. For comparison results of hydrographic sections from SO163/2 are included.

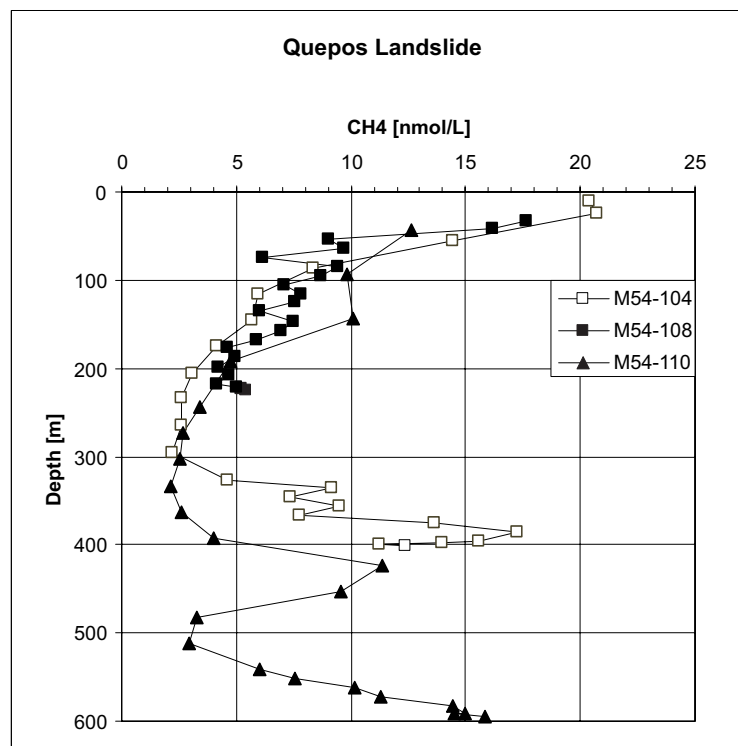


Figure 5.6.14: Methane content in the water column above Quepos Landslide. Station 108 is located at the top of the headwall, station 104 at the bottom of the headwall and station 110 on the slide mass.

5.7. Biomarker sampling

(B. Manzke)

Biomarkers are organic molecules found in the geological record whose basic hydrocarbon structural features have remained well preserved. They are thus often regarded as “chemical fossils” and can provide valuable information about the biological origins and subsequent transformation of organic matter in the geosphere over long timescales.

The biomarkers (hopanoids and isoprenoids) that are to be investigated here are produced by methane – consuming bacteria.

Hopanoids are mainly derived from bacteriohopanepolyols synthesised as membrane stabilising compounds by many different bacteria. They are absent in archaeobacteria; their role as structural components is fulfilled by acyclic isoprenoids.

In order to obtain samples of the biomarkers and their precursors the upper sediment and water column at methane seeps must be sampled.

The precursors (bacteriohopanepolyols) are present in bacteria only. To obtain these compounds bacteria must be sampled by filtering water through a 14 cm GF – Filter. Two filtering options were available:

1. filtering water from water bottles (either CTD – rosette or bottom water sampler)
2. using a KIEL in situ PUMP (KISP) secured to a TV guided VESP – MUC or TV guided MUC which are then positioned over or near a methane seep.

All filters were packed in aluminum foil and frozen at – 80°C after sampling.

The degradation products of bacteriohopanepolyols are hopanoids present in sediments. To investigate these biomarkers sediment was sampled as well. Whenever undisturbed surface sediment was available a sample was taken. Two complete cores from the MUC were also taken and frozen immediately at –20°C. They were later packed and frozen at – 80°C.

The KISP consists of 5 main parts: the filter holder, the battery pack, the electronic unit, the pump and the flow meter. A pressure compensation technique is used allowing constant flow rates with depth. The operation of the unit is controlled by software and all essential data is recorded. The build-in computer controls the time and duration of pumping. This proved to be a problem because it was difficult to estimate the time needed to find the right sampling site. This resulted in usually too early starts of pumping when the sampling site has not been reached.

The energy is supplied by battery packs with Ni/Cd rechargeable batteries. The encountered problem here was that the batteries were sometimes not working properly. At times the pumping time was reduced to a few minutes.

The pumping rate can be selected and kept constant between 1 and 200 l/h. To get the maximum amount of material on the filter the pumping rate was always at 100%. The usual bottom time was about 1 h and so was the pumping time.

The sampling technique was kept the same for the duration of the cruise.

5.8 Trace element and isotope studies

(D. Garbe-Schoenberg, S. Klauke, S. Purkl, J. Scholten, A. Eisenhauer)

The knowledge of fluid sources, chemical composition of expelled fluids, exchange rates between basement, sediments, fluids and seawater, transport pathways, and residence times of fluids is of general importance for the understanding of material budgets and cycling in subduction zones. For these objectives a variety of chemical analyses and isotopic measurements were conducted on-board ship and will be performed in the shore-based laboratories.

Trace elements

The chemical composition of fluids sampled during leg M 54/3 - pore water, vent fluid, bottom seawater, normal seawater – is the result of variable mixtures of fluid components from different sources and origins, e.g.: (i) low-salinity/ high alkalinity fluids rich in sulfide and methane assumed to represent ascending fluids formed by heating of the sediments and basalt of the subducted slab. The ultimate origin of the freshened water is still under debate relating it to fossil water aquifers, gas hydrates, membrane filtration by clays, removal of interlayer water from clay minerals and opal; (ii) fresh water from *in-situ* gas hydrate destabilization, (iii) a local fluid source essentially pore water that interacted with local sediment; (iv) normal seawater. The distribution of selected trace elements is characteristic for the different fluid components and can be used for the identification and discrimination of the fluid components and their sources. Another aspect is the identification and quantification of one or more trace elements in the water column above active vents which can be used as a conservative fluid tracer for mass balance calculations.

Fluid sampling during leg 54/3a focused on carbonate mounds (Mound Culebra, Mounds # 10, 11, and 12) where active venting of fluids was manifested by rich vent communities - notably at Mound 12 – and chemical anomalies (methane) were observed in the bottom water. Probably, deep fluids emerge at these sites as is evidenced from over-solidified clasts in the sediments. This may suggest a mud-diapiric origin of at least some of these mounds. *In-situ* destabilizing gas-hydrates play a role in pore water composition at Mound 11. In contrast, fluids from probably shallower depths are released at Jaco Scarp. Consequently, leg 54/3 allowed the sampling of fluids with markedly different chemical composition, originating from probably contrasting sources and depths.

Methods

Fluid samples were obtained by means of (i) pressing pore water from sediments obtained with gravity (GC, see Table 5.8.1), multi-corer (TV-MUC), and TV-guided grab sampler (TV-G) ; (ii) bottom-water sampler (BWS), (iii) Niskin sampling rosette (CTD), and (iv) Niskin bottles mounted on a TV-guided VESP-MUC frame. In addition, time-series samples were taken from incubation experiments with VESP, and Benthic Chamber Lander, respectively. Pore water was pressed through 0.2 μm cellulose acetate membrane filters in all-Teflon devices pressurized with Argon. Immediately after filtration, all samples (1-2 ml) were acidified with a few drops of subboiled concentrated nitric acid. Water samples with larger volumes (BWS, SW, VF) were pressure-filtrated through 0.2 μm Nuclepore PC membrane filters in Sartorius filtration units and acidified to pH 1 with subboiled concentrated nitric acid. Procedural blanks were processed in regular intervals. All work was done in a class 100 clean bench using all plastic labware. Rinse water was ultrapure (>18.2 Mohm) dispensed from a Millipore Milli-Q system.

A total of 216 pore water and 128 water samples were taken (Table 5.8.1). After return to the home labs in Kiel selected samples will be analysed for trace element composition (e.g., I, Br, B, Li, Al, Ti, Cs, Ba, Sr, Y-REE, Fe, Mn, Cr, V, Cu, Co, Ni, Pb, U, Mo, As, Sb, W) by ICP-mass spectrometry using both collision-cell quadrupole and high resolution sector-field based instrumentation.

Isotopes

Radioisotopes of the natural uranium-thorium decay chains are supplied to vent fluids and pore waters by water/sediment-, water/rock-interaction and by alpha recoil. Apart from the chemical composition of the sources the concentration of the radionuclides in the vent fluids depend to a larger extend on the transit time between the reaction zone and the discharge zone at the sediment surface. By measuring e. g. ^{224}Ra ($T_{1/2} = 3.6$ d), ^{222}Rn ($T_{1/2} = 3.8$ d), ^{228}Ra ($T_{1/2} = 5.7$ a), ^{210}Pb ($T_{1/2} = 22$ a) and ^{226}Ra ($T_{1/2} = 1600$ a), information on vent fluid residence times and discharge rates can be estimated.

During M 54/3a samples for radionuclide measurements were obtained by means of CTD, Bottom Water Sampler, VESP-MUC and TV-MUC. For ^{222}Rn analysis one litre of water was filled in an extraction apparatus and a water-immiscible scintillation cocktail (MaxiLight) was added. The sample was shaken for 1.5 hours and the organic phase was transferred into a low diffusive LS-vial which was stored for isotope equilibration three hours. Two liquid scintillation counters (Gurdian and Triathler) were available for on-board ^{222}Rn measurements. Samples were counted for three hours. Final calibration of the procedure and calculations of specific activities will be performed in the home lab.

At two locations samples were analysed for ^{224}Ra and ^{226}Ra . Sample volume varied between two and four litres. After adding a yield tracer (^{225}Ra) target nuclides were extracted from seawater matrix using radium selective extraction Disks (Empore Radium Rad Disks). The radium fraction can be stripped from the disk using EDTA/ammonium acetate in alkaline solution. For alpha-spectrometric assay further sample treatment includes low pressure column-chromatography and electrodeposition. Samples were counted on-board in an octal alpha-spectrometer (OCTÊTE PC). Beta-emitting ^{228}Ra also present on prepared alpha-sources will be determined in the home lab, waiting for ingrowth of alpha-emitting daughters.

Additional water samples (two to five litres) were taken for the determination of ^{228}Ra , ^{226}Ra , ^{210}Pb and e. g. Sr, Nd in the home lab.

5.8.1 Smooth Cocos plate segment off Nicaragua and Northern Costa Rica

Vent fluids were sampled at Mound 10 and more detailed at Mound Culebra. Details of the stations are given in Table 5.8.1.1. In order to determine the flux rates of the vent fluids, changes of radioisotope concentration with time were determined using the VESP-MUC at Mound Culebra (Stat. 131). The VESP-MUC was positioned for about one hour on a sediment surface covered with vent fauna (Calypptogena) which are indicative of the emanation of vent fluids. After deployment of the VESP-MUC three samples were obtained after 10 min, 30 min and 60 min. No significant differences in the uncorrected ^{222}Rn activities were observed. From two samples (131/1, 131/5) ^{224}Ra and ^{226}Ra activities were determined. Measured $^{224}\text{Ra}/^{226}\text{Ra}$ activity ratio (0.04 ± 0.02 , 0.05 ± 0.02) showed no significant differences with time.

Table 5.8.1.1: List of water and vent samples obtained in the area off smooth Cocos plate.

Station	Water depth (m)	Bulk sample
<i>Mound 10</i>		
125 CTD	2248,2244,2238,2234	x, x ,x, x
<i>Mound Culebra</i>		
114 CTD	1487, 1436, 1198	x, x, x
119-2 TVMUC (c)	1613	
128 BWS	1538	x, x
129-2 TV-MUC	1540	
131 VESP-MUC	1535	

5.8.2 Rough plate segment

At nine stations in the area of the rough plate, vent and water sampling for the determination of radioisotopes was conducted (Table 5.8.2.1). At the Jaco Scarp escarpment dense populations of Pogonophora were observed indicating strong discharge of vent fluids. In order to sample these fluids the VESP-MUC was lowered along the escarpment accompanied by time controlled water sampling. Two out of the five samples were measured for ^{224}Ra and ^{226}Ra activities. The ^{226}Ra activity concentration was similar to those measured at stat. 131. ^{224}Ra activity concentration was below the detection limit of 0.2mBq/l.

Further vent sampling using the VESP-MUC was conducted at Mound 12. The VESP-MUC was positioned on a Bathymodiolus field and was deployed for 1.20 min; The uncorrected ^{222}Rn concentrations measured in the five water samples showed a slight increase with time.

Table 5.8.2.1: List of water and vent samples obtained in the area of rough plate segment.

Station	Water depth (m)	Bulk sample
<i>Jaco Scarp</i>		
151 CTD	1742,1700,1450	x, x, x
173-3 VESP-MUC	1729,1734, 1753, 1805,1833	
180 CTD	2192,2176,2167	
<i>Mound 11</i>		
135 CTD	1004,1001,997	x
137-1 TV-MUC	1024	
142-1 BWS	1020	x, x
<i>Mound 12</i>		
167 CTD	1573,1563,1543,1504,1444, 1345,1200,1002	x,x,x,x,x, x, x,x
186 VESP-MUC	1008	

5.9 Lander deployments

(P. Linke, H. Sahling, M. Poser, M. Türk, B. Bannert, W. Queisser, K. Stange)

Introduction

The interrelationship between mass transfer, pore water chemistry and biological activities in vent ecosystems is the central topic for the deployment of benthic landers. On one hand, the development of chemolithoautotrophic microbial and symbiotic communities is dependent on the transfer rates of reduced inorganic substrates, on the other hand this mass transfer is modified by their activities. The continuous supply and transfer of methane and reduced sulfur compounds as energy substrates for chemoautotrophic bacteria and symbioses are of major importance for the establishment, the maintenance and the extent of these prolific benthic communities.

Measurements of aqueous flow rates (water, chloride and nutrients), of the control parameters of fluid expulsion and transient flow pattern, the determination of concentrations of methane, reduced sulfur compounds (sulfide, elemental sulfur, thiosulfate), and of their transformation rates are important parameters for the determination of mass balances in various subduction zone settings.

Methods

Our basic concept to sample fluids and to measure the fluid and gas flow is the channeling of the effluent from the sea floor into a semi-enclosed benthic chamber with a large opening at the bottom and a small exhaust port at the top (Linke et al., 1994). After deployment of the chamber the internal volume is initially flooded with ambient seawater and is then slowly replaced by vented fluids. Sequentially timed water samples are collected inside the chamber. Changes in the concentration of dissolved components within this time series are used to calculate flux rates (Carson et al., 1990). Parallel to this, a thermistor flowmeter is mounted in the exhaust port of the chamber to record the *in situ* fluid flow rate.

During cruise M54/3A two video-guided devices were used for the deployment of a benthic chamber from a conventional research vessel on a cold seep at the seafloor (VEnt SamPler - VESP). The ship's coaxial cable is used for bidirectional transmission of the video images, commands, data, and power supply of the underwater units (ADITEC/SCHOLZ). The instrument is towed in view of the seafloor approx. 2 – 3 m above the sediment and is deployed when signs of seepage become visible (e.g. clam clusters, bacterial mats). During deployment the given slack of the cable is kept away from the moored instrument by floatation attached to the cable (FLOATATION TECHNOLOGY).

In the first device, the barrel is attached to the central piston of a modified multicorer frame which operates on a water hydraulic basis and assures gentle deployment of the barrel once the frame settles on the sea floor (Linke et al., 1994). VESP is equipped with five 5L water bottles (HYDRO-BIOS) and a programmable data logger (TATTETALE) mounted within the barrel which is activated from the surface telemetry unit to start the water-sampling cycle. The benthic barrel is a commercially available 55-gallon polyethylene barrel with a large opening at the bottom and a small exhaust port at the top.

Since this VESP system requires a permanent cable connection to the ship for bidirectional power, video signal and data transmission which limits the deployment time (up to 2 hours) we developed a concept to deploy an autonomous lander system with a launcher and disconnect it from the ship's cable after its video-guided deployment on a suspected seep site. The 2 VESP-Landers are equipped with an improved chamber to obtain both direct water flow and samples expelled from active sites and are designed as instrument carriers for a variety of different measurements which could be integrated within these systems. The landers are designed to stay on the seafloor for several days recording the different parameters (e.g. temperature, conductivity, methane, fluid flow, microseismicity etc.) and would take samples prior to the recovery of the instrument by acoustic release of the additional weight.

In the configuration used during cruise M54/3A the VESP-launcher carried a video camera (DEEP-SEA POWER & LIGHT) and floodlights (OKTOPUS) on the front which can be switched with a PC-controlled telemetry surface unit (ADITEC/SCHOLZ).

The attached lander (Fig. 5.9.1) is disconnected from the launcher by a mechanic release (NICHYU GIKEN KOGYO). The lander carries a floatation unit with up to 14 BENTHOS floats and 2 glass instrument housings for power supply and ARGOS transmitters. Pieces of train tracks are used as weights and are dropped by paired acoustic transponder releasers (OCEANO RT 661 B1S & RT 361 BS). For spotting and recovery the lander is equipped with a radio beacon, strobe light (NOVATECH) and flag.

Beneath the floatation unit the lander has a wide open space for carrying various instruments like i.e. benthic chambers. The chambers of the 2 landers used on the M54/3A cruise are pyramidal stumps made of titanium or stainless steel with a height of 30 cm. The bottom (surface) area covers 1 m² and the exchangeable top area (40 x 40 cm) was equipped with ports for the thermistor flowmeter and for different other sensors. The chambers are suspended within the lander frame during deployment by strong rubber bands and lowered on the seafloor by its own weight. To facilitate water exchange during deployment and recovery valves are opened by rubber bands and kept close through spring action when the chamber is placed on the seafloor. Both VESP-Landers are equipped with a motor-driven syringe sampler with 7 x 50 ml glass syringes attached to the chamber to obtain water samples in a time series during deployment. To obtain a larger sample at the end of the deployment both landers carry a single 1.7-L water bottle mounted within and another as a bottom water reference sample outside the chambers respectively. Both are tripped simultaneously at the end of the deployment when the acoustic releasers are activated and provide water samples for the analysis of dissolved seep fluid species.

Environmental parameters, e.g. conductivity, temperature, and pressure, are continuously recorded by storage CTD probes (SBE19plus and Micro FSI). Furthermore, the bottom water velocities close to the funnel outlet are recorded by MAVS 3-axis acoustic current meters (NOBSKA); the bottom water regime above the landers is recorded by acoustic doppler current profilers (RDI). Additionally, VESP-Lander II was equipped with a GEOLON seismometer. The electronic and mechanical design is based on the experiences with the GEOMAR OBS. During deployment the seismometer is attached to a level arm and is released from its hook when the launcher is disconnected from the lander. The level arm is kept at an horizontal position above the seismometer which falls to sea floor from about 1 m height. This should ensure the coupling of the seismometer to the sea floor. At this time the only connection from the seismometer to the Lander is a cable and an attached rope which will take the pull load while rising to the sea surface later. A movement or current on the instrument is thus not transmitted mechanically to the seismometer. All three channels are preamplified within the seismometer housing and recorded by a GEOLON-MLS data logger. Parallel to these three channels the standard hydrophone is recorded on the fourth channel.

The video-guided deployment, autonomous measurement and retrieval of the Benthic Chamber Lander (BC-Lander; Fig. 5.9.2) is similar to that of the VESP-Lander. Its basic frame is a stainless steel tripod that carries 18 - 21 BENTHOS glass spheres for buoyancy and ballast attached by release toggles to each of the three legs.

Two acoustic release units that provide parallel redundancy control of the ballast. A radio beacon and strobe aid in relocation of the lander at the surface and an ARGOS system to track it in case of a premature release. The frame carries a platform to which various experimental packages can be attached. The lander is comparably small (2 m wide, 2.50 m high) and thus easy to handle. For the measurements of benthic material turnover, the frame was equipped with 4 squared Delrin benthic chambers supported by a stainless-steel frame that is attached to the lander. The chamber lid carries a central stirrer. Each chamber represents an autonomous module with its own control unit and power supply with the rechargeable NiCd-battery packs (6 V, 10 Ah) integrated into a glass sphere. The chambers are driven into the sediment by a motor enclosing a sediment surface area of 20 x 20 cm with overlying bottom water. At the end of each incubation a shutter is closed by a 2nd motor in order to retrieve the sediment. Once the shutter is closed the chamber

VESP-Lander

for the measurement of fluid flow and environmental control parameters

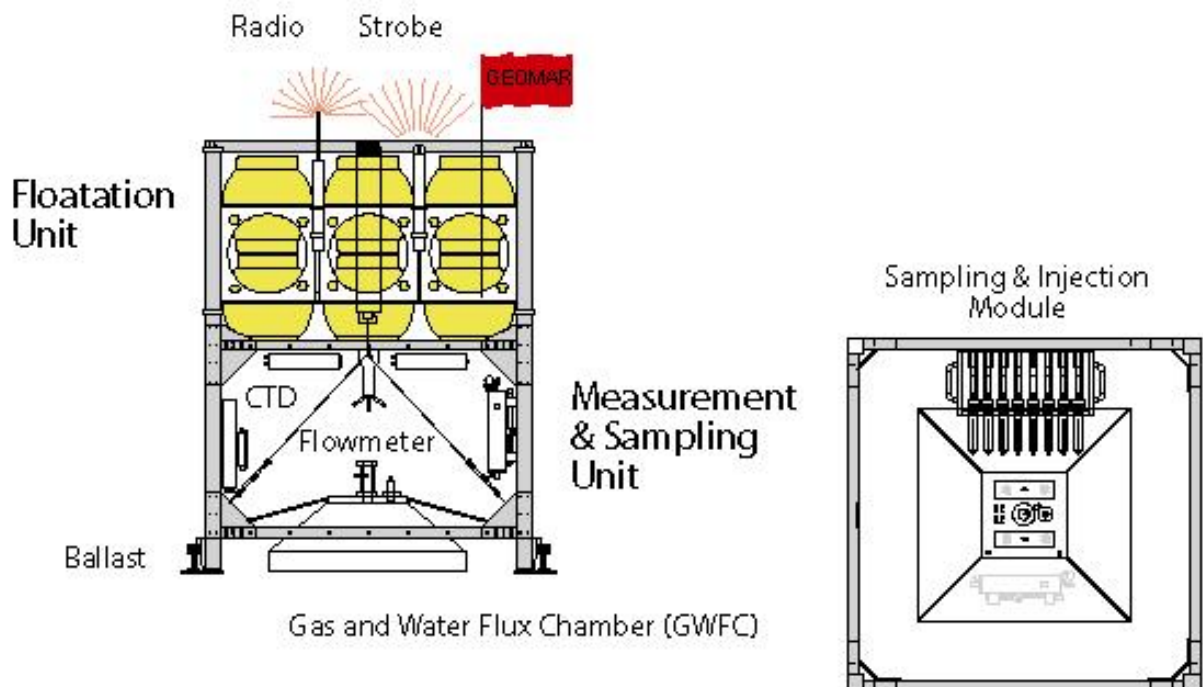
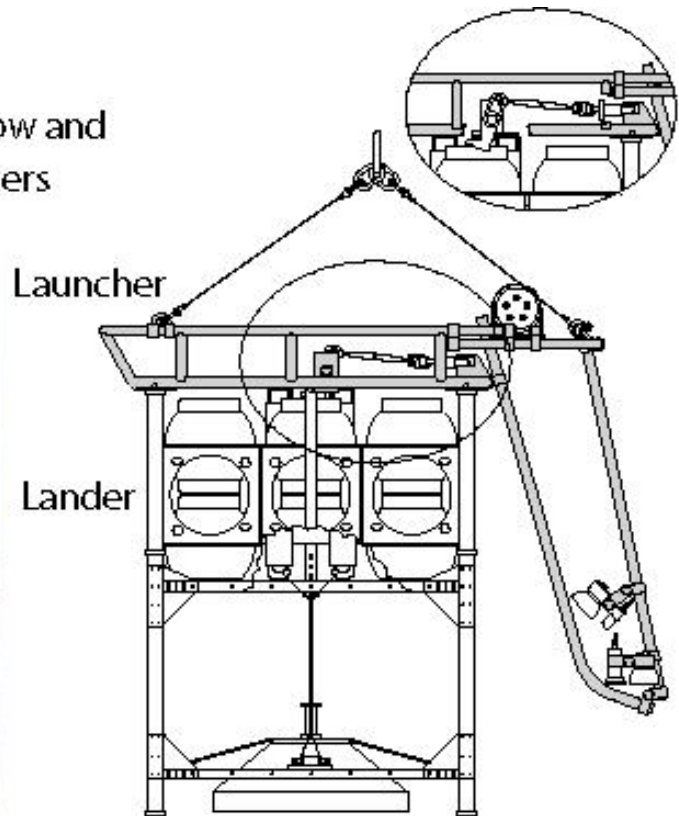
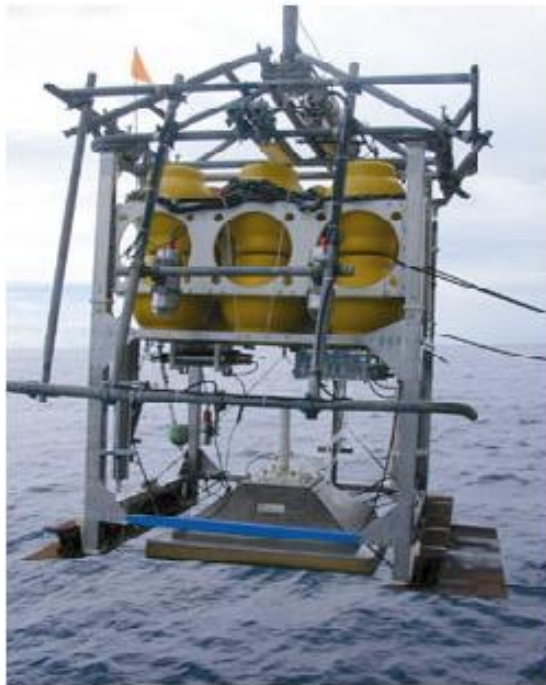
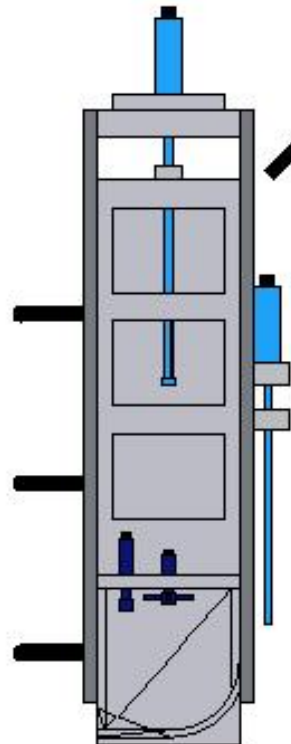
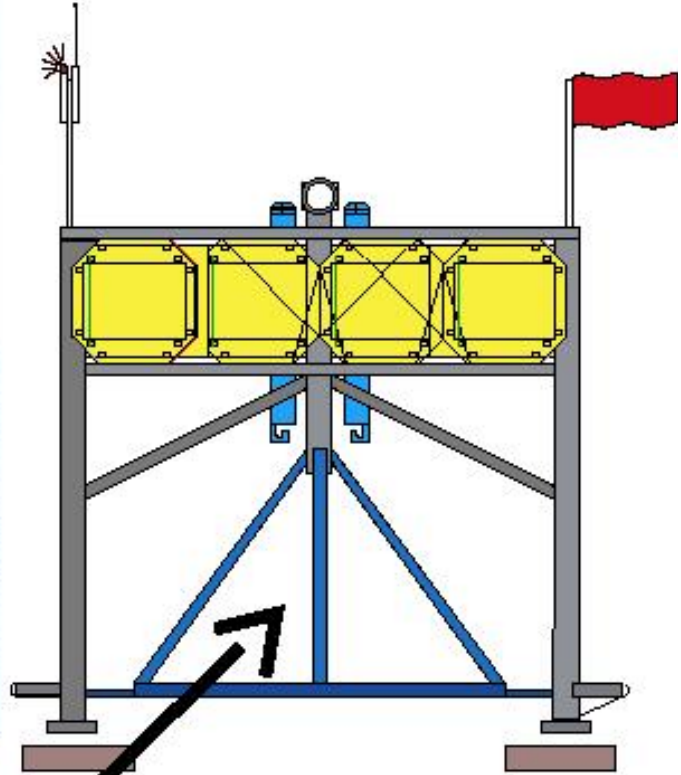


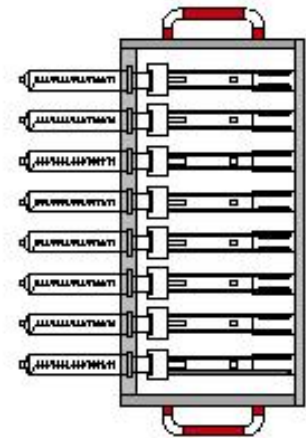
Figure 5.9.1: The VESP-Lander with the Launcher on top; enlarged the release mechanism. The Lander consists of the floatation unit and the measurement & sampling unit.

Benthic Chamber Lander

for the incubation of sediments to quantify benthic turnover rates



benthic chamber module



syringe water-sampler module

Figure 5.9.2: The GEOMAR benthic chamber lander consisting of: lander frame (top), benthic chamber modules (left) and water sampler/injection modules attached to a benthic chamber (right).

is slowly heaved out of the sediment by the first motor and the lander can be called back to the surface by acoustic command. During each incubation, a syringe water sampler equipped with glass syringes takes 7 water samples of 50 ml each from the benthic chamber at pre-set time intervals. The concentration change of chemical constituents (e.g. oxygen, methane, nutrients) over time allows quantification of benthic turnover rates. Sediment community oxygen consumption (SCOC) measurements were performed by precision Winkler titration and measured in situ by a prototype of a planar optrode which was provided by AANDERAA.

Results

During M 54/3 the VESP-Lander and the BC-Lander were deployed at four different locations. A short summary of the BCL deployments is given in Table 5.9.1; results of the VESP-Lander deployments are described below.

Table 5.9.1: Summary of BCL deployments during the cruise M 54/3. Data for pore water and nutrients were provided by Ch. Hensen and K. Nass, CH₄-data were provided by G. Rehder and S. Mau.

Station No.	Area	No.	Chamber recovery	PW	O ₂	CH ₄	Nutrients
124/132	Mound 10	K1	-	-			
		K2	-	-			
		K3	-	-	x	x	
		K4	-	-	x	x	
144/149	Mound 11	K1	11 cm	10 cm	x	x	x
		K2	8 cm, inclined	10 cm		x	
		K3	8.5 cm, inclined	-	x	x	x
		K4	7 cm, inclined	-	x	x	x
166/174	Mound 12	K1	12 cm, with bacteria	11 cm	x	x	x
		K2	12 cm, without bacteria	-	x	x	x
		K3	13 cm, bacteria	-	x	x	x
		K4	15 cm, with few bacteria	12 cm	x	x	x
181/185	Jaco Scarp	K1	2 cm sediment	-	x	x	
		K2	10 cm, some gravel, brown sediments	10 cm	x	x	x
		K3	empty	-	x	x	
		K4	2 cm sediment	-	x	x	x

5.9.1 Smooth Cocos Plate segment off Nicaragua and Northern Costa Rica

Mound Culebra

VESP-Lander Station 130/189

At this station, VESP-Lander I was deployed for almost 14 days. The uncalibration flow data revealed a flow pattern which can be divided into 2 phases (Fig. 5.9.1.1). Whereas the first phase (16.9. – 22.9.02) represents a period of more vigorous flow, the second phase (22.9. – 28.9.02) clearly reflects the impact of tidal induced currents. This is reflected in the methane concentrations with elevated values in the first period and reduced values in the second period. The same pattern is depicted in the ADCP data set (Fig. 5.9.1.2).

Mound #10

BC-Lander Station 124/132

On this station, the lander did not recover any sediment, due to the roughness of the sediment surface. The only samples that were retrieved were a complete set of 7 syringes with bottom water from chamber K3 and 3 samples from chamber K4.

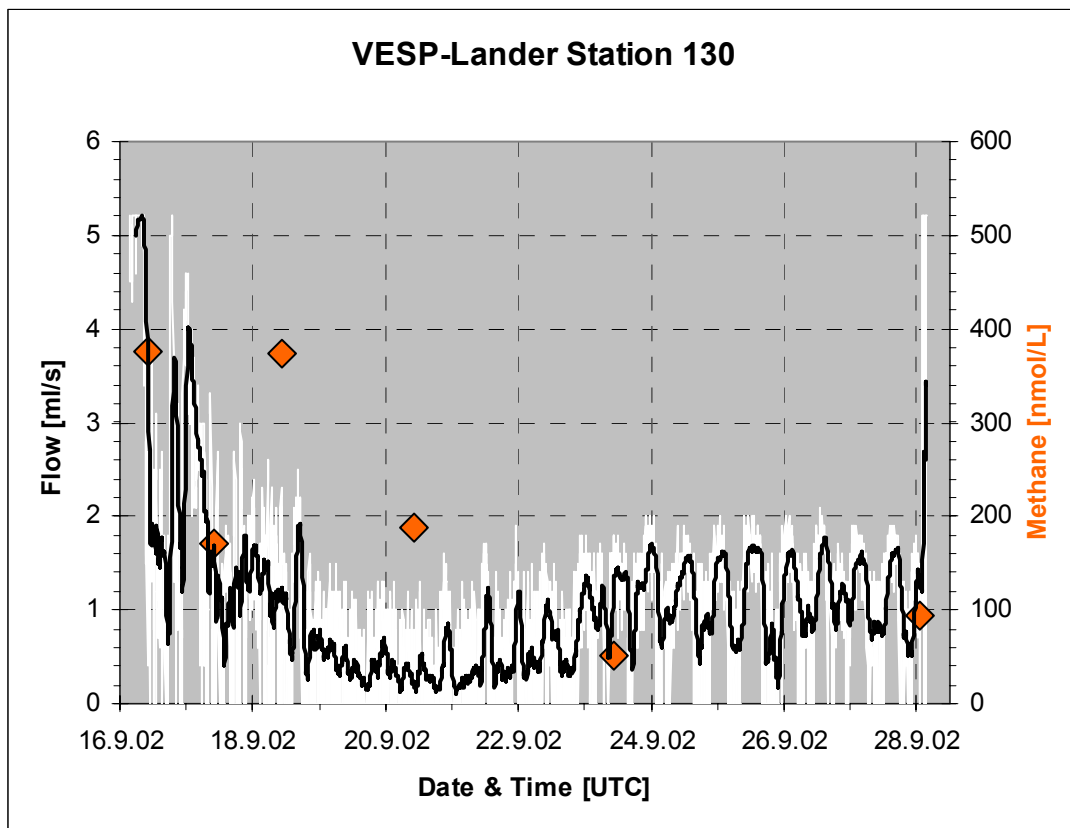


Figure 5.9.1.1: Uncalibrated flow data plotted together with methane concentrations derived from the syringe sampler (Data provided by Rehder & Mau).

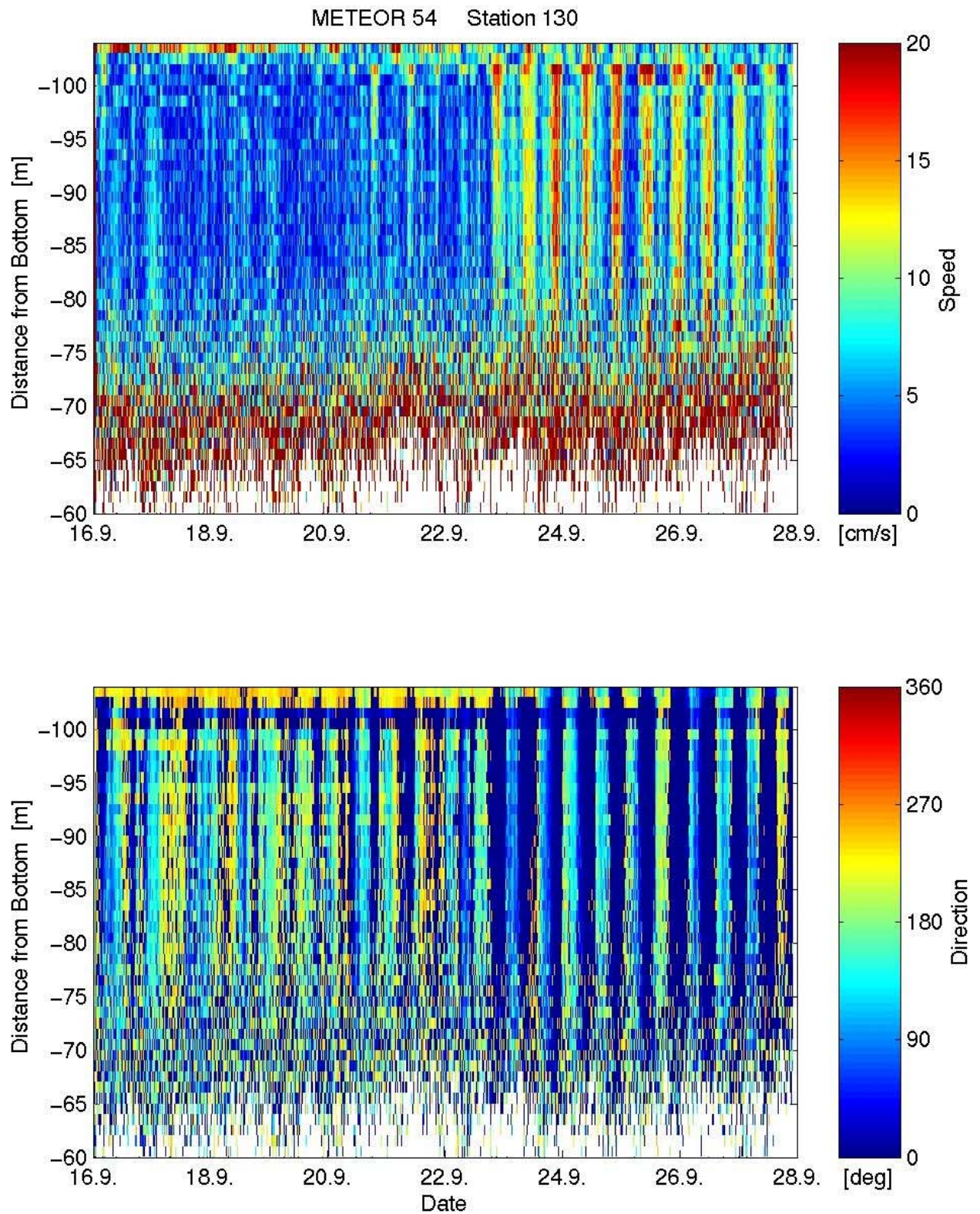


Figure 5.9.1.2: ADCP-data reflecting bottom water current speed and direction in 60 to 105 m distance above seafloor. Note the 2 phases before and after 22 September 2002.

5.9.2 Rough Plate segment off Costa Rica

Mound #11

BC-Lander Station 144/149

The deployments at Mound 11 and 12 yielded the most complete data sets, consisting of a time series of methane, oxygen and nutrient concentrations in the enclosed bottom water of the chamber, as well as the porewater composition from the recovered sediments. These data clearly show that, at both stations, the lander was deployed on sediments that were influenced by fluid venting. Furthermore, the data show considerable variability between the four different chambers of each deployment reflecting the patchy distribution of venting.

VESP-Lander Station 146/154

At this station, VESP-Lander I was deployed for 48 hours. The deployment revealed 2 events in the flow data set (Fig. 5.9.2.1). Unfortunately, the thermistor flowmeter can not distinguish the flow direction (outflow/inflow szenarios) like the flowmeter of Tryon et al. (1999).

Nevertheless, both events occurred at high tide and are again reflected in the ADCP data set (Fig. 5.9.2.2) which reflects the impact of the bottom water velocities on the flow measurements.

Mound #12

VESP-Lander Station 165/175

This deployment revealed the highest fluid flow rates measured on this cruise (Fig. 5.9.2.3). Some of the measured events are again reflected the ADCP-data (Fig. 5.9.2.4).

BC-Lander Station 166/174

Here, we present the data of BCL 166 chamber K1 as an example of vigorous chemical release and turnover at the vent sites (Fig. 5.9.2.5 & Fig. 5.9.2.6).

The lander was deployed in the SW area of Mound 12. The surface of the recovered sediments in chamber K1 contained filaments of sulfur-oxidizing bacteria in low density. Methane and sulfide concentrations in the porewater were high, the chloride concentrations decreased considerably with sediment depth. The oxygen and nitrate concentration decreased significantly in the chamber water during the deployment interval. It is known that both electron donators are used by sulfur-oxidizing bacteria to oxidise sulfide in order to gain energy. The consumption rates can be calculated (Tab. 5.9.2.1) for a given chamber geometry (approx. 4.5 l volume, 20 x 20 cm area). Sulfide accumulated in the chamber after oxygen and nitrate had been depleted. The increase in alkalinity in the course of time can be explained by methane oxidation. In order to compare the consumption rates with the rates of methane and sulfide that are released (and partly oxidized), the values are converted to oxygen equivalents (Tab. 5.9.2.1). These values indicate that the nitrate and oxygen consumption can be completely explained by the release of sulfide and methane at this locations.

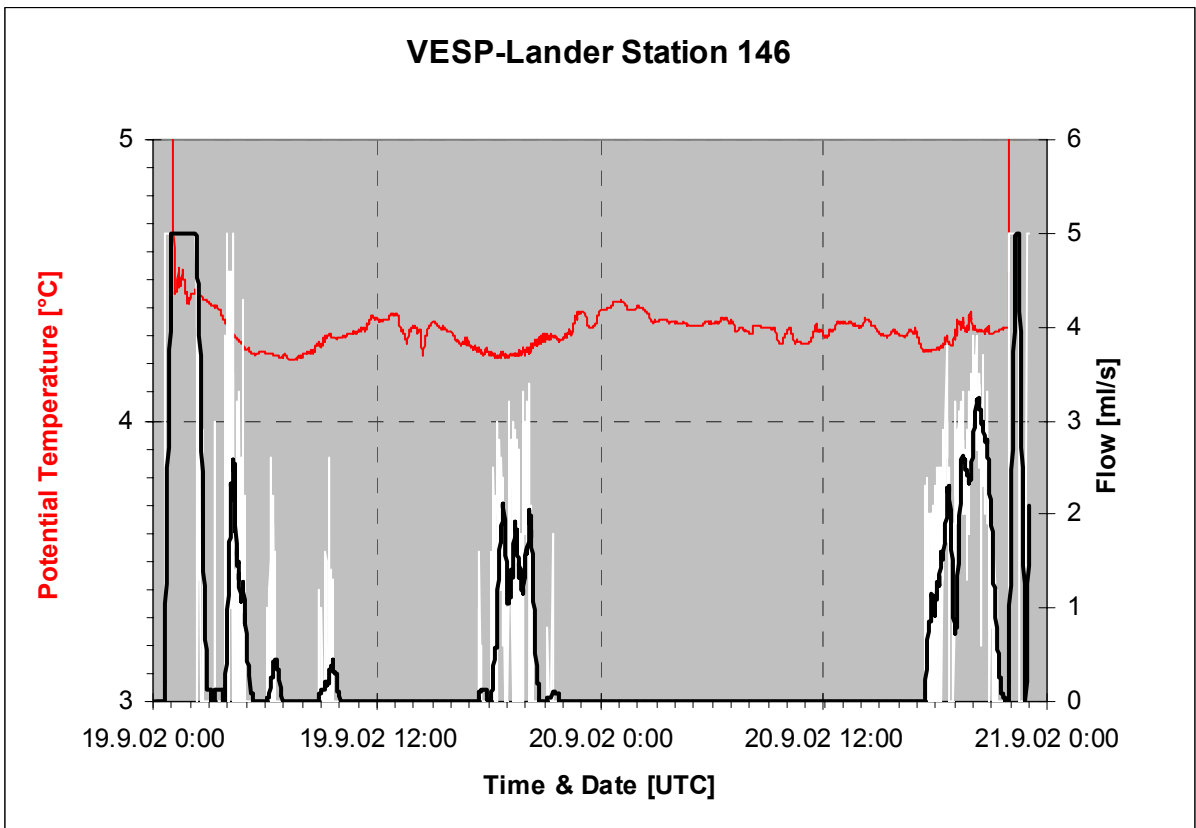
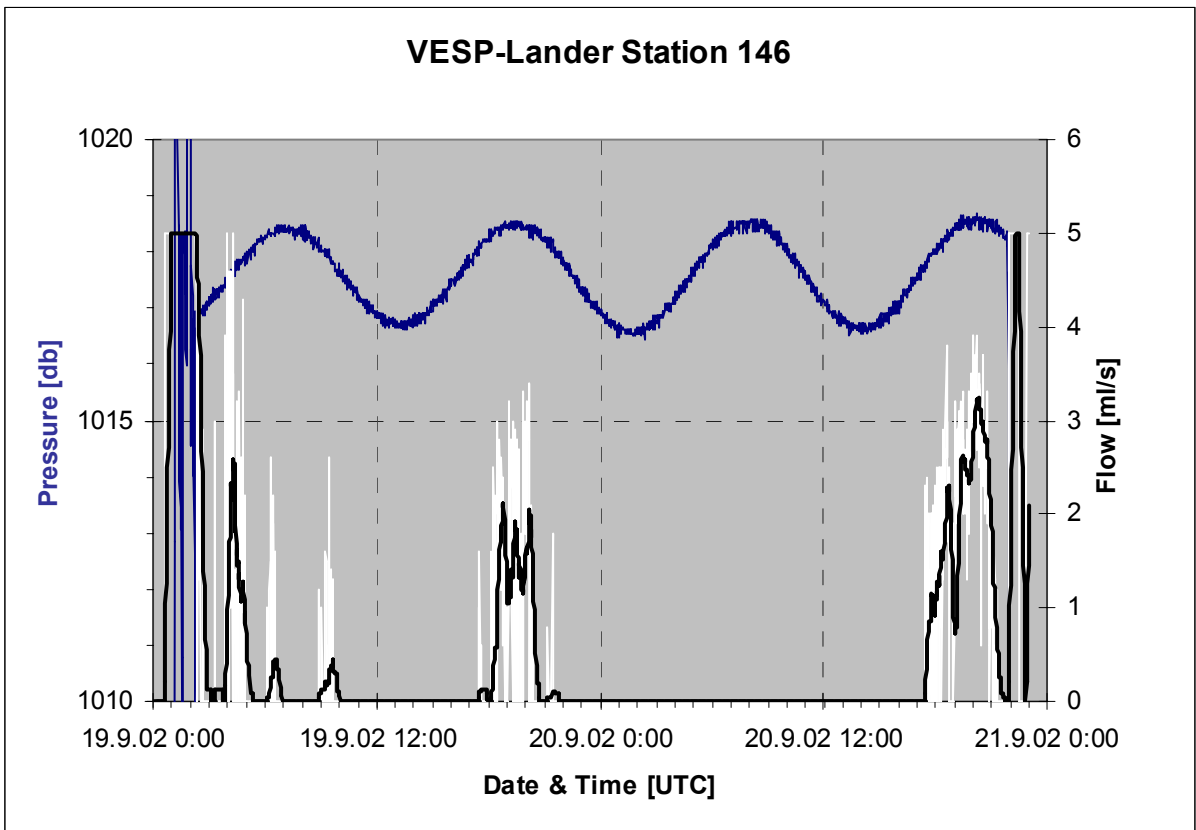


Figure 5.9.2.1: Uncalibrated flow data and time course of pressure and temperature.

METEOR 54 VESP-Lander Station 146

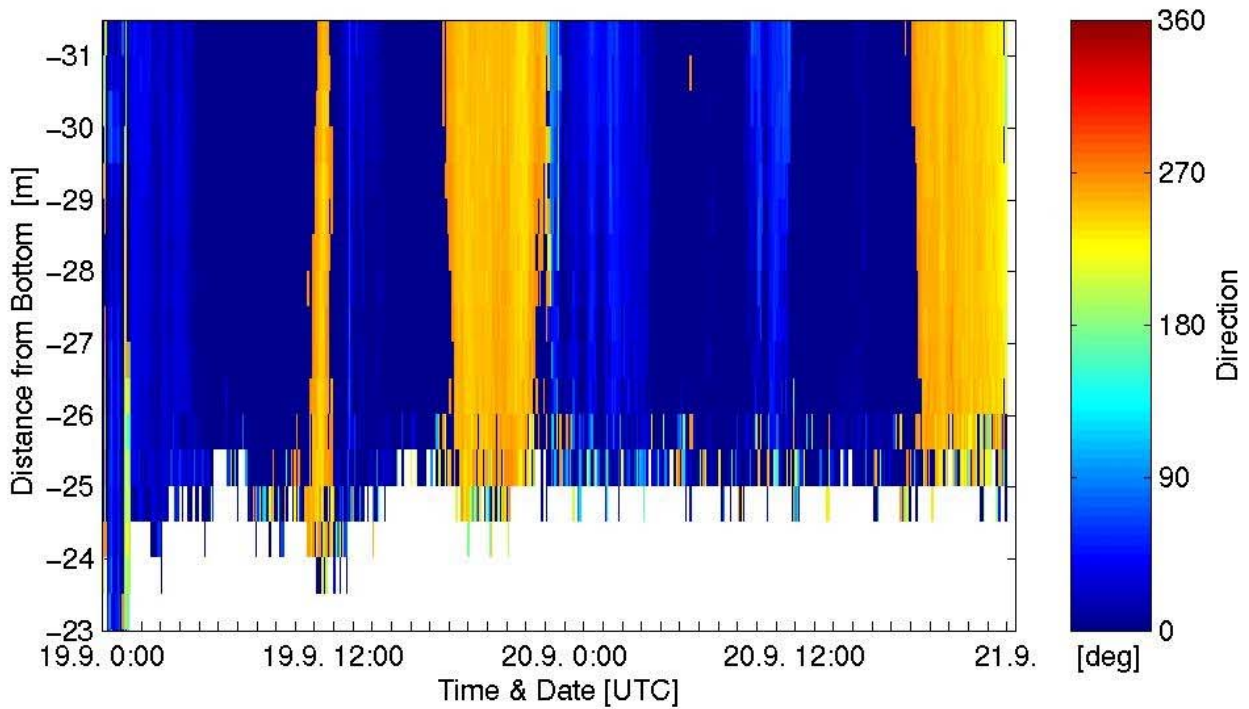
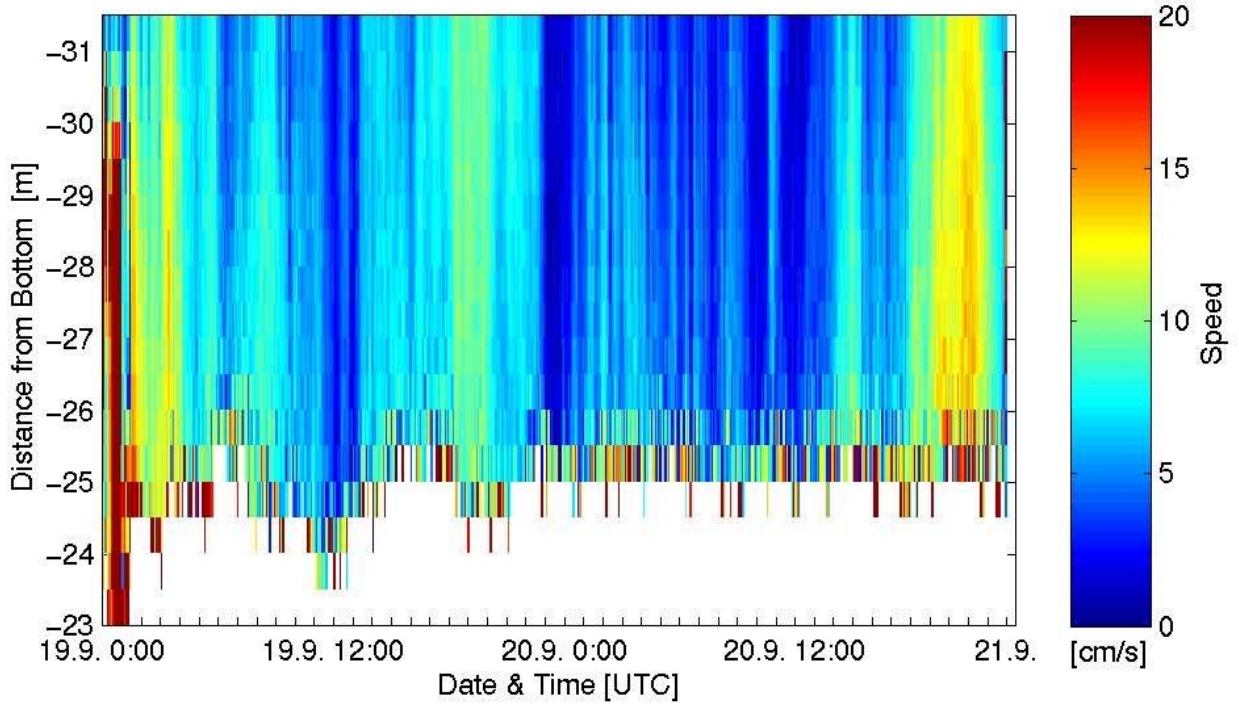


Figure 5.9.2.2: ADCP-data reflecting bottom water current speed and direction in 25 to 31 m distance above seafloor.

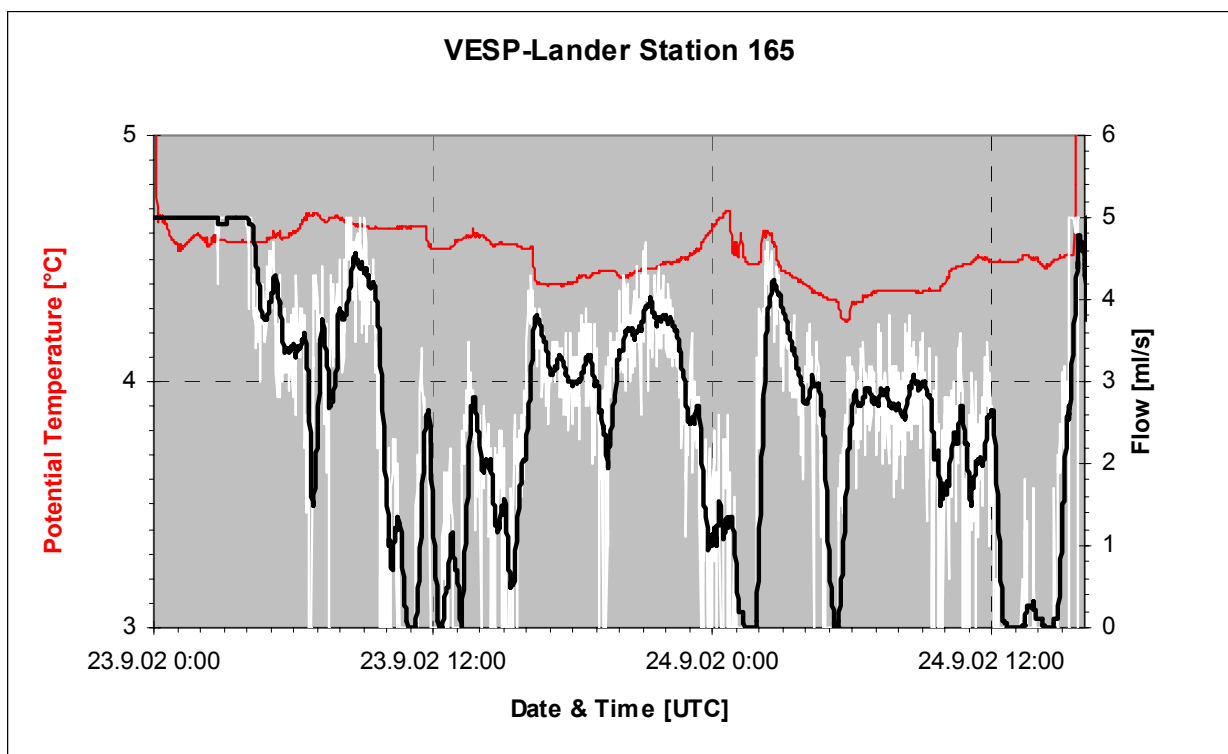
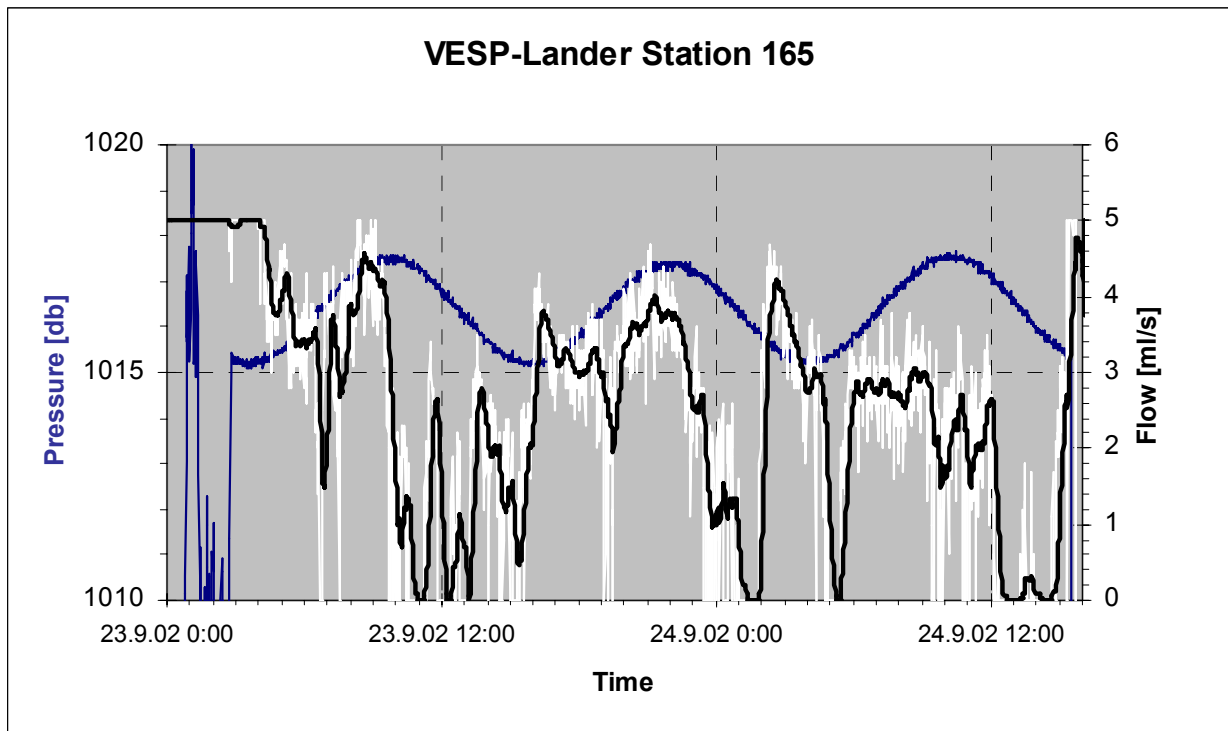


Figure 5.9.2.3: Plot of the uncalibrated flow data with pressure and temperature.

METEOR 54 VESP-Lander Station 165

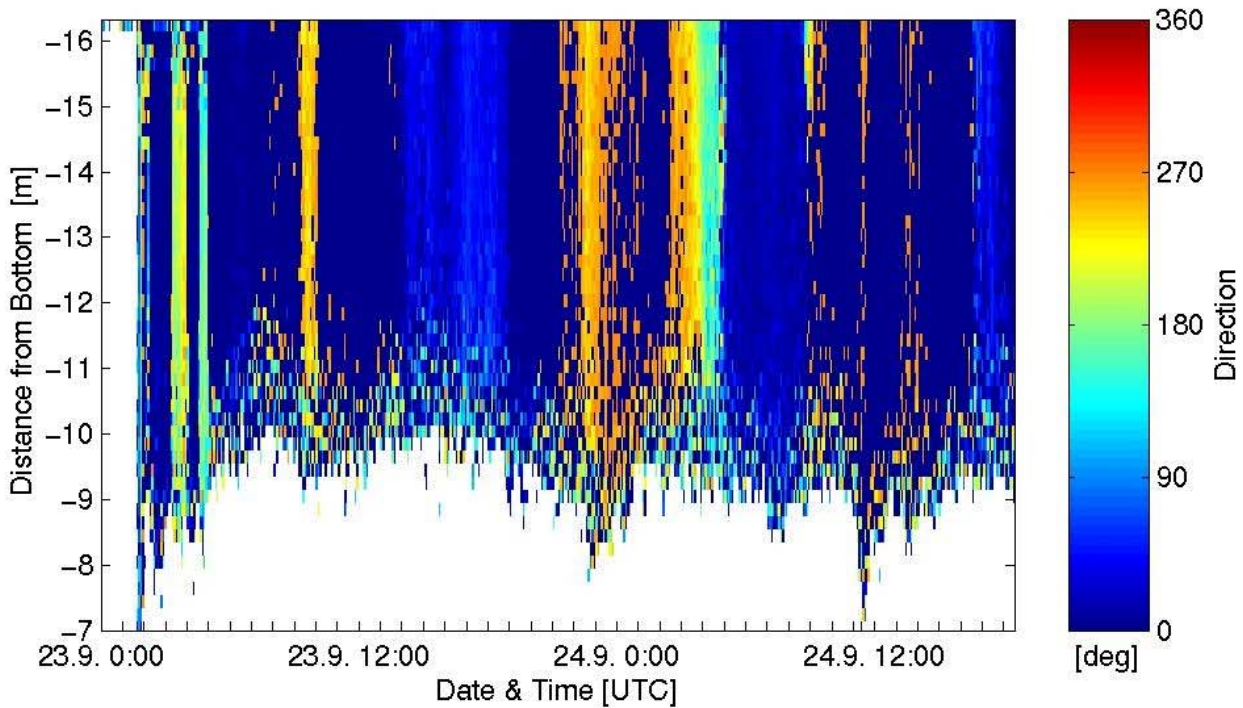
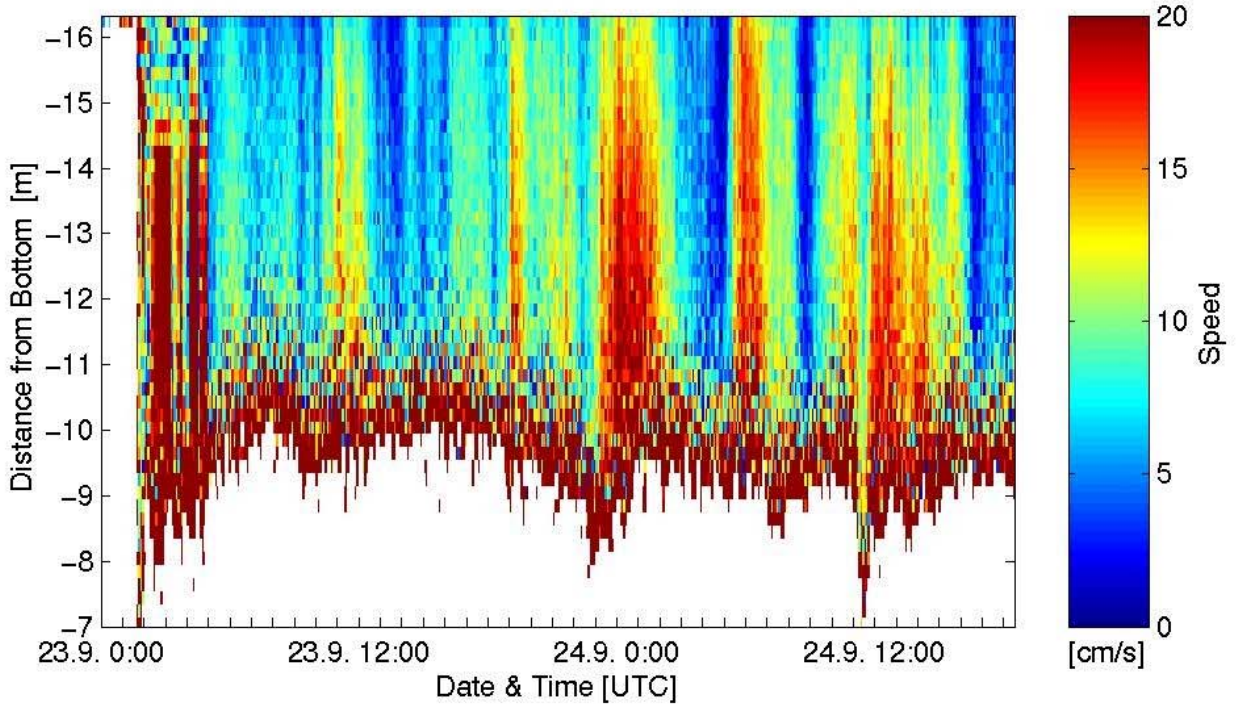


Figure 5.9.2.4: ADCP data with speed and direction of the bottom water 9 to 10 m above the seafloor.

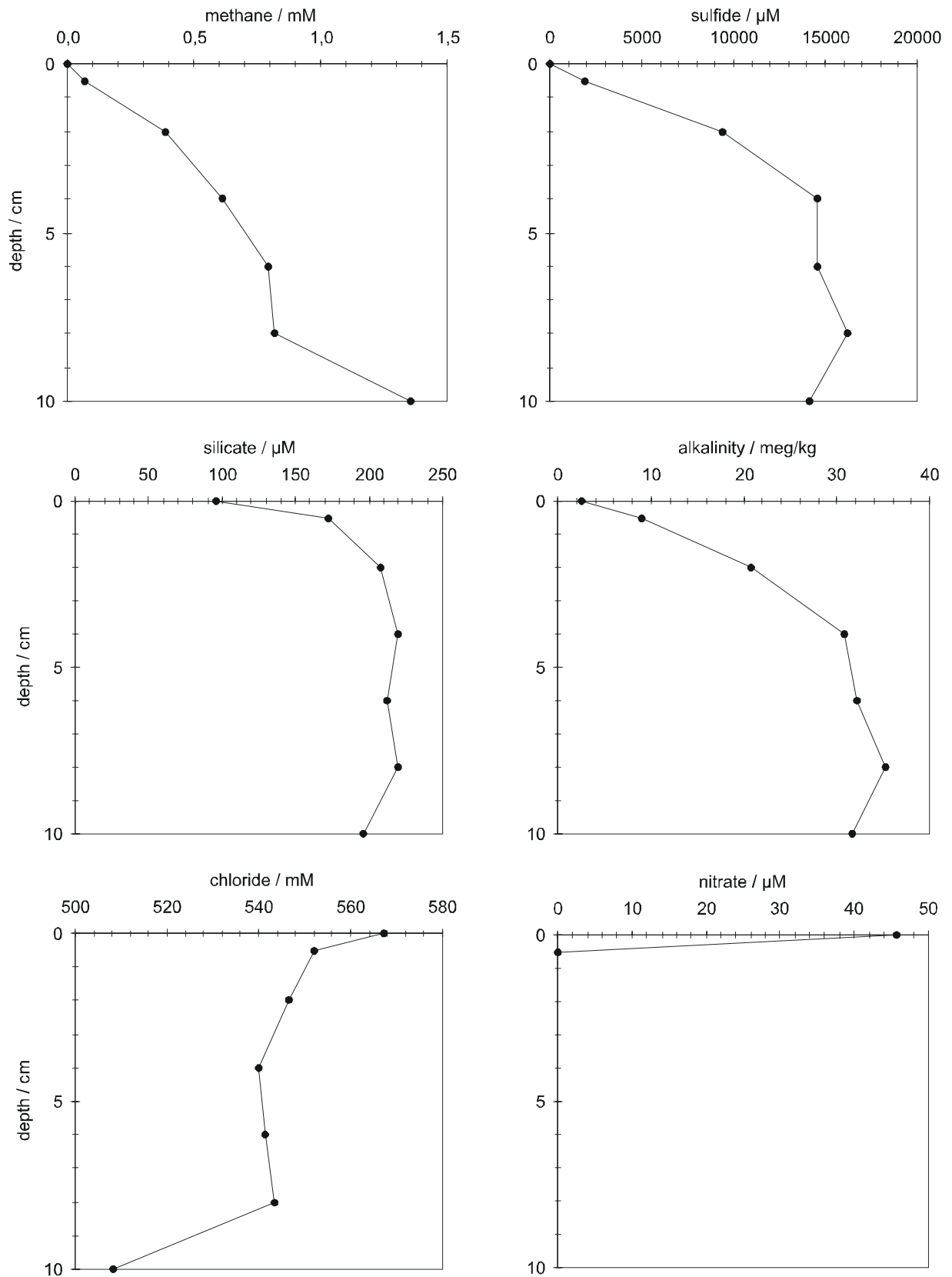


Figure 5.9.2.5: The chemical composition of porewater in the sediments retrieved in chamber K1, BCL 166 at Mound 12. The sharp gradients indicate the release of a low-chlorinity methane-rich fluids.

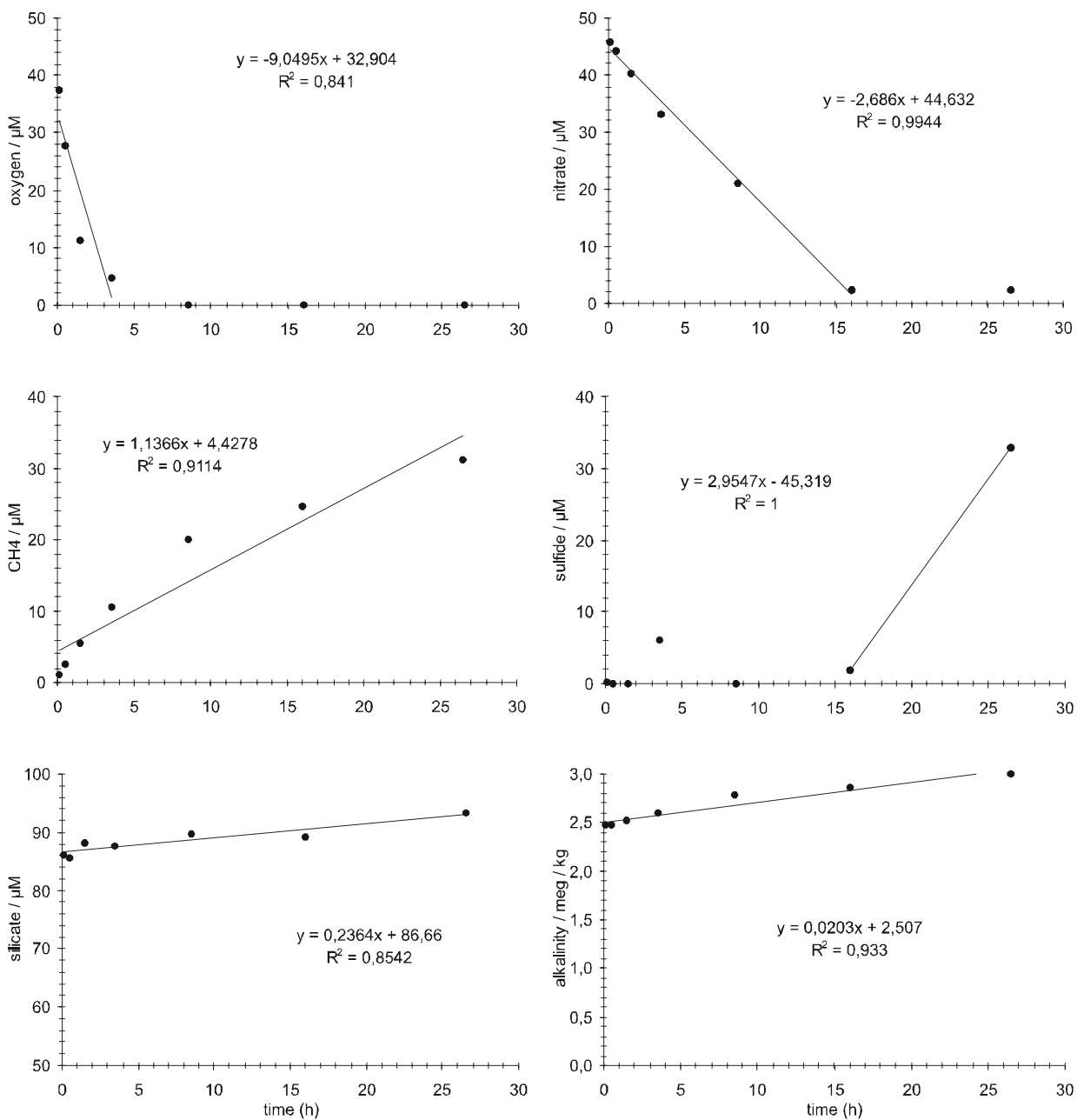


Figure 5.9.2.6: The concentration change of chemical constituents in the chamber water in the course of time (BCL 166, K1, Mound 12). When oxygen and nitrate were completely oxidised the sulfide concentration increases rapidly. The alkalinity increase can be explained by vigorous methane oxidation.

Table 5.9.2.1: Fluxes of chemical compounds in chamber K1, BCL 166 at Mound 12 during the deployment period. The fluxes were calculated as 'oxygen equivalent' in order to compare the total consumption with the total release. The result reveals that oxygen and nitrate is depleted due to the high amounts of sulfide and methane released.

	Flux / mmol m ⁻² d ⁻¹	Flux oxygen equivalent / mmol m ⁻² d ⁻¹
Oxygen consumption	24.4	~24
Nitrate consumption	7.3	~11
Total consumption		~35
Sulfide release (hour 16 to 26.5)	8	16
Methane oxidized (based on Alkalinity released)	27	54
Total release		~70
Methane release	3.1	6.2

Jaco Scarp

VESP-Lander Station 184/190

The Lander was deployed at a clam field close to the scarp. Due to the steep slope the Lander slid at least 1 meter on the train tracks that are used as ballast. The Lander was retrieved on Leg M54/3b. On October 2nd at 23:00 UTC, from 9°7,16' N 84°50,64' W at a water depth of 1818 m.

The deployment site was a narrow plateau at Jaco Scarp characterised by a large field of Vent clams, which indicated fluid venting. Close to this position a benthic chamber lander (BCL) had been deployed beforehand for a short time experiment.

After retrieval of the system the water samples were filled into prepared bottles for preservation and storage and the data of the electronic instruments were read out. Data processing and analysing of the samples will be done at GEOMAR.

References

- Carson B., Suess E., Strasser J.C. (1990) Fluid Flow and Mass Flux Determinations at Vent Sites on the Cascadia Margin Accretionary Prism. *J. Geophys. Res.* 95/B6: 8891-8897.
- Linke P, Suess E, Torres M, Martens V, Rugh WD, Ziebis W, Kulm LD (1994) *In situ* measurement of fluid flow from cold seeps at active continental margins. *Deep-Sea Res.* I 41: 721-739
- Tryon, M.D., K.M. Brown, M.E. Torres, A.M. Trehu, J. McManus, R.W. Collier (1999): Measurements of transience and downward fluid flow near episodic methane gas vents, Hydrate Ridge, Cascadia, *Geology* 2, 1075-1078.

Appendix A

Station List

METEOR 54/2

Station list

			Time (UTC)					Begin / on seafloor		End / off seafloor			
Date 2002	St. No. M 54/	Instrument	Begin	on sea-floor	off sea-floor	End	Duration hh:mm	Latitude N°	Longitude W°	Latitude N°	Longitude W°	Water depth (m)	Recovery Remarks
14.08.	1	GC-6m	12:12	12:19	12:20	12:33	00:21	11°28.91	87°00.02	11°28.91	87°00.02	148	5m
14.08.	2	GC-MTL	15:24	15:46	15:53	16:20	00:56	11°20.11	87°18.35	11°20.11	87°18.35	1205	7,45m / 7 MTL
14.08.	3-1	CTD	18:31			19:39	01:08	11°07.00	87°30.90	11°07.00	87°30.90	5326	test run
14.08.	3-2	CTD	20:08	21:50	21:51	00:26	04:18	11°07.00	87°30.90	11°07.00	87°30.90	5337	22 bottles
15.08.	4-1	HF	01:20	02:30	02:41		00:11	11°14.00	87°30.68	11°14.00	87°30.68	4168	HF-3m
	4-2	HF		03:50	04:05		00:15	11°14.38	87°30.28	11°14.38	87°30.28	4115	
	4-3	HF		05:15	05:24		00:09	11°14.78	87°29.87	11°14.78	87°29.87	4100	
	4-4	HF		06:38	06:47		00:09	11°15.17	87°29.53	11°15.17	87°29.53	4027	
	4-5	HF		08:00	08:06		00:06	11°15.57	87°29.12	11°15.57	87°29.12	3727	failed
	4-6	HF		09:05	09:12		00:07	11°15.94	87°28.74	11°15.94	87°28.74	3638	
	4-7	HF		10:15	10:24		00:09	11°16.34	87°28.36	11°16.34	87°28.36	3498	
	4-8	HF		11:33	11:40		00:07	11°16.72	87°27.98	11°16.72	87°27.98	n.d.	
	4-9	HF		12:28	12:36	13:49	00:08	11°17.12	87°27.60	11°17.12	87°27.60	n.d.	
15.08.	5	DR	15:45	16:58	19:47	21:00	05:15	11°11.44	87°21.24	11°16.01	87°16.16	2947-1719	mainly claye stone
15.08.	6	GC-MTL	22:58	00:27	00:35	02:00	03:02	11°07.01	87°30.91	11°07.01	87°30.90	5320	4.5m/10 MTL
16.08.	7-1	HF	08:12	09:20	09:36		00:16	11°01.22	87°34.20	11°01.22	87°34.20	3874	HF-3m
	7-2	HF		10:31	10:38		00:07	11°01.62	87°42.76	11°01.62	87°42.76	3894	
	7-3	HF		11:32	11:39		00:07	11°02.00	87°42.38	11°02.00	87°42.38	3898	
	7-4	HF		12:28	12:43		00:15	11°02.40	87°42.00	11°02.40	87°42.00	3950	
	7-5	HF		13:39	13:48	15:01	00:09	11°02.79	87°41.61	11°02.79	87°41.61	4125	
16.08.	8	CTD	16:18	17:53	17:54	20:11	03:53	11°04.74	87°34.17	11°04.74	87°34.17	4992	21 bottles
16.08.	8-1	HF	21:00			00:45	03:45	11°04.76	87°34.22	11°04.76	87°34.22	4996	HF-6m, test
17.08.	9	MUC	03:26	03:50	03:51	04:25	00:59	11°20.11	87°18.26	11°20.11	87°18.26	1184	7
17.08.	10-1	HF	05:30	05:52	06:13		00:21	11°24.52	87°20.54	11°24.52	87°20.54	948	HF-6m
	10-2	HF		06:56	07:11		00:15	11°24.89	87°19.99	11°24.89	87°19.99	916	
	10-3	HF		07:58	08:07		00:09	11°25.29	87°19.59	11°25.29	87°19.59	891	
	10-4	HF		08:53	09:08		00:15	11°25.68	87°19.22	11°25.68	87°19.22	855	
	10-5	HF		09:52	10:00		00:08	11°26.07	87°19.83	11°26.07	87°19.83	824	
	10-6	HF		10:46	11:03		00:17	11°26.47	87°18.44	11°26.47	87°18.44	797	
	10-7	HF		11:44	11:56	12:25	00:12	11°26.85	87°18.05	11°26.85	87°18.05	760	
17.08.	11-1	GC-MTL	17:06	17:59	18:06	18:50	01:44	11°06.80	87°51.42	11°06.80	87°51.42	3344	0.5m rock charts/MTL

METEOR 54/2													
Station list													
			Time (UTC)					Begin / on seafloor		End / off seafloor			
Date 2002	St. No. M 54/	Instrument	Begin	on sea-floor	off sea-floor	End	Duration hh:mm	Latitude N°	Longitude W°	Latitude N°	Longitude W°	Water depth (m)	Recovery Remarks
17.08.	11-2	GC	19:42	20:34	20:35	21:20	01:38	11°06.03	87°49.82	11°06.03	87°49.82	3334	4.4m
17.08.	11-3	CTD	22:20	23:28	23:29	00:59	02:39	11°06.77	87°51.45	11°06.77	87°51.45	3350	22
18.08.	12-1	HF	03:00	03:53	04:04		00:11	11°06.41	87°38.05	11°06.41	87°38.05	4906	HF-6m
	12-2	HF		05:01	05:12		00:11	11°06.81	87°38.05	11°06.81	87°38.05	4911	
	12-3	HF		06:02	06:14		00:12	11°07.21	87°37.73	11°07.21	87°37.73	4888	
	12-4	HF		07:01	07:15		00:14	11°07.58	87°36.92	11°07.58	87°36.92	4899	
	12-5	HF		08:08	08:20		00:12	11°07.96	87°36.55	11°07.96	87°36.55	5065	
	12-6	HF		09:06	09:16		00:10	11°08.34	87°36.14	11°08.34	87°36.14	5240	
	12-7	HF		10:11	10:22		00:11	11°08.74	87°35.76	11°08.74	87°35.76	5313	
	12-8	HF		11:17	11:28		00:11	11°09.13	87°35.40	11°09.13	87°35.40	5328	
	12-9	HF		12:26	12:36		00:10	11°09.52	87°35.01	11°09.52	87°35.01	5457	
	12-10	HF		13:37	13:47		00:10	11°09.91	87°34.63	11°09.91	87°34.63	5445	
	12-11	HF		14:51	15:02		00:11	11°10.30	87°34.25	11°10.30	87°34.25	5313	
	12-12	HF		15:54	16:04	17:30	00:10	11°10.70	87°33.87	11°10.70	87°33.87	5120	
18.08.	13	PC	20:00	20:21	20:22	21:15	01:15	11°20.12	87°18.30	11°20.11	87°18.30	1200	3.5m
18.08.	14	GC	23:12	00:51	00:52	02:25	03:13	11°08.61	87°34.00	11°08.61	87°34.00	5412	9.8m
19.08.	15	CTD	03:40	05:03	05:05	07:19	03:39	11°03.34	87°40.11	11°03.34	87°40.11	4383	22
19.08.	16	GC	19:18	19:57	19:58	21:00	01:42	10°18.10	86°18.19	10°18.10	86°18.19	1551	carbonate stone in CC
19.08.	17	GC	21:30	22:01	22:02	22:30	01:00	10°17.57	86°18.57	10°17.57	86°18.57	1673	7.7+2m
19.08.	18	GC	23:00	23:35	23:36	23:57	00:57	10°17.92	86°18.47	10°17.92	86°18.47	1551	5.53m
20.08.	19	CTD	00:35	01:05	01:10	02:27	01:52	10°18.17	86°18.38	10°18.17	86°18.38	1640	22
20.08.	20-1	HF	02:47	03:26	03:34		00:08	10°18.43	86°18.98	10°18.43	86°18.98	1692	HF-3m
	20-2	HF		04:09	04:25		00:16	10°18.25	86°18.84	10°18.25	86°18.84	1690	
	20-3	HF		05:00	05:08		00:08	10°18.08	86°18.66	10°18.08	86°18.66	1683	
	20-4	HF		05:34	05:50		00:16	10°17.97	86°18.55	10°17.97	86°18.55	1617	
	20-5	HF		06:17	06:25		00:08	10°17.91	86°18.48	10°17.91	86°18.48	1553	
	20-6	HF		06:53	06:55		00:02	10°17.83	86°18.40	10°17.83	86°18.40	1529	failed
	20-7	HF		07:24	07:26		00:02	10°17.79	86°18.31	10°17.79	86°18.31	1529	failed
	20-8	HF		07:55	08:11		00:16	10°17.79	86°18.22	10°17.79	86°18.22	1562	
	20-9	HF		08:38	08:45		00:07	10°17.78	86°18.13	10°17.78	86°18.13	1617	
	20-10	HF		09:17	09:32		00:15	10°17.60	86°18.03	10°17.60	86°18.03	1618	
	20-11	HF		10:20	10:28		00:08	10°17.41	86°17.84	10°17.41	86°17.84	1611	

METEOR 54/2

Station list

Date 2002	St. No. M 54/	Instrument	Time (UTC)					Begin / on seafloor		End / off seafloor		Water depth (m)	Recovery Remarks
			Begin	on sea-floor	off sea-floor	End	Duration hh:mm	Latitude N°	Longitude W°	Latitude N°	Longitude W°		
	20-13	HF		12:29	12:37		00:08	10°17.62	86°17.29	10°17.62	86°17.29	1931	
	20-14	HF		13:31	13:47	14:17	00:16	10°18.80	86°18.92	10°18.80	86°18.92	1492	
20.08.	21	GC-MTL	14:57	15:19	15:30	16:15	01:18	10°17.91	86°18.48	10°17.91	86°18.48	1548	4.5m/+5 MTL
20.08.	22	GC-MTL	16:29	16:56	17:03	17:35	01:06	10°17.99	86°18.29	10°17.99	86°18.29	1532	4.6m/+6 MTL
20.08.	23	GC-MTL	19:10	19:35	19:43	20:04	00:54	10°17.81	86°18.25	10°17.81	86°18.25	1530	2.4m/+5 MTL
20.08.	24	GC-MTL	21:34	21:57	22:04	22:30	00:56	10°17.67	86°18.32	10°17.67	86°18.32	1615	5.4m/+5 MTL
20.08.	25	CTD	23:10	23:39	23:55	01:06	01:56	10°17.99	86°18.30	10°18.00	86°18.32	1530	20
21.08.	26-1	HF	02:49	03:48	04:03		00:15	10°05.24	86°24.19	10°05.24	86°24.19	3492	HF-3m
	26-2	HF		04:58	05:05		00:07	10°05.65	86°25.08	10°05.65	86°25.08	3439	
	26-3	HF		07:37	07:53		00:16	10°06.03	86°23.42	10°06.03	86°23.42	3288	
	26-4	HF		08:45	08:53		00:08	10°06.42	86°23.03	10°06.42	86°23.03	3265	
	26-5	HF		09:47	10:02		00:15	10°06.80	86°22.66	10°06.80	86°22.66	3170	
	26-6	HF		10:57	11:04		00:07	10°07.18	86°22.26	10°07.18	86°22.26	3039	
	26-7	HF		11:54	12:08		00:14	10°07.57	86°21.87	10°07.57	86°21.87	3077	
	26-8	HF		13:11	13:17		00:06	10°07.95	86°21.49	10°07.95	86°21.49	2827	
	26-9	HF		14:13	14:20		00:07	10°08.34	86°21.10	10°08.34	86°21.10	2709	
	26-10	HF		15:09	15:21	16:13	00:12	10°08.73	86°20.71	10°08.73	86°20.71	2620	
21.08.	27	GC-MTL	17:21	17:51	17:58	18:15	00:54	10°17.86	86°18.37	10°17.86	86°18.37	1530	0.3m/2 MTL lost
21.08.	28	CTD	19:00	19:36	19:38	20:48	01:48	10°17.93	86°18.15	10°17.93	86°18.15	1532	22
21.08.	29	GC	21:13	21:41	17:42	22:10	00:57	10°17.87	86°18.37	10°17.87	86°18.37	1529	1.5m
21.08.	30	GC	22:34	23:04	23:05	23:37	01:03	10°18.19	86°18.26	10°18.19	86°18.26	1627	0.6m
22.08.	31	MUC	00:10	00:44	00:45	01:17	01:07	10°17.90	86°18.27	10°17.90	86°18.27	1514	7x0.4m
22.08.	32	GC	01:56	02:23	02:24	02:52	00:56	10°18.06	86°18.55	10°18.06	86°18.55	1656	5.8m
22.08.	33-1	HF	03:25	03:54	04:10		00:16	10°17.89	86°18.40	10°17.89	86°18.40	1527	HF-3m
	33-2	HF		04:16	04:25		00:09	10°17.87	86°18.37	10°17.87	86°18.37	1530	
	33-3	HF		04:30	04:38	05:08	00:08	10°17.85	86°18.37	10°17.85	86°18.37	1527	
22.08.	34-1	HF	07:37	09:15	09:24		00:09	09°59.55	86°30.00	09°59.55	86°30.00	4708	HF-6m; data corrupted
	34-2	HF		12:31	12:46		00:15	09°55.73	86°33.88	09°55.73	86°33.88	4193	HF 3m
	34-3	HF		13:44	13:52		00:08	09°56.11	86°33.48	09°56.11	86°33.48	4188	
	34-4	HF		14:56	15:04	16:12	00:08	09°56.47	86°33.10	09°56.47	86°33.10		
22.08.	35	GC	19:26	20:37	20:38	21:35	02:09	09°41.20	86°14.58	09°41.20	86°14.58	4403	7.7m
22.08.	36	GC	22:20	23:17	23:18	00:15	01:55	09°40.02	86°11.02	09°40.02	86°11.02	4183	5.8m
23.08.	37-1	HF	01:33	02:13	02:29		00:16	09°48.18	86°03.40	09°48.18	86°03.40	2514	HF-3m
	37-2	HF		03:25	03:32		00:07	09°48.58	86°03.04	09°48.58	86°03.04	2470	

METEOR 54/2
Station list

		Time (UTC)						Begin / on seafloor		End / off seafloor			
Date 2002	St. No. M 54/	Instrument	Begin	on sea-floor	off sea-floor	End	Duration hh:mm	Latitude N°	Longitude W°	Latitude N°	Longitude W°	Water depth (m)	Recovery Remarks
	37-3	HF		04:24	04:40		00:16	09°48.98	86°02.68	09°48.98	86°02.68	2422	
	37-4	HF		05:28	05:35	06:20	00:07	09°49.39	86°02.33	09°49.39	86°02.33	2380	
23.08.	38-1	HF	09:40	10:29	10:44		00:15	09°51.84	86°00.16	09°51.84	86°00.16	1926	HF-3m
	38-2	HF		11:33	11:39		00:06	09°52.24	85°59.81	09°52.24	85°59.81	1824	
	38-3	HF		12:31	12:49	13:21	00:18	09°52.66	85°59.45	09°52.66	85°59.45	1682	
23.08.	39-1	GC-MTL	16:06	16:24	16:31	16:36	00:30	09°49.81	85°40.81	09°49.81	85°40.81	105	0.3m
23.08.	39-2	GC-MTL	16:54	16:57	17:01	17:05	00:11	09°49.82	85°40.81	09°49.82	85°40.82	105	0.3m
23.08.	40	GC	18:16	18:20	18:21	18:30	00:14	09°50.27	85°44.07	09°50.28	85°44.05	230	2.7m
23.08.	41-1	GC	20:28	21:06	21:07	21:46	01:18	09°48.99	86°02.68	09°48.99	86°02.68	2422	5.3m
23.08.	41-2	MUC	22:15	22:57	22:59	23:45	01:30	09°49.00	86°02.67	09°49.00	86°02.67	2421	6x0.4m
24.08.	42-1	HF	01:22	02:29	02:44		00:15	09°37.59	86°12.73	09°37.59	86°12.73	4154	HF-3m
	42-2	HF		03:29	03:37		00:08	09°37.98	86°12.38	09°37.98	86°12.38	4169	
	42-3	HF		04:27	04:42		00:15	09°38.40	86°12.03	09°38.40	86°12.03	4350	
	42-4	HF		07:26	07:32		00:06	09°38.80	86°11.65	09°38.80	86°11.65	4368	
	42-5	HF		08:20	08:33		00:13	09°39.17	86°11.31	09°39.17	86°11.31	4316	
	42-6	HF		09:41				09°39.61	86°10.95	09°39.61	86°10.95		failed
	42-7	HF		10:57	11:06		00:09	09°40.04	86°10.58	09°40.04	86°10.58	4077	
	42-8	HF		12:09				09°40.44	86°10.22	09°40.44	86°10.22	3980	
	42-9	HF		13:20	13:28		00:08	09°40.85	86°09.88	09°40.85	86°09.88	3890	
	42-10	HF		14:24	14:39	15:44	00:15	09°41.24	86°09.51	09°41.24	86°09.51	3799	
24.08.	43-1	HF	18:31	19:33	19:48		00:15	09°23.88	85°59.87	09°23.88	86°59.87	3815	HF-3m
	43-2	HF		20:52	20:54		00:02	09°24.26	85°59.56	09°24.26	85°59.56	3841	
	43-3	HF		22:11	22:19	23:30	00:08	09°24.70	85°59.19	09°24.70	85°59.19	3888	
	44	HF											no existence
25.08.	45	GC	15:53	16:26	16:25	16:53	01:00	09°07.85	84°50.20	09°07.85	84°50.20	1343	0.2m
25.08.	46	GC	18:13	18:43	18:44	19:10	00:57	09°07.09	84°50.74	09°07.09	84°50.74	1858	0.2m
25.08.	47	CTD	19:45	20:21	20:24	21:49	02:04	09°07.24	84°50.65	09°07.25	84°50.61	1803	22
25.08.	48-1	GC	23:02	23:20	23:21	23:38	00:36	09°10.41	84°48.25	09°10.41	84°48.25	761	2.5m
26.08.	48-2	GC	00:13	00:26	00:27	00:40	00:27	09°10.41	84°48.25	09°10.41	84°48.25	760	2.8m
26.08.	49-1	HF		04:40	04:55		00:15	08°49.83	84°51.05	08°49.83	84°51.05	3468	HF-3m
	49-2	HF		06:10	06:20		00:10	08°49.41	84°51.34	08°49.41	84°51.34	3331	
	49-3	HF		07:27	07:43		00:16	08°48.93	84°51.60	08°48.93	84°51.60	3289	1st therm. out of order

METEOR 54/2

Station list

			Time (UTC)					Begin / on seafloor		End / off seafloor			
Date 2002	St. No. M 54/	Instrument	Begin	on sea-floor	off sea-floor	End	Duration hh:mm	Latitude N°	Longitude W°	Latitude N°	Longitude W°	Water depth (m)	Recovery Remarks
	49-4	HF		08:39	08:46		00:07	08°48.46	84°51.84	08°48.46	84°51.84	3279	2nd therm. out of order
	49-5	HF		09:39	09:54		00:15	08°47.98	84°52.11	08°47.98	84°52.11	3772	3rd therm. out of order
	49-6	HF		10:43	10:50		00:07	08°47.49	84°52.36	08°47.49	84°52.36	3284	
	49-7	HF		11:41	11:58		00:17	08°47.01	84°52.63	08°47.01	84°52.63	3264	
26.08.	50	CTD	15:20	15:58	16:01	17:31	02:11	09°06.90	84°50.86	09°06.90	84°50.85	1922	22
26.08.	51	GC	18:37	18:52	18:53	19:25	00:48	09°09.04	84°49.19	09°09.04	84°49.19	838	0.2m, carbonate stone
26.08.	52	GC	20:04	20:29	20:30	20:56	00:52	09°07.23	84°50.65	09°07.23	84°50.65	1802	0.34m, clay clasts
26.08.	53	CTD	21:35	22:12	22:14	23:42	02:07	09°06.22	84°51.84	09°06.20	84°51.85	2025	22
27.08.	54	GC	00:16	00:47	00:48	01:17	01:01	09°07.31	84°50.56	09°07.31	84°50.56	1758	0.3m
27.08.	55-1	HF		03:36	03:50		00:14	08°56.05	84°47.74	08°56.05	84°47.74	2882	HF-3m
	55-2	HF		04:49	04:56		00:07	08°56.53	84°47.49	08°56.53	84°47.49	2790	1st therm. out of order
	55-3	HF		05:53	06:08		00:15	08°57.00	84°47.23	08°57.00	84°47.23	2732	3rd therm. out of order
	55-4	HF		07:01	07:03		00:02	08°57.48	84°47.00	08°57.48	84°47.00	2633	no data
	55-5	HF		09:00	09:15		00:15	08°58.94	84°46.22	08°58.94	84°46.22	2285	
	55-6	HF		10:07	10:14		00:07	08°59.41	84°45.97	08°59.41	84°45.97	2153	
	55-7	HF		11:06	11:21		00:15	08°59.89	84°45.71	08°59.89	84°45.71	2045	
	55-8	HF		12:06	12:13		00:07	09°00.37	84°45.44	09°00.37	84°45.44	1917	
	55-9	HF		12:59	13:14		00:15	09°00.85	84°45.18	09°00.85	84°45.18	1829	
27.08.	56	GC-MTL	15:44	16:39	16:46	18:00	02:16	08°55.61	84°58.01	08°55.61	84°58.01	3535	5.9m
27.08.	57	GC-MTL	19:07	20:02	20:09	21:10	02:03	08°49.70	84°51.21	08°49.70	84°51.21	3462	7.2m
27.08.	58-1	CTD	23:10	23:27	23:28	00:29	01:19	09°10.43	84°48.25	09°10.44	84°48.26	760	21
28.08.	58-2	MUC	00:42	00:55	00:56	01:23	00:41	09°10.43	84°48.25	09°10.43	84°48.25	757	5x0.2m
28.08.	59-1	HF		02:13	02:27		00:14	09°10.40	84°48.64	09°10.40	84°48.64	785	HF-3m
	59-2	HF		02:59	03:07		00:08	09°10.41	84°48.47	09°10.41	84°48.47	772	
	59-3	HF		03:41	03:56		00:15	09°10.42	84°48.30	09°10.42	84°48.30	757	
	59-4	HF		04:23	04:30		00:07	09°10.41	84°48.26	09°10.41	84°48.26	759	
	59-5	HF		04:52	05:05		00:13	09°10.43	84°48.21	09°10.43	84°48.21	755	
	59-6	HF		05:28	05:35		00:07	09°10.43	84°48.12	09°10.43	84°48.12	740	
	59-7	HF		06:08	06:24		00:16	09°10.45	84°47.92	09°10.45	84°47.92	738	
28.08.	60-1	HF		07:46	08:01		00:15	09°09.21	84°49.45	09°09.21	84°49.45	819	HF-3m
	60-2	HF		08:23	08:32		00:09	09°09.15	84°49.36	09°09.15	84°49.36	802	
	60-3	HF		08:53	09:02		00:09	09°09.08	84°49.25	09°09.08	84°49.25	833	

METEOR 54/2

Station list

			Time (UTC)					Begin / on seafloor		End / off seafloor			
Date 2002	St. No. M 54/	Instrument	Begin	on sea-floor	off sea-floor	End	Duration hh:mm	Latitude N°	Longitude W°	Latitude N°	Longitude W°	Water depth (m)	Recovery Remarks
	60-4	HF		09:21	09:38		00:17	09°09.03	84°49.18	09°09.03	84°49.18	839	
	60-5	HF		10:02	10:10		00:08	09°08.98	84°49.10	09°08.98	84°49.10	826	
	60-6	HF		10:29	10:44		00:15	09°08.91	84°49.02	09°08.91	84°49.02	834	
	60-7	HF		11:06	11:13		00:07	09°08.85	84°48.92	09°08.85	84°48.92	835	
	60-8	HF		11:48	11:57		00:09	09°08.75	84°48.74	09°08.75	84°48.74	881	
	60-9	HF		12:25	12:38		00:13	09°08.63	84°48.58	09°08.63	84°48.58	861	
	60-10	HF		13:04	13:11		00:07	09°08.53	84°48.40	09°08.53	84°48.40	854	
28.08.	61	GC	14:00	14:20	14:21	14:36	00:36	09°10.46	84°47.76	09°10.46	84°47.76	744	
28.08.	62-1	CTD	15:15	15:30	15:31	16:32	01:17	09°09.04	84°49.18	09°09.03	84°49.18	837	22
28.08.	62-2	GC	16:43	16:58	16:59	17:18	00:35	09°09.02	84°49.18	09°09.02	84°49.18	825	2.8m
28.08.	63	GC	18:05	18:16	18:17	18:45	00:40	09°09.11	84°49.28	09°09.11	84°49.28	815	3.3m
28.08.	64	GC	19:31	19:45	19:46	20:13	00:42	09°10.54	84°48.27	09°10.54	84°48.27	750	5.5m
28.08.	65	MUC	20:35	20:45	20:46	21:18	00:43	09°10.44	84°47.75	09°10.44	84°47.75	743	5X0.2
28.08.	66	CTD	22:10	22:45	22:46	00:09	01:59	09°05.41	84°49.64	09°05.40	84°49.64	1960	22
29.08.	67-1	HF		01:40	02:00		00:20	09°06.53	84°42.09	09°06.53	84°42.09	1232	HF-6m
	67-2	HF		02:54	03:05		00:11	09°07.00	84°41.83	09°07.00	84°41.83	1191	
	67-3	HF		04:02	04:26		00:24	09°07.47	84°41.57	09°07.47	84°41.57	1151	
	67-4	HF		05:31	05:54		00:23	09°07.95	84°41.31	09°07.95	84°41.31	1108	
	67-5	HF		06:54	07:05		00:11	09°08.43	84°41.04	09°08.43	84°41.04	1076	
	67-6	HF		08:03	08:19		00:16	09°08.90	84°40.80	09°08.90	84°40.80	1021	
	67-7	HF		09:15	09:25		00:10	09°09.42	84°40.52	09°09.42	84°40.52	965	
	67-8	HF		10:23	10:45		00:22	09°09.87	84°40.27	09°09.87	84°40.27	897	
	67-9	HF		11:52	12:04		00:12	09°10.36	84°40.04	09°10.36	84°40.04	851	
29.08.	68	GC	14:56	15:02	15:03	15:10	00:14	09°24.71	84°22.51	09°24.71	84°22.51	54	5.6m
29.08.	69-1	GC	18:50	19:20	19:21	19:50	01:00	09°01.97	84°37.27	09°01.97	84°37.27	1427	-
29.08.	69-2	CTD	19:55	20:22	20:24	21:34	01:39	09°01.98	84°37.28	09°01.98	84°37.26	1427	22
29.08.	70-1	GC	21:46	22:16	22:17	22:47	01:01	09°01.91	84°37.26	09°01.91	84°37.26	1422	carbonate concretion
29.08.	70-2	GC	22:49	23:20	23:21	23:50	01:01	09°01.91	84°37.26	09°01.91	84°37.26	1434	carbonate concretions
30.08.	71-1	HF		02:33	02:41		00:08	08°50.35	84°50.82	08°50.35	84°50.82	3437	HF-3m
	71-2	HF		04:11	04:25		00:14	08°50.83	84°50.56	08°50.83	84°50.56	3466	
	71-3	HF		05:33	05:47		00:14	08°51.30	84°50.29	08°51.30	84°50.29		
	71-4	HF		06:38	06:45		00:07	08°51.78	84°50.07	08°51.78	84°50.07		

METEOR 54/2

Station list

			Time (UTC)					Begin / on seafloor		End / off seafloor			
Date 2002	St. No. M 54/	Instrument	Begin	on sea-floor	off sea-floor	End	Duration hh:mm	Latitude N°	Longitude W°	Latitude N°	Longitude W°	Water depth (m)	Recovery Remarks
	71-5	HF		07:42	07:49		00:07	08°52.25	84°49.82	08°52.25	84°49.82	3568	
	71-6	HF		08:41	08:52		00:11	08°52.74	84°49.56	08°52.74	84°49.56	3422	
	71-7	HF		09:47	10:01		00:14	08°53.22	84°49.29	08°53.22	84°49.29	3414	
	71-8	HF		10:49	10:56		00:07	08°53.70	84°49.03	08°53.70	84°49.03	3309	
	71-9	HF		11:42	11:49		00:07	08°53.17	84°48.79	08°53.17	84°48.79	3251	
30.08.	72	GC	14:13	14:37	14:38	15:02	00:49	09°01.96	84°37.20	09°01.96	84°37.20	1430	carbonate concretions
30.08.	73-1	CTD	15:40	16:06	16:08	17:11	01:31	09°02.01	84°37.24	09°02.03	84°37.24	1446	22
30.08.	73-2	GC	17:27	18:02	18:03	18:30	01:03	09°02.03	84°37.24	09°02.03	84°37.24	1450	2.8(+1.3)m
30.08.	74	GC	18:57	19:23	19:24	20:00	01:03	09°02.05	84°37.31	09°02.05	84°37.31	1445	2.8(+1.55)m
30.08.	75	GC	20:22	20:45	20:46	21:18	00:56	09°01.98	84°37.24	09°01.98	84°37.24	1430	2.8(+1.4)m
30.08.	76-1	MUC	21:40	22:02	22:03	22:27	00:47	09°02.00	84°37.25	09°02.00	84°37.25	1438	1x0.3m
30.08.	76-2	MUC	22:42	23:07	23:09	23:40	00:58	09°02.00	84°37.25	09°02.00	84°37.25	1441	6x0.3m
31.08.	77-1	HF		05:46	06:02		00:16	08°48.60	84°48.29	08°48.60	84°48.29	3393	HF-3m
	77-2	HF		06:53	07:00		00:07	08°49.07	84°48.05	08°49.07	84°48.05		
	77-3	HF		08:00	08:12		00:12	08°49.55	84°47.80	08°49.55	84°47.80	3540	
	77-4	HF		09:10	09:17		00:07	08°50.04	84°47.54	08°50.04	84°47.54	3558	
	77-5	HF		10:15	10:30		00:15	08°50.52	84°47.26	08°50.52	84°47.26	3568	
	77-6	HF		11:20	11:35		00:15	08°50.99	84°47.02	08°50.99	84°47.02	3544	
31.08.	78	GC-MTL	14:22	14:47	14:53	15:20	00:58	09°02.01	84°37.25	09°02.01	84°37.25	1447	5.8m
31.08.	79	CTD	15:35	16:00	16:01	17:06	01:31	09°01.95	84°37.25	09°01.94	84°37.25	1426	22
31.08.	80	GC-MTL	17:39	18:00	18:07	18:50	01:11	09°02.04	84°37.29	09°02.07	84°37.29	1448	8.6m
31.08.	81-1	GC	20:30	20:48	20:49	21:12	00:42	09°09.20	84°41.97	09°09.20	84°41.97	931	5.8m
31.08.	81-2	MUC	21:33	21:52	21:53	22:19	00:46	09°09.19	84°41.99	09°09.19	84°41.99	932	4x0.25m
01.09.	82-1	HF		01:23	01:39		00:16	08°55.13	84°18.43	08°55.13	84°18.43	1077	HF-3m
	82-2	HF		02:09	02:17		00:08	08°55.24	84°18.45	08°55.24	84°18.45	1069	
	82-3	HF		02:50	02:57		00:07	08°55.34	84°18.45	08°55.34	84°18.45	1049	
	82-4	HF		03:21	03:28		00:07	08°55.44	84°18.45	08°55.44	84°18.45	1037	
	82-5	HF		03:57	04:10		00:13	08°55.54	84°18.45	08°55.54	84°18.45	1031	
	82-6	HF		05:36	05:43		00:07	08°55.15	84°18.34	08°55.15	84°18.34	1069	
	82-7	HF		06:17	06:24		00:07	08°55.24	84°18.34	08°55.24	84°18.34	1052	
	82-8	HF		06:51	06:57		00:06	08°55.34	84°18.34	08°55.34	84°18.34	1037	
	82-9	HF		07:17	07:33		00:16	08°55.44	84°18.34	08°55.44	84°18.34	1039	

METEOR 54/2

Station list

			Time (UTC)					Begin / on seafloor		End / off seafloor			
Date 2002	St. No. M 54/	Instrument	Begin	on sea-floor	off sea-floor	End	Duration hh:mm	Latitude N°	Longitude W°	Latitude N°	Longitude W°	Water depth (m)	Recovery Remarks
	82-10	HF		07:56	08:03		00:07	08°55.54	84°18.34	08°55.54	84°18.34	1042	
	82-11	HF		08:57	09:04		00:07	08°55.14	84°18.25	08°55.14	84°18.25	1043	
	82-12	HF		09:27	09:37		00:10	08°55.24	84°18.25	08°55.24	84°18.25	1047	
	82-13	HF		09:57	10:12		00:15	08°55.34	84°18.24	08°55.34	84°18.24	1019	
	82-14	HF		10:30	10:38		00:08	08°55.45	84°18.24	08°55.45	84°18.24	1029	
	82-15	HF		11:00	11:15		00:15	08°55.55	84°18.25	08°55.55	84°18.25	1036	
	82-16	HF		11:32	11:39		00:07	08°55.54	84°18.15	08°55.54	84°18.15	1036	
	82-17	HF		12:01	12:15		00:14	08°55.45	84°18.14	08°55.45	84°18.14	1041	
	82-18	HF		12:32	12:38		00:06	08°55.35	84°18.14	08°55.35	84°18.14	1043	
	82-19	HF		12:53	13:07		00:14	08°55.25	84°18.14	08°55.25	84°18.14	1047	
	82-20	HF		13:22	13:28		00:06	08°55.15	84°18.14	08°55.15	84°18.14	1051	
	82-21	HF		13:50	14:05		00:15	08°55.15	84°18.06	08°55.15	84°18.06	1044	
	82-22	HF		14:27	14:34		00:07	08°55.24	84°18.05	08°55.24	84°18.05	1044	
	82-23	HF		14:56	15:10		00:14	08°55.34	84°18.05	08°55.34	84°18.05	1044	
	82-24	HF		15:29	15:36		00:07	08°55.44	84°18.04	08°55.44	84°18.04	1036	
	82-25	HF		15:54	16:09		00:15	08°55.54	84°18.04	08°55.54	84°18.04	1032	
01.09.	83	GC	17:07	17:23	17:24	17:47	00:40	08°55.79	84°18.74	08°55.79	84°18.74	1005	0.2m
01.09.	84	GC	18:20	18:36	18:37	18:55	00:35	08°55.80	84°18.61	08°55.80	84°18.61	980	2.8(+0.1)m
01.09.	85	GC	19:24	19:39	19:40	20:01	00:37	08°55.84	84°18.65	08°55.84	84°18.65	968	-
01.09.	86	CTD	20:10	20:33	20:36	21:36	01:26	08°55.79	84°18.71	08°55.78	84°18.74	1003	22
01.09.	87	MUC	21:51	22:14	22:15	22:38	00:47	08°55.94	84°18.65	08°55.94	84°18.65	1000	7x0.3m
02.09.	88-1	HF		01:17	01:32		00:15	08°39.08	84°19.22	08°39.08	84°19.22	2226	HF-3m
	88-2	HF		02:28	02:36		00:08	08°39.53	84°18.94	08°39.53	84°18.94	2130	
	88-3	HF		03:21	03:36		00:15	08°39.98	84°18.63	08°39.98	84°18.63	1954	
	88-4	HF		04:25	04:32		00:07	08°40.44	84°18.34	08°40.44	84°18.34	1857	
	88-5	HF		05:17	05:32		00:15	08°40.91	84°18.05	08°40.91	84°18.05	1738	
	88-6	HF		06:24	06:31		00:07	08°41.37	84°17.77	08°41.37	84°17.77		
	88-7	HF		07:27	07:42		00:15	08°41.83	84°17.48	08°41.83	84°17.48	1558	
	88-8	HF		08:38	08:45		00:07	08°42.28	84°17.10	08°42.28	84°17.10	1496	
	88-9	HF		09:37	09:52		00:15	08°42.74	84°16.91	08°42.74	84°16.91	1424	
	88-10	HF		10:58	11:05		00:07	08°43.22	84°16.60	08°43.22	84°16.60	1307	
	88-11	HF		12:03	12:18		00:15	08°43.88	84°16.32	08°43.88	84°16.32	1168	

METEOR 54/2

Station list

			Time (UTC)					Begin / on seafloor		End / off seafloor			
Date 2002	St. No. M 54/	Instrument	Begin	on sea-floor	off sea-floor	End	Duration hh:mm	Latitude N°	Longitude W°	Latitude N°	Longitude W°	Water depth (m)	Recovery Remarks
02.09.	89	GC	14:15	14:43	14:44	15:10	00:55	08°55.89	84°18.69	08°55.89	84°18.69	997	2.3m
02.09.	90	GC	15:24	16:18	16:19	16:41	01:17	08°55.93	84°18.55	08°55.93	84°18.55	1009	2.8(+0.3)m
02.09.	91	GC	17:05	17:21	17:22	17:47	00:42	08°55.77	84°18.57	08°55.77	84°18.57	1010	2.8m
02.09.	92	GC	18:40	18:57	18:58	19:30	00:50	08°55.88	84°18.77	08°55.88	84°18.77	1012	2.8m
02.09.	93	CTD	19:54	20:15	20:16	21:22	01:28	08°55.84	84°18.51	08°55.82	84°18.55	1014	22
02.09.	94	GC	21:30	21:51	21:52	22:20	00:50	08°55.81	84°18.64	08°55.81	84°18.64	994	4.7m
03.09.	95-1	HF		01:15	01:32		00:17	08°34.04	84°22.38	08°34.04	84°22.38	2837	HF-3m
	95-2	HF		02:43	02:50		00:07	08°34.50	84°22.11	08°34.50	84°22.11	2853	
	95-3	HF		03:44	03:58		00:14	08°34.96	84°21.81	08°34.96	84°21.81	2856	
	95-4	HF		04:50	04:57		00:07	08°35.42	84°21.53	08°35.42	84°21.53	2873	
	95-5	HF		05:51	06:05		00:14	08°35.88	84°21.24	08°35.88	84°21.24	2919	
	95-6	HF		06:56	07:03		00:07	08°36.33	84°20.96	08°36.33	84°20.96	2801	
	95-7	HF		07:51	08:06		00:15	08°36.79	84°20.65	08°36.79	84°20.65	2705	
	95-8	HF		08:56	09:03		00:07	08°37.26	84°20.36	08°37.26	84°20.36	2668	
	95-9	HF		09:50	10:03		00:13	08°37.12	84°20.08	08°37.12	84°20.08	2566	
	95-10	HF		10:57	11:13		00:16	08°38.17	84°19.80	08°38.17	84°19.80	2436	
03.09.	96	CTD	14:15	14:33	14:34	15:32	01:17	08°55.84	84°18.64	08°55.85	84°18.64	986	22
03.09.	97-1	GC	15:47	16:05	16:06	16:30	00:43	08°55.91	84°18.69	08°55.91	84°18.69	999	-
03.09.	97-2	GC	16:40	16:59	17:00	17:25	00:45	08°55.90	84°18.70	08°55.90	84°18.70	1001	3.8m
03.09.	98	GC	19:29	19:52	19:53	20:24	00:55	09°01.94	84°37.25	09°01.94	84°37.25	1428	carbonate concretions
03.09.	99	CTD	22:30	22:46	22:47	23:46	01:16	08°55.82	84°18.64	08°55.80	84°18.63	991	22
04.09.	100	GC	00:03	00:23	00:24	00:55	00:52	08°55.25	84°18.24	08°55.25	84°18.24	1044	2.8m
04.09.	101-1	HF		04:22	04:37		00:15	08°30.03	84°07.25	08°30.03	84°07.25	1708	HF-3m
	101-2	HF		05:39	05:47		00:08	08°29.55	84°07.48	08°29.55	84°07.48	1861	
	101-3	HF		06:35	06:51		00:16	08°29.07	84°07.72	08°29.07	84°07.72	1999	
	101-4	HF		07:39	07:48		00:09	08°28.57	84°07.96	08°28.57	84°07.96	2192	
	101-5	HF		08:40	08:55		00:15	08°28.08	84°08.20	08°28.08	84°08.20	2270	
	101-6	HF		09:35	09:42		00:07	08°27.59	84°08.44	08°27.59	84°08.44	2248	
	101-7	HF		10:33	10:47		00:14	08°27.09	84°08.69	08°27.09	84°08.69	2235	
	101-8	HF		11:35	11:50		00:15	08°26.60	84°08.95	08°26.60	84°08.95	2238	
04.09.	102	GC	15:57	16:11	16:13	16:48	00:51	08°55.38	84°18.31	08°55.38	84°18.31	1039	2.3m
04.09.	103	GC	17:20	17:40	17:41	18:00	00:40	08°55.90	84°18.70	08°55.90	84°18.70	994	-

METEOR 54/2													
Station list													
			Time (UTC)					Begin / on seafloor		End / off seafloor			
Date 2002	St. No. M 54/	Instrument	Begin	on sea-floor	off sea-floor	End	Duration hh:mm	Latitude N°	Longitude W°	Latitude N°	Longitude W°	Water depth (m)	Recovery Remarks
04.09.	104	CTD	18:55	19:06	19:07	19:56	01:01	08°51.00	84°12.97	08°51.02	84°12.97	408	22
04.09.	105	GC	20:14	20:22	20:23	20:50	00:36	08°51.20	84°13.01	08°51.20	84°13.01	414	3m
04.09.	106	GC	22:15	22:37	22:38	23:10	00:55	08°45.55	84°17.09	08°45.55	84°17.09	1012	5.8m
05.09.	107-1	HF		01:58	02:19		00:21	08°30.03	84°07.26	08°30.03	84°07.26	1706	HF-6m
	107-2	HF		03:07	03:20		00:13	08°30.51	84°07.02	08°30.51	84°07.02	1594	
	107-3	HF		04:07	04:28		00:21	08°31.00	84°06.78	08°31.00	84°06.78	1481	
	107-4	HF		05:12	05:24		00:12	08°31.49	84°06.54	08°31.49	84°06.54	1419	
	107-5	HF		06:14	06:38		00:24	08°31.96	84°06.31	08°31.96	84°06.31	1278	
	107-6	HF		07:18	07:28		00:10	08°32.45	84°06.07	08°32.45	84°06.07	1159	
	107-7	HF		08:18	08:22		00:04	08°32.94	84°05.83	08°32.94	84°05.83	1071	failed
	107-8	HF		09:10	09:29		00:19	08°33.44	84°05.57	08°33.44	84°05.57	930	
	107-9	HF		10:17	10:28		00:11	08°33.92	84°05.34	08°33.92	84°05.34	809	
	107-10	HF		11:23	11:35		00:12	08°34.40	84°05.10	08°34.40	84°05.10	687	
05.09.	108	CTD	14:05	14:11	14:12	14:58	00:53	08°51.40	84°12.70	08°51.42	84°12.70	225	22
05.09.	109	GC-MTL	16:00	16:13	16:20	16:32	00:32	08°55.31	84°18.26	08°55.31	84°18.26	1000	2.4m, gas hydrate
05.09.	110	CTD	17:35	17:48	17:49	18:38	01:03	08°49.84	84°13.78	08°49.84	84°13.75	600	22
06.09.	111-1	HF		00:57	01:23		00:26	09°06.84	84°50.88	09°06.84	84°50.88	1946	HF-3m
	111-2	HF		02:40	02:47		00:07	09°07.42	84°50.50	09°07.42	84°50.50	1649	
	111-3	HF		03:48	04:04		00:16	09°07.63	84°49.88	09°07.63	84°49.88	1325	
	111-4	HF		04:55	05:02		00:07	09°07.89	84°50.21	09°07.89	84°50.21	1342	
	111-5	HF		06:30	06:46		00:16	09°08.42	84°49.88	09°08.42	84°49.88	941	
06.09.	112	HF	14:14	-	-	17:04	02:50	09°27.55	85°56.66	09°27.55	85°56.66	3684	HF-6m
06.09.	113-1	HF		19:23	19:37		00:14	09°38.04	85°47.57	09°38.04	85°47.57	1634	HF-3m
	113-2	HF		20:29	20:36		00:07	09°37.94	85°47.92	09°37.94	85°47.92	1690	
	113-3	HF		21:25	21:40		00:15	09°37.52	85°48.27	09°37.52	85°48.27	1775	
	113-4	HF		22:32	22:39		00:07	09°37.11	85°48.64	09°37.11	85°48.64	1839	
	113-5	HF		23:29	23:44		00:15	09°37.68	85°48.99	09°37.68	85°48.99	1906	
	113-6	HF		00:30	00:36		00:06	09°36.28	85°49.33	09°36.28	85°49.33	1892	
													end of M54-2

METEOR 54/3A													Station list	
			Time (UTC)					Begin / on seafloor		End / off seafloor				
Date 2002	St. No. M 54/	Instrument	Begin	on sea-floor	off sea-floor	End	Duration hh:mm	Latitude N°	Longitude W°	Latitude N°	Longitude W°	Water depth (m)	Recovery Remarks	
Start of M54-3														
11.09.	114	CTD	05:32	06:03	06:04	07:20	00:01	10°17,89	86°18,37	10°17,90	86°18,36	1499		
11.09.	115-1	OFOS	16:35	-	-	17:40	01:05	11°05,65	87°38,22	11°05,65	87°38,22	4535	electrical failure	
11.09.	115-2	OFOS	19:45	-	-	20:00	00:15	11°05,60	87°38,20	11°05,60	87°38,20	4534	electrical failure	
11.09.	115-3	OFOS	22:47	00:05	05:20	07:00	05:15	11°05,64	87°38,21	11°06,82	87°34,37	4533	2 videos	
12.09.	116	GC	15:52	16:16	16:17	16:44	00:01	10°18,33	86°18,85	10°18,34	86°18,85	1683	8.25m	
12.09.	117-1	OFOS	18:02	18:32	19:56	20:25	01:24	10°18,32	86°18,00	10°17,69	86°18,96	1602	1 video	
12.09.	117-2	OFOS	20:56	21:30	22:39	23:18	01:09	10°18,73	86°18,67	10°17,78	86°18,99	1632	1 video	
12.09.	118	CTD	23:40	00:50	00:50	01:43	00:00	10°17,57	86°18,56	10°17,56	86°18,56	1670		
13.09.	119-1	TV-MUC	02:25	02:54	02:54	03:25	00:00	10°18,10	86°18,36	10°18,10	86°18,35	1613	premature touchdown	
13.09.	119-2	TV-MUC	03:25	03:54	03:56	04:25	00:02	10°18,09	86°18,39	10°18,04	86°18,47	1613	6 cores	
13.09.	120	OFOS	13:42	15:11	16:42	18:12	01:31	11°06,01	87°38,46	11°06,40	87°37,91	4565	1 video	
13.09.	121	OFOS	19:07	20:17	21:22	22:40	01:05	11°03,79	87°40,98	11°04,27	87°40,25	4025	1 video	
13.09.	122	TV-G	01:54	03:10	03:44	05:15	00:34	11°05,67	87°38,07	11°05,81	87°37,90	4603	calcareous ooze	
14.09.	123-1	TV-MUC	17:00	17:45	19:47	20:45	02:02	10°00,45	86°11,46	10°00,46	86°11,40	2268	4 cores	
14.09.	123-2	TV-MUC	21:13	22:09	23:51	00:40	01:42	10°00,30	86°11,41	10°00,43	86°11,45	2263	1 core	
15.09.	124	BC-L	02:40	03:45			-03:45	10°00,37	86°11,43			2304		
15.09.	125	CTD	06:35	07:16	07:16	08:36	00:00	10°00,47	86°11,44	10°00,47	86°11,44	2260		
15.09.	126	VESP-L1	08:45	10:15	10:20		00:05	10°00,42	86°11,46	10°00,43	86°11,43	2296	failure, no separation	
15.09.	127	CTD	11:55	12:41	12:41	14:00	00:00	10°00,72	86°11,58	10°00,72	86°11,58	2380		
15.09.	128	BWS	16:25	17:33	17:54	18:50	00:21	10°18,00	86°18,30	10°17,99	86°18,30	1538		
15.09.	129-1	TV-MUC	18:51	19:25	19:34	19:15	00:09	10°17,91	86°18,32	10°17,91	86°18,32	1523	little recovery	
15.09.	129-2	TV-MUC	19:20	20:57	21:28	22:00	00:31	10°17,90	86°18,33	10°17,98	86°18,31	1540	4 cores	
15.09.	129-3	TV-MUC	22:23	23:02	00:26		01:24	10°18,02	86°18,23	10°18,07	86°18,40	1544		
16.09.	130	VESP-L2	02:25	03:14	03:16		00:02	10°17,99	86°18,31	10°18,00	86°18,32	1543		
16.09.	131	VESP	05:40	06:20	06:44		00:24	10°17,99	86°18,29	10°17,96	86°18,36	1535		
16.09.	132	BC-L	14:00			15:17	00:00	10°00,24	86°11,37	10°00,39	86°11,30	2386	no sediment	
16.09.	133	GC	15:39	16:16	16:17	16:55	00:01	10°00,45	86°11,47	10°00,45	86°11,47	2298	4,1m	
16.09.	134	TV-G	17:55	18:38	19:59	20:30	01:21	10°00,37	86°11,44	10°00,52	86°11,41	2258		
17.09.	135	CTD	10:45	11:11	11:11	12:05	00:00	8°55,37	84°18,27	8°55,37	84°18,27	1022		
17.09.	136-1	GC	12:48	13:04	13:06	13:22	00:02	8°55,32	84°18,26	8°55,32	84°18,27	1025		
17.09.	136-2	GC	14:06	14:28	14:30	14:50	00:02	8°55,32	84°18,25	8°55,33	84°18,25	1023	2.3m	

METEOR 54/3A
Station list

			Time (UTC)					Begin / on seafloor		End / off seafloor			
Date 2002	St. No. M 54/	Instrument	Begin	on sea-floor	off sea-floor	End	Duration hh:mm	Latitude N°	Longitude W°	Latitude N°	Longitude W°	Water depth (m)	Recovery Remarks
17.09.	137-1	TV-MUC	16:04	16:33	16:51	17:20	00:18	8°55,31	84°18,26	8°55,37	84°18,23	1024	4 cores
17.09.	137-2	TV-MUC	18:06	18:33	19:57	20:21	01:24	8°55,33	84°18,28	8°55,35	84°18,21	1023	failure
17.09.	138	TV-MUC	20:38	21:04	21:27	22:00	00:23	8°55,35	84°18,23	8°55,36	84°18,23	1024	4 cores
17.09.	139	TV-MUC	22:13	22:41	00:11	00:40	01:30	8°55,35	84°18,23	8°55,34	84°18,22	1025	1 core
18.09.	140	GC	01:25	01:42	01:43	02:02	00:01	8°55,35	84°18,24	8°55,34	84°18,25	1020	1.85m
18.09.	141	CTD	05:49	06:26	06:26	07:40	00:00	9°06,08	84°49,72	9°06,08	84°49,72	1930	
18.09.	142-1	BWS	11:15	12:05	12:25	12:45	00:20	8°55,34	84°18,24	8°55,35	84°18,24	1020	
18.09.	142-2	CTD	13:00	13:24	13:24	14:12	00:00	8°55,34	84°18,24	8°55,34	84°18,24	1018	
18.09.	143	GC	14:48	15:00	15:00	15:15	00:00	8°55,34	84°18,26	8°55,34	84°18,26	1019	1.52m
18.09.	144	BC-L	17:42	18:25	18:25	19:10	00:00	8°55,39	84°18,22	8°55,39	84°18,22	1023	
18.09.	145	VESP-L1	21:00	21:32	21:32	22:00	00:00	8°55,36	84°18,25	8°55,36	84°18,25	1023	failure, no separation
19.09.	146	VESP-L1	00:35	01:08	02:16	02:38	01:08	8°55,44	84°18,20	8°55,39	84°18,22	1023	
19.09.	147	OFOS	06:03	06:23	15:31	15:59	09:08	9°07,83	84°48,80	9°07,45	84°50,54	1640	3 videos
19.09.	148	TV-G	16:40	17:20	18:31	19:10	01:11	9°07,24	84°50,19	9°06,80	84°50,09	1677	shells, gravel
19.09.	149	BC-L rec.					00:00					1800	rec. of stat. 144 BC-L
20.09.	150	CTD	01:00	01:28	01:28	02:30	00:00	8°55,95	84°18,72	8°55,95	84°18,72	1008	
20.09.	151	CTD	06:15	06:58	06:58	08:50	00:00	9°07,24	84°50,88	9°07,21	84°50,57	1780	+ in situ pump
20.09.	152	CTD	10:15	11:05	12:20	13:15	01:15	9°04,01	84°52,60	9°04,01	84°52,60	2430	
20.09.	153	TV-G	14:03	14:44	16:39	17:20	01:55	9°07,34	84°50,50	9°07,16	84°50,63	1698	
20.09.	154	VESP-L1 rec.	21:55					8°55,40	84°18,37				rec. of stat. 146 VESP-L
20.09.	155	GC	22:55	23:10	23:11	23:39	00:01	8°55,36	84°18,23	8°55,36	84°18,23		1.75m
20.09.	156	OFOS	03:40	04:16	15:45	16:25	11:29	9°07,23	84°50,57	9°07,00	84°50,43	1852	3 videos
20.09.	157	CTD	16:30			17:12	00:00	9°07,10	84°50,37	9°07,10	84°50,37		
21.09.	158	VESP-MUC	18:07	18:45	20:01	20:50	01:16	9°07,25	84°50,44	9°06,98	84°50,46	1888	failure
21.09.	159	GC	22:02	22:24	22:24	23:00	00:00	9°07,20	84°50,63	9°06,92	84°50,43	1816	0.58m
21.09.	160	VESP-MUC	23:29	00:09	01:16	02:02	01:07	9°07,15	84°50,41	9°06,92	84°50,43	1890	+ in situ pump
22.09.	161	OFOS	06:14	06:35	13:07	13:38	06:32	8°56,06	84°18,71	8°56,57	84°18,86	1023	
22.09.	162	CTD	13:55	14:21	14:21	15:21	00:00	8°55,94	84°18,55	8°55,94	84°18,55	1018	
22.09.	163-1	TV-MUC	15:58	16:17	16:59	17:22	00:42	8°55,90	84°18,87	8°55,69	84°18,81	1022	3 cores
22.09.	163-2	TV-MUC	17:46	18:36	19:48	20:32	01:12	8°55,90	84°18,87	8°55,69	84°18,81	1017	+ in situ pump
22.09.	163-3	TV-MUC	20:27	20:56	21:28	21:52	00:32	8°55,78	84°18,83	8°55,68	84°18,83	1024	
22.09.	164	GC	22:25	22:37	22:38	22:55	00:01	8°55,69	84°18,82	8°55,88	84°18,70	1022	2.9m

METEOR 54/3A													
Station list													
			Time (UTC)					Begin / on seafloor		End / off seafloor			
Date 2002	St. No. M 54/	Instrument	Begin	on sea-floor	off sea-floor	End	Duration hh:mm	Latitude N°	Longitude W°	Latitude N°	Longitude W°	Water depth (m)	Recovery Remarks
22.09.	165	VESP-L1	23:30	00:10	02:46		02:36	8°55,88	84°18,74	8°55,87	84°18,85	1020	
23.09.	166-1	BC-L	04:30	05:00	05:00	05:30	00:00	8°55,59	84°18,79			1043	failure, no separation
23.09.	166-2	BC-L	06:45	07:14	07:25	07:45	00:11	8°55,66	84°18,82	8°55,72	84°18,85	1022	
23.09.	167	CTD	08:50	09:25	09:25	10:40	00:00	8°52,00	84°22,99	8°52,00	84°22,99	1608	
23.09.	168	BWS	11:47	12:21	13:02	13:40	00:41	8°55,74	84°18,81	8°55,74	84°18,81	1014	5 bottles + in situ pum
23.09.	169	CTD	13:37	14:03	14:03	15:03	00:00	8°55,72	84°18,82	8°55,72	84°18,82	1065	
23.09.	170	PS	18:00	18:00	20:30	20:30	02:30	9°11,50	84°41,00	9°12,50	84°39,83	560	
23.09.	171	GC	21:10	21:23	21:29	21:45	00:06	9°11,67	84°39,81	9°11,67	84°39,81	611	3.2m
23.09.	172	TV-G	23:14	23:35	23:41	00:00	00:06	9°09,01	84°49,15	9°09,01	84°49,14	827	
23.09.	173-1	VESP-MUC	01:11	01:53	02:50	03:27	00:57	9°07,19	84°50,05	9°07,00	84°50,50	1867	
23.09.	173-2	VESP-MUC	04:09	04:50	05:52	06:35	01:02	9°07,21	84°50,49	9°07,00	84°50,50	1845	
24.09.	173-3	VESP-MUC	07:20	07:58	08:51	09:28	00:53	9°07,20	84°50,49	9°06,98	84°50,51	1868	
24.09.	174	BC-L rec.	14:00	14:03	14:03	15:00	00:00	8°55,55	84°18,60	8°55,55	84°18,60		rec. of stat. 166 BC-L
24.09.	175	VESP-L1 rec.	15:30				00:00	8°55,67	84°18,80				rec. of stat. 165 VESP-L
24.09.	176-1	VESP-MUC	17:09	17:43	18:06	18:52	00:23	8°55,88	84°18,71	8°55,81	84°18,58	1007	5 bottles
24.09.	176-2	VESP-MUC	20:16	20:39	21:29	21:57	00:50	8°55,87	84°18,72	8°55,69	84°18,81	1022	5 bottles
24.09.	177	TV-G	23:23	23:48	01:33	01:56	01:45	8°55,25	84°18,30	8°55,30	84°18,22	1033	
25.09.	178	OFOS	05:14	05:58	11:04	11:36	05:06	8°27,57	84°08,38	8°26,19	84°10,81	2125	2 videos
25.09.	179	GC	19:00	19:25	19:28	19:53	00:03	8°59,55	84°43,70	8°59,55	84°43,70	1938	1.9m
25.09.	180	CTD	21:14	22:00	22:00	23:15	00:00	9°05,53	84°50,47	9°05,53	84°50,47	2220	
25.09.	181	BC-L	23:44	00:40	00:40	01:30	00:00	9°07,22	84°50,60	9°07,22	84°50,20	1798	
26.09.	182	OFOS	03:01	03:14	10:12	10:25	06:58	9°11,97	84°39,77	9°11,81	84°39,57	545	
26.09.	183	CTD	10:53	11:11	11:11	12:00	00:00	9°11,59	84°39,74	9°11,59	84°39,74	615	
26.09.	184	VESP-L1	14:00	14:58	15:11	15:55	00:13	9°07,20	84°50,60	9°07,15	84°50,64	1826	
26.09.	185	BC-L rec.	16:15	16:15	16:20	17:00	00:05	9°06,89	84°50,21	9°06,89	84°50,21	1865	rec. of stat. 181 BC-L
26.09.	186	VESP-MUC	20:45	21:14	23:56	00:30	02:42	8°55,62	84°18,83	8°55,82	84°18,76	1008	5 bottles
27.09.	187	BWS	00:52	01:27	01:27	02:35	01:08	8°55,94	84°18,73	8°55,94	84°18,73	1009	
27.09.	188	VESP-MUC	02:45	03:14	06:24	06:53	03:10	8°55,80	84°18,65	8°55,83	84°18,69	1009	
27.09.	189	VESP-L2 rec.	02:00				00:00	10°18,08	86°18,39	10°18,08	86°18,39	1590	rec. of stat. 130 VESP-L
End M54-3a													

METEOR 54/3B

Station list

			Time (UTC)					Begin / on seafloor		End / off seafloor			
Date 2002	St. No. M 54/	Instrument	Begin	on sea-floor	off sea-floor	End	Duration hh:mm	Latitude N°	Longitude W°	Latitude N°	Longitude W°	Water depth (m)	Recovery Remarks
Begin M54-3b													
02.10.	195	OBH			02:04	02:20		9,4695	-84,754	9,4695	-84,754	320	recovery
02.10.	194	OBH			03:15	03:29		9,46883333	-84,877833	9,46883333	-84,877833	560	recovery
02.10.	193	OBH			04:57	05:37		9,3365	-85,106667	9,3365	-85,106667	1880	recovery
02.10.	38	OBH			06:41	07:40		9,24133333	-85,946833	9,24133333	-85,946833	1760	recovery
02.10.	197	OBS			08:16	09:00		9,3365	-84,886333	9,3365	-84,886333	1724	recovery
02.10.	196	OBH			09:54	10:18		9,36033333	-84,753833	9,36033333	-84,753833	666	recovery
02.10.	198	OBH			11:03	11:20		9,25216667	-84,734667	9,25216667	-84,734667	284	recovery
02.10.	141	OBH			11:44	12:01		9,21933333	-84,684333	9,21933333	-84,684333	334	recovery
02.10.	140	OBH			12:29	12:51		9,171	-84,6355	9,171	-84,6355	901	recovery
02.10.	139	OBH			13:23	13:39		9,22033333	-84,559167	9,22033333	-84,559167	358	recovery
02.10.	301	OBH		14:32				9,25933333	-84,500167	9,25933333	-84,500167	310	deployment
02.10.	302	OBH		15:33				9,26183333	-84,358167	9,26183333	-84,358167	326	deployment
02.10.	303	OBH		16:30				9,13933333	-84,385833	9,13933333	-84,385833	655	deployment
02.10.	304	OBH		17:20				9,03016667	-84,413333	9,03016667	-84,413333	1159	deployment
02.10.	305-1	OBH		18:30				9,08433333	-84,507667	9,08433333	-84,507667	1028	deployment
02.10.	42	OBH			19:10	19:57		9,08683333	-84,519667	9,08683333	-84,519667	1507	recovery
02.10.	207	OBH			20:23	20:48		9,1195	-84,717	9,1195	-84,717	1143	recovery
02.10.	306	OBH		21:02				9,11766667	-84,7165	9,11766667	-84,7165	1155	recovery
02.10.	199	OBH/OBT			21:35	22:16		9,20783333	-84,785667	9,20783333	-84,785667	729	recovery
02.10.	200	OBH/OBT			22:40	23:00		9,15816667	-84,826667	9,15816667	-84,826667	815	recovery
02.10.	201	OBS			00:32	01:25		9,16966667	-84,933667	9,16966667	-84,933667	2078	recovery
03.10.	39	OBH			03:50	04:51		9,0905	-84,044333	9,0905	-84,044333	2496	recovery
03.10.	203	OBH			05:35	06:40		8,96983333	-85,082833	8,96983333	-85,082833	3619	recovery
03.10.	40	OBH			07:30	09:10		8,89283333	-84,9745	8,89283333	-84,9745	3420	recovery
03.10.	204	OBH			09:46	10:40		8,83433333	-84,830333	8,83433333	-84,830333	3474	recovery
03.10.	307	OBS		10:24				8,83366667	-84,833	8,83366667	-84,833	3487	deployment
03.10.	308	OBH		12:51				8,65333333	-84,546333	8,65333333	-84,546333	2167	deployment
03.10.	309	OBS		14:05				8,58	-84,379833	8,58	-84,379833	2841	deployment
03.10.	310	OBH		15:37				8,76333333	-84,386	8,76333333	-84,386	1850	deployment
03.10.	311	OBH		16:34				8,77083333	-84,51	8,77083333	-84,51	2548	deployment
03.10.	313	OBH		17:31				8,88416667	-84,471667	8,88416667	-84,471667	1996	deployment
03.10.	312	OBH		18:25				8,88	-84,58	8,88	-84,58	2614	deployment
03.10.	41	OBH			19:07	20:04		8,93733333	-84,725667	8,93733333	-84,725667	2593	recovery
03.10.	205	OBH			20:36	21:17		9,00133333	-84,834833	9,00133333	-84,834833	2210	recovery
03.10.	202	OBH			21:46	20:34		9,03383333	-84,934833	9,03383333	-84,934833	2236	recovery
03.10.	190	VESP			22:59	23:51		9,12233333	-84,8455	9,12233333	-84,8455		recovery
04.10.	206	OBS			00:48	01:32		9,03616667	-84,716833	9,03616667	-84,716833	1726	recovery
04.10.	314	OBH		03:15				8,961	-84,464	8,961	-84,464	1618	deployment

METEOR 54/3B			Station list										
Date 2002	St. No. M 54/	Instrument	Time (UTC)				Begin / on seafloor		End / off seafloor		Water depth (m)	Recovery Remarks	
			Begin	on sea-floor	off sea-floor	End	Duration hh:mm	Latitude N°	Longitude W°	Latitude N°			Longitude W°
04.10.	316	OBS		05:07				8,9665	-84,317333	8,9665	-84,317333	908	deployment
04.10.	317	OBH		05:55				9,06	-84,28	9,06	-84,28	520	deployment
04.10.	318	OBS		06:55				9,177	-84,254333	9,177	-84,254333	354	deployment
04.10.	319	OBH		08:15				9,05266667	-84,195667	9,05266667	-84,195667	282	deployment
04.10.	320	OBH		09:03				9,00116667	-84,1815	9,00116667	-84,1815	220	deployment
04.10.	321	OBH		09:55				8,89466667	-84,203167	8,89466667	-84,203167	282	deployment
04.10.	322	OBH		10:51				8,79	-84,26	8,79	-84,26	796	deployment
04.10.	323	OBH		11:38				8,79533333	-84,164833	8,79533333	-84,164833	205	deployment
04.10.	305-1	OBH			14:12	14:46		9,086	-84,5105	9,086	-84,5105	1021	recovery
04.10.	305-2	OBH		17:01				9,1	-84,506667	9,1	-84,506667	1038	deployment
04.10.	1-1	HS	19:30			22:00		8,788	-84,253167	8,62166667	-84,085	500	profile segment
04.10.	1-2	HS	22:00			02:00		8,62166667	-84,085	8,408	-83,7085		profile segment
05.10.	1-3	HS	02:00			06:00		8,408	-83,7085	8,29266667	-83,17		profile segment
05.10.	2-1	HS	07:40			10:00		8	-83,166667	7,6	-83,166667		profile segment
05.10.	2-2	HS	10:00			13:41		7,6	-83,166667	7,00066667	-83,165833		profile segment
05.10.	3	HS	13:41			14:16		7,00066667	-83,165833	7	-83,085		profile
05.10.	4	HS	14:16			21:45		7	-83,085	8,25583333	-83,0835		profile
05.10.	5	HS	21:45			22:28		8,25583333	-83,0835	8,1835	-83,000667		profile
05.10.	6	HS	22:28			00:57		8,1835	-83,000667	7,7525	-83		profile
06.10.	7	HS	00:57			01:07		7,7525	-83	7,75233333	-83,023667		profile
06.10.	8	HS	01:07			03:51		7,7525	-83,023667	8,16666667	-83,021667		profile
06.10.	9	HS	03:51			04:12		8,16666667	-83,021667	8,195	-83,052667		profile
06.10.	10	HS	04:12			06:32		8,195	-83,052667	7,81583333	-83,052667		profile
06.10.	11	HS	06:32			06:52		7,81583333	-83,052667	7,8175	-83,103333		profile
06.10.	12	HS	06:52			09:35		7,8175	-83,103333	8,2635	-83,109		profile
06.10.	13	HS	09:35			09:47		8,2635	-83,109	8,269	-83,141667		profile
06.10.	14	HS	09:47			12:28		8,269	-83,141667	7,8195	-83,1345		profile
06.10.	15	HS	12:28			12:50		7,8195	-83,1345	7,8195	-83,198167		profile
06.10.	16	HS	12:50			15:59		7,8195	-83,198167	8,31	-83,1945		profile
06.10.	17	HS	15:59			16:08		8,31	-83,1945	8,31466667	-83,2145		profile
06.10.	18	HS	16:08			17:15		8,31466667	-83,2145	8,1345	-83,223333		profile
06.10.	19	HS	17:15			18:19		8,1345	-83,223333	8,21816667	-83,0665		profile

Abbreviations:	Annotations:
CTD (Conductivity temperature depth)	No of bottles
TV-MUC (TV-Multicorer)	No of filled cores, recovery
MUC (Multicorer)	No of filled cores, recovery
GC (Gravity Corer)	recovery
PC (Piston Corer)	recovery
TV-G (TV-Grab sampler)	
DR (Dredge)	
OFOS (Ocean floor observation system)	all Lat./Long. positions are ship's positions
VESP (Vent Sampler)	
VESP-L (Vent Lander)	
BC (Benthic Chamber lander)	
BWS (Bottom Water Sampler)	
HF (Heat Flow detector)	
MTL (Miniatur Temperature Logger)	No of MTL attached to GC
HS (Hydrosweep)	
PS (Parasound)	
TP (Transponder)	
PDR 18 kHz (Precision Depth Recorder)	
PDR 20 kHz (Precision Depth Recorder)	
OBS (Ocean Bottom Seismometer)	
OBH (Ocean Bottom Hydrophone)	
OBT (Ocean Bottom Tiltmeter)	
ISP (In Situ Pump)	

Stationsprotokoll Reise

M 54.3B

		Winden, Seile, Kabel:				
Winde	bestückt mit	RF-Nummer	aktuelle Länge	aufgelegt	Zustand	Bemerkungen
W 01	COSA 8 8 mm	720090	6000	Sep 01	2	keine
W 02	Kabel 11 mm	728570	6233	Sep 01	3-4	
W 03	Kabel 11 mm	728569	6043	Sep 01	3-4	
W 05	Kurtleine 20 mm	727406	3000	Aug 98	2	Winde ausgelagert HH
W 06	Kurtleine 20 mm	727406	3000	Aug 98	2	Winde ausgelagert HH
W 09	Kabel 11 mm	725331	8190	Sep 01	2	keine
W 11	Seil 18 mm	720088	11011	Aug 01	3	
W 12	Kabel 18 mm	725578	7830 ???	Sep 99	3	0 - 1000 m = Zustand 4
W 13	Netzsondenkabel	Erstaurüst.	2732	Feb 86	3-??	Alter des Kabels 15 Jahre

Winde	Einsatzzeit		Arbeitslänge m	max. gest. Länge	Bemerkungen
	vorherige	diese Reise			
W 01	17,8	0,0	17,8	1000	1000 Sept. 01 neu aufgelegt W 01 spult nicht optimal, Kunststoffseil ist nicht formstabil
W 02	418,9	6,8	425,7	1525	5639 Sept. 01 neu aufgelegt
W 03	428,4	27,3	455,7	2353	5517 Sept. 01 neu aufgelegt
W 04	425,3	0,0	425,3	0	z.Z Meteorleine
W 09	3,6	0,0	3,6	0	5005 Sept. 01 neu aufgelegt
W 11	560,3	0,0	560,3	0	5647 Aug. 01 neu aufgelegt
W 12	626,7	162,5	789,2	4907	7692 11.01 auf 8000m gekürzt

Abkürzungen im Stationsprotokoll:

KL	Kabellänge		
SL	Seillänge		
HS	Hydrosweep		
PN	Parasound		
WT	Wassertiefe		
Pl	Pinger		

Eingesetzte seilgebundene Geräte

Schwerlot 3 m		Einsätze
Schwerlot 6 m		4
CTD/ROS		7
TV MUC		16
VESP MUC		16
TVG		7
		6
OFOs		10
BWS		4
VESP launching		7
BC Launching		4
		81

Eingesetzte nicht seilgebundene Geräte

	Thermosalinograph	Einsätze
	Hydrosweep-/Parasound-Echolotsysteme	
	Schiffs-ADCP + 38KHz ADCP im Lotschacht	
	Kreiselpumpe Schiff	

Geräteverluste:

keine

Bemerkungen:

Zeitangaben : Alle in UTC, Position nach GPS
Tiefenangaben: Wenn nicht anders vermerkt, Parasountlot im NBS-Modus

Stationsinformationer					Bemerkungen	Meteorologische Beobachtungen															
2002	Station		Winde	Lottiefe		Zeit	Breite			Länge			Wind			Luft		Wasser		Dünung	
	Gerät	Nr.	Datum	W		[m]	[UTC]	Grad	Min	N	Grad	Min	W	dd	ff	N	Druck	Temp.	Temp.	Richt.	Periode
							[°]			[°]			[Bft.]			[hPa]	[°C]	[°C]	[°]	[s]	[m]
					21:45	aufgetaucht															
				729	22:16	an Bord	9	12,47		84	47,14										
OBH/OBT	200	01.10.02		815	22:40	ausgelöst															
					22:53	gesichtet															
					23:00	an Deck	9	9,49		84	49,60										
OBS	201	01.10.02			23:31	ausgelöst															
		02.10.02			0:32	2. Auslösung															
					1:14	gesichtet															
				2078	1:25	an Deck	9	10,18		84	56,02										
OBH	39	02.10.02		2496	02:20	ausgelöst							E'l	2	o,r	1011,9	27,4	28,1	9		
					3:50	2. Auslösung															
					4:35	aufgetaucht															
					4:51	an Deck	9	5,43		84	2,66										
OBH	203	02.10.02			5:35	ausgelöst															
					6:19	aufgetaucht															
				3619	6:40	an Deck	8	58,19		85	4,97										
OBH	40	02.10.02		3420	7:30	ausgelöst															
					8:38	aufgetaucht															
					9:10	an Deck	8	53,57		84	58,47										
OBH	204	02.10.02		3474	9:46	ausgelöst															
					10:22	aufgetaucht															
					10:40	an Deck	8	50,06		84	49,82										
OBS	307	02.10.02		3487	10:24	ausgesetzt	8	50,02		84	49,98										
OBH	308			2167	12:51	ausgesetzt	8	39,20		84	32,78										
OBS	309			2841	14:05	ausgesetzt	8	34,80		84	22,79		N	2	o,r	1011,3	26,6	28,0	9		
OBH	310			1850	15:37	ausgesetzt	8	45,80		84	23,16										
OBH	311			2548	16:34	ausgesetzt	8	46,25		84	30,60										
OBH	313			1996	17:31	ausgesetzt	8	53,05		84	28,30										
OBH	312			2614	18:25	ausgesetzt	8	52,80		84	34,80										
OBH	41	02.10.02			19:07	ausgelöst															
					19:54	augetaucht															
				2593	20:04	an Deck	8	56,24		84	43,54										
OBH	205	02.10.02		2210	20:36	ausgelöst															
					21:03	aufgetaucht															
					21:17	an Deck	9	0,08		84	50,09										
OBH	202	02.10.02			21:46	ausgelöst															
					22:15	gesichtet															
				2236	20:34	an Deck	9	2,03		84	56,09										
VESP	190	02.10.02			22:59	ausgelöst															
					23:37	aufgetaucht															
					23:51	an Deck	9	7,34		84	50,73										
OBS	206	03.10.02		1726	0:48	ausgelöst							E'l	2	o	1008,4	27,3	28,2	9		

Appendix B

Weather

The Weather during M54/3

When the METEOR left Caldera, Puntarenas, Costa Rica, on September 10th, 2002, the Inertropical Convergence Zone, short ITCZ, was around 10 N south of Mexico, bending southward to 7 N south of Panama. A Tropical Wave had passed the port the night before and was on its way further west. The METEOR followed it so that light southeasterly winds were reported when the ship rounded the Nicoya peninsula to work in Nicaraguan waters first. There, winds turned to light westerlies until September 15th, when the next Tropical Wave arrived west of the Nicoya peninsula. During its passage, winds turned east and later south, but force restricted itself to 4 Bft. One day later winds were back to light and variable again.

Meanwhile on September 13th a Tropical Depression had passed the southernmost Windward Islands on its way west. On September 16th it passed the Netherlands ABC Islands, staying just a few miles north off their shores. The path of the depression then turned more northwestward. On September 18th, the Depression had passed Jamaica and it had been given a name instead of the number „10“ it had been allocated already when still being in the Atlantic. From now on it was being referred to as Tropical Storm „Isidore“. While the METEOR returned to Costa Rican waters where light local wind systems reigned Tropical Storm „Isidore“ passed the Cayman Islands and on September 20th the twister reached Hurricane status, maximum sustained winds being 75 kts and gusts reaching even 90 kts. These data were being confirmed by Miami as well as by Havana radar and by flights of Air Force Reserve Hurricane Hunter Aircraft using dropsondes to report a central sea level pressure of 979 mb. „Isidore“ then passed the Isle of Youth and the western tip of Cuba until September 21st, central pressure falling to 964 mb as stated in the reports of the Hurricane Tracking Center in Houston, maximum sustained winds rising to 85/105 kts. The next day saw „Isidore“ near the northern coast of Yucatan moving due west, maximum sustained winds even rising to 110/135 kts.

By this time the METEOR was no longer totally unmolested. A low was being induced near Central America's southern coast, bands of clouds extending from the Hurricane to the low to show the connection. There were northwesterly winds of 5 Bft, a wind force seldom being reached during M 54 in the Pacific. „Isidore“ was forecast to move into the Bay of Campeche but instead went inland, devastating the town of Merida while itself being weakened by the sudden increase in friction as well as by the sudden dwindling of supply of energy from the surface. Therefore „Isidore“ was downgraded to Tropical Storm again on September 24th, maximum sustained winds being still 50/60 kts. Its further path was due north, making a second landfall in the Mississippi Delta on September 26th where torrential rainfall was reported. The remnants of „Isidore“ moved past Nashville and further northeast.

Meanwhile on September 23rd another Tropical Depression had entered the Caribbean via Trinidad and Tobago, too, initially being allocated the number „13“. During the next day when the developing twister just had passed these islands it was named „Lili“ and so was upgraded to Tropical Storm, too. On September 26th, „Lili“ passed the Netherlands Antilles, taking much the same path as „Isidore“ had done. On METEOR's position on the Costa Rican coast winds were light and variable notwithstanding daily thundery showers. „Lili“ then experienced a phase of weakness on September 28th while on Haiti's south coast, but the twister recovered and accelerated, thereby developing to Hurricane strength, and was positioned well north of Yucatan on October 2nd with a central pressure of 954 mb and maximum sustained winds of 95 kts. This time, a low on Central America's south coast was induced, too, but it showed up between El Salvador and Tehuantepec and so our research ship continued unmolested, winds being light mainly from the west. On October 3rd, „Lili“ made her landfall west of New Orleans, La., where several hundred thousands of people were on the run from her. NASA Control Houston had to be shut down for some time resulting in a delay of a start of the spacecraft „Atlantis“. On October 4th, President Bush declared all of the state of Louisiana a disaster area.

Quite in contrast, no one aboard the research vessel had to worry about the weather all of the time the METEOR spent in the Pacific Ocean in 2002.

Appendix C

OBS/OBH/OBT Station List

INST.	LAT (N)	LON (W)	Deployed	DEPTH	REL.	ANT.	REC.	SKEW	SENSOR	Other Sensors	REMARKS
	D:M	D:M	Recovered	(m)	CODE	CH.	REC.	(ms)	HYDRO.		
OBH 38	09:14.271	84:56.637	28.04.02/ 01.10.02	1752	03BD+0355	D	000713	238	DPG 93		
OBH 39	09:05.280	85:02.560	28.04.02/ 01.10.02	2496	03B6+0355	C	991249	629	DPG 75		
OBH 40	08:53.328	84:58.432	28.04.02/ 01.10.02	3420	03B5+0355	C	991237	-409	DPG 91		
OBH 41	08:56.043	84:43.428	28.04.02/ 01.10.02	2615	03B3+0355	C	991242	-279	DPG 87		
OBH 42	09:05.173	84:39.092	28.04.02/ 01.10.02	1481	03B8+0355	C	991250	496	DPG 92		
OBH 139	09:13,023	84:33,508	12.05.02/ 01.10.02	379	03B7+0355	C	991247	165	OAS 02		
OBH 140	09:10,017	84:37,993	12.05.02/ 01.10.02	939	03BB+0355	A	10405	-69	OAS 04		
OBH 141	09:13,016	84:41,022	12.05.02/ 01.10.02	351	03B9+0355	A	10402	not determine	OAS 29		no skew determined
OBH 193	09:19,989	85:06,063	16.05.02/ 01.10.02	1880	3659	C	991238	-355	HTI 502		
OBH 194	09:28,015	84:52,503	16.05.02/ 01.10.02	560	039A+0355	D	707	-548	OAS 18		
OBH 195	09:28,001	84:44,997	16.05.02/ 01.10.02	324	0387+0355	B	991256	-388	OAS 30		
OBH 196	09:21,531	84:45,034	16.05.02/ 01.10.02	413	3624	C	10401	-614	HTI 302		
OBS 197	09:20,022	84:53,006	16.05.02/ 01.10.02	1745	03BA+0355	C	10404	485	HTI 702	Owen 22 (4,5Hz)	no coupling
OBH 198	09:14,975	84:44,001	16.05.02/ 01.10.02	291	3674	C	991243	146	OAS 27		
OBT 199	09:12,016	84:46,990	16.05.02/ 02.10.02	734	03B1+0355	D	20303	-582	TM 4949	Tiltmeter	
OBH 199	09:12,016	84:46,990	16.05.02/ 02.10.02	734	03B1+0355	D	20303	188	HTI 802		
OBT 200	09:09,419	84:49,601	16.05.02/ 02.10.02	824	03B2+0355	C	20302	not determine	TM 4948	Tiltmeter	power failure on 04.09.02
OBH 200	09:09,419	84:49,601	16.05.02/ 02.10.02	824	03B2+0355	C	991259	-440	HTI 602		
OBS 201	09:10,013	84:56,020	16.05.02/ 02.10.02	2080	0397+0355	D	991252	-161	OAS 31	LG 01 (4,5 Hz)	no data
OBH 202	09:01992	84:56,010	17.05.02/ 02.10.02	2237	0386+0355	D	991236	-209	HTI 102		
OBH 203	08:57,974	85:05,004	17.05.02/ 02.10.02	3561	3614	D	706	500	OAS 18		
OBH 204	08:50,000	84:49,995	17.05.02/ 02.10.02	3474	3629	D	991246	-270	OAS 38		
OBH 205	08:59,985	84:49,996	17.05.02/ 02.10.02	2210	3669	B	991241	401	HTI 902		
OBS 206	09:01,996	84:43,006	17.05.02/ 02.10.02	1726	03BC+0355	D	10403	7344	OAS 46	Owen 21 (4,5Hz)	no coupling
OBH 207	09:07,000	84:43,003	17.05.02/ 02.10.02	1159	3609	C	711	-305	OAS 22		

INST.	LAT (N)	LON (W)	Deployed	DEPTH	REL.	ANT.	REC.	SENSOR	Other Sensors	REMARKS
	D:M	D:M	Recovered	(m)	CODE	CH.		HYDRO.		
OBH 301	09:15.56	84:30.03	01.10.02	311	03BD+0355	C	000713	DPG 93		
OBH 302	09:15.71	84:21.48	01.10.02	326	039A+0355	D	000707	OAS 318		
OBH 303	09:08.36	84:23.15	01.10.02	656	0387+0355	A	991256	OAS 30		
OBH 304	09:01.81	84:24.81	01.10.02	1156	03B7+0355	A	991247	OAS 02		
OBS 305	09:05.06	84:30.47	01.10.02/ 01.10.02	1025	03B4+0355	D	000712	DPG 86	PMD 509	
OBS 305	09:05.01	84:30.40	03.10.02	1038	03B4+0355	D	000712	DPG 86	PMD 509	
OBH 306	09:07.06	84:42.99	01.10.02	1157	03BB+0355	C	991238	OAS 27		
OBS 307	08:50.03	84:50.03	01.10.02	3488	03B6+0355	D	010407	DPG 78	Webb 2352	
OBH 308	08:39.20	84:32.78	01.10.02	2167	03B5+0355	D	000711	OAS 22		
OBS 309	08:34.80	84:22.79	01.10.02	2840	03B2+0355	C	991243	OAS "dnu"	PMD 539	
OBH 310	08:45.81	84:23.16	01.10.02	1849	3614	B	991237	DPG 91		
OBH 311	08:46.26	84:30.60	01.10.02	2550	3659	C	010402	OAS 29		
OBH 312	08:52.81	84:34.81	01.10.02	2613	3629	C	991250	DPG 92		
OBH 313	08:53.05	84:28.29	01.10.02	1993	03B9+0355	C	991246	OAS 38		
OBH 314	08:57.66	84:27.84	01.10.02	1617	0386+0355	D	010405	OAS 06		
OBT 315	08:52.55	84:20.60	01.10.02	1312	03B1+0355	B	020303	TM		
OBT 315	08:52.55	84:20.60	01.10.02	1312	03B1+0355	B	990701	HTI 802		
OBS 316	08:57.88	84:19.04	01.10.02	909	0397+0355	C	991242	DPG 74	PMD 540	
OBH 317	09:03.60	84:16.80	01.10.02	519	03B3+0355	D	10409	DPG 77		
OBH 318	09:10.53	84:15.27	01.10.02	354	3609	D	10401	HTI 302		
OBH 319	09:03.16	84:11.74	01.10.02	283	3674	C	991236	OAS 01		
OBH 320	09:00.08	84:10.89	01.10.02	220	03B8+0355	C	10403	HTI 902		
OBH 321	08:53.69	84:12.20	01.10.02	284	03BC+0355	C	000706	HTI 002		
OBH 322	08:47.41	84:15.60	01.10.02	796	3624	C	991259	HTI 102		
OBH 323	08:47.72	84:09.89	01.10.02	206	03BA+0355	D	991249	DPG 87		

Appendix D

Heatflow Instrumentation, Methodology and Maps

Instrumentation and methodology for geothermal investigations

(N.Kaul, H.-H. Gennerich, B. Heesemann, M. Müller, I. Grevemeyer)

Heat Probe and Shipboard Operation

On cruise M54/2 two heat flow probes of a Lister type (Lister, 1979; Hyndman et al., 1979) violin bow design (Figures A.HF.1), from the University of Bremen, Meerestechnik und Sensorik were used to obtain temperature gradients and *in-situ* thermal conductivities. Both instruments are capable of k-determinations by a pulsed heat source method. They differ remarkably by size. The Small Heat flow Probe (SHP) has an active length of 3 m and a weight of about 500 kg in air, the Giant Heat flow Probe (GHP) is capable of 6 m penetration. It has a weight in air of app. 1200 kg.

Additionally, autonomous Miniature Temperature data Loggers (MTL) were used routinely on gravity and piston corers to gain sediment temperatures and thermal gradients.

Small Heat flow Probe (SHP)

The active length of the sensor string is 3 m, with 11 thermistors spaced every 0.3 m. Two 8-channel 16 bit A/D converters are used to record the digital data into solid state memory. This instrument is used in conjunction with an online data transmission and a bottom finding pinger. On this cruise, following instruments and settings were in service:

Parameters of 3m-Lister-type heat probe:

Probe #:	#6846
Stings:	5/7/2000, 6/7/2000, 17/7/2000, 1/96
Heating current:	8 A
Heat pulse:	600 J/m
Pulse duration:	20 sec
Sample rate:	10 sec
Online data transmission:	2400 Baud net via coax wire
Wire:	7200 m 18 mm deep sea cable (W12) with coax

The *Lister* type heat probe has the capability of autonomous operation for at least 48 hours due to memory and power capacity. During a single deployment a minimum of 20 heat pulses, equating to 20 sets of thermal conductivity measurements, can be made. Data security is guaranteed by twofold recording into solid state memory and on deck data logging.

Giant Heat flow Probe (GHP)

This brand new tool is designed with an active length of 6 m to cope with transient bottom water temperature variations in shallow water. Shallow in term of stable bottom water temperatures means less than approximately 2500 m water depth. The new probe has a capacity of 72 hours of internal data storing. Additionally, it is equipped with an online data transmission, to allow permanent control during operation. For control of penetration depth, a downward looking acoustic pinger is mounted onto the probe. This pinger gives distance information with a resolution of up to several centimeters. The sensor string contains 22 thermistors, spaced every 0.28 m and several loops of heater wire. The outer and inner diameters of the sensor tube are 14 and 7 mm, respectively. A heat pulse is generated for thermal conductivity determination. The amount of energy dissipated by the wire is controlled by precise voltage and current measurements.



Figure A.HF.1: Giant Heat flow Probe.

Parameters of 6m-Lister-type heat probe:

Probe #:	#34 and #39
Stings:	#1, #2, #3
Heating current:	variable, up to 20 A.
Heat pulse:	variable, up to 1200 J/m
Pulse duration:	20 sec
Sample rate:	1 sec
Online data transmission:	FSK (9600 Baud) via coax wire
Wire:	7200 m 18 mm deep sea cable (W12) with coax

Operation

Measurements are made in the so called ‘pogo-style’, performing many penetrations in a row at small distances. Each penetration consists of raising the probe some hundred meters above the sea floor from the previous penetration, slowly moving the ship to the next penetration site and letting the wire angle become nearly vertical before dropping the probe into the sediment for the next penetration. Once the probe is in the bottom it is left undisturbed for 7-10 minutes for the equilibrium temperature measurements and another 7 minutes if a thermal conductivity measurement is made. For the penetration spacing used in this survey, transit between penetration points lasts about 30 – 45 minutes, a recording cycle in the sea floor is either 7 or 14 minutes, yielding a rate of about one hour per penetration. Transit speed is governed by the tradeoff between keeping the wire angle small and minimizing the time between penetration points.

Winch speed during payout and retrieval of wire is 1.2 – 1.5 m/s, so the initial penetration velocity is 1.2 m/s for the smaller probe and 1.5 m/s for the larger one. Deployment of the instrument is amidships on the starboard side, employing a beam crane and one assistance winch. This procedure ensures safe operation even during medium sea state and minimum interference due to the ships vertical movement during station work. Three deckhands are necessary during deployment. A bottom finding pinger is mounted 30 m above the instrument and can be monitored via an Atlas DESO pinger recorder, switched to passive mode. This set-up is useful as a backup in case of other failures. Rope tension can be monitored in all labs, which turned out to be a most sensible instrument to determine the penetration moment.

To achieve spatially high resolution of heat flow determinations, penetrations were usually positioned 500 and 1000 m apart, depending on targets, which were chosen from bathymetric maps and seismic records. Occasionally, a 90 or 180 m spacing was used to cope with small scale objects.

Miniature Temperature data Loggers (MTL)

Autonomous temperature loggers were used in conjunction with the gravity and piston corers. A detailed description of the loggers is given by Pfender and Villinger (2002). These temperature loggers were mounted onto the core barrel.

Parameters of autonomous temperature data loggers:

Instruments:	18540022B, 12B, 14B, 15B, 16B, 17B, 18B, 19B, 23B, 24B, 25B, 27B, 28B, 29B
Sample rate:	1 sec
Recording length:	18:03 h potential maximum @ 1 sec.
Spacing:	0.90 – 1.80 m

Between five and up to ten instruments were mounted on the core barrel. It turned out that the optimal configuration is achieved with three instruments spaced 1.8 m and mounted at 50° offset from each other. All instruments operated normal within water depth up to 5500 m.

Thermal conductivity measurements on gravity-cores

(M. Heesemann)

To provide constraints on the thermal conductivity of sediments, samples from the seabed are analyzed by the needle probe method to supplement thermal conductivities obtained by *in situ* measurements with the Lister probes. Measurements were carried out using a transient needle-probe method. At the stations where temperature measurements using miniature temperature loggers (MTL) were made, the knowledge of the thermal conductivities is important, because it is essential in order to compute the heatflow. Furthermore, the measurements can be correlated to other physical properties of the sediments.

Instrumentation and operation

The employed needle-probes (Fig. A.HF.2) are manufactured by TeKa, Berlin. The brass tube of the probes is 6 cm in length and 2 mm in diameter. A heating wire inside of the tube is driven by a linear power supply (Armel LPS 301) to create a pulse with a defined amount of heat. The temperature decay after a heatpulse is measured by a thermistor, which is placed in the middle of the brass tube. We used a digital multimeter (Keithley Modell 2000) to acquire resistivity readings from the thermistor and to trigger the heatpulse, the latter is done by an add-on card (Keithley 2000-SCAN Card). Finally, the whole setup is controlled by a quick-basic program running on an IBM-PC compatible computer that is connected to the multimeter via a RS-232 link.



Figure A.HF.2: Two of the five employed needle-probes embedded in the sediments of a split-core, and the linear power supply (left) as well as the digital multimeter (right) in the background.

Five measurements per core section were performed using five different needle-probes. The probes were evenly spaced along the length of the section, unless some parts of the sediments were disturbed by prior sampling procedures. Each measurement contains:

100 s of temperature drift measurement, which indicates the thermal condition of the core

5 s of heating with 350 mA heating current. The total amount of applied heat Q is a function of the heating time and the heating current.

200 s of temperature decay measurements - at a sample rate of one resistivity / temperature reading per second - from which the thermal conductivity k is derived.

Data processing

Thermal conductivity k is calculated from the temperature measurements $T(t)$ by using the equation

$$T(t) = \frac{Q}{4\pi} \cdot \frac{1}{k} \cdot \frac{1}{t + t_{st}} + T_0 + d \cdot t$$

Here, t is a vector of times, after the heat-pulse took place, at which temperature measurements were performed. Q denotes the applied heat, T_0 the sediment temperature prior to heating, and d a factor representing a linear temperature drift. The time-shift t_{sft} is an empirical constant which was introduced by Villinger and Davis (1987).

In this equation $T(t)$, t and Q are measured and k , t_{sft} , T_0 and d are unknown parameters. These unknown parameters including the thermal conductivity are calculated by fitting the measured data by a least squares method. Since the equation is not linear in its parameters, an iterative method is used to perform the fit. For this task the function FMINS of Matlab® is utilized. An example of thermal conductivities as a function of depth is shown in Fig. A.HF3.

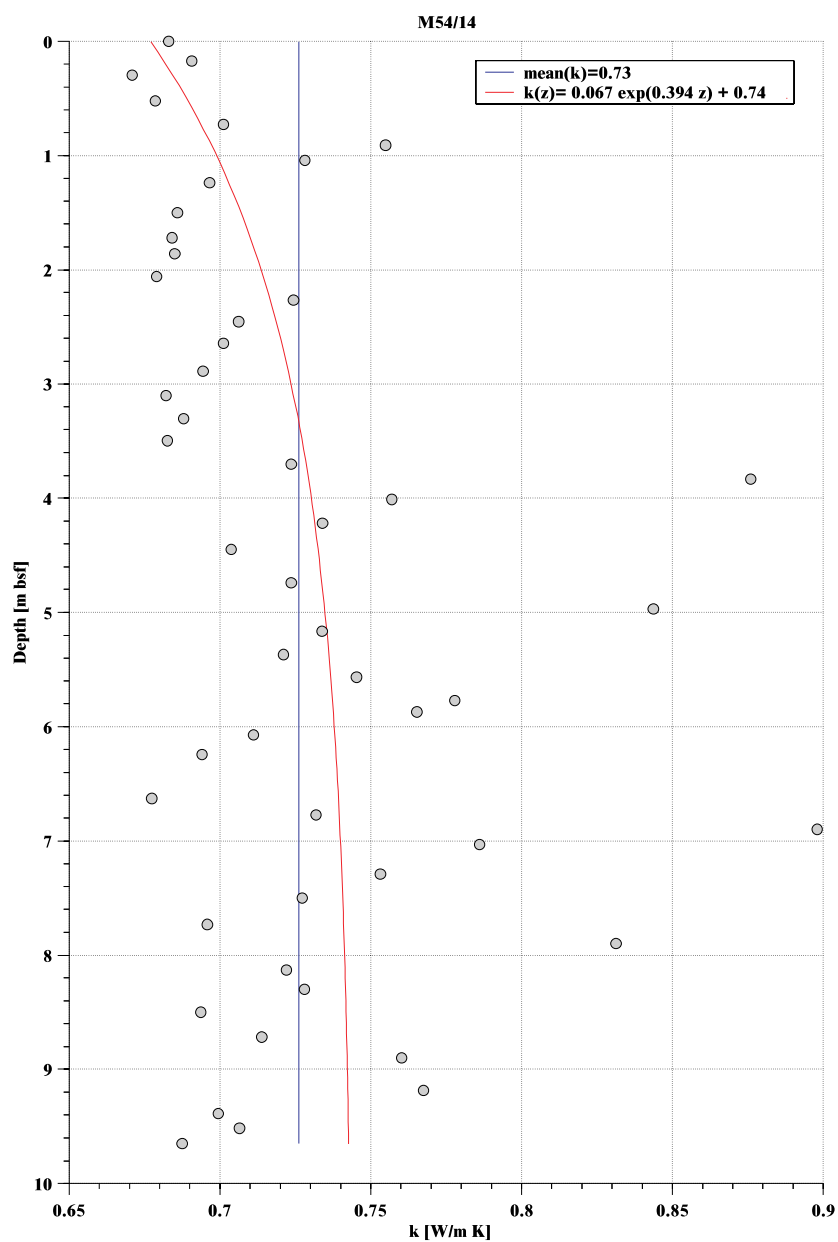


Figure A.HF.3: Thermal conductivities of core M54/14.

Heat flow data reduction

(N. Kaul and I. Grevenmeyer)

Processing temperature data includes calibration of thermistor sensors, calculation of sediment temperatures and temperature gradients, correction for probe tilt during penetration, and calculation of thermal conductivities. While the 7 minute wait is not long enough for the sediment temperatures to return to equilibrium after the frictional disturbance of penetration (Fig. A.HF.4), it is long enough to extrapolate to an equilibrium temperature with a high degree of precision. Each temperature-time series, from each thermistor, is extrapolated to an equilibrium temperature by the program T2C (Hartmann and Villinger, 2002). Because the calibration of each thermistor by the manufacturer is only good to 0.1°C, a secondary calibration is applied. This is usually done in deep marine environment (> 3000 m water depth) where negligible thermal gradients exist within the limits of observation. In other marine environments temperature gradients in the water column are surveyed with a CTD. For the secondary calibration purposes the heat flow probe is allowed to equilibrate at a certain depth (usually 200 m above seafloor). At this depth temperatures are calibrated to the CTD, including the local temperature gradient.

Fourier's law of heat conduction in one-dimension shows that heat flow (Q) is the product of the thermal gradient dT/dz and thermal conductivity k . If these terms are constant over the depth of the measurements then the calculation of heat flow is trivial. However if these values are changing proportionately to each other, as is the case for a constant basal heat flux, then heat flow can be derived from Bullard's (1939) relation given by,

$$\Delta T = Q \sum \Delta z_i / k_i,$$

Where Δz_i is the thickness and k_i is the thermal conductivity over the i th interval. In this case heat flow can easily be calculated as the slope of the line given by the summation. An example is given in Fig. A.HF.5). To properly calculate the temperature gradient a correction for the penetration tilt angle is applied. In most cases the tilt angle is less than 10° and the tilt correction is modest. Determination of thermal conductivity requires the knowledge of the amount of heat, dissipated into the sediment. Therefore a pulsed heat source is used, producing a set of 11 (22) thermal conductivities. Along with measurements on core samples a detailed characterization could be archived, yielding heat flow anomalies with tight error bounds. Because thermal conductivities are sensitive to the sediment porosity over the depth range of the measurements, these measurements generally reflect the reduction of porosity within the upper three meters of sediment.

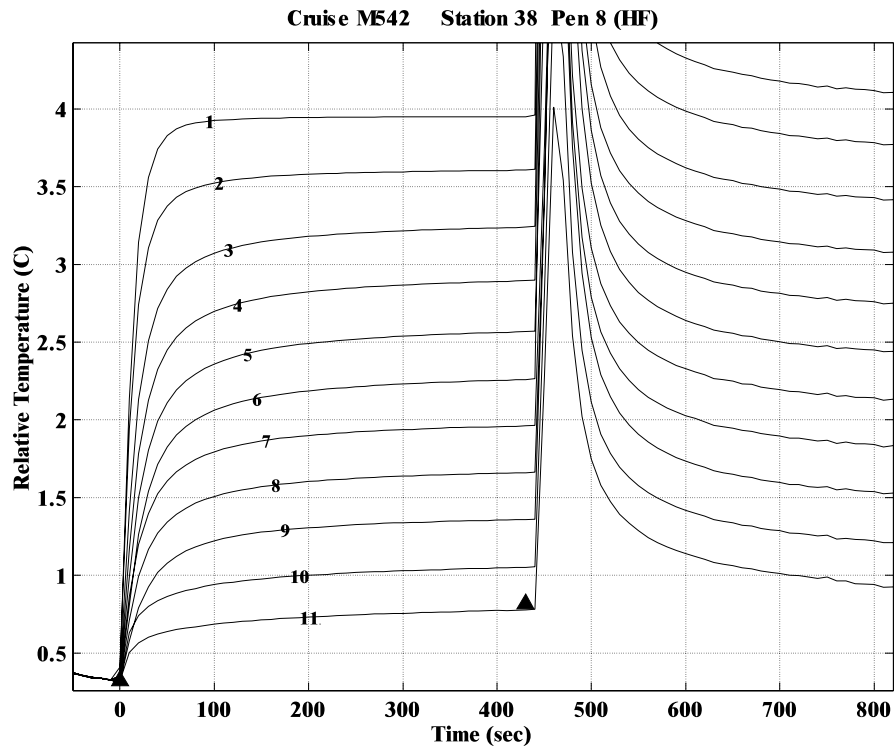


Figure A.HF.4: Frictional heating pulse and defined heat pulse.

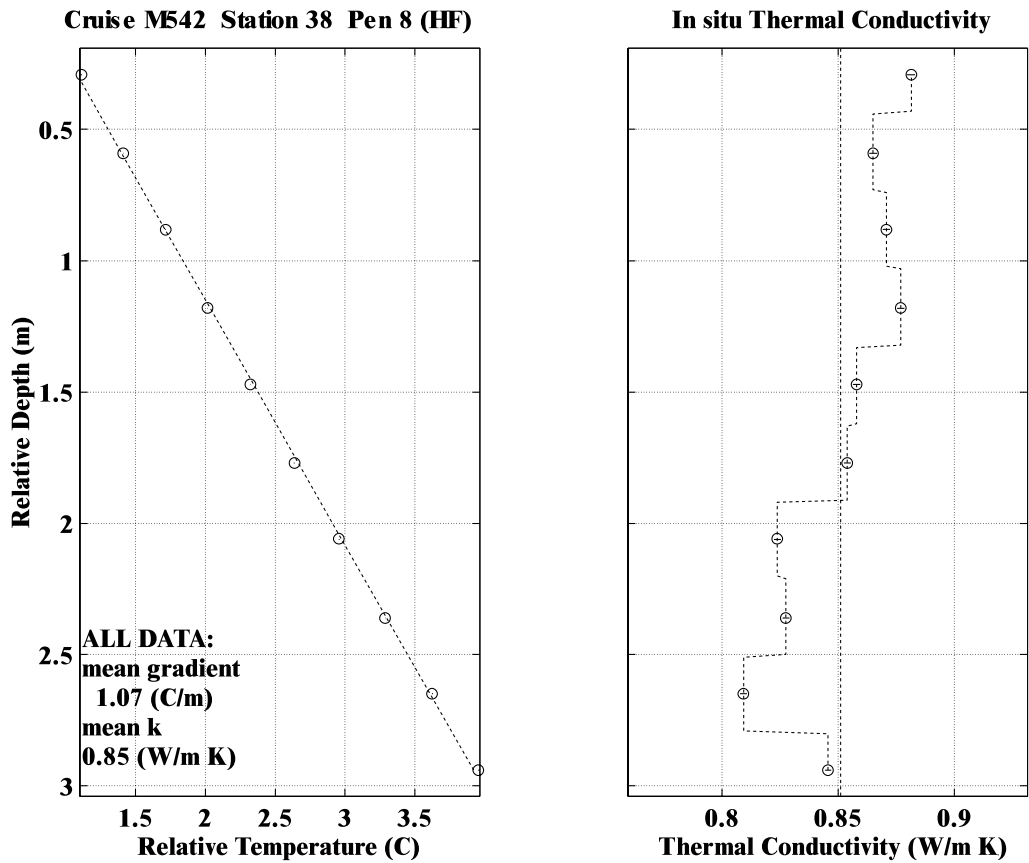


Figure A.HF.5: Thermal gradient and in situ thermal conductivity.

Table. A.HF: Station codes and location of heat flow surveys.

Station name	Station number	Station code	N	Description
NIC1	M54/4	HF02	9	middle slope
	M54/7	HF04	5	incoming plate
	M54/10	HF06	7	upper slope
	M54/12	HF08	12	incoming plate, trench, lower slope
NIC2	M54/26	HF14	10	middle slope
	M54/34-1	HF17	1	no data
	M54/34-2	HF18	3	incoming plate
Mound Culebra	M54/20	HF09	14	Mound Culebra transect
	M54/33	HF16	3	top Mound Culebra
CR1	M54/37	HF19	4	middle slope
	M54/	HF20	3	middle/upper slope
	M54/42	HF22	10	incoming plate, trench, lower slope
CR2	M54/43	HF23	3	incoming plate
	M54/112	HF42	1	no data
	M54/113	HF43	6	middle/upper slope
CR3	M54/49	HF24	7	incoming plate
	M54/55	HF25	9	middle slope
	M54/67	HF30	9	upper slope
	M54/71	HF31	9	incoming plate
	M54/77	HF32	6	incoming plate
Jaco Scarp	M54/59	HF28	7	top Jaco Scarp, OFOS11, TVG3(SO163)
	M54/60	HF29	10	top Jaco Scarp, OFOS12, TVG7(SO163)
	M54/111	HF41	5	Jaco Scarp, OFOS2(SO144)
Mound11	M54/82	HF35	25	3D survey mud dome „Mound11“
CR4	M54/88	HF36	11	middle slope
	M54/95	HF37	10	incoming plate, trench, lower slope
CR5	M54/101	HF38	8	incoming plate, trench, lower slope
	M54/107	HF39	10	middle slope

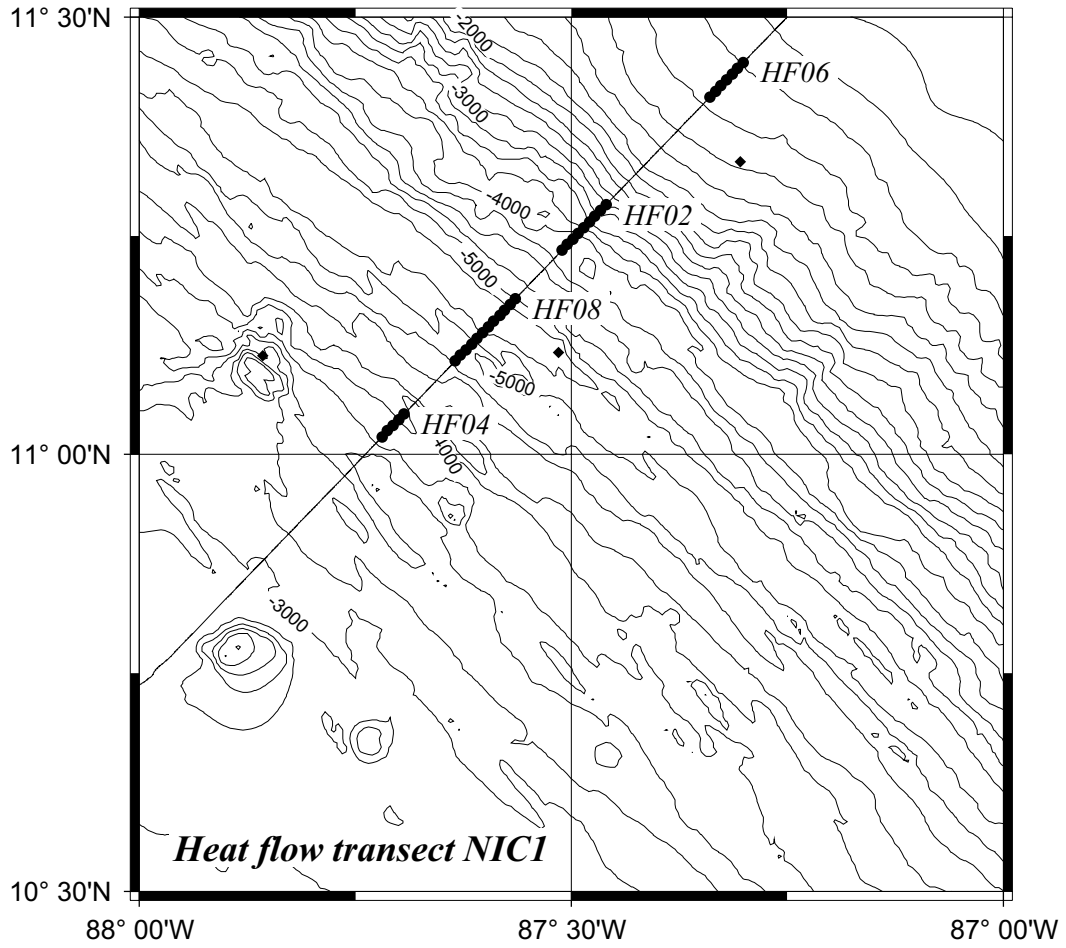


Figure A.Map.HF.1: Detailed map of heat flow transect NIC1.

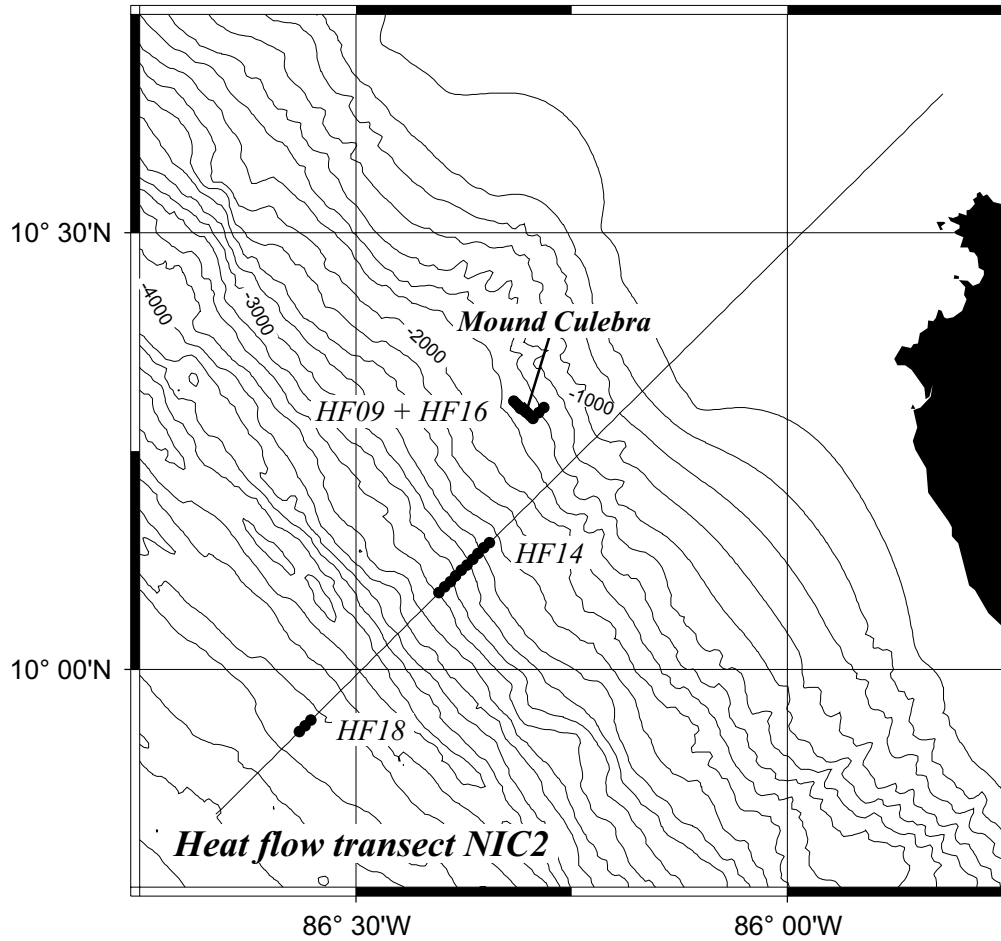


Figure A.Map.HF.2: Detailed map of heat flow transect NIC2.

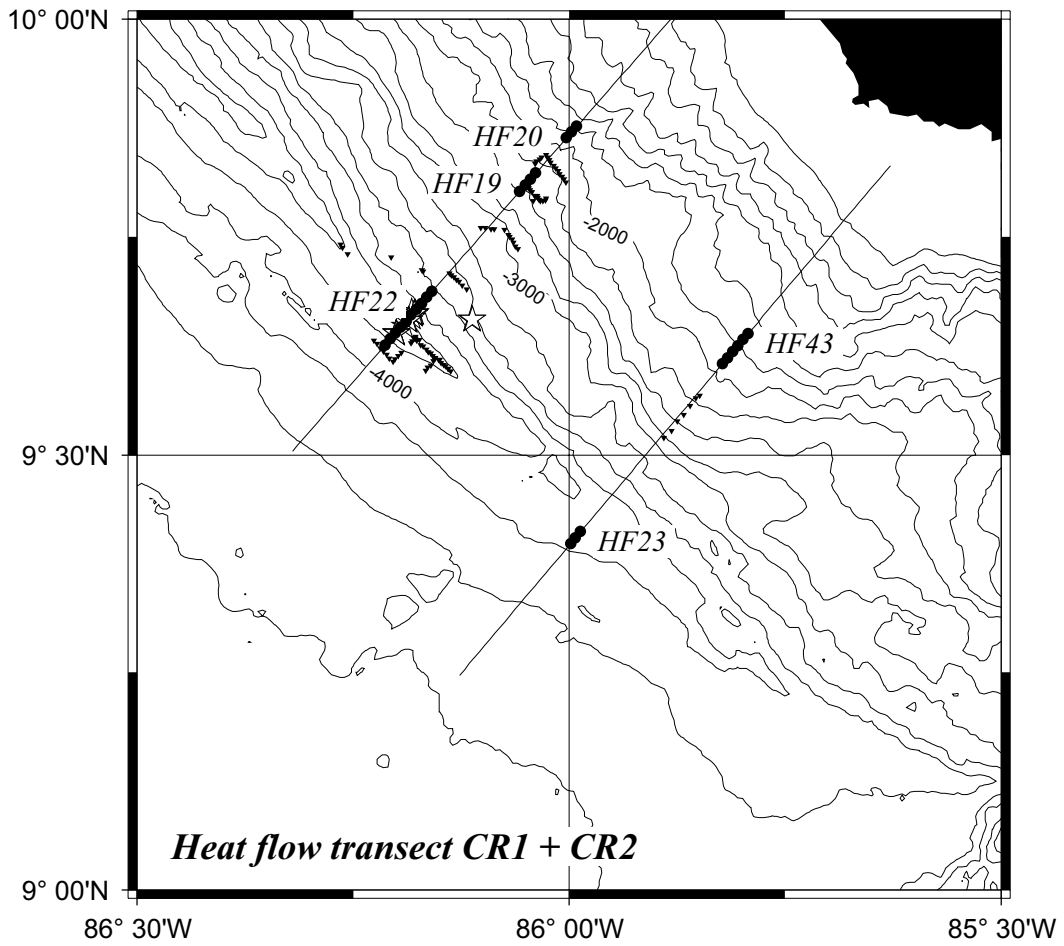


Figure A.Map.HF.3: Detailed map of heat flow transect CR1 and CR2.

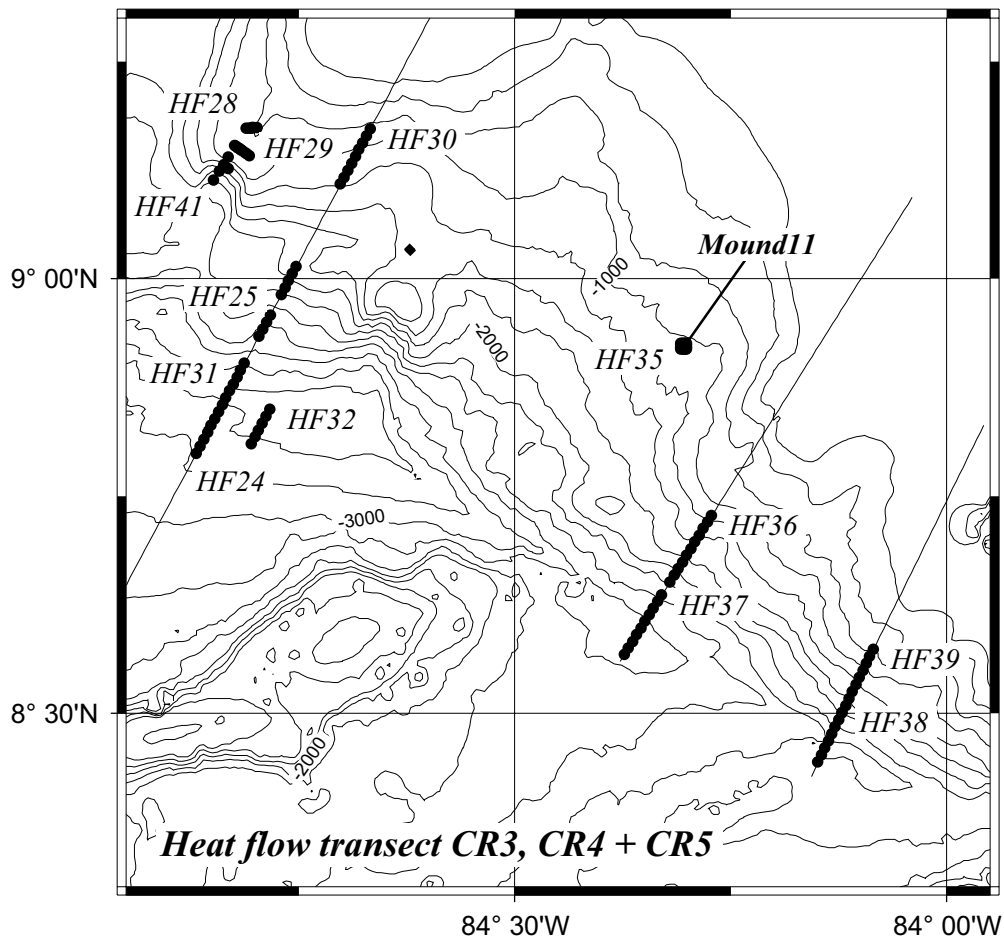
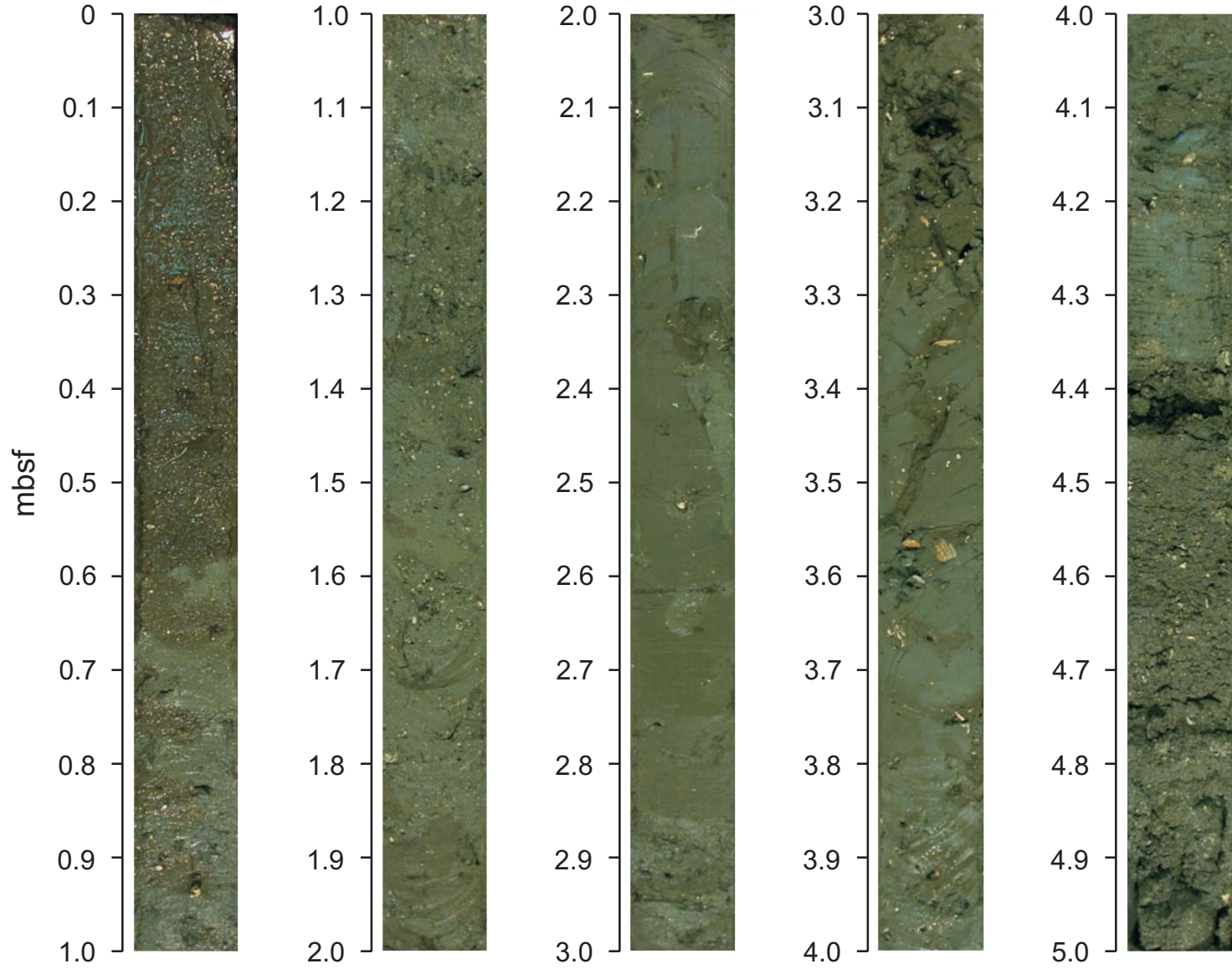


Figure A.Map.HF.4: Detailed map of heat flow transect CR3, CR4, CR5.

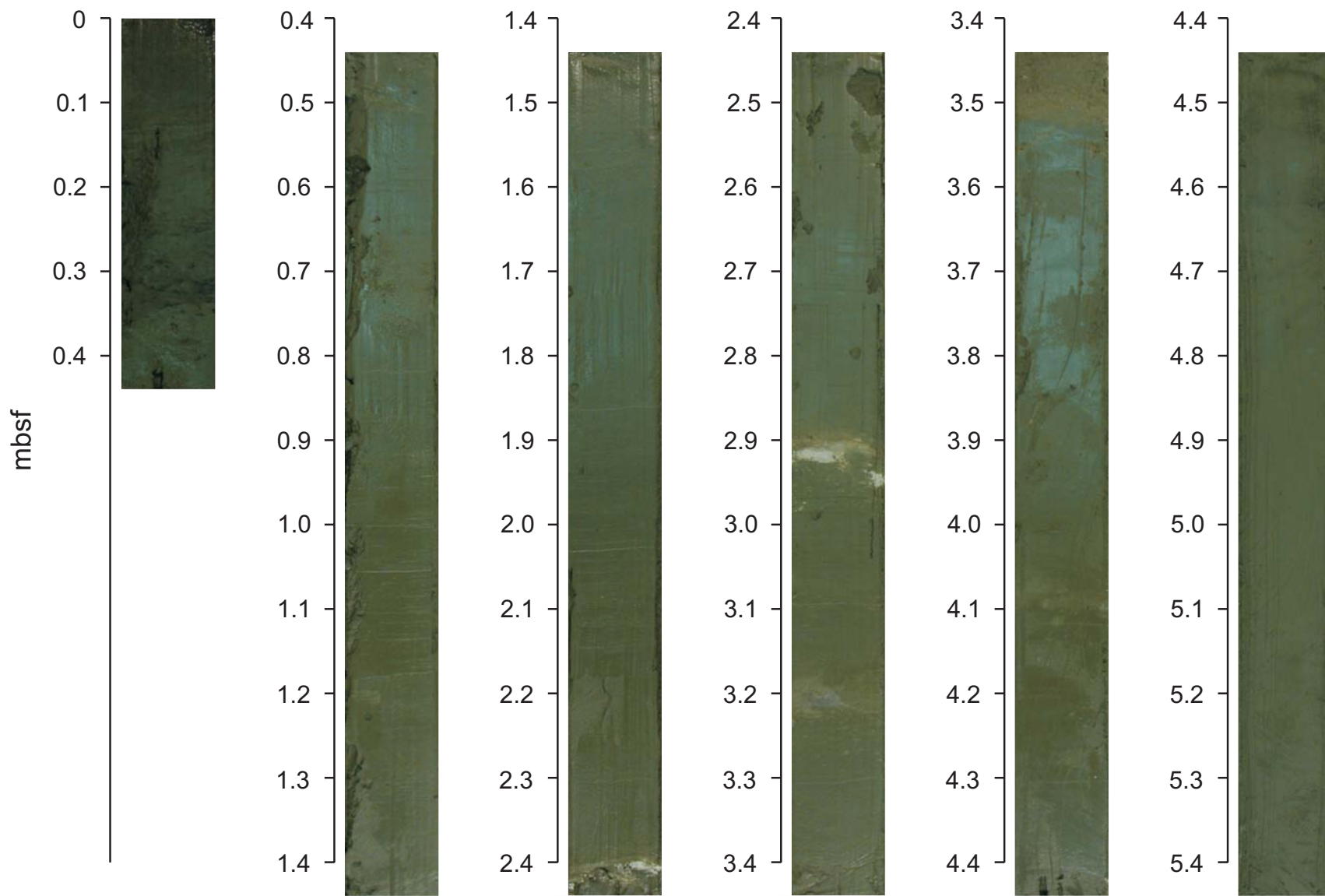
Appendix E

Core Photography

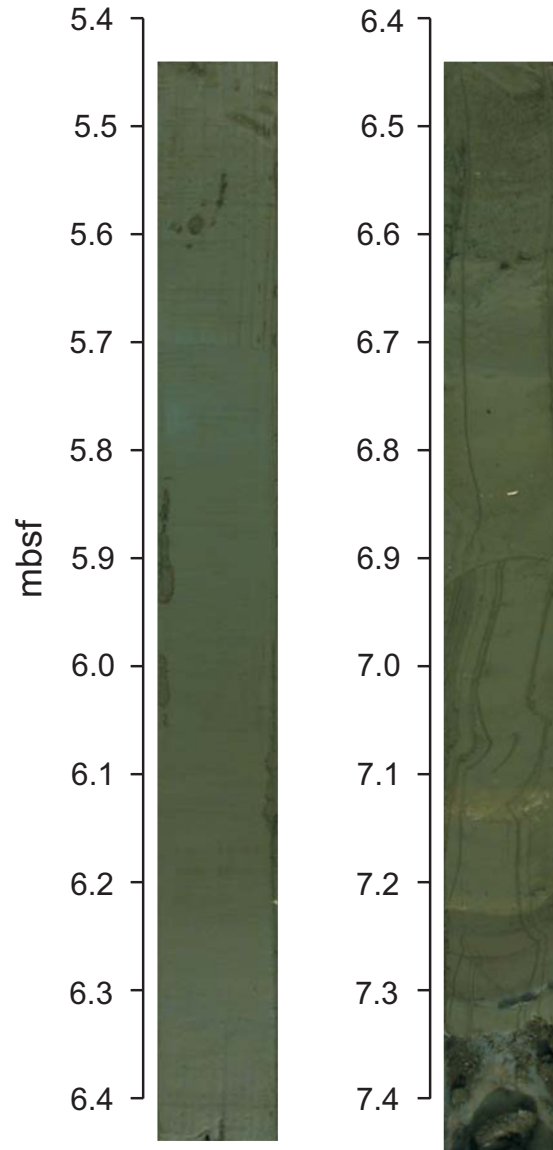
Core M 54-1 (0-5.0 m)



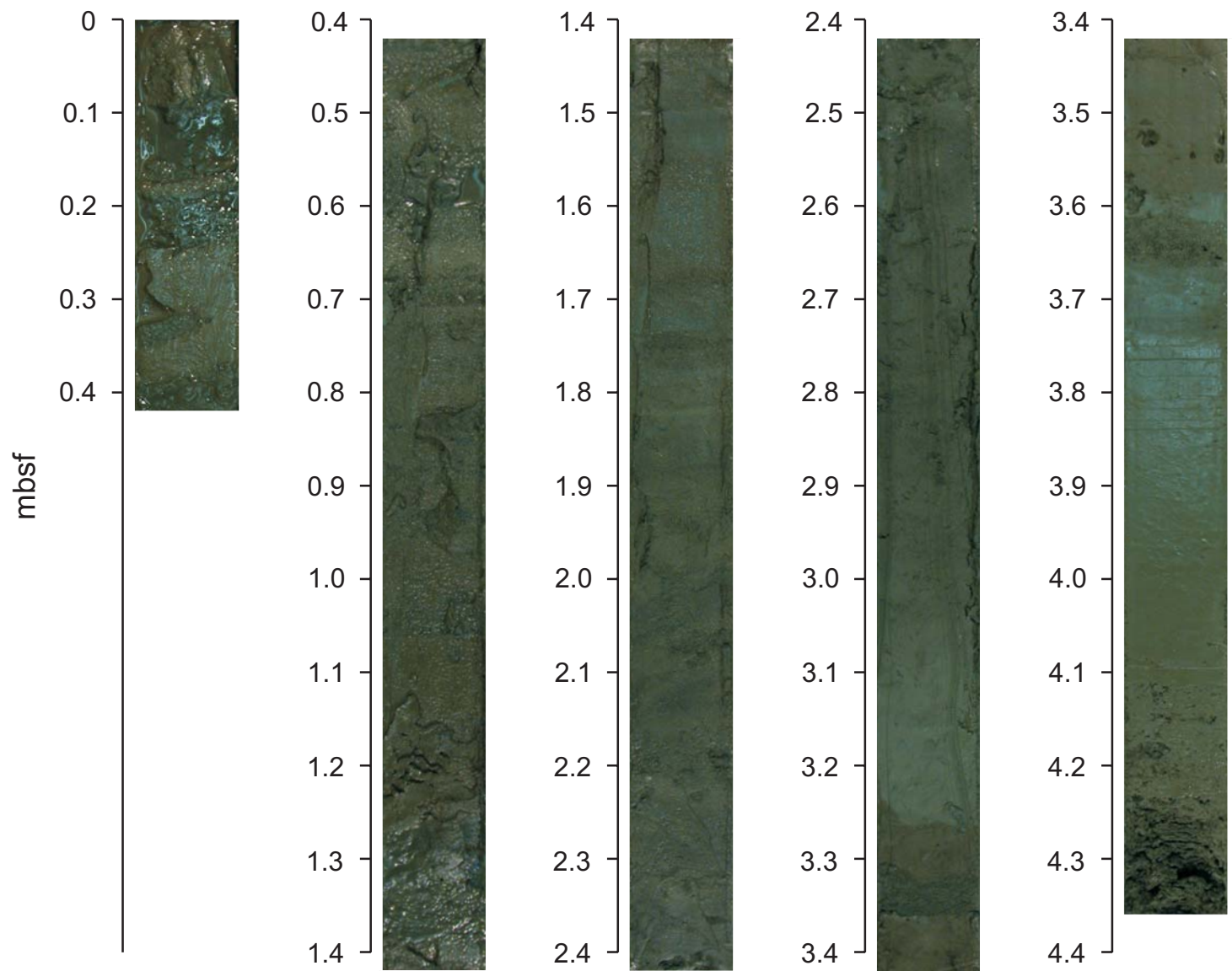
Core M 54-2a (0-7.45 m)



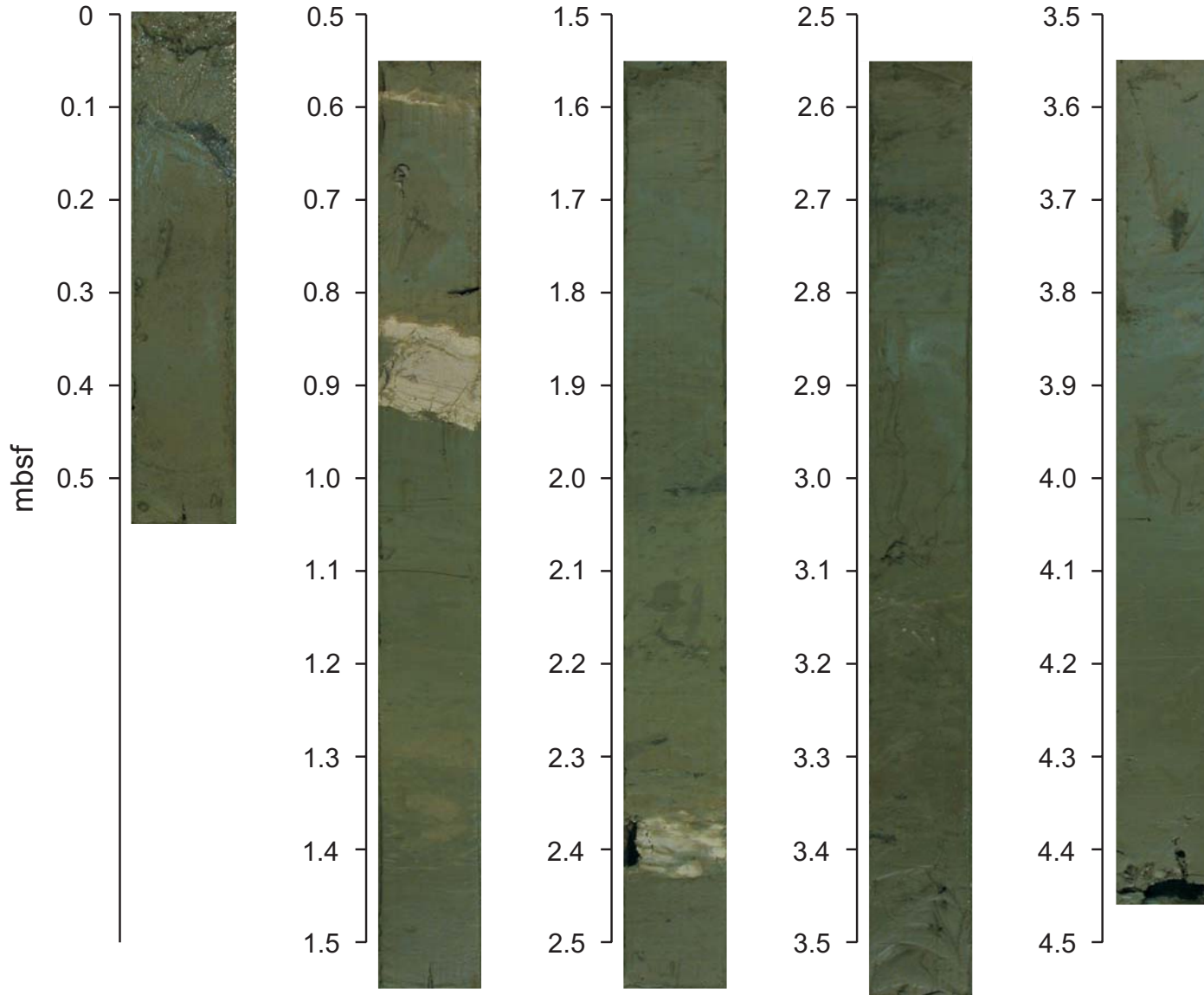
Core M 54-2b (0-7.45 m)



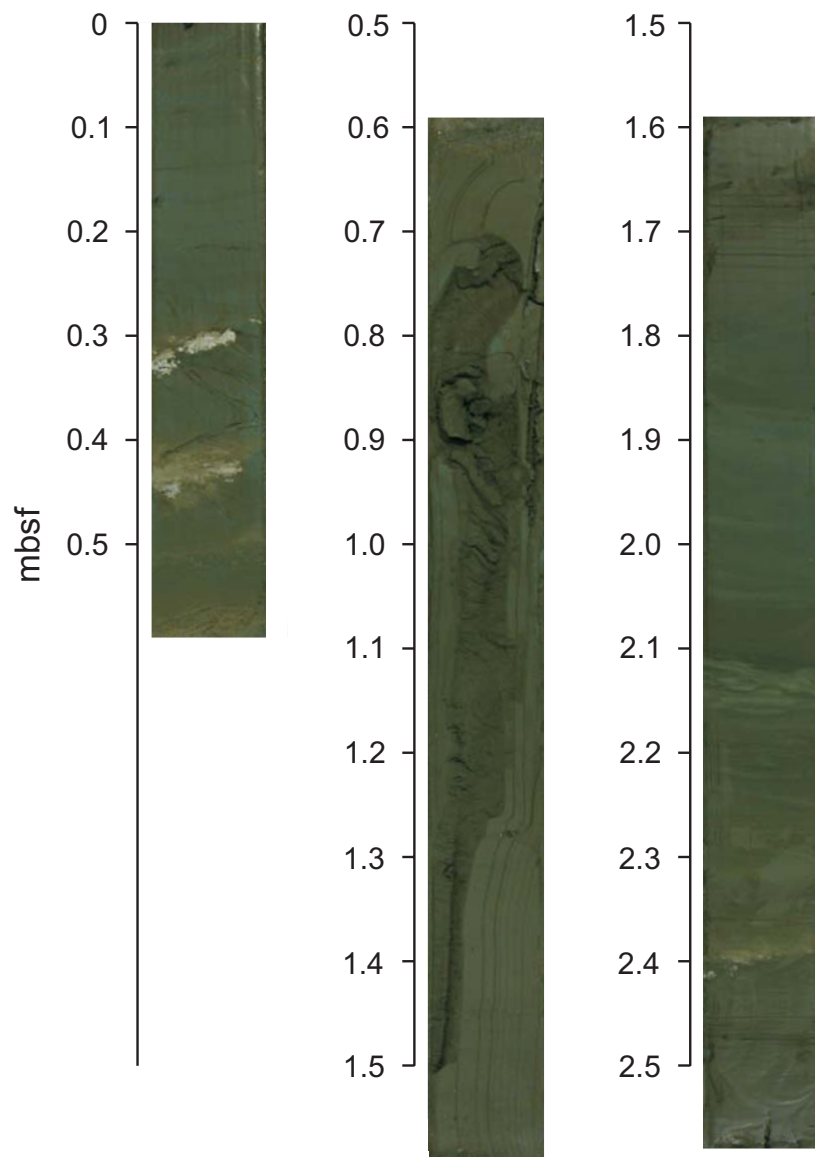
Core M 54-6 (0-4.36 m)



Core M 54-11/2 (0-4.46 m)

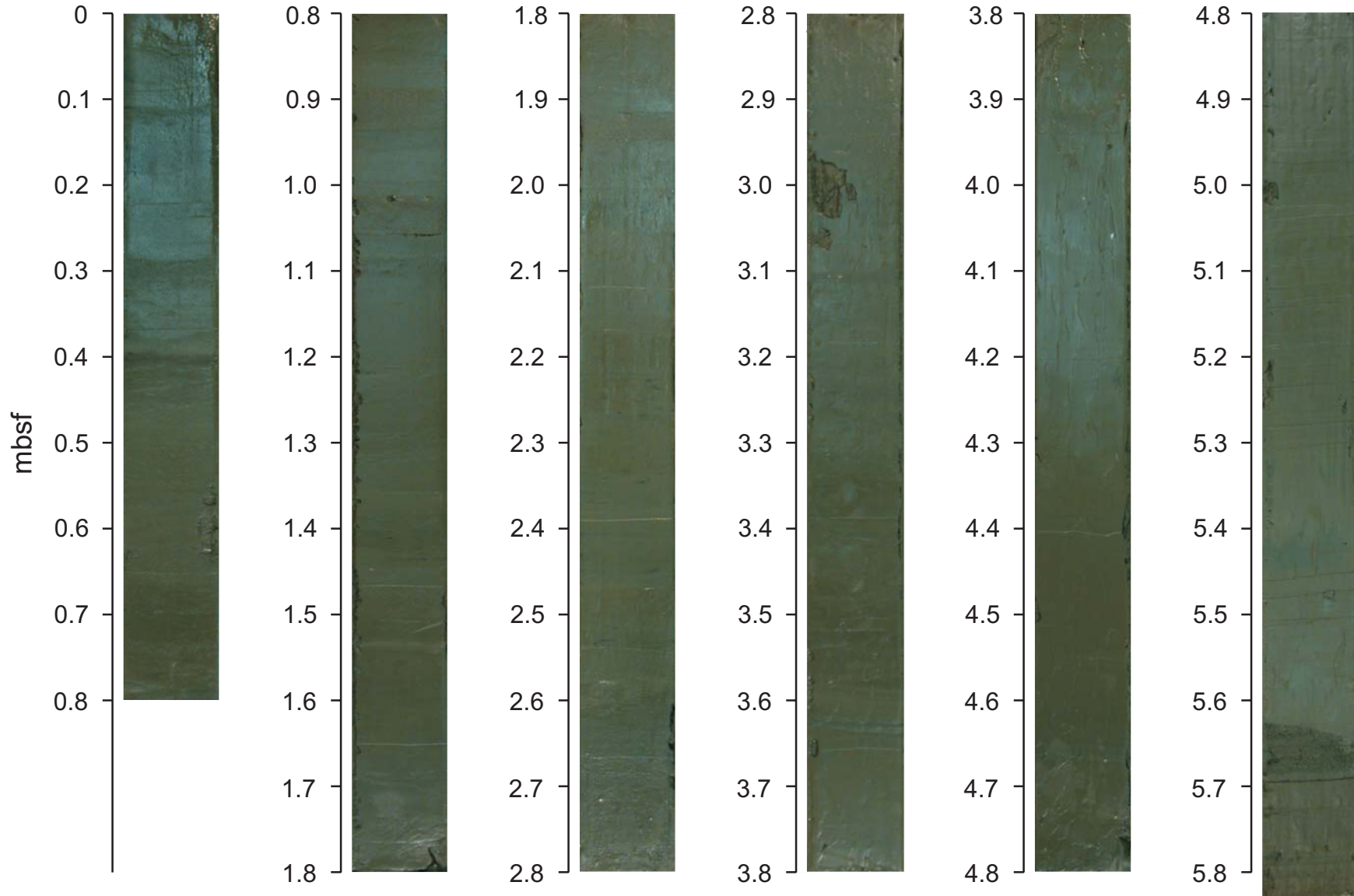


Core M 54-13 (0-2.58 m)

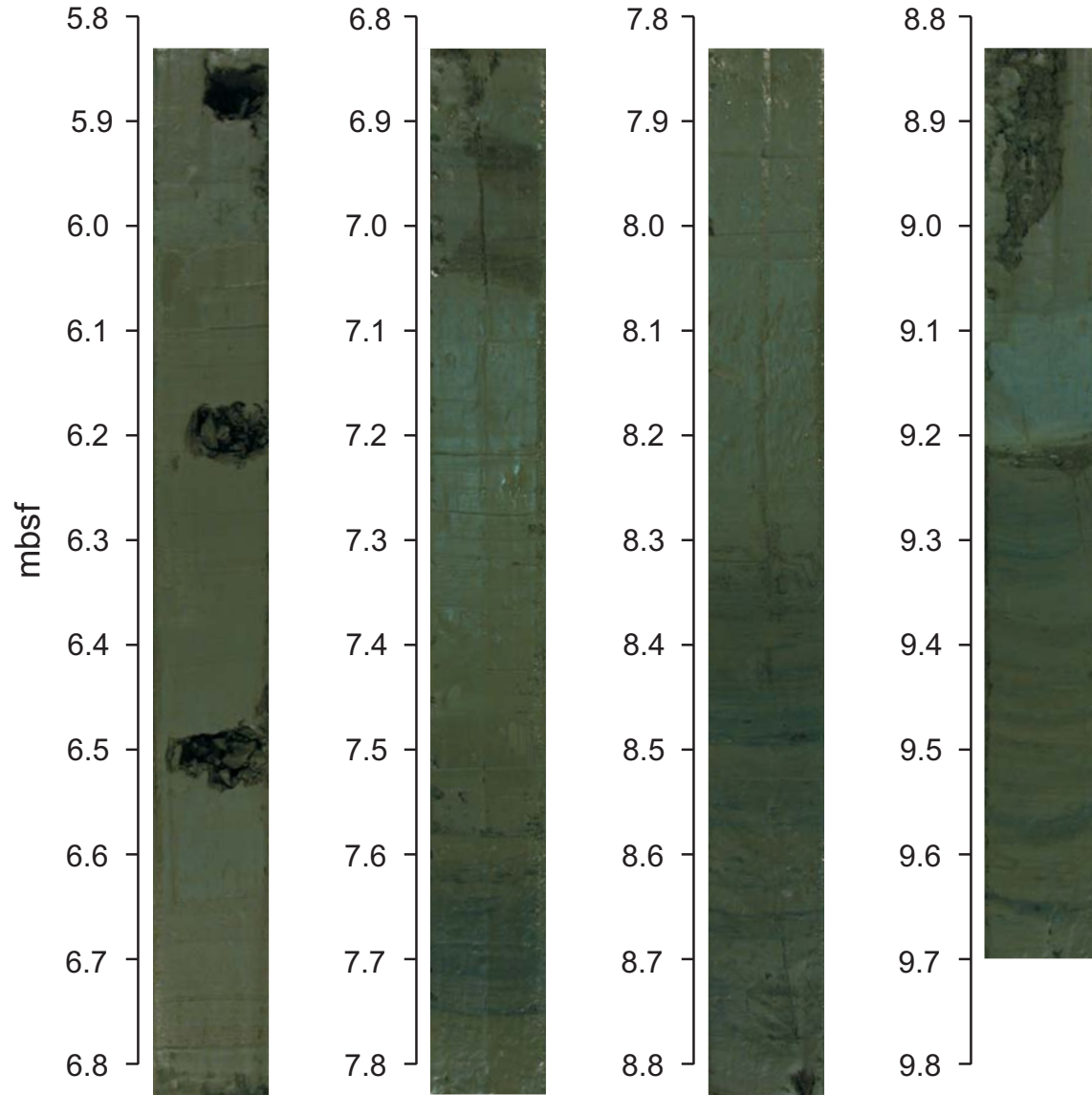


Core M 54-14a (0-9.7 m)

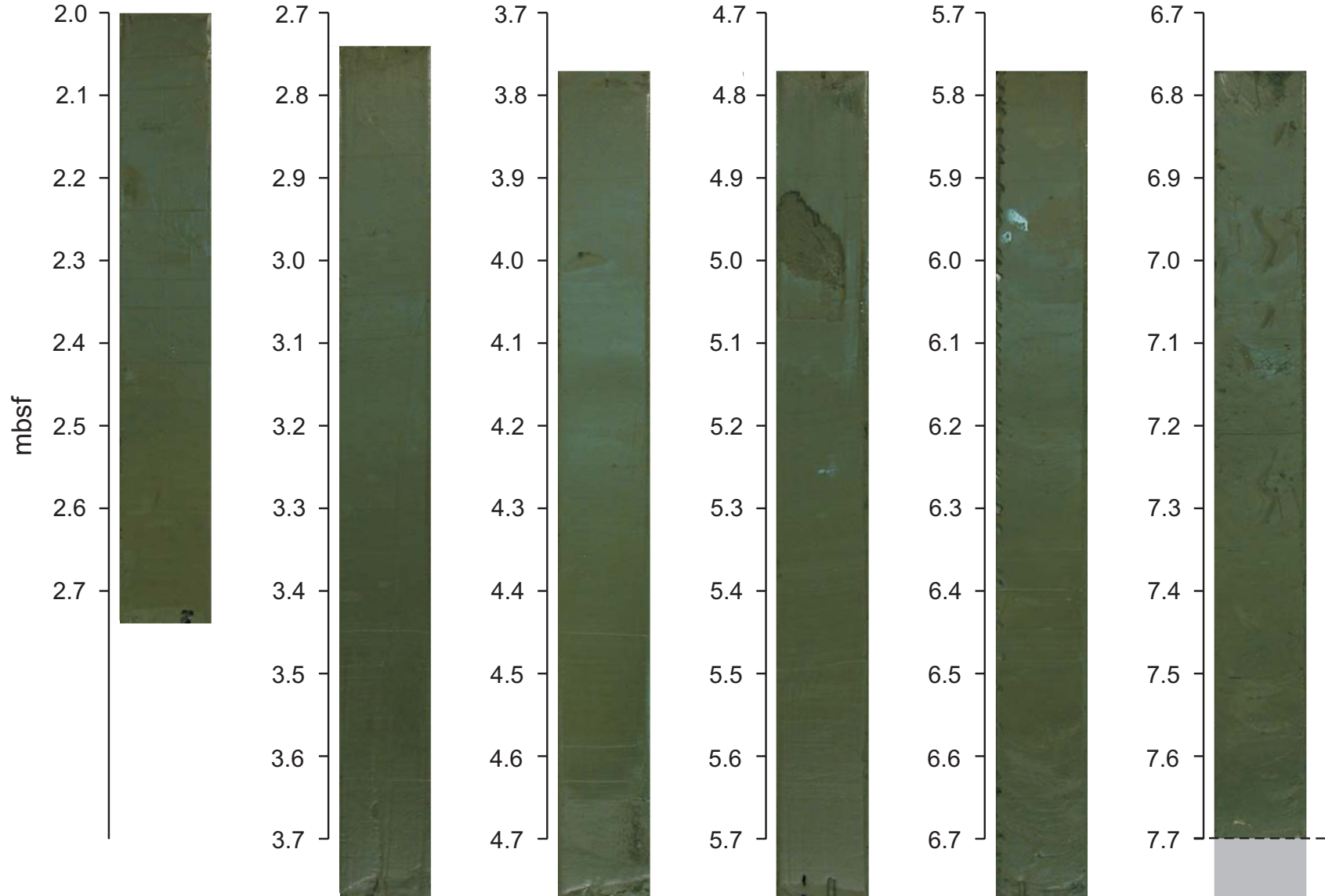
220



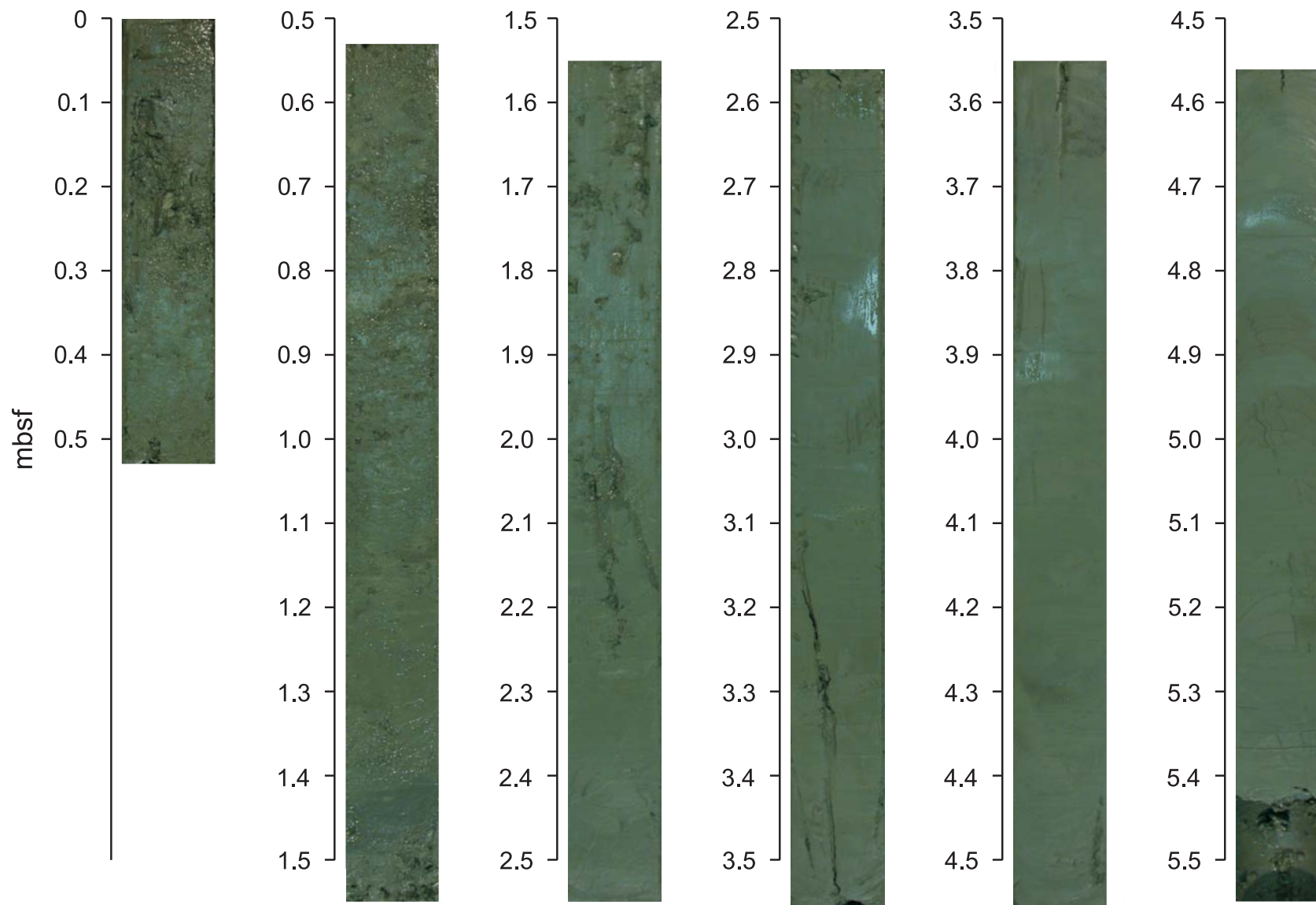
Core M 54-14b (0-9.7 m)



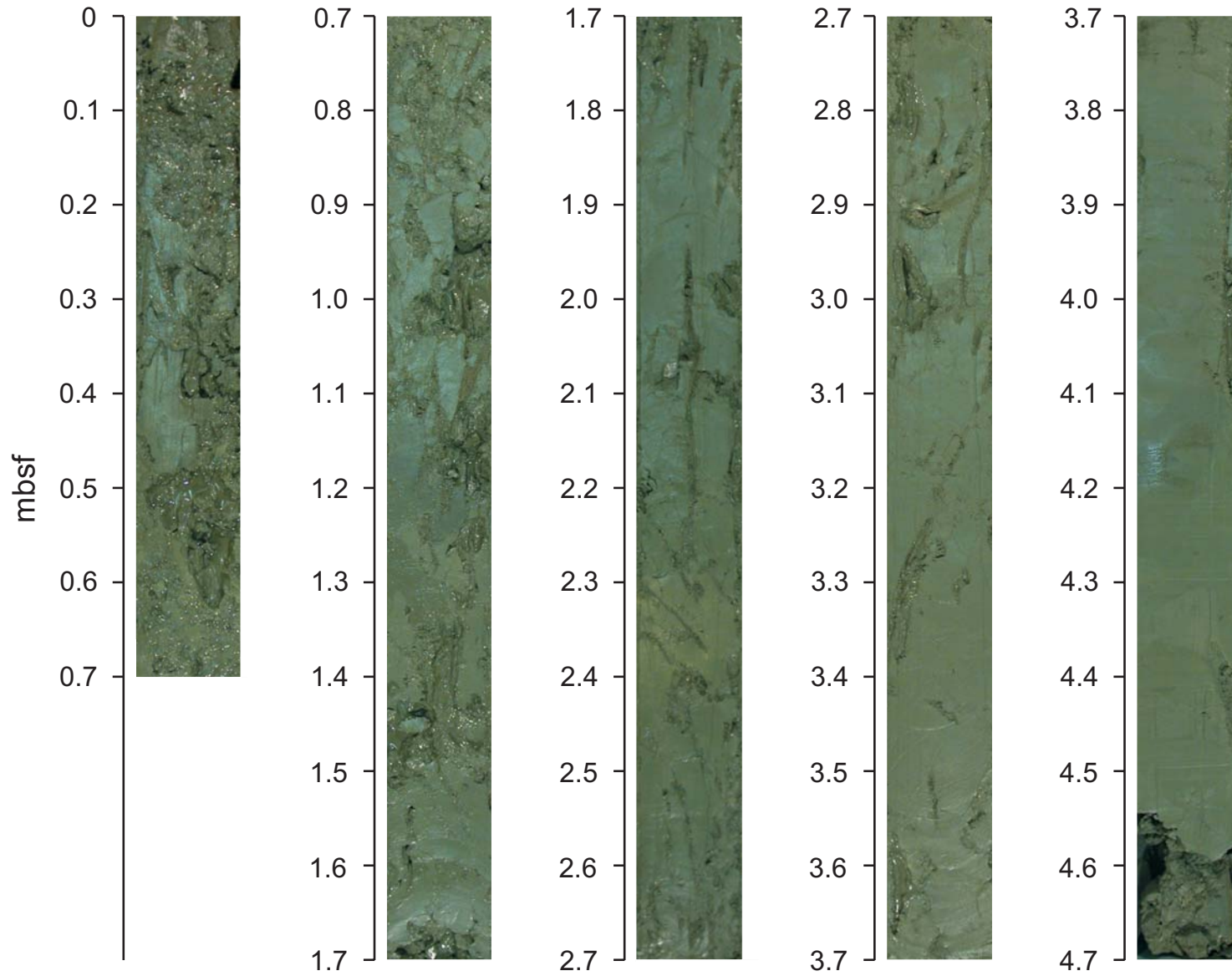
Core M 54-17 (2.0-7.77 m) - Mound Culebra, SW Base



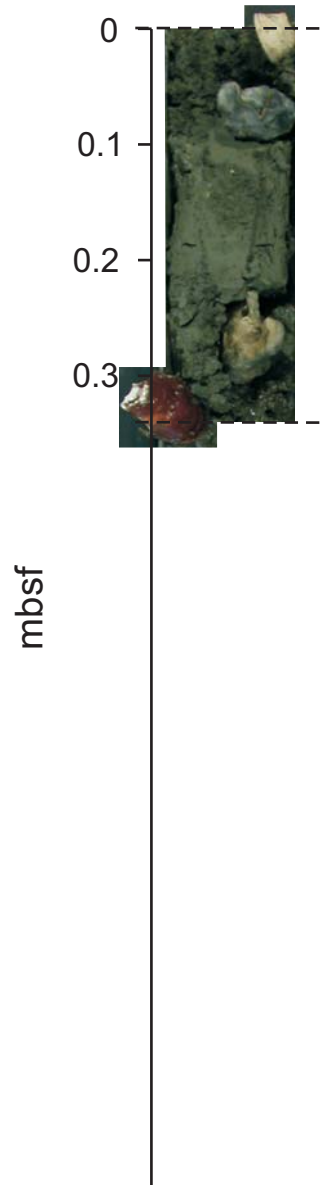
Core M 54-18 (0-5.55 m) - Mound Culebra, NW Top



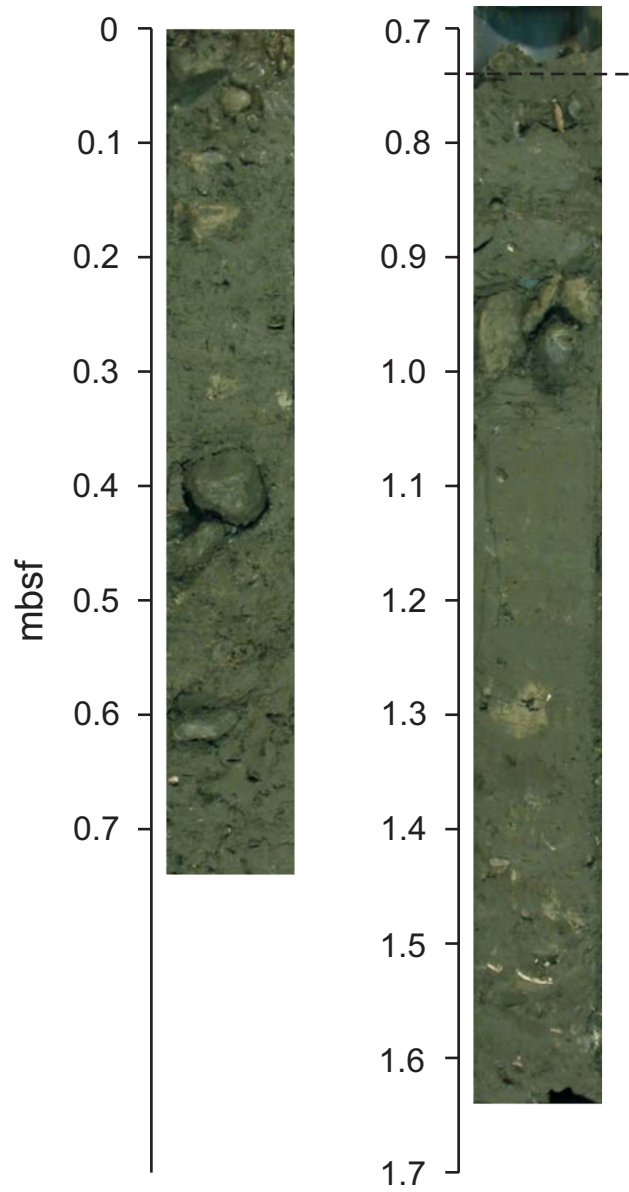
Core M 54-21 (0-4.70 m) - Mound Culebra, NW Top



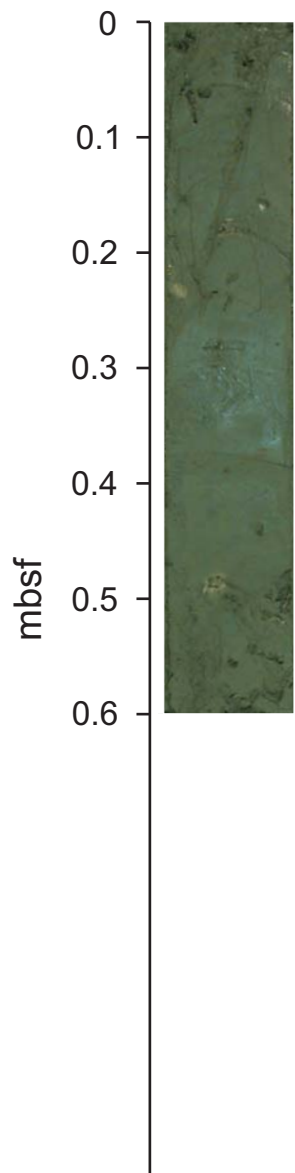
Core M 54-27 (0-0.34 m) - Mound Culebra, Top



Core M 54-29 (0-1.67 m) - Mound Culebra, Top

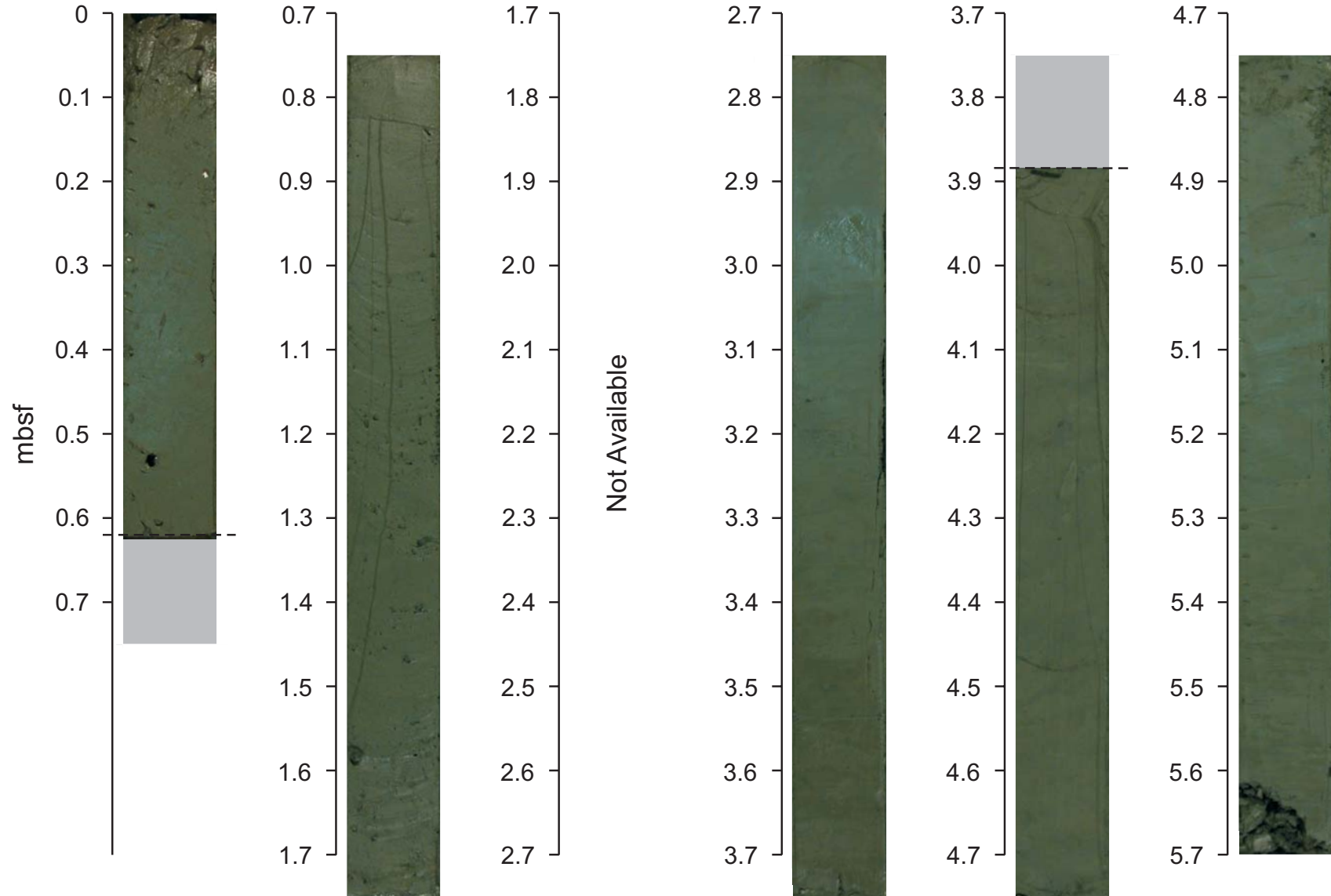


Core M 54-30 (0-0.6 m) - Mound Culebra, N Base

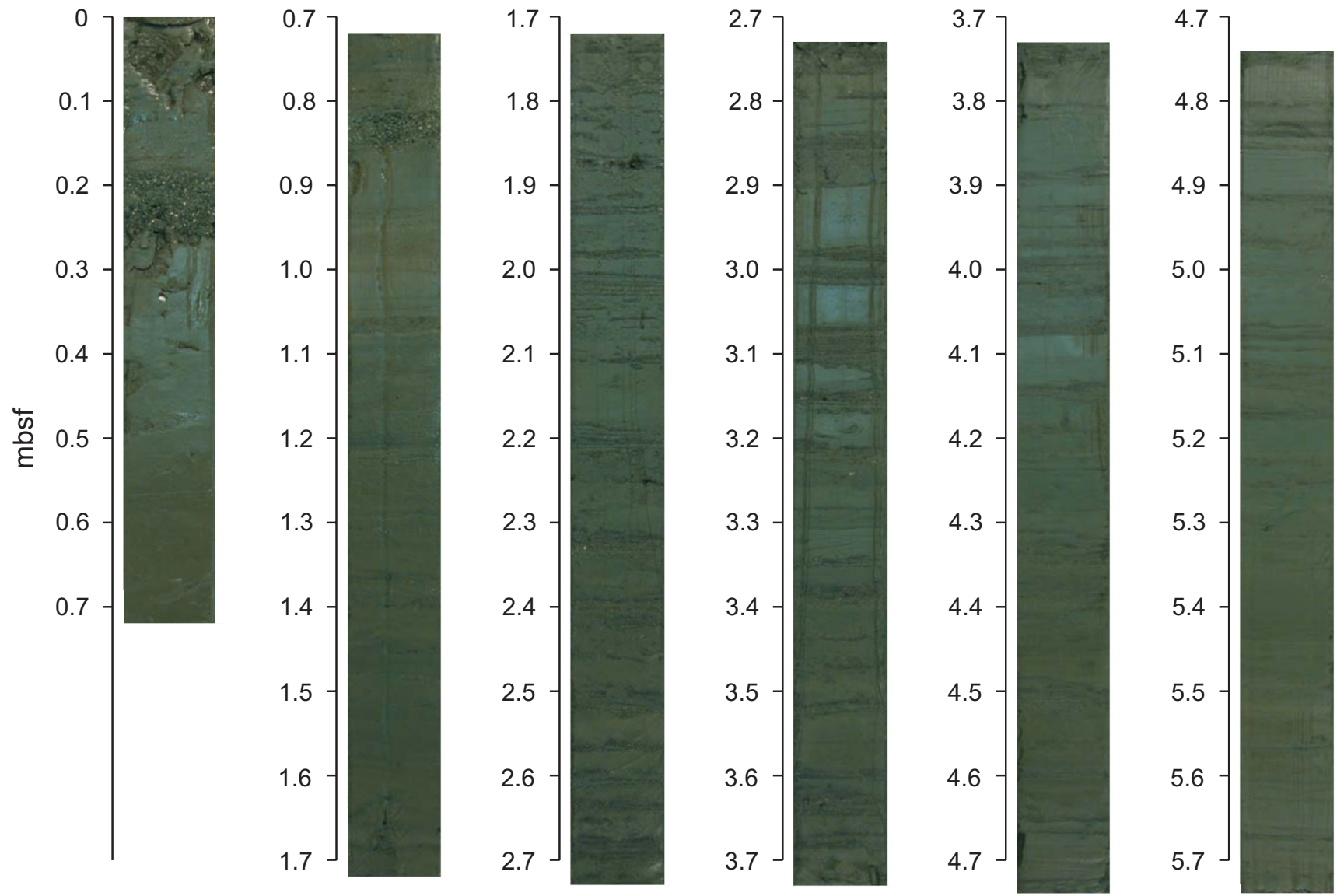


Core M 54-32 (0-5.70 m) - Mound Culebra, NW Slope

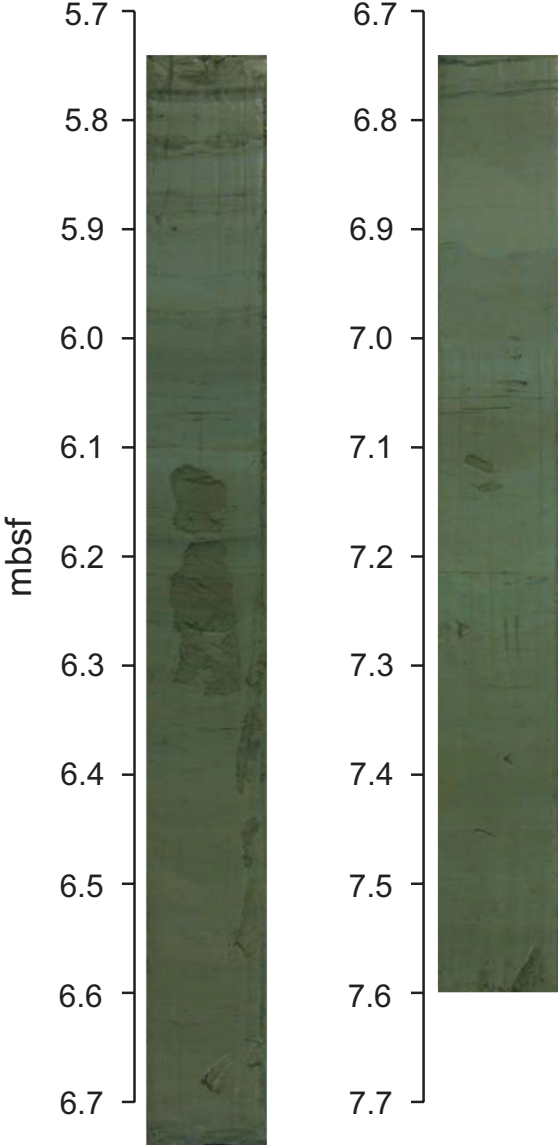
228



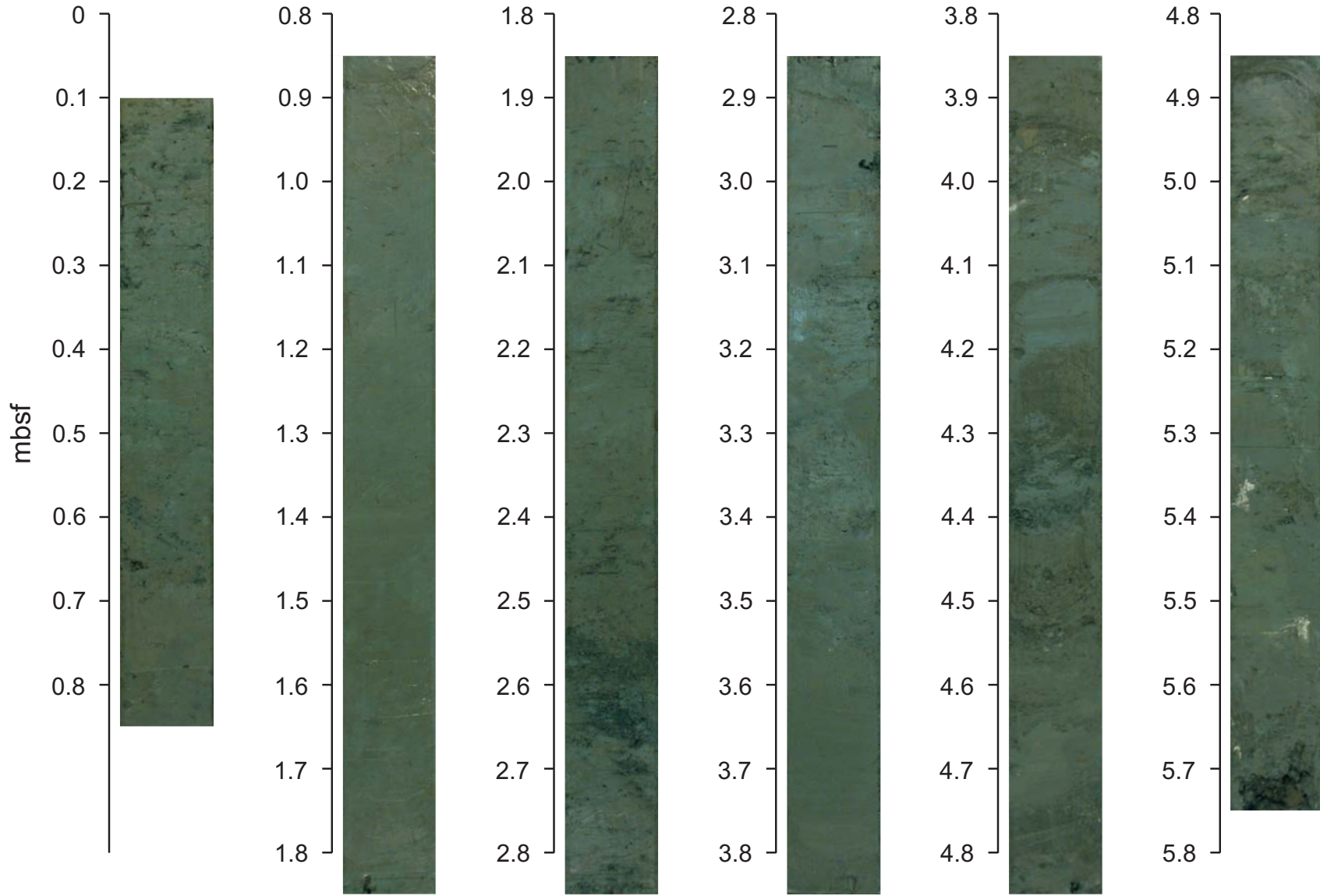
Core M 54-35a (0-7.6 m) - Trench



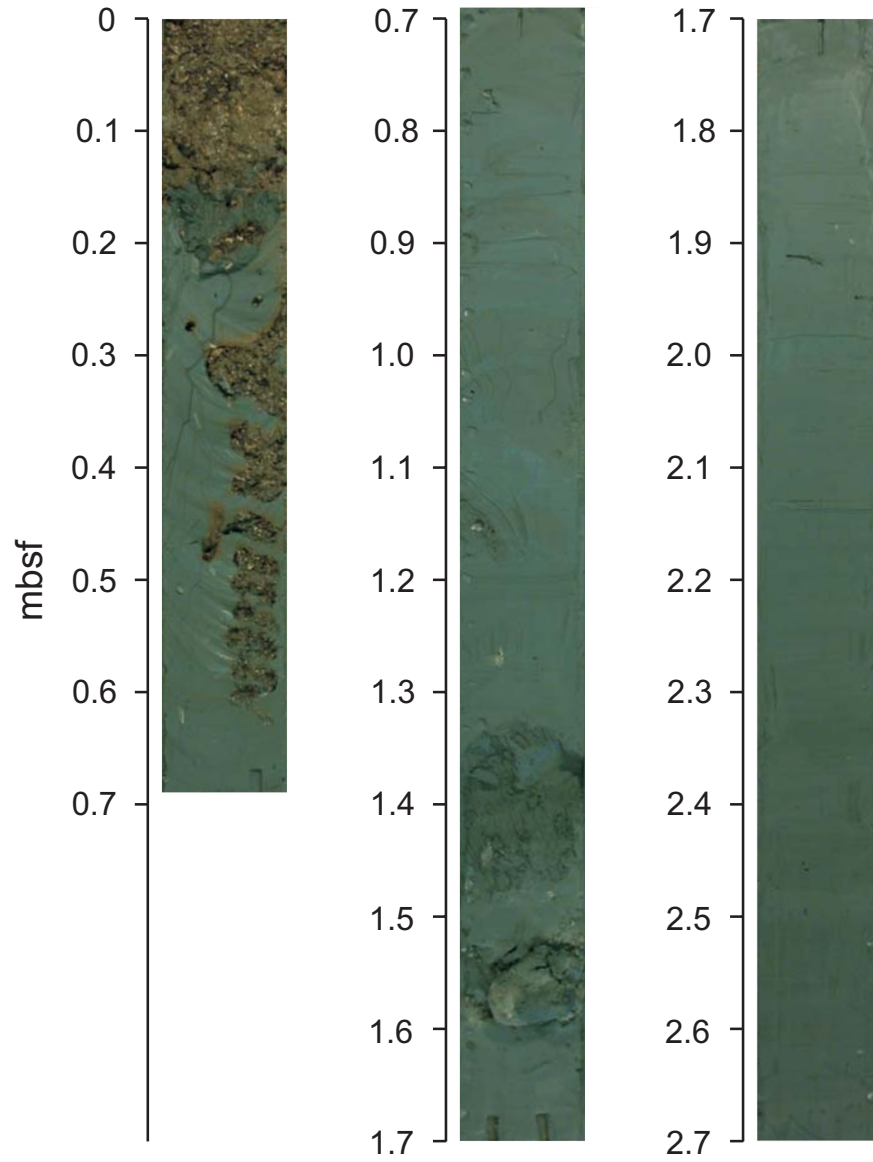
Core M 54-35b (0-7.6 m) - Trench



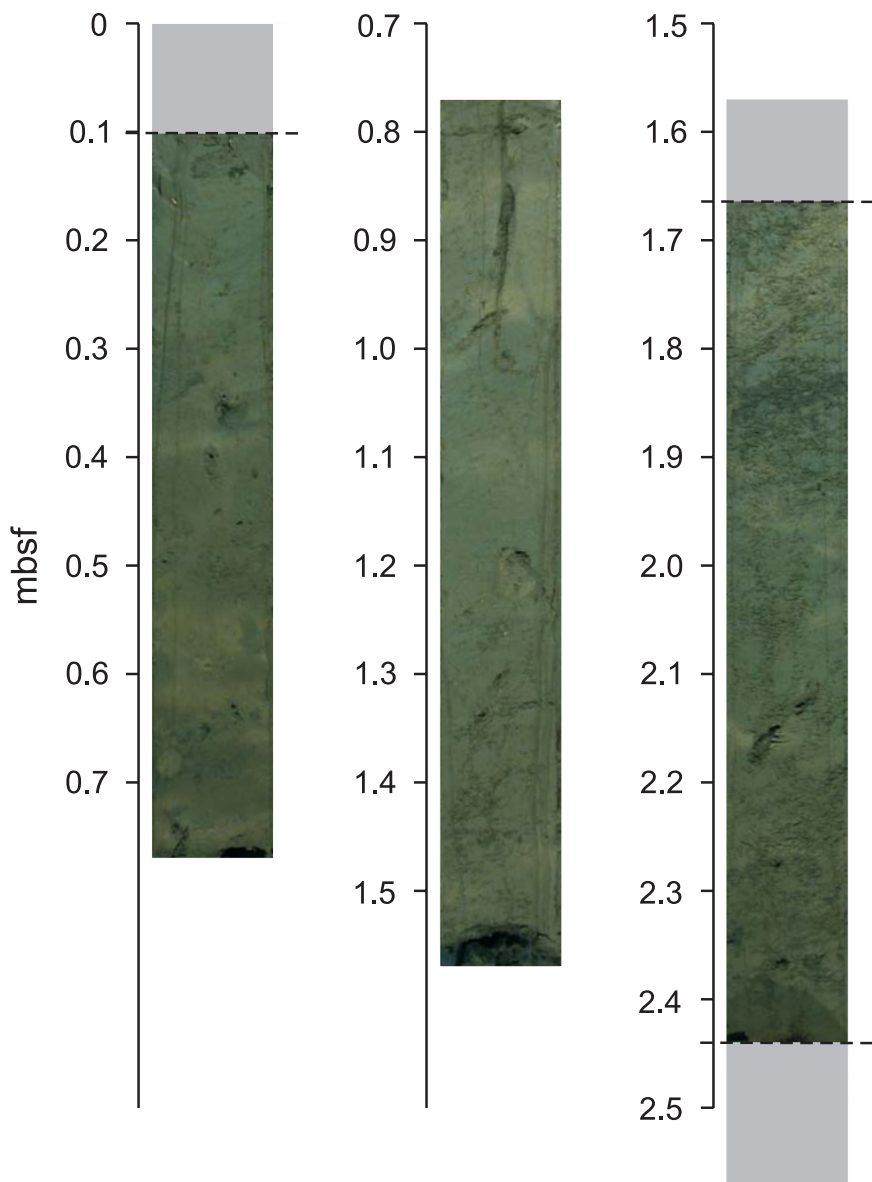
Core M 54-36 (0.1-5.72 m) - Trench



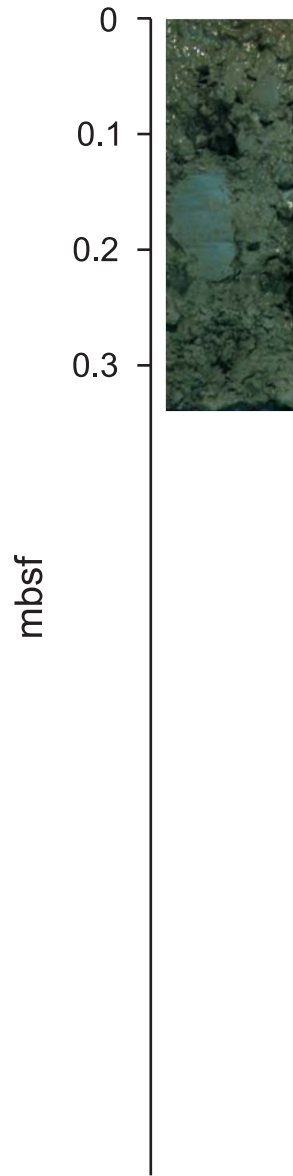
Core M 54-40 (0-2.70 m) - Trench



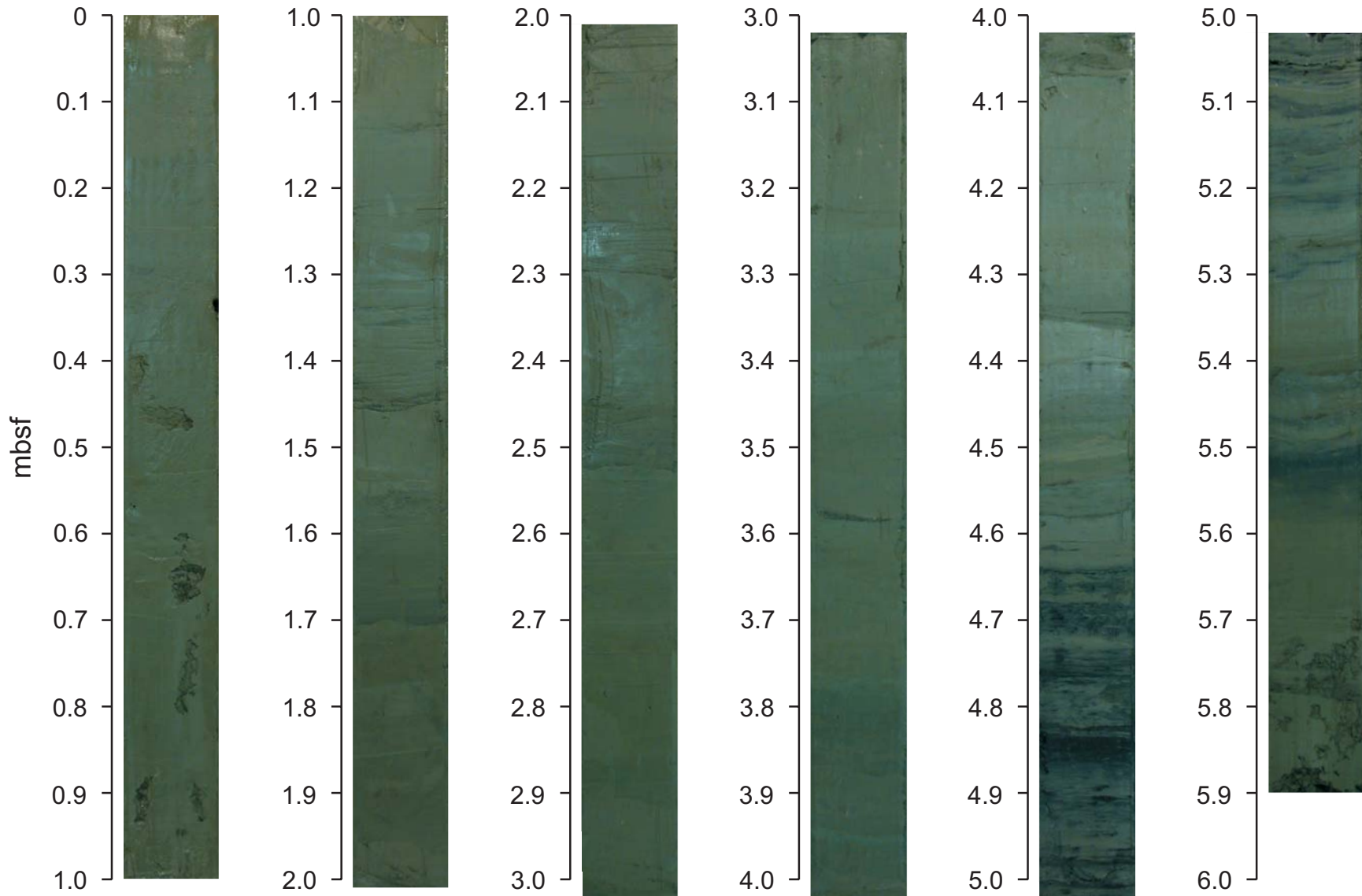
Core M 54-48/1 (0-2.57 m) - Jaco Scarp, Central Bulge



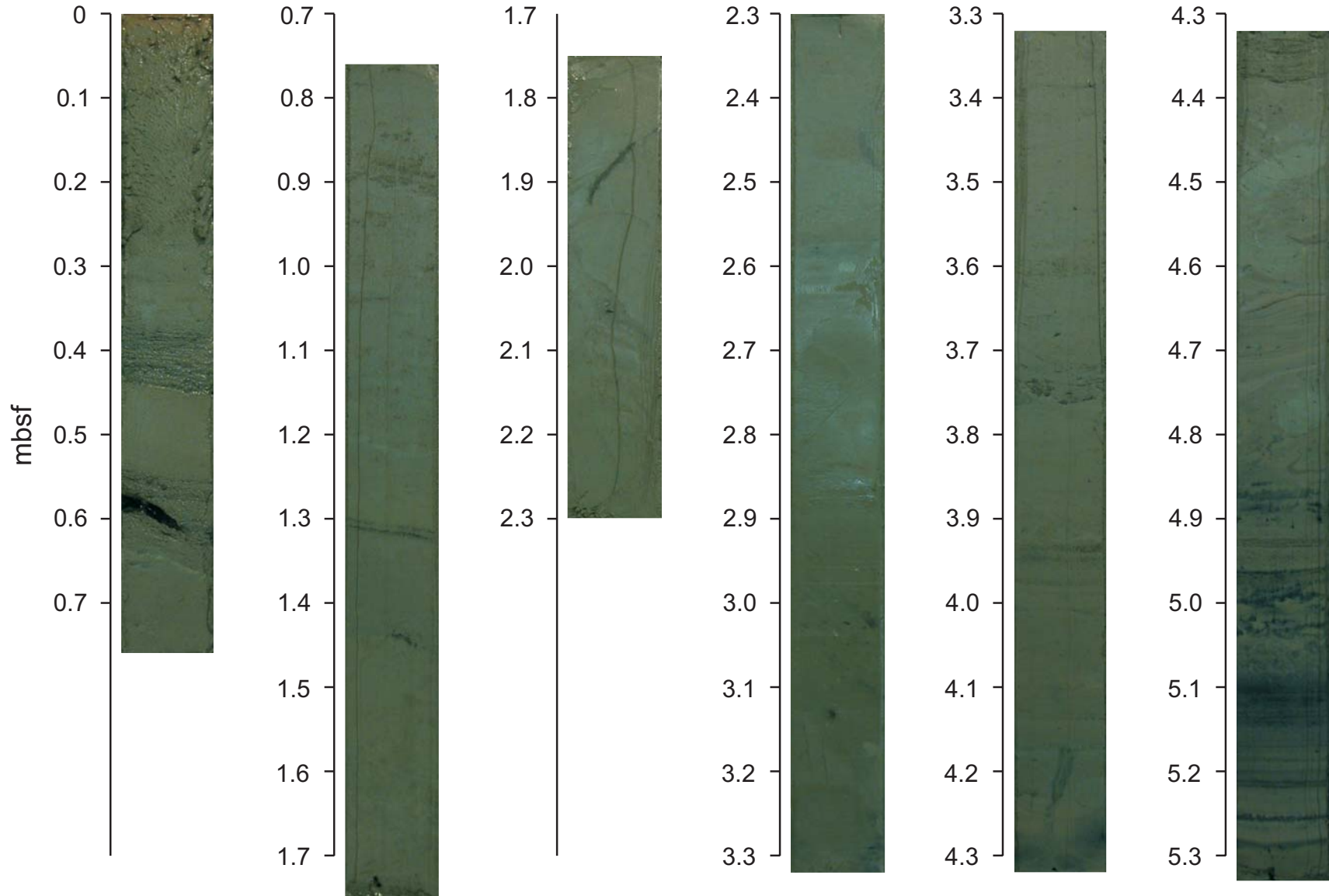
Core M 54-52 (0-0.34 m) - Jaco Scarp, Central Bulge



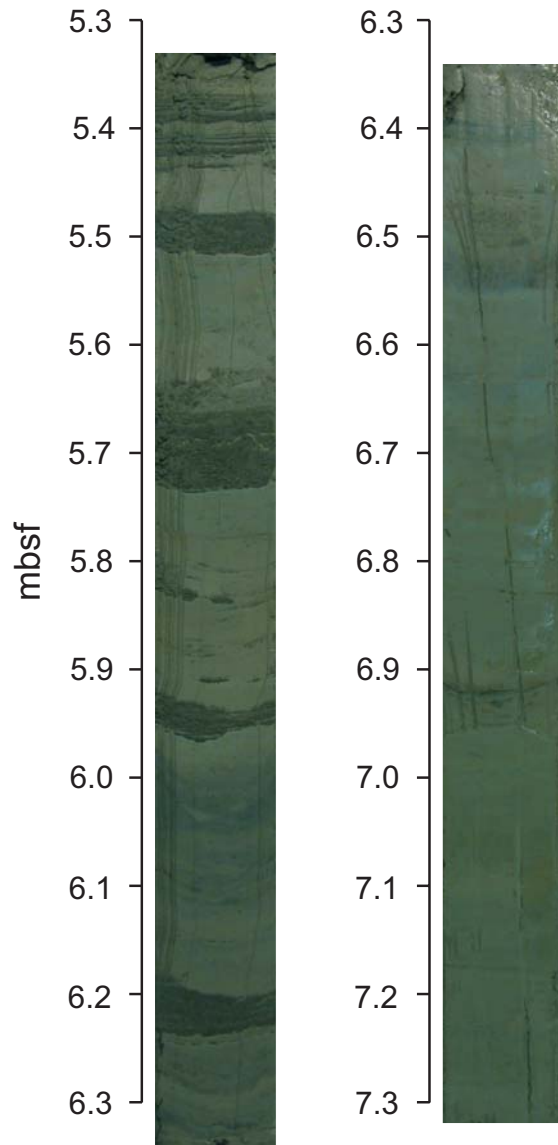
Core M 54-56 (0-5.9 m) - Jaco Scarp, SW Trench



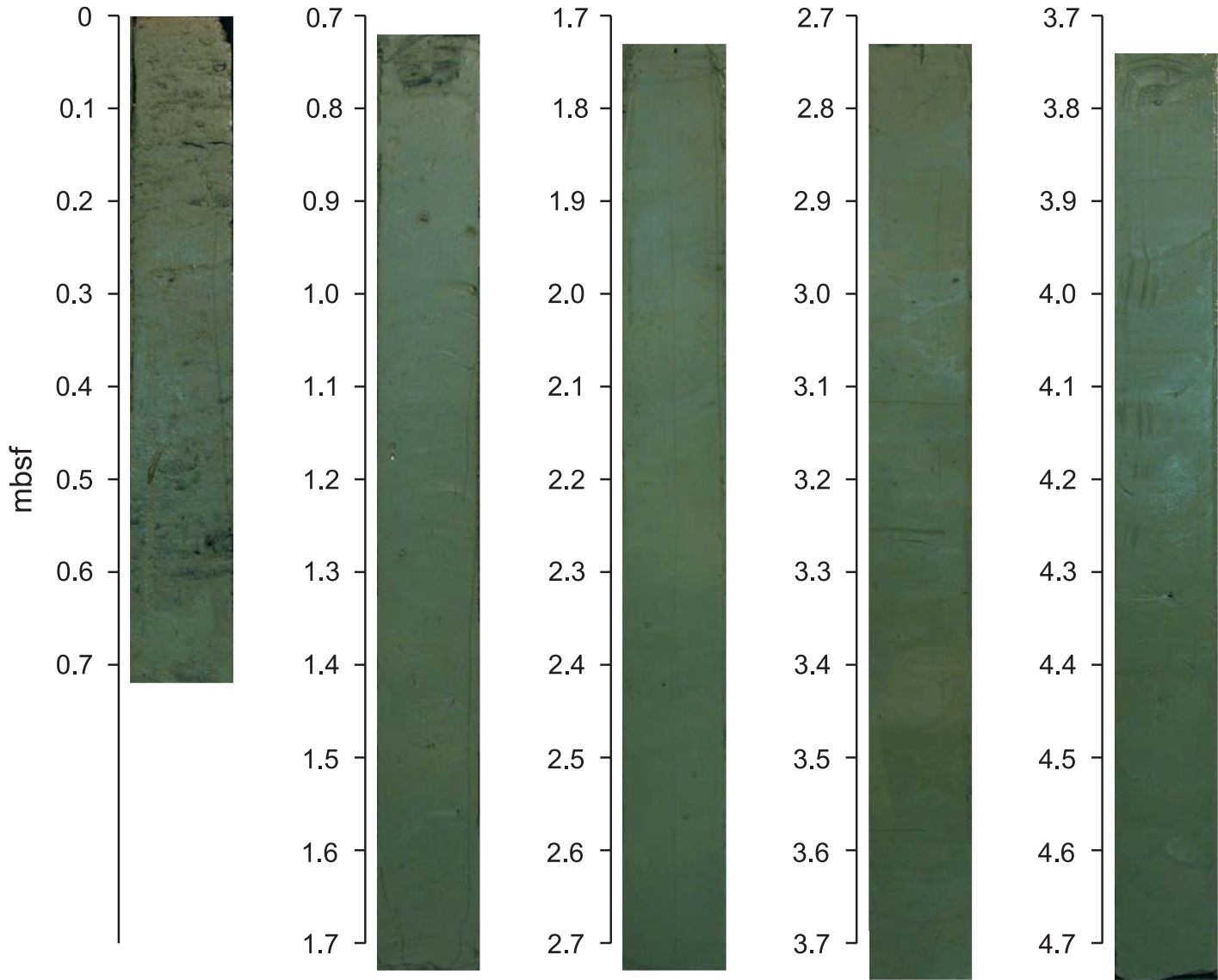
Core M 54-57a (0-7.32 m) - Jaco Scarp, SW Trench



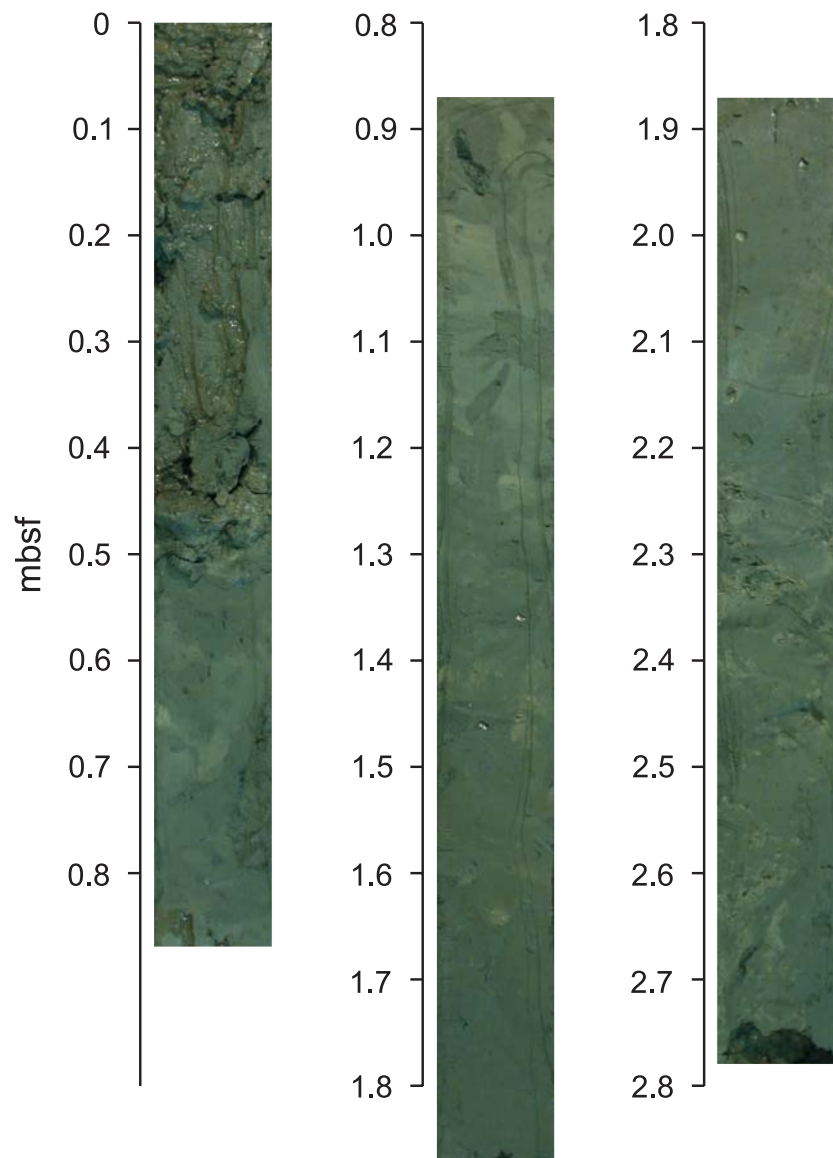
Core M 54-57b (0-7.32 m) - Jaco Scarp, SW Trench



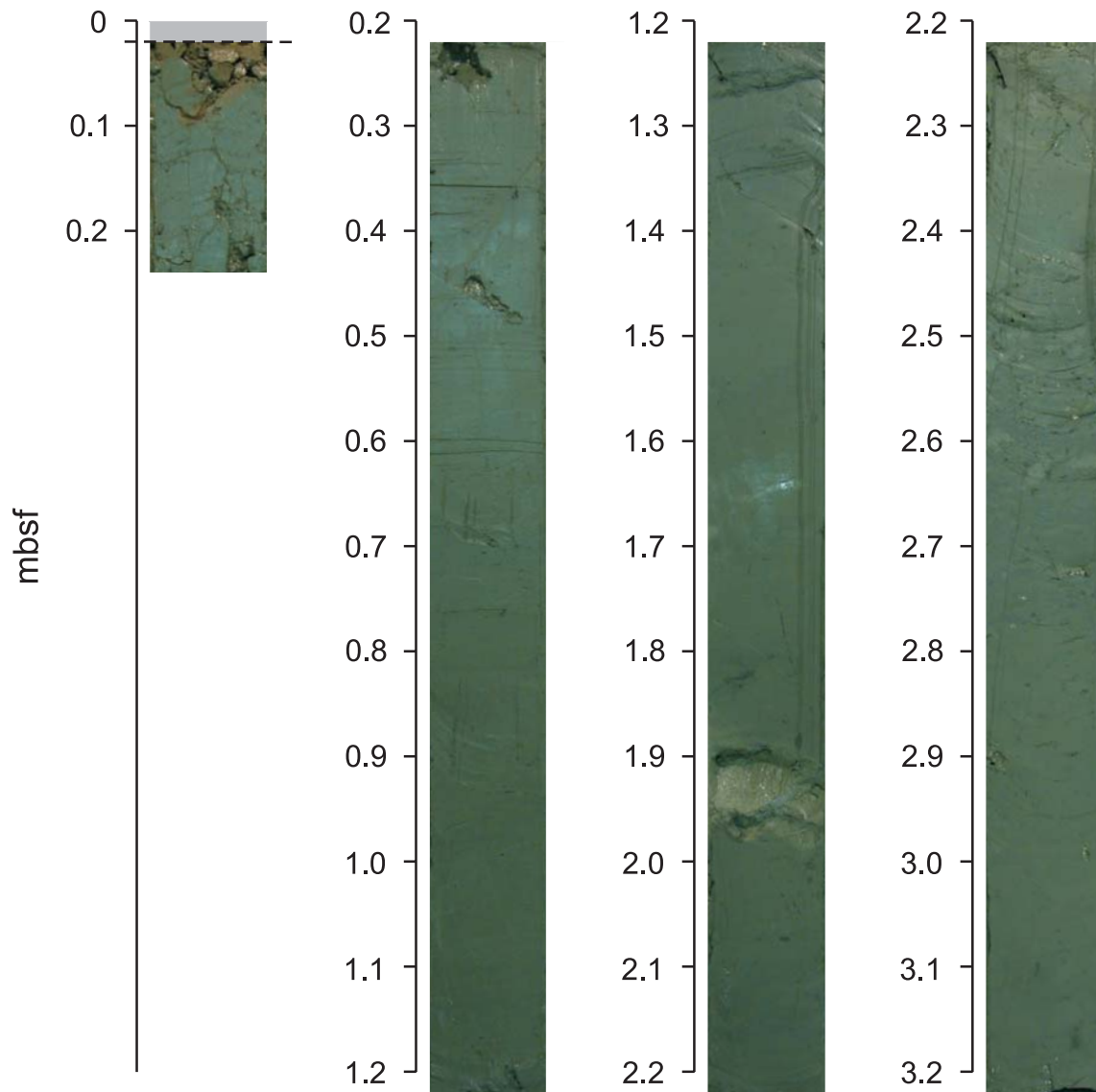
Core M 54-61 (0-4.74 m) - Jaco Scarp, Central Bulge



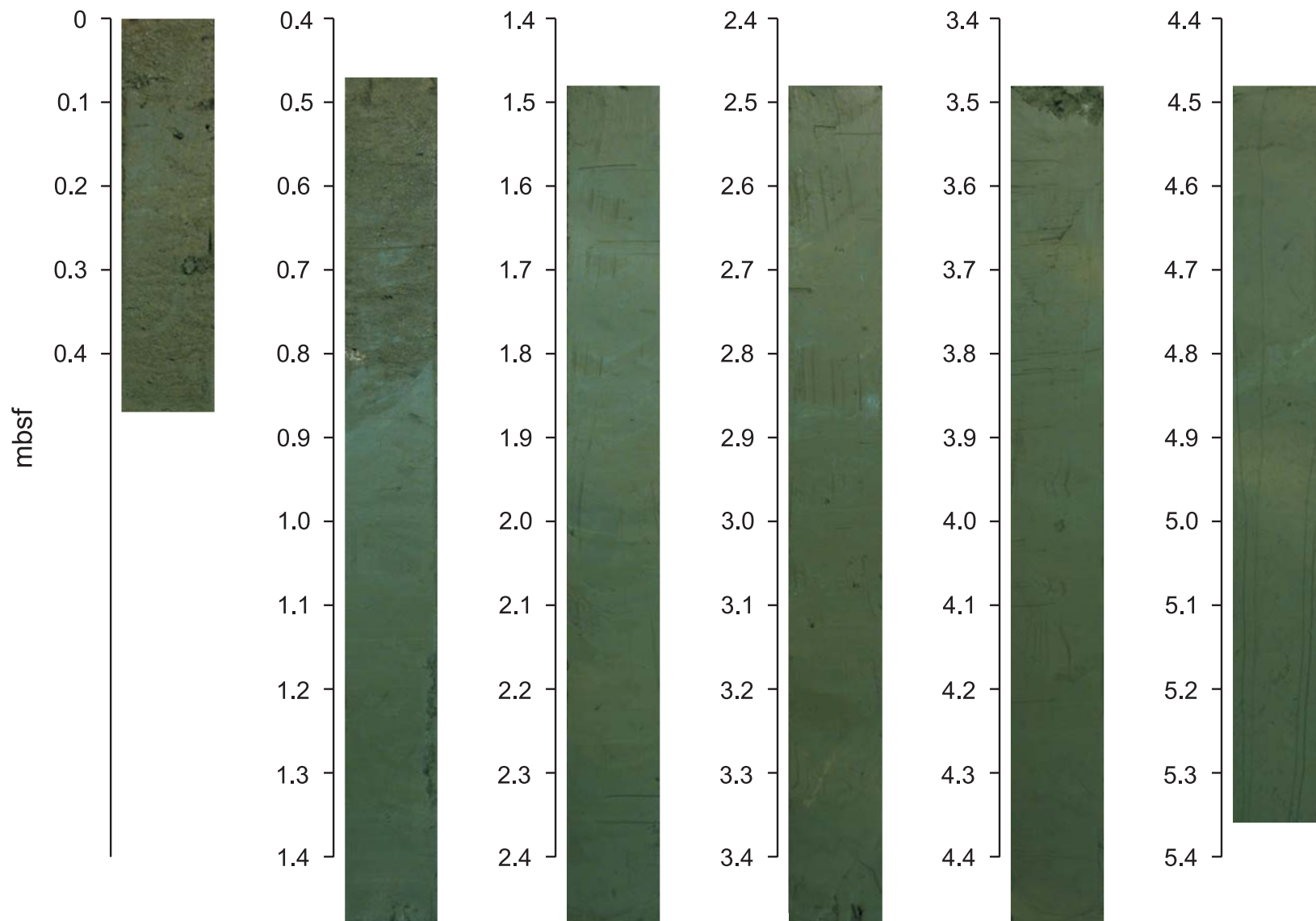
Core M 54-62/2 (0-2.78 m) - Jaco Scarp, Central Bulge



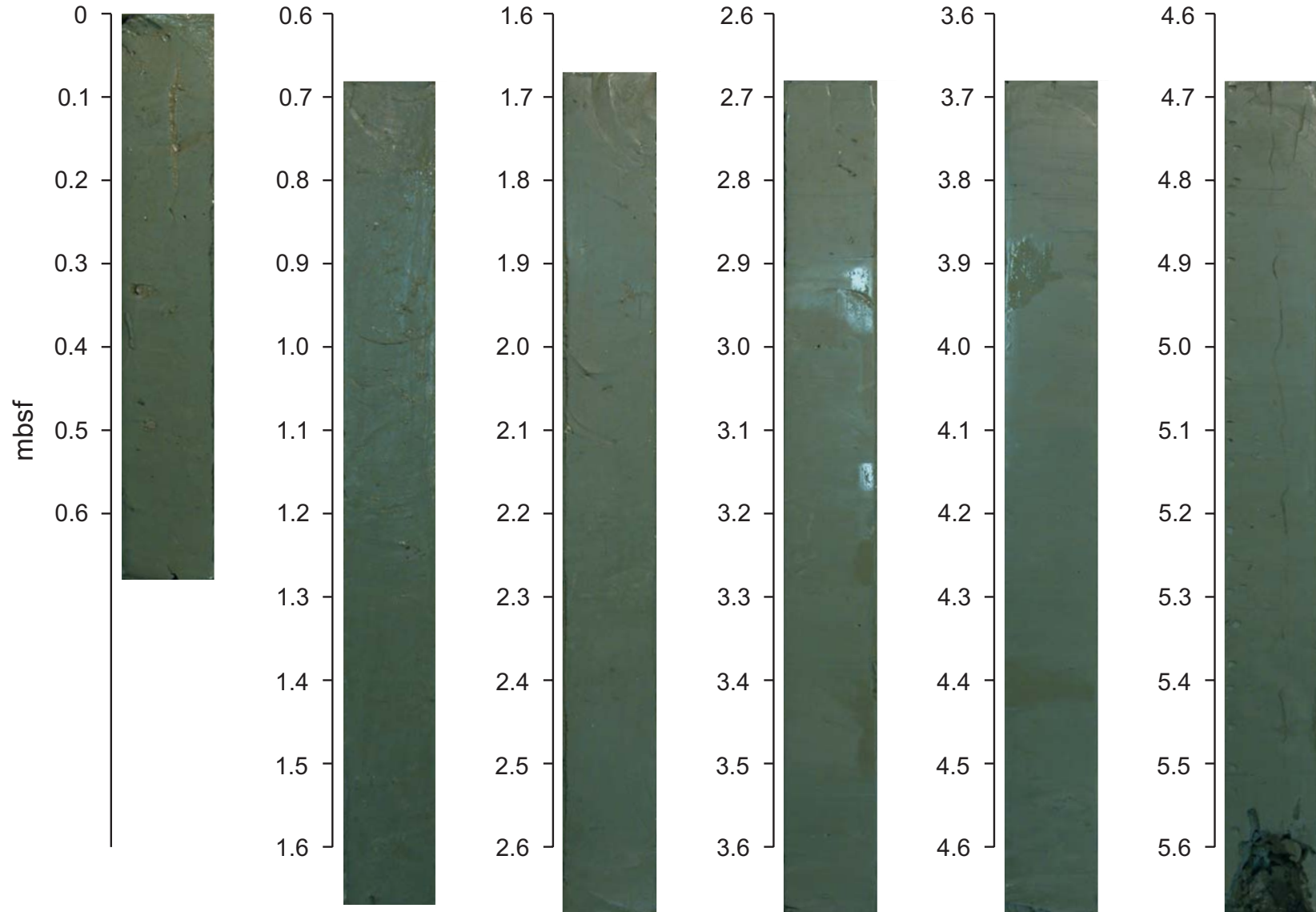
Core M 54-63 (0-3.24 m) - Jaco Scarp, Central Bulge



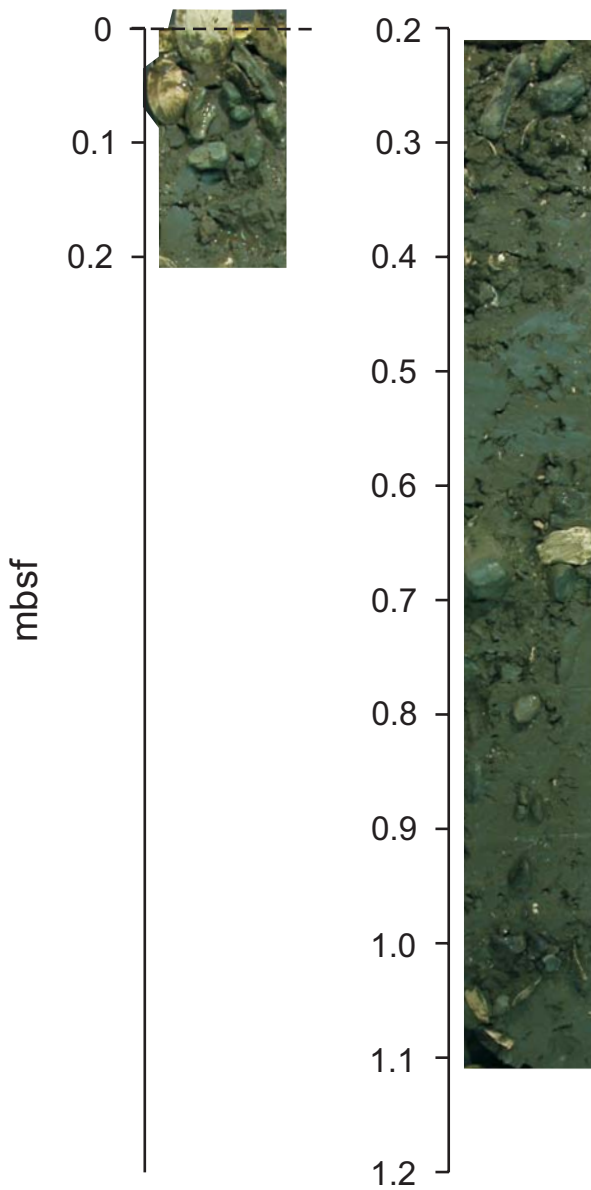
Core M 54-64 (0-5.36 m) - Jaco Scarp, Central Bulge



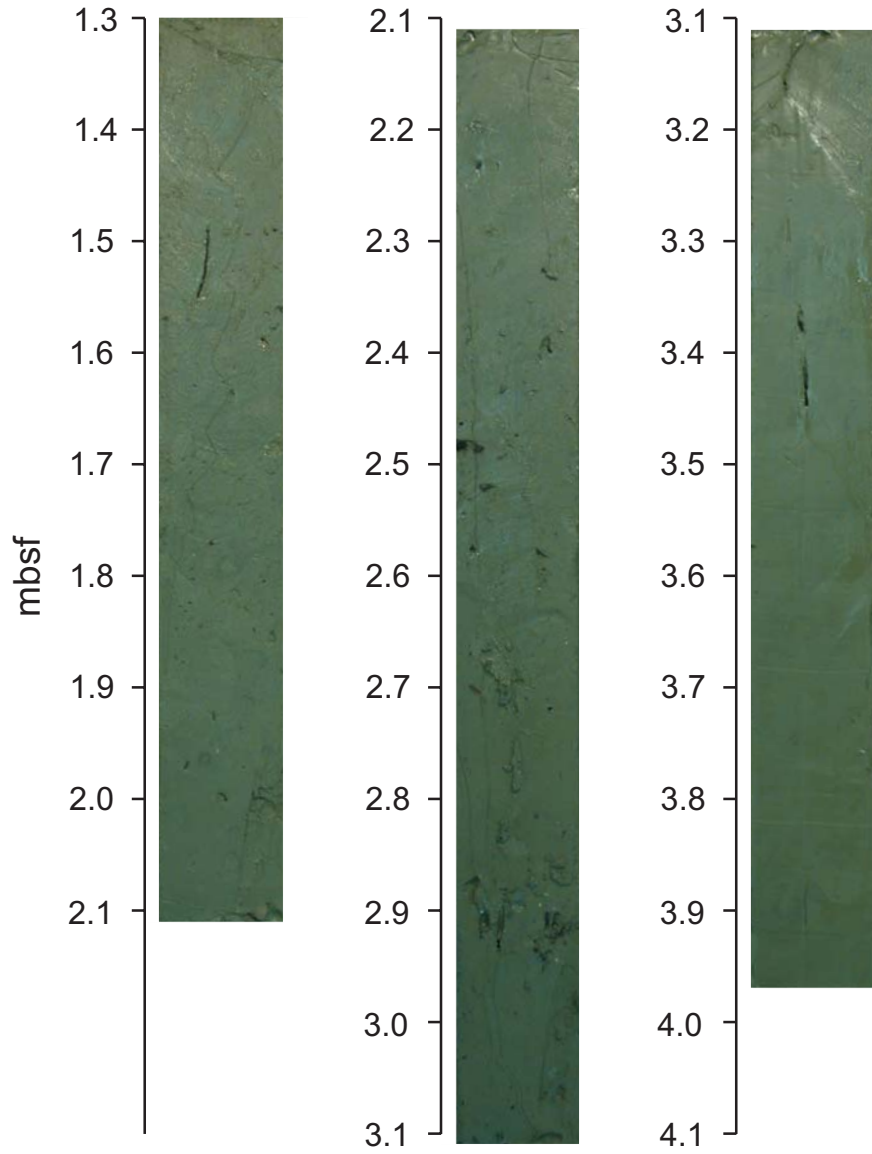
Core M 54-68 (0-5.68 m) - Southern Area



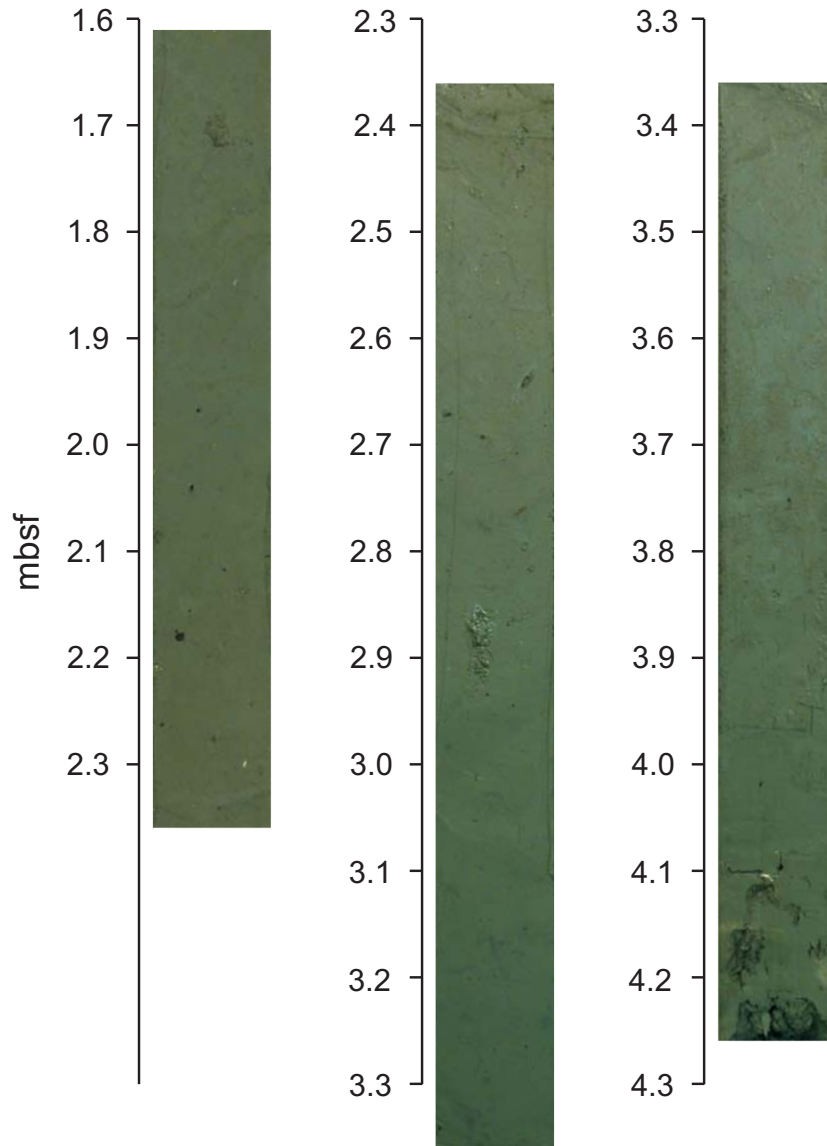
Core M 54-69/1 (0-1.11 m) - Mound Quepos, Top



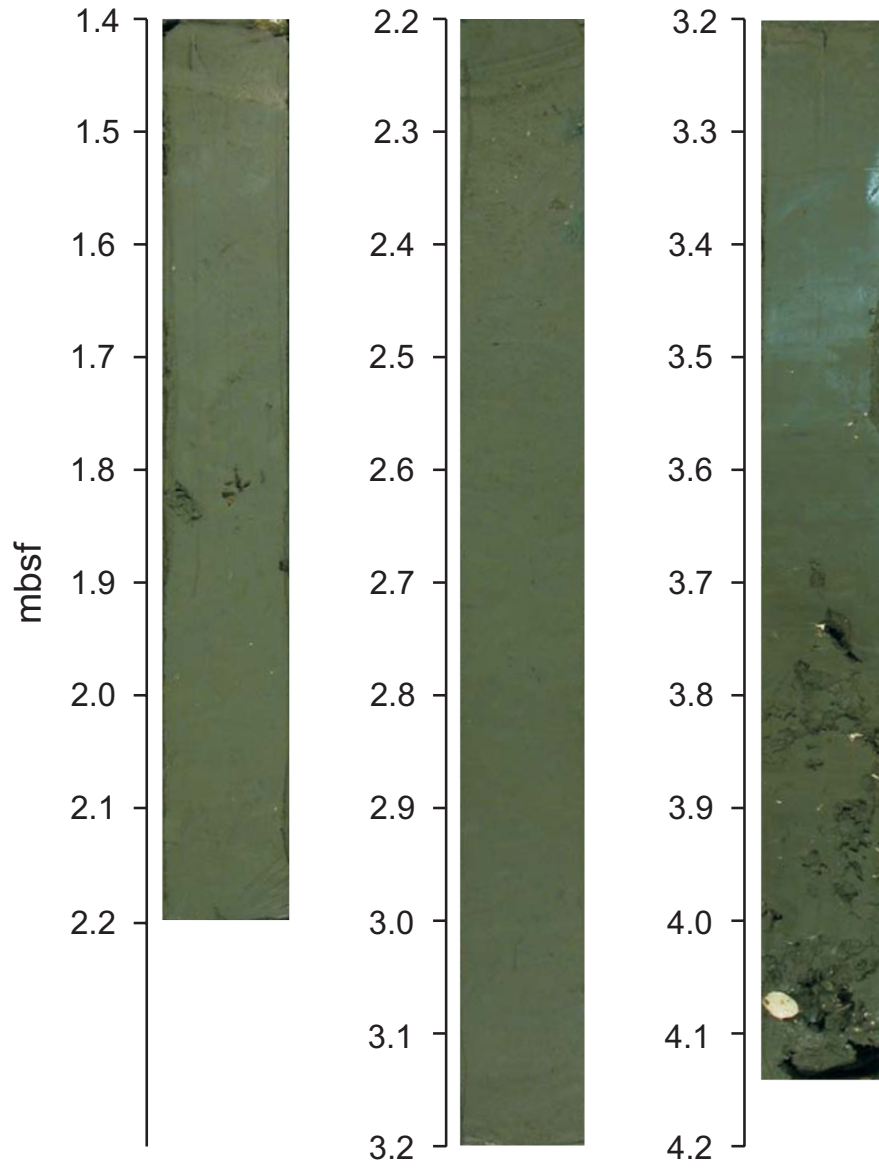
Core M 54-73/2 (1.3-3.97 m) - Mound Quepos, N Slope



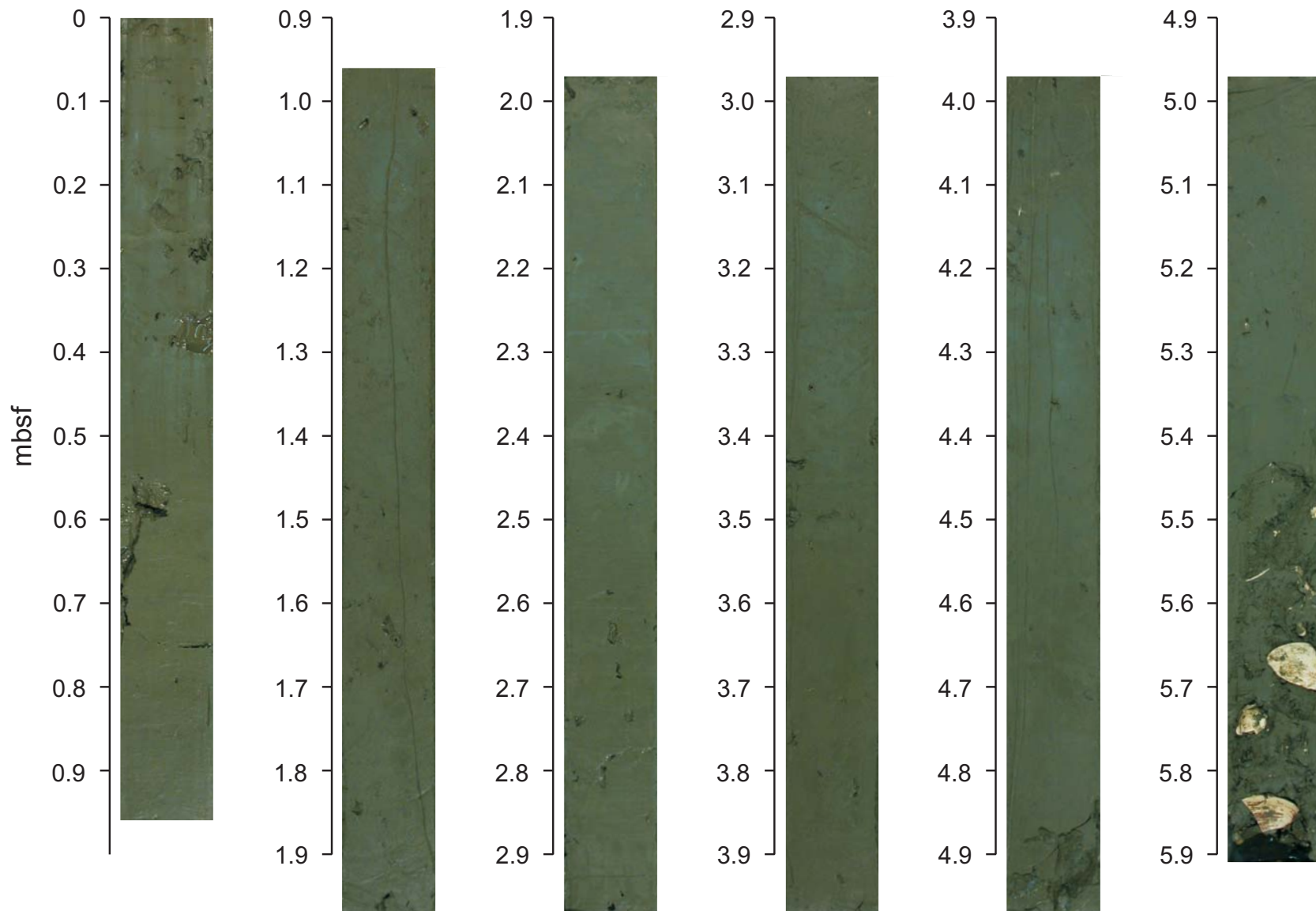
Core M 54-74 (1.61-4.26 m) - Mound Quepos, NW Slope



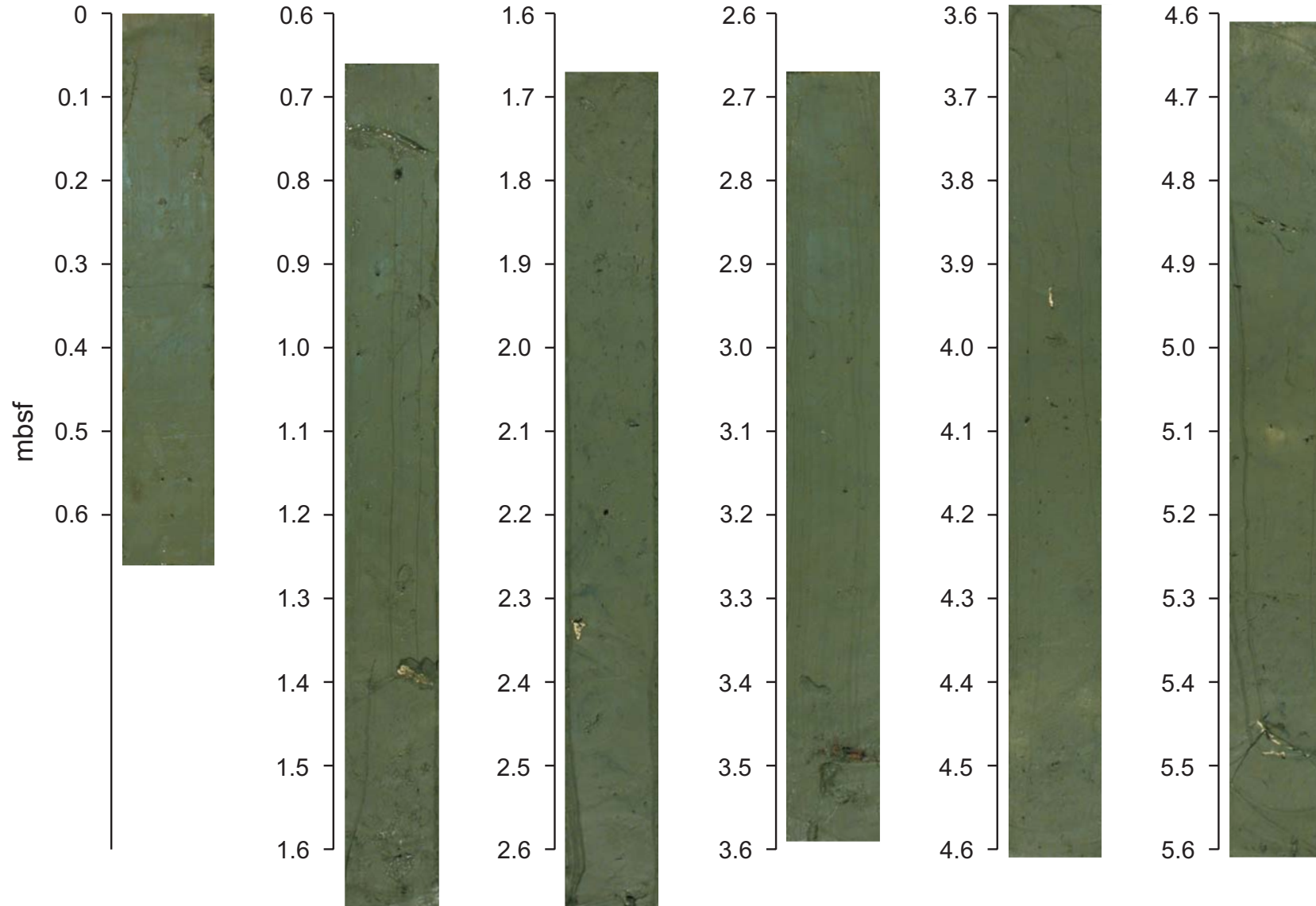
Core M 54-75 (1.4-4.14 m) - Mound Quepos, Top



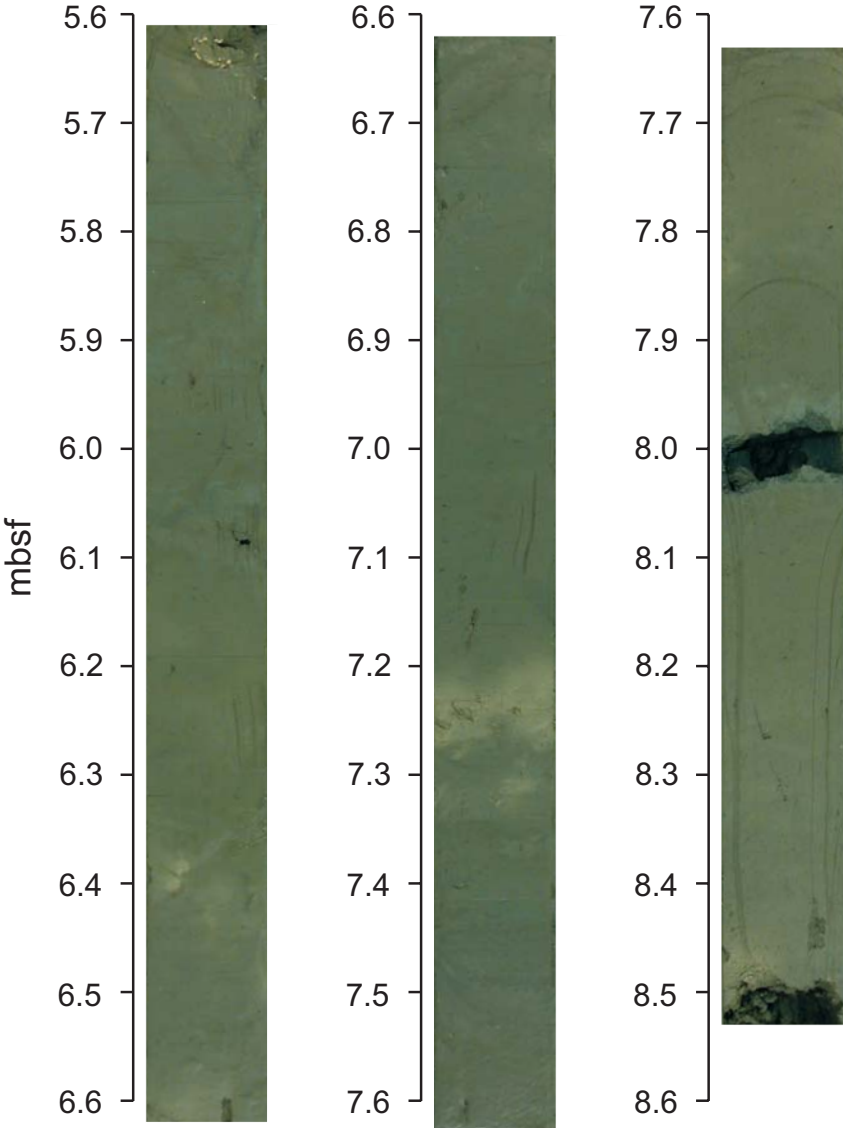
Core M 54-78 (0-5.91 m) - Mound Quepos, N Slope



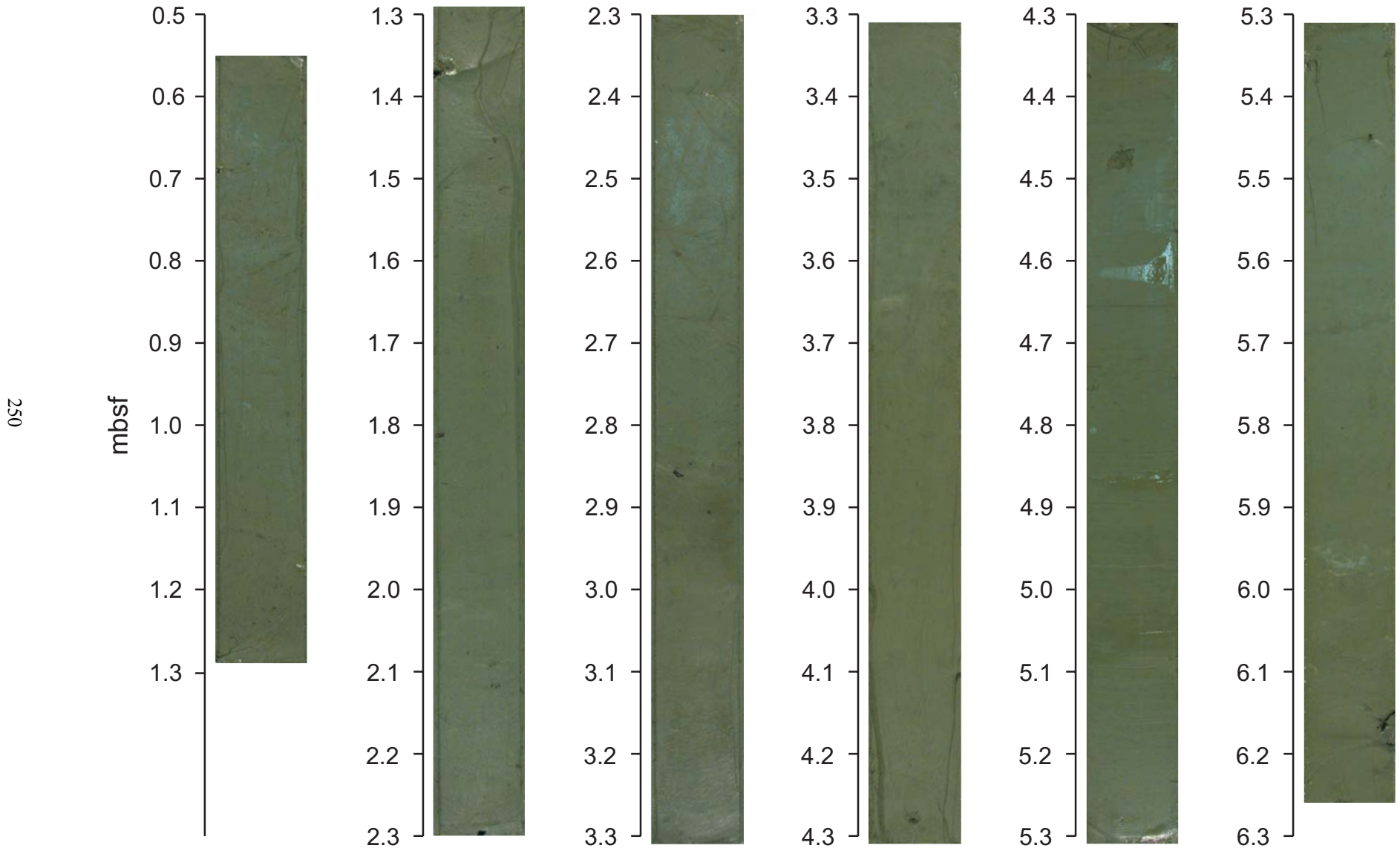
Core M 54-80a (0-5.8 m) - Mound Quepos, N Slope



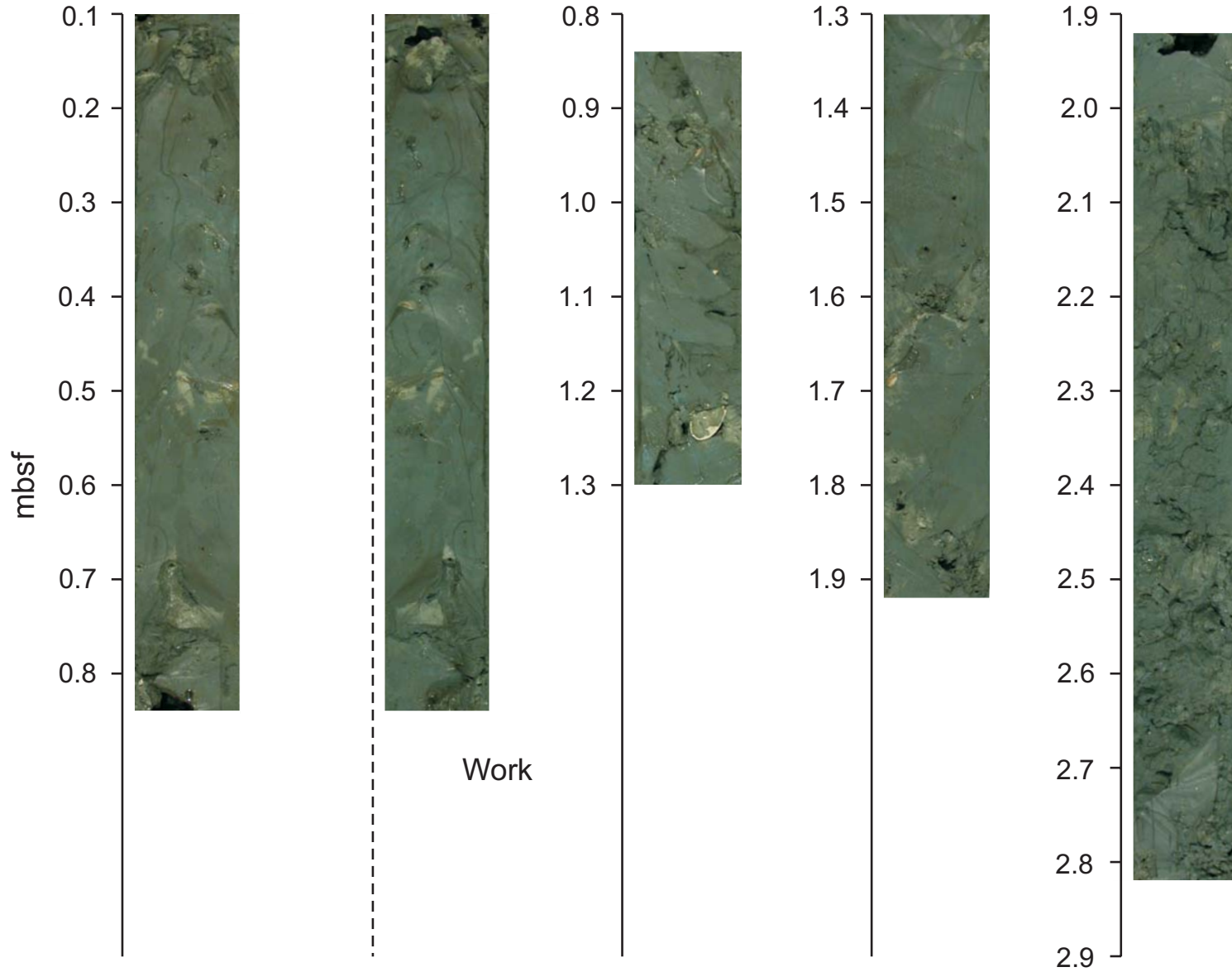
Core M 54-80b (0-5.8 m) - Mound Quepos, N Slope



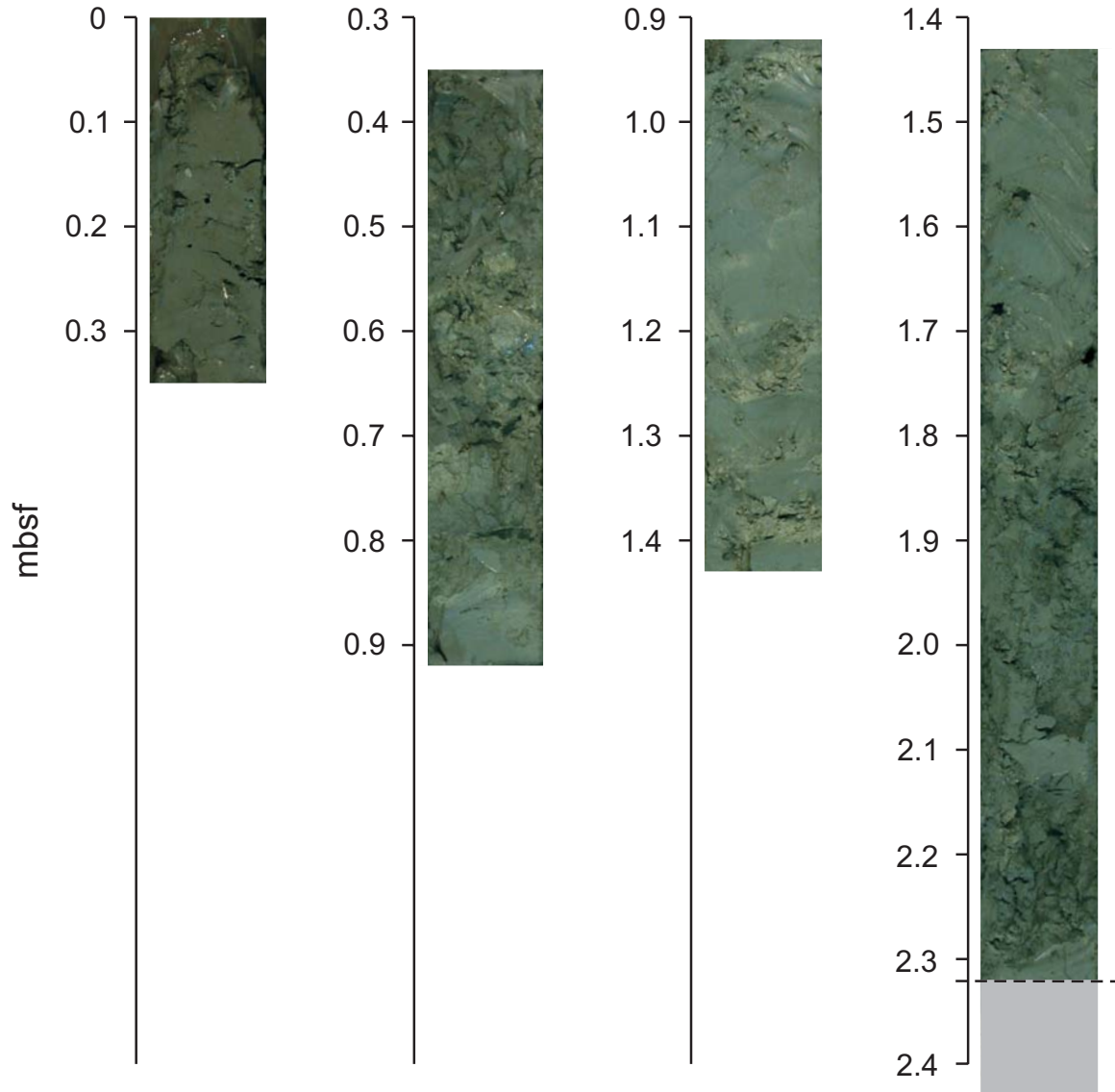
Core M 54-81/1 (0.55-6.26 m) - Jaco Scarp, E Slope



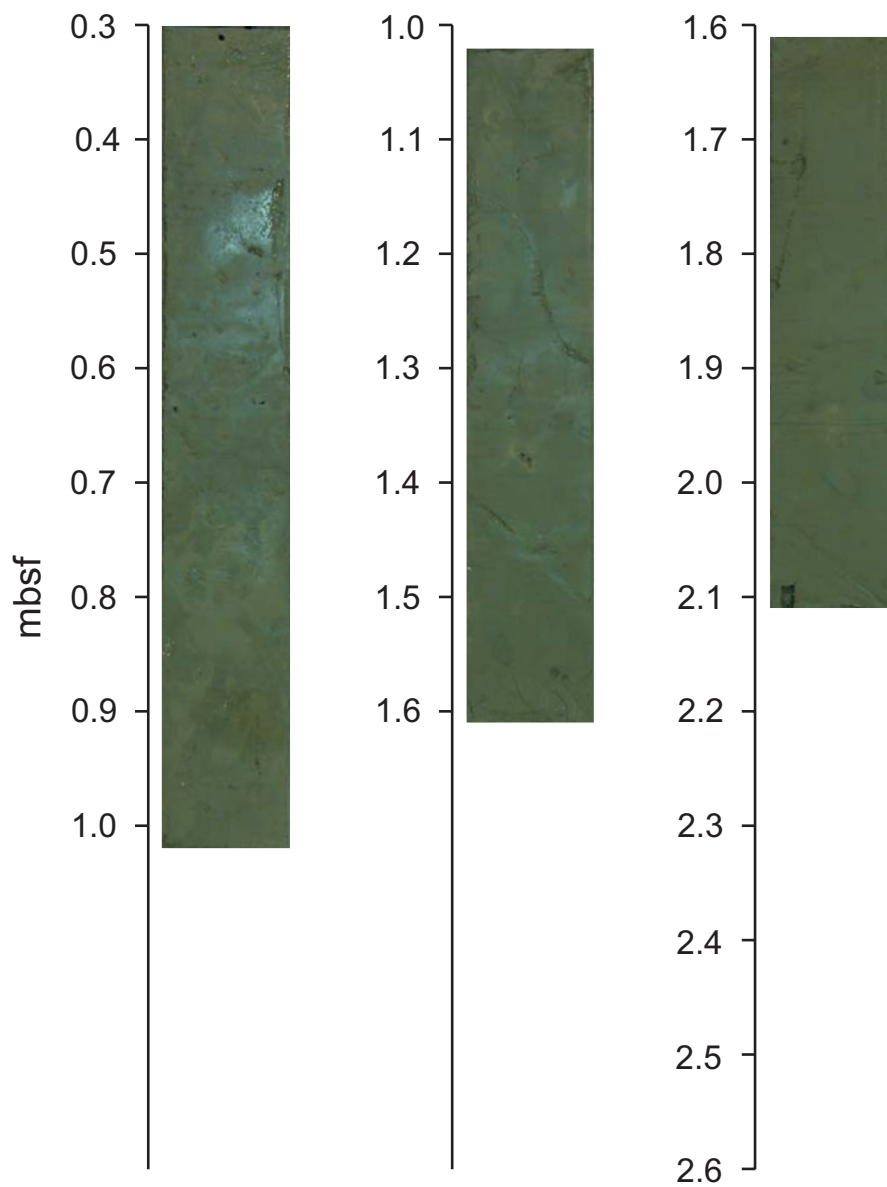
Core M 54-84 (0.1-2.82 m) - Mound 12, S Slope



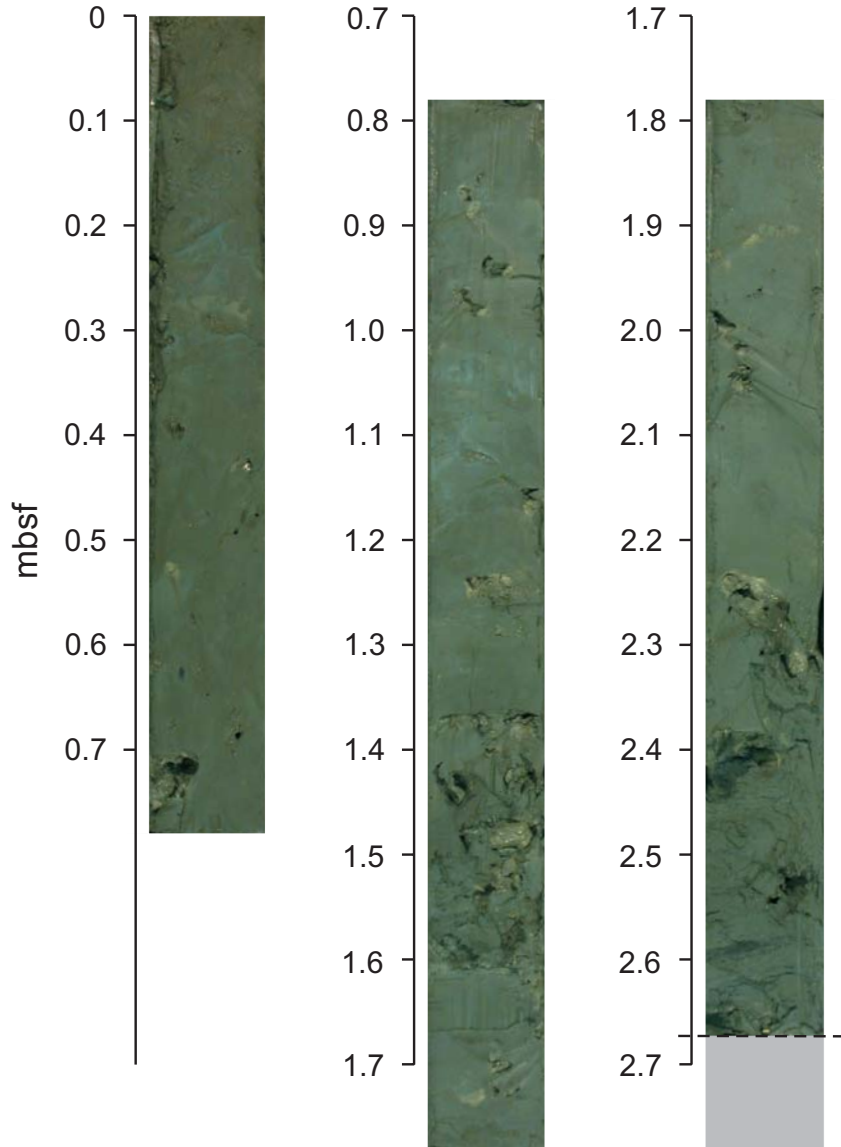
Core M 54-89 (0-2.43 m) - Mound 12, NW Slope



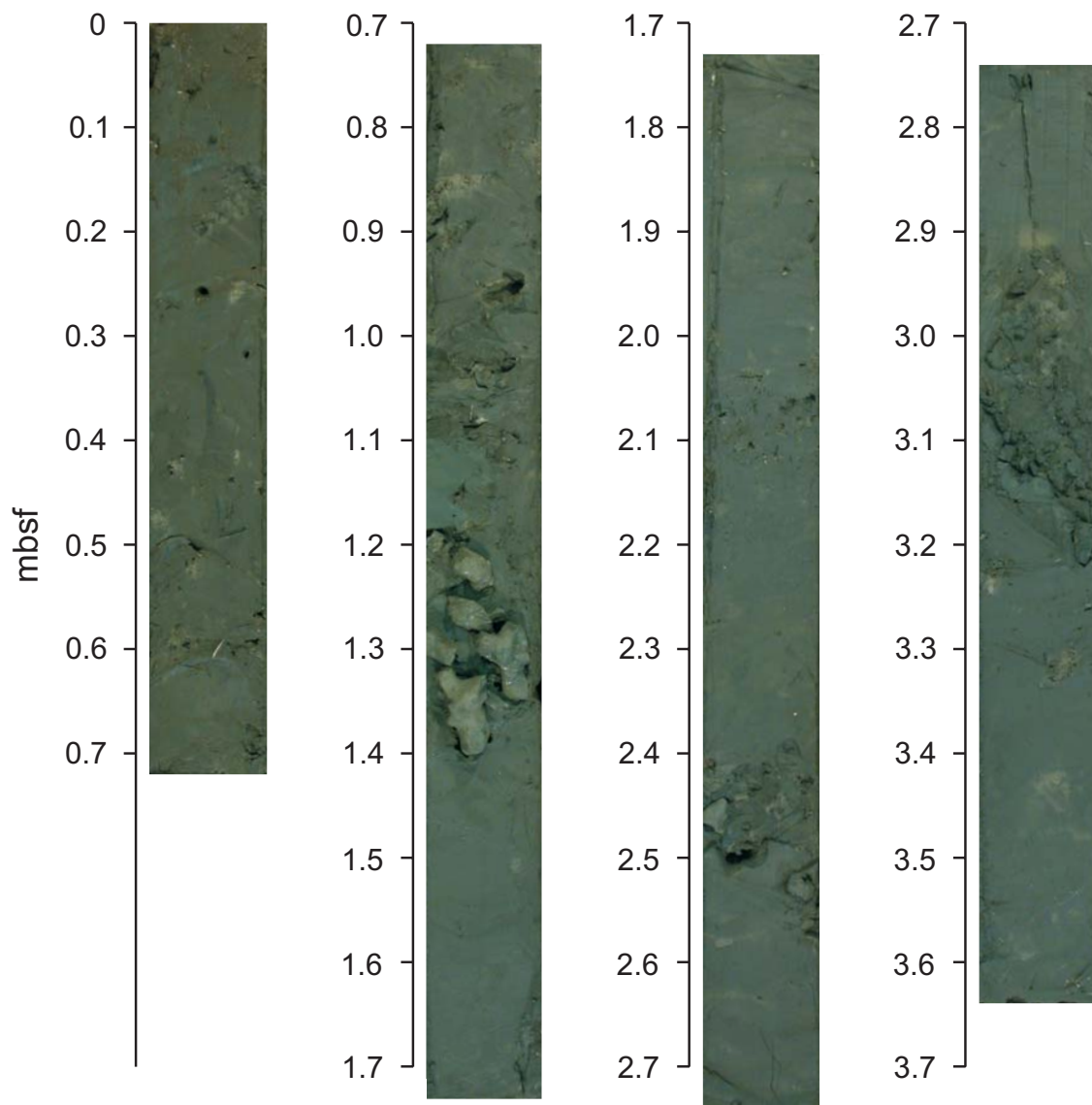
Core M 54-90 (0.3-2.11 m) - Mound 12, E Base



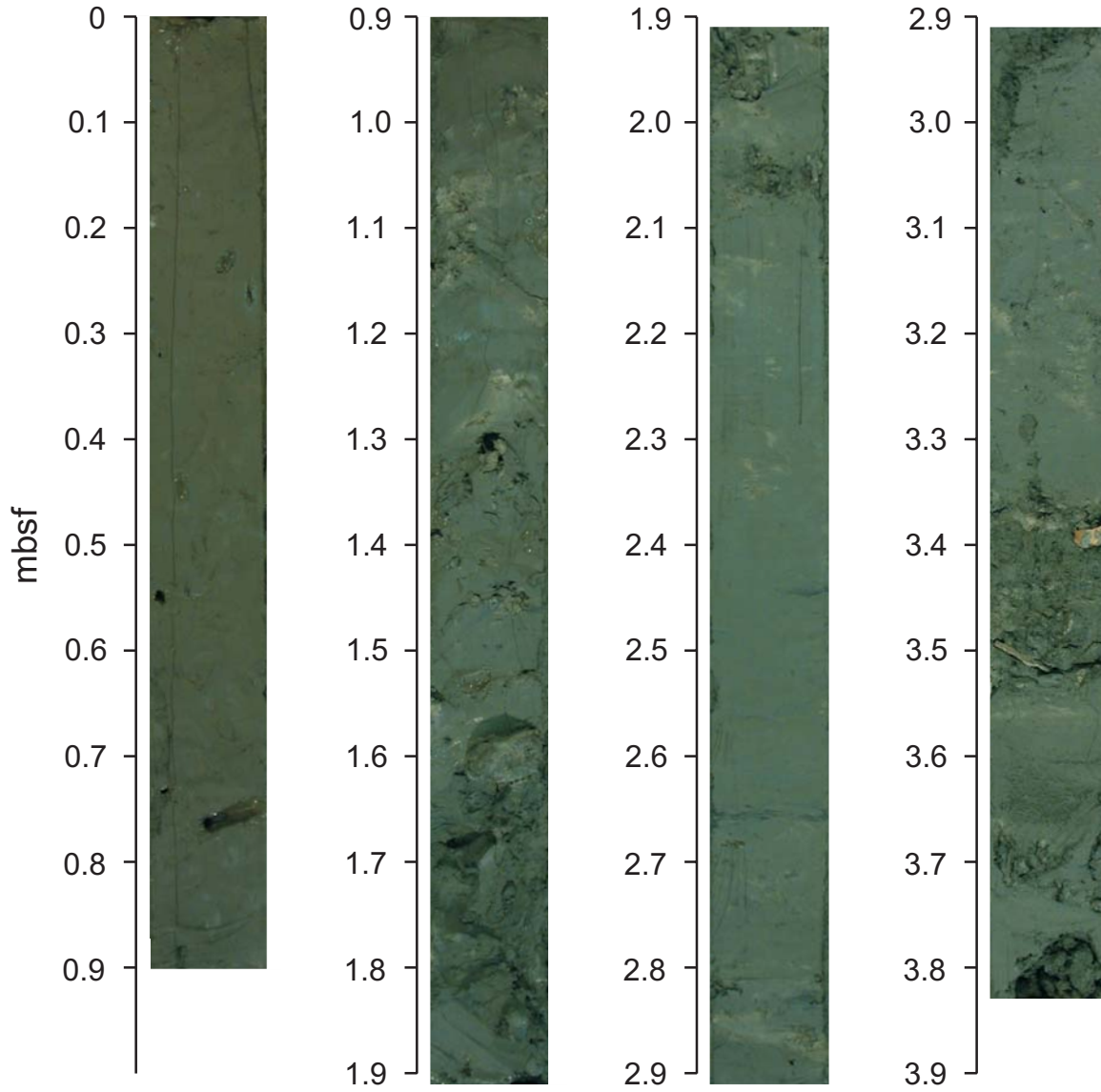
Core M 54-92 (0-2.78 m) - Mound 12, NW Base



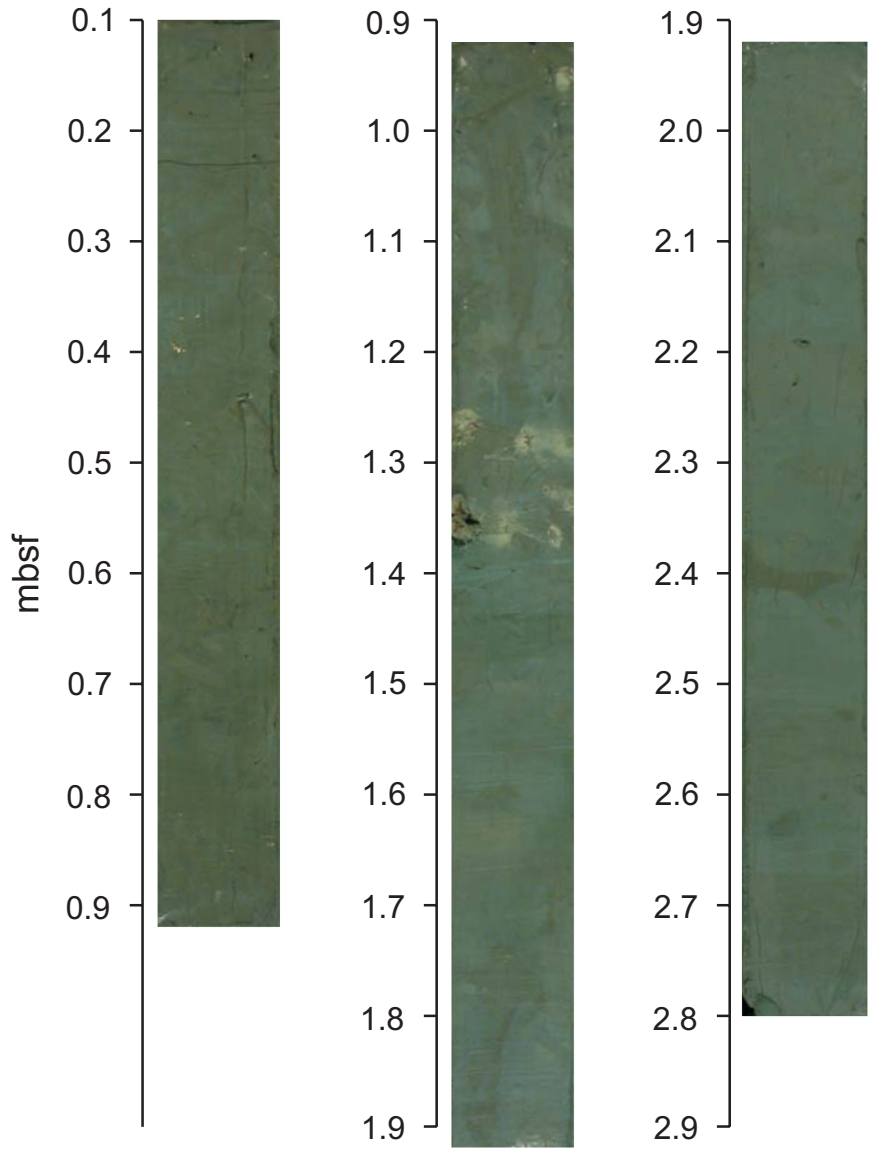
Core M 54-94 (0-3.64 m) - Mound 12, S Slope



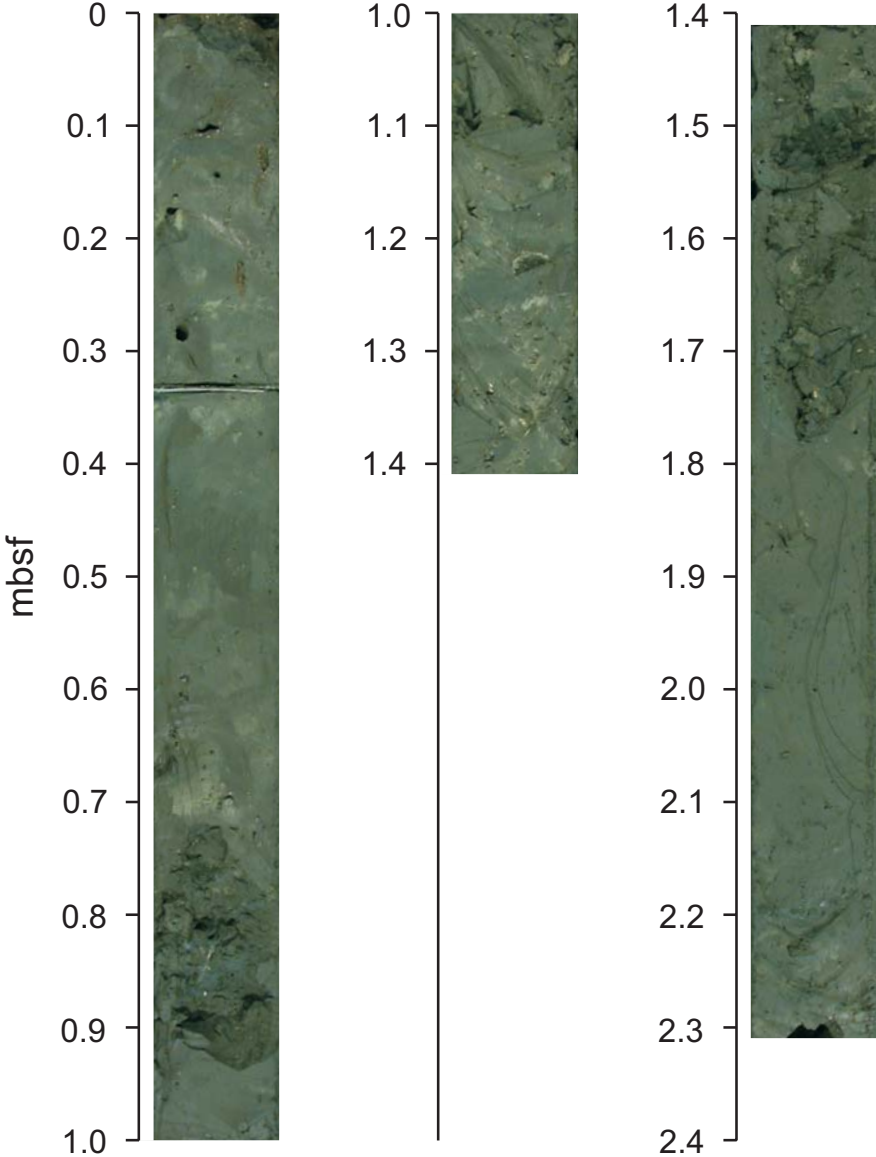
Core M 54-97/2 (0-3.83 m) - Mound 12, NW Slope



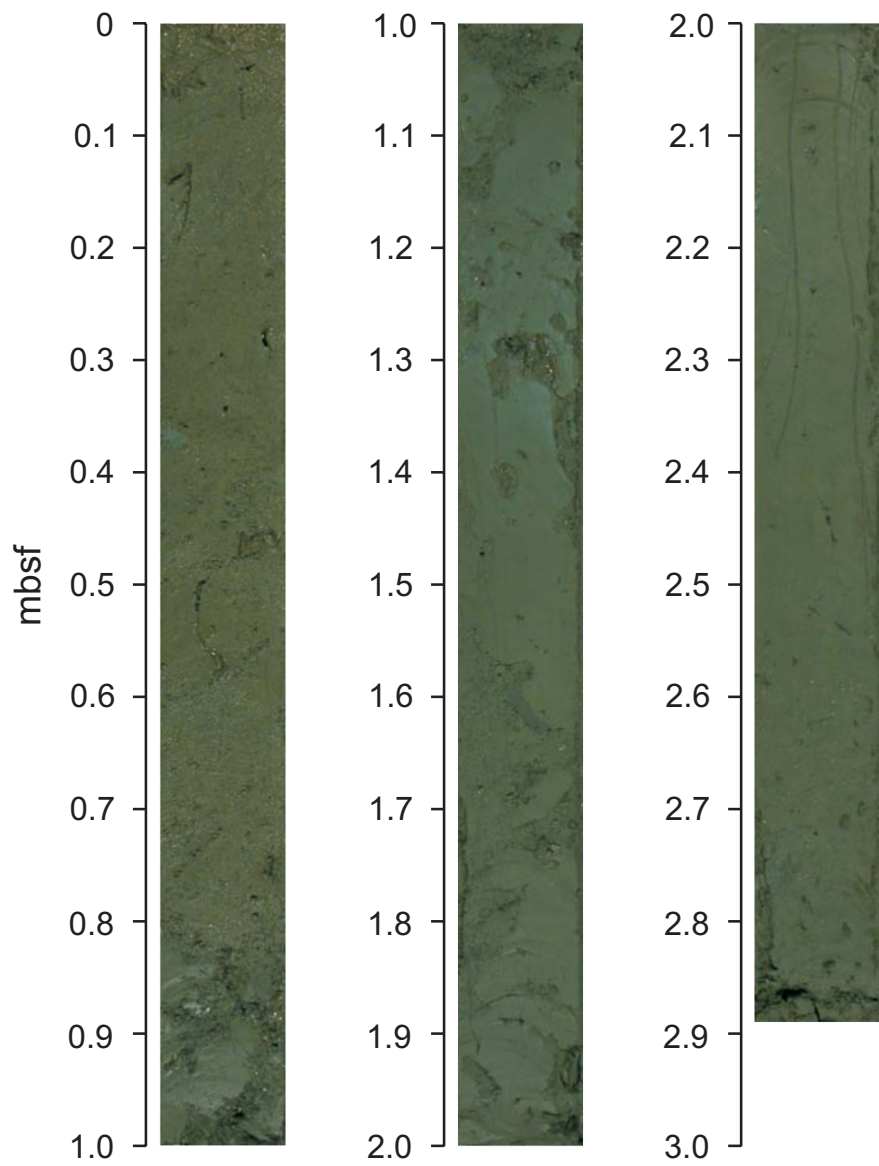
Core M 54-100 (0.1-2.80 m) - Mound 11, S Base



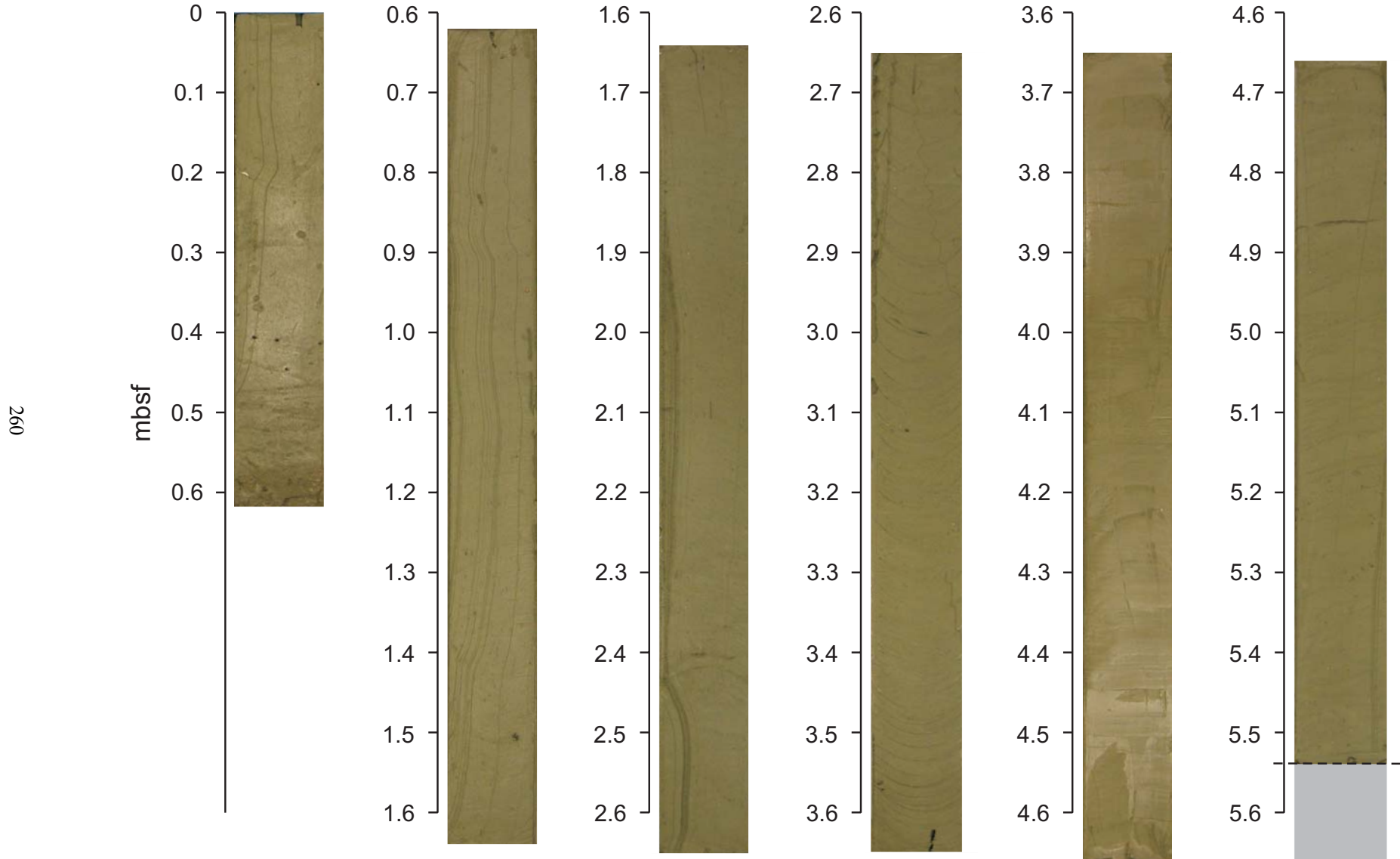
Core M 54-102 (0-2.31 m) - Mound 11, NW Slope



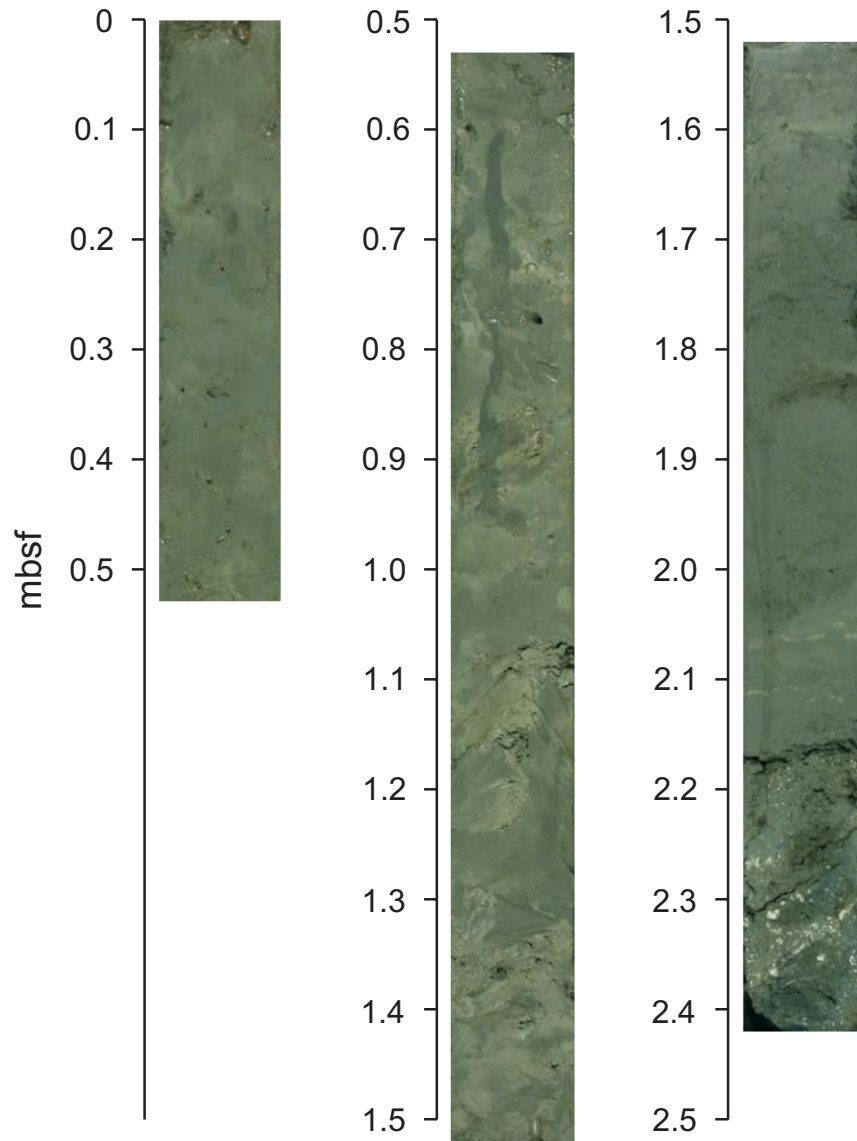
Core M 54-105 (0-2.89 m) - Mound 11, SE Slope



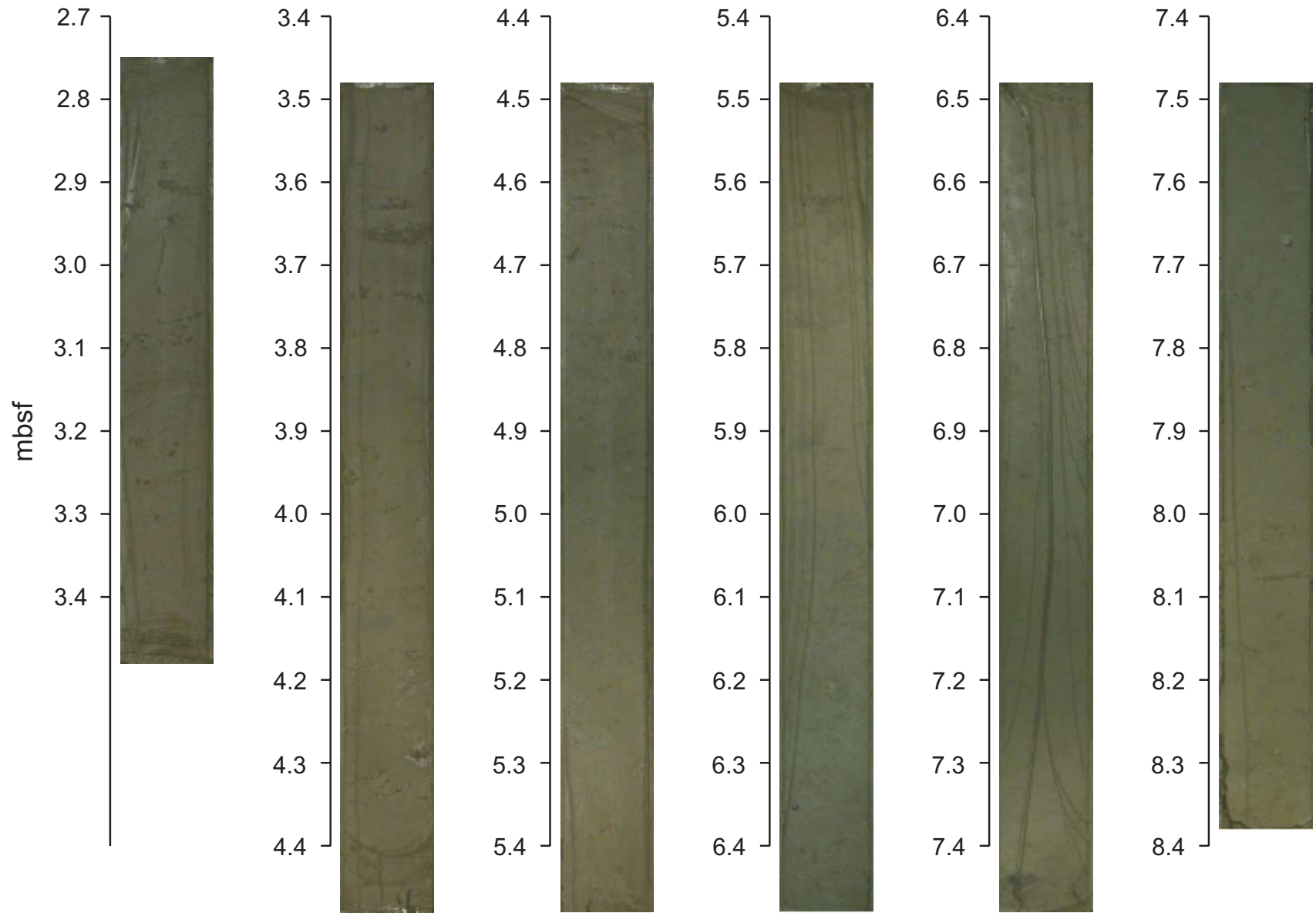
Core M 54-106 (0-5.66 m) - Mound 11, N Slope



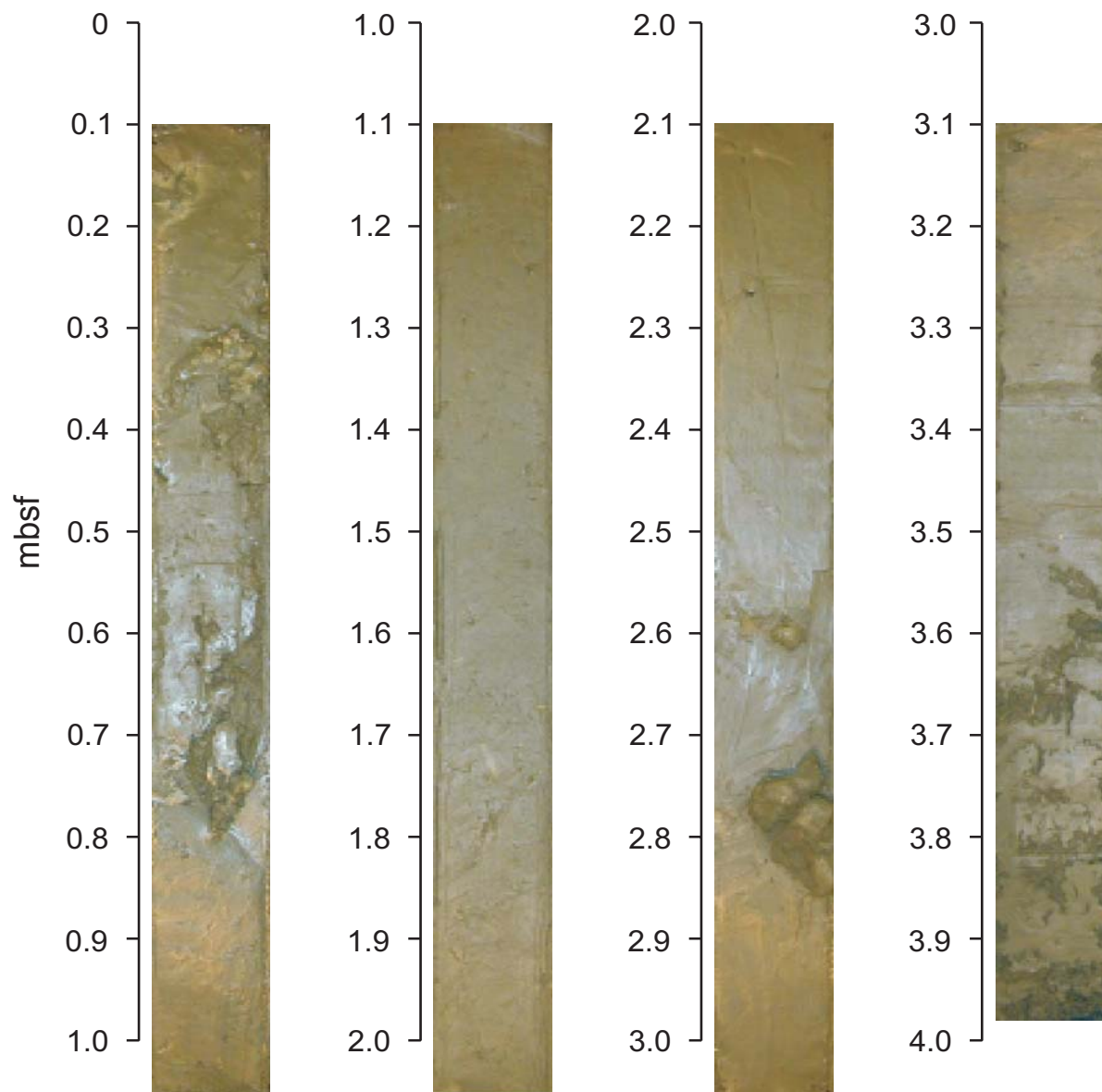
Core M 54-109 (0-2.42 m) - Mound 11, S Slope



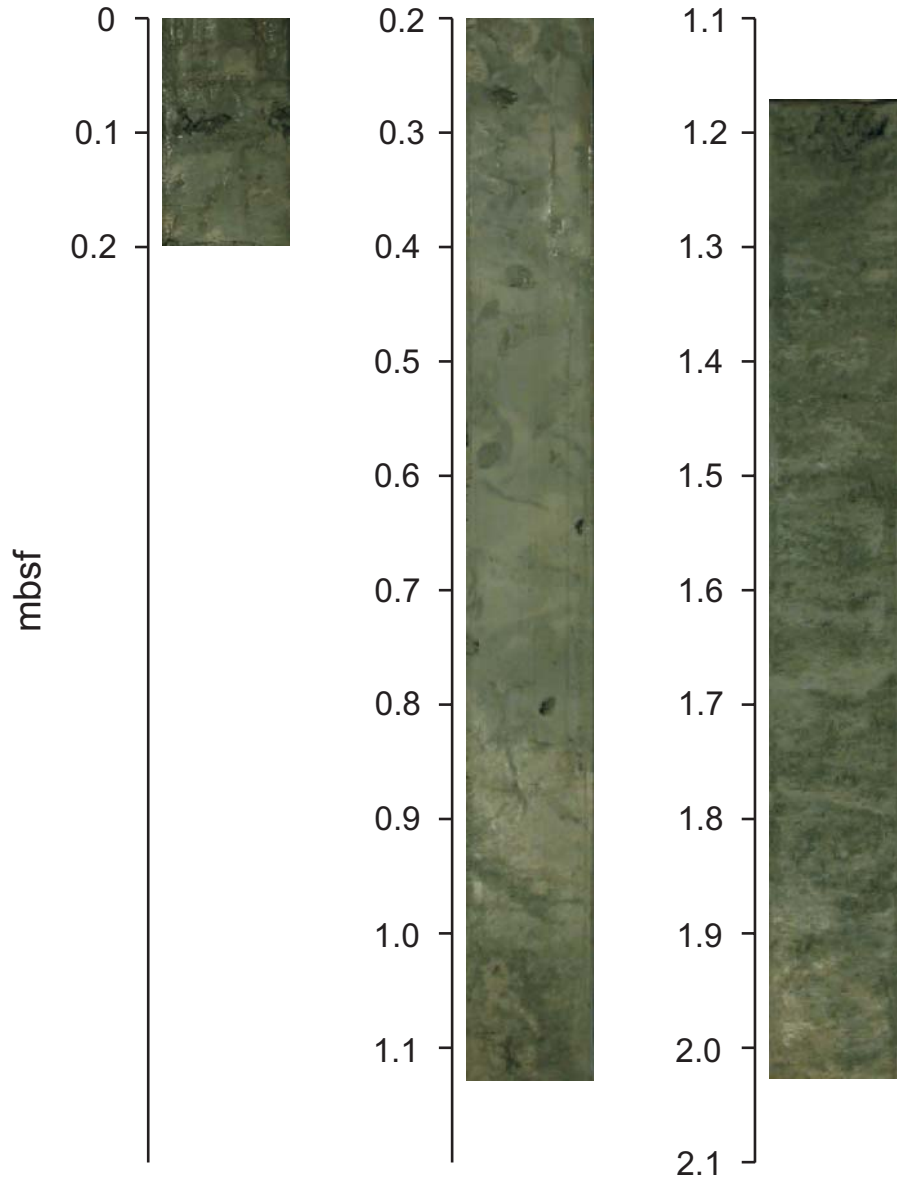
Core M 54-116 (2.75-8.38 m) - Mound Culebra, NW Slope



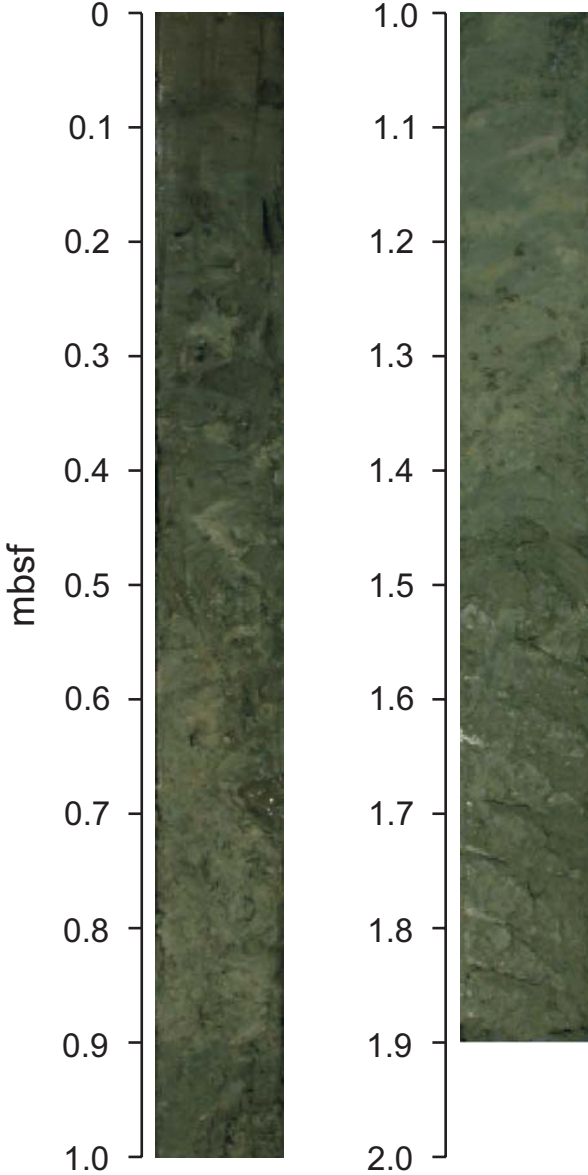
Core M 54-133 (0.1-3.98 m) - Mound 10, W Slope



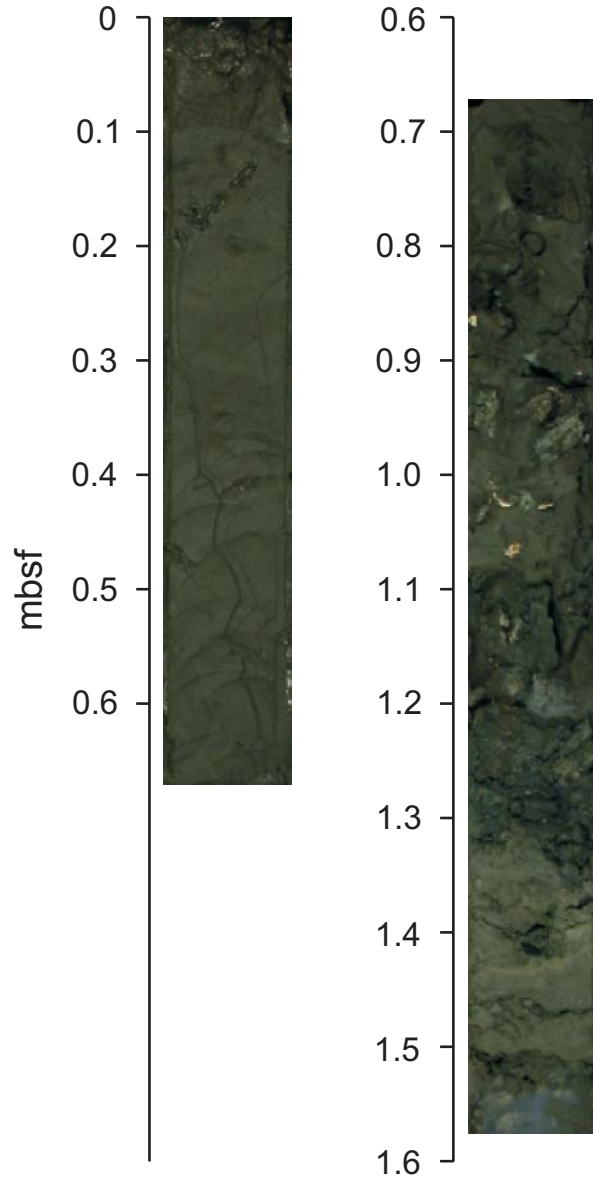
Core M 54-136/2 (0-? M) - Mound 11, S Top



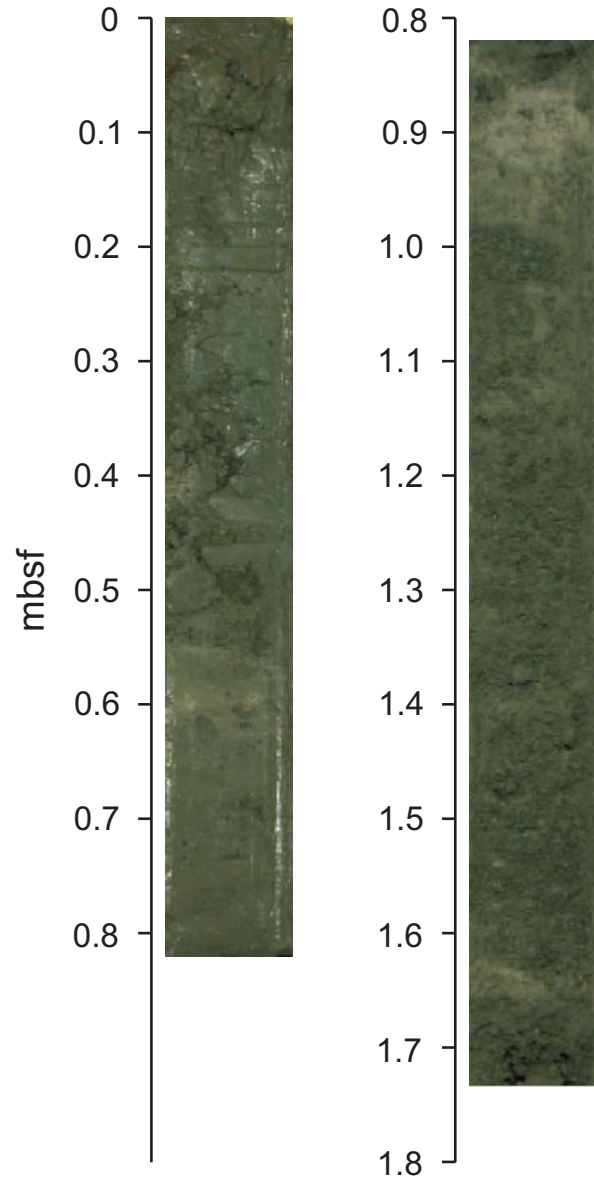
Core M 54-140 (0-1.9 m) - Mound 11, Top



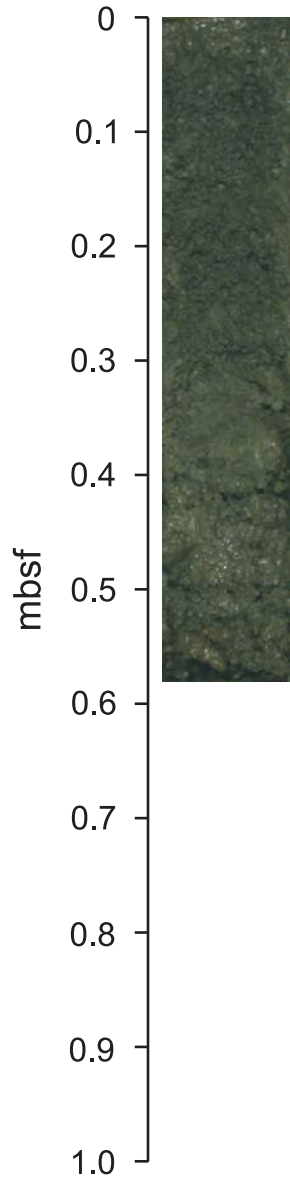
Core M 54-143 (0-1.57 m) - Mound 11, W Top



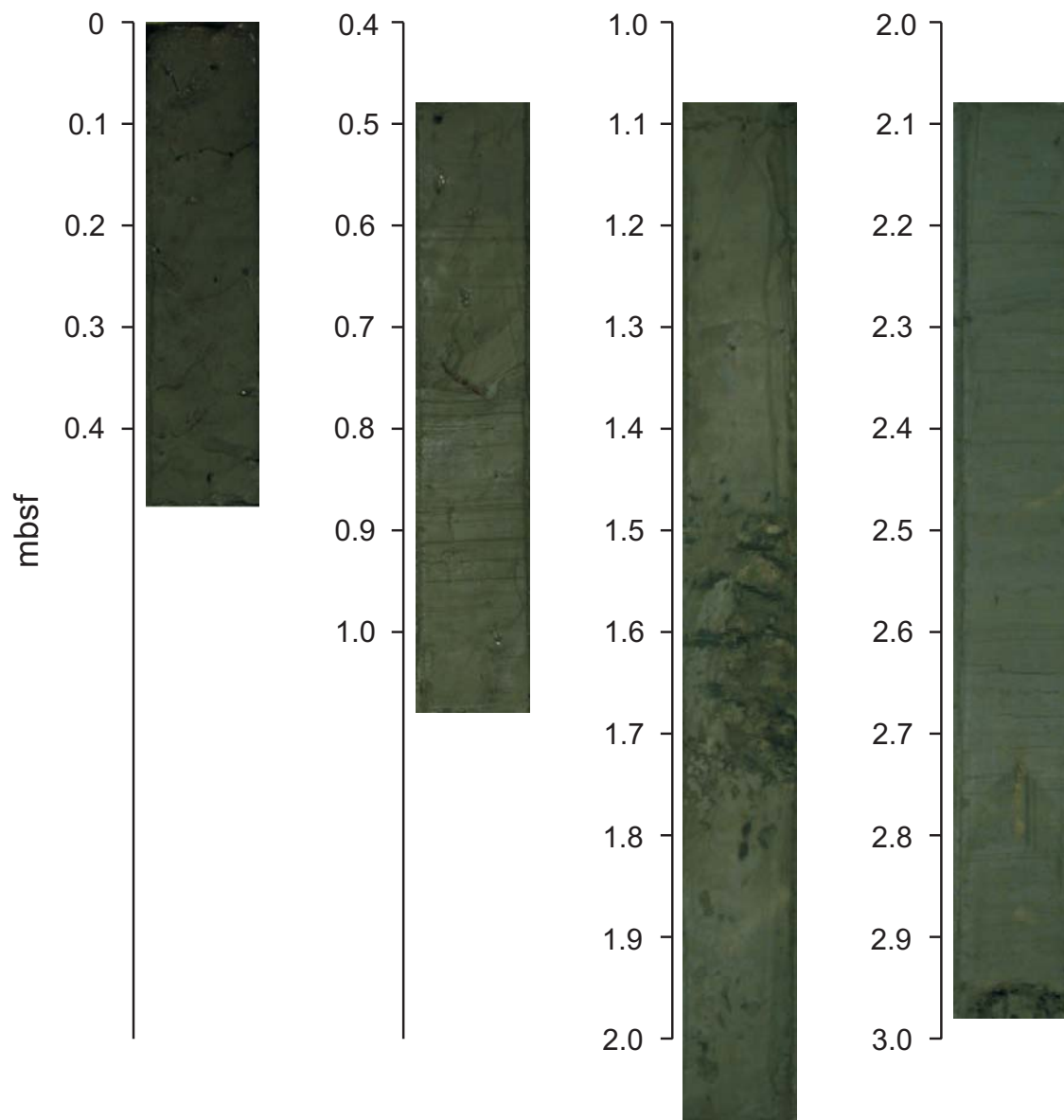
Core M 54-155 (0-1.74 m)



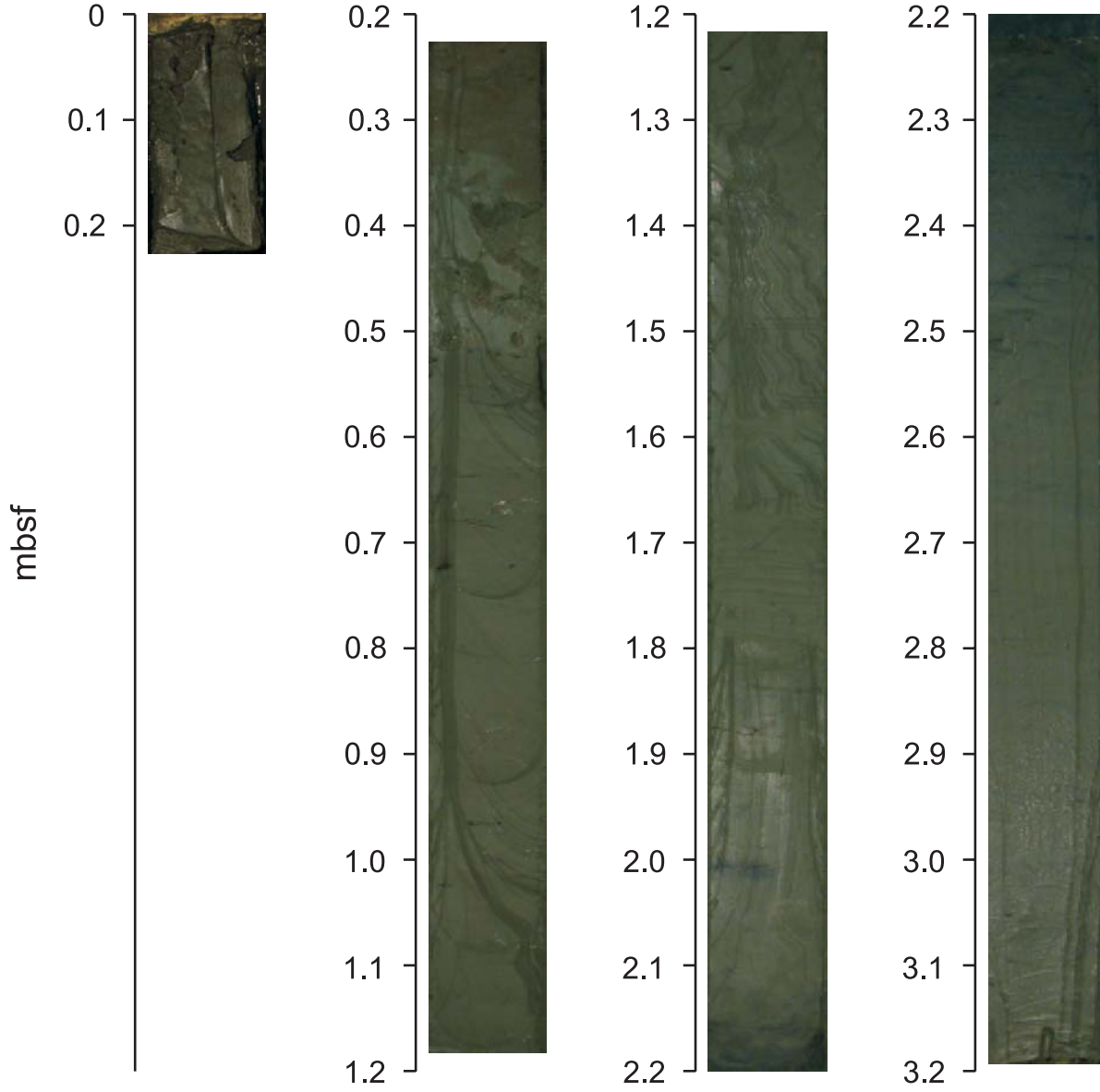
Core M 54-159 (0-0.58 m) - Jaco Scarp, Central Bulge



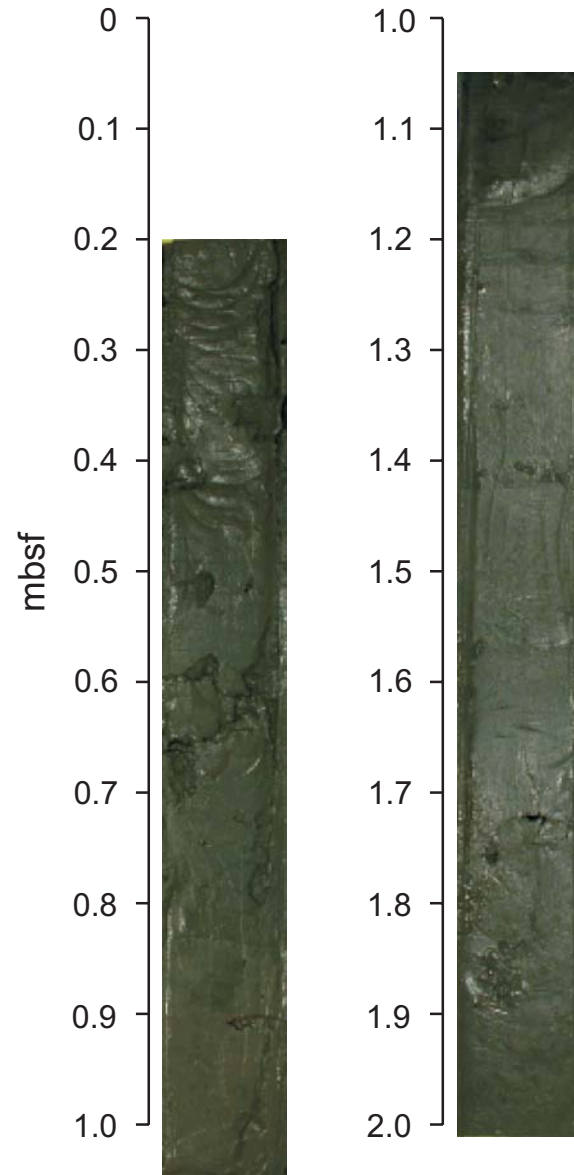
Core M 54-164 (0-2.98 m) - Mound 12, NW Slope



Core M 54-171 (0-? M) - BGR Slide



Core M 54-179 (0-2.01 m)



Appendix F

Core Description Plates

Legend for stratigraphic columns

Lithology

	clay		clayey silt		clayey sand		Scaly clay
	Silty clay		Silt		Silty sand		Consolidated clay
	Sandy clay		sandy silt		sand		Sequence of turbidite

Structures

S	bioturbated (<30% of sediment)
SS	bioturbated (<30-60% of sediment)
SSS	bioturbated (>60% of sediment)
Δ	turbidite
?Δ	possible turbidite

—	erosiv contact
WW	wavy bedding

Various accessories

	White ash layer
	Black ash layer
	Carbonate layer
	Lenses/channels

Fossils

	shells
	shell fragments

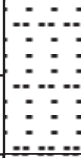
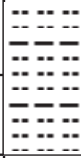
Lithology

ME54-1

m	Lithol.	Struct.	Color	Description
0		S	olive gray 5Y3/2	0-50cm: muddy sediment
		SSS		
		⊕	Grayish olive 10Y4/2	50-300cm: shell fragments, bioturbated
1		SSS		
		⊕	5GY3/2	111-114/134-139/145-163cm: sandy silt lenses
		SSS		
		⊕		
		SSS		185-200cm: claye silt inflow
2		⊕		
		SSS		
		⊕		
		SSS		
3		⊕		300-400cm: mussell shells (~4cm) bioturbated
		SSS		
		⊕		
4				

Lithology

ME54-1

m	Lithol.	Struct.	Color	Description
4		⊗ SSS	5GY3/2	400-500cm: mussell shell fragments bioturbated
5		⊗ SSS		500cm-end of core
6				
7				
8				

Lithology

ME54-2

m	Lithol.	Struct.	Color	Description
0			5GY3/2	20-21cm: black ash layer
				24-35cm: thin ash layers and lenses of silty sand
				44-52cm: volcanic clastics
1			olive gray 5Y3/2	120-123cm: volcanic clastics
2				208cm: foraminifera
			5GY3/2	240-242cm: white ash layer
				255cm: white ash lens
3			5Y3/2	290-298cm: white ash
				319-325cm: black ash layer
4				388cm: sand lense

Lithology

ME54-2

m	Lithol.	Struct.	Color	Description
4	[Lithology pattern: alternating horizontal lines and dashes]	[Structure: mostly empty]	5GY3/2	461-463cm: black ash layer
5				669-673cm: black ash layer
6				699cm: black ash layer
7				708-711cm: white ash layer 717-719cm: white ash layer 719-721cm: black ash layer 725-728cm. black ash layer 734cm-end of core
8	[Lithology pattern: mostly empty]	[Structure: mostly empty]	[Color: mostly empty]	


Lithology

ME54-6

m	Lithol.	Struct.	Color	Description
0				
1		—	olive gray 5Y3/2	61-65cm: black ash lens 67-94cm: thin black ash lenses 107-113cm: thin black ash lenses
2		?Δ		
3		?Δ		H ₂ S
4		?Δ	5YR2/1	
4		?Δ	5Y3/2	

Lithology

ME54-6

	Lithol.	Struct.	Color	Description
4			5Y3/2	408-436cm: rippup clasts
				436cm-end of core
5				
6				
7				
8				


Lithology

ME54-11-2

m	Lithol.	Struct.	Color	Description
0			olive gray 5Y3/2	12-20cm: black ash layer
				59-62cm: white ash layer 5Y6/1, light olive gray
1				83-96cm: white ash layer 5Y6/1
2				200-202cm: black ash layer 5YR2/1-brownish black
			5Y6/1	234-242cm: white ash layer with sandy erosive base
3			5Y3/2	262-400cm: reworked black and white ash
				340-356cm: volcanic clasts (basalts, 2-3mm)
				372-378cm: sand lens
4				

Lithology

ME54-11-2

m	Lithol.	Struct.	Color	Description
4			5Y3/2	400-446cm: reworked black ash
				446cm-end of core
5				
6				
7				
8				

Lithology

ME54-13

m	Lithol.	Struct.	Color	Description
0	[Dotted pattern]	[Horizontal lines]	olive gray 5Y3/2	0-29cm: reworked black ash
				29-34cm: white ash layer, 5Y6/1, light olive gray
	[Dotted pattern]	[Horizontal lines]	olive gray 5Y3/2	41-47cm: white ash layer, 5Y6/1
1				0-358cm: foraminifera in whole core
	[Dotted pattern]	[Horizontal lines]	olive gray 5Y3/2	210-237cm: reworked ash, wavy bedding
2				237-241cm: white ash layer with erosive base
	[Dotted pattern]	[Horizontal lines]	olive gray 5Y3/2	268-286cm: reworked white ash
3				350-356cm: black ash layer 5YR2/1-brownish black
	[Dotted pattern]	[Horizontal lines]	olive gray 5Y3/2	358cm: end of core
4				

Lithology

ME54-14

m	Lithol.	Struct.	Color	Description
0			olive gray 5Y3/2	0-80cm: reworked black ash
1				102cm: white 1cm concretions, opal-A? Zeolites?
2				136-143cm: reworked black ash
				192-272cm: reworked black ash
3				292-360cm: reworked black ash
4				360-362cm: black ash layer

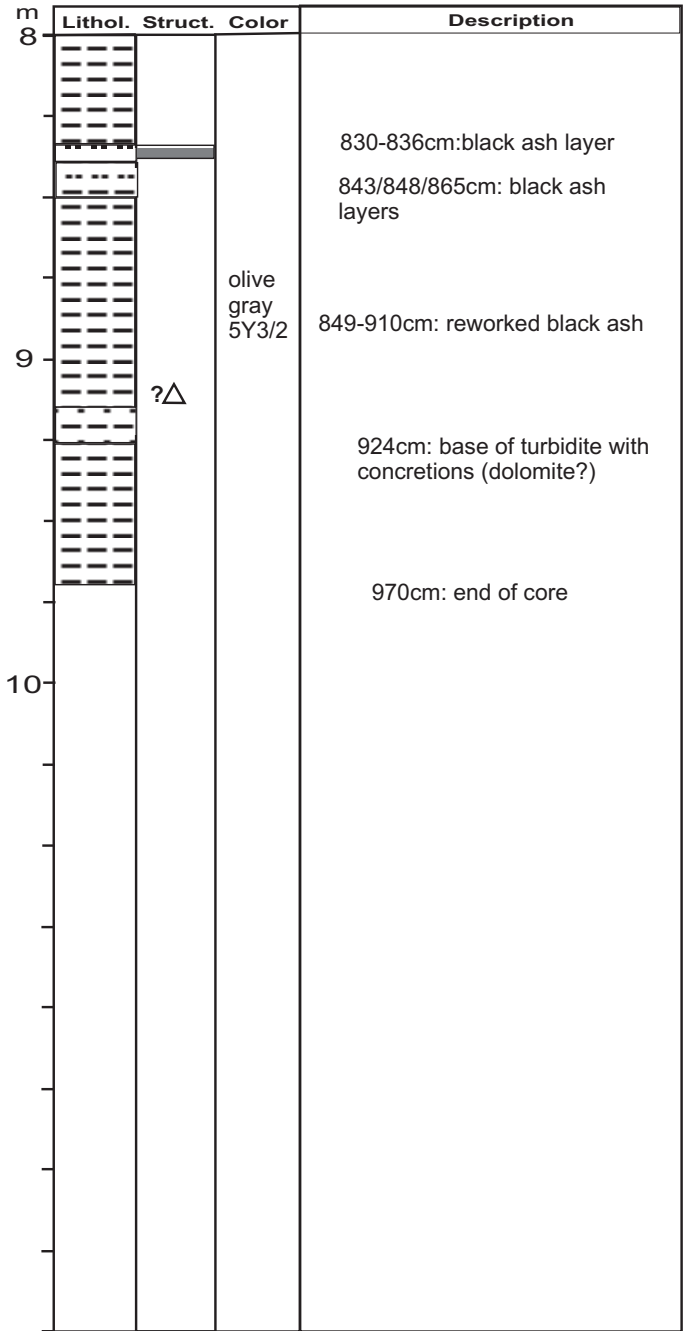
Lithology

ME54-14

m	Lithol.	Struct.	Color	Description	
4			olive gray 5Y3/2		
5					
6				?Δ	
7				?Δ	689-708cm: reworked black ash
8					757-774cm: reworked black ash



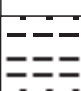
Lithology

ME54-14



Lithology

ME54-17

m	Lithol.	Struct.	Color	Description
0				0-200cm: lost
1				
2			olive gray 5Y3/2	
3				
4				376-417cm: volcanic clasts (altered basalt fragments)

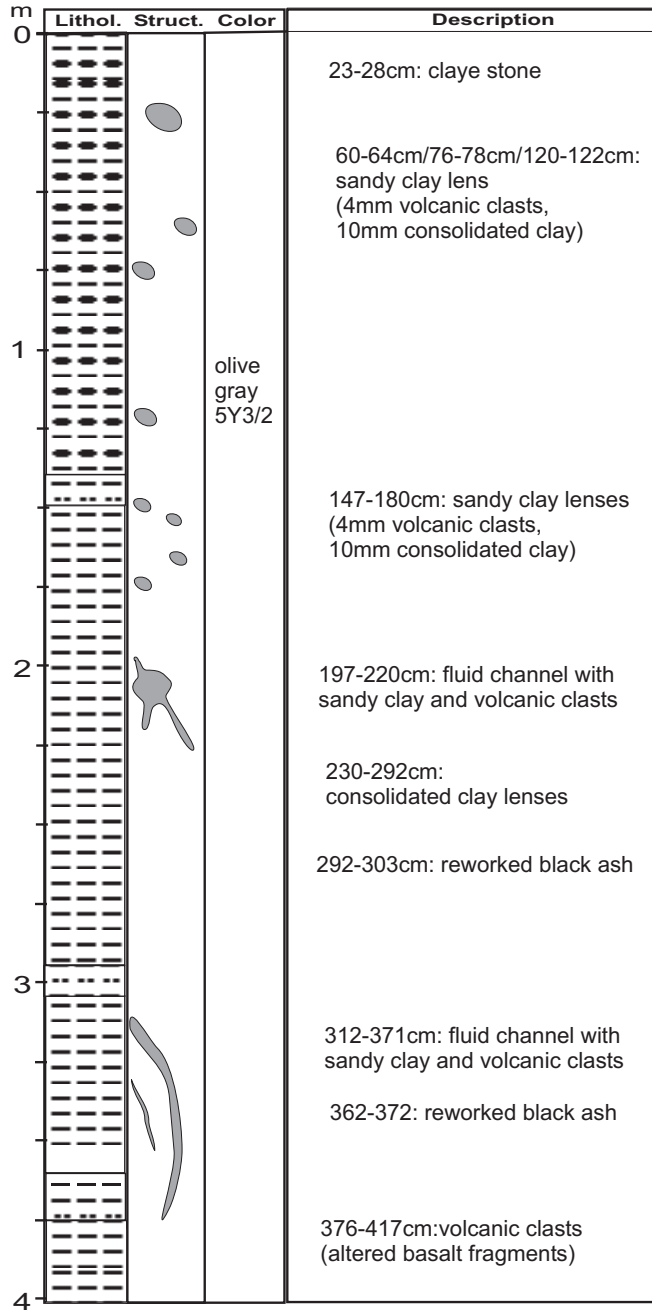
Lithology

ME54-17

m	Lithol.	Struct.	Color	Description
4	[Pattern: horizontal dashes]			
5	[Pattern: horizontal dashes]			
6	[Pattern: horizontal dashes]			577-677cm: volcanic clasts (2-5mm, altered basalts?)
7	[Pattern: horizontal dashes]			677cm: sand lens with erosive base (glass, altered basalts)
7	[Pattern: horizontal dashes]			682-677cm: reworked black ash
7	[Pattern: horizontal dashes]			706-770cm: altered volcanic clasts (serpentinites, zeolites, chloritoites)
8	[Pattern: horizontal dashes]			770cm: end of core Core catcher: scaly clay

Lithology

ME54-18



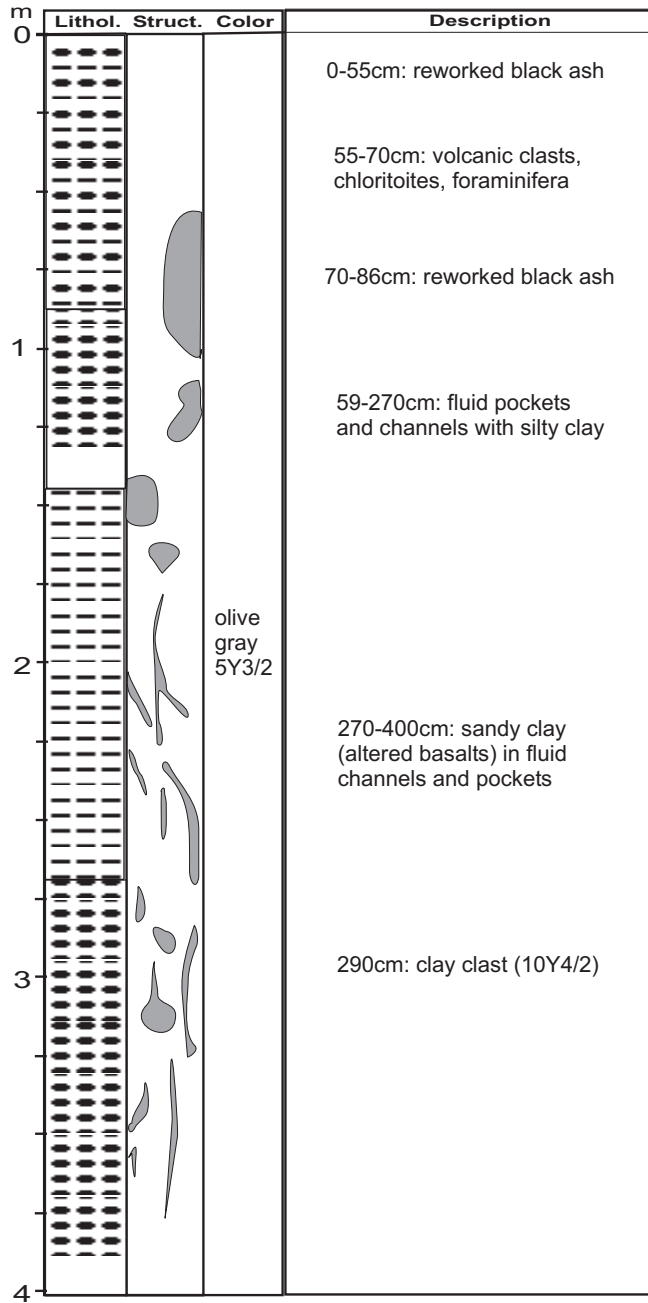
Lithology

ME54-18

m	Lithol.	Struct.	Color	Description
4				
				422-436cm: reworked black ash
5				
				540cm: end of core
6				
7				
8				


Lithology

ME54-21



Lithology

ME54-21

m	Lithol.	Struct.	Color	Description
4			5Y3/2	<p>400-470cm: sandy clay and altered basalts in fluid channels</p> <p>470cm: end of core</p>
5				
6				
7				
8				


Lithology

ME54-22

m	Lithol.	Struct.	Color	Description
0				
1			olive gray 5Y3/2	
2				330-335cm: consolidated clay (5GY5/2)
3				380-390cm: carbonate clasts (1-3mm)
4				

Lithology

ME54-22

m	Lithol.	Struct.	Color	Description
4			5Y3/2	<p>400-464cm: consolidated clay with scaly clay</p> <p>465cm: end of core</p>
5				
6				
7				
8				

Lithology

ME54-23

m	Lithol.	Struct.	Color	Description
0			olive gray 5Y3/2	0-30cm: carbonate clasts (1-3mm)
1				100-130cm: carbonate clasts (1-3mm)
2				170-175cm: carbonate stone
240cm: end of core				
3				
4				

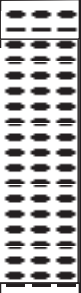
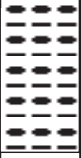

Lithology

ME54-24

m	Lithol.	Struct.	Color	Description
0			olive gray 5Y3/2	0-120cm: altered volcanic clasts (10mm)
1				
2				
3				
4				

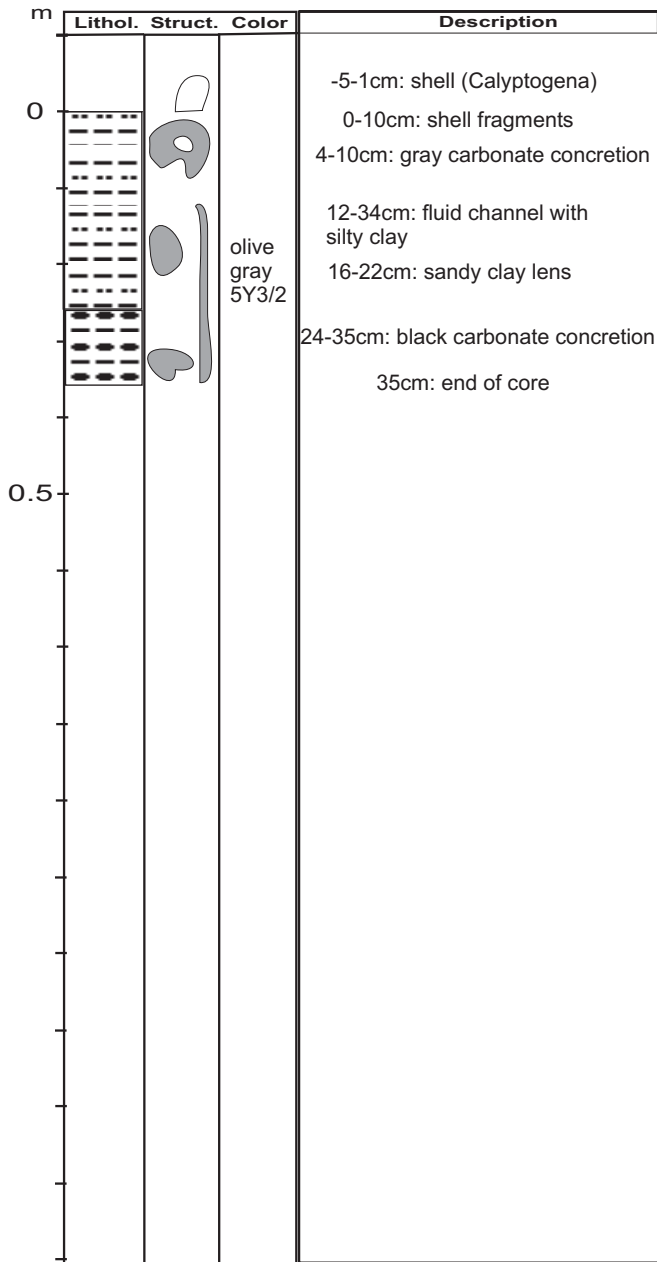
Lithology

ME54-24

m	Lithol.	Struct.	Color	Description
4			5Y3/2	
				
5				540cm: end of core
8				

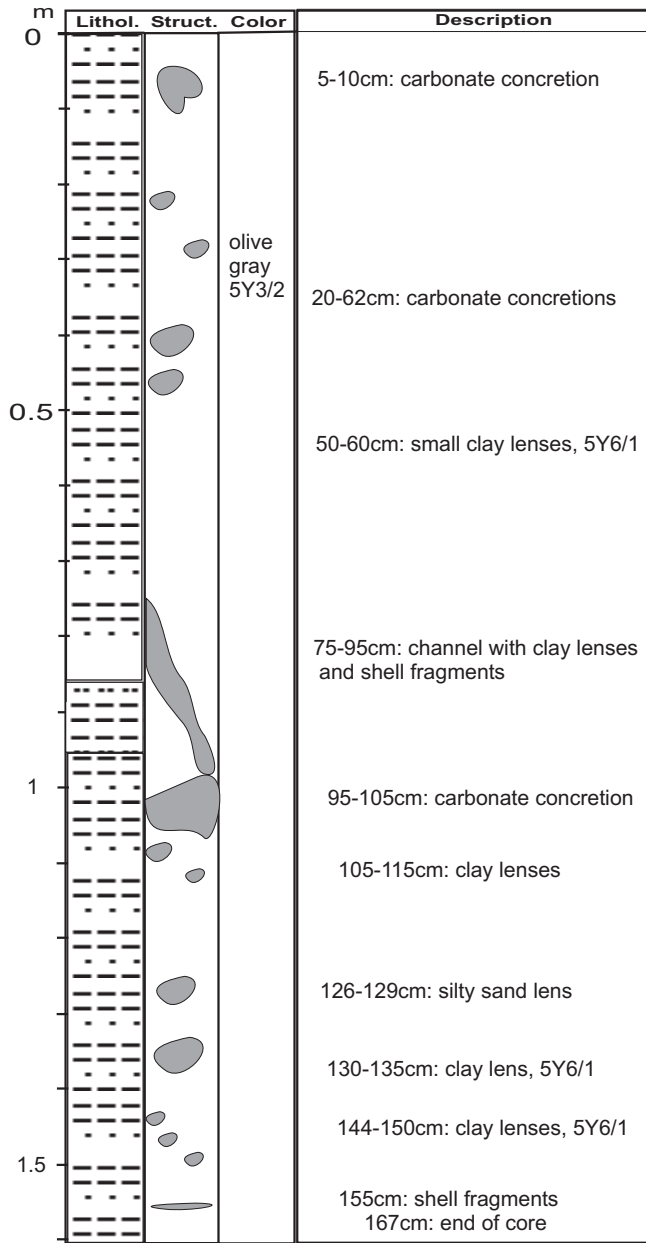
Lithology

ME54-27



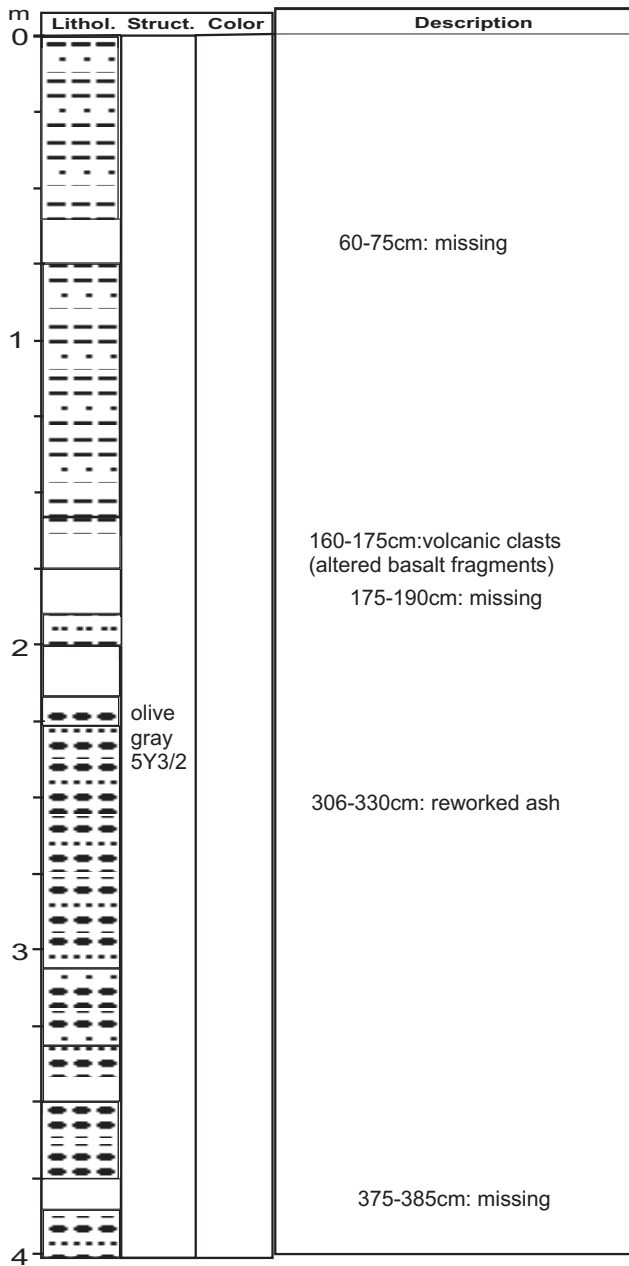
Lithology

ME54-29



Lithology

ME54-32



Lithology

ME54-32

m	Lithol.	Struct.	Color	Description
4				425-430cm: silty clay lens
5				570cm: end of core
6				
7				
8				

Lithology

ME54-35

m	Lithol.	Struct.	Color	Description
0		△	olive gray 5Y3/2	
		△		
		△		
		△		
1		△		
		△		
		△		
		△		
		△		
		△		
		△		
		△		
		△		
		△		
2		△		
		△		187-400cm: thin reworked ash layers
		△		
		△		
		△		
		△		
		△		
		△		
3		△		
		△		
		△		
		△		
		△		
		△		
		△		
		△		
		△		
4		△		

Lithology

ME54-35

m	Lithol.	Struct.	Color	Description
4		△		
5		△		
6		△		610-680cm: reworked ash layers
7				693cm: erosive ash lens
8				760cm: end of core

Lithology

ME54-36

m	Lithol.	Struct.	Color	Description
0			olive gray 5Y3/2	10-13cm: 10YR4/2
1				10-56cm: clay clasts, ash- and sand lenses
2				85-196cm: reworked ash
3				234-323cm: clay clasts with basalts (1-2mm)
4				329-360cm: clay clasts with basalts (1-2mm)
				385-400cm: clay clasts with basalts (1-2mm)
				394-399cm: clay clasts

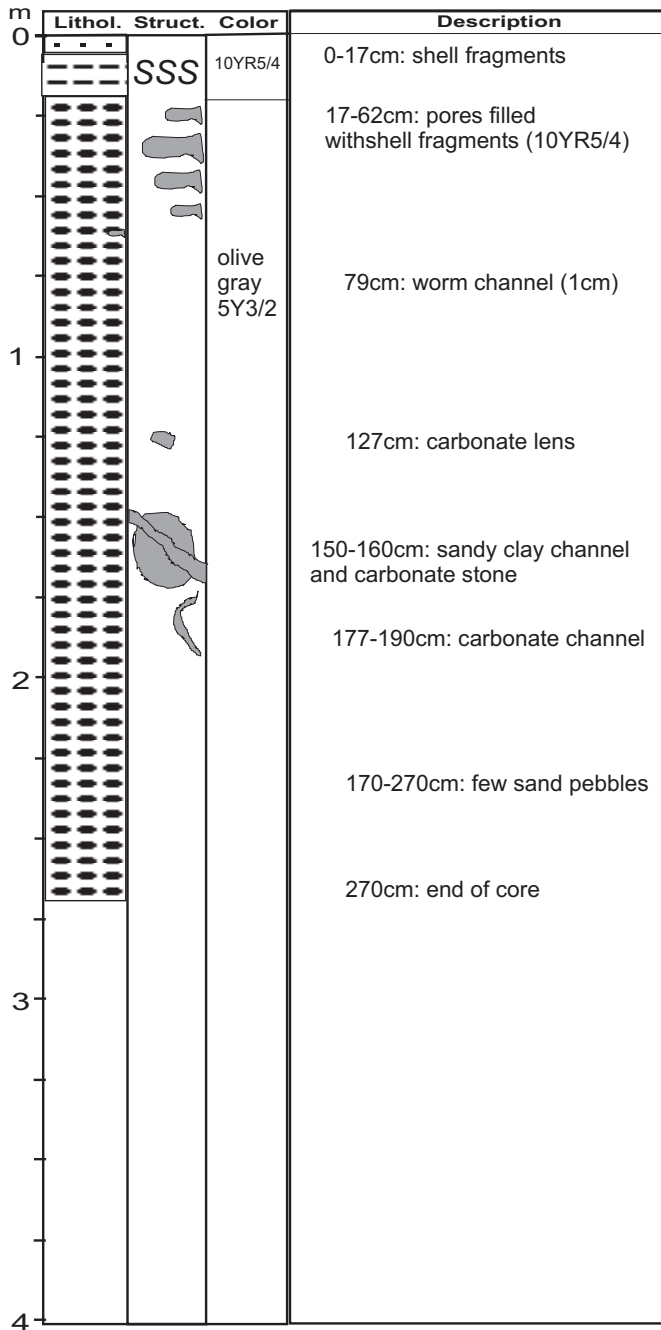
Lithology

ME54-36

m	Lithol.	Struct.	Color	Description
4				404cm: claye sand (carbonate) 411-420cm: clay clast 432-440cm: rippup clay clast 446cm: basalt (6mm)
5				485-572cm: reworked (mixed) sediment (sand/clay/carbonate) 503/525/539/555/569cm: claye sand lenses (carbonate), 5Y7/2
6				572cm: end of core
7				
8				

Lithology

ME54-40



Lithology

ME54-41-1

m	Lithol.	Struct.	Color	Description
4			olive gray 5Y3/2	430-500cm: reworked black ash
5				560cm: end of core
6				
7				
8				

Lithology

ME54-41-1

m	Lithol.	Struct.	Color	Description
0				
			olive gray 5Y3/2	0-340cm: foraminifera
1				
				140-340cm: claye sand lenses
2				
3				
				340-360cm: reworked black ash
4				

Lithology

ME54-48-1

m	Lithol.	Struct.	Color	Description
0				0-18cm: shell fragments 12-15cm: reworked ash 18-52cm: lenses of porous silty clay (5cm) 33cm: reworked ash layer
1			olive gray 5Y3/2	52-77cm: lenses of porous silty clay 62-72cm: reworked ash 73cm: white mineral in carbonate mud 79-148cm: porous silty clay/ sandy clay lenses
2				148-183cm: gap in sediment 183-250cm: porous silty clay lenses and tubes 250-260cm: reworked ash lenses 260cm: end of core
3				
4				

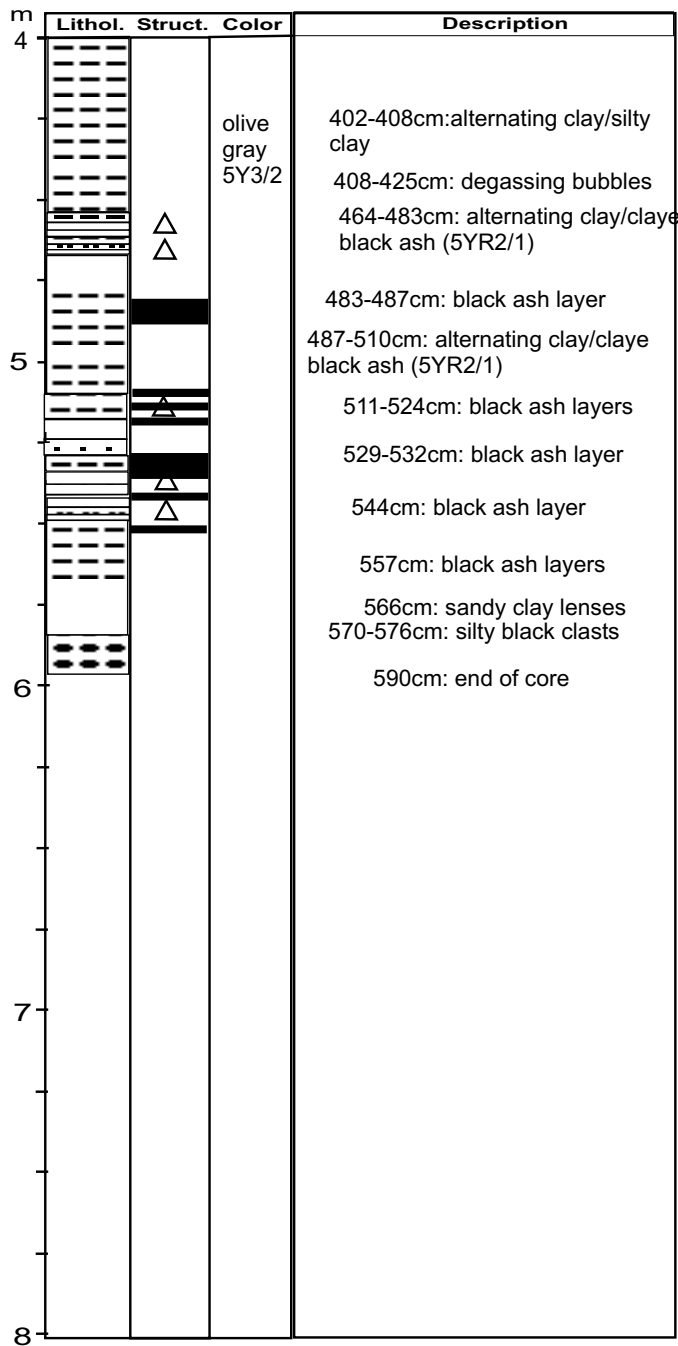
Lithology

ME54-48-2

m	Lithol.	Struct.	Color	Description
0			olive gray 5Y3/2	0-280cm: H ₂ S
				15-40cm: carbonate mud
				60-100cm: carbonate clasts (5mm)
1				100-130cm: claye clasts, high water content
				130-150cm: carbonate clasts
				150-160cm: carbonate concretion (chimney, 10cm), high water content
				180-182cm: carbonate concretions
2				195-205cm: claye clasts, high water content
				205-225cm: carbonate clasts
				218cm: reddish minerals, turn to brown at air contact:
	225-235cm: claye clasts, high water content			
	235-280cm: high porosity			
	260cm: carbonate clasts			
	280cm: end of core			
3				
4				

Lithology

ME54-56



Lithology

ME54-56

m	Lithol.	Struct.	Color	Description
0	[Symbol: horizontal dashes]		olive gray 5Y3/2	
	[Symbol: horizontal dashes]			
	[Symbol: horizontal dashes]			
	[Symbol: horizontal dashes]			
	[Symbol: horizontal dashes]			
	[Symbol: horizontal dashes]			
	[Symbol: horizontal dashes]			
	[Symbol: horizontal dashes]			
	[Symbol: horizontal dashes]			
	[Symbol: horizontal dashes]			
1	[Symbol: horizontal dashes]			114cm: sandy lens
	[Symbol: horizontal dashes]			132-147cm: alternating clay/silty clay (black ash); erosive bottom
	[Symbol: horizontal dashes]			156-171cm: alternating clay/silty clay (black ash); erosive bottom:
2	[Symbol: horizontal dashes]			171-201cm: silty clay lenses (3-5cm)
	[Symbol: horizontal dashes]			223-231cm: alternating clay/sandy black ash
	[Symbol: horizontal dashes]			245-253cm: alternating clay/sandy black ash
	[Symbol: horizontal dashes]			253cm: flame structure
	[Symbol: horizontal dashes]			302-326cm: firm clay lenses
	[Symbol: horizontal dashes]			324cm: silty clay layer
3	[Symbol: horizontal dashes]			326-350cm: degassing bubbles
	[Symbol: horizontal dashes]			338cm: brownish clay lens
	[Symbol: horizontal dashes]			351-357cm: clay fissure
4	[Symbol: horizontal dashes]			

Lithology

ME54-57

m	Lithol.	Struct.	Color	Description
4			olive gray 5Y3/2	415-433cm: flame structure (sandy clay)
				433-490cm: dense 10cm clasts at top; laminar bedding at middle; conduit bedding at bottom
5				490-497cm: alternating sandy clay/clay
				497-510cm: clay mixed with black ash layers
				574-596cm: sandy lenses
6				634-682cm: alternating clay/sandy clay (black ash)
				689-695cm: alternating claye sand/ sandy clay
7				712cm: sandy clay lens
				721cm: reworked sandy clay lens (black ash)
				732cm: end of core
8				


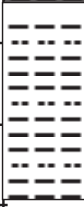
Lithology

ME54-57

m	Lithol.	Struct.	Color	Description
0		△		0-4cm: clay, dark yellowish brown (10YR4/2)
		△		
			olive gray 5Y3/2	
1				131cm: claye sand (black ash layer)
				144cm: silty sand lens (black ash)
2				184-193cm: silty clay (black ash)
				260cm: sandy clay lens (green)
3				298-332cm: black ash lenses and carbonate clasts
4				393-401cm: inverse grading

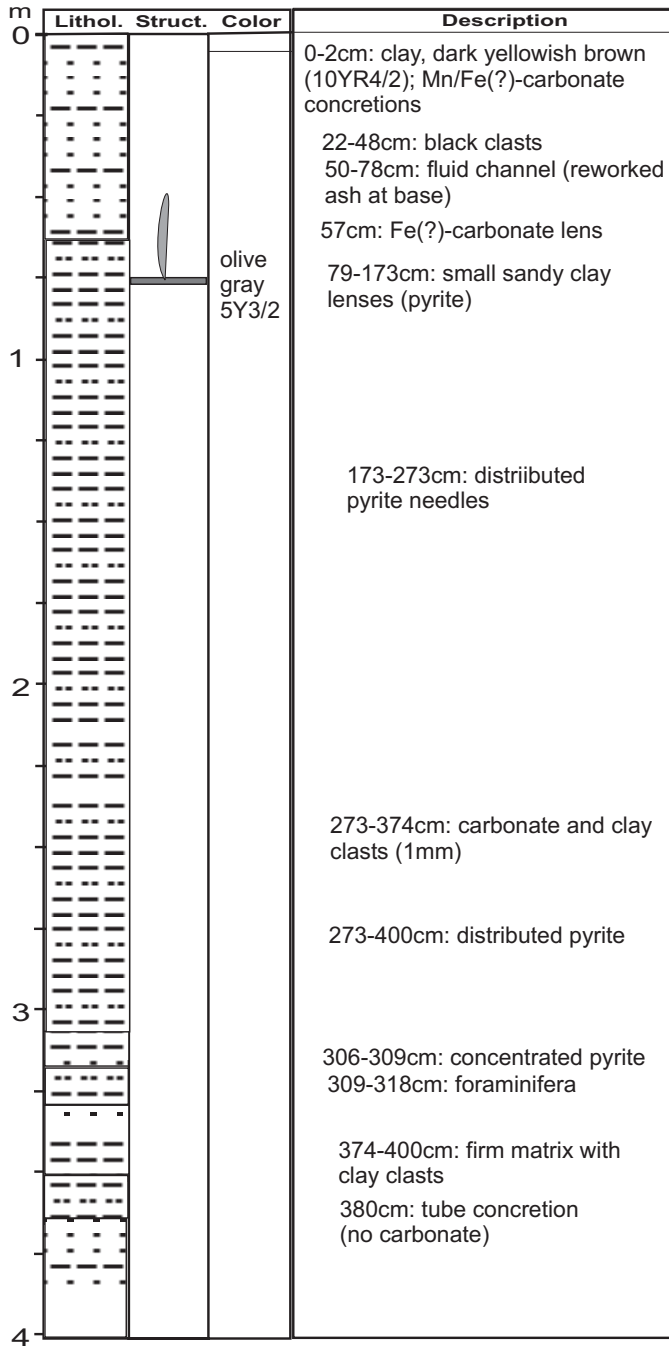
Lithology

ME54-61

m	Lithol.	Struct.	Color	Description
4				
			olive gray 5Y3/2	400-474cm: firm sandy and silty clay 400-474cm: distributed clay clasts and pyrite
5				474cm: end of core
6				
7				
8				

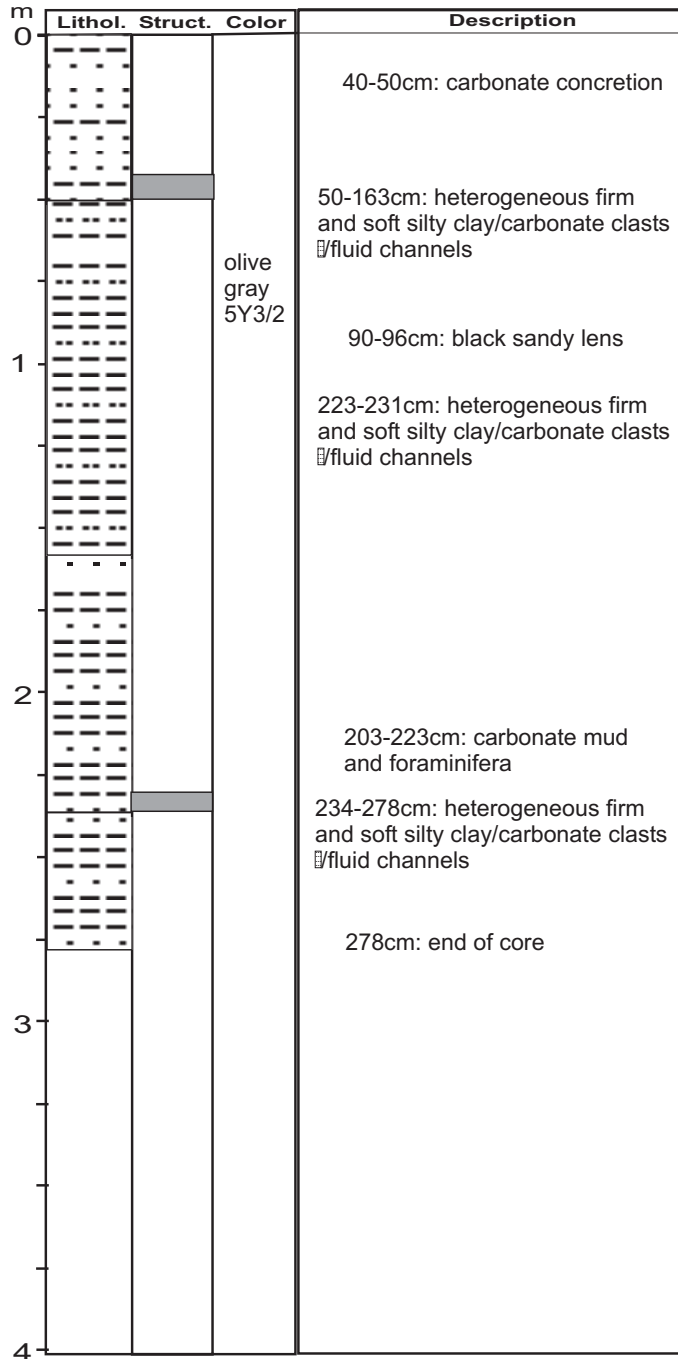
Lithology

ME54-61



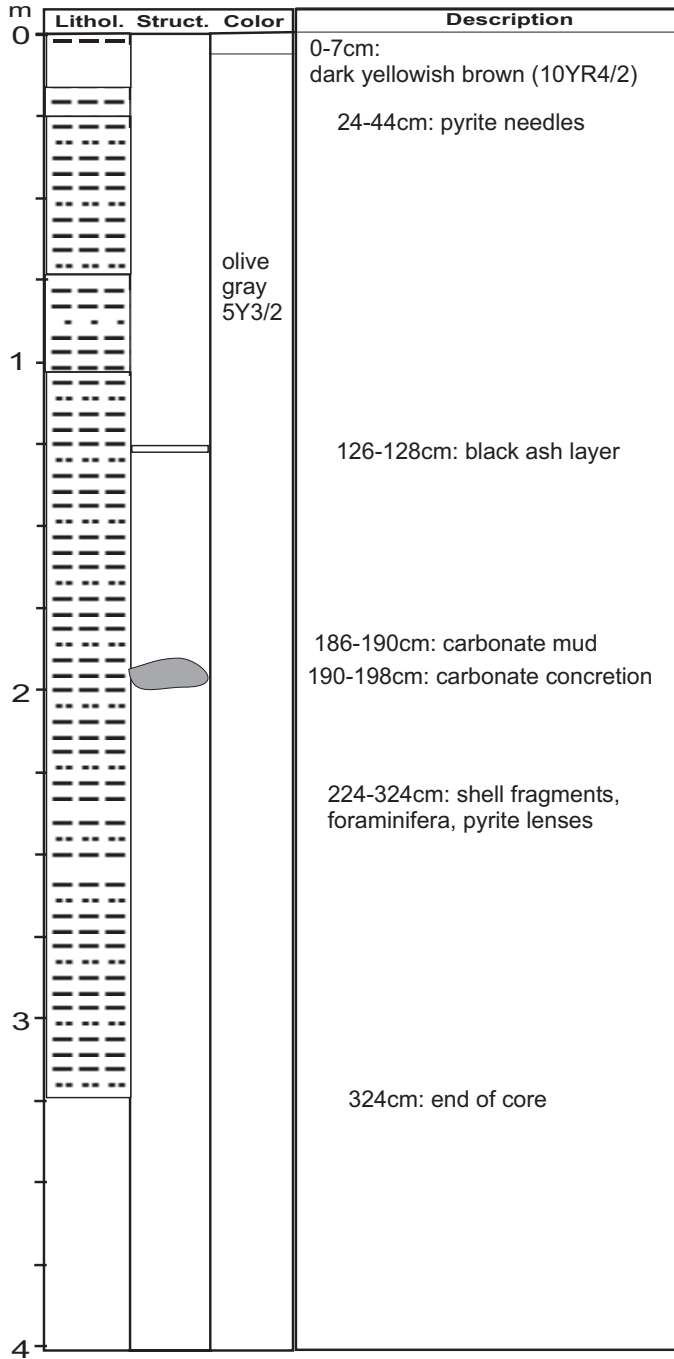
Lithology

ME54-62-2








Lithology

ME54-63



Lithology

ME54-64

m	Lithol.	Struct.	Color	Description
4			5Y3/2	418/440cm: clayey sand lens
				400-495cm: pyrite needles
				461-463cm: clay lens, carbonate mud on top
5				500-536cm: thin channels filled with firm clay
				536cm: end of core
6				
7				
8				


Lithology

ME54-64

m	Lithol.	Struct.	Color	Description
0				
				47-86cm: coral fragments, altered glass, volcanic clasts, pyroxene, olivine, foraminifera, carbonate clasts
			olive gray 5Y3/2	80cm: lens of shell fragments
				82-90cm: fracture
1				208-214cm: clayey sand lens
				148-248cm: pyrite needles
				253-509cm: various fractures, contacts consist of carbonate mud
2				
3				
				354-400cm: foraminifera, pyrite needles
				359cm: carbonate mud lens
4				

Lithology

ME54-68

m	Lithol.	Struct.	Color	Description
4			5Y3/2	400-568cm: pyrite needles, shell and snale fragments, foraminifera
5				568cm: end of core
6				
7				
8				

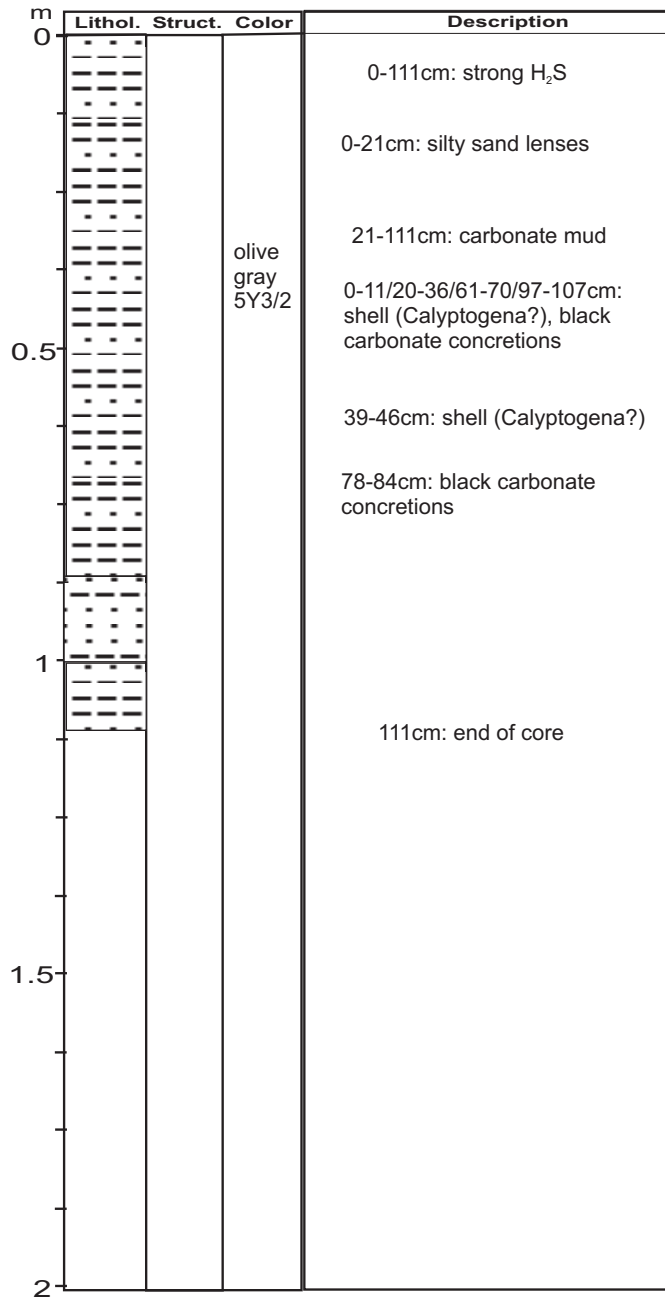
Lithology

ME54-68

m	Lithol.	Struct.	Color	Description
0			olive gray 5Y3/2	5-21cm: porous fluid channel
				33/39/76cm: porous lens
1				86-400cm: pyrite needles, shell and snale fragments, foraminifera
2				
3				354-400cm: foraminifera, pyrite needles
4				359cm: carbonate mud lens

Lithology

ME54-69-1



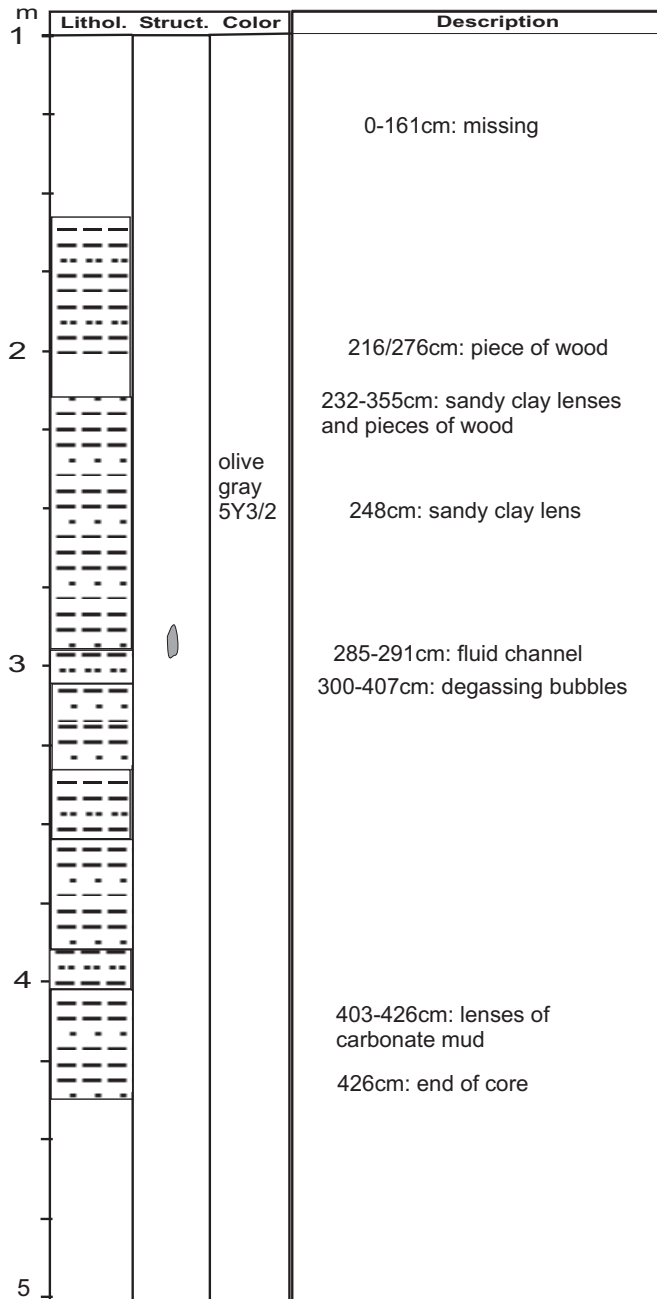
Lithology

ME54-73-2

m	Lithol.	Struct.	Color	Description
0				0-130cm: missing
1			olive gray 5Y3/2	
2				248/252/296cm: lenses filled with wood
3				290-300cm: fluid pores 311-361cm: black concretions (<0.5cm) 335-345cm: fluid channel
4				361-397cm: pyrite, shell fragments foraminifera 397cm: end of core

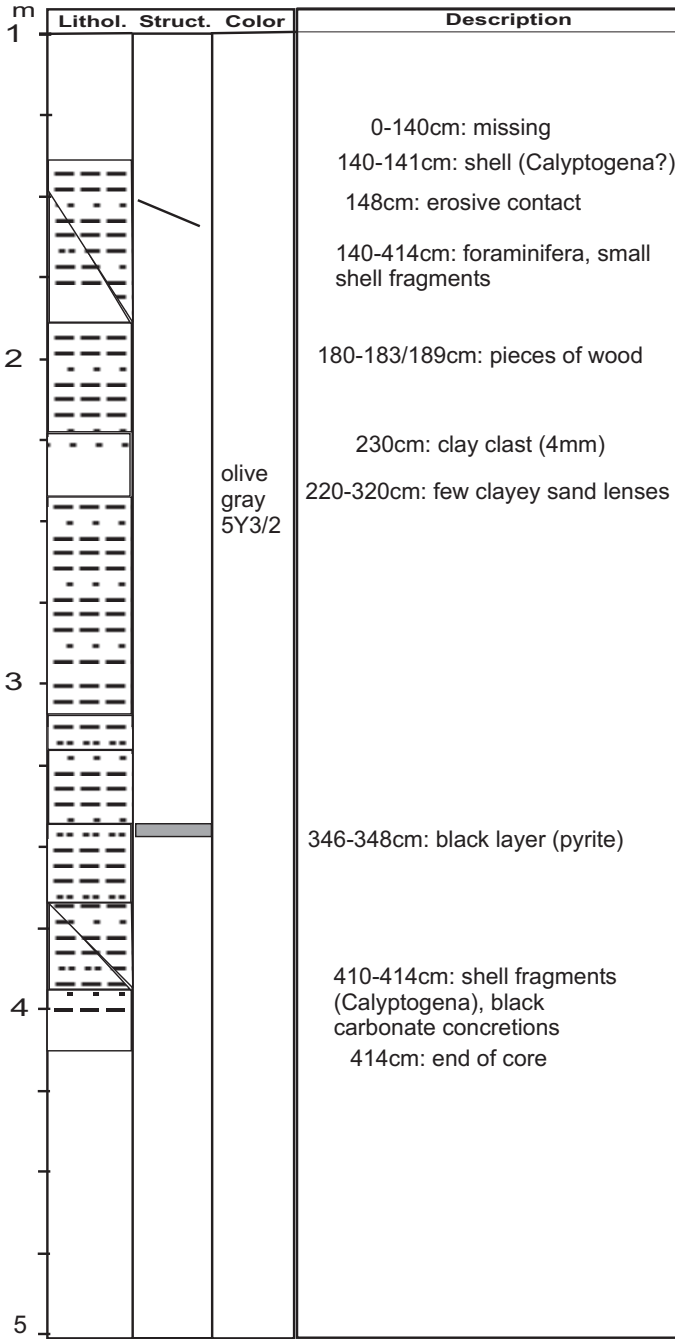
Lithology

ME54-74



Lithology

ME54-75



Lithology

ME54-78

m	Lithol.	Struct.	Color	Description
4			5Y3/2	409-413cm: carbonate lens
5				543-591cm: ~6cm shell fragments (Calyptogena?)
6				591cm: end of core
7				
8				

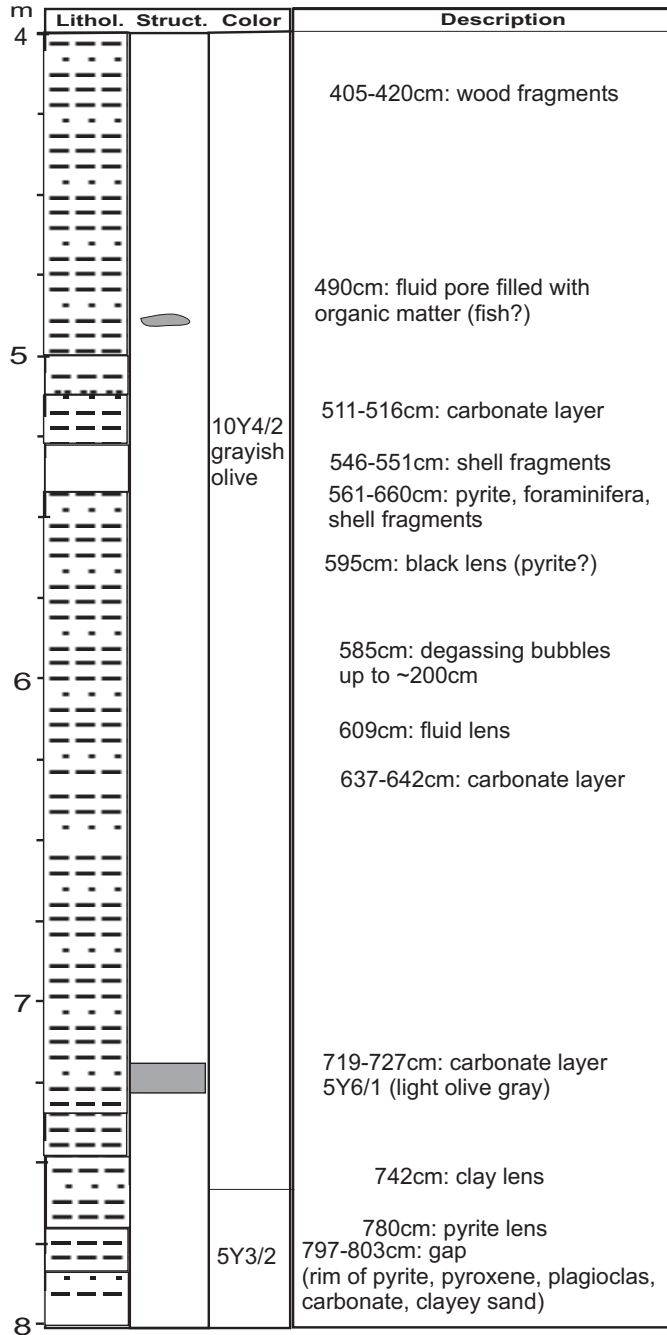
Lithology

ME54-78

m	Lithol.	Struct.	Color	Description
0			olive gray 5Y3/2	25-26cm: carbonate mud layer
1				0-591cm: foraminifera in whole core
2				96-196cm: small fluid lenses
3				162cm: fluid lens
4				166cm: piece of wood
				237-285cm: fluid pores
				297-397cm: shell fragments, pyrite (increase to top)
				354-400cm: foraminifera, pyrite needles
				359cm: carbonate mud lens
				378-385cm: sandy clay lens

Lithology

ME54-80



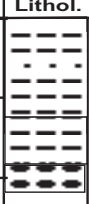
Lithology

ME54-80

m	Lithol.	Struct.	Color	Description
0	[Lithology symbols: horizontal dashes, dots, and vertical lines]		olive gray 5Y3/2	0-853cm: H ₂ S, pyrite needles, foraminifera
				0-763cm: carbonate mud
1				26-167cm: mixed silty and sandy clay lenses/clasts (chaotic structure)
				171cm: silty clay lens
2	[Lithology symbols: horizontal dashes, dots, and vertical lines]		olive gray 5Y3/2	189-195cm: porous clayey sand lens
				219-233cm: shell fragments
				244/248/250cm: clayey sand lens
				269/275/310cm: clay lens
3	[Lithology symbols: horizontal dashes, dots, and vertical lines]		olive gray 5Y3/2	347-348cm: wood layer
				387cm: organic matter (fish?)
				393cm: shell fragments
4				

Lithology

ME54-80

m	Lithol.	Struct.	Color	Description
8			olive gray 5Y3/2	763-857cm: strong H ₂ S, foraminifera 840-853cm: pyrite, carbonate mud 853cm: strong degassing through core catcher 853cm: end of core
9				
10				
11				
12				

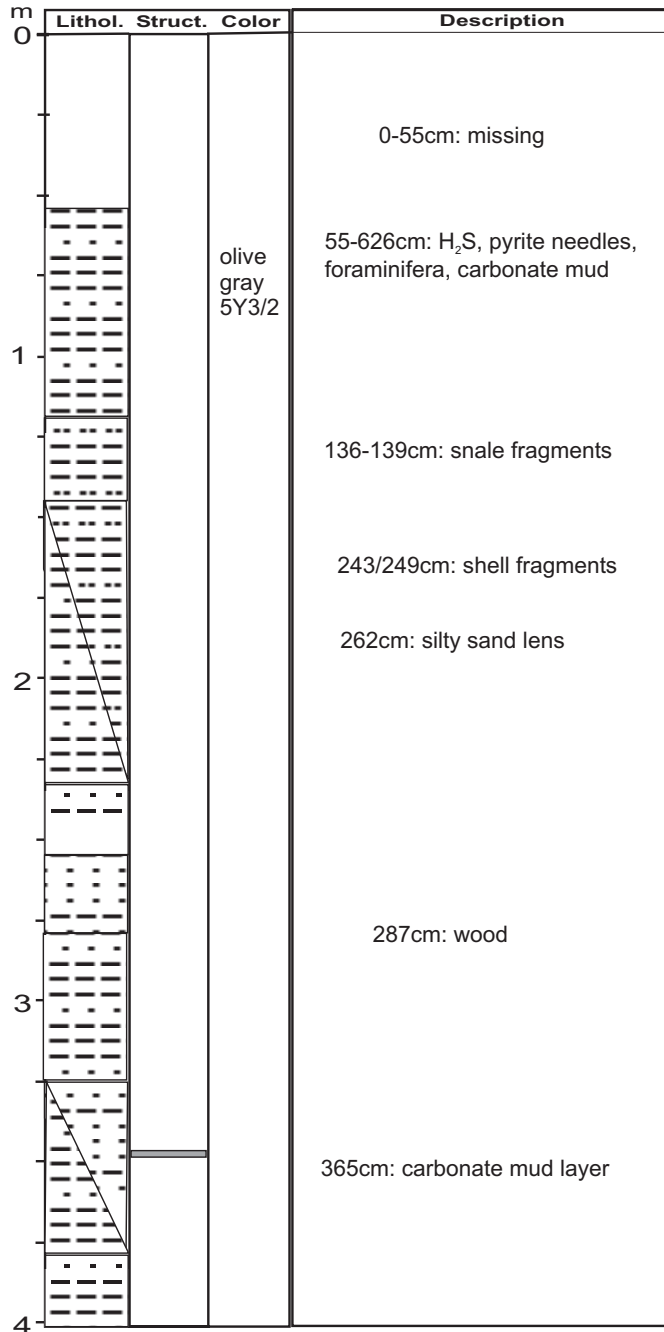
Lithology

ME54-81-1

m	Lithol.	Struct.	Color	Description
4	[Hatched pattern]		5Y3/2	409cm: pyrite lens
5				540cm: wood
				561cm: clayey sand layer
6				590-626cm: carbonate layer 5Y6/1 (light olive gray)
				610cm: reworked black ash lens 626cm: end of core
7				
8				

Lithology

ME54-81-1



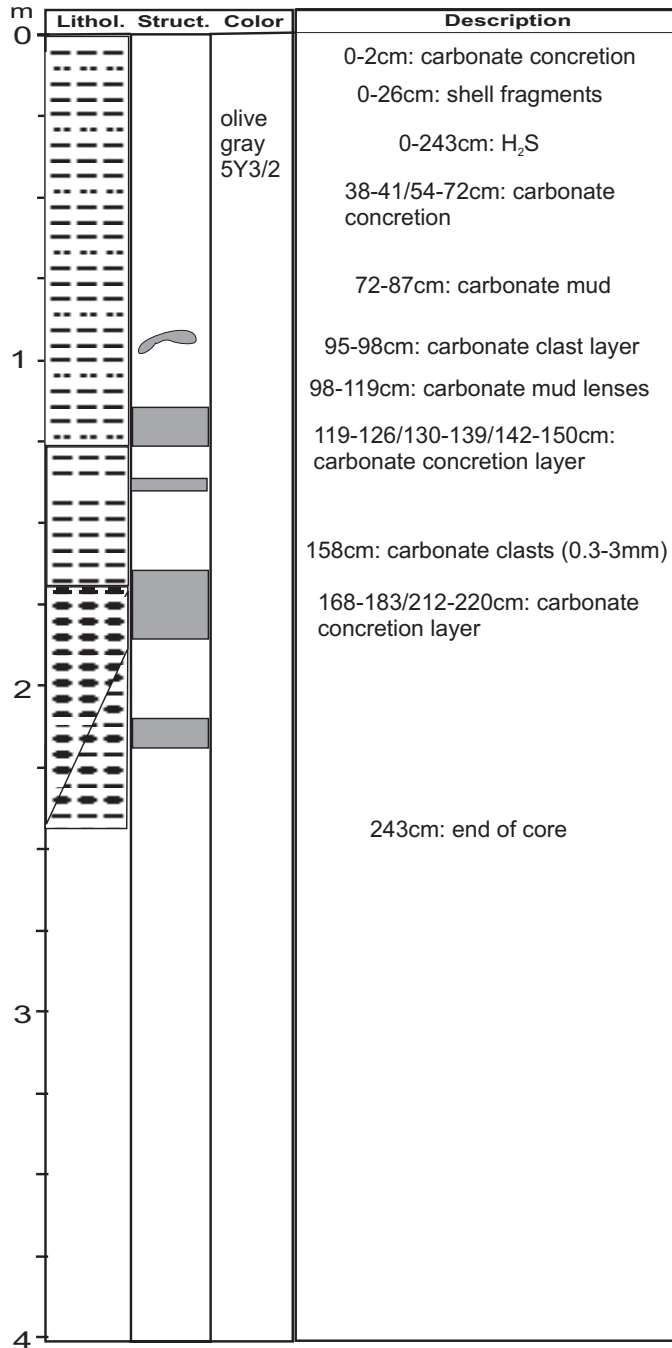
Lithology

ME54-84

m	Lithol.	Struct.	Color	Description
0			olive gray 5Y3/2	0-10cm: missing
				0-282cm: foraminifera
				13-20cm: carbonate chimney
				41cm: shell fragment
				41-54cm: carbonate lenses/clasts
				54cm fluid lens with sandy clay
				65-75cm: carbonate layer and chimney
				89-98cm: carbonate layer, shell fragments, siderite?
1				132cm: shell fragments (3cm), carbonate clasts
				157cm: heterogeneous (mixed) structure to top
			135-152cm: fluid channel	
			157-168cm: carbonate layer	
			168cm: shell fragment (4cm)	
			177-192cm: carbonate clasts (siderite?)	
2			196-200cm: carbonate layer	
			206-230cm: carbonate layer	
			192-282cm: porous (solid) lenses with clayey matrix	
			239-254/249-254/269-275cm: carbonate layer	
3			282cm: end of core	
4				

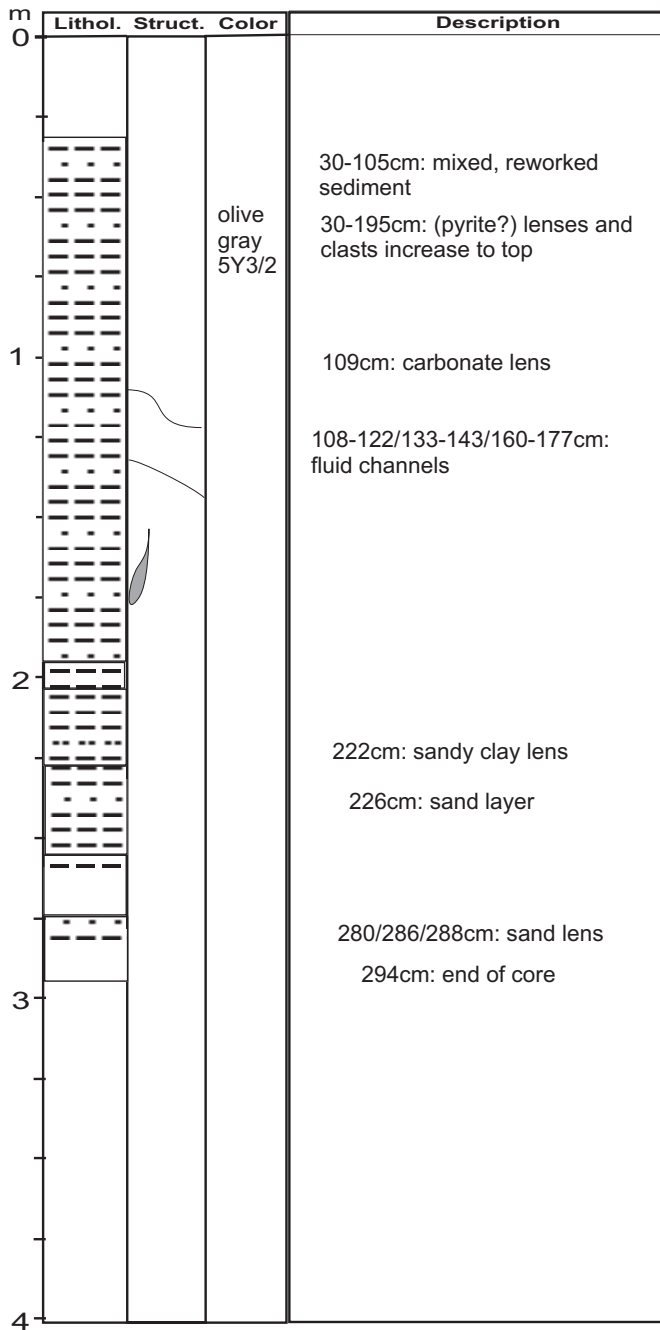
Lithology

ME54-89



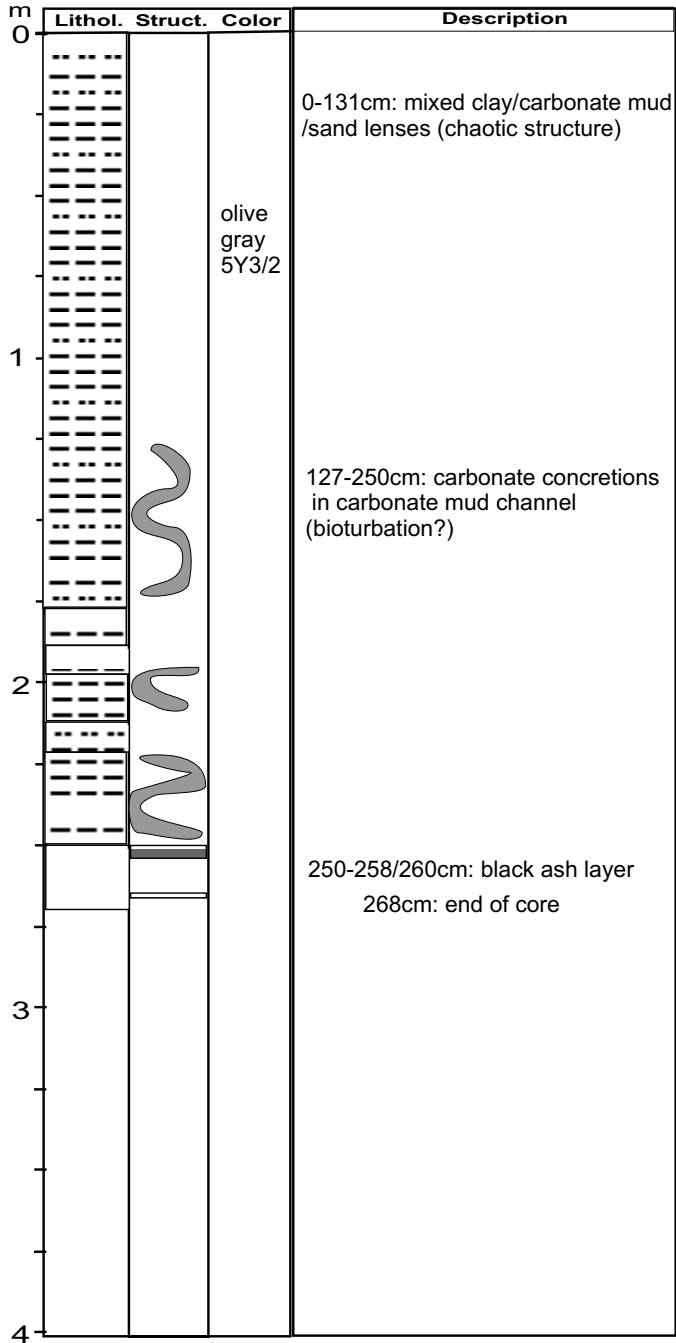
Lithology

ME54-90



Lithology

ME54-92



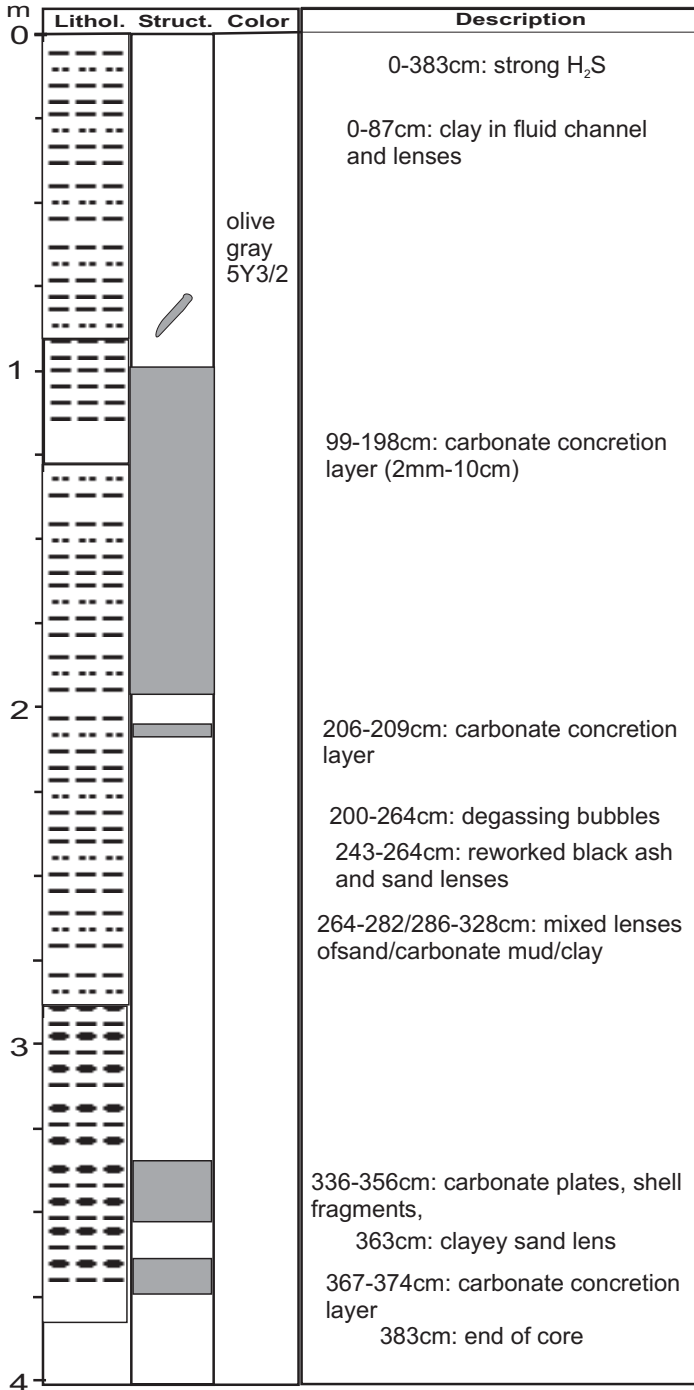
Lithology

ME54-94

m	Lithol.	Struct.	Color	Description		
0			olive gray 5Y3/2	14-138cm: mixed clay/carbonate mud/sand lenses (chaotic structure)		
				25-28cm: carbonate mud lenses and concretions		
				26-56cm: carbonate mud channel and concretions		
				56cm: shell fragment		
1						105-113/240-250cm: carbonate concretion layer
2						
3						292cm: shell fragment
						292-320cm: carbonate mud lenses and concretions
						320-362cm: carbonate mud lenses
						362cm: end of core
4						

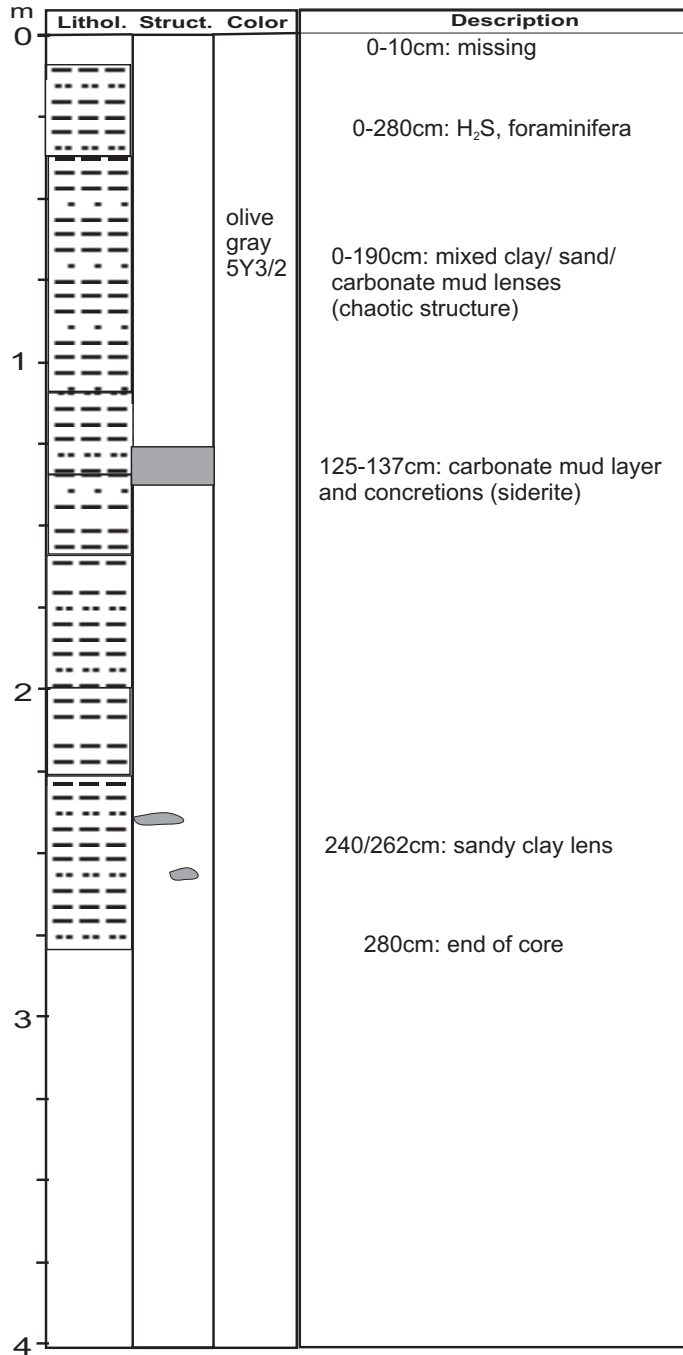
Lithology

ME54-97-2



Lithology

ME54-100



Lithology

ME54-102

m	Lithol.	Struct.	Color	Description
0			olive gray 5Y3/2	0-30cm: carbonate clasts (2mm) 0-231cm: H ₂ S, foraminifera 20-40cm: reworked carbonate mud layer and concretions
1				66-95cm: reworked carbonate mud layer shell fragments, carbonate concretions
2				102-186cm: carbonate mud layer, shell/ shale fragments, carbonate concretions (6cm)
3				219-231cm: carbonate mud lenses 231cm: end of core
4				

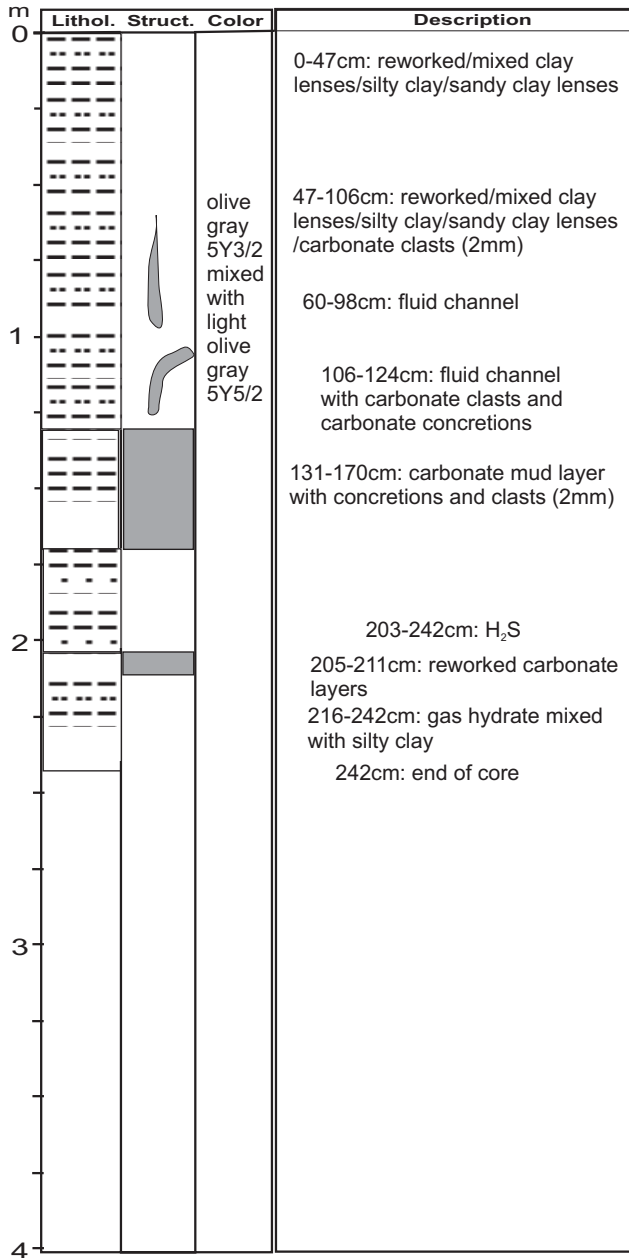
Lithology

ME54-105

m	Lithol.	Struct.	Color	Description
0				0-289cm: H ₂ S
			olive gray 5Y3/2	0-80cm: clay lenses
1				80-200cm: foraminifera, shell fragments, carbonate clasts in clayey sand lenses
				80-200cm: mixed/reworked scaly clay/clayey sand
2				210-263cm: degassing bubbles
				260-265/270-277cm: sandy clay lenses
3				263cm: end of core
4				

Lithology

ME54-109



ME54-116-GC

LATITUDE: 10°18.34'N
 LON: 86°18.85'W
 WATER DEPTH: 1682 m
 DATE: 12.09.2002
 TIME: 16.17.34

Cm	Lithol.	Struct.	Color	Description
250				This core begins at 275 cm under the sea floor
300		Homogenous		
350			olive green	275-748 cm: olive green soft calcareous clay with few nanofossils (about 1%), the structure is homogenous
400				281-283 cm, 307-309 cm, 320-323 cm: porous layer?
450				363 cm-365 cm: olive gray clayey silt lens, sharp top and bottom contact, volcanic ash?
500				589-592 cm: dark green clayey silt lens, 4.5x2.5 cm
550				636 cm: greenish black silt lens, 1x0.8 cm
600				651-653 cm: a layer of greenish black sandy silt
650				720 cm: microorganism fragments, grain size is about 1 mm
700				748-838: olive green calcareous silty clay, foraminifera is common.
750				806.5 cm: layer contains small pores
800				Strong H ₂ S smells at the bottom of the core
850				838cm: end of core

ME54-133-GC

LATITUDE: 10° '
 LON: 86° '
 WATER DEPTH: m
 DATE: 17.09.2002
 TIME:

Cm	Lithol.	Struct.	Color	Description
0				0-10 cm: semi-liquified layer, dark green calcareous silty clay
50				10-210 cm: dark green calcareous silty clay
100			dark green	14-24 cm: light yellow silty clay spot 14 cm: carbonate concretion, 1x1 cm
150				32-38 cm: carbonate concretion chimney, 4x7 cm (sampled)
200				170 cm: and 172-176 cm: light yellow color spot
250				210-310 cm: dark green clay
300				210-262 cm,: porous sediments containing numerous small holes, with a diameter of about 0.5 mm
350				228 cm: carbonate concretion, 2.5x1.5 cm
400				263 cm: carbonate concretion, 5x3 cm
450				279-290 cm: 2 carbonate concretions, about 10x4.5 cm (sampled)
				288-340 cm: gas bubbles on the surface, the diameters of bubbles are in the range of 1-10mm
				The whole core strong H₂S smell
				398 cm: end of the core
				Note: all of the carbonate concretions have been sampled

ME54-136-2-GC

LATITUDE: 8°55.33'N
 LON:84°18.25'W
 WATER DEPTH: m
 DATE: 17.09.2002
 TIME:

Cm	Lithol.	Struct.	Color	Description
0				0-13 cm: dark green semi-liquified calcareous silty clay
				13-21 cm: dark green calcareous clay, mottled
50		SSS	dark green	21-121 cm: gray green and light gray calcareous clay mottled, rich in organism traces (horizontal and low angle worm tubes). The pattern usually shows a sharp contact. The sediments in the color of light gray are drier, and often contains consolidated carbonates in the size of about 0.5 cm
100		Mottled		29-30.5 cm: horizontal worm tube, unfilled, diameter: 1.3 cm, 40-42 cm: worm tube, filled with dark green clay, 2x1.5 cm, moisture 45-47 cm: worm tube, filled with dark green clay, 2.5x3.5 cm, moisture 48-50.5 cm: worm tube, filled with dark green clay, 2x1.5 cm, drier
150		S		51-53 cm, 54-56, 56-59, 61-64 cm: as above, moisture 64-67 cm: worm trace, 0.5x7 cm, different color, sharp contact 68-69.5 cm: worm tube, unfilled, 1.5x1 cm 79-81, 83-84.5 cm: same as above, surrounding sediments contain bubbles 88-121 cm: light gray clay, dry and stiff, containing carbonate consolidation
200				121-211 cm: dark green calcareous clay (the section has been compressed 6 cm, the original length is 90 cm) 127-211cm: mottled light gray calcareous clay 128-143 cm, 189-203 cm: moisture. 153-161, 175-179, 183-189, 203-211 cm: dry and stiff, contain consolidated carbonates
250				210 cm: end of the core

ME54-140-GC

LATITUDE: 8°55.35'N
 LON:84°18.24'W
 WATER DEPTH: 1018 m
 DATE: 17.09.2002
 TIME:

Cm	Lithol.	Struct.	Color	Description
0				0-9 cm: dark green semi-liquelied calcareous silty clay
50			dark green	9-190 cm: dark green calcareous clay mottled with greenish calcareous gray clay. The patterns usually show sharp contacts, the sediments in the color of greenish gray are drier and stiff, often containing consolidated carbonates pebbles
100		Mottled		64-67 cm: carbonate concretion, 2x3 cm
150		SSS		104-106 cm: same as above, 1x1 cm 111-113 cm: reddish gray silt lens, volcanic ash
200				190 cm: end of the core

ME54-143-GC

LATITUDE: 8°55.33'N
 LON:84°18.26'W
 WATER DEPTH: 1021m
 DATE: 17.09.2002
 TIME:

Cm	Lithol.	Struct.	Color	Description
0				0-13 cm: dark green semi-liquified calcareous silty clay
50			dark green	13-157 cm: dark green calcareous clay 67-75 cm: dense texture 75-79 cm: carbonate nodule, light gray, 2.5x2 cm, micrite 85-87 cm: same as above, 3x1.3 cm 88-89 cm: same as above, 1x1 cm 91-96 cm: same as above, 5x4 cm 97-99 cm: same as above, 2x1 cm, and 10x5 cm 99-108 cm: shell fragments
100				104-124 cm: this layer contains very important evidence for gas hydrate
150				104-110 cm: black carbonate crust, about 10x15 cm, 2 cm thick, granular surface easy flaked off. Under the microscope, they are composed of authigenetic aragonite needles and micrite. In this layer, it also contain white crystals looks like barite 110-124 cm: carbonate concretions 119-126 cm: a big hole, about 9x6 cm, filled with water, surrounded by black volcanic ashes, porous and soft. Probable gas hydrate layer, which apparently broke up when the core was exposed to ambient temperature and pressure 126-134 cm: carbonate concretion
200				134-143 cm: light gray clay, dense texture 143-157 cm: dark green calcareous clay 157 cm: end of the core

ME54-155-GC

LATITUDE: 8°55.36'N
 LON:84°18.23'W
 WATER DEPTH: 1018m
 DATE: 20.09.2002
 TIME:

Cm	Lithol.	Struct.	Color	Description
0				0-3 cm: olive green semi-liquefied calcareous silty clay
20				3-130 cm: olive green calcareous clay
40				8-11 cm: carbonate nodule, 5x4 cm
60				33-41 cm: high water content
80				40-43 cm: yellowish gray calcareous sandy clay, containing carbonate concretion
100				47-50 cm: carbonate nodule, 2.5x3.5 cm
120				55-63 cm: yellowish gray calcareous clay
140				60-62.5 cm: a worm tube filled with dark green calcareous clay, sharp contact
160				87-95 cm: mottled yellowish calcareous gray clay
180				98 cm: a shell fragment
				130-174 cm: sediments looks much drier, granular appearance
				164 cm: reddish gray volcanic ash lens
				174 cm: end of core
				Strong H ₂ S smell
				Sampling: 44-46, 87-95, 100, 160-164 cm

ME54-159-GC

LATITUDE: 9°07.20'N
 LON:84°50.63'W
 WATER DEPTH: m
 DATE: 21.09.2002
 TIME:

Cm	Lithol.	Struct.	Color	Description
0				
20			olive green	0-58 cm: olive green gravelly sand, calcareous, talus
40		Talus		
60				58 cm: end of the core

ME54-164-GC

LATITUDE: 8°55.69'N
 LON:84°18.82'W
 WATER DEPTH: 1022m
 DATE: 22.09.2002
 TIME:

Cm	Lithol.	Struct.	Color	Description
0		SSS		0-10 cm: olive green semi-liquefied calcareous silty clay
30				10-48 cm: olive green calcareous clay. Strong bioturbation. Worm tubes, some of them were filled with dark green clay, horizontal orientation, diameter: 0.5-0.8 cm (empty tube), 1-2 cm (filled tube)
60		SS		48-108 cm: olive green calcareous clay 50-51 cm, 57-57.8 cm: worm tube, unfilled, 0.8 cm diameter 73-76 cm: piece of wood, 1x6 cm 78-85 cm: dark green clay lump, 6x8 cm, where water content is higher than in the surrounding sediments
90				108-208 cm: yellowish green calcareous clay mixed with volcanic ash layers and carbonare concretion. The color is getting darker under ash layers and changes into dark green (175-208) 146-146.5, 148-149, 150-156 cm: grayish black volcanic ash spots or lenses, size: 0.5-6 cm, fine sand 155-158, 159-163, 171-172.5 cm: grayish black volcanic ashlayers, fine sand 165.5-175, 176-176.5, 178.5-182.5, 196-196.5, 198-200 cm: volcanic ash spots or lenses, carbonate nodule: 4x6 cm, light gray
120				208-298 cm: dark green calcareous clay mixed with grayish dark fine sandy volcanic ash or interbedded with very thin volcanic ash layers 214.5, 219.5, 229.5-230.5, 257, 264 cm: volcanic ash layers, the layers are very thin. Between layers, the sediments contain spotted ash 246-249 cm: light yellow vertical worm tube, sharp contact, filled with light yellow clay 286-288 cm: yellow diagenetic lump, strong H ₂ S smell
150				298 cm: end of core
180				Sampling: 154-156, 119-121, 161-162, 180-182, 175-177, 161-162, 172-176, 179-183, 219-220, 226-228 cm
210				
240				
270				
300				

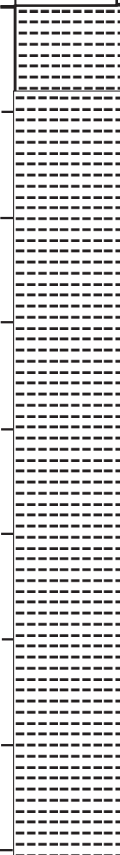

ME54-171-GC

LATITUDE: 9°11.67'N
 LON:84°39.81'W
 WATER DEPTH: 610m
 DATE: 23.09.2002
 TIME:

Cm	Lithol.	Struct.	Color	Description
0	[Dotted pattern]			0-22 cm: dark green calcareous clay
				22-36 cm: yellowish green calcareous clay with light green lump
50				36-54 cm: light green calcareous clay
				54 cm: erosive contact
		⊗		54-120 cm: dark green calcareous clay, stiff 56, 57, 65, 68.5, 73, 82, 86.5, 90, 93, 97, 99, 100, 101, 105, 110, 114, 121 cm: shell fragments (some still intact, parallel to stratification). The surface layer of the shells has been dissolved to some extent, so it is thin and white and looks like mica with bare eyes. Composition: calcite crystal
100				66, 68, 71, 74.5, 98, 104.5 cm: contain brownish black material, looks like rich in ferric oxide
150				120-197 cm: dark green calcareous clay, stiff 124, 186 cm: brownish black layer (ferric oxide?) 130, 136.5, 138, 145, 175, 179, 188, 198 cm: shell fragments 182 cm: black sandy volcanic ash lens
200		⊗		197-243.5 cm: dark green calcareous clay , black stained, stiff 197-199 cm: dark green clay with black stained layers 213-218 cm: dark green clay with nonhomogenous black stain, the stain extent is stronger than the upper layer, no sharp contact 231, 236, 241, 243, 245 cm: shell fragments
250				243-312 cm: greenish dark calcareous clay, stiff. This layer is darker than the layers above
300				312 cm: end of the core
350				

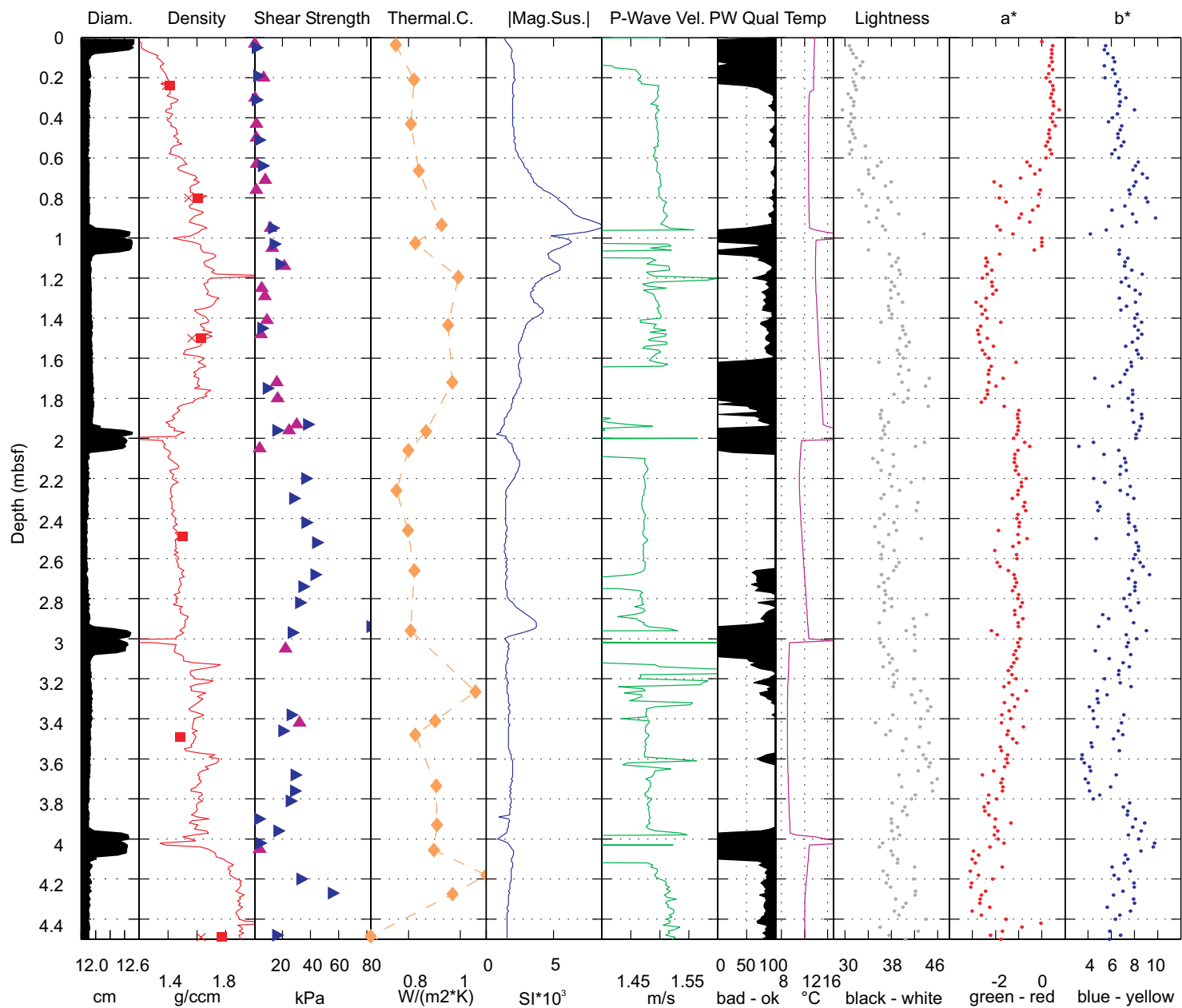
ME54-179-GC

LATITUDE: 8°59.55'N
 LON: 84°43.70'W
 WATER DEPTH: 1938m
 DATE: 25.09.2002
 TIME:

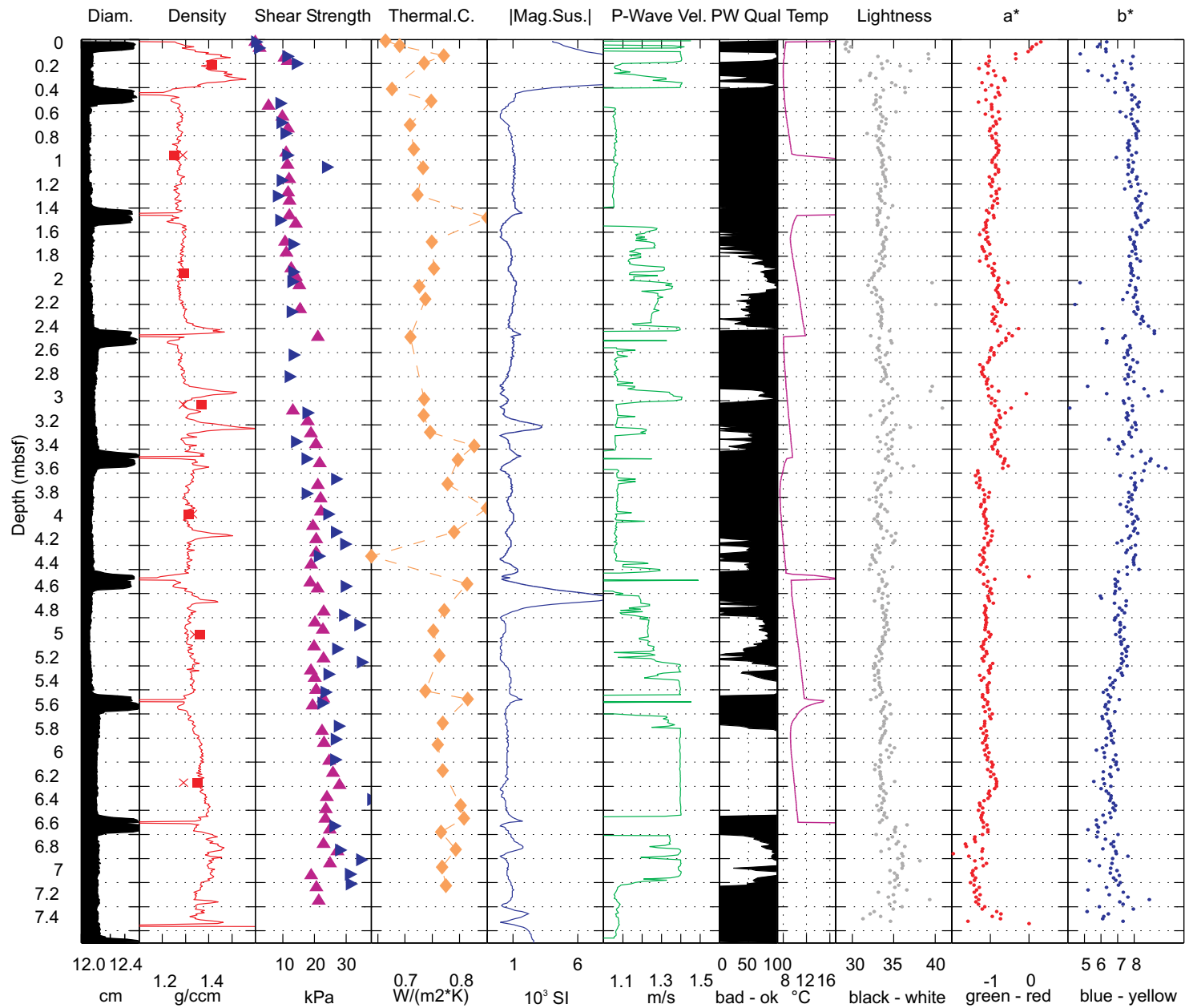
Cm	Lithol.	Struct.	Color	Description		
0		SS		0-20 cm: olive green calcareous clay, semi-liquefied		
				20-82 cm: olive green calcareous clay, homogenous		
50					52 cm: an unfilled worm tube, diameter 1 cm, horizontal angle: about 70 degree	
					82-189 cm: greenish gray mix with mottled olive green calcareous clay. Nonhomogenous in color.	
100					89, 119 cm: an unfilled worm tube, horizontal, diameter 1 cm, water inside	
					149-150 cm: greenish gray calcareous silty clay	
150					189 cm: unconformity surface, shell fragments below the surface	
					189-201 cm: olive green calcareous clay, more stiff than the layer above	
200						195-201 cm: dark stained calcareous clay
					201 cm: end of the core	
250						
300						

Appendix G

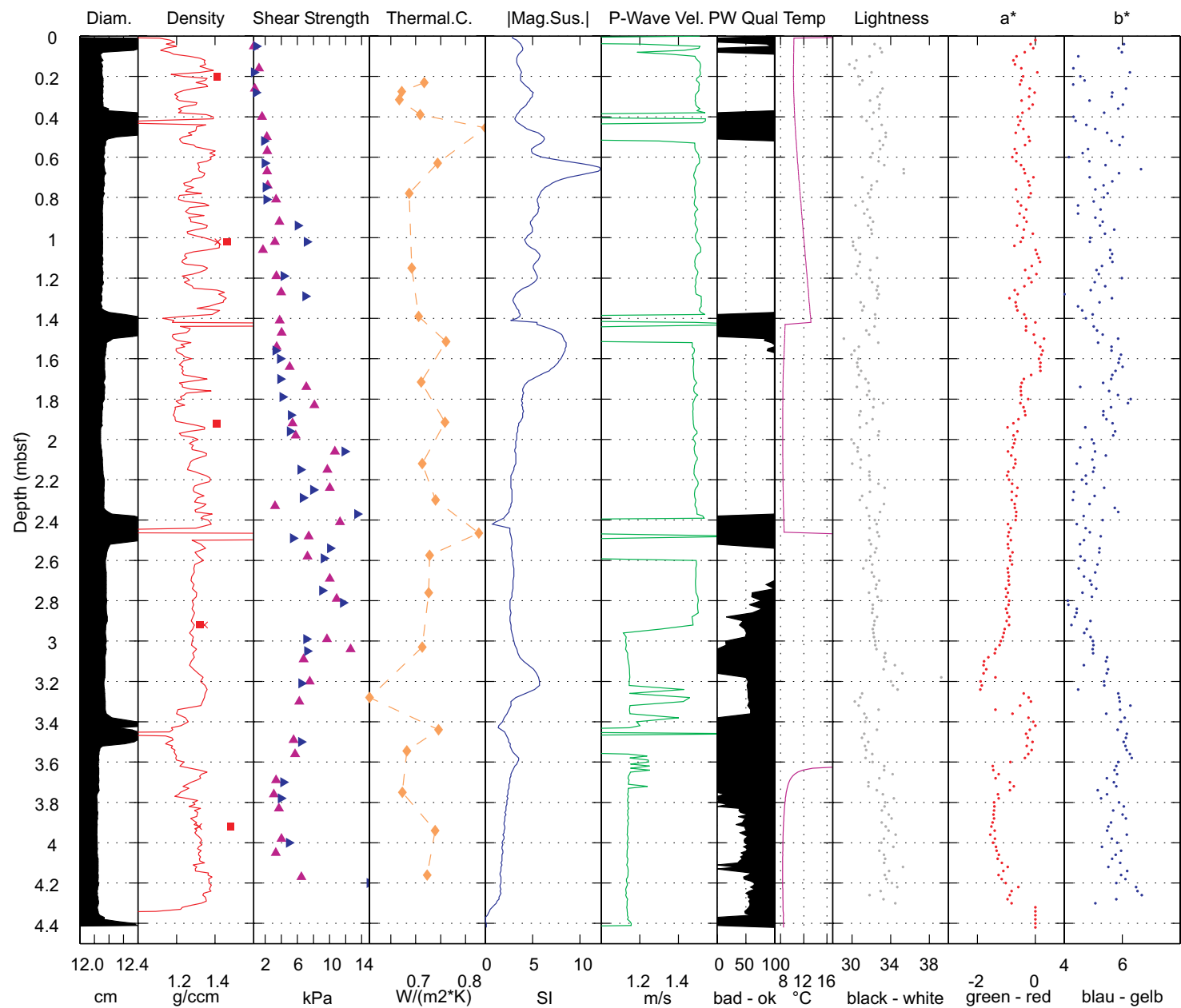
Logging Plates



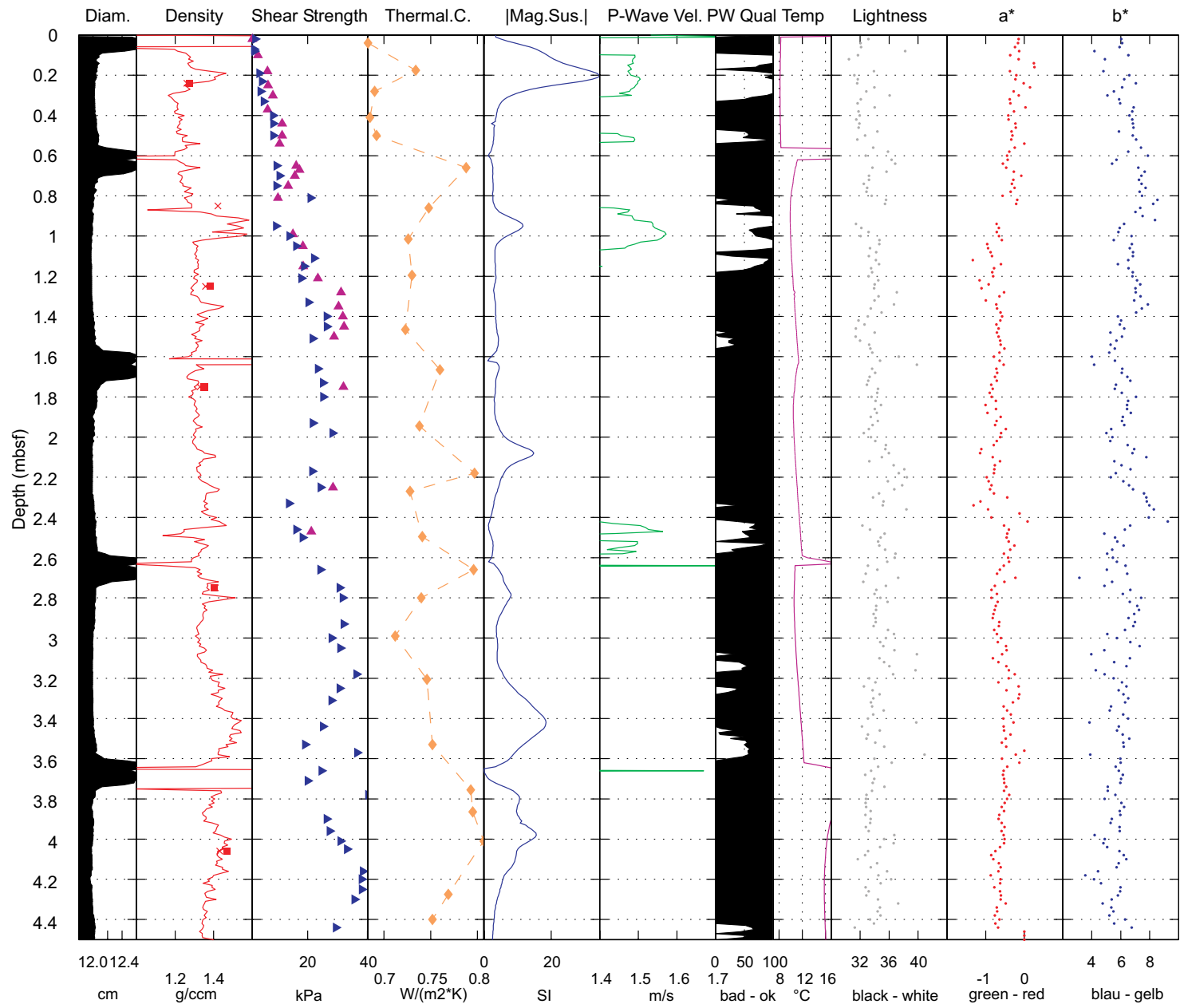
Core M 54-1



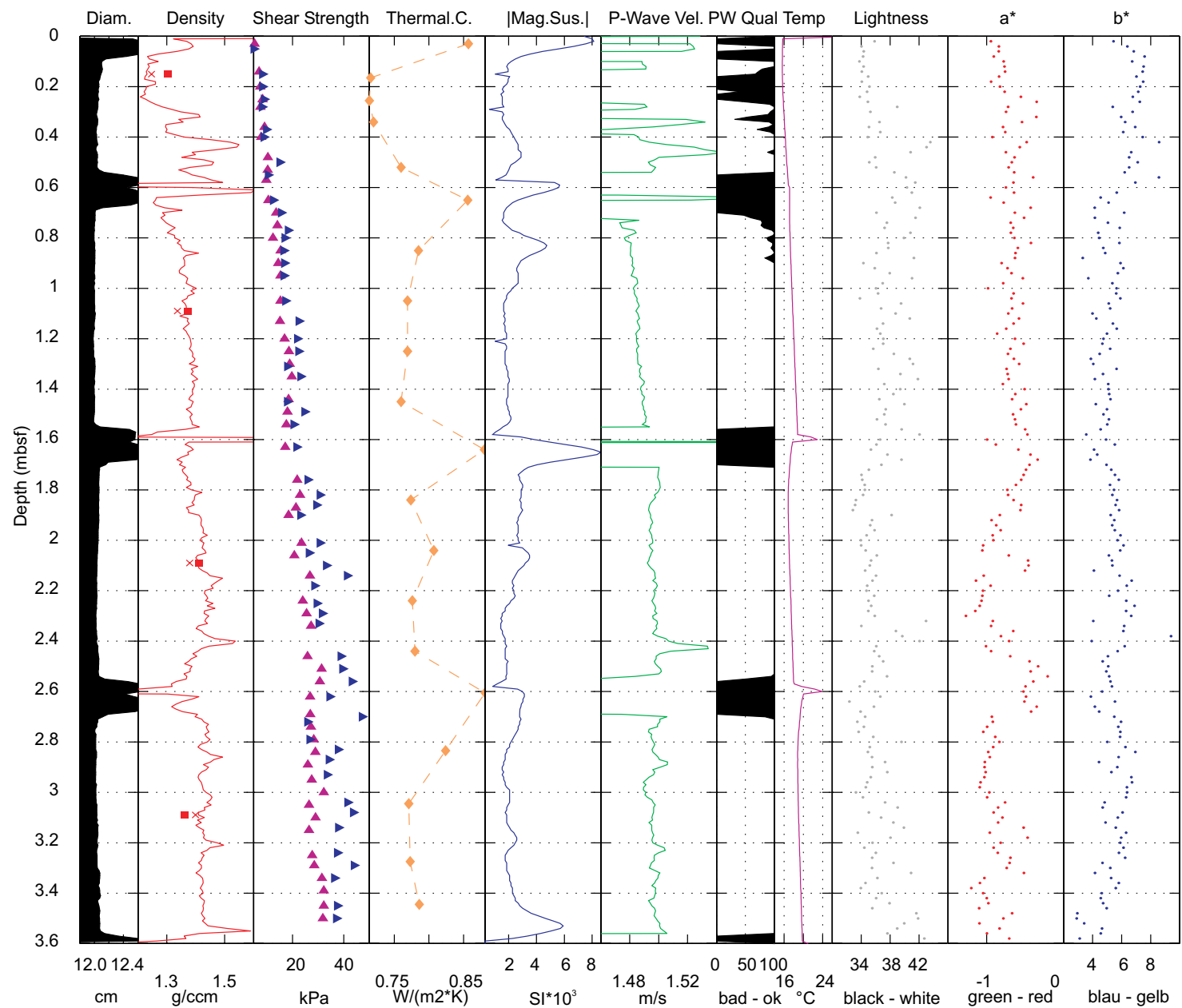
Core M 54-2



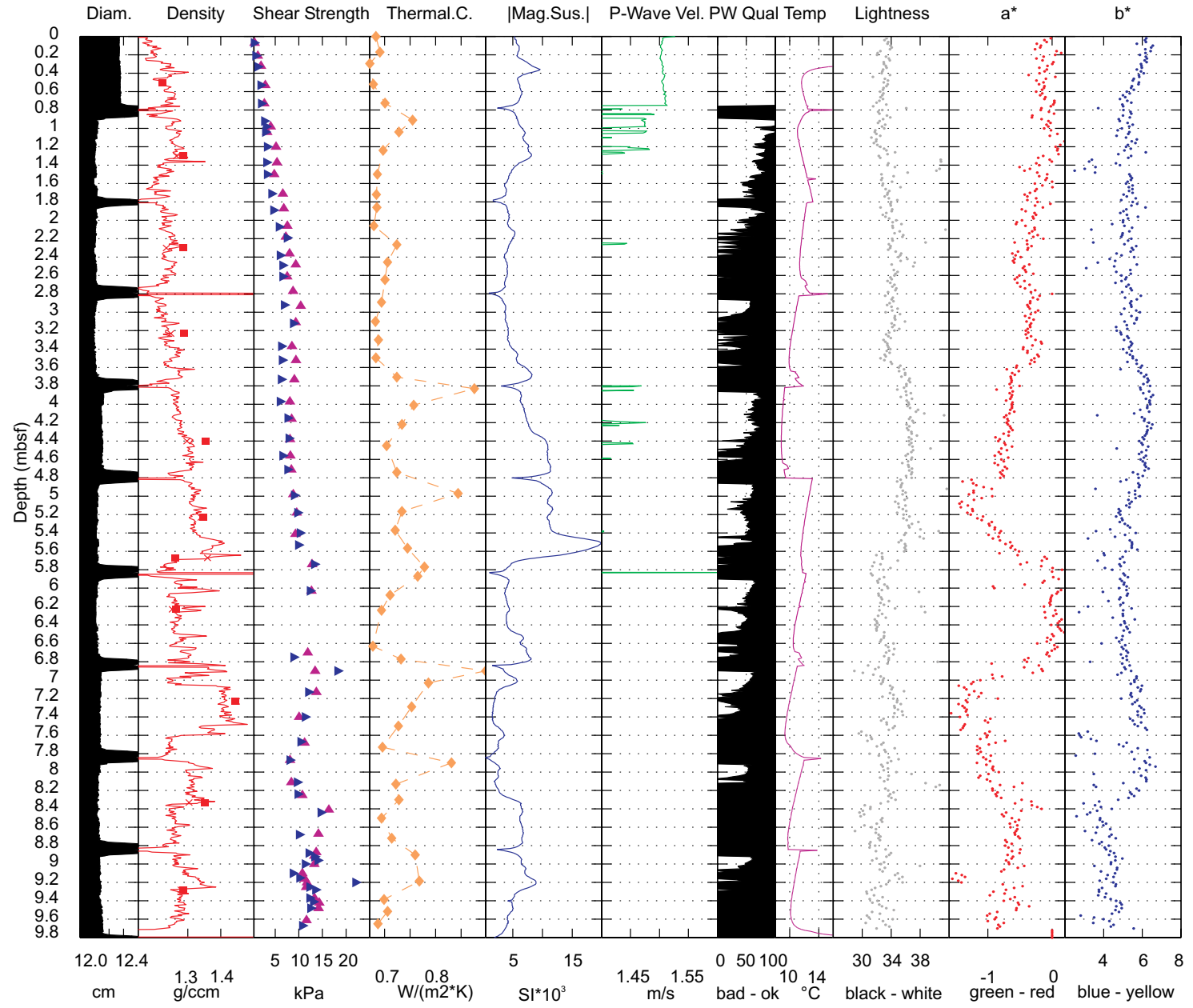
Core M 54-6



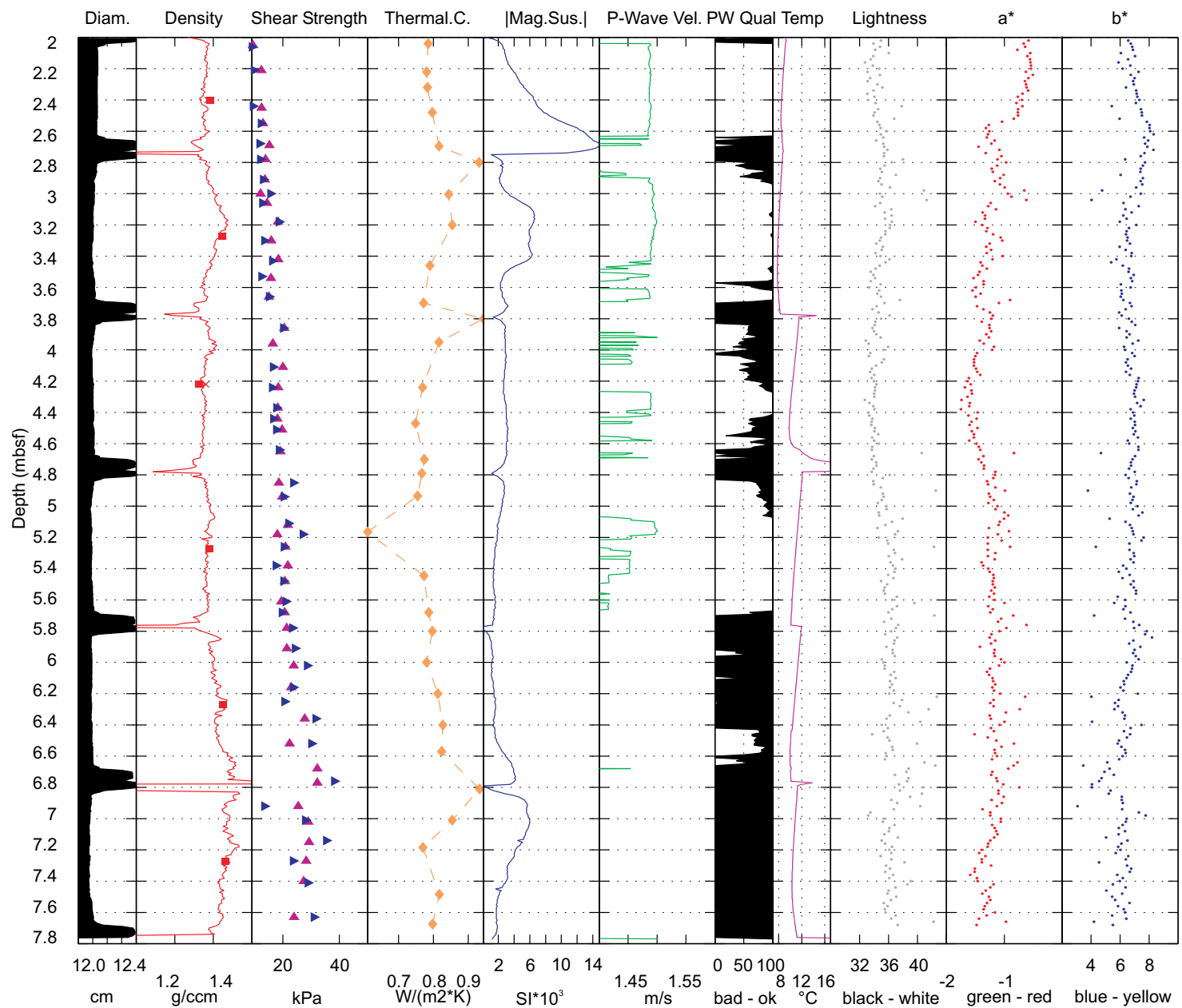
Core M 54-11/2



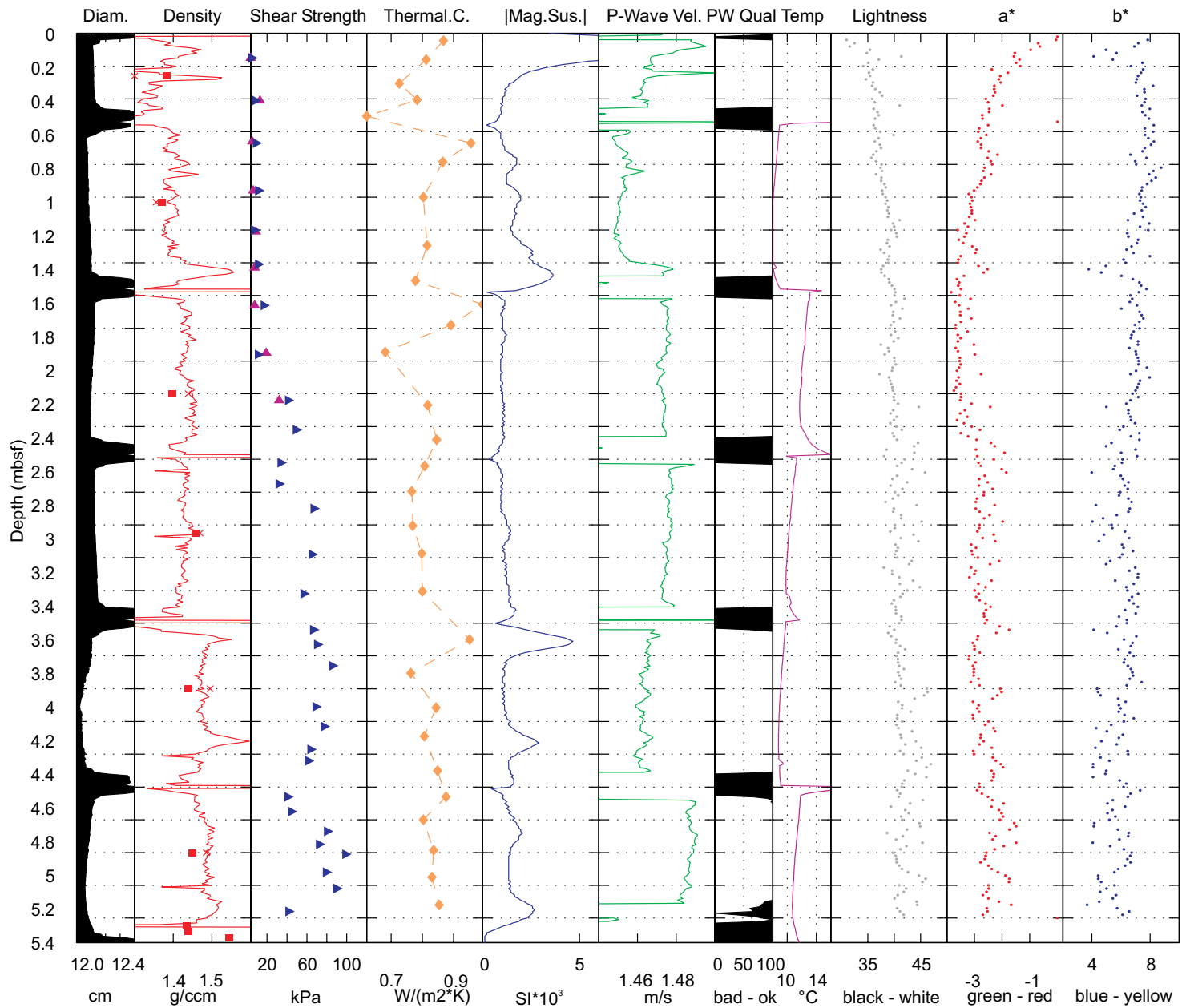
Core M 54-13



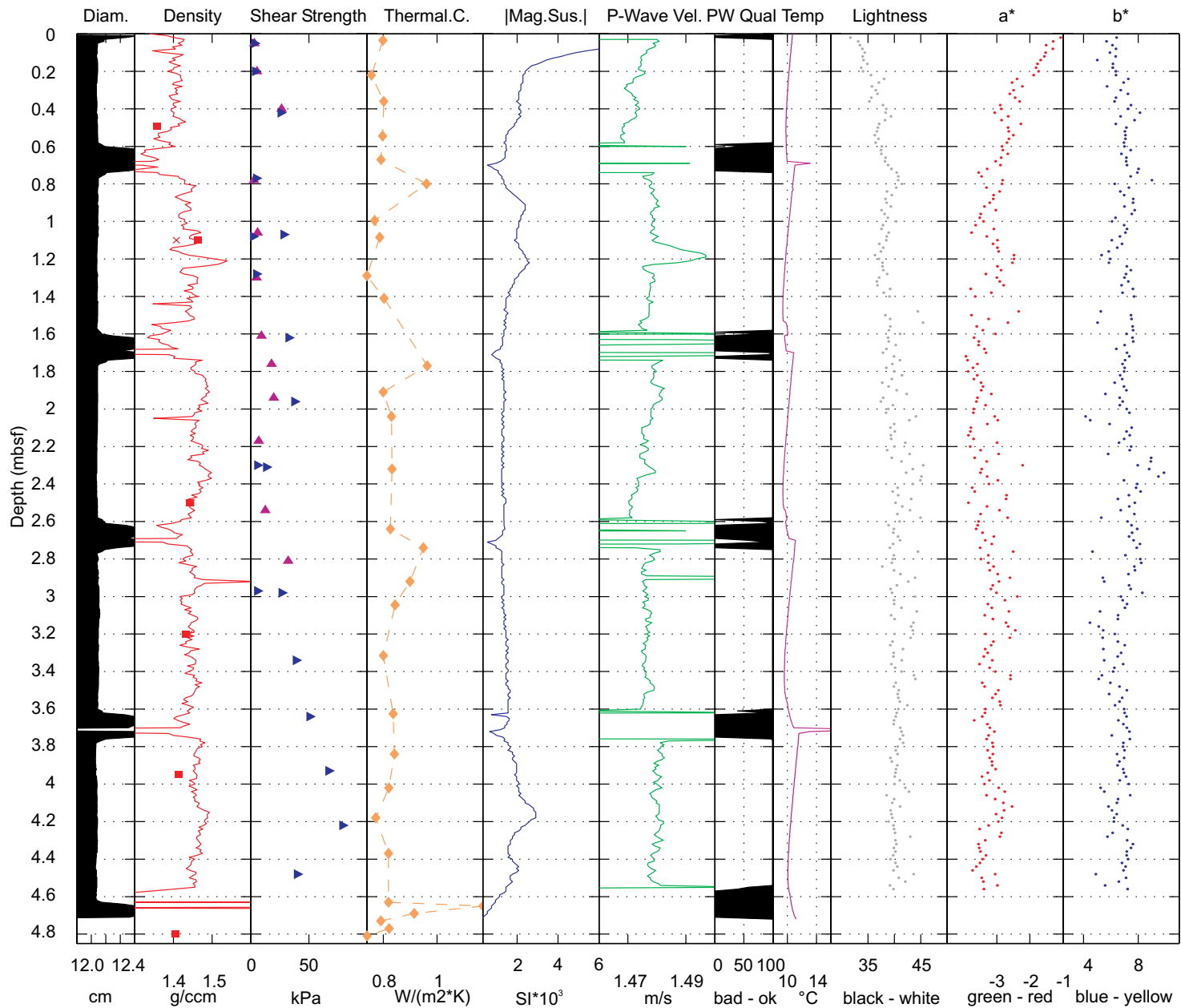
Core M 54-14



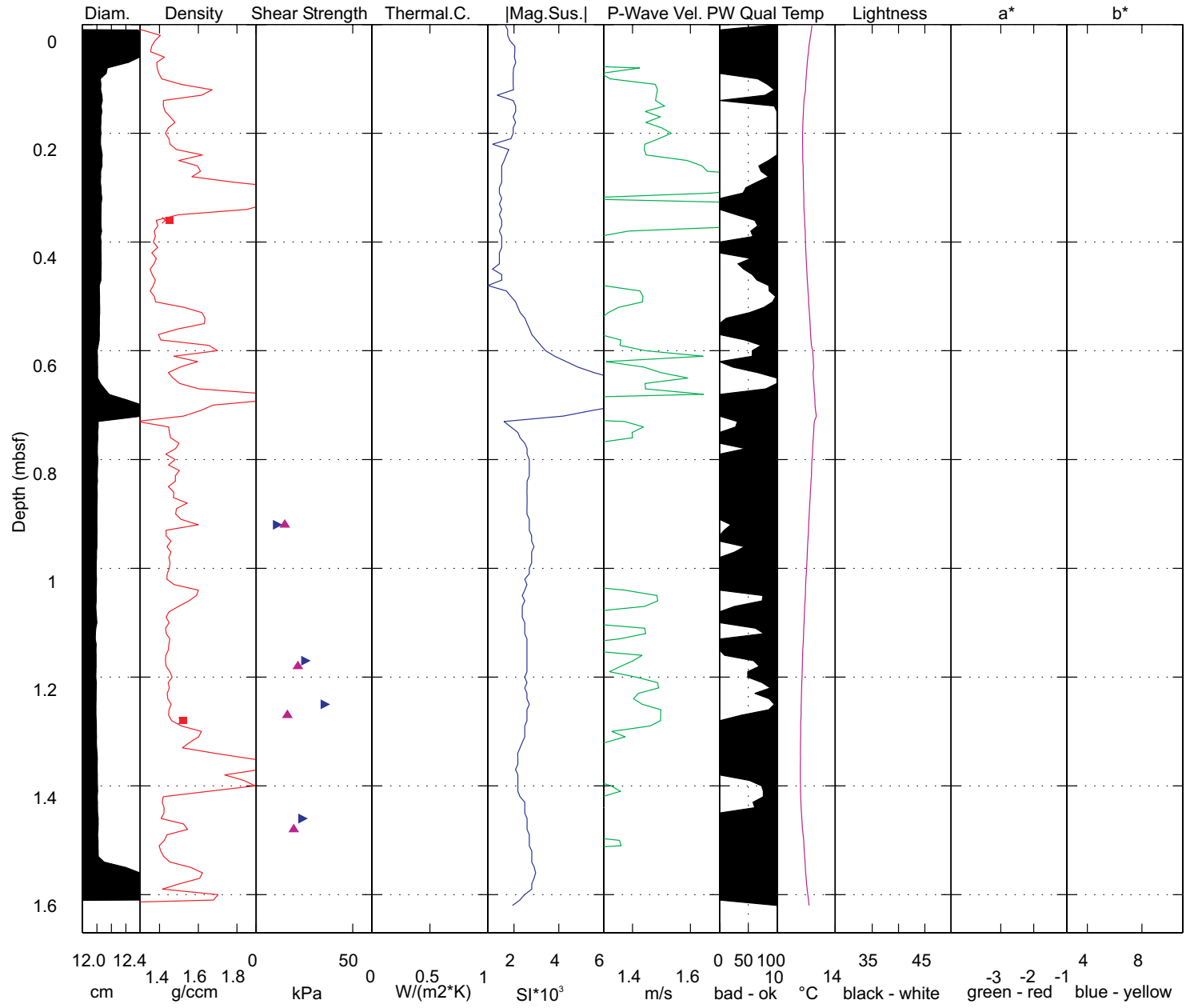
Core M 54-17 - Mound Culebra, SW Base



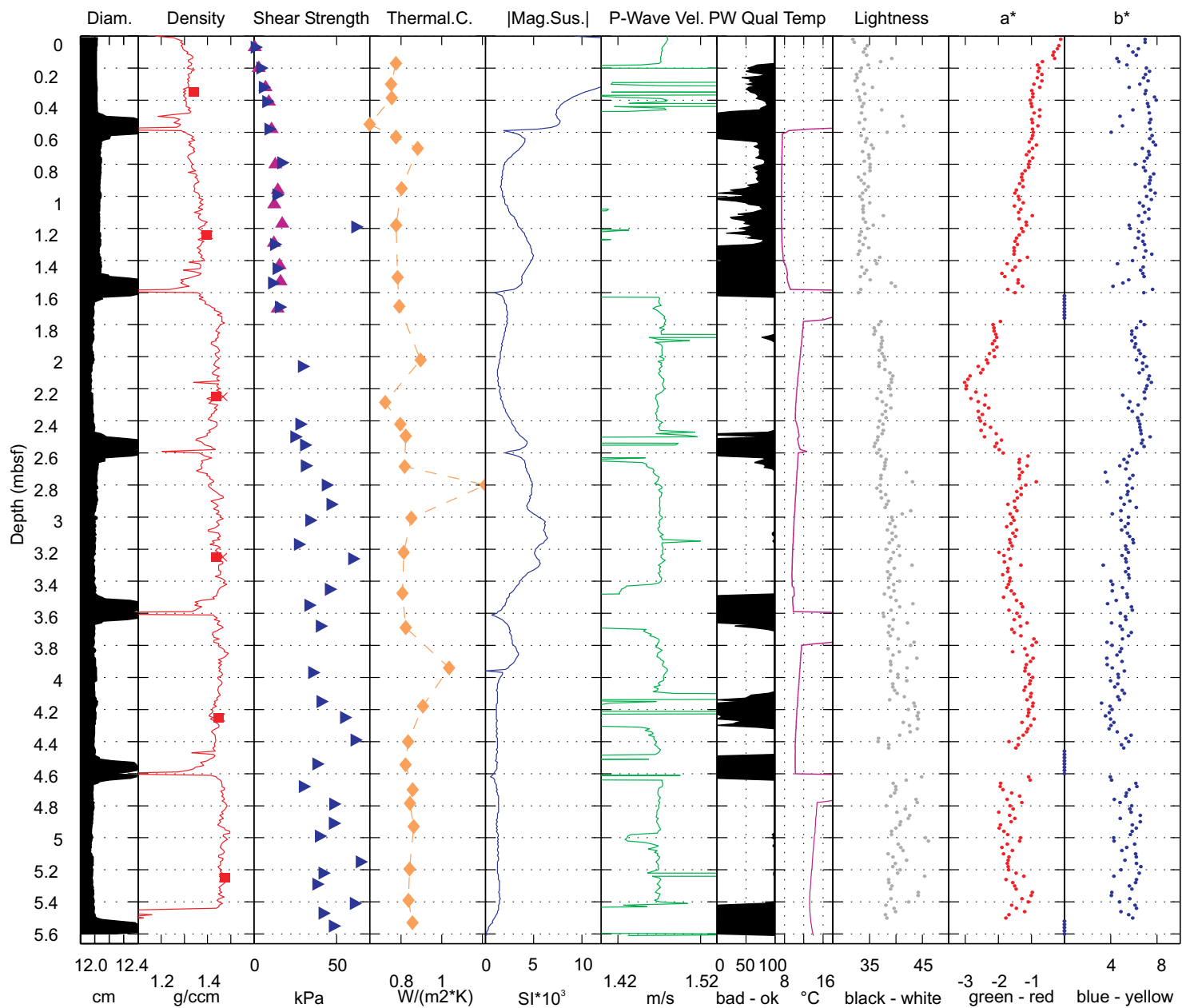
Core M 54-18 - Mound Culebra, NW Top



Core M 54-21 - Mound Culebra, NW Top



Core M 54-29 - Mound Culebra, Top



Core M 54-32 - Mound Culebra, NW Slope